12

AMSAA

ARMY MATERIEL SYSTEMS ANALYSIS ACTIVITY

AD A128964

PROCEEDINGS
FOURTH MEETING OF THE COORDINATING GROUP
ON
MODERN CONTROL THEORY

27-28 OCTOBER 1982
OAKLAND UNIVERSITY
ROCHESTER, MICHIGAN 48063

DTIC
S APR 26 1983 D
H

DISTRIBUTION STATEMENT A
Approved for public release;
Distribution Unlimited

DTIC FILE COPY

U S ARMY MATERIEL SYSTEMS ANALYSIS ACTIVITY
ABERDEEN PROVING GROUND, MARYLAND 21005

83 04 26 012

DISPOSITION

Destroy this report when no longer needed. Do not return it to the originator.

DISCLAIMER

The findings in this report are not to be construed as an official Department of the Army position unless so specified by other official documentation.

WARNING

Information and data contained in this document are based on the input available at the time of preparation. The results may be subject to change and should not be construed as representing the DARCOM position unless so specified.

TRADE NAMES

The use of trade names in this report does not constitute an official endorsement or approval of the use of such commercial hardware or software. The report may not be cited for purposes of advertisement.

COMPONENT PART NOTICE

THIS PAPER IS A COMPONENT PART OF THE FOLLOWING COMPILATION REPORT:

(TITLE): Proceedings of the Meeting of the Coordinating Group on Modern Control Theory (4th) Held at Rochester, Michigan on 27-28 October 1982, Part I.

(SOURCE): Army Materiel Systems Analysis Activity

Aberdeen Proving Ground, MD 21005

TO ORDER THE COMPLETE COMPILATION REPORT USE AD-A128 964.

THE COMPONENT PART IS PROVIDED HERE TO ALLOW USERS ACCESS TO INDIVIDUALLY AUTHORED SECTIONS OF PROCEEDINGS, ANNALS, SYMPOSIA, ETC. HOWEVER, THE COMPONENT SHOULD BE CONSIDERED WITHIN THE CONTEXT OF THE OVERALL COMPILATION REPORT AND NOT AS A STAND-ALONE TECHNICAL REPORT.

THE FOLLOWING COMPONENT PART NUMBERS COMPRISE THE COMPILATION REPORT:

AD#:	TITLE:
P001 062	Wideband Modern Control of Microprocessor-Based Tracking and Pointing Systems.
P001 063	Discrete-Time Disturbance Accommodating Control of a Helicopter Gun-Turret System.
P001 064	Firing Data Comparison of Classical and Modern Turret Controllers.
P001 065	Development of a Combat Vehicle Support Plan Using Modern System Theory.
P001 066	Closed Loop Methodology Applied to the Combat Vehicle Support Plan.
P001 067	Controllability of Disturbed Reticle Tank Fire Control Systems.
P001 068	Endgame Performance Tradeoff Study of a Special Class of Interceptors.
P001 069	Applications of Heuristic and Game-Theoretic Paradigms to Fire Control.
P001 070	Application of Modern Control Theory and Adaptive Control Concepts to the Guidance and Control of a Terminally Guided Anti-Tank Weapon.
P001 071	Free-Flight Rocket Guidance with the Spinning Plug Nozzle.
P001 072	Boost-Phase Steering for Surface-Launched Cruise Missiles.
P001 073	Closed-Loop Bullet Tracking Algorithms for Digital Fire Control Systems.
P001 074	DARPA (Defense Advanced Research Projects Agency) Program Intelligent Task Automation (ITA).
P001 075	Vision Systems for Intelligent Task Automation.
P001 076	A Robotic Tank Gun Autoloader.
P001 077	Experiments in Nonlinear Adaptive Control of Mechanical Linkage Systems.
P001 078	Multi-Resolution Clutter Rejction.
P001 079	An Optimal Integral Submarine Depth Controller.
P001 080	Regulator Design for Linear Systems Whose Coefficients Depend on Parameters.

COMPONENT PART NOTICE (CON'T)

AD#:		TITLE:
P001 081		A Nonlinear Liapunov Inequality.
P001 082		Nonlinear Control for Robotic Applications.
P001 083		Integrated Simulation of Vehicular Systems with Stabilization.
P001 084		Full Scale Simulation of Large Scale Mechanical Systems.
P001 085		VATT (Video Automatic Target Tracker) - The Gunner's 'Invisible' Aid.
P001 086		A Modern Control Approach to Gun Firing Accuracy Improvements.
P001 087		A Modern Control Theory View of HIMAG Test Data.
P001 088		Maneuvering Vehicle Path Simulator.
P001 089		Improving Air-to-Ground Gunnery Using an Attack Autopilot and A Moveable Gun.
P001 090		A Fire Coordination Center for Lightweight Air Defense Weapons.
P001 091		Closed-Form Control Algorithm for Continuous-Time Disturbance-Utilizing Control Including Autopilot Lag.
P001 092		Control of a Spinning Projectile.
P001 093		Information Enhancement and Homing Missile Guidance.
P001 094		Robustifying the Kalman Filter via Pseudo-Measurements.

DTIC
SELECTED
S JUN 9 1983 D
A

Accession For	
NTIS GRA&I	☑
DTIC TAB	☐
Unannounced	☐
Justification	
By	
Distribution/	
Availability Codes	
Dist	Avail and/or Special
A	

This document has been approved for public release and sale; its distribution is unlimited.

UNCLASSIFIED
SECURITY CLASSIFICATION OF THIS PAGE (When Data Entered)

REPORT DOCUMENTATION PAGE		READ INSTRUCTIONS BEFORE COMPLETING FORM
1. REPORT NUMBER	2. GOVT ACCESSION NO. AD-A128964	3. RECIPIENT'S CATALOG NUMBER
4. TITLE (and Subtitle) Proceedings of the Fourth Meeting of the Coordinating Group on Modern Control Theory (27-28 Oct 1982) Oakland University, Rochester, Michigan 48063		5. TYPE OF REPORT & PERIOD COVERED Conference
		6. PERFORMING ORG. REPORT NUMBER
7. AUTHOR(s) H. Cohen (Chairman)		8. CONTRACT OR GRANT NUMBER(s)
9. PERFORMING ORGANIZATION NAME AND ADDRESS Director US Army Materiel Systems Analysis Activity Aberdeen Proving Ground, MD 21005		10. PROGRAM ELEMENT, PROJECT, TASK AREA & WORK UNIT NUMBERS DA Project No. 1R665706M541
11. CONTROLLING OFFICE NAME AND ADDRESS Director US Army Materiel Systems Analysis Activity ATTN: DRXSY-MP, Aberdeen Proving Ground, MD 21005		12. REPORT DATE October 1982
		13. NUMBER OF PAGES 642
14. MONITORING AGENCY NAME & ADDRESS (if different from Controlling Office) Cdr, US Army Materiel Development & Readiness Command, 5001 Eisenhower Avenue, Alexandria, VA 22333		15. SECURITY CLASS. (of this report) UNCLASSIFIED
		15a. DECLASSIFICATION/DOWNGRADING SCHEDULE
16. DISTRIBUTION STATEMENT (of this Report) Approved for public release; distribution unlimited		
17. DISTRIBUTION STATEMENT (of the abstract entered in Block 20, if different from Report)		
18. SUPPLEMENTARY NOTES		
19. KEY WORDS (Continue on reverse side if necessary and identify by block number) Control Theory, Kalman Filtering, Man-Model, Maneuvering Target, Fire Control, Missile Guidance and Control, Robotics, Artificial Intelligence		
20. ABSTRACT (Continue on reverse side if necessary and identify by block number) Report documents papers presented at fourth meeting of the coordinating group on modern control theory with emphasis on military weapon systems.		

DD FORM 1 JAN 73 1473 EDITION OF 1 NOV 65 IS OBSOLETE

UNCLASSIFIED
SECURITY CLASSIFICATION OF THIS PAGE (When Data Entered)

TABLE OF CONTENTS

Title	Page
AGENDA	iv
ACKNOWLEDGEMENT	xi
WIDEBAND MODERN CONTROL OF MICROPROCESSOR-BASED TRACKING AND POINTING SYSTEMS William J. Bigley, Vincent J. Rizzo	3
DISCRETE-TIME DISTURBANCE ACCOMMODATING CONTROL OF A HELICOPTER GUN-TURRET CONTROL SYSTEM N. P. Coleman, R. Johnson, E. Carroll	25
FIRING DATA COMPARISON OF CLASSICAL AND MODERN TURRET CONTROLLERS Gerald A. Strahl	45
DEVELOPMENT OF A COMBAT VEHICLE SUPPORT PLAN USING MODERN SYSTEM THEORY A. Fermelia	67
CLOSED LOOP METHODOLOGY APPLIED TO THE COMBAT VEHICLE SUPPORT PLAN A. Fermelia	87
CONTROLLABILITY OF DISTURBED RETICLE TANK FIRE CONTROL SYSTEMS Paul G. Cushman	105
ENDGAME PERFORMANCE STUDY OF A SPECIAL CLASS OF INTERCEPTORS Johnathan Korn, Sol W. Gully	123
APPLICATIONS OF HEURISTIC AND GAME-THEORETIC PARADIGMS TO FIRE CONTROL Max Mintz, Terry L. Neighbor, Walter Dziwak, S. S. Wolff	133
APPLICATION OF MODERN CONTROL THEORY AND ADAPTIVE CONTROL CONCEPTS TO THE GUIDANCE AND CONTROL OF A TERMINALLY GUIDED ANTITANK WEAPON R. D. Ehrich	155
FREE-FLIGHT ROCKET GUIDANCE WITH THE SPINNING PLUG NOZZLE W. E. Judnick, Aryeh H. Samuel	179
BOOST-PHASE STEERING FOR SURFACE-LAUNCHED CRUISE MISSILES D. J. Fromnes	197
CLOSED-LOOP BULLET TRACKING ALGORITHM FOR DIGITAL FIRE CONTROL SYSTEMS R. S. Baheti	225

Title	Page
DARPA INTELLIGENT TASK AUTOMATION (ITA) E. van Reuth, E. C. Levinthal	247
VISION SYSTEMS FOR INTELLIGENT TASK AUTOMATION C. P. Christensen, R. A. Geesey, C. M. Stickley	259
A ROBOTIC TANK GUN AUTOLOADER Stephen Derby	263
EXPERIMENTS IN NONLINEAR ADAPTIVE CONTROL OF MECHANICAL LINKAGE SYSTEMS T. M. Depkovich	277
## FORCE FEEDBACK SENSORS FOR ROBOT ADAPTIVE CONTROL Robert De Moyer, Eugene Mitchell, John Vranish	Dupe of AD-P000 962
CHALLENGES IN ROBOTIC AND ARTIFICIAL INTELLIGENCE FOR NBC REMOTE DETECTION AND RECONNAISSANCE Kirkman Phelps, William R. Loerop, Bernard W. Fromm	297
ROBOT DECONTAMINATING SYSTEMS Mathew Kaufman	313
MULTI-RESOLUTION CLUTTER REJECTION Allen Gorin	333
AN OPTIMAL INTEGRAL SUBMARINE DEPTH CONTROLLER M. J. Dundics	341
## MODERN CONTROL TECHNIQUES APPLICABLE TO THE SPACE SHUTTLE MAIN ENGINE Richard E. Brewster, Esmat C. Bekir, Thomas C. Evatt.	Dupe of AD-P000 963
REGULATOR DESIGN FOR LINEAR SYSTEMS WHOSE COEFFICIENT DEPEND ON PARAMETERS E. W. Kamen, P. P. Khargonekar	359
A NONLINEAR LIAPUNOV INEQUALITY Leon Lotin	367
NONLINEAR CONTROL FOR ROBOTIC APPLICATIONS William H. Boykin, Allon Guez	375
INTEGRATED SIMULATION OF VEHICULAR SYSTEMS WITH STABILIZATION George M. Lance, Gwo-Gee Liang, Mark A. McCleary.	387
FULL SCALE SIMULATION OF LARGE SCALE MECHANICAL SYSTEMS Edward J. Haug, Gerald Jackson	411
VEHICLE SUSPENSION DYNAMIC OPTIMIZATION ## Edward J. Haug, Vikram N. Sohoni, Sang S. Kim, Hwal-G Seong	Dupe of AD-P000 964

Title	Page
// COMPONENT MODE ANALYSIS OF LARGE SCALE INERTIA VARIANT MECHANICAL SYSTEMS WITH FLEXIBLE ELEMENTS AND CONTROL SYSTEMS Dupe of AD-P000 965 Ahmed Schaban, Roger A. Wehage	
VATT - The Gunner's "Invisible" Aid J. A. Wes	437
A MODERN CONTROL APPROACH TO GUN FIRING ACCURACY IMPROVEMENTS Robert J. Talir, Donald L. Ringkamp, Fred W. Stein	447
A MODERN CONTROL THEORY VIEW OF HIMAG TEST DATA R. A. Scheder, A. T. Green, B. C. Culver	467
MANEUVERING VEHICLE PATH SIMULATOR T. R. Perkins, H. H. Burke, J. L. Leathrum	487
IMPROVING AIR-TO-GROUND GUNNERY USING AN ATTACK AUTOPILOT AND A MOVEABLE GUN Dr. Edward J. Bauman, CPT Randall L. Shepard	507
A FIRE COORDINATION CENTER FOR LIGHTWEIGHT AIR DEFENSE WEAPONS William C. Cleveland	535
CLOSED-FORM CONTROL ALGORITHM FOR CONTINUOUS-TIME-DISTURBANCE-UTILIZING CONTROL INCLUDING AUTOPILOT LAG Jerry Bosley, Wayne Kendrick	547
CONTROL OF A SPINNING PROJECTILE N. A. Lehtomaki, J. E. Wall, Jr.	555
INFORMATION ENHANCEMENT AND HOMING MISSILE GUIDANCE Jason L. Speyer and David G. Hull	597
ROBUSTIFYING THE KALMAN FILTER VIA PSEUDO-MEASUREMENTS Dr. G. A. Hewer and Robert J. Sacks.	623

// Handouts provided; will appear as Part II of Proceedings

Accession For
NTIS GRA&I
DTIC TAB
Unannounced
Justification
By
Distribution/
Availability Codes
Dist | Avail and/or Special
A

FOURTH MEETING

OF

COORDINATING GROUP ON MODERN CONTROL THEORY

27-28 OCTOBER 1982

OAKLAND UNIVERSITY
MEADOW BROOK HALL
Rochester, Michigan 48063

AGENDA

WEDNESDAY, 27 OCTOBER 1982

ROOM #1 - MORNING

SESSION I: Weapon Stabilization and Control (Chairman - Dr. Ronald Beck)

WELCOMING STATEMENT -

0900 - Wideband Modern Control of Microprocessor-Based Tracking and Pointing Systems
by William J. Bigley, Vincent J. Rizzo
Lockheed Electronics Company, Inc.
Plainfield, New Jersey 07061

0930 - Discrete-Time Disturbance Accommodating Control of a Helicopter Gun-Turret System
by N. P. Coleman, R. Johnson, E. Carroll
US Army Armament Research & Development Command
Dover, New Jersey 07801

1000 - Firing Data Comparison of Classical and Modern Turret Controllers
by G. A. Strahl
Ware Simulation Section
US Army Armament Research & Development Command
Rock Island, IL 61299

1030 - Development of a Combat Vehicle Support Plan Using Modern System Theory
by A. Fermelia
Martin-Marietta Aerospace
Denver Division (Mail Stop 0570)
P. O. Box 179
Denver, CO 80201

1100 - Closed Loop Methodology Applied to the Combat Vehicle Support Plan
by A. Fermelia
Martin-Marietta Aerospace
Denver Division (Mail Stop 0570)
P. O. Box 179
Denver, CO 80201

1130 - Controllability of Disturbed Reticle Tank Fire Control Systems
by Paul G. Cushman
Ordnance Systems
General Electric Company
Pittsfield, Mass. 01201

ROOM #2 - MORNING

SESSION II: Missile/Air Defense Fire Control (Chairman - Mr. Herbert E. Cohen)

0900 - Endgame Performance Study of a Special Class of Interceptors
by Dr. Jonathan Korn
ALPHATECH, Inc.
3 New England Executive Park
Burlington, Mass. 01803

0930 - Applications of Heuristic and Game-Theoretic Paradigms to Fire Control
by Max Mintz
Dept of Systems Engineering
University of Pennsylvania
Philadelphia, PA 19104

Terry L. Neighbor
Advanced Development Branch
Air Force Flight Dynamics Laboratory
Wright-Patterson AFB, OH 45433

Walter Dziwak
US Army Armament Research & Development Command
Fire Control & Small Caliber Weapon Systems Laboratory
Dover, NJ 07801

Stephen S. Wolff
US Army Armament Research & Development Command
Ballistic Research Laboratory
Aberdeen Proving Ground, MD 21005

1000 - Application of Modern Control Theory and Adaptive Control Concepts to the Guidance and Control of a Terminally Guided Anti-Tank Weapon
by R. D. Ehrich
Missile Systems Division
Rockwell International
Columbus, OH 43216

1030 - Free-Flight Rocket Guidance with the Spinning Plug Nozzle
by W. E. Judnick and A. H. Samuel
Battelle-Columbus Laboratories
505 King Avenue
Columbus, OH 43201

1100 - Boost-Phase Steering for Surface-Launched Cruise Missiles
by D. J. Fromnes
General Dynamics Convair Division
P. O. Box 80847
San Diego, CA 92138

1130 - Closed-Loop Bullet Tracking Algorithms for Digital Fire Control Systems
by Radhakisan S. Baheti
Corporate Research & Development
General Electric Company
Schenectady, NY 12345

ROOM #1 - AFTERNOON

SESSION III: Robotics (Chairman - Professor Nan K. Loh)

1300 - DARPA Intelligent Task Automation (ITA)
by Dr. Edward C. van Reuth
Dr. Elliott C. Levinthal
Defense Advanced Research Projects Agency
1400 Wilson Boulevard
Arlington, VA 22209

1330 - Vision Systems for Intelligent Task Automation
by Dr. C. Paul Christensen
Dr. Roger A. Geesey
Dr. C. Martin Stickley
The BDM Corporation
7915 Jones Branch Drive
McLean, VA 22102

1400 - A Robotic Tank Gun Autoloader
by S. J. Derby
Benet Weapons Laboratory, LCWSL
US Army Armament Research & Development Command
Watervliet Arsenal
Watervliet, NY 12189

1430 - Experiments in Nonlinear Adaptive Control of Mechanical Linkage Systems
by T. M. Depkovich
Martin-Marietta Aerospace
Denver Division (Mail Stop 0570)
P. O. Box 179
Denver, CO 80201

H. Elliott
Department of Electrical & Computer Engineering
University of Massachusetts
Amherst, MA 01003

1500 - Force Feedback Sensors for Robot Adaptive Control
by Robert DeMoyer, Eugene Mitchell
US Naval Academy
Mail Drop 14A
Annapolis, MD 21402

John Vranish
Naval Surface Weapons Center
NSWC Robotics R&D Laboratory
Dhalgren, VA

1530 - Challenges in Robotic and Artificial Intelligence for NBC Remote Detection and Reconnaissance
by Kirkman Phelps, William R. Loerop, Bernard W. Fromm
Chemical Systems Laboratory
US Army Armament Research & Development Command
Aberdeen Proving Ground, MD 21005

1600 - Robot Decontaminating Systems
by M. B. Kaufman
Chemical Systems Laboratory
US Army Armament Research & Development Command
Aberdeen Proving Ground, MD 21005

1630 - Multi-Resolution Clutter Rejection
by Dr. Allen Gorin
Image Processing Lab
Lockheed Electronics Company
Plainfield, NJ

ROOM #2 - AFTERNOON

SESSION IV: Control Theory & Applications (Chairman - Mr. Toney Perkins)

1300 - An Optimal Integral Submarine Depth Controller
by M. J. Dundics
Director of Program Development
Tracor Incorporated
19 Thames St
Groton, CT 06340

1330 - Modern Control Techniques Applicable to the Space Shuttle Main Engine
by Richard E. Brewster, Esmat C. Bekir, Thomas C. Evatt
Rockwell International
Columbus, OH 43216

1400 - Regulator Design for Linear Systems Whose Coefficients Depend on Parameters
by E. W. Kamen, P.P. Khargonekar
Center for Matehmatical System Theory
Department of Electrical Engineering
University of Florida
Gainesville, Florida 32611

1430 - A Nonlinear Liapunov Inequality
by Leon Kotin
Center for Tactical Computer Systems
US Army Communications-Electronics Command
Fort Monmouth, NJ 07703

1500 - Nonlinear Control for Robotic Applications
by William H. Boykin, Allon Guez
System Dynamics Incorporated
1219 N. W. 10th Avenue
Gainesville, FL 32601

1530 - Integrated Simulation of Vehicular Systems with Stabilization
by George M. Lance, Gwo-Gee Liang, Mark A. McCleary
Center for Computer Aided Design
College of Engineering
The University of Iowa
Iowa City, Iowa 52242

1600 Full Scale Simulation of Large Scale Mechanical Systems
by Edward J. Haug, Gerald Jackson
Center for Computer Aided Design
College of Engineering
The University of Iowa
Iowa City, Iowa 52242

1630 - Vehicle Suspension Dynamic Optimization
by Edward J. Haug, Vikram N. Sohoni, Sang S. Kim, Hwal-G Seong
Center for Computer Aided Design
College of Engineering
The University of Iowa
Iowa City, Iowa 52242

1700 - Component Mode Analysis of Large Scale Inertia Variant Mechanical Systems with Flexible Elements and Control Systems
by Ahmed Schaban, Roger A. Wehage
Center for Computer Aided Design
College of Engineering
The University of Iowa
Iowa City, Iowa 52242

THURSDAY, 28 OCTOBER 1982

ROOM #1 - MORNING

SESSION V: Gun Fire Control (Chairman - Dr. Norman Coleman)

0900 - VATT - The Gunner's "Invisible" Aid
by J. A. Wes
Northrop Corporation
Electro-Mechanical Division
Anaheim, CA 92801

0930 - A Modern Control Approach to Gun Firing Accuracy Improvements
by Robert J. Talir, Donald L. Ringkamp, Fred W. Stein
Emerson Electric Company
8100 W. Florissant Avenue
St. Louis, Missouri 63136

1000 - A Modern Control Theory View of HIMAG Test Data
by R. A. Scheder, A. T. Green, B. C. Culver
Delco Electronics Division
General Motors Corporation
Coleta, CA 93117

1030 - Maneuvering Vehicle Path Simulator
by T. R. Perkins, H. H. Burke, J. L. Leathrum
US Army Materiel Systems Analysis Activity
Aberdeen Proving Ground, MD 21005

1100 - Improving Air-to-Ground Gunnery Using an Attack Autopilot and a Moveable Gun
by Dr. Edward J. Bauman
Department of Electrical Engineering
University of Colorado
Colorado Springs, CO 80907

Captain Randall L. Shepard
Department of Astronautics
USAF Academy, CO 80840

ROOM #2 - MORNING

SESSION VI: Missile Stabilization & Control (Chairman - Dr. Donald R. Falkenburg)

0900 - A Fire Coordination Center for Lightweight Air Defense Weapons
by William C. Cleveland
LADS Program Office
Ford Aerospace & Communications Corporation
Newport Beach, CA 92660

0930 - Closed-Form Control Algorithm for Continuous-Time Disturbance-Utilizing Control Including Autopilot Lag
by Jerry Bosley
Wayne Kendrick
Computer Sciences Corporation
Huntsville, AL 35898

1000 - Control of a Spinning Projectile
by N. A. Lehtomaki, J. E. Wall, Jr.
Honeywell Systems and Research Center
2600 Ridgway Parkway
Minneapolis, Minnesota 55413

1030 - Information Enhancement and Homing Missile Guidance
by Jason L. Speyer and David G. Hull
Department of Aerospace Engineering & Engineering Mechanics
University of Texas
Austin, Texas 78712

1100 - Robustifying the Kalman Filter via Pseudo-Measurements
by Dr. G. A. Hewer and Robert J. Sacks
RF Anti-Air Branch
Weapons Synthesis Division
Naval Weapons Center
China Lake, CA 93555

ACKNOWLEDGEMENT

I would like to take this opportunity to thank Sharon Betts of the Protocol Office, US Army Tank-Automotive Command for her invaluable assistance in arranging this meeting and to Professor Nan Loh, Oakland University and Dr. Ronald Beck, US Army Tank-Automotive Command, for their dedicated work in developing an outstanding technical program. Lastly, to Otto Renius, US Army Tank-Automotive Command for the support and encouragement he has provided and to Dean Mohammed S. Ghausi, Dean of the School of Engineering, Oakland University for making these beautiful facilities available.

HERBERT E. COHEN
Chairman
Coordinating Group on
Modern Control Theory

Next page is blank.

SESSION I: WEAPON STABILIZATION AND CONTROL

27 OCT 1982

(MORNING)

ROOM #1

FOURTH MEETING OF THE COORDINATING

GROUP ON MODERN CONTROL THEORY

HOSTED BY: OAKLAND UNIVERSITY
ROCHESTER, MICHIGAN

Next page is blank.

AD P001062

WIDEBAND MODERN CONTROL OF MICROPROCESSOR-BASED TRACKING AND POINTING SYSTEMS

William J. Bigley
Vincent J. Rizzo
Lockheed Electronics Company, Inc. (LEC)
Plainfield, New Jersey 07061

ABSTRACT

This paper describes recent results of a multi-year research effort to develop wideband, high accuracy tracking and weapon pointing control systems through the practical implementation of *modern control* theory in a state-of-the-art, microprocessor-based, weapon control system.

Linear Quadratic (LQ) control laws were applied to an existing weapon system at the hardware level in order to optimize plant performance in the presence of certain non-linearities and mechanical resonance constraints. This hardware approach has enabled us to apply *modern control* theory to the development of fast response, large scale weapon systems without the degrading limitations usually associated with the plant hardware.

Two different optimal control techniques were developed and demonstrated with existing weapon system equipment. One technique was applied to the weapon pointing rate loops, and the other was used to control the electro-optical target tracking sensor subsystem. A practical design procedure, based upon an extensive library of computer programs, that was developed to analyze, simulate, program, and implement deterministic type *modern control* systems with higher order dynamics is also described in this paper.

INTRODUCTION

Modern control theory has been commonly applied to tracking filters, and similar predictive type control functions, where system dynamics are well defined and relatively simple to model. If the higher order system dynamics are not or cannot be accurately modeled, application of *modern control* theory is confined to low bandwidth loops.

The purpose of this research project was to develop practical *modern control* techniques for optimizing wideband plant hardware rate loops in the presence of certain non-linearities and high order dynamic constraints such as mechanical resonance.

The work described here is the latest effort in a long term R&D program that was initiated in 1976 to develop wideband microprocessor based control systems with modern and adaptive control capabilities. The first breakthrough came in 1977 when the Resonance Equalization technique (patented) was developed to eliminate rate loop bandwidth restrictions caused by mechanical drive resonance.[1] By 1979 techniques for implementing microprocessor control of wideband sampled data feedback loops were developed and demonstrated in an all-digital, multiloop control system for LEC's improved version of the U.S. Army Vulcan Air Defense System (IVADS).[2] In the subject research project, many of these new classical control techniques for overcoming bandwidth restrictions were utilized in developing wideband *modern control* methods.

At present, classically designed weapon control systems have dynamic limitations against the threats of high performance air and surface targets. More advanced and sophisticated feedback control techniques for future weapon control systems are necessary to meet the demand for greater accuracy and faster response at reasonable cost. The demand for such wideband super accurate tracking systems is particularly high in mobile weapon systems and gun netting systems.

The practical on-line modeling of plants containing high order dynamics, non-linearities, and noise uncertainties are the major problems constraining the effective use of *modern control* theory on wideband target tracking systems.

Large inertia systems suffer from low resonance frequencies, saturation, friction and deadband constraints. The resonance problem limits bandwidth and causes instability. The others result in increased synchronization time and large following errors. If resonance frequencies and resonance gain amplitude were stationary, fixed frequency compensation would overcome them. However, resonance frequencies vary with signal level due to deadspace (i.e. backlash) and amplitude varies with speed due to coulomb friction. Saturation causes large overshoots during synchronization and small signal following errors are limited to a narrow linear region. Correcting resonance problems mechanically results in costly overdesign of mechanical drive trains. System uncertainties due to combinations of component changes, environmental conditions and other unknown random effects result in less than optimum performance.

The problem addressed in this paper is: how to combine today's *modern control* theory (optimal/adaptive), present microprocessor computing power, and newly developed classical techniques for counteracting hardware limitations in order to achieve practical, and cost effective, wideband inertially stabilized tracking and weapon pointing systems.

Two subsystems in the Lockheed IVAD weapon system were chosen as subjects for this research: the gun rate loops and the inertially stabilized sight loops. Using Linear Quadratic control theory (LQ) as the basis, one version was developed for the gun loops and another version was developed for the sight loops. Both methods are briefly described in this paper.

THE SPECIMEN WEAPON SYSTEM

For the purposes of developing wideband *modern control* techniques, the IVADS system was chosen because it already contained the microprocessor control ability required.

The IVADS gun fire control system is based on a director type system concept developed and patented by LEC.[3] It is presently configured for man-in-the-loop optical tracking operation. A simplified diagram of one of the two similar axes (elevation over azimuth) is presented in figure 1. In the initial system, all feedback loops are analog. Outside the loops, the digital central processor performs ballistics and rate-aid functions. These are injected into the system for feed-forward and leadangle control. Each axis is composed of three interrelated subsystems: (1) Gyro Stabilized Gun Sight, (2) VPS-2 Range Only Radar Control System, and (3) Gun Control System. In this version of the system, the man is the Track Error Sensor. In the version presently being produced for the Spanish Navy, Meroka, a tracking radar is also used as the Track Error Sensor.

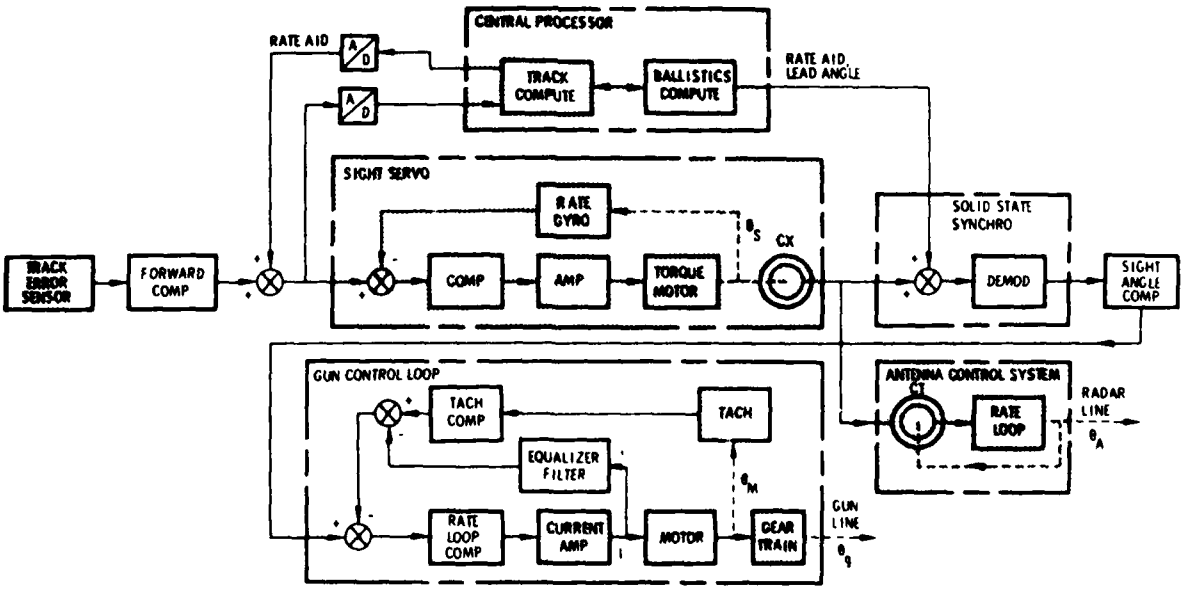


Figure 1. Analog Sharpshooter Control System (Single Axis)

All control functions that are depicted by unshaded boxes in figure 1 were implemented in the microprocessor for two axes control. This resulted in the digital control system shown in figure 2. To eliminate the need for the solid-state synchro module shown in figure 1, the sight synchro transmitter signal in the digital system is routed directly through the central processor to the microprocessor.

In this project, *modern control* techniques were applied to the "Gun Control Loop" and the "Sight Servo" subsystems shown in figure 1. Eventually, the entire fire control system will be optimally controlled.

In the chosen specimen system shown in figure 2, the block Sight Rate Loop is analog. In the process of applying one version of LQ control to this inertial rate loop, the Sight Rate Loop became an all-digital design.

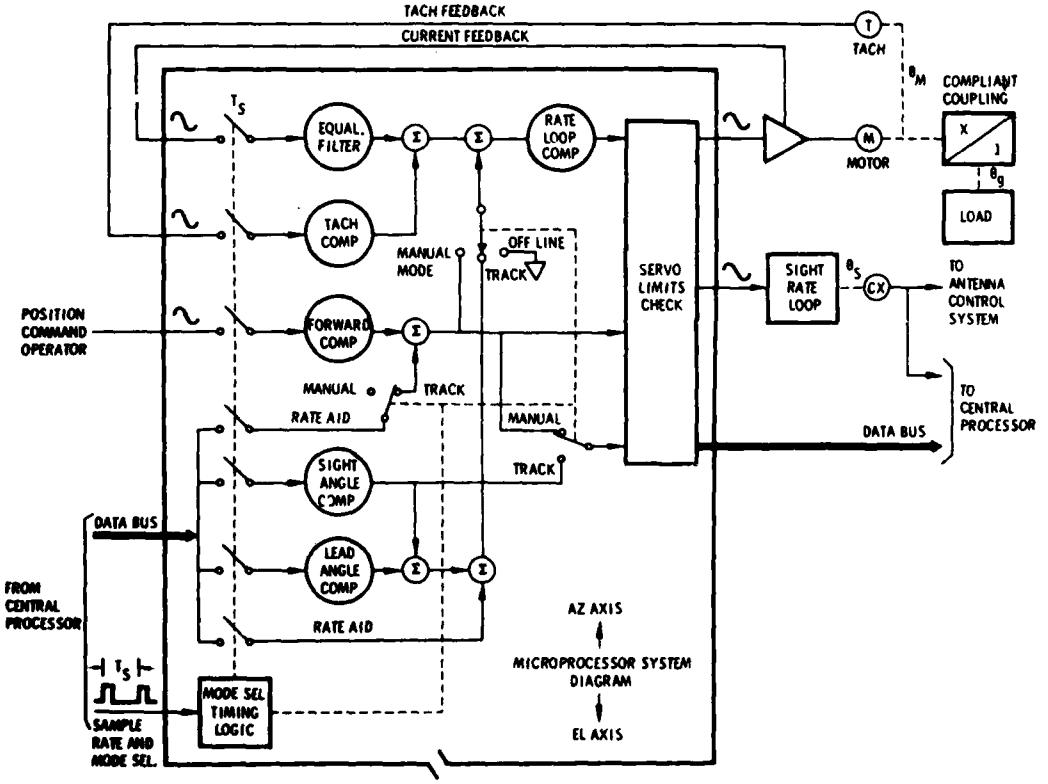


Figure 2. Digital Sharpshooter Control System (Two Axes)

GENERALIZED COMPUTER AIDED DESIGN TECHNIQUE

COMPUTER AIDED DESIGN TECHNIQUES

In the process of developing this wideband optimal rate loop, a computer aided design procedure evolved which later proved to be very useful in future designs of *modern control* systems. The following major tasks are performed in this design procedure:

1. Develop modeling techniques for plant nonlinearities and high order dynamics.

2. Select performance indices to achieve optimal design goals.

3. Ensure a practical solution by finding the optimal feedback solution and checking it with realistic system simulation methods.

4. Compare test results to evaluate the hardware model, the mathematical model, and the original classical model.

The format of this paper generally follows the pattern of the design procedure itself.

Since most tracking and weapon pointing control systems have similar topographies, a series of computer aided analysis and design techniques were formulated into a procedure for producing highly accurate and reliable *modern control* system designs in a cost effective manner. This design procedure is described in figure 3.

All the apriori information about the existing or proposed servo plant and desired system is gathered as the first step. If, for example, the servo plant exists, frequency response and step response test data are measured. For proposed designs, the motor, gear ratio, and servoamplifier characteristics are usually known. Either way, the measured data or catalog data is applied to the modeling effort in block A of figure 3.

PERFORMANCE GOALS

As a basis for comparison, the following performance goals were selected:

1. Increase rate loop bandwidth significantly beyond the mechanical antiresonance frequency in the servo plant and do so with high relative stability.

2. Reduce settling and synchronizing time below normal classical response times.

3. Reduce following error while providing a relatively wide linear operating region.

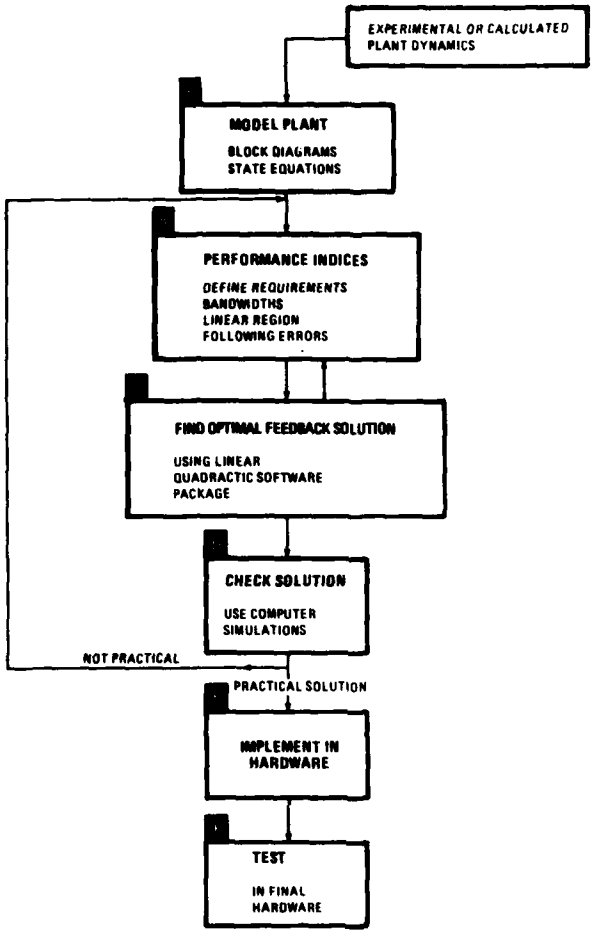


Figure 3. Design Flow Chart

This paper describes how these performance goals were achieved by applying a form of the Linear Quadratic (LQ) optimal design algorithm (4) to the power servo drive in an existing weapon pointing system. The deterministic methods described are considered a major step towards our ultimate goal of applying the more powerful stochastic *modern control* theory to achieve the super accurate tracking performance required in laser pointing systems. The LQ control theory is well known in the field of *modern control*. A good description of the theory is provided in references (4) and (5).

DEVELOPING THE GUN PLANT MODEL

The effectiveness of applying any optimizing theory is largely dependent on the validity of the model representing the plant or the process. Because the LQ control system is a "full state feedback" system, some of the states to be fed back through an optimal gain must come from an accurate model of the plant if they cannot be measured directly in the plant. With this in mind, a hybrid method for generating an accurate model of an existing plant was developed and validated.

An analog state variable diagram of the plant components is shown in figure 4. This familiar diagram contains all the usual plant non-linearities. Most of the parameters and nonlinearities are either well known or can be measured. Because the non-linearities are amplitude dependent, they cause the system in figure 4 to have frequency responses that vary with the input signal level.

One important objective in the modeling phase is to obtain the elements of the state variable equation of the plant to be optimally controlled:

$$\dot{\bar{X}} = \bar{A}\,\bar{X} + \bar{B}\,\bar{u} \qquad (1)$$

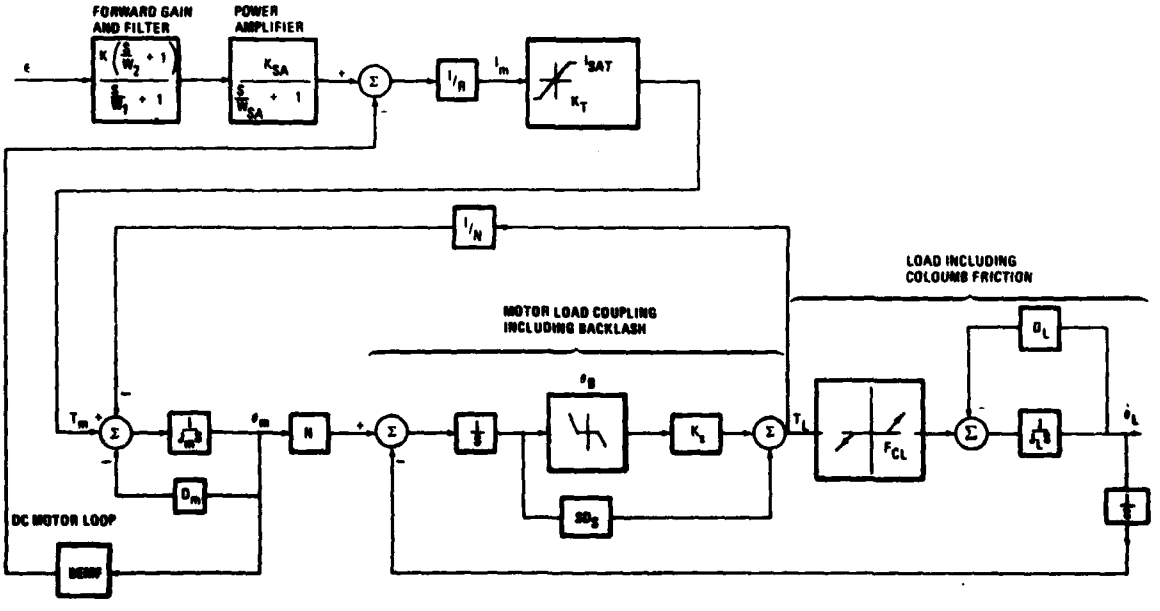


Figure 4. Single Axis Gun Drive Block Diagram

Two frequency responses were measured on the existing weapon system plant; one at a low signal level, and one at a high signal level. The results are shown in figure 5. Observe in figure 5 that the anti-resonance frequency, W_{AR}, increases with increasing excitation level. This is due to the change in effective gear train compliance (K_S) as a function of the ratios of input to backlash. The effects of coulomb friction are also apparent at low frequency in the amplitude change with signal level.

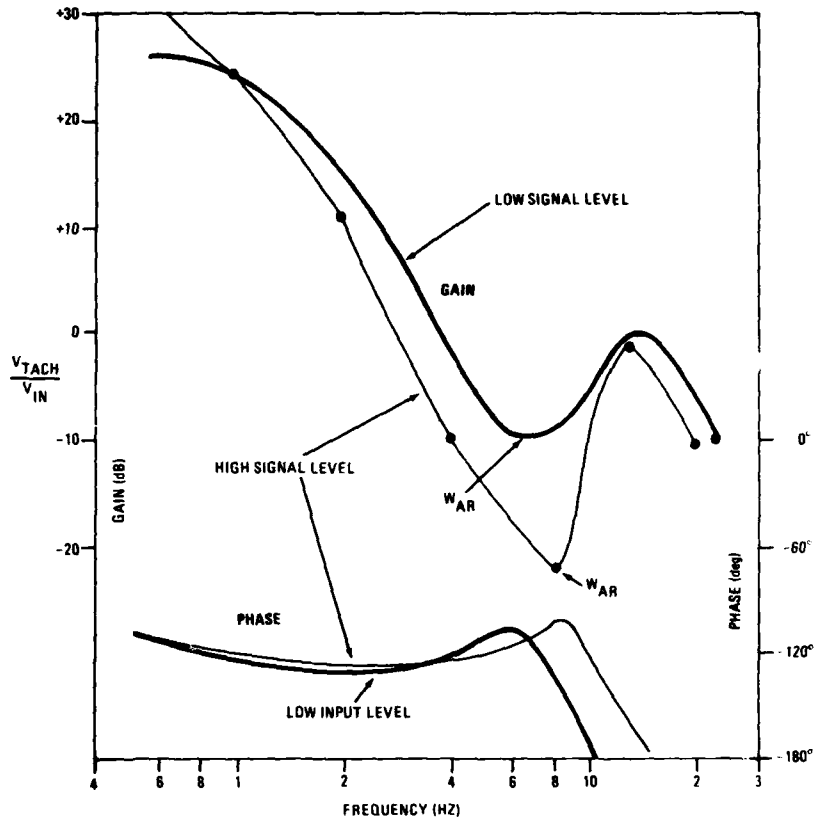


Figure 5. Open Loop Frequency Response of Gun Plant

A linear transfer function block diagram of the filter, amplifier, and loaded motor is shown in figure 6. The measured frequency response data in figure 5 and the math model in figure 6 were processed through a least squares curve fitting computer program to match both models and determine the unknown model coefficients. The coefficients determined in this way are average over the range of signal level. It is possible, however, to obtain several solutions by curve fitting different operating regions. Thus, a series of optimal gains can be found to suit each operating region. For simplicity, only one operating region is considered in this paper.

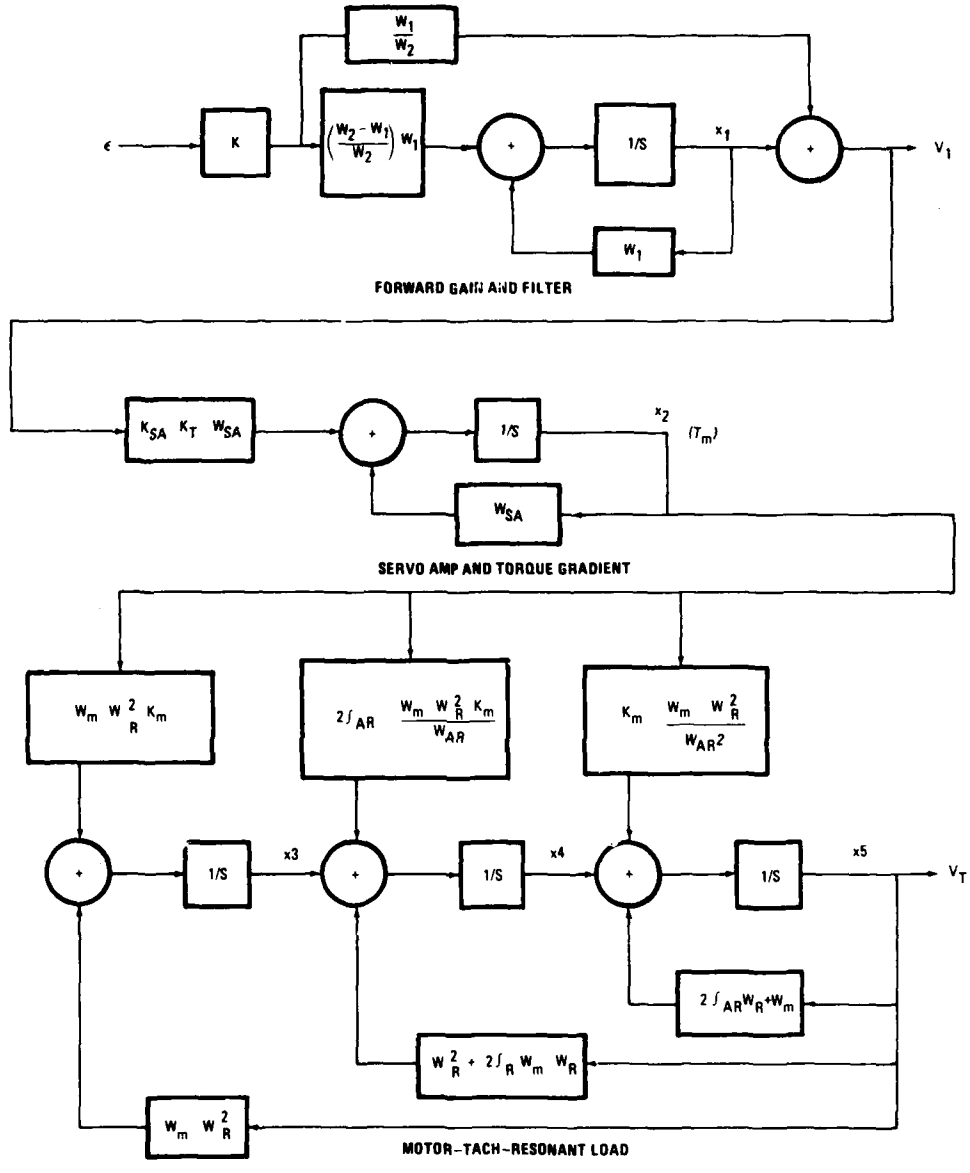


Figure 7. State Model of Gun Plant

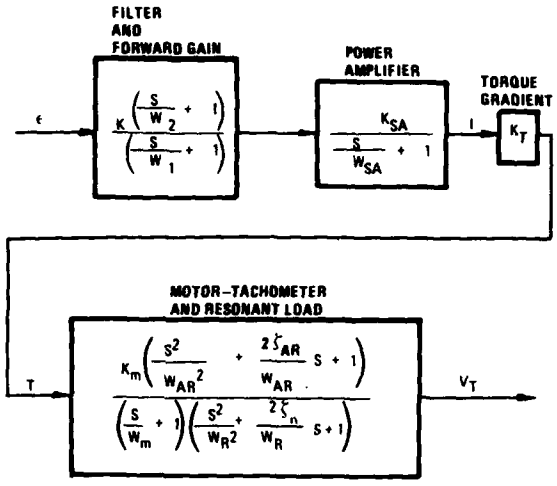


Figure 6. Transfer Function Model of Gun Plant

The state variable model of the plant shown in figure 7 is generated from the transfer functions shown in figure 6. The state matrix equation of the plant is derived from figure 7 and shown in equation 2.

$$\dot{\bar{X}} = \bar{A}\,\bar{X} + \bar{B}\,\bar{\varepsilon} \tag{2}$$

where:

$$\bar{X} = \begin{pmatrix} x_1 \\ T_m \\ x_3 \\ x_4 \\ V_t \end{pmatrix}; \quad \bar{A} = \begin{pmatrix} -W & 0 & 0 & 0 & 0 \\ (KW_sK_t) & -W_s & 0 & 0 & 0 \\ 0 & W_mW_r^2K_m & 0 & 0 & -W_mW_R^2 \\ 0 & \dfrac{2\zeta_{ar}W_mW_R^2Km}{W_{AR}} & 1 & 0 & -(W_r^2+2\zeta_RW_mW_r) \\ 0 & \dfrac{W_mW_R^2K_m}{W_{AR}^2} & 0 & 1 & -2\zeta_RW_r+W_m) \end{pmatrix}; \quad \bar{B} = \begin{pmatrix} \dfrac{(W_2-W_1)}{W_2} & (W_1)K \\ K_{SA}K_tW_{SA}K\,\dfrac{W_1}{W_2} & \\ 0 & \\ 0 & \\ 0 & \end{pmatrix}$$

and,

x_1 = Servo compensation Feedback

$x_2 = T_m$ = Motor Torque

x_3 = Proportional to change in acceleration

x_4 = Proportional to acceleration

$x_5 = V_t$ = Proportional to motor speed

GUN PERFORMANCE INDICES AND THE OPTIMAL SOLUTION

To optimize the selected performance indices by using the LQ algorithm, the indices are expressed mathematically and initially incorporated in a quadratic cost function, J, of the form:

$$J = \int \sum_{i=1}^{n} \frac{(x_i)^2}{(x_i^*)^2} + \frac{(\mu)^2}{(\mu^*)^2} \qquad (3)$$

where: x_i = system states

x_i^* = maximum allowable value of each system state

μ_i = control inputs

μ_i^* = maximum allowable control

Referring to the states defined in figure 7, the following performance goals, and associated performance indices, were chosen:

1. Maximum Bandwidth

   Bandwidth of a loop generally increases with increased open loop gain. The bandwidth of the velocity state is a function of the feedback gain associated with that state. By giving the highest weight to the speed performance index, wide bandwidth is assured (x_5 = tach voltage, V_T):

$$\left(\frac{x_5}{x_5^*}\right)^2 = \left(\frac{x_5}{V_T^*}\right)^2 \qquad (4)$$

   In the cost functional, if the chosen V_T^* decreases, the optimal gain associated with speed will increase to minimize speed variations and increase bandwidth. In this case, for example, V_T^* was chosen equal to approximately (V_T maximum)10^{-3}.

2. Minimum Following Error, ε

To maintain the following error less than a desired value of ε^* radian per second, set the control index in equation 3 to:

$$\left(\frac{\bar{\mu}}{\bar{\mu}^*}\right)^2 = \left(\frac{\varepsilon}{\varepsilon^*}\right)^2 \qquad (5)$$

3. Maximum Linear Range

Torque saturation primarily determines the linear range of the system. Therefore, the performance index associated with this goal is the torque state variable x_2, which is measureable as a function of motor current:

$$\left(\frac{x_2}{x_2^*}\right)^2 \qquad (6)$$

where x_2^* is selected equal to the current limit setting of the amplifier, because maximum current is proportional to maximum torque.

4. Minimum Settling and Synchronizing Time

This performance goal is related to the bandwidth, following error, and torque performance indexes. Therefore, the goal is achieved automatically by virtue of accomplishing the first three.

After substituting the chosen performance indices in the cost function (equation 3)., it is transformed to the following matrix form in order to process it in the LQ algorithm program:

$$\bar{J} = \int \bar{X}\,\bar{Q}\,\bar{X}^1 + \bar{\varepsilon}\,\bar{R}\,\bar{\varepsilon}^1 \; dt \qquad (7)$$

where:

$$\bar{R} = \left(\frac{1}{\bar{\varepsilon}^*}\right)^2 \qquad (8)$$

$$\bar{Q} = \begin{vmatrix} 0 & 0 & 0 & 0 & 0 \\ 0 & (x_2^*)^{-2} & 0 & 0 & 0 \\ 0 & 0 & 0 & 0 & 0 \\ 0 & 0 & 0 & 0 & 0 \\ 0 & 0 & 0 & 0 & (x_5^*)^{-2} \end{vmatrix} \qquad (9)$$

$\bar{J}$ (equation 7), A (equation 2), and B (equation 2) are placed in the optimization computer program, which is based on the LQ algorithm. The computer program outputs the optimal feedback gain matrix, G_{OPT}. Using G_{OPT}, the complete closed loop system implementation is diagramed as shown in figure 8.

Two states, (x_3 and x_4) cannot be physically measured in the hardware. Therefore, an analytical model of the fullstate feedback system is made in the microprocessor and states x_3 and x_4 are extracted for optimal feedback as shown in figure 8.

Once the solution check step and the hardware implementation step (blocks D & E in figure 3) are completed, the test phase shown in block F of figure 3 was performed.

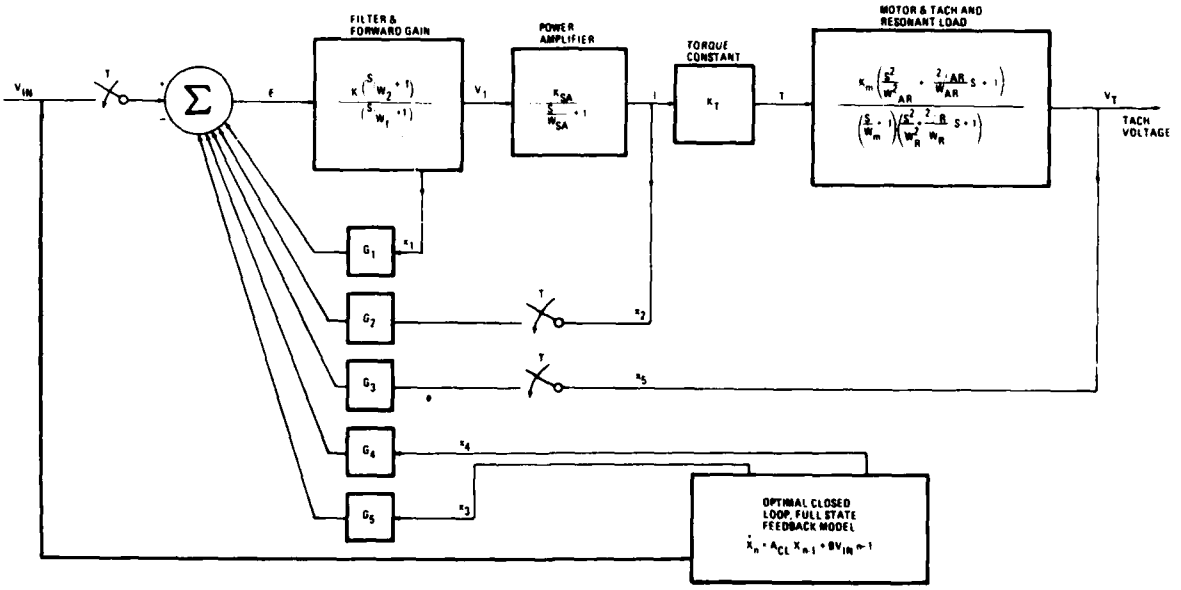


Figure 8. Optimal Wideband Gun Rate Loop

TEST RESULTS OF GUN CONTROL

The frequency response of the LQ model and the typical classical model were measured and plotted in figure 9. The results of the frequency response tests clearly indicate bandwidths are well beyond the usual and classical range of 6Hz to 8Hz for high powered resonant plants.

Step response tests were also performed on the LQ model and the classical model. The step response test results shown in figure 10 indicate achievement of established performance goals. Although wide bandwidth is evident in figure 9, the linear range shown in figure 10 is very large for this high inertia system.

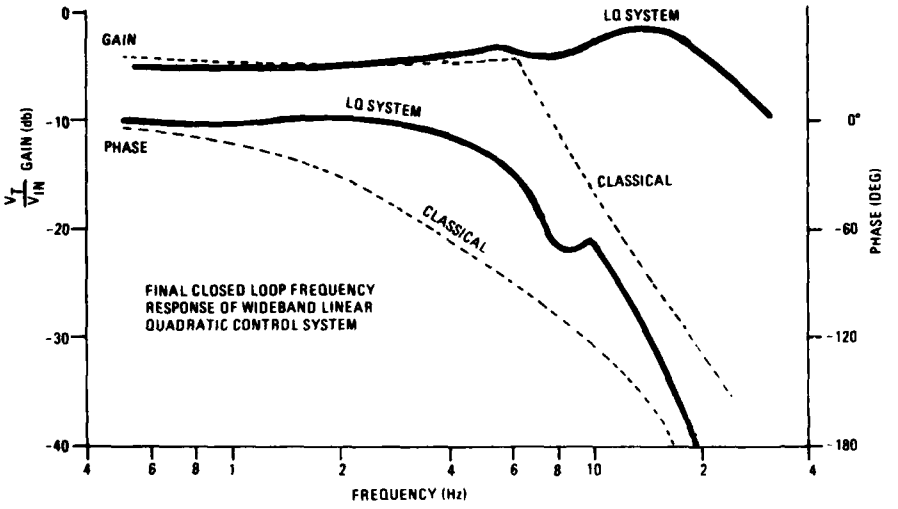


Figure 9. Frequency Response of Gun LQ Model and Classical Model

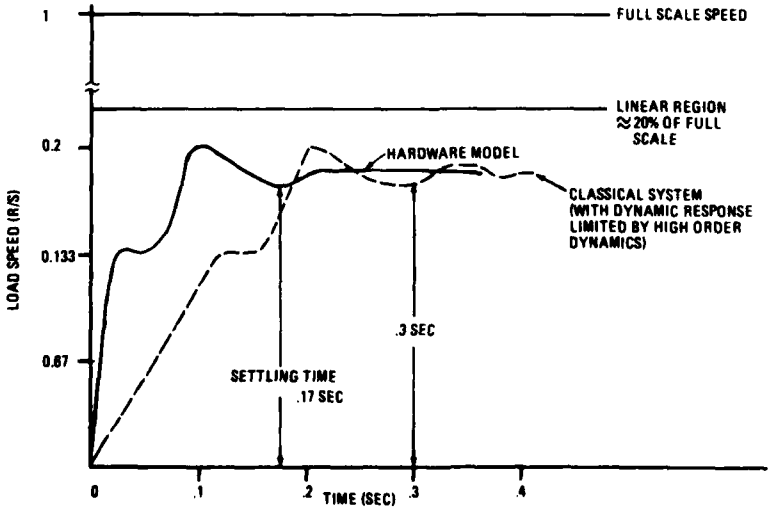


Figure 10. Step Response, Gun Velocity

LQ CONTROL OF GYRO STABILIZED SIGHT SYSTEM

The main objective in the design of the sight system is to maintain the rate following errors at a minimum over the frequency range required to reject external disturbances.

The approach chosen to achieve this objective is to design a system having the topography shown in figure 11.

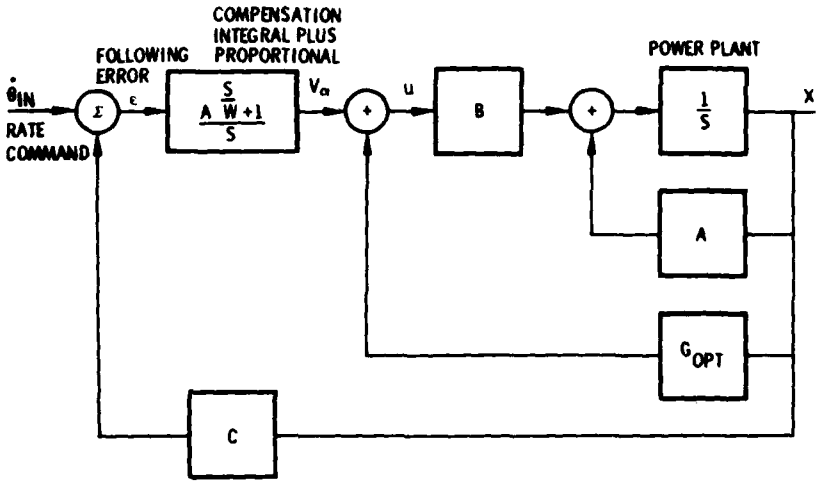


Figure 11. Optimal Wideband Gyro Stabilized Sight System

This rate feedback system is TYPE 1 which guarantees zero steady state velocity following error. The forward gain A, lead segment W and full state feedback matrix G_{OPT} must be chosen to minimize the following error over the frequency range of interest, while still achieving the maximum speed and acceleration requirements of the system.

SIGHT STATE MODEL

With this in mind, a three state plant model was developed using a curve fitting technique for frequency response over the frequency range of operation. This technique is similar to the one described for the gun drive. The three states chosen were:

1. $\dot{\theta}_m$ = motor speed
2. $\Delta\theta$ = $[\theta_m - \theta_L]$ = spring windup, proportional to load torque and acceleration
3. $\dot{\theta}_L$ = Load speed

Based on a state variable diagram similar to the one in figure 7, the plant state equation shown in equation 10 was derived.

$$\dot{\bar{X}} = \bar{A}\bar{X} + \bar{B}\bar{U} \tag{10}$$

$$\begin{pmatrix} \ddot{\theta}_m \\ \dot{\theta} \\ \ddot{\theta}_L \end{pmatrix} = \begin{pmatrix} \left(\frac{D_m}{J_m} + \frac{K_V K_T}{J_m R} + \frac{D_S}{N J_m}\right) & \frac{-K_s}{NJ_m} & \frac{D_s}{NJ_m} \\ \frac{1}{N} & 0 & -1 \\ \frac{D_S}{NJ_L} & \frac{K_S}{J_L} & \frac{-D_L+D_S}{J_L} \end{pmatrix} \begin{pmatrix} \dot{\theta}_m \\ \Delta\theta \\ \dot{\theta}_L \end{pmatrix} + \begin{pmatrix} \frac{K_T K}{J_m R} \\ 0 \\ 0 \end{pmatrix} U$$

Since the equivalent friction D_L varies with speed and equivalent spring constant K_S is a function of the ratio of speed and backlash, a number of solutions can be found as a function of speed. An optional A, W and G_{OPT} can be selected for each region of speed. Note however, careful attention must be paid to making a smooth transition between regions of operation in order to avoid large transients in the system.

PERFORMANCE INDICES

The mathematical form of the cost functional (see reference 4 for explanation) is shown in equation 11.

$$\bar{J} = \int \bar{\varepsilon}' \, \bar{Q}_{11} \, \bar{\varepsilon} + \bar{U}' \bar{Q}_{22} \bar{U} + \dot{\bar{U}}' \bar{R} \, \dot{\bar{U}} \tag{11}$$

where $\bar{Q}_{11}$, $\bar{Q}_{22}$, and $\bar{R}$ are weighting matrices chosen to penalize the system for too much error or too much control.

$\bar{Q}_{11}$ elements are chosen to limit the maximum following error allowable between the commanded speed ($\dot{\theta}_{IN}$) and the load speed (θ_L). For example, as $\bar{Q}_{11}$ approaches ∞, ε approaches 0.

Q_{22} elements are chosen to limit the maximum allowable difference between the plant command of speed (V_α) and torque, and the actual load speed ($\dot{\theta}_L$).

$\bar{R}$ elements are chosen to limit the allowable difference between plant command of acceleration and jerk, and the actual acceleration and jerk.

SEARCH FOR A PRACTICAL SOLUTION

Having decided on the performance indices for the sight, the next step was to perform an iterative search of a number of LQ solutions for various values of Q_{11}, Q_{22} and R in order to achieve a practical system. In addition to some obvious reasons for eliminating certain solutions, the following two criteria were chosen to reject certain solutions:

1. Discard solutions with bandwidth beyond 25 Hz since the model is valid for the frequency region below 25 Hz.

2. An open loop gain of 40 dB minimum at 1 radian/second is required to reject known load disturbances.

A summary of optimization solutions about one operating point is shown in table 1. Note that wide variations in Q_{11}, Q_{22} and R produce significant variations in closed loop bandwidth but less variation in open loop gain at 1 radian/second fre- quency. The last set of parameters shown in table 1 was chosen for the practical system solution implementation phase.

Table 1. Summary of Optimization Solution Results For One Operating Point

Q_{11}	Q_{22}	R	Open Loop Gain (dB) @ 1 Rad/Sec	Closed Loop Bandwidth (Hz)
10^3	.01	.01	40	10.0
10^3	1.0	1.0	35	3.65
10^6	.09	.09	48	35.0
10^3	.1	.1	38	7.7
$2x10^3$	.01	1.0	42	15.5
$2x10^5$	.01	.0001	52	82.5
$2x10^3$	.05	.0001	45	33
$2x10^4$	.05	.25	47	36
10^5	.05	1.0	46	38
10^5	.05	10	44	23 Selected

Using the last optimal solution in table 1, the wideband inertially stabilized sight rate loop shown in figure 12 was implemented in the laboratory for testing. As shown in figure 12, all of the control functions are performed in the microprocessor. The value for A and W in the integral-plus-proportional compensation was provided by the chosen solution. Three states θ_m; θ_L; $\Delta\theta$ are fed back around the plant through optimal gains G_1, G_2 and G_3 respectively. Since the θ state (spring deflection) cannot be measured easily in the hardware, a model of the system is used to generate this state.

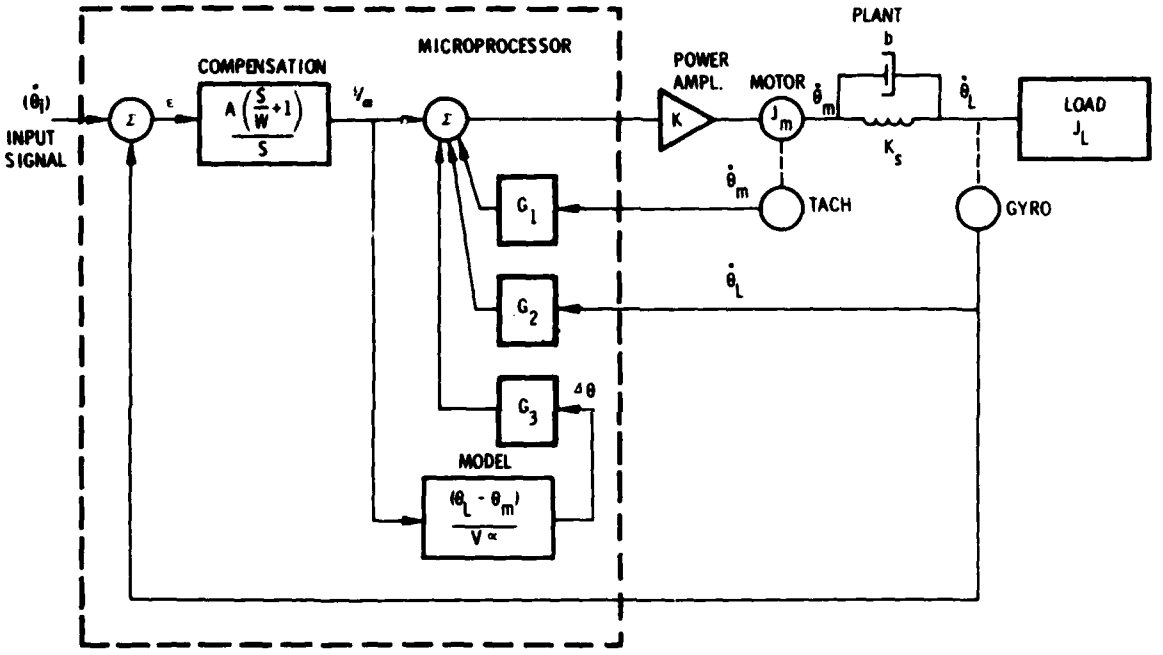


Figure 12. Optimal Wideband Gyro Stabilized Sight System

SIGHT SYSTEM RESPONSE

Using the BODE simulation language developed at Lockheed, frequency response tests were run on the Sight System defined in figure 12 and table 1. The open loop response shown in figure 13 indicates sufficient stability margin is achieved along with the desired level of open loop gain at 1 radian/second (0.167 Hz). The closed loop response of the simulated system is shown in figure 14. Studying the gain and phase curves, one sees the desired loop bandwidth criteria is also achieved in the simulation model of the Sight System.

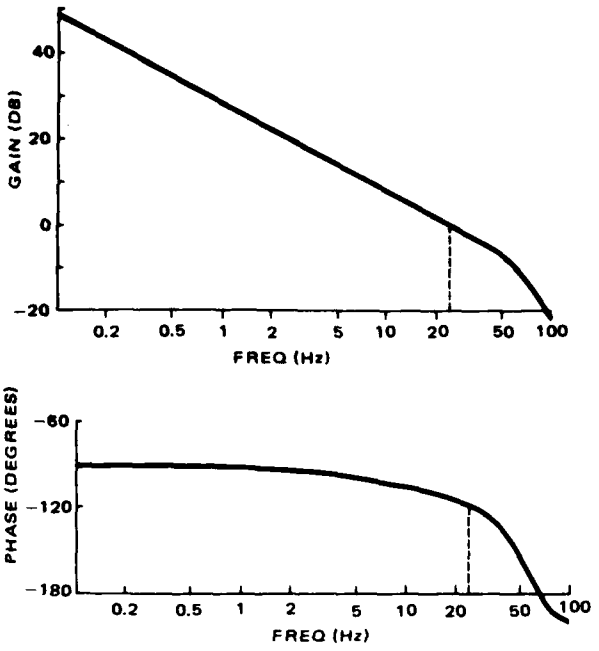


Figure 13. Open Gyro Loop Response, Simulated Sight System

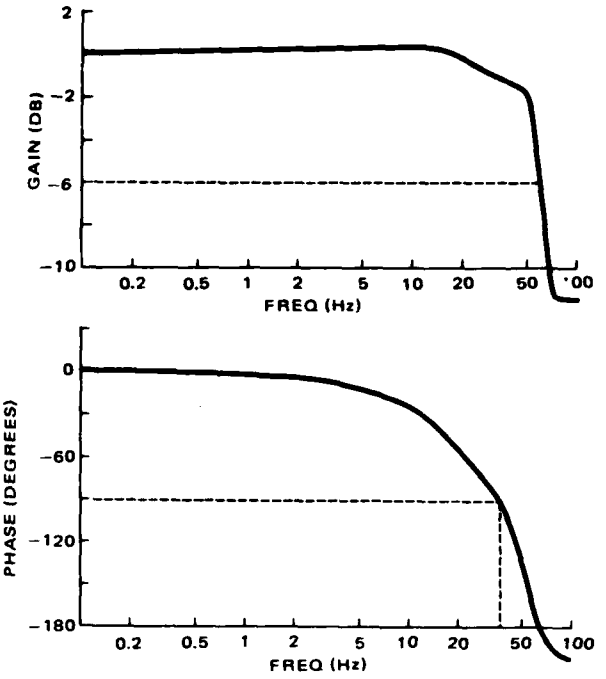


Figure 14. Closed Rate Loop Response, Simulated Sight System

CONCLUSIONS

This paper is the fifth in a series concerning a multi year IR&D program to develop advanced microprocessor based control systems using *modern control* and distributive processing capabilities. The authors describe two applications of Linear Quadratic control theory to improve response of an existing weapon control servo plant containing high order dynamics (resonance) and non-linearities. A deterministic, full-state feedback rate loop is developed to optimize bandwidth, following error, and linear operating range for the gun plant and the inertial gun sight. Test results confirm that a wideband *modern control* system can be achieved in the presence of high order resonance dynamics and non-linearities in a cost effective and practical manner.

The development results described in this paper reinforce the validity of the authors' approach to the practical implementation of modern control theory. That is: apply it at the hardware level and solve the hardware induced problems before using it at the higher system levels. In this way, the performance constraints caused by hardware are reduced and more effective use of modern control theory can be made.

NOMENCLATURE

V_{IN} = Input command to plant
ε = Following error
R = Armature resistance (varies as function of temperature)
J_m = Motor inertia
D_m = Motor viscious friction
D_L = Load viscious friction
D_s = Equivalent damping in gear train and shaft coupling between motor/load.
N = Gear ratio
K_s = Spring constant (compliance between motor to load) varies as ratio of input displacement to backlash
F_{cl} = Load coulomb friction
J_L = Load inertia
θ_B = Backlash
I_s = Saturation current
I_m = Armature current
$W_{aR} = \sqrt{\frac{K_s}{J_L}}$ Anti-resonance frequency

$W_R = \sqrt{\frac{K_s}{J_L || J_m}}$

ζ_{AR} = Damping ratio at W_{AR}
ζ_R = Damping ratio at W_R
$\dot{\theta}_i$ = Load position
$\dot{\theta}_m$ = Motor speed
$\dot{\theta}_L$ = Load speed
K_v = BEMF constant
K_T = Motor torque constant
K = Amplifier gain
W_{SA} = Amplifier break
W_1, W_2 = Forward filter breaks
T_m = Motor torque
T_L = Load torque
V_α = Command voltage, sight plant

ACKNOWLEDGEMENTS

The authors wish to convey their appreciation for the valuable assistance and advice given them during the course of this work by William Buntemeyer of Lockheed Electronics Company.

REFERENCES

1. Bigley, William J. and Vincent J. Rizzo, "Resonance Equalization in Feedback Control Systems," ASME Paper #78-WA/DSC-24, presented at Winter Annual Meeting, San Francisco, Calif. December 15, 1978.

2. Rizzo, Vincent J. and William J. Bigley, "Microprocessor Based Control System," Proceeding of the IEEE 1980 National Aerospace and Electronics Conference, Vol. 2, pp 211-218, Dayton, Ohio, May 1980.

3. Bigley, William J. and John D. Vandenberg, "Human Supervision and Microprocessor Control of an Optical Tracking System," Proceedings of the 17th Annual Conference on Manual Control, U.C.L.A., California, 16 June 1981.

4. Athans, Michael, Modern Control Theory, Part 2 Deterministic Optimal Control, Cambridge, Mass.: Massachusetts Institute of Technology, 1974.

5. Athans, Michael and Peter L. Falk, Optimal Control, New York: McGraw Hill Book Company, 1966.

Next page is blank.

DISCRETE-TIME DISTURBANCE ACCOMMODATING CONTROL OF A HELICOPTER GUN-TURRET SYSTEM

N.P. Coleman, R. Johnson, and E. Carroll
U.S. Army Armament Research and Development Command
Dover, New Jersey 07801

AD P001063

ABSTRACT

The design and implementation of a microprocessor-based disturbance accommodating controller for the XM-97 helicopter gun-turret control system is considered. A two-state observer is used to estimate and suppress recoil induced torque disturbances associated with weapon firing. Both nonfiring and firing test results are presented.

INTRODUCTION

The design of high performance controllers for a helicopter gun-turret system using modern control and observer theory has been investigated by Coleman et al [1] - [3]. The continuous time optimal controller and observer developed in [1] were implemented using standard analog components, while the discrete time controller developed in [2] and [3] were implemented in fixed point assembly code using a 16 bit 8086 based microprocessor. Due to the limitations of the controller hardware in [1] - [3], only two-state linear quadratic (LQ) controllers and LQ controllers with first order recoil torque observers were implemented.

The purpose of this paper is to present some preliminary results, which demonstrate the performance of higher order disturbance accommodating controllers for the XM-97 turret, which permit improved suppression of recoil induced disturbances at the firing frequency of 10 Hertz.

A detailed description of the XM-97 turret system and associated system dynamic equations may be found in [1] - [3]. Briefly, the system consists of a three-barrel, 20mm automatic cannon and a turret drive system mounted under the noise section of a Cobra helicopter. For test purposes, the gun-turret and helicopter airframe are suspended from a six-degree-of-freedom simulator as shown in Fig. 1. The gun-turret control system is essentially an inertial load driven by a pulse width modulated split series DC motor through a compliant gear box. The system consists of two controllers: one controller positions the gun turret in azimuth and the other elevates and depresses the gun cradle and the gun. The two controllers are functionally similar and independent. The only difference between the two controllers is the gear ratio N, which is N = 620 for the azimuth channel and N = 810 for the elevation channel. Both controllers employ angular position feedback and angular velocity feedback.

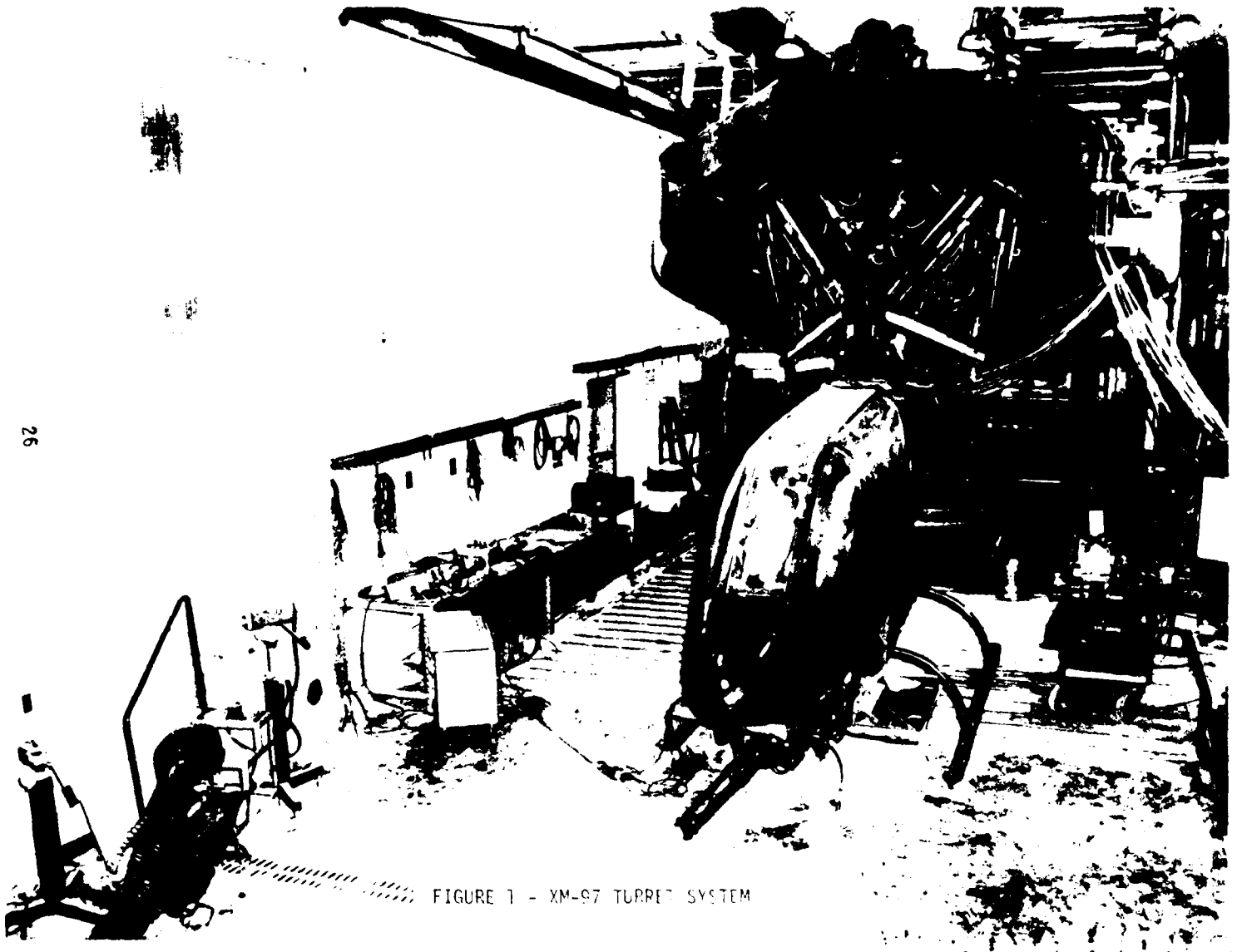


FIGURE 1 - XM-97 TURRET SYSTEM

DISCRETE-TIME DISTURBANCE ACCOMMODATING CONTROLLER DESIGN

The design of a continuous-time disturbance accommodating controller for the XM-97 helicopter gun-turret control system has been investigated in [1]. The design problem was formulated as shown in Fig. 2, with the dynamics of the open-loop system described by (for both the azimuth and elevation channels)

$$\dot{\underline{x}}(t) = A\underline{x}(t) + Bu(t) + Fv_r + Gw(t), \quad \underline{x}(0) = \underline{x}_0, \qquad (1)$$

where

$$\underline{x}^T(t) = [x_1(t)\ x_2(t)],$$

$x_1(t) = x_r(t) - x'_1(t)$

= error between the position command input x_r (radians) and the actual gun-turret angular position $x'_1(t)$ (radians),

$x_2(t) = Nv_r - x'_2(t)$

= error between the velocity command v_r (radians/second) and the actual motor angular velocity $x'_2(t)$ (radians/second),

$x_r(t) = x_r + v_r t$

= step-plus-ramp position command input (radians),

$u(t)$ = control input (volts),

and A, B, and F are constant matrices given by

$$A = \begin{bmatrix} 0 & \frac{1}{N} \\ 0 & \frac{3.84\times10^3}{J} \end{bmatrix} \triangleq \begin{bmatrix} 0 & a_{12} \\ 0 & -a_{22} \end{bmatrix},$$

$$B = \begin{bmatrix} 0 \\ \frac{-80.25}{K} \end{bmatrix} \triangleq \begin{bmatrix} 0 \\ -b_{12} \end{bmatrix}, \quad F = \begin{bmatrix} 0 \\ \frac{3.84\times10^{-3}N}{J} \end{bmatrix}$$

$$\triangleq \begin{bmatrix} 0 \\ f_{12} \end{bmatrix}, \quad G = \begin{bmatrix} 0 \\ \frac{1}{NJ} \end{bmatrix} \triangleq \begin{bmatrix} 0 \\ -g \end{bmatrix}$$

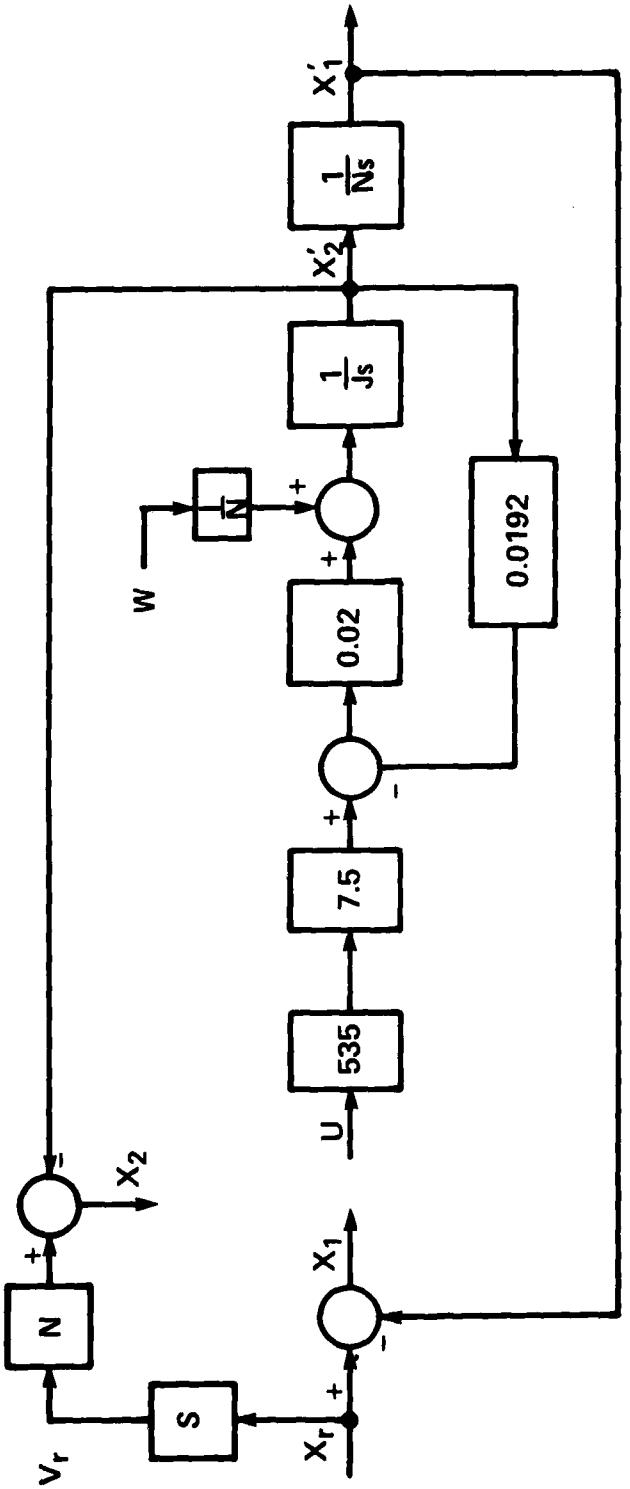


FIG 2. OPEN LOOP HELICOPTER TURRET CONTROL SYSTEM

To design a suitable microprocessor-based controller for the helicopter gun-turret control system, equation (1) is first discretized by using a sampling interval T seconds as follows:

$$\underline{x}(k+1) = A_d\underline{x}(k) + B_d u(k) + F_d v_r + G_d w(k), \quad \underline{x}(0) = \underline{x}_o, \tag{2a}$$

where $\underline{x}(k) \triangleq \underline{x}(kT)$, $u(k) \triangleq u(kT)$,

$$A_d \triangleq e^{AT} = \begin{bmatrix} 1 & a_{d12} \\ 0 & a_{d22} \end{bmatrix} \tag{2b}$$

$$B_d \triangleq \int_o^T e^{At} B dt = \begin{bmatrix} b_{d11} \\ b_{d12} \end{bmatrix} \tag{2c}$$

$$F_d \triangleq \int_o^T e^{At} F dt = \begin{bmatrix} f_{d11} \\ f_{d12} \end{bmatrix} \tag{2d}$$

$$G_d \triangleq \int_o^T e^{AT} G dt = \begin{bmatrix} g_{d12} \\ g_{d12} \end{bmatrix} \tag{2e}$$

and the components in the A_d, B_d, F_d, and G_d matrices can be computed easily for each of the azimuth and elevation channels.

The design objective is to drive $\underline{x}(k)$ to the zero state and at the same time minimizing a quadratic performance measure. To achieve the objective, the control u(k) is first split into three parts as

$$u(k) = u_{fb}(k) + u_{ff}(k) + u_w(k) \tag{3}$$

where $u_{fb}(k)$ is the feedback component responsible for driving the state $\underline{x}(k)$ to the zero state, $u_{ff}(k)$ is the feedforward component responsible for accommodating the velocity command v_r, and u_w is the feedforward component responsible for accommodating the disturbance torque w(k), i.e,

$$B_d u_{ff}(k) + F_d v_r = 0, \tag{4a}$$

$$B_d u_w(k) + G_d w(k) = 0. \tag{4b}$$

Using (1), (2), and (4), it is not difficult to show that

$$u_{ff}(k) = \frac{f_{12}}{b_{12}} v_r = 4.785Nx10^{-5}v_r \triangleq k_r v_r . \qquad (5a)$$

$$u_w(k) = \frac{-gw(k)}{b_{12}} = -k_w w(k) \qquad (5b)$$

which when substituted into (2) yields

$$\underline{x}(k+1) = A_d\underline{x}(k) + B_d u_{fb}(k) \quad \underline{x}(0) = \underline{x}_o . \qquad (6)$$

Equation (6) may be written (by adding and substracting the same term $-B_d R_d^{-1} S_d^T \underline{x}(k)$ on the right-hand side of the equation[1],) as

$$\underline{x}(k+1) = A_{eq}\underline{x}(k) + B_d u_{eq}(k), \quad \underline{x}(0) = \underline{x}_o , \qquad (7)$$

where R_d and S_d are constant matrices, and

$$A_{eq} \triangleq A - B_d R_d^{-1} S_d^T , \qquad (8)$$

$$u_{eq}(k) \triangleq u_{fb}(k) + R_d^{-1} S_d^T \underline{x}(k). \qquad (9)$$

Consider the performance measure

$$J_d = \sum_{k=0}^{\infty} [x^T(k)Q_d\underline{x}(k) + 2\underline{x}^T(k)S_d\underline{u}_{fb}(k) \qquad (10)$$

$$+ \underline{u}^T_{fb}(k)R_d\underline{u}_{fb}(k)]$$

which may be written as

$$J_{eq} = \sum_{k=0}^{\infty} [\underline{x}^T(k)Q_{eq}\underline{x}(k) + \underline{u}^T_{eq}(k)R_d\underline{u}_{eq}(k)], \qquad (11)$$

---

[1]The reason for using (7) is the provide a discrete time equivalent of a desired continuous time optimal control design.

where $J_d \equiv J_{eq}$, and

$$Q_{eq} \triangleq Q_d - S_d R_d S_d^T, \tag{12}$$

while $\underline{u}_{eq}$ is as defined in (9). In (10), the matrices Q_d, S_d, and R_d can be computed directly from the continuous time LQ cost functional weighting matrices as shown below. This now allows computation of the discrete time equivalent of the continuous time controller designs developed in [1].

More precisely, the optimal control problem posed by (6) and (10), or (7) and (11) *is equivalent to the following* continuous time optimal control problem:

Given the continuous-time system,

$$\dot{\underline{x}}(t) = A\underline{x}(t) + B\underline{u}(t), \; \underline{x}(0) = x_o \tag{13}$$

find the optimal control which minimizes the performance measure

$$J(u) = \int_o^\infty [\underline{x}^T(t)Q\underline{x}(t) + \underline{u}^T(t)R\underline{u}(t)]dt, \tag{14}$$

where Q and R are respectively symmetric positive-semidefinite and *symmetric positive-definite* weighting matrices. The continuous-time system described by (13) may be discretized as shown in (2). The corresponding discrete-time version of (14) is then given by (10) with the following substitutions [4]:

$$Q_d = \int_o^T e^{A^T t} Q e^{At} dt \tag{15}$$

$$R_d = \int_o^T [R + B_d^T(t)QB_d(t)]dt, \tag{16}$$

$$S_d = \int_o^T e^{A^T t} QB(t)dt, \tag{17}$$

$$B(t) = \int_o^T e^{A\sigma} Bd\sigma \tag{18}$$

We observe that although there is no cross-product term of the form $\underline{x}^T(t)S\underline{u}(t)$ used in (14), the cross-product term due to S_d in (10) is generally nonzero, unless $Q = 0$ as may be seen from (17).

We remark also that the cross-product term in (10) may be dropped if one is not interested in establishing the corresponding relationships between the continuous-time and the associated discrete-time optimal control problems.

Now, the optimal control which minimizes the performance measure J_d given by (1) subject to (6) is given by

$$u_{fb}(k) = -(R_d + B_d^T K_d B_d)^{-1}(B_d^T K_d A_d + S_d^T)\underline{x}(k) \tag{19a}$$

$$= k_1 x_1(k) + k_2 x_2(k) \tag{19b}$$

$$= k_1[x_r(k) - x_1'(k)] + k_2[Nv_r - x_2'(k)], \tag{19c}$$

where k_1 and k_2 are constants, and K_d is the symmetric positive-definite solution of the algebraic matrix Riccati equation

$$K_d = A_d^T K_d A_d + Q_d - (B_d^T K_d A_d + S_d^T)^T k(R_d + B_d^T K_d B_d)^{-1}(B_d^T K_d A_d + S_d^T)' \tag{20a}$$

$$= A_{eq}^T K_d A_d + Q_{eq} - A_{eq}^T K_d B_d (R_d + B_d^T K_d B_d)^{-1} B_d^T K_d A_{eq}. \tag{20b}$$

Equation (20b) follows from (20a) by simple algebraic manipulations.

Similarly, the optimal control which minimizes J_{eq} given by (11) subject to (7) is given by

$$u_{eq}^o(k) = -(R_d + B_d^T K_d B_d)^{-1} B_d^T K_d A_{eq}\underline{x}(k), \tag{21}$$

where K_d is the symmetric positive-definite solution of (20). As expected, substitution of (21) into (9) yields (19).

Combining (5) and (19), the total control is given by

$$u(k) = -(R_d + B_d^T K_d B_d)^{-1}(B_d^T K_d A_d + S_d^T)\underline{x}(k) + k_r v_r - k_w w(k) \tag{22a}$$

$$= k_1 x_1(k) + k_2 x_2(k) + k_r v_r - k_w w(k) \tag{22b}$$

Substituting (22) into (29) yields the optimal helicopter gun-turret control system

$$\underline{x}(k+1) = [A_d - B_d(R_d + B_d^T K_d B_d)^{-1}(B_d^T K_d A_d + S_d^T)]\underline{x}(k),$$
$$\underline{x}(0) = \underline{x}_o. \tag{23}$$

TWO-STATE RECOIL OBSERVER

Implementation of the disturbance accommodating control law (22) requires that an estimate be made of the disturbance term w(k). This estimate is made using a reduced order observer obtained by modeling the disturbance as a sinusoid of frequency f = 10 Hertz, i.e.,

$$\dot{\underline{w}}(t) \triangleq \begin{bmatrix} \dot{w}_1(t) \\ \dot{w}_2(t) \end{bmatrix} = \begin{bmatrix} 0 & 1 \\ -(2\pi f)^2 & 0 \end{bmatrix} \begin{bmatrix} w_1(t) \\ w_2(t) \end{bmatrix} \tag{24}$$
$$= A_w \underline{w}(t)$$
$$w(t) = w_1(t)$$

Augmenting the disturbance dynamics with the XM-97 plant dynamics results in the dynamical system

$$\begin{bmatrix} \dot{\underline{x}}(t) \\ \dot{\underline{w}}(t) \end{bmatrix} = \begin{bmatrix} A & \tilde{G} \\ 0 & A_w \end{bmatrix} \begin{bmatrix} \underline{x}(t) \\ \underline{w}(t) \end{bmatrix} + \begin{bmatrix} B \\ 0 \end{bmatrix} u(t) + \begin{bmatrix} F \\ 0 \end{bmatrix} V_r$$

where

$$\tilde{G} = [G \ \underline{0}] = \begin{bmatrix} 0 & 0 \\ -g & 0 \end{bmatrix}$$

and the measurement equation is given by

$$y(t) = \underline{x}(t).$$

It is readily shown [1] that this system is completely observable. It is possible, therefore, to estimate the disturbance vector $\underline{w}(t)$ using a reduced order observer, [1] and [6]. The discrete-time observer equations required for microprocessor

implementation are obtained by first transforming (25) into discrete form

$$\begin{bmatrix} \underline{x}(k+1) \\ \underline{w}(k+1) \end{bmatrix} = \begin{bmatrix} A_d & \tilde{G}_d \\ 0 & A_{wd} \end{bmatrix} \begin{bmatrix} \underline{x}(k) \\ \underline{w}(k) \end{bmatrix} + \begin{bmatrix} B_d \\ 0 \end{bmatrix} u(k) \qquad (26)$$

$$+ \begin{bmatrix} F_d \\ 0 \end{bmatrix} V_r$$

where $x(k) = x(kT)$, $u(k) = u(RT)$, T = sample time, A_d, B_d, F_d are defined by (2),

$$\tilde{G}_d \triangleq \int_0^T e^{At} \tilde{G}\, dt \qquad (27a)$$

and

$$A_{wd} \triangleq e^{A_w T} . \qquad (27b)$$

The discrete-time estimate of the disturbance state vector $w(k)$ evolves according to

$$\hat{\underline{w}}(k+1) = \underline{z}(k) + H\underline{x}(k) \qquad (28a)$$

$$z(k+1) = (A_{wd} - H\tilde{G}_d)z(k) + [(A_{wd} - H\tilde{G}_d)H - HA_d]\underline{x}(k) \qquad (28b)$$

$$-HB_d u'(k)$$

where $u'(k) = k_1 x_1(k) + k_2 x_2(k) - k_w \hat{w}(k)$.

The observer gain matrix H detrmines the observer dynamics and is given by the solution of the quadratic minimization problem [5], [6]:

$$\text{minimize } J(v(k)) = \sum_{k=0}^{\infty} e'(k)\tilde{Q}e(k) + v'(k)\tilde{R}\, v(k), \qquad (29)$$

$$\tilde{Q} \geq 0,\ R > 0$$

subject to $e(k+1) = A'_{wd}e(k) + \tilde{G}_d'v(k)$.

Furthermore, the observer gain matrix H can be expressed in the form

$$H = (\tilde{G}_d P \tilde{G}_d' + \tilde{R})^{-1}\, \tilde{G}_d P A'_{wd} \qquad (30)$$

where P is the solution of the discrete matrix Ricatti equation

$$P = A_{wd}PA'_{wd} - A_{wd}P\tilde{G}_d(\tilde{R}+\tilde{G}_dP\tilde{G}'_d)^{-1}\tilde{G}_dP\tilde{G}_d + \tilde{Q} \qquad (31)$$

The control law (26) can now be implemented as

$$u(k) = k_1x_1(k) + k_2x_2(k) + k_rv_r - k_w\hat{w}(k) \qquad (32)$$

with $\hat{w}(k)$ given by (28).

IMPLEMENTATION

The microprocessor used to execute the discrete-time disturbance accommodating controller for the XM-97 gun-turret system is shown in figure 3. The processor consists of two intel SBC 86/12 (16 bit, 8086 based) single board computers, each with an 8087 floating point numeric processor, an SBC 732 combination A/D and D/A board (12 bits), and prom memory board configured as shown in figure 4. A CRT display and keyboard, serially interfaced to the 86/12 monitor provides the capability for quick parameter adjustment during testing. Except for the initialization and driver subroutines, all code was written in PL/M-86. Also, floating point number format was used exclusively to simplify coding. Total execution time for both elevation and azimuth channels is 2 milliseconds.

The initialization and driver subroutines were coded in assembly language in order to minimize execution time and memory overhead. The "INITS" routine initializes all the ports, timers, and interupts. "DAOT" converts the 32 bit floating point result to the 16 bit representation recognized by the analog output board, and clips the values to a predetermined value (±10 volts) prior to passing the data. "ADIN" converts the 16 bit data from the analog input board to 32 bit floating point.

TEST RESULTS

Preliminary nonfiring and firing tests of the discrete-time disturbance accommodating control law (26) were carried out for values of the Q and R control weighting matrices given by

$$Q = \begin{bmatrix} 5 & 0 \\ 0 & 0 \end{bmatrix}, \quad R=1$$

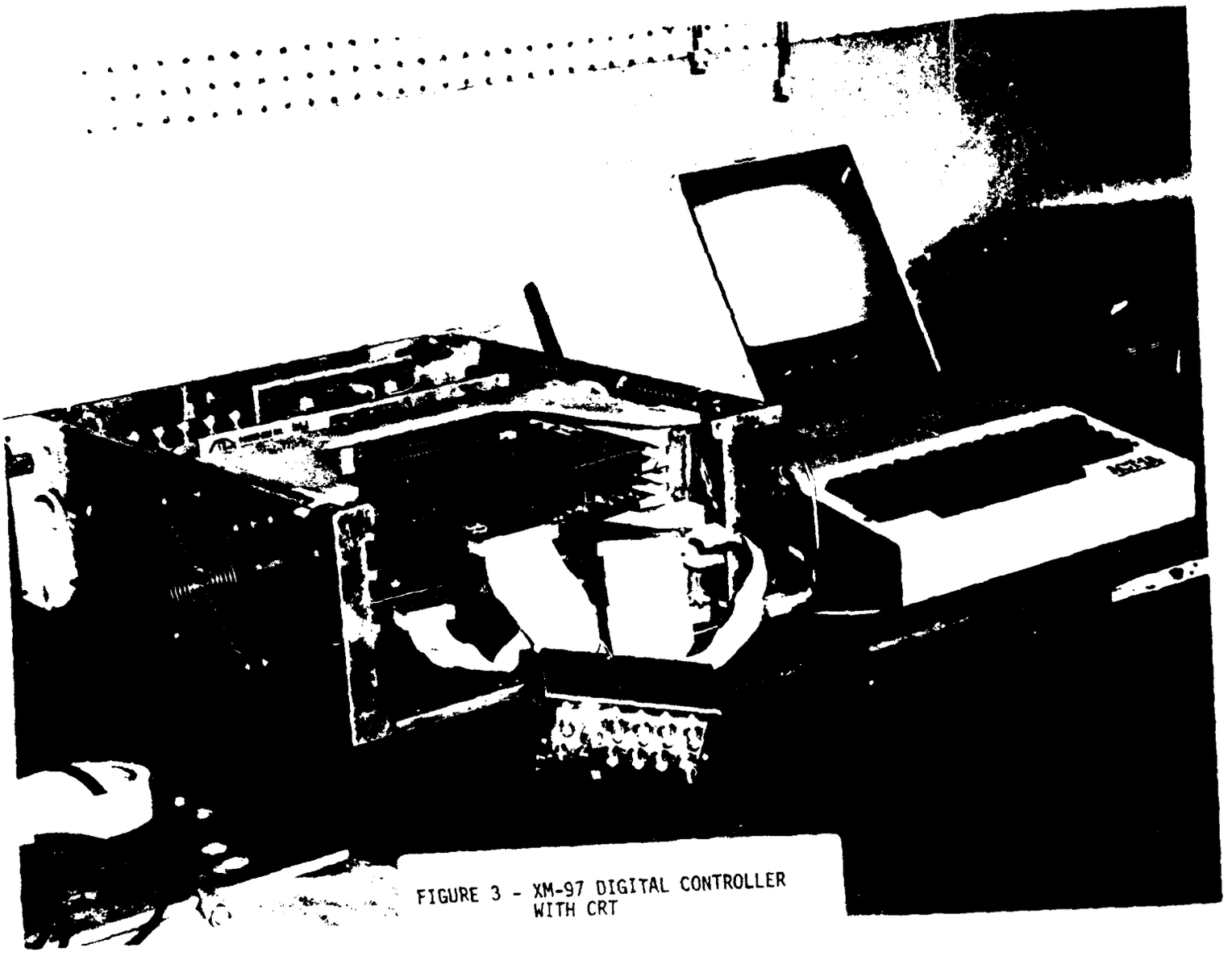


FIGURE 3 - XM-97 DIGITAL CONTROLLER WITH CRT

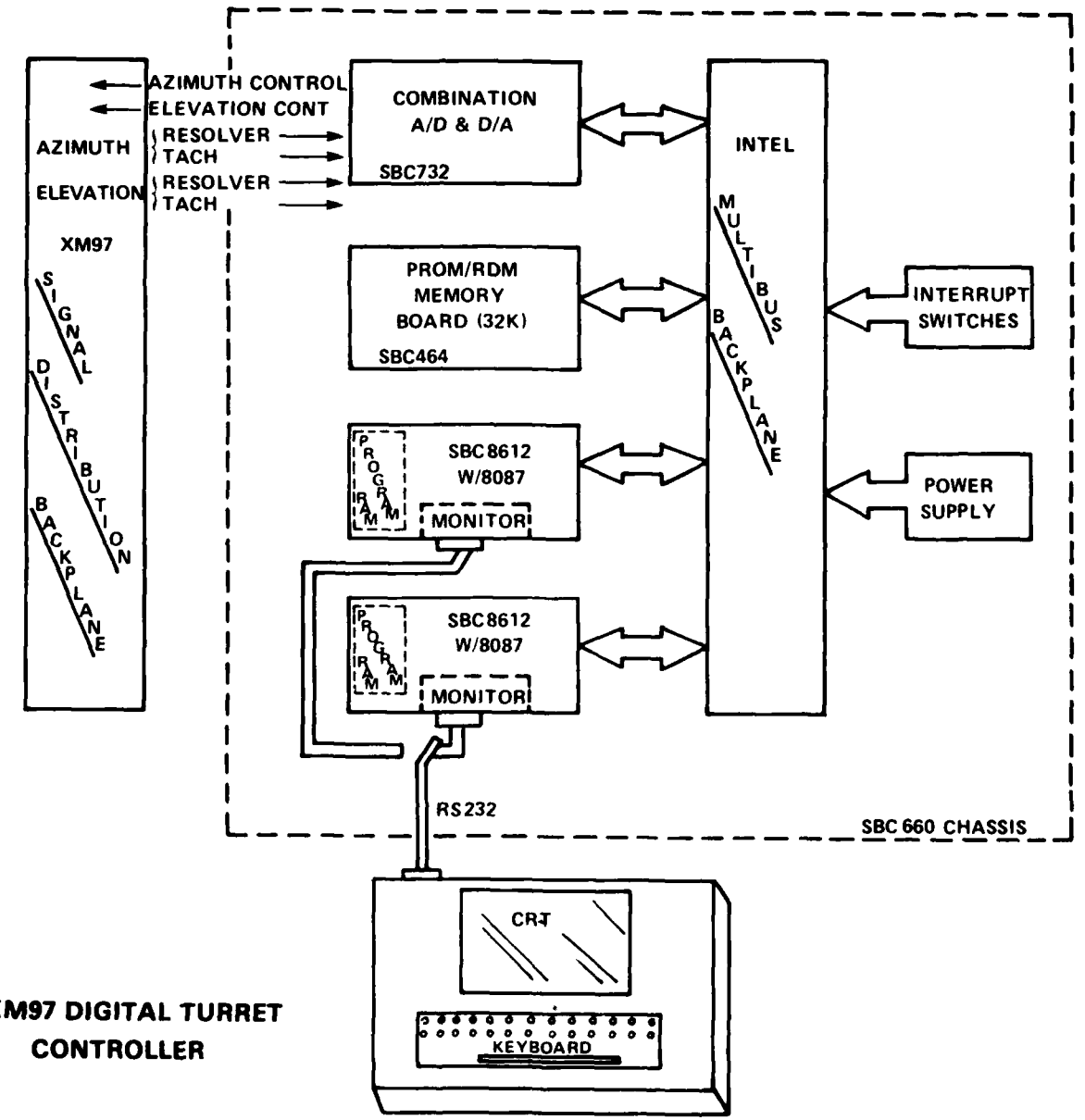


FIG. 4. XM97 DIGITAL TURRET CONTROLLER

and values of the $\tilde{Q}$ and $\tilde{R}$ observer weighting matrices

$$\tilde{Q} = \begin{bmatrix} 0 & 0 \\ 0 & 100 \end{bmatrix}$$

$$\tilde{R} = \begin{bmatrix} .001 & 0 \\ 0 & .001 \end{bmatrix}$$

The equivalent continuous time observer and closed loop plant poles associated with the given weighting matrices are located at $-10.10 \pm j63.65$ and $-19.22 \pm j19.2$, respectively.

Although no attempt was made to optimize the performance of the observer design (28), nevertheless the control law (32) proved much superior to the original XM-97 controller design in both nonfiring and firing tests. Figures 5a and 5b compare the step response of the original XM-97 controller and the discrete-time control law (32), respectively, while figures 6a and 6b compare the resolver output error for the two systems during a 20-round burst fired at 600 rounds per minute. Typical shot groups for the original XM-97 system and (32) are shown in figures 7a and 7b, respectively, and illustrate the capability of the discrete-time disturbance accommodating controller to suppress recoil induced disturbances. It should also be noted that the dispersion associated with the first three rounds is due to vertical motion of the airframe which is not corrected for by either controller.

Finally, we remark that several modifications of the control law (32) are in progress. One modification will permit on-line estimation of the disturbance frequency w_r and tuning of the observer and control gain parameters. The details of this disturbance adaptive control law will be reported elsewhere.

CONCLUSION

The design and implementation of a discrete-time disturbance accommodating control law for a helicopter gun-turret system has been investigated. The investigation addresses problems associated with control law design, observer design, and software/hardware implementation using an 8087 based microprocessor. Preliminary test results illustrate the great potential of disturbance accommodating control methods in the design of high performance weapon pointing systems.

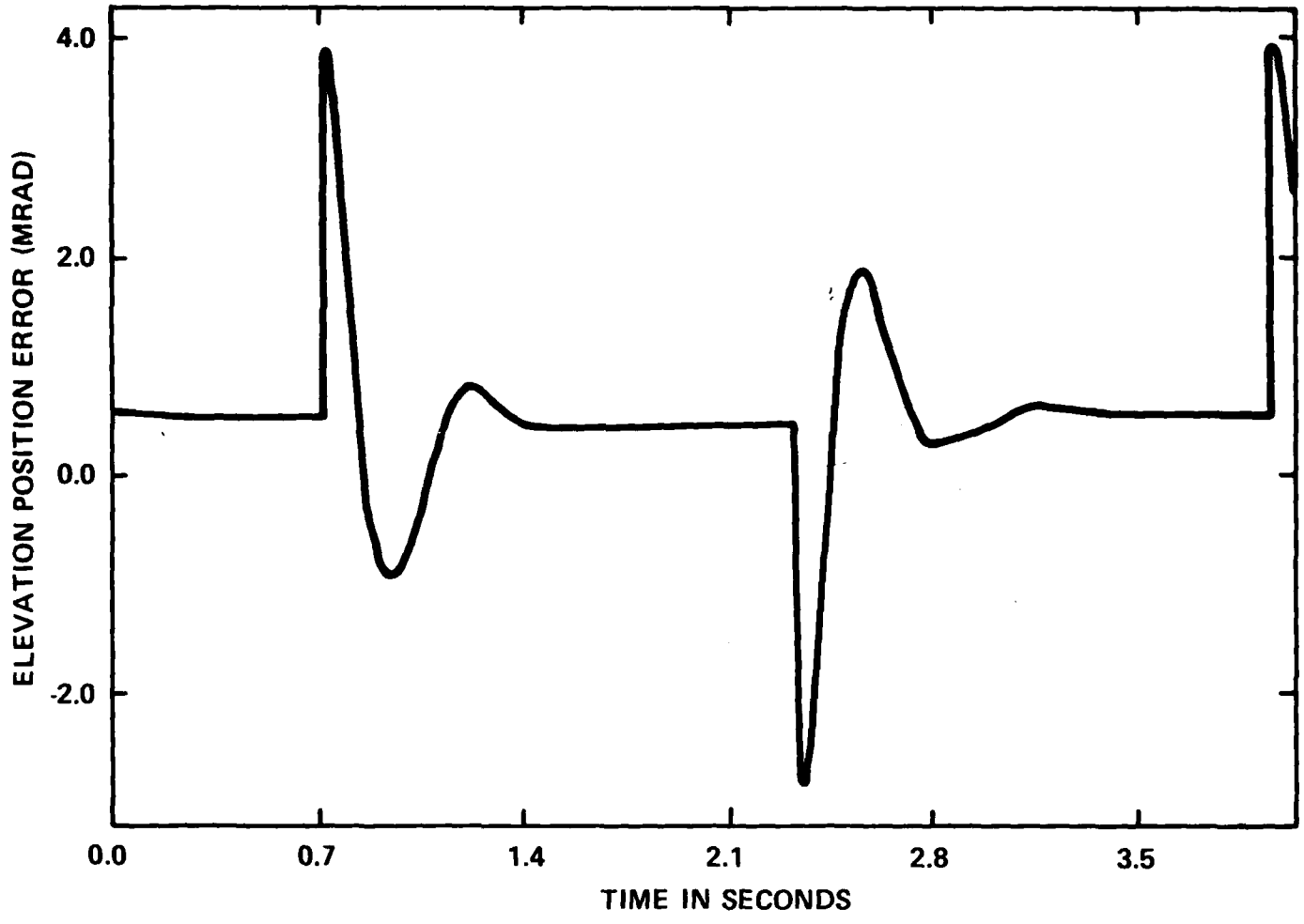


FIG. 5a. STEP RESPONSE OF ORIGINAL XM97 TURRET

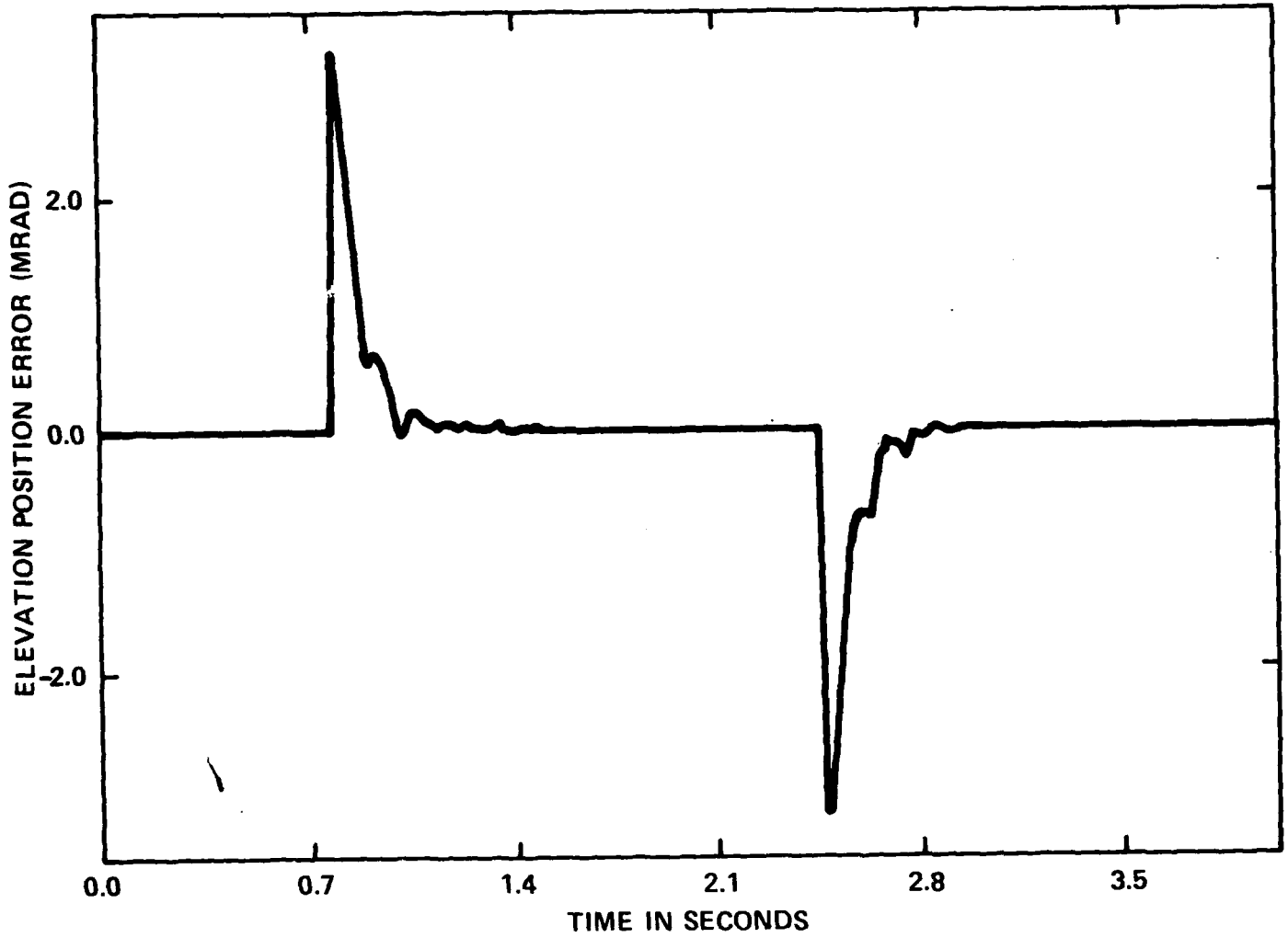


FIG. 5b. STEP RESPONSE OF DISCRETE-TIME DISTURBANCE ACCOMODATING CONTROL SYSTEM

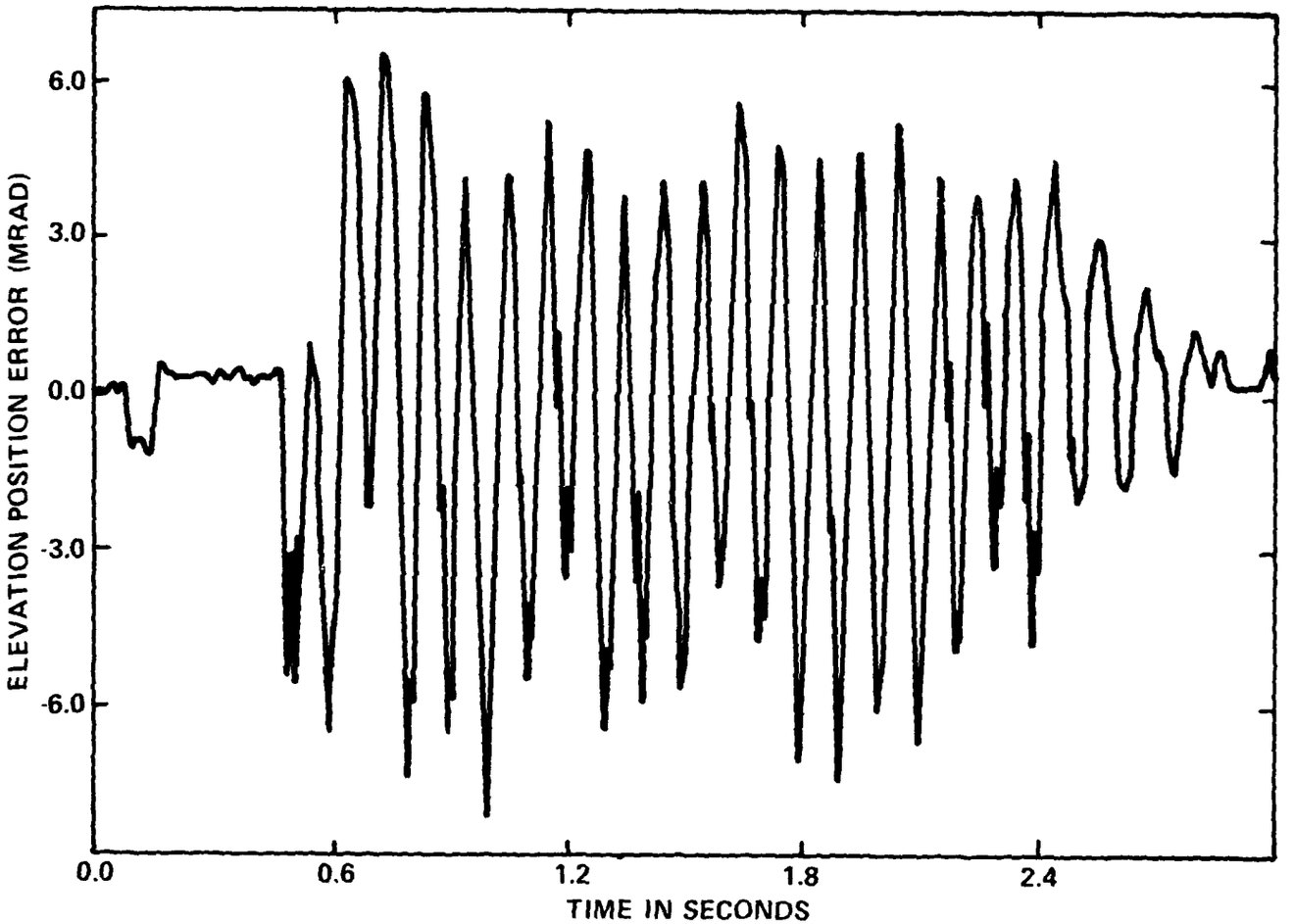


FIG. 6a. RESOLVER OUTPUT DURING 20-ROUND FIRING BURST OF ORIGINAL XM97 TURRET SYSTEM

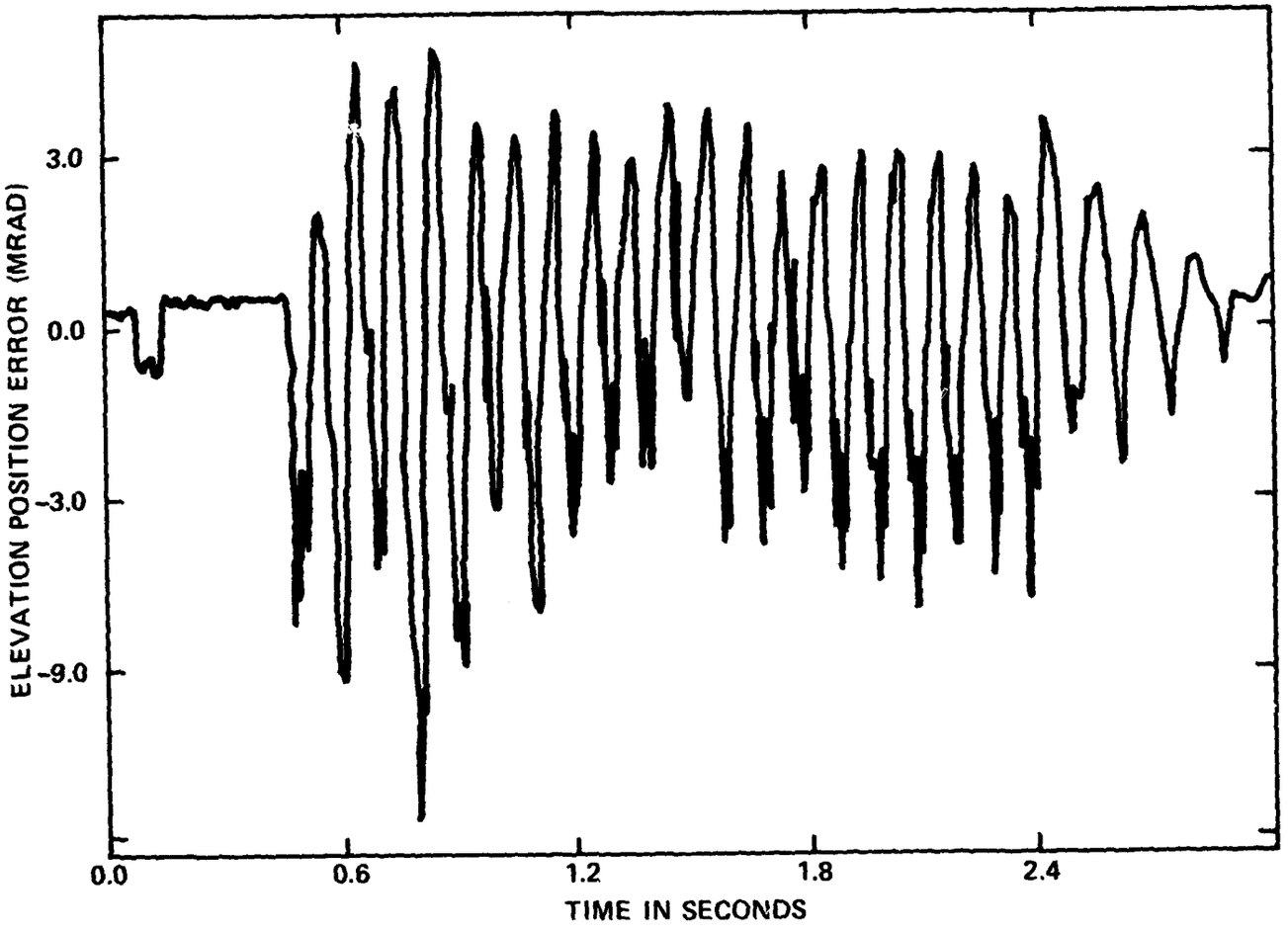


FIG. 6b. RESOLVER OUTPUT DURING 20-ROUND FIRING BURST w/DISCRETE TIME DISTURBANCE ACCOMODATING CONTROL SYSTEM



FIGURE 7a - 20 ROUND SHOT GROUP FIRED USING THE DISCRETE-TIME DISTURBANCE ACCOMMODATING CONTROLLER

FIGURE 7b - 20 ROUND SHOT GROUP FIRED FROM THE ORIGINAL XM-97 TURRET

ACKNOWLEDGMENT

The authors would like to thank Mr. D. Farnsworth, H. Plude, R. Peterson, and R. Radkiewicz, of the Ware Simulation Center, Rock Island Arsenal, IL, for conducting tests and providing data presented in this paper. The authors also acknowledge the valuable assistance and advice provided by Professor N.K. Loh of Oakland University, and Dr. J. Korn of Alphatech Inc.

REFERENCES

[1] Coleman, N.P. et al, "Application of Modern Control Theory to the Design of a Helicopter Turret Control System," Proceedings of the Second Meeting of the Coordinating Group on Modern Control Theory, APG, MD, Part 1, December 1980, pp. 1-20.

[2] Coleman, N.P. and Loh, N.K., "Microprocessor - Based Optimal Controllers for a Helicopter Turret Control System," Proceedings of the Nineteenth Annual Allerton Conference on Communication, Control, and Computing, Sep 1981, pp. 659-668.

[3] Loh, N.K. and Coleman, N.P., "Microprocessor Controlled Optimal Helicopter Turret Control System," submitted to 1982 American Control Conference to be held at Arlington, VA, 14-16 June 1982.

[4] Dorato, P. and Levis, A.H., "Optimal Linear Regulator: The Discrete-Time Case," IEEE Transactions on Automatic Control, Vol. AC-16, December 1971, pp. 613-620.

[5] Kovn, J., Carroll, E., and Johnson, R., "Microcomputer Implementation of Control Algorithms for Weapon Pointing and Stabilization," Proceedings of the Army Numerical Analysis and Computers Conference, Feb 1981, pp. 443-469.

[6] Gully, S.W., "Inertial Platform Synthesis Employing Observers to Accommodate Disturbances and Coupling," Proceedings of the 1976 IEEE Conference on Decision and Control, Dec 1976, pp. 65-77.

[7] Coleman, N.P. and Gully, S.W., "Microcomputer Control Algorithms for Weapon Pointing and Stabilization," IEEE Control Systems Magazine, Vol. 1, No. 3, Sep 1981, pp. 22-28.

AD P001064

FIRING DATA COMPARISON OF CLASSICAL AND MODERN TURRET CONTROLLERS

G. A. Strahl
Ware Simulation Section
US Army Armament Research and Development Command
Rock Island, IL 61299

ABSTRACT

Analysis of firing test data has proved the validity of using modern optimal control techniques to improve the dispersion characteristics of helicopter gun turrets. Statistical analysis was performed on firing data from tests conducted at the Ware Simulation Center at Rock Island Arsenal involving helicopter turret controllers designed using classical and modern control theory. This analysis showed that the gun turret systems operated by modern optimally designed controllers demonstrated statistically significant smaller firing dispersion than systems operated by classically designed controllers.

INTRODUCTION

This paper reports on work accomplished at the Ware Simulation Center (WSC) located at Rock Island, IL. Results were obtained from projects using a prototype XM97 turret and a production Universal Turret System both of which were mounted on a AH-1G Cobra helicopter fuselage. This fuselage was suspended from the Six-Degree-Of-Freedom (6-DOF) simulator at the Ware Center. Part of the work was funded by the Fire Control and Small Caliber Weapon Systems Laboratory of the Army Armament Research and Development Command located at Dover, NJ.

Optimal controllers were developed for the two helicopter turrets using modern control theory. These controllers were then implemented using a general test bed controller. Testing was then conducted to compare the optimal controllers performance with the performance of the turret's original classically designed controllers. Identical step and firing tests were performed with each controller. All tests were conducted under identical conditions at the Ware Simulation Center.

Test results indicate that the optimal controllers perform better than the original controllers. Step responses show that the optimal controllers can return the weapon to its original sight line following a disturbance faster than the original systems, and the firing tests show that the optimally controlled turrets have the tightest firing patterns.

A statistical analysis of the firing data shows the performance superiority of the optimal controllers. First a performance criterion for the multi-barrel weapon system was developed by comparing its hard stand and helicopter mounted firing patterns. Then the firing data was analyzed using an analysis of variance technique. This analysis showed that optimal controllers had statistically significant better performance than the original controllers

TESTING

TEST FACILITIES

The Ware Simulation Center (WSC) is located in Building 25 on Rock Island Arsenal, Rock Island, IL. The organization is part of the Technical Support Directorate of ARRADCOM. Test facilities at building 25 include two 100 meter and two 1000 inch (25.4m) indoor ranges capable of handling ammunition up to 30mm. One of the 1000 inch ranges is equipped with an environmental chamber capable of producing temperatures between -70 and +165°F (-57 to +74°C). The other 1000 inch range contains the 6-DOF simulator and was used for all testing reported in this paper. The 6-DOF can suspend helicopter fuselages and armored vehicle turrets up to 20,000 pounds (9071.9 Kg). [1]

An AH-1G Cobra helicopter without its rotor blades and tail section was suspended from the 6-DOF and used for the testing. The simulator's hydraulic actuators are operated by an electronic adaptive control system, which enables realistic flight motions and hovering conditions to be input to the suspended helicopter (figure 1).

A project was undertaken at WSC whose objective was to implement and test controllers designed using modern control theory. New controllers were designed first for the prototype XM97 turret and later for the Universal Turret System. Both turrets fit on the AH-1G helicopter and mount the M197 20mm 3-barrel gun which fires in a rotating Gatling style. Each turret contains an original classically designed controller that commands electrical motors in the azimuth and elevation axises.

THEORETICAL BACKGROUND

The new controllers were designed using standard optimal control theory. Details of the approach and particular design can be found in the references [2, 3]. Briefly, the system being controlled is

represented by the general, linear, time invariant equations:

$$\dot{\underline{x}}(t) = A\underline{x}(t) + B\underline{u}(t) + F\underline{v}(t) \qquad (1)$$

$$\underline{y}(t) = C\underline{x}(t) \qquad (2)$$

where all vectors and matrices are of the appropriate dimensions. The vectors are: x = state vector, u = control vector, v = input vector and u = control vector.

The elements of the A, B, F, and C matrices are found from the mathematical model of the system. The simple, known model shown in figure 2 was used for the XM97. The three state variables shown were chosen using experiment and experience to properly control the system. System equations shown below are easily derived from the figure:

$$\begin{bmatrix}\dot{x}_1(t)\\ \dot{x}_2(t)\\ \dot{x}_3(t)\end{bmatrix} = \begin{bmatrix}0 & 1/N & 0\\ 0 & 0 & 66.66\\ 0 & 96 & -500\end{bmatrix}\begin{bmatrix}x_1(t)\\ x_2(t)\\ x_3(t)\end{bmatrix} + \begin{bmatrix}0\\ 0\\ 2.006X10^7\end{bmatrix}u(t) + \begin{bmatrix}0\\ 0\\ -96N\end{bmatrix}v(t) \qquad (3)$$

$$y(t) = \begin{bmatrix}1 & 0 & 0\\ 0 & 1 & 0\\ 0 & 0 & 1\end{bmatrix} x(t) \qquad (4)$$

where N = gear ratio = 620 for azimuth and 810 for elevation.

A more detailed mathematical model for the UTS was derived from experimental data [4]. In both systems, non-linear elements were approximated by linear transfer functions.

The control vector, u(t), is found by the equation:

$$\underline{u}(t) = -K\underline{x}(t) \qquad (5)$$

where K is a time-invariant matrix determined by minimizing the performance index:

$$J = \int_0^\infty [Q\underline{x}(t) + R\underline{u}(t)]dt \qquad (6)$$

where Q and R are weighting matrices chosen to provide the desired system performance.

As can be seen from (5) the optimal control consists of the system states multiplied by simple constant terms. Using (5) in (1) the closed loop system is represented by:

$$\dot{\underline{x}}(t) = [A-BK]\underline{x}(t) + F\underline{v}(t) \qquad (7)$$

The complete XM97 optimal controller is shown in figure 4.

Later in the program, it was decided to include a state, torque disturbance, in the controller that is not measurable but had to be estimated using Luenberger Observer Theory [5]. In general, to use this theory (1) and (2) are partioned into two parts, one containing the measurable states $\underline{x}_1$ and one containing the unmeasurable states, $\underline{x}_2$:

$$\begin{bmatrix} \dot{\underline{x}}_1(t) \\ \hline \dot{\underline{x}}_2(t) \end{bmatrix} = \begin{bmatrix} A_{11} & A_{12} \\ \hline A_{21} & A_{22} \end{bmatrix} \begin{bmatrix} \underline{x}_1(t) \\ \hline \underline{x}_2(t) \end{bmatrix} + \begin{bmatrix} B_1 \\ \hline B_2 \end{bmatrix} \underline{u}(t) + \begin{bmatrix} F_1 \\ \hline F_2 \end{bmatrix} \underline{v}(t) \qquad (8)$$

$$\underline{y}(t) = \left[\begin{array}{c:c} I & 0 \end{array}\right] \begin{bmatrix} \underline{x}_1(t) \\ \hline \underline{x}_2(t) \end{bmatrix} = \underline{x}_1(t) \qquad (9)$$

The unmeasurable state $\underline{x}_2$ is estimated by [6]

$$\underline{x}_2(t) = \underline{p}(t) + L\underline{x}_1(t) \qquad (10)$$

where

$$\begin{aligned} \dot{\underline{p}}(t) &= (A_{22} - LA_{12})\underline{p}(t) + (B_2 - LB_1)\underline{u}(t) \\ &+ [(A_{21} - LA_{11}) + (A_{22} - LA_{12})L]\underline{x}_1(t) \end{aligned} \qquad (11)$$

The components of the matrix, L, are chosen using trial and error and experience to allow $\underline{x}_2$ to converge quickly to the actual state vector $\underline{x}_2$. Luenberger observers can be used also to estimate states that are measurable but for reasons of economy or reliability it is better to estimate. An example of such a state is vehicle hull rate which can be measured with a gyroscope. However, gyroscopes are expensive and in the severe military environment, are often unreliable. Thus, in this case, using an estimator may be an attractive alternative to measuring the state.

IMPLEMENTATION

The new controllers were implemented on the turrets by changing only the control electronics and using existing power amplifiers and motors. Implementing a modern controller requires measuring the states,

conditioning the signals, multiplying the signals by the desired theoretical gains, forming the estimated state signal, summing all signals to make the control input, and sending this control input to the power amplifier. All of these functions except measuring the states were performed by a test bed controller called the Modular Turret Controller (MTC).

The MTC consists of a mother board with 32 slots each accepting one electronic board. Sixteen boards control the elevation channel and sixteen control the azimuth channel. Most cards have an identical framework consisting of four operational amplifiers and an associated programmer card. The configuration of its programmer card determines the function an amplifier will perform. Possible functions are summation, multiplication, or integration. Different combinations of programmer cards allows each circuit card to perform a desired larger function such as solving a differential equation (figure 3).

The MTC can implement controllers on a wide variety of systems. The linear control theory on which the controllers are based is equally applicable to electrical, hydraulic, or pneumatic systems, and the implemented controller on the MTC can be easily changed by putting different programmer cards in the circuit cards.

Several controllers have been implemented using the MTC, including two and three state controllers both with and without Luenberger Observers for the XM97 and a three state controller for the UTS. Identical tests were conducted using the original and optimal controllers for both turrets and the results used to compare their performance.

TEST RESULTS

STEP TESTS

In the step tests, a square wave voltage is input to the system resolver which commands the controller to move the turret to a new position in a similar manner to a gunner commanding the turret to move with his control handle in actual flight. How quickly a controller can move the turret to its commanded position is a good measure of its effectiveness. A comparison of the original and optimal controllers' step responses is shown in figures 4 and 5. In each response, the turret has reached its commanded position when the error is zero.

Two features can be seen from figures 4 and 5. One, the production UTS performs much better than the prototype XM97, for both original and optimal controllers. Second, the optimal controllers move the turret to the commanded position much faster than the original controllers in both turrets.

An analysis of the step responses reveals how the optimal controllers achieve better performance. Considering the two turrets separately, the step responses for the first 0.30 seconds are the same for both controllers. However, at this time, the original controllers overshoot the desired position at least once and lose time returning from this overshoot.

The 5% settling time, the time it takes for the error to become 5% of its peak value, is used to quantitatively compare the controllers performance. A smaller settling time indicates a quicker move to the commanded position and a more effective controller. The average 5% settling times are shown below:

Controller	5% Settling Time (Sec)
XM97 - Original	0.68
UTS - Original	0.35
XM97 - Optimal	0.26
UTS - Optimal	0.21

FIRING TESTS

To establish baseline data for firing tests the M197 gun was fired from a hardstand. The M197 produced a firing pattern wherein rounds from the same barrel landed in the same area, that is rounds 1, 4, 7, 10, 13, 16, and 19 from barrel 1 are in one group, rounds 2, 5, 8, 11, 14, 17, and 20 from barrel 2 are in another group, and rounds 3, 6, 9, 12, 15, and 18 are in a third group (see figure 6).

Numerous firing tests were conducted to compare the performances of the optimal and original controllers. All firing tests were accomplished from the AH-1G helicopter suspended from the 6-DOF simulator. Each test consisted of a 20 round burst from the 3 barrel 20mm M197 gun. Targets were taken at the end of the WSC 1000 inch range. Each round was color coded so that each target hole could be identified with a round number.

Targets from the XM97 and UTS firing tests also show that rounds fired from the same barrel are in general proximity to each other. In fact, some target patterns approached those shown in the hardstand tests, thus indicating a very good controller. The degree that a test firing pattern resembles that of a hardstand firing pattern is a good indicator of controller performance; therefore, the standard deviation or dispersion of shots from each particular barrel was chosen as one performance measure of the original and optimal controllers.

The impact point of the first round of each barrel in a burst (that is, the first three rounds of a burst) was eliminated from this analysis due to the mechanisms of the helicopter and the finite response time of the controllers. When the M197 gun fires, the recoil force causes the helicopter to pitch quickly downward. This pitching motion is so quick that the control system cannot react fast enough to effectively control the first three rounds of a burst. This behavior is very similar for all controllers tested. After the first three rounds, however, the controller can affect the weapon line and can keep the round impact points in fairly close proximity. Since any controller cannot affect the impact points of the first three rounds, these rounds are not included in the controller performance analysis.

The average standard deviations of the round impact points for the XM97 and UTS original and optimal controllers are shown in the table:

	Standard Deviation--means(mr)					
	Barrel 1		Barrel 2		Barrel 3	
Controller	AZ	EL	AZ	EL	AZ	EL
XM97 Original	1.25	3.90	1.42	2.73	1.32	2.36
XM97 Optimal	1.10	1.98	1.40	2.16	1.35	1.64
UTS Original	1.03	1.62	1.34	1.39	0.77	1.65
UTS Optimal	0.97	1.53	0.67	1.43	0.64	1.75

Generally, the optimal controllers provide smaller dispersion than the original controllers. Also, the UTS with an optimal or original controller has smaller dispersion than the prototype XM97 turret system.

FIRING DATA ANALYSIS

ANALYSIS OF VARIANCE APPROACH

A statistical analysis was performed using the firing data to compare the controllers' performance in more detail. An analysis of variance (ANOVA) technique was employed to determine if the type of controller used had a statistically significant effect on shot dispersion and if any statistical difference exists in the barrel shot dispersion depending on whether it was fired first, second, or third. The analysis was done separately on the azimuth and elevation channels.

The basis of the technique is to calculate test statistics from the data and compare them to a critical statistic to accept or reject a hypothesis about the data. There were two hypotheses tested in this ANOVA for each channel. The first hypothesis was that the means of the data for the different controllers are equal. Notationally, this hypothesis can be stated: H_o: $\mu_{\text{original XM97}} = \mu_{\text{optimal XM97}} = \mu_{\text{original UTS}} = \mu_{\text{optimal UTS}}$.

This hypothesis can also be interpreted as meaning that the controller used has no effect on shot dispersion. The second hypothesis was that the means of the barrel shot groups are the same, or $H_o: \mu_1 = \mu_2 = \mu_3$. This hypothesis also can be interpreted as saying that when the barrel is fired it has no effect on the shot dispersion of that barrel. The alternative to each hypothesis is that at least two of the means differ.

Test statistics are determined from the mean sum of squares of the data and are compared to a critical statistic obtained from a table of F-statistics. To aid the calculation process, first a table of data and preliminary calculations is set. Tables for the elevation and azimuth channels are shown below. In each table a T-notation short hand for column and row summation is used, that is:

$$T_{i.} = \sum_{j=1}^{3} x_{ij}, \quad T_{.j} = \sum_{i=1}^{4}, \quad \text{and} \quad T_{..} = \sum_{i=1}^{4} \sum_{j=1}^{3} xij.$$

Data and Preliminary Calculations Table

Azimuth

	Barrel Firing Number				
Controller	First	Second	Third	$T_{i.}$	$T_{i.}^2$
Original XM97	1.25	1.42	1.32	3.99	15.9201
Optimal XM97	1.10	1.40	1.35	3.85	14.8225
Original UTS	1.03	1.34	0.77	3.14	9.8596
Optimal UTS	0.97	0.67	0.64	2.28	5.1984
$T_{.j}$	4.35	4.83	4.08	$T_{..}=13.26$, $\sum_{i=1}^{4} T_{i.}^2=45.8006$	
$T_{.j}^2$	18.9225	23.3289	16.6464	$\sum_{j=1}^{3} T_{.j}^2 = 58.8978$	

Elevation

	Barrel Firing Number				
Controller	First	Second	Third	$T_{i.}$	$T_{i.}^2$
Original XM97	3.90	2.73	2.36	8.99	80.8201
Optimal XM97	1.98	2.16	1.64	5.78	33.4084
Original UTS	1.62	1.39	1.65	4.66	22.1841
Optimal UTS	1.53	1.43	1.75	4.71	21.7156
$T_{.j}$	9.03	7.71	7.40	$T_{..}=24.14$, $\sum_{i=1}^{4} T_{i.}^2=158.1282$	
$T_{.j}^2$	81.5409	59.4441	54.76	$\sum_{j=1}^{3} T_{.j}^2 = 195.745$	

Next, the test statistics are calculated according to formulae:

$$F_{\text{Test, Controller}} = \frac{MS_{\text{Controller}}}{MS_{\text{Error}}} = \frac{SS_{\text{Controller}}/3}{SS_{\text{Error}}/6}$$

$$F_{\text{Test, Barrel}} = \frac{MS_{\text{Barrel}}}{MS_{\text{Error}}} = \frac{SS_{\text{Barrel}}/2}{SS_{\text{Error}}/6}$$

where

$$SS_{\text{Controller}} = \text{Sum of squares (controller)} = \frac{\sum_{i=1}^{4} T_{i.}^2}{3} - \frac{T_{..}^2}{12}$$

$$SS_{\text{Barrel}} = \text{Sum of squares (barrel)} = \frac{\sum_{j=1}^{3} T_{.j}^2}{4} - \frac{T_{..}^2}{12}$$

$$SS_{\text{Error}} = \text{Sum of squares (error)} = \sum_{i=1}^{4}\sum_{j=1}^{3} x_{ij}^2 - \sum_{i=1}^{4} \frac{T_{i.}^2}{3} - \sum_{j=1}^{3} \frac{T_{.j}^2}{3} + \frac{T_{..}^2}{12}$$

The calculations are summarized in the ANOVA Table below:

Source	Sum of Squares	Degree of* Freedom	MS	F_{Test}	F_{Critical}
		AZIMUTH			
Controller	0.61457	3	0.20486	5.4981	3.2888
Barrel	0.07215	2	0.03608	0.9683	3.4633
Error	0.22358	6	0.03726		
Total	0.91030	11			
		ELEVATION			
Controller	4.14777	3	1.38259	7.20474	3.2888
Barrel	0.37462	2	0.18731	0.97608	3.4633
Error	1.15138	6	0.19190		
Total	5.67377	11			

* One less than number of data points used to calculate a given mean.

The critical statistic, $F_{critical}$, is obtained from a standard table of F-statistics, and its value depends on the degrees of freedom of the mean squares involved and the level of confidence, , chosen for the analysis. If an value of 0.10, which corresponds to having 90% confidence in the results is used, then

$$F_{critical,\ controller} = F\ (df_{controller},\ df_{error}) \qquad (12)$$

$$= F_{0.10(3,6)} = 3.2888$$

and

$$F_{critical,\ barrel} = F\ (df_{barrel}, df_{error}) = F_{0.10(2,6)} \qquad (13)$$

$$= 3.4633$$

A hypothesis can be rejected if $F_{test} > F_{critical}$. Thus, for both azimuth and elevation, the hypothesis about controller means can be rejected, but the hypothesis about barrel means cannot be rejected. The first conclusion indicates that for both channels at least two of the shot dispersion means for the different controllers are different or, in other words, the type of controller does affect the shot dispersion. The second conclusion says that whether a given barrel is fired first, second, or third in a burst does not affect the burst dispersion.

Since at least two of the controller data means differ, more information about the controller performance can be determined by application of the most-significant-difference (MSD) test. Also known as the multiple-t test, this method is used to determine which data means are different to a statistically significant extent. While the data summary shows that the standard deviation means are smaller for the optimal and UTS controllers, the MSD test will tell which differences can be called significant within a confidence level of 90%.

In the MSD, test differences between data are compared to a calculated MSD number. Any difference that is larger than the MSD number is statistically significant. The MSD number is calculated from the equation

$$MSD = \sqrt{2}\ S_{\bar{x}}\ t_{0.10,df_{error}} \quad \text{where } S_{\bar{x}} = \sqrt{MS_E/m} \qquad (14)$$

where MS_E = mean square error and m = number of data points involved in calculating the controller means. Since it has been shown that the barrel firing position is not significant, a new ANOVA Table is constructed ignoring barrel effects:

Table 1. ANOVA Table -- Ignoring Barrel Effects

Source	Sum of Squares	Degree of* Freedom	MS	F	$F_{Critical}$
		AZIMUTH			
System	0.61457	3	0.20486	5.5412	2.9238
Error	0.29573	(8)	(0.03697)		
Total	0.91030	11			
		ELEVATION			
System	4.14777	3	1.38259	7.2482	2.9238
Error	1.52600	(8)	(0.19075)		
Total	5.67377	11			

* One less than number of data points used to calculate a given mean.

The required MS_E and df_{error} numbers are circled in the Table. Thus, for azimuth: $S_{\bar{x}} = \sqrt{(.03697)/3} = 0.11100$ and for elevation: $S_{\bar{x}} = \sqrt{(.19075)/3} = 0.25216$. So the following MSD numbers can be calculated: for azimuth: $MSD = (\sqrt{2})(0.111)t_{10,8} = (.157)(1.397) = 0.219$, and for elevation: $MSD = (\sqrt{2})(0.25216)(1.397) = 0.498$. The calculation of the differences and comparison of them to the MSD number is facilitated by the construction of the tables shown below

Table 2. Azimuth Mean Ranking and Difference Tables

	System	Test Replications 1	2	3	Total	Mean
A:	Original XM97	1.25	1.42	1.32	3.99	1.330
B:	Optimal XM97	1.10	1.40	1.35	3.85	1.283
C:	Original UTS	1.03	1.34	0.77	3.14	1.047
D:	Optimal UTS	0.97	0.67	0.64	2.28	0.760

Table 2 (Cont.)

Mean Rank: Largest: System A
2nd Largest: System B
2nd Smallest: System C
Smallest: System D

		A 1.330	B 1.283	D 1.047
D:	0.760	[0.570]	[0.523]	[0.287]
C:	1.047	[0.283]	[0.236]	---
B:	1.283	0.047	---	---

Table 3. Elevation Mean Ranking and Difference Tables

	System	Test Replications 1	2	3	Total	Mean
A:	Original XM97	3.90	2.73	2.36	8.99	2.9967
B:	Optimal XM97	1.98	2.16	1.64	5.78	1.9267
C:	Original UTS	1.62	1.39	1.65	4.66	1.5533
D:	Optimal UTS	1.53	1.43	1.75	4.71	1.5700

Mean Rank: Largest: System A
2nd Largest: System B
2nd Smallest: System D
Smallest: System C

		A 2.9967	B 1.9267	C 1.5700
C:	1.5533	[1.4434]	0.3734	0.0167
D:	1.5700	[1.4267]	0.3567	--
B:	1.9267	[1.0700]	--	--

In the tables, every difference that exceeds the MSD number is circled and corresponds to two means that come from different statistical populations. For azimuth, every difference except the B - A = 0.047 entry is circled which means that there is no statistically significant difference between the performance of controller A and controller B. However, there are statistically significant differences between all other controller combinations, that is, (A,D), (B,D), (C,D), (A,C), and (B,C). In elevation, there is no statistically significant difference between controllers (B,D), (C,D), and (B,D) but there is between controllers (A,C), (A,D), and (A,B).

The MSD method shows that the optimal UTS controller provided statistically improved performance over the original system in azimuth. In elevation, however, there is no significant difference between the original and optimal controller's performance. The reverse condition was found for the XM97, where the optimal controller was significantly better than the original controller in elevation, but no significant difference existed in azimuth.

One difference between the XM97 and UTS firing tests is that poistion gyro feedback was used in elevation for the XM97 test. This position gyro feedback provided a correction for the pitch rotation caused by the weapon recoil force. Gyro feedback was not used in azimuth in the XM97 test and was not used in either channel in the UTS test due to failure of the gyro package. The change in weapon-pointing angle caused by the recoil force is much larger in elevation than in azimuth; and, without elevation gyro feedback, the controller's performance is degraded due to the larger error input. In fact, the larger error input may mask any improvement that would be possible with the UTS optimal controller. In azimuth, with much smaller recoil force, the UTS optimal controller performed much better than the UTS original controller.

The optimal UTS controller was designed very quickly (in less than a week) without knowledge of an accurate mathematical model. Improved performance could be obtained from an optimal controller designed more thoroughly and with the knowledge of an accurate mathematical model. It is quite possible that the model used to design the UTS optimal controller was in more error in elevation than azimuth and that this prevented the UTS optimal controller from being significantly better than the original in elevation as it was in azimuth.

OVERALL PATTERN ANALYSIS

Another method of evaluating the performance of the original and optimal UTS controllers is by comparison of the overall dispersion of their firing patterns. The particular dispersion measure that is used in

this report is a determination of the 80% dispersion circle (that is, the smallest diameter circle that can be drawn on the target that contains 80% of the rounds fired). The radius of that circle is considered the 80% dispersion.

This overall dispersion criteria corresponds to a helicopter manufacturer specification that requires the UTS to fire a 100 round burst wherein 80% of the rounds fall within a circle of diameter not greater that 12 milliradians.

Average 80% dispersion is shown below for each controller and the hardstand firing:

Test Condition	Average 80% Dispersion
XM97 with original controller	4.20 mr
XM97 with optimal controller	3.63 mr
UTS with original controller	3.27 mr
UTS with optimal controller	2.74 mr
M197 gun on hardstand	2.31 mr

These results show that the optimal controller provides a tighter firing pattern for the XM97 and UTS. In fact, the UTS optimal controller firing pattern while having an 80% dispersion near that of the hardstand pattern, it also has the same rounds from each barrel grouping (see figure 6)..

SUMMARY

New controllers have been designed for two helicopter turrets using modern linear optimal control theory. The optimal controllers have been implemented on a test bed controller. The new controllers' and original classically designed turret controllers' performances have been compared using step and firing test data. Several analytical and statistical tools have been employed in this comparison. The data analysis shows that improved performance is obtained in both turrets through use of an optimal controller.

REFERENCES

[1] Radkiewicz, R. J., "Simulation Testing of Weapon Systems", Technical Report ARTSD-TR-81001, US Army Armament Research and Development Command, Dover, NJ 07801, October 1981.

[2] Kwakernaak, H., and Sivan, R., Linear Optimal Control Systems, New York, John Wiley and Sons, Inc., 1972.

[3] Loh, N. K., et.al., "Design and Implementation of an Optimal Helicopter Turret Control System", J. of Interdis. Model. and Simul., Vol. 3, pp. 31-46, January 1980.

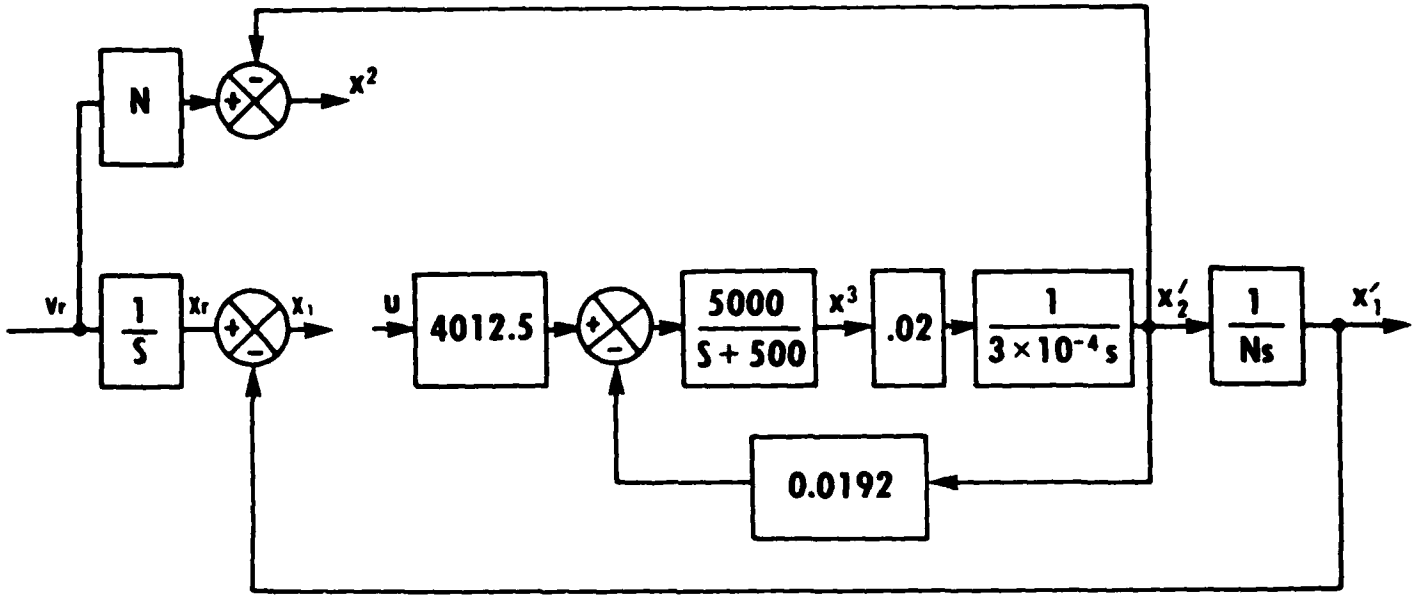
[4] Strahl, G. A., and Peterson, R. A., "UTS Model Determination and Controller Performance Testing", Technical Report ARTSD-TR-81005, US Army Armament Research and Development Command, Dover, NJ 07801, April 1982.

[5] Luenberger, D. G., "Observers for Multivariable Systems", IEEE Trans. Automat. Contr., Vol. AC-11, pp. 190-197, April 1966.

[6] Gopinath, B., "On the Control of Linear Multiple Input-Output Systems", Bell System Technical Journal, Vol. 50, pp. 1063-1080, March 1971.



XM97 BLOCK DIAGRAM



$$N = \text{GEAR RATIO} = \begin{cases} 620 \text{ IN AZIMUTH} \\ 810 \text{ IN ELEVATION} \end{cases}$$

STATE VARIABLES

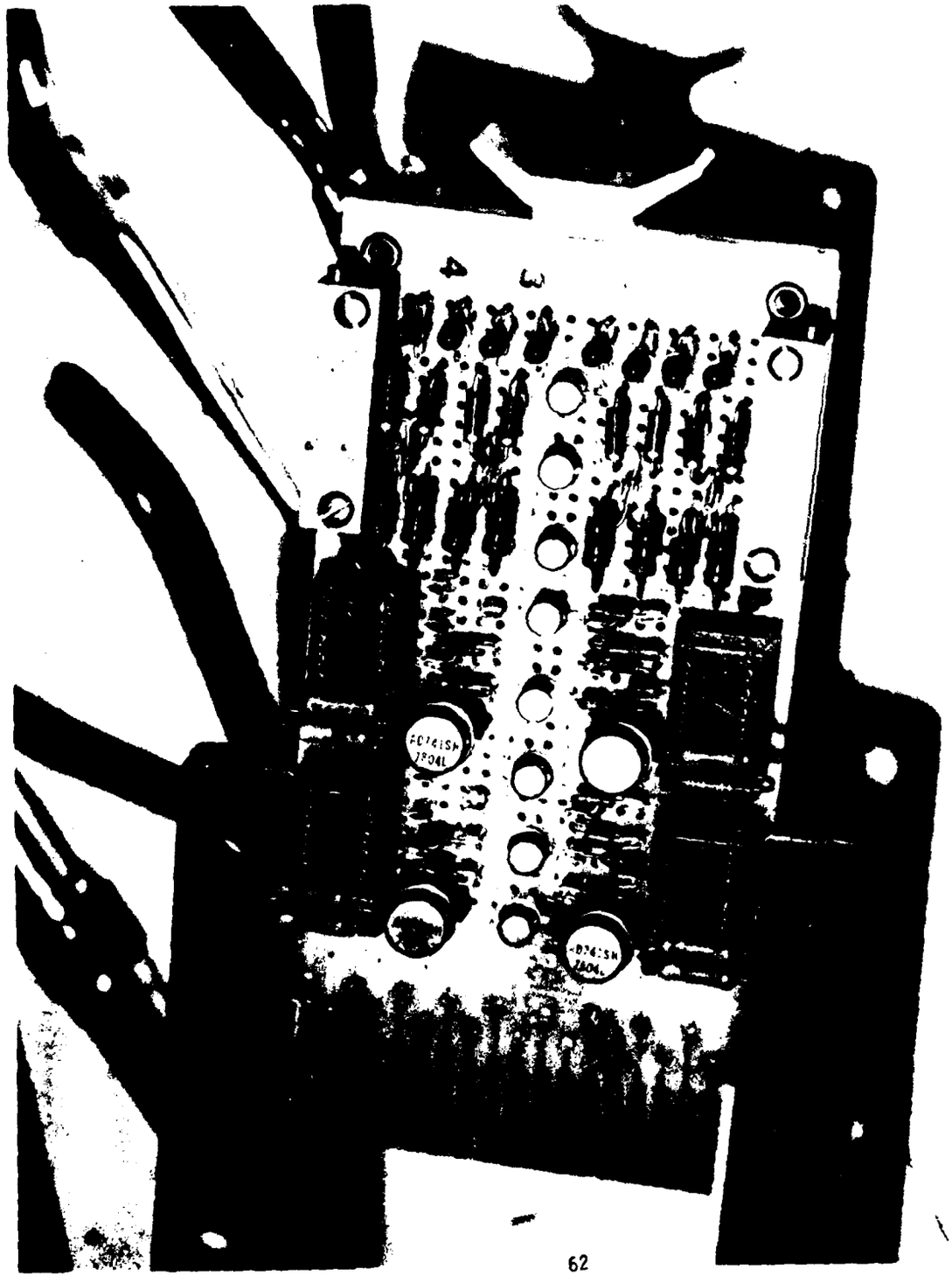
x_1 = ANGULAR POSITION ERROR (RADIANS)

x_2 = MOTOR ANGULAR VELOCITY (RADIANS/SEC)

x_3 = MOTOR ARMATURE CURRENT (AMPERES)

OPTIMAL CONTROL IMPLEMENTATION

FIGURE 2



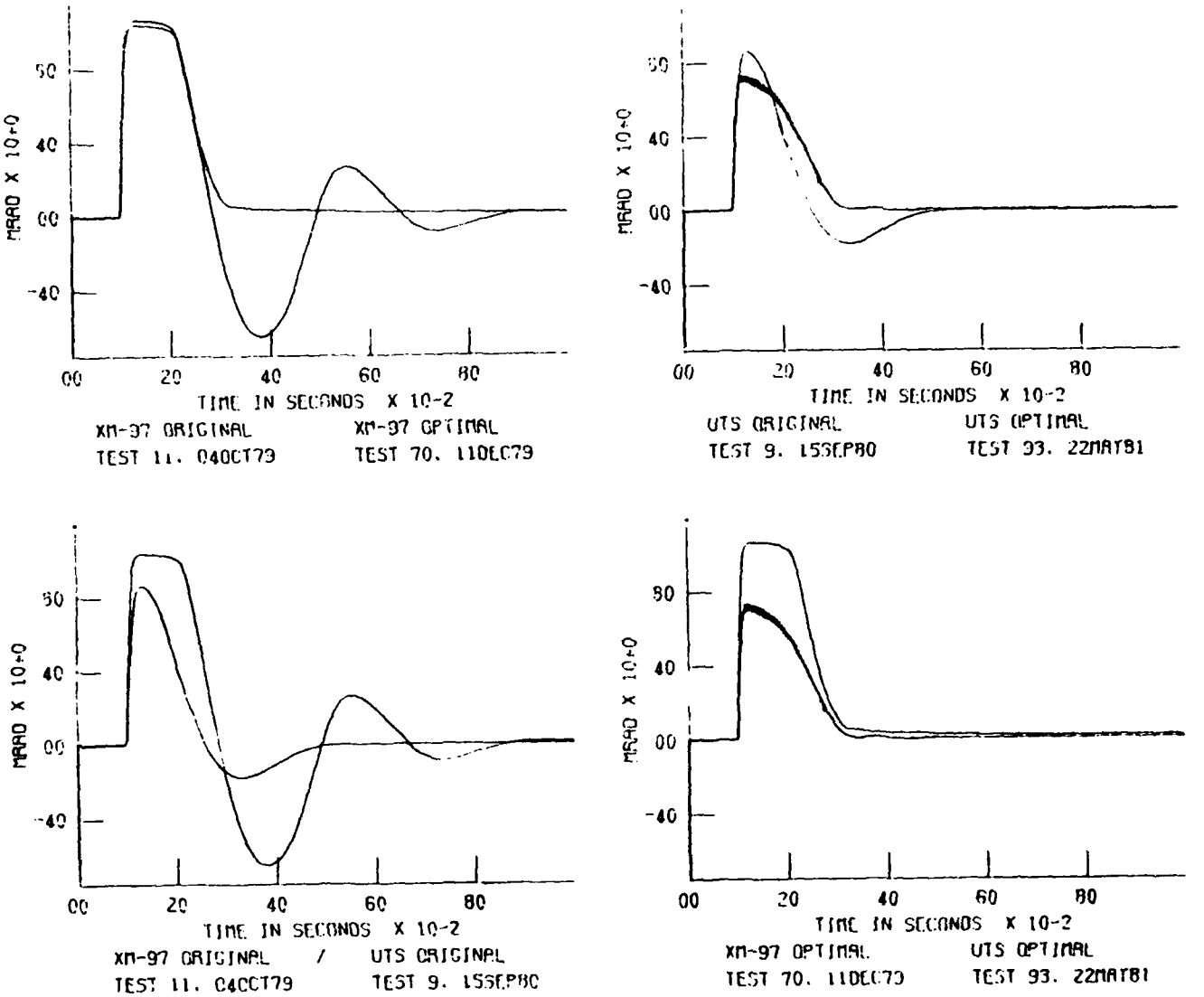
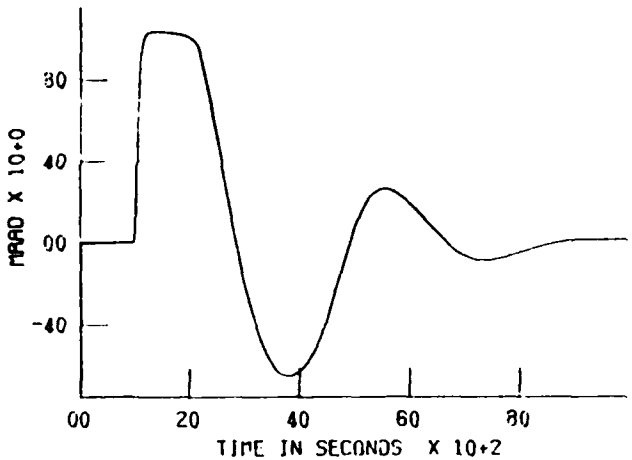
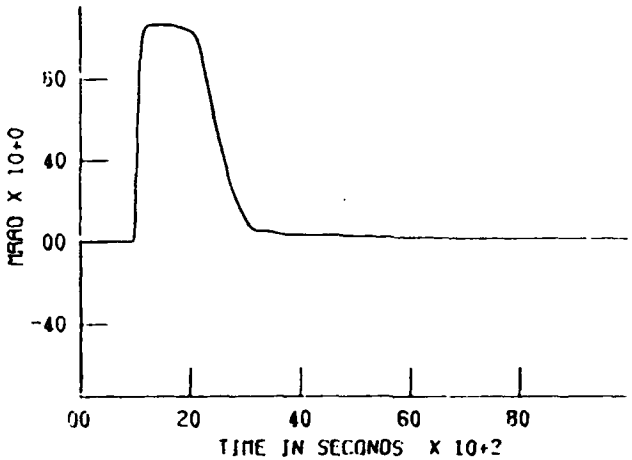

MRAD X 10+0
50
40
00
-40
00
20
40
60
80
TIME IN SECONDS X 10-2
XM-97 ORIGINAL
TEST 11. 040CT79
XM-97 OPTIMAL
TEST 70. 11DEC79
UTS ORIGINAL
TEST 9. 15SEP80
UTS OPTIMAL
TEST 93. 22MAY81
XM-97 ORIGINAL / UTS ORIGINAL
TEST 11. 04OCT79
TEST 9. 15SEP80
XM-97 OPTIMAL
TEST 70. 11DEC79
UTS OPTIMAL
TEST 93. 22MAY81

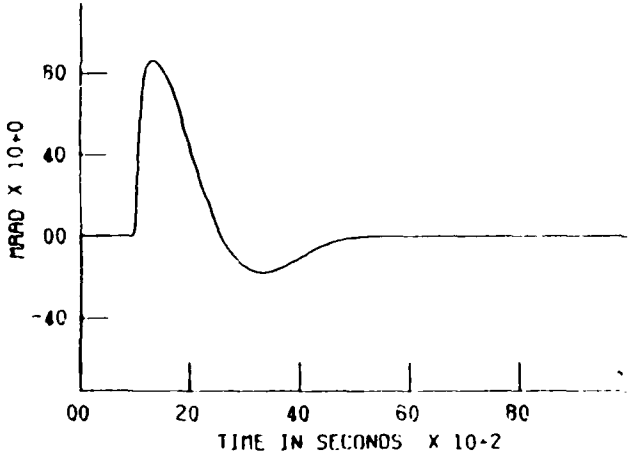
FIGURE 4



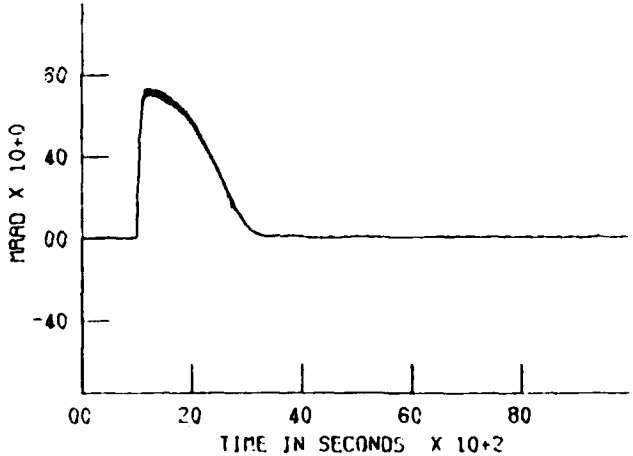
DEMODULATED AZIMUTH ERROR - FILTER = 100HZ
TEST 011. 040CT79 ORIGINAL XM-97 CONTROLLER



TRK 01A FILTERED DEMODULATED AZIMUTH ERROR
TEST 070. 11DEC79 OPTIMAL XM-97 CONTROLLER



TRK 01A DEMODULATED AZIMUTH ERROR - FILT = 100HZ
U.T.S. TEST 003. 155EPBO UTS ORIGINAL CONTROLLER



AZ D'MOD ERROR - UTS
TEST 093. MTC/UTS. 22MAY81 UTS OPTIMAL CONTROLLER

FIGURE 5

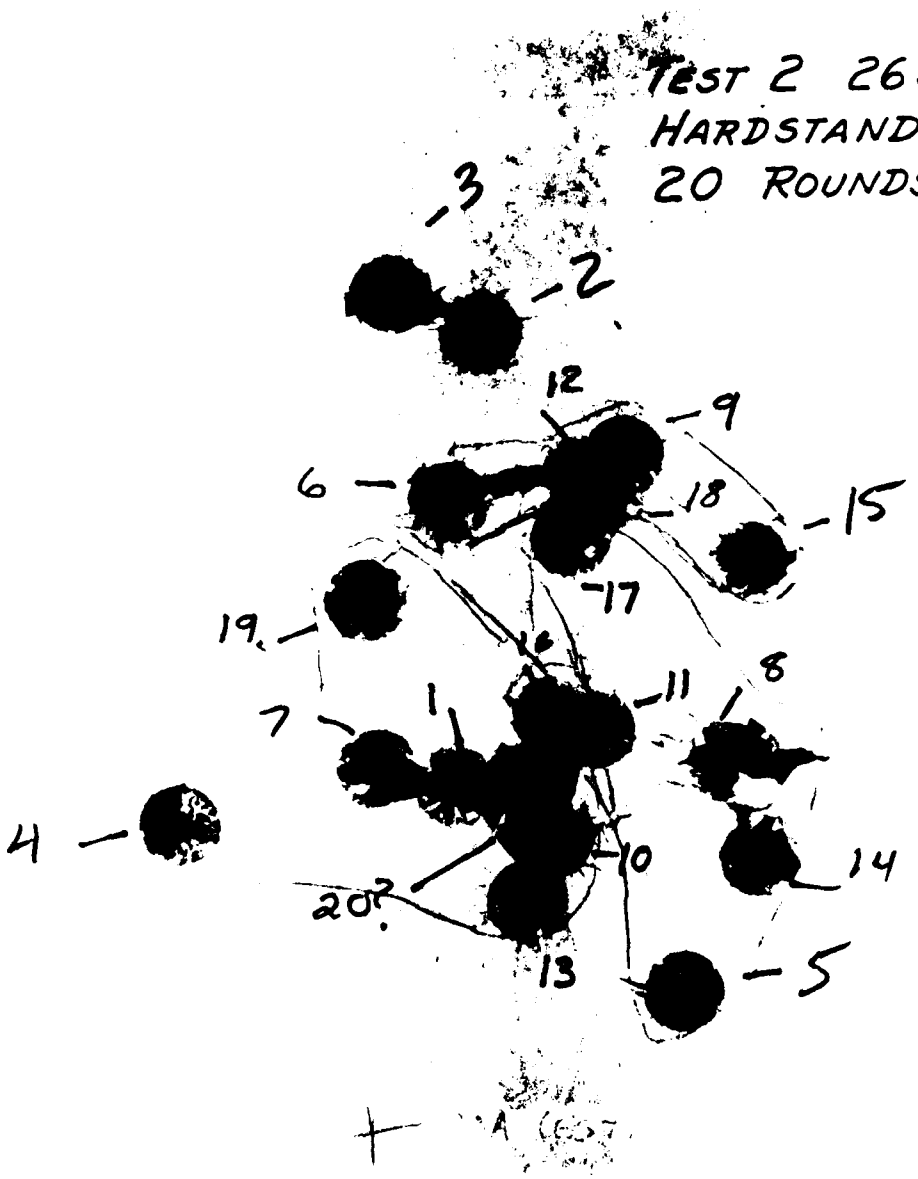


FIGURE 6

Next page is blank.

AD P001065

DEVELOPMENT OF A COMBAT VEHICLE SUPPORT PLAN USING MODERN SYSTEM THEORY

by

A. Fermelia

I. INTRODUCTION

Due to the nature of the USSR/Warsaw Pact threat to the U.S. and its NATO allies, it is considered by military analysts that any future land combat will be characterized by high engagement rate battles. Therefore, the armed combat vehicle will play a major role if the U.S. and their allies hope to defeat such a threat. Since intelligence sources have indicated that Warsaw Pact nations have a numerical superiority in combat vehicles, the U.S. Army's Training and Doctrine Command maintains the NATO forces must achieve a three-to-one kill ratio in order to achieve victory. In addition, due to an effective range of 2000 meters for USSR equipment, doctrine requires "fire on the move" whenever the range of engagement is less than 2000 meters and "shoot and scoot" tactics for engagements at more than 2000 meters.

In order to develop combat vehicles that will achieve a three-to-one kill ratio, the Dynamic Capability Development Tank Program, D^2T, was created. This program is intended to address the component design of the combat vehicle, i.e., the ballistic computer, range finder, target tracker, etc. However, the D^2T Program will not answer the overall question: What is the system's probability of survival under saturation attack? This question can only be answered by formulation of a viable "Combat Vehicle Support Plan." This paper provides a methodology for development of such a plan.

The Combat Vehicle Support Plan (CVSP) is illustrated in Figure 1. Development of such a plan consists of three phases:

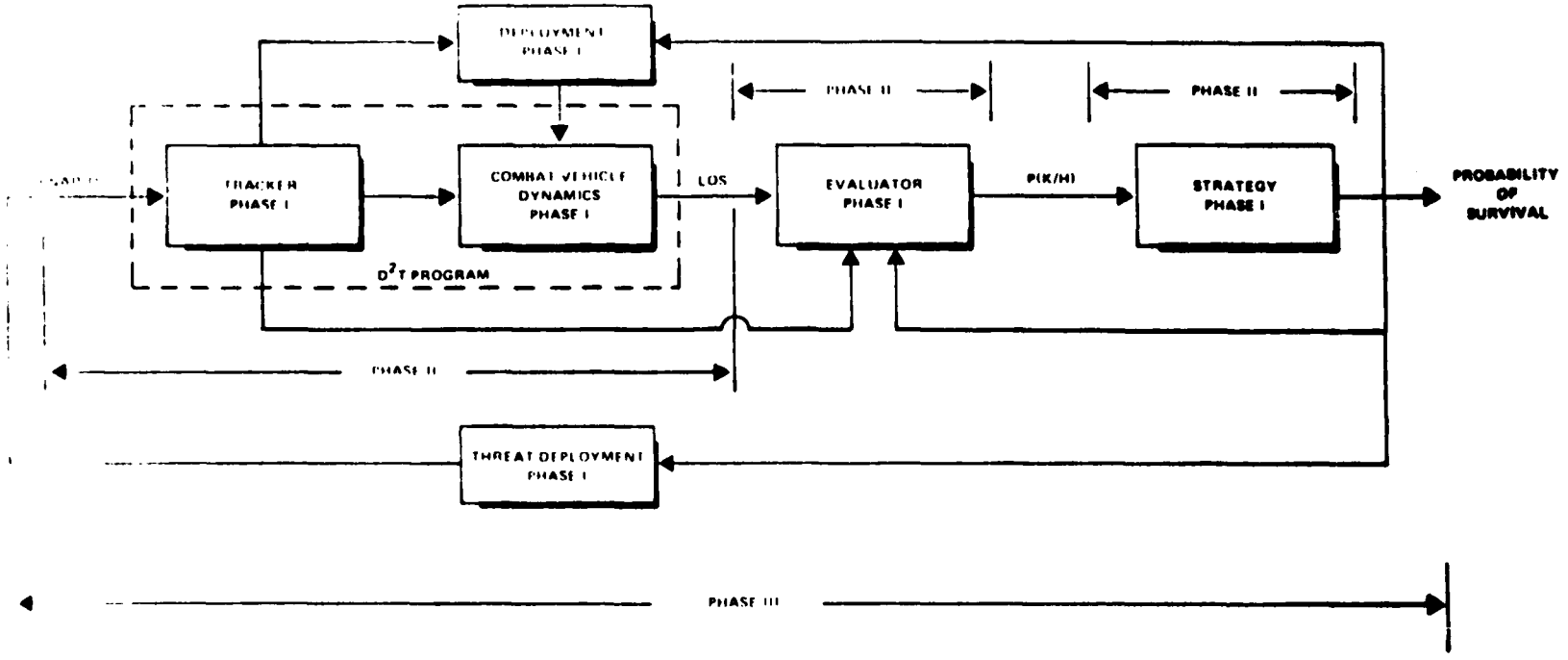


Figure 1. Development Phases of Combat Vehicle Support Plan
Phase I: Data Base
Phase II: Performance Analysis
Phase III: Force on Force Simulations

Phase I - Data Base

Phase II - Performance Analysis

Phase III - Force-on-Force Simulations

Phase I development will produce a data base of 1) existing combat vehicle performance, 2) numbers of vehicles in respective arsenals, 3) determination of likely threat scenarios, and 4) defeat requirements. Completion of Phase I yields information that would allow definition of inputs/outputs of each block defined in Figure 1.

In Phase II, an "open loop" performance analysis of the CVSP is obtained. This consists of relating inputs to outputs for all blocks given in Figure 1, i.e., definition of "transfer functions." Outputs for this phase are these "transfer functions" and sensitivities associated with them. It should be noted that benefit to the D^2T Program and the CVSP can be achieved in the development of this phase; that is, the evaluation of the combat vehicle fire control system is a subtask of Phase II.

A force-on-force simulation assures the viability of the CVSP. Phase III output results of a force-on-force simulation. This can be obtained by "closing the loop" of Figure 1. This "closure" may take the form of employing existing models (Carmonette, Tape, etc.) or creation of a new code.

II. TECHNICAL DISCUSSION

The design of future combat vehicles will be driven by the theory that future land combat will be characterized by high-engagement-rate battles. Hence the problem of survivability under saturation attack must be addressed. The role of a Combat Vehicle Support Plan (CVSP) is a key factor in addressing this problem. Figure 2 illustrates the components of the CVSP.

The CVSP is designed to blend doctrine, tactics, strategy, and intelligence to improve the probability of survival. Doctrine maintains that in order to

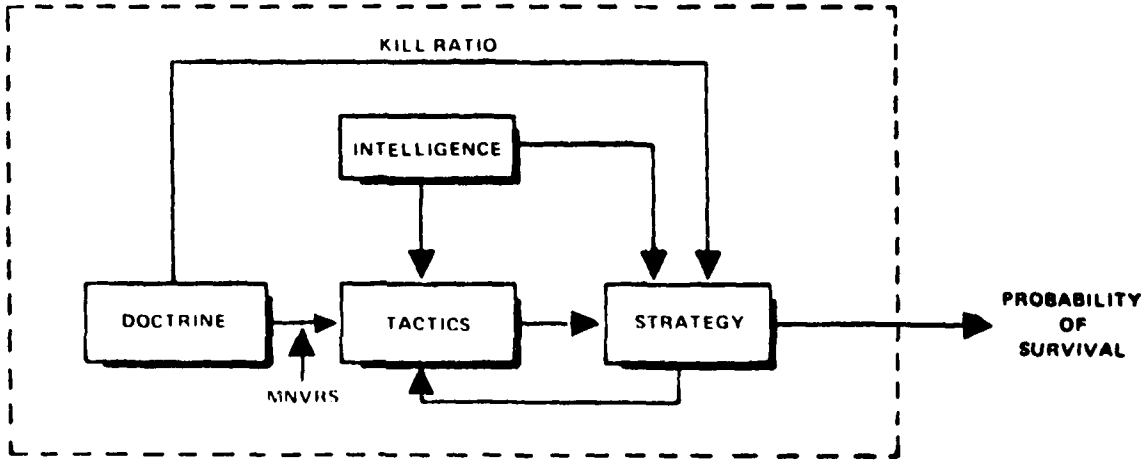


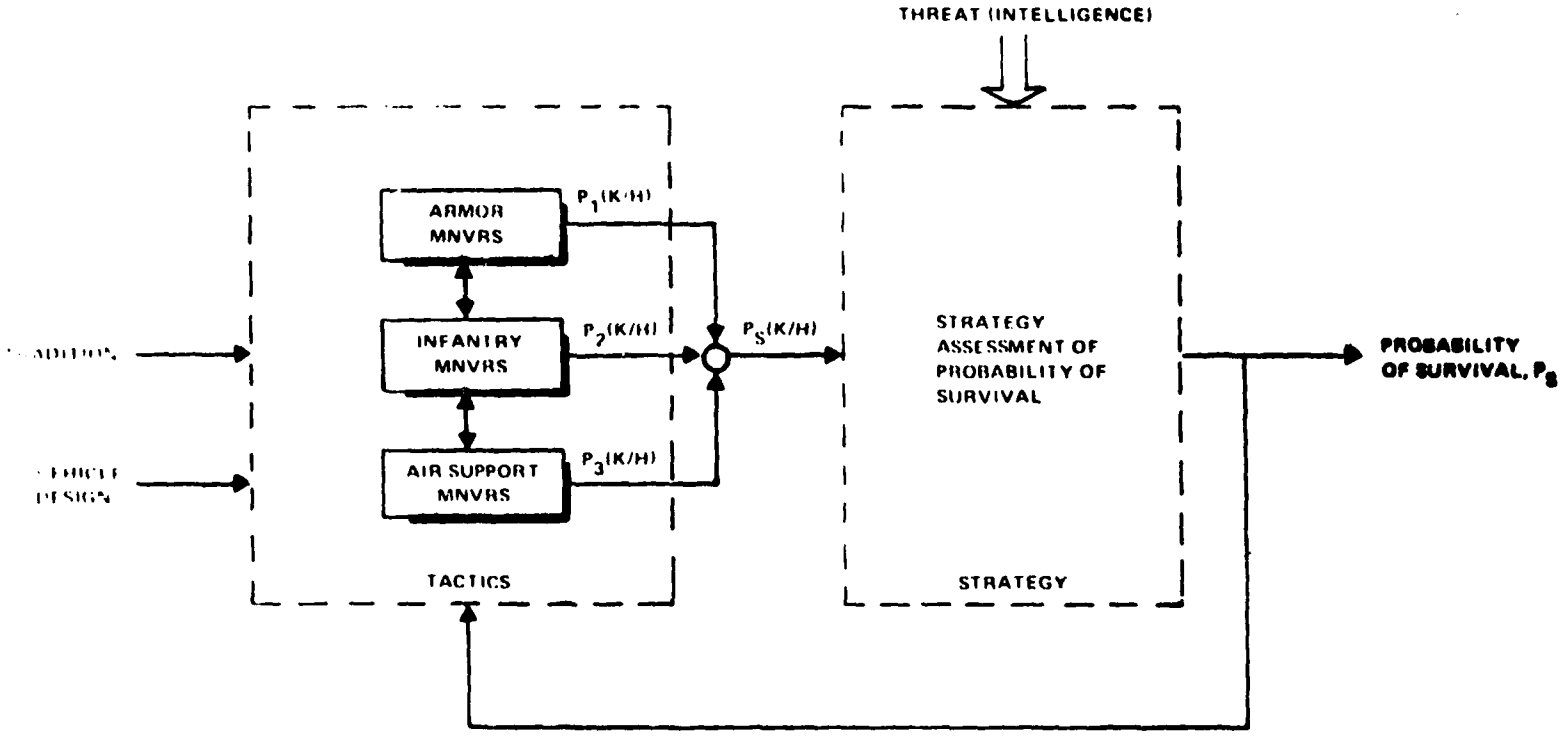
Figure 2. Combat Vehicle Support Plan (CVSP)

overcome the numerical superiority of the Warsaw Pact forces, American forces must achieve a three-to-one kill ratio. This can be achieved only by developing tactical and operational capabilities that call for "fire on the move" whenever the engagement range is less than 2000 meters. Beyond 2000 meters, "shoot and scoot" tactics will be utilized. This implies that the combat vehicle must be developed which has superior hit probability at long ranges and must be highly maneuverable at short ranges.

Tactics defines the utilization of forces in order to achieve a "system" probability of kill given a hit. The constituents of such forces are armor, infantry, and air support. Figure 3 portrays the role of tactics in the overall CVSP. It should be noted that the system probability of hit depends on maneuver capability or effective range.

Since the output of system tactics is the probability of kill given a hit, P(K/H), a mechanism for obtaining this performance must be understood. Examination of Figure 4 clarifies this mechanization. The P(K/H) associated with the combat vehicle is determined by an evaluator. The functions of the evaluator are: count and name threats; note time between threats; for each threat, estimate probability of killing the combat vehicle; determine whether threat can be engaged; given an engagement, perform damage assessments; assess the probabilities of mobility kill, firepower kill, catastrophic kill; and take the above information and relate it to combat vehicle P(K/H).

In order to answer the question whether a threat can be engaged, vehicle dynamics must be understood. Vehicle dynamics are driven by decisions to "fire on the move" or "shoot and scoot." The result of the maneuver decision manifests itself in terms of the gun line of sight (LOS). The LOS is subject to errors such as servo-mechanism jitter, etc. Therefore, since P(K/H) for a given combat vehicle will be sensitive to the LOS, complete knowledge of system dynamics is imperative.


THREAT (INTELLIGENCE)
ARMOR MNVRS
INFANTRY MNVRS
AIR SUPPORT MNVRS
$P_1(K/H)$
$P_2(K/H)$
$P_3(K/H)$
$P_S(K/H)$
STRATEGY ASSESSMENT OF PROBABILITY OF SURVIVAL
PROBABILITY OF SURVIVAL, P_S
TACTICS
STRATEGY

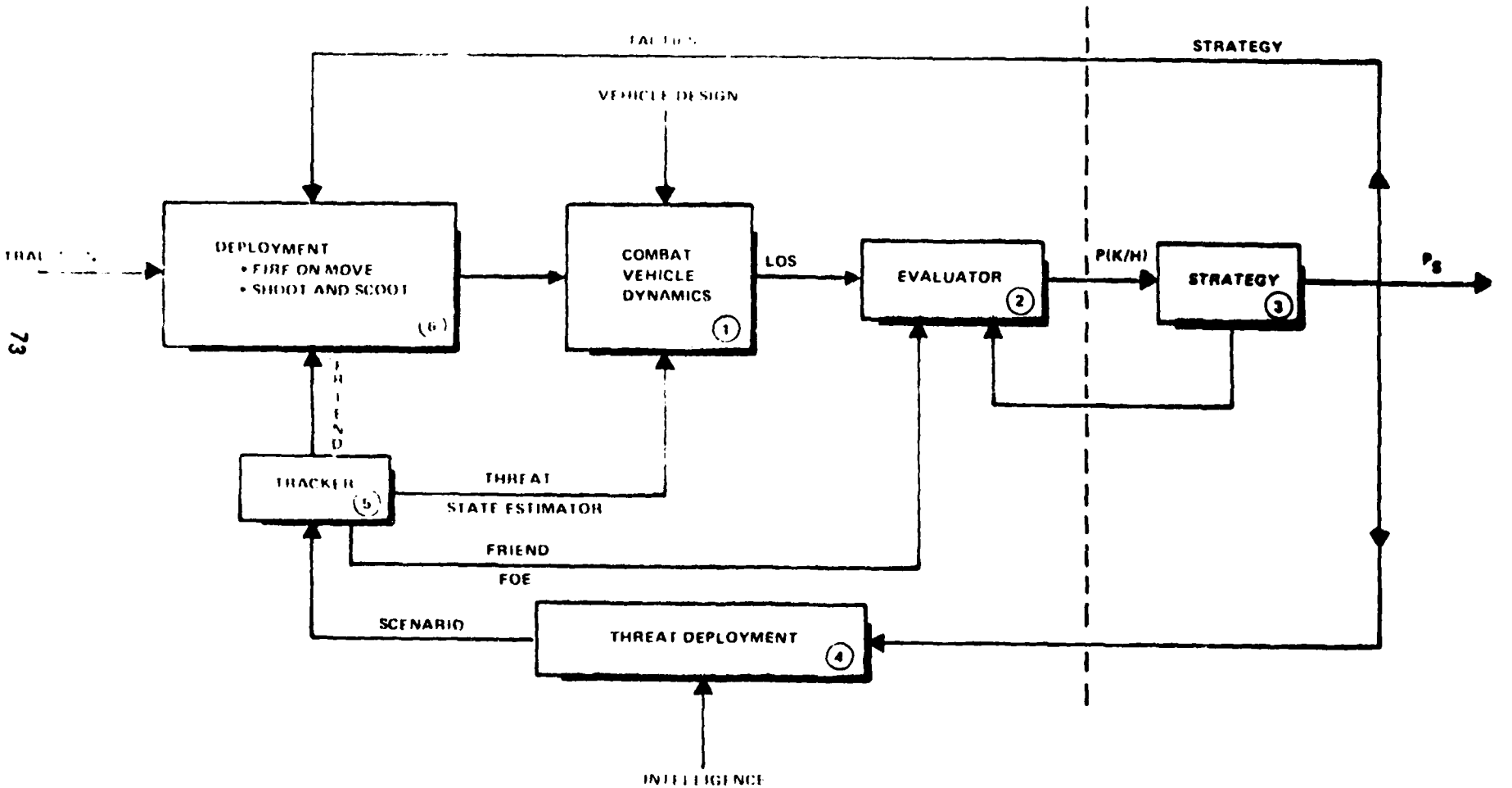
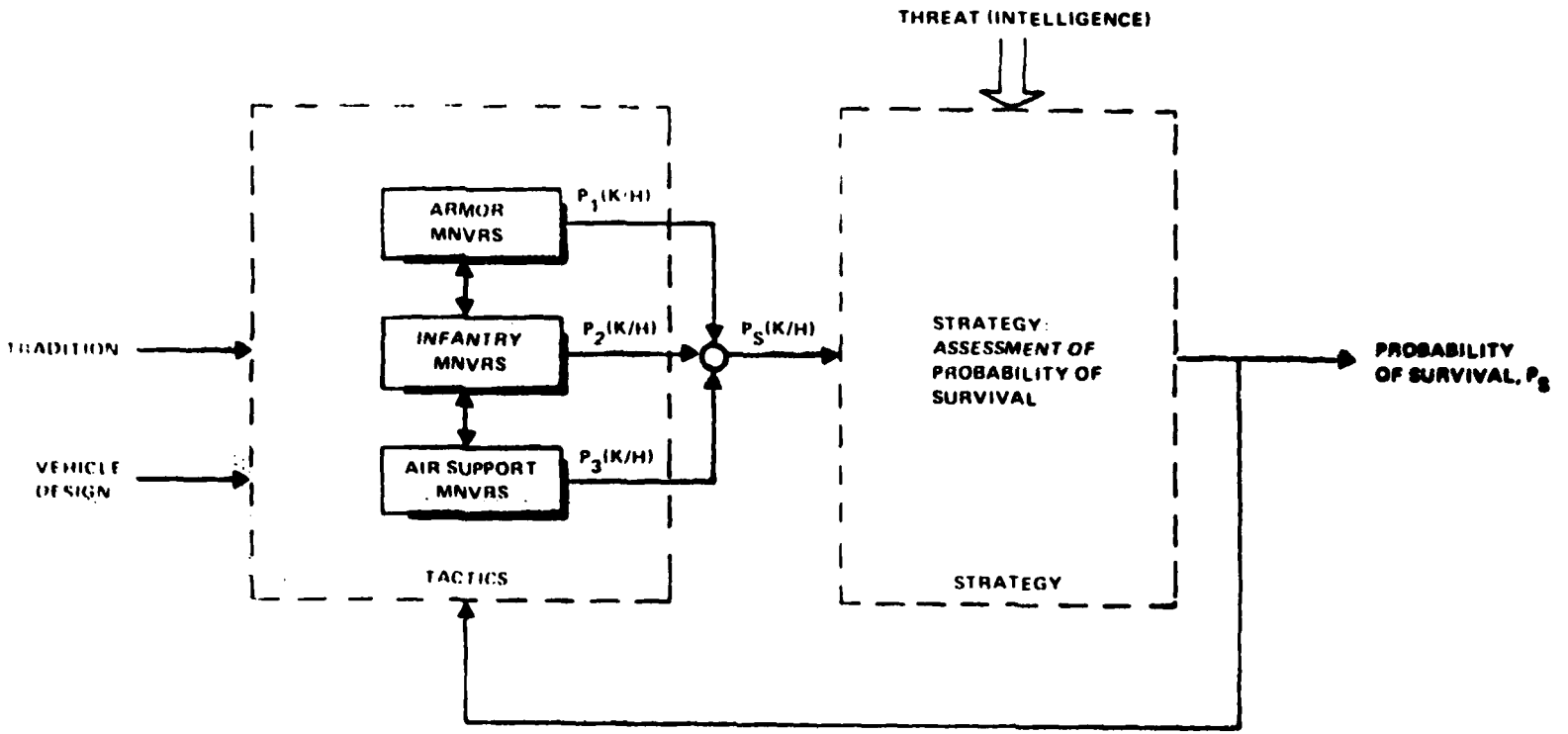


Figure 4. Integration of Combat Vehicle


THREAT (INTELLIGENCE)
ARMOR MNVRS
INFANTRY MNVRS
AIR SUPPORT MNVRS
$P_1(K/H)$
$P_2(K/H)$
$P_3(K/H)$
$P_S(K/H)$
TRADITION
VEHICLE DESIGN
TACTICS
STRATEGY: ASSESSMENT OF PROBABILITY OF SURVIVAL
STRATEGY
PROBABILITY OF SURVIVAL, P_S

Inputs to the combat vehicle dynamics, in addition to deployment patterns, consist of vehicle design constraints and tracker information. Vehicle design constraints may be considered to be fuel, turning radius, gimbal constraints, etc. The function of the tracker is to answer the following questions:

1. Has any new threat appeared?
2. Has combat vehicle maneuvered?
3. Has any threat changed trajectory?
4. Has a currently-engaged threat been killed?

The above questions can be answered by solving the problems of:

i. detection
ii. identification
iii. acquisition
iv. engagement

associated with the tracking sensors.

Strategy, in this paper, is defined as the assessment of the probability of survival; that is, the employment of a given strategy can be evaluated by the optimization of a performance index. This index will be defined as the probability of survival calculated from all current information available to the combat vehicle. Such information includes a probability of the threat killing an asset, given no defensive action; a probability of the combat vehicle negating the threat, given that action is taken; a time commitment required for such defensive action; and a time to go until the threat reaches a critical keep-out range.

The problem of formulating a Combat Vehicle Support Plan can be supported by the development of the following Phases:

Phase I: Develop a data base

Phase II: Performance evaluation

Phase III: Implement force-on-force simulations

A. Phase I

The purpose of the Phase I effort is to obtain a data base of:

1) existing combat vehicle performance,

2) numbers of vehicles in respective arsenals,

3) determination of likely threat scenarios, and

4) defeat requirements.

The relationship between the items listed above and the CVSP can be clarified by examination of Figure 4.

1) Combat Vehicle Performance is associated with blocks 1 and 2 of Figure 4. This index of performance is given by a probability of kill given a kit, P(K/H). As illustrated in Figure 4, this parameter is a requirement in order to determine probability of survival (Ps). Therefore, the data base associated with item 1) is a P(K/H) associated with the following vehicles:

U.S. Forces

- o M60 Tank Series (A1, A2, A3)
- o M113 APC Series (A1, A2)
- o M109 SP Howitzer Series (A1, A2)
- o XM1 Tank
- o XM2 Infantry Fighting Vehicle (TOW)
- o Gen. SPT Rocket System
- o V-150 Scout/Military Police Vehicle

Warsaw Pact

- o Tanks (T-54, T-55, T-62, T-64, T-72, T-80)
- o BMP Infantry Fighting Vehicle
- o BRDM APC
- o Howitzers - 122mm and 152mm
- o ZSU23-4 Air Defense Gun

It is assumed that the P(K/H) associated with each vehicle will be a function of:

- o Ammunition utilized in main gun
- o Range of target
- o Cant angle
- o Crosswind
- o Muzzle velocity variation
- o Parallax compensation
- o Drift compensation
- o Air temperature
- o Air density
- o Optical path bending
- o Zeroing
- o Others

Since the P(K/H) is associated with the LOS, there will be no P(K/H) unless there is a probability of hit, P(H), and no P(H) unless the sight is lined up on the target. Therefore, factors which address the main gun's LOS must be understood. Several errors affect gun systems' LOS. Some of these errors are: tracking, lay error, tracking rate and acceleration error, target motion estimation, lead calculation, lead insertion, evasive bias, range error, servo mechanism jitter, and human errors. This list incorporates many of the tracker functions discussed previously (Block 5 of Figures 4 and 5). Phase I efforts quantify the errors for each vehicle listed previously.

2) Once numbers of vehicles in respective arsenals are determined, the force-on-force mission can be performed. These numbers are then to be utilized in support of blocks 2, 3, 4, and 6 of Figure 4.

3) Once potential threat scenarios are given, this data is used for definition of block 4 of Figure 4. Threat deployment definition is obtained by: a) identifying threat areas which require further definition to support the

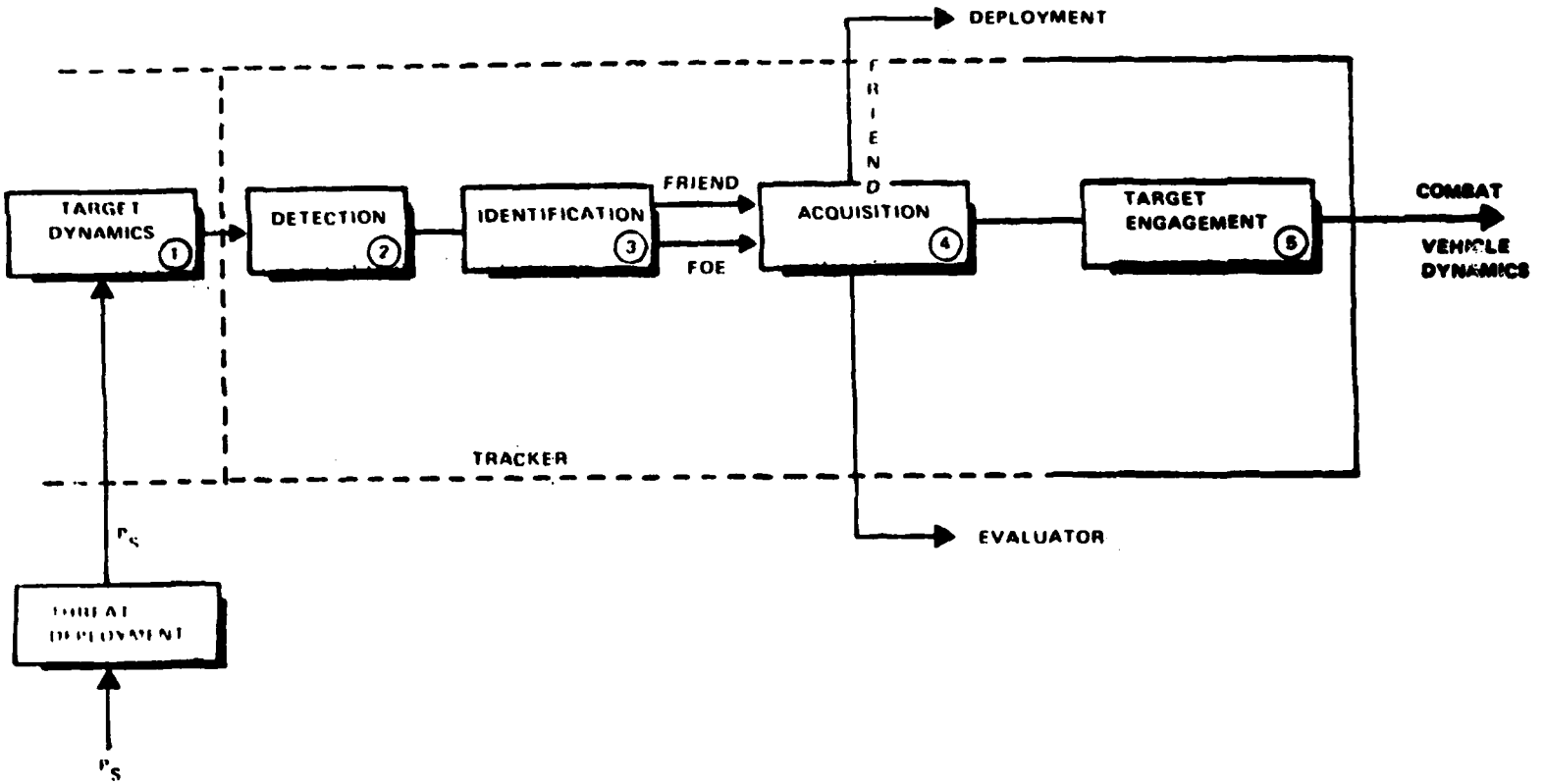


Figure 5. Tracker Functions

Utilization of Ps as defined above implies that a relationship between it and P(K/H) can be obtained.

Regarding the P(K/H), it is clear that for a given range, this probability (data base) is valid. However, in a given scenario, it will change due to threat and changing range. Hence in Phase II, the P(K/H) will be updated to consider range variation and threat exposure. Utilizing the definition of conditional probability

$$P(K/H) = P(K,H)/P(H),$$

the probability of hit, P(H), can be obtained via

$$P(H) = \frac{t}{N}\left[1 - \frac{tm}{N})P(H)_{LE} + \frac{tm}{N} P(H)_{RW}\right].$$

The terms expressed in P(H) may be further clarified by the definitions

$t \triangleq$ number of remaining threat

$N \triangleq$ number of threat

$tm \triangleq$ number of threat that has been mobility killed

$P(H)_{LE} \triangleq$ probability of hit as function of leading edge of moving threat (function of range)

$P(H)_{RM} \triangleq$ probability of hit of stationary target (this would be a data base P(H))

Task 4 will survey the communication devices that can be utilized to allow identification of friend or foe. These communication devices will consist of radio devices, television, and the BIF* system. Information gained from this survey will be utilized to determine a reasonable time line for engagement rates. This information will also be utilized in support of the tracker functions, i.e., the identification function of the tracker can be supported via the communication systems (see Figures 4, 5, and 6). It is also interesting to note that this data will be required in the definition of the combat vehicle fire control system (Figure 5).

---

*BIF - Battlefield identification of friend or foe

system design efforts and preparing assessments based on DOD-approved intelligence. The threat of USSR/Warsaw Pact nations will be clearly defined with respect to present, near, and future time frames. If threat time frame is not covered in approved intelligence, threat assessment can be based on such considerations as hard evidence, R&D trends, projected technological capability, and oeprational feasibility; by b) making necessary projections in accordance with guidelines indicated in a) above for threat assessment gaps identified and deemed essential to the concept design process; and c) by accessing intelligence organizations.

4) A measure of defeat is obtained by assigning probabilities associated with vehicle's/gun's ability to obtain mobility kill, firepower kill, and catastrophic kill. Referring again to Figure 4, this information is required to obtain blocks 1, 2, 3, and 4. Specifically, the probability of survival will give a measure of the defeat requirements. For example, questions must be answered as to: How does increase in firepower kill relate to probability of survival? How does mobility kill relate to probability of survival? As in the discussion of P(K/H), data exists that relates the probabilities of mobility, firepower, and catastrophic kill with respective vehicle/gun systems. This data is to be data based for utilization in Phase II.

B. Phase II

The purpose of this phase is to perform an "open loop" performance analysis; in other words, determine input/output relationships of each block in Figure 4. Establishment of these relationships will provide an evaluation of the combat vehicle fire control system. Specifically, this analysis will involve the following tasks:

1. Define probability of survival (Ps)
2. Relate the P(K/H) to Ps

3. Relate LOS to the P(K/H).

4. Relate friend-or-foe information to P(K/H).

5. Relate Ps to threat deployment.

6. Relate Ps to own deployment.

7. Relate threat state estimate to LOS (This analysis will result in evaluation of the combat vehicle fire control system.).

8. Perform a sensitivity analysis.

Tasks 1, 2, 3, 5, and 6 may be accomplished by defining a suitable probability of survival (Ps). A definition of Ps* which may be utilized is given by

$$Ps = \prod_{n=1}^{N} 1 - P_{tn}[1 - P_{wn}(1 - P_N)]$$

where

$Ps \triangleq$ probability of survival

$P_{tn} \triangleq$ threat kill probability

$P_{wn} \triangleq$ weapon kill probability

$P_N \triangleq$ leakage probability, i.e., the probability of failing to engage a threat for the required time given N threats generated at a rate of λ.

Further clarification of Ps may be given by defining

$P_N \triangleq$ probability that threat n is not engaged

$(1 - P_N) \triangleq$ probability that target n is engaged

$P_{wn}(1 - P_N) \triangleq$ probability that threat n is killed

$1 - P_{wn}(1 - P_N) \triangleq$ probability that threat n is not killed

$P_{tn}[1 - P_{wn}(1 - P_N)] \triangleq$ probability that threat n kills combat vehicle

$1 - P_{tn}[1 - P_{wn}(1 - P_N)] \triangleq$ probability that threat n fails to kill combat vehicle

$Ps \triangleq$ probability that every threat fails to kill combat vehicle

*Probability of survival defined by Dr. C. Whitney of Charles Stark Draper Laboratory. This has been utilized in threat action planning regarding the high energy laser systems. Note that this index is valid for survival against N indentical threats.

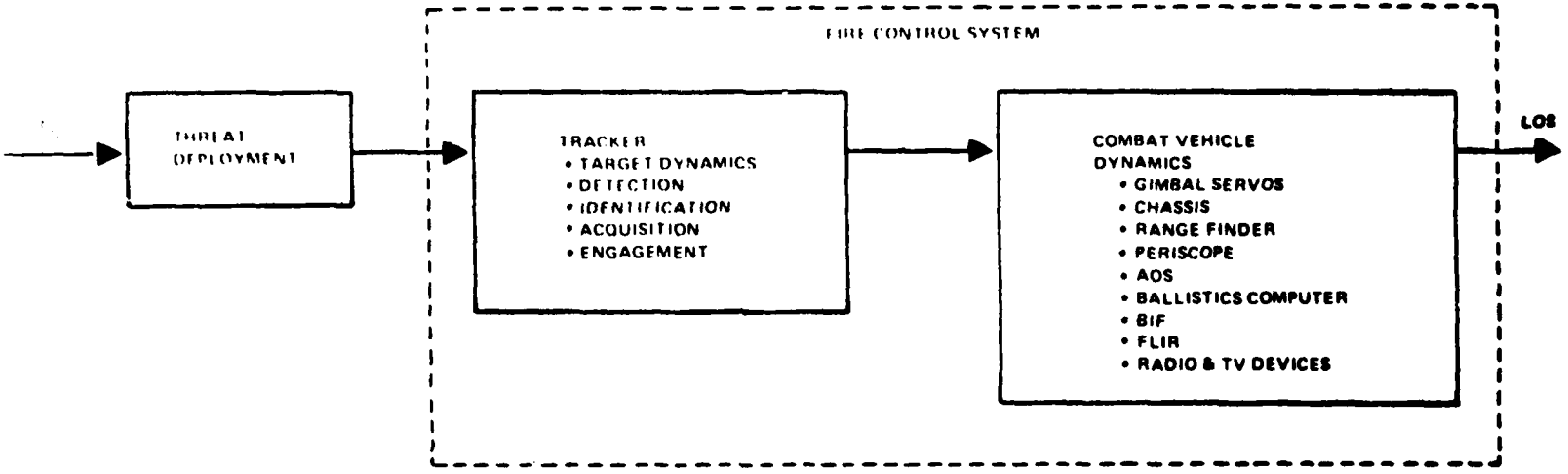


Figure 6. Combat Vehicle Fire Control System Components

Task 7, relating the threat state estimate to LOS, is treated next. Determination of this relationship essentially results in evaluation of the combat vehicle's fire control system. Specifically, this task will be broken down into subtasks of systems requirements definition, modeling, and testing/validation.

System requirements consists of defining requirements and bases for these requirements on the combat vehicle's LOS accuracy.

Modeling efforts will consist of modeling existing candidate tracking sensors and vehicle dynamics. Data can be obtained from hardware manufacturers regarding system performance, transfer functions, etc. Tracker functions to be considered in the modeling effort are: target dynamics, detection, identification, acquisition, and engagement. Functional interaction of the vehicle's gimbal servos, chassis, rangefinder, periscope, AOS, ballistics computers, BIF, FLIR, radio, television devices, etc., must also be understood.

Components of the fire control system model will be validated via system test. Since the D^2T Program will be testing existing candidate tracking sensors, this task effort would "dovetail" that specific laboratory effort. Models generated can be utilized in definition of tests to be conducted and defining instrumentation required in order to obtain meaningful test results. In addition, the application of closed loop methodology will yield a systematic method of assuring that subsystem components comply to design specifications.

Sensitivity analysis is performed under Task 8. This task addresses the sensitivity of the probability of survival with respect to the propability of kill given a hit as well as a function of vehicle line of sight. This sensitivity can be obtained by expressing the above parameters in terms of their independent variables and obtaining partial derivatives with respect to these variables. In the event that analytical expression may not be found, expected

values for such partials can be obtained via existing data or by empirical means.

C. Phase III

Viability of the CVSP is assured by "closing the loop" as shown in Figure 4. In essence, the closure of the open loop presented in Phase II will amount to a force-on-force engagement. The accomplishment of this objective can be optimized by using the closed loop methodology of system modeling. This method of modeling is presented in the companion paper and will not be discussed in this paper.

III. SUMMARY

Due to the theory that future land combat will be characterized by high engagement rate battles, there exists an immediate need to develop a combat vehicle support plan (CVSP). Such a plan is to be developed in three phases:

Phase I - Data base

Phase II - Performance analysis

Phase III - Force-on-force simulations

In order to develop combat vehicle strategy, the threat possessed by the USSR/Warsaw Pact nations must be clearly defined with respect to present, near, and future time frames. Comparative data concerning the respective combat vehicles must be obtained. This data consists of associating a probability of kill/hit with vehicles from respective forces. An understanding of this threat can be obtained by evaluating the effectiveness, numbers of vehicles, and kill criterion of the respective forces.

The effectiveness of the combat vehicle is to be determined by associating a performance index to each vehicle in the respective arsenals. This index is defined to be the probability of kill given a hit.

In order to determine defeat requirements, the combat vehicle's ability to achieve mobility, firepower, and catastrophic kill is to be addresses, i.e., probabilities associated with the above-mentioned items must be determined.

Sources of error are catalogued according to weapon system and possible improvements to overcome the problem. Investigation of current hardware subsystems such as the auto-tracker must be evaluated to determine how they will reduce the known sources of error. Also in support of error analysis, a technology review is to be conducted. This should consist of current, near, and projected state of the art.

In order to perform a performance analysis on a combat vehicle support plan, a systems approach is utilized in order to relate data base parameters obtained in Phase I. In effect, this will constitute an open loop analysis; it will relate probability of kill given a hit to probability of survival, line of sight to probability of kill given a hit, and friend or foe information to probability of kill given a hit; evaluate vehicle fire control system; perform a sensitivity analysis; and incorporate D^2T technology into analysis.

Incorporation of the CLM tool as a means of performing force-on-force analysis will result in an optimal method to assess one-on-one, one-on-many, and many-on-many engagement scenarios.

Next page is blank.

AD P001066

CLOSED LOOP METHODOLOGY APPLIED TO THE COMBAT VEHICLE SUPPORT PLAN

by
A. Fermelia

I. INTRODUCTION

The analysis of any physical system must begin by characterizing the specific process to be modeled. This characterization must consider: (1) the system type, (2) governing equations of the process, and (3) system questions to be answered. Table 1 illustrates these notions.

Systems may be typed as being either deterministic or stochastic. A deterministic system is defined as one which incorporates no uncertainty; the stochastic type as one which includes uncertainty in the model. Since physicist recognizes that these laws are expressed by partial differential equations (PDEs), ordinary differential equations (ODEs), and algebraic equations (AEs); the governing equations of the process must be given by PDEs, ODEs, AEs, or a combination of the three. To answer the system questions, one must solve the governing equations. In the case of the deterministic type system, this may be easily obtained; however, the stochastic system presents additional concerns.

The solution of a stochastic system may be obtained by defining and solving the estimation, identification, and control (EIC) problems associated with the given process. This study will illustrate the need for solving the EIC problems as the pertain to the development of a combat vehicle support plan (CVSP).

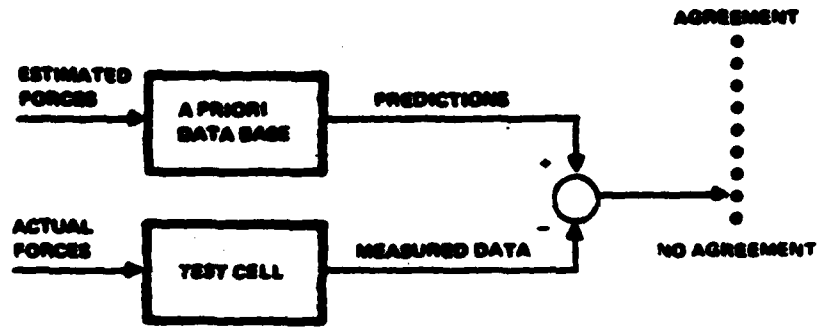
Having introduced the terms OLM and CLM, further clarification of these notions will be given at this time. OLMs are described generally by systems which lack feedback from the operation which is occuring. An OLM is illustrated in figure 1.

The open loop methodology in figure 1 makes use of a priori data base to provide predictions of outputs, which are compared with measured data from the test cell. Results can range from complete agreement to no agreement at all. In addition, the confidence level of the results of a given test are typically low until a large statistical data base indicates the attributes of the samples. Typically, as one begins to accumulate test data, the predictions are adjusted to accommodate these data. This "knob tweaking" is usually conducted by methods which are far from being rigorous mathematically.

Because OLMs have considerable shortcomings, the need for a more systematic approach has become evident in recent years. Modern system theory provides such an approach based on CLMs which form the bases for most applications where feedback is used to control the system. The CLM is illustrated in figure 2 using adaptive procedures which provide a model with quantified confidence levels. Modern system theory recognizes the potential differences in predictions and results that can be attributed to forcing function uncertainty, incorrect estimates of constituents in the governing equations, and the possibility that the model order is insufficient to describe these systems. The adaptive processor design attempts to accommodate these uncertainties and to systematically drive the difference between predictions and test data to a minimum.

Table I Analysis of Physical Systems

- Types of Systems
  1. Deterministic, i.e., Noise-Free System
  2. Stochasitic, i.e., Systems with Noise
- System Description
  1. Ordinary Differential Equations } Linear or
  2. Partial Differential Equations } Nonlinear
  3. Algebraic Equations
- System Questions to be Answered
  1. Solution to Governing Equations
  2. Estimation
  3. Identification
  4. Control



RESULTS IN:

1) AN EXCELLENT MODEL
2) A GOOD MODEL
3) A FAIR MODEL
4) A POOR MODEL
5) AN UNACCEPTABLE MODEL

Figure 1. OLM System Approach

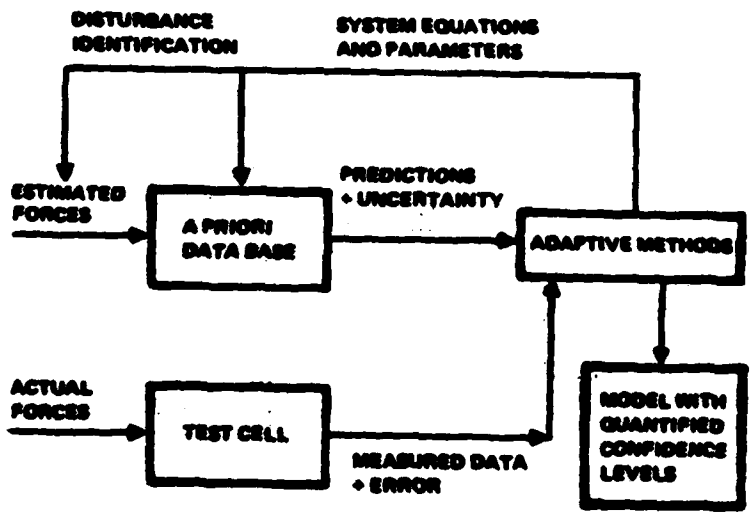


Figure 2. CLM Using Adaptive Procedures

Having stated that OLM and CLM are essentially techniques for controlling the comparison error, the discussion will now turn toward the theoretical aspects required to obtain the systematic results of the CLM. This is introduced by presentation of the thesis:

> "Control of the error which results from the comparison of data obtained from the true system to that produced by a priori data base will result in:
>
> a) obtaining a classification set, which implies the system can be modeled. This in turn implies that the system equations can be solved, or
>
> b) denial of the classification set, which implies that the system cannot be modeled."

Acceptance of this thesis implies that the solution of the control problem is imperative to model the system.

In presenting the thesis, the term "classification set" has been introduced. Since the set has significant impact, it needs further clarification at this time.

The notion of a set is generally defined in mathematical terms. In particular, this set, C, may be given as the set which contains the following elements: independent variables, dependent variables, coefficients of the governing equations, and the sensor output. In mathematical parlance, then, this set can be written as:

$$C_{\Delta} \left\{ \begin{array}{cccc} \text{INDEPENDENT} & \text{DEPENDENT} & \text{COEFFICIENTS} & \text{SENSOR} \\ \text{VARIABLES} & \text{VARIABLES} & \text{OF} & \text{OUTPUT} \\ & & \text{EQUATIONS} & \end{array} \right\} \quad (1)$$

Since this definition for the classification set holds for the propagation of a signal through any system, the elements of this set will be obtained from the equations which govern the evolution of ROBSIM control signal. Equation (2) shows the relationship of estimation, identification, and control to the classification set. For example, a solution to the estimation problem will yield estimates of the independent and dependent variables. Similarly, the solution to control encompasses solution of both estimation and identification in addition to providing an estimate of sensor output.

$$C_{\Delta} \left\{ \begin{array}{cccc} \underbrace{\text{INDEPENDENT}}_{\text{ESTIMATION}} & \underbrace{\text{DEPENDENT}}_{\text{ESTIMATION}} & \underbrace{\text{COEFFICIENTS OF EQUATIONS}}_{\text{IDENTIFICATION}} & \text{SENSOR OUTPUT} \\ \text{VARIABLES} & \text{VARIABLES} & & \end{array} \right\} \quad (2)$$

$$\underbrace{\qquad\qquad\qquad\qquad\qquad\qquad\qquad\qquad}_{\text{CONTROL}}$$

Before further clarification of the classification set is feasible, the basic elements of the physical process must be considered. To do this for the OLM, a lower layer of figure 1 must be produced. This second layer is shown in figure 3. From this figure, two basic elements may be defined as being 1) the subsystem under evaluation, and 2) a measurement device. The subsystem under investigation produces a measureable set, M, and the measurement device acting on this set produces the output, Z. In addition to illustrating the basic elements, figure 3 shows the basis for their physical makeup.

However, the description of the process does not allow total definition of the classification set. For example, the only elements of the classification set that are illustrated are the measureable set, M, and the signature set, Z. In addition, the measureable set contains only some of the dependent variables, none of the independent variables, and none of the coefficient set.

This fact requires a further peeling back of the layers in order to completely define the notion of the classification set. Unfortunately, the third layer given by figure 4 is still not sufficient to completely identify this set. However, additional element members can be defined. Specifically, some members of the observable set, O, are distinguishable as well as all of the independent variable (internal and external stimuli). A further reduction is required in order to obtain the complete dependent variable and coefficient sets. At this juncture a description of the specific problem of interest is required. Since this is the case, further clarification of the classification set will be postponed until application to a specific example.

Since definition of the system level problems will involve terms such as *state variable*, *control vector*, and *observations*, these notions will now be defined. Consider the fourth layer schematic of figure 1 as shown by figure 5.

The figure represents a typical system in terms of its characteristics, independent, and dependent variables. Dependent variables are defined as state variables and independent variables are designated as the control variables. System characteristics may be quantified as: lay error, tracking error, evasive bias, servo mechanism jitter, etc. The location of these quantities is internal to block 1 through n. In figure 5 the independent variables are designated by the p multi-inputs, u. The dependent variables, $\underline{x}$, are imbedded in the system components designated by blocks 1 through n . It should be noted that the measureable set (outputs of the system) generally does not consist of all dependent or state variables.

The measurable set is acted on by the sensor system. This action takes place dynamically and statically. Specifically, these measureables enter into the sensing device and are subjected to phase and amplitude distortion (dynamics) and ultimately sensed as a "voltage" (static). Hence, dynamics of the sensor must be accounted for in addition to dynamics of the system. In this sense, dynamics attributable to the sensor are typically augmented to the state vector with dimension n to produce a system state of dimension n+1. Due to the fact that sensing devices have errors associated with them, the signature produced by the sensor will be corrupted by this uncertainty. This is designated by the quantity, v, in figure 5. Addition of the noise quantity produces a signature set designated by the term, Z.

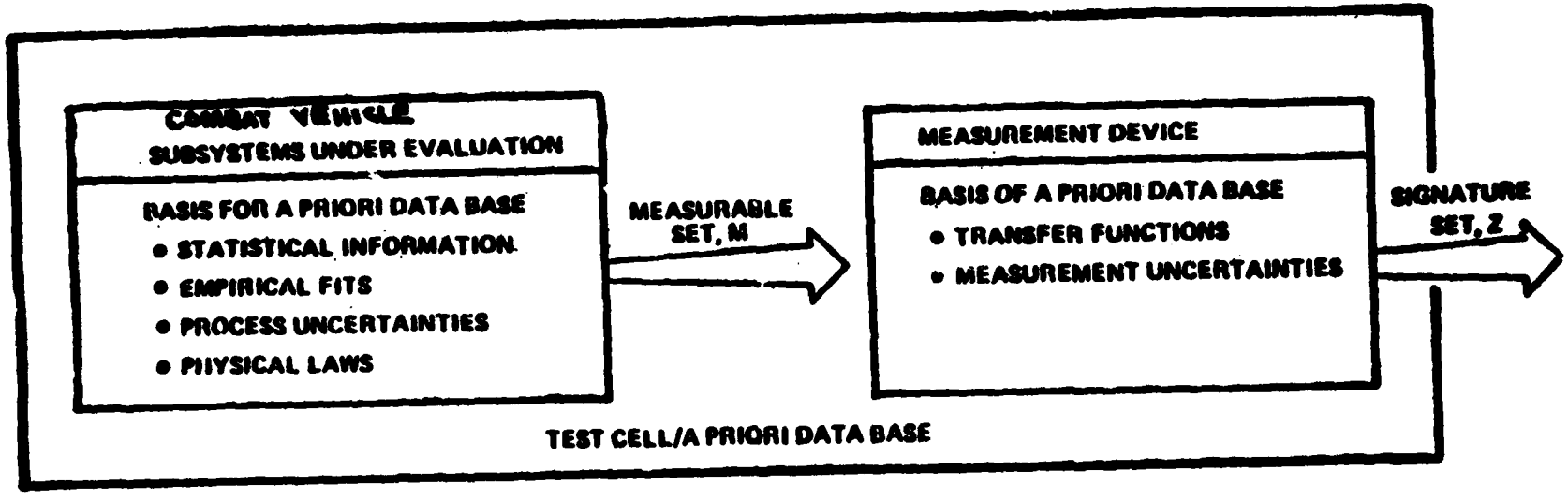


Figure 3. Second Layer of Physical Process

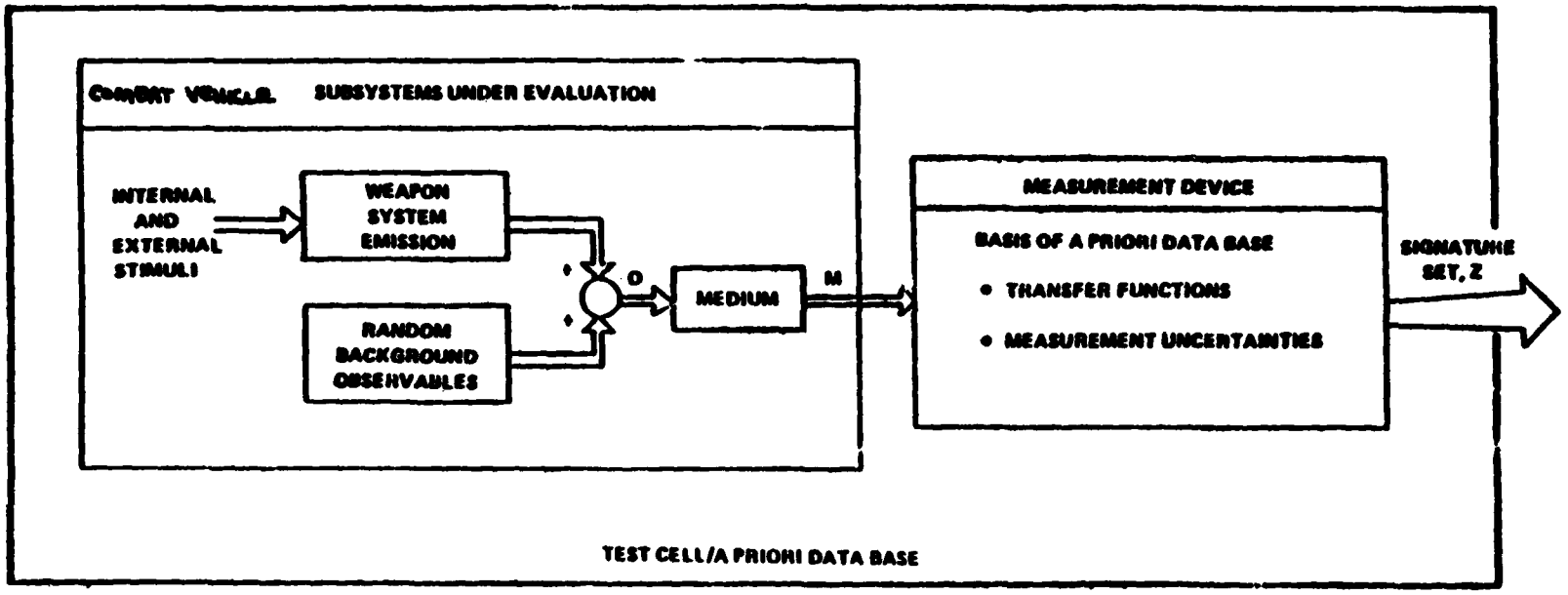


Figure 4. Third Layer Mechanization

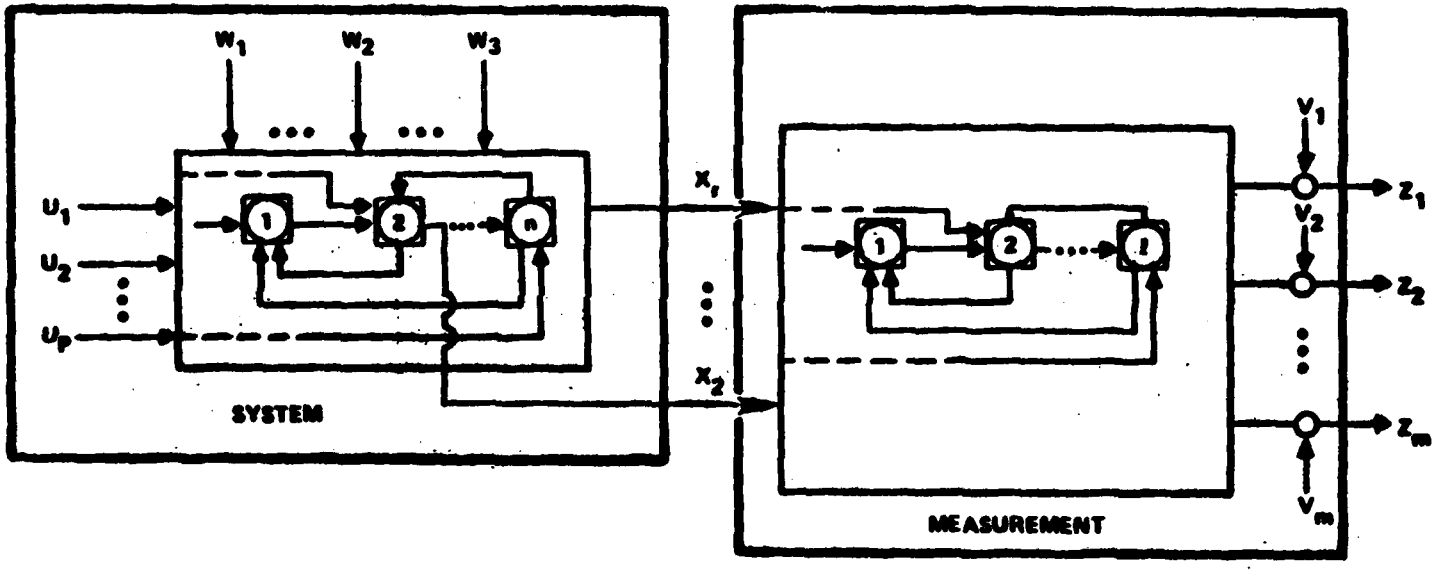


Figure 5. Fourth Layer A Priori Model

II. CLM APPLIED TO THE CVSP

This section will illustrate the application of the CLM to modeling of a force-on-force problem. Specifically the problem that is to be answered is: What effect does the blending of intelligence information, vehicle maneuverability, a pre-battle deployment plan, and adversary position information have on the survivability of the combat vehicle under attack.

As developed in reference [1], the elements of the combat vehicle support plan are shown in figure 6. Definition of the system state vector would be incomplete without accounting for background uncertainties. The uncertainties are represented by the w terms illustrated in figure 5.

A mathematical equivalent CVSP is shown in figure 7. Examination of the figure indicates the role of friendly intelligence and one's own measure of probability of survival at a given time, k+1. As shown intelligence, I_1, operates on the error resulting from the expected difference, e(k), between the combat vehicle's probability of survival, P_s, and that of the adversary's, P_s. Combining this information with the measure of the combat vehicle's own P_s through M_1 provides an update of current decision information, $\underline{r}$ (k). This data is then adjoined to the a priori deployment plan to produce the decision command, $\underline{u}$ (k), for the combat vehicle.

The combat vehicle receives this command and translates it into a particular maneuver characterized by the state vector, $\underline{x}_1$. This information is fed into the tracker box, T_1, along with information regarding the state of the adversary, $\underline{x}_2$. Using this information the combat vehicle residents can determine the line of sight, L_1, required to engage the adversary. Line of sight information and its associated errors are evaluated in order to determine when and where to engage the adversary. At a given pre-selected engagement range, the battle is assumed to commence. Once the battle has begun the probability of a kill given a hit, P_1, and confidence level associated with this probability is computed [1]. This information is then modified by a pre-defined factor, a, and summed with the weighted value of the adversary's probability of kill given a hit, P_2. From this combination the probability of survival, P_s of the combat vehicle is determined. At this juncture, information is recursively fed back to repeat the procedure just described.

In developing the game to be played by the friendly combat vehicle, information is required with respect to the adversary's plan. In addition, since the winner of the game will be designated by the combatant who achieves the maximum survival and survival rate, the mathematical description of the game is incomplete without consideration of the adversary's plan.

Under the assumption that the top level structure of the adversary's plan is the same as the friendly's, figure 8 can be drawn to illustrate the complete game. As shown in the figure the flow of the adversary's process is the same as described above. However it should be noted that although it is mechanized the same, the transfer functions acting on the input signals are entirely different. Using this figure the governing equations can now be written as:

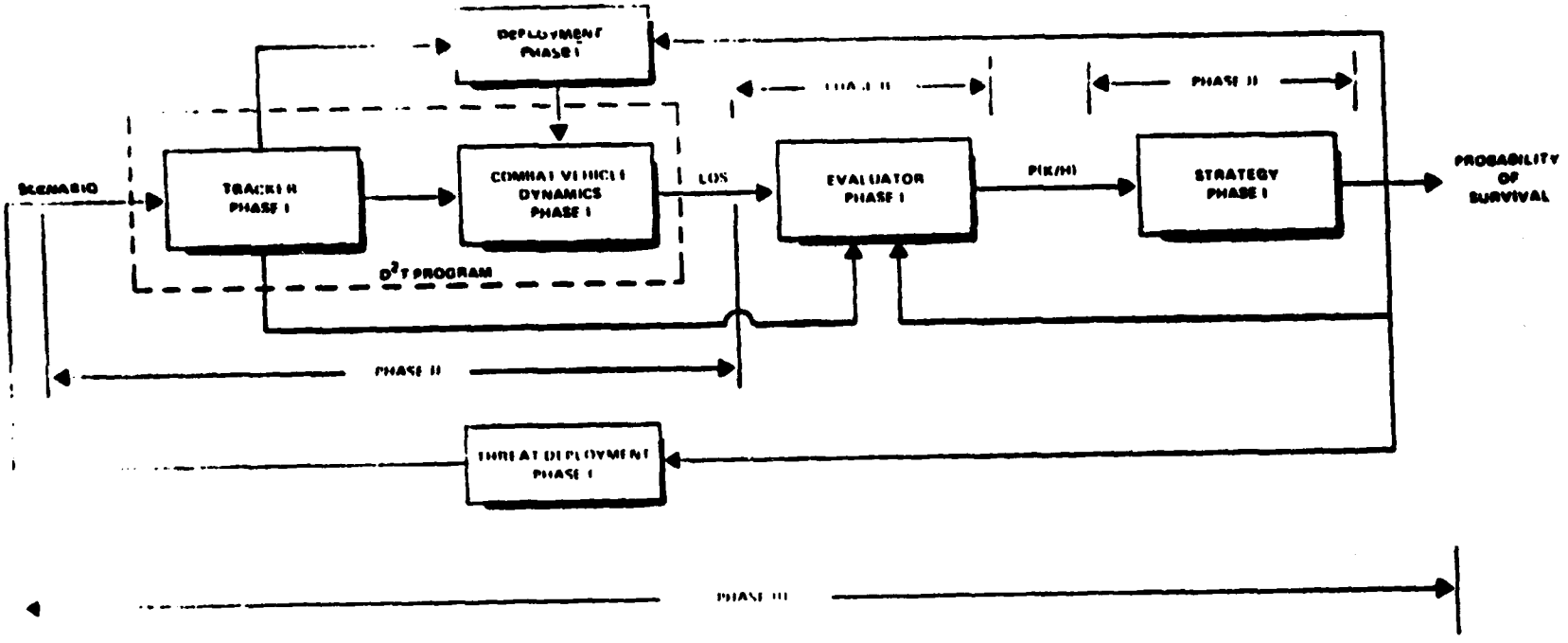


Figure 6. Development Phases of Combat Vehicle Support Plan
Phase I: Data Base
Phase II: Performance Analysis
Phase III: Force on Force Simulations

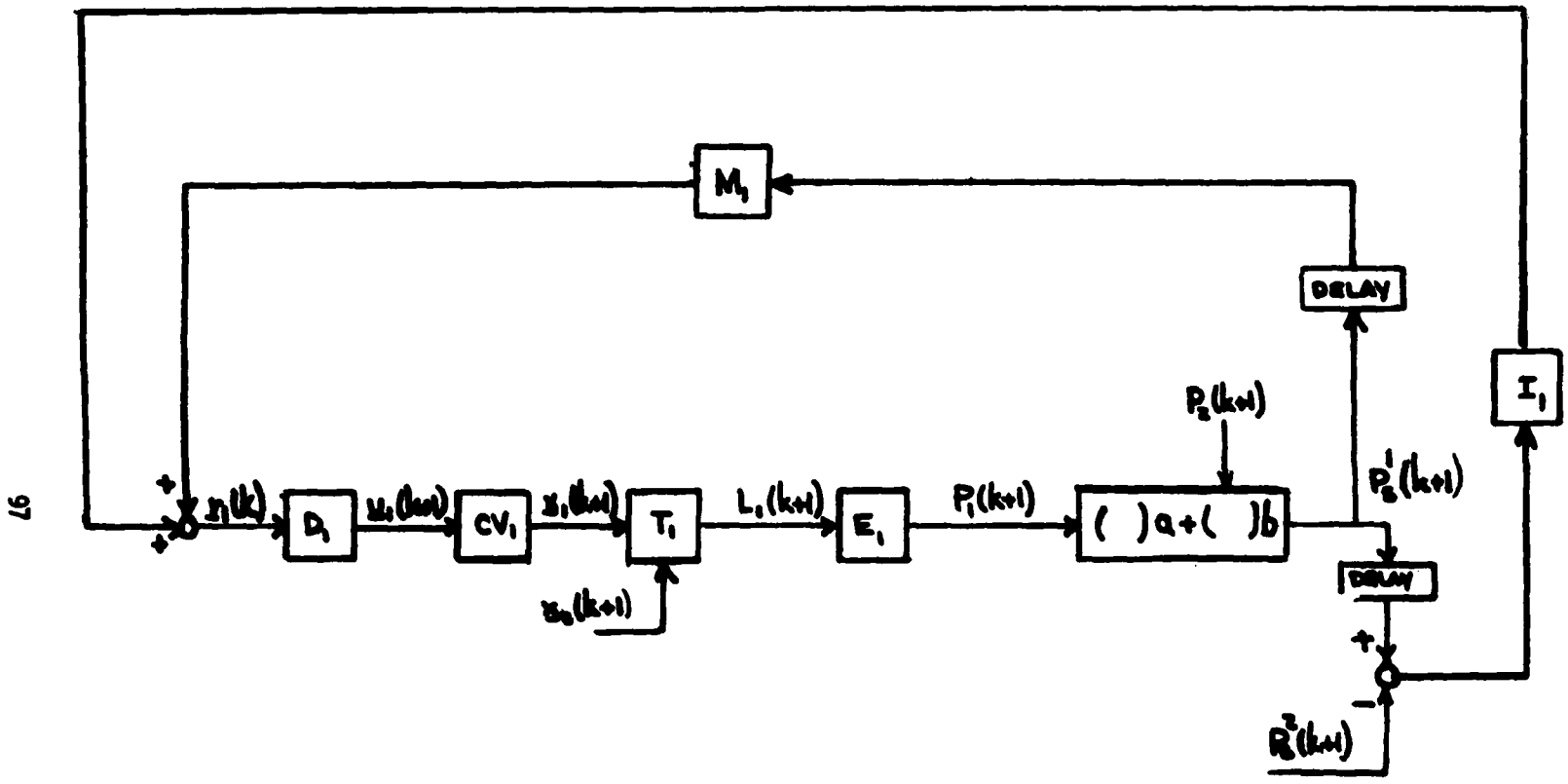


Figure 7. Mathematical Equivalent CVSP

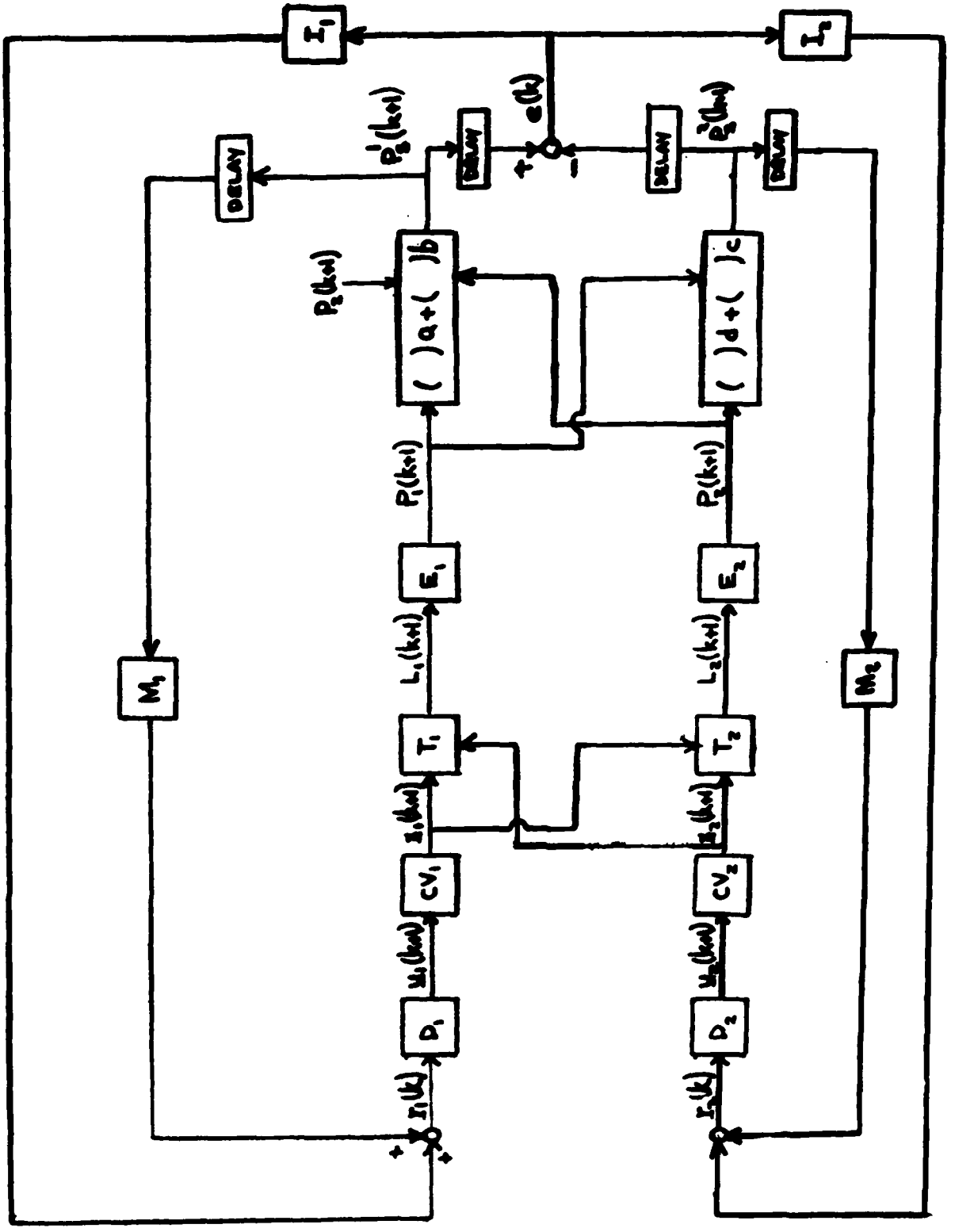


Figure 8. Composite Force-on-Force

$$\underline{x}_1(k+1) = \phi_1(k+1,k)\,\underline{x}_1(k) + \Theta_1(k+1,k)\,\underline{u}_1(k) + \underline{w}_1(k) \quad (1)$$

$$\underline{x}_2(k+1) = \phi_2(k+1,k)\,\underline{x}_2(k) + \Theta_2(k+1,k)\,\underline{u}_2(k) + \underline{w}_2(k) \quad (2)$$

$$\underline{u}_1(k+1) = \phi_3(k+1,k)\,\underline{u}_1(k) + \underline{r}_1(k) + \underline{w}_3(k) \quad (3)$$

$$\underline{u}_2(k+1) = \phi_4(k+1,k)\,\underline{u}_2(k) + \underline{r}_2(k) + \underline{w}_4(k) \quad (4)$$

$$r_1(k) = I_1(k)\,e(k) + M_1(k)\,P_s^1(k) \quad (5)$$

$$r_2(k) = I_2(k)\,e(k) + M_2(k)\,P_s^2(k) \quad (6)$$

$$e(k) = P_s^1(k) - P_s^2(k) \quad (7)$$

$$P_s^1(k+1) = a(k+1)\,P_1(k+1) + b(k+1)\,P_2(k+1) + v_1(k+1) \quad (8)$$

$$P_s^2(k+1) = c(k+1)\,P_1(k+1) + d(k+1)\,P_2(k+1) + v_2(k+1) \quad (9)$$

$$P_1(k+1) = E_1(k+1)\,L_1(k+1) \quad (10)$$

$$P_2(k+1) = E_2(k+1)\,L_2(k+1) \quad (11)$$

$$L_1(k+1) = T_1(k+1)\left[\underline{z}_1(k+1) - \underline{z}_2(k+1)\right] \quad (12)$$

$$L_2(k+1) = T_2(k+1)\left[\underline{z}_2(k+1) - \underline{z}_1(k+1)\right] \quad (13)$$

$$\underline{z}_1(k+1) = H_1(k+1)\,\underline{x}_2(k+1) + \underline{v}_3(k+1) \quad (14)$$

$$\underline{z}_2(k+1) = H_2(k+1)\,\underline{x}_1(k+1) + \underline{v}_4(k+1) \quad (15)$$

where the subscripts 1 and 2 refer to friendly and adversary forces respectively. Further clarification of the terms presented above will now be given.

Consider the equations pertaining to the subscript 1. The state, $\underline{X}_1$, of the combat vehicle is given to be a n_1 x 1 vector; dynamics which describe its maneuverability are given by the n_1 x n_1 dynamics matrix, ϕ_1; response of the vehicle to decision commands (the p_1 x 1 vector $\underline{u}_1$) is brought about by the matrix product of $\underline{u}$ and the n_1 x p_1 decision matrix, θ_1; uncertainty in the state propagation due to wind gusts, terrain constraints, and other forces are represented by the n x 1 random disturbance vector $\underline{w}_1$. Similarly the state propagation of the adversary is given by:

$\underline{X}_2 \triangleq n_2 \times 1$ state vector

$\underline{U}_2 \triangleq p_2 \times 1$ decision vector

$\underline{W}_2 \triangleq n_2 \times 1$ disturbance vector

$\phi_2 \triangleq n_2 \times n_2$ dynamics matrix

$\Theta_2 \triangleq n_2 \times p_2$ decision matrix

The decision vector, $\underline{u}_1$, is comprised of an update of current decision information given by the P_1 x 1 vector, $\underline{r}_1$, and the a priori deployment plan given by the matrix product of the p_1 x p_1 a prior decision matrix, θ_3, and $\underline{u}_1$. Similarly the decision vector, $\underline{u}_2$, is obtained from (4) where

$\phi_4 \triangleq p_2 \times p_2$ a priori decision matrix, and

$\underline{r}_2 \triangleq p_2 \times 1$ current decision information

Equation (5) shows that current information is a function of intelligence in the form of the product of the p_1 x 1 intelligence vector, I_1, and the scalar error, e. In addition, the measurement of the own force probability of survival is accounted for by the product of the p_1 x 1 weighting matrix M_1 and the scalar probability. Definition of the adversaries current information vector, $\underline{r}_2$, is similar to that given for the friendly force.

The scalar probability of survival for each force is given as a linear combination of each others probability of kill. In addition, uncertainty with respect to the ability to measure this parameter is incorporated by inclusion of the scalar measurement error terms v.

Evaluation of the probability of kill given a hit is given by the product of the 1 x 3 evaluation vector E and the respective 3 x 1 line of sight vector, L. The line of sight vector is determined from the 3 x m tracker matrix, T, operating on the difference between own force state measurements and adversary measurements. These measurements are given by the m x 1 vectors, $\underline{z}$, as shown in equations (14) and (15). Inclusion of sensor uncertainty is given by the vector m x 1 vectors $\underline{v}_3$ and $\underline{v}_4$.

Having described the equations governing the system, these equations can be manipulated into composite state and measurement equations given by:

$$\begin{pmatrix} \underline{x}_1 \\ \underline{u}_1 \\ \hline \underline{x}_2 \\ \underline{u}_2 \end{pmatrix}_{k+1} = \left(\begin{array}{cc|cc} \phi_1 & \Theta_1 & 0 & 0 \\ 0 & \phi_3 & 0 & 0 \\ \hline 0 & 0 & \phi_2 & \Theta_2 \\ 0 & 0 & 0 & \phi_4 \end{array}\right) \begin{pmatrix} \underline{x}_1 \\ \underline{u}_1 \\ \hline \underline{x}_2 \\ \underline{u}_2 \end{pmatrix}_k$$

$$+ \begin{pmatrix} 0 & 0 \\ \dfrac{I_1}{0} & \dfrac{M_1 - I_1}{0} \\ I_2 & M_2 - I_2 \end{pmatrix} \begin{pmatrix} P_s^1 \\ P_s^2 \end{pmatrix} + \begin{pmatrix} \underline{w}_1 \\ \underline{w}_2 \\ \underline{w}_3 \\ \underline{w}_4 \end{pmatrix}_k \qquad (16)$$

$$\begin{pmatrix} P_s^1 \\ P_s^2 \\ \hline \underline{z}_1 \\ \underline{z}_2 \end{pmatrix} = \left(\begin{array}{cc|cc} H_3 & 0 & H_4 & 0 \\ H_5 & 0 & H_6 & 0 \\ \hline 0 & 0 & H_1 & 0 \\ H_2 & 0 & 0 & 0 \end{array}\right) \begin{pmatrix} \underline{x}_1 \\ \underline{u}_1 \\ \underline{x}_2 \\ \underline{u}_2 \end{pmatrix} + \begin{pmatrix} \underline{v}_1 \\ \underline{v}_2 \\ \underline{v}_3 \\ \underline{v}_4 \end{pmatrix} \qquad (17)$$

where

$$H_3 \triangleq (bE_2T_2 - aE_1T_1)H_2$$

$$H_4 \triangleq (aE_1T_1 - bE_2T_2)H_1$$

$$H_5 \triangleq (dE_2T_2 - cE_1T_1)H_2$$

$$H_6 \triangleq (cE_1T_1 - dE_2T_2)H_1$$

Using equations (16) and (17), the question posed at the beginning of this section will now be re-addressed. The use of the CLM to determine the effect of intelligence, vehicle maneuverability, pre-battle deployment plan, and adversary position information on vehicle survivability can now be demonstrated.

Before initiation of the same certain ground rules will be established in order to assess the value of employment of the CLM approach. Therefore assume that:

1. All measurements are available to friendly forces and adversary. For example, numbers representing the left hand side of (17) are given to both combatants. However, it will be assumed that the standard deviation on the sensor uncertainty is not known, i.e., the sigma on v_3 is not known to force 2 and the sigma on v_4 is not known to force 1. In addition, weightings given by coefficients, a, b, c, d, and respective evaluator functions (the E's) are known only to their respective forces.

2. Information given in equation (16) regarding Force 1 and 2 are known only by the respective combatants. For example, equation (16) has been written such that the composite dynamic matrix and the composite control matrix are partitioned to correspond to friendly and adversary forces. That being the case, only those elements contributing to the propagation of state, $\underline{x}_1$, are known to those who favor $\underline{x}_1$ combatants.

3. Friendly forces will use the CLM to obtained the total system classification set. Adversary forces will use information based on OLM techniques to gain insight into friendly identification.

Once the a prior model has been established, the next step for application of the CLM is to identify the classification set elements. By writing (16) and (17) into their respective equivalents given by:

$$\underline{z}(k+1) = \underline{\Phi}(k+1,k)\,\underline{z}(k) + \underline{\Theta}(k+1,k)\,\underline{y}(k) + \underline{W}(k) \qquad (18)$$

$$\underline{y}(k+1) = H(k+1,k)\,\underline{z}(k) + \underline{V}(k+1) \qquad (19)$$

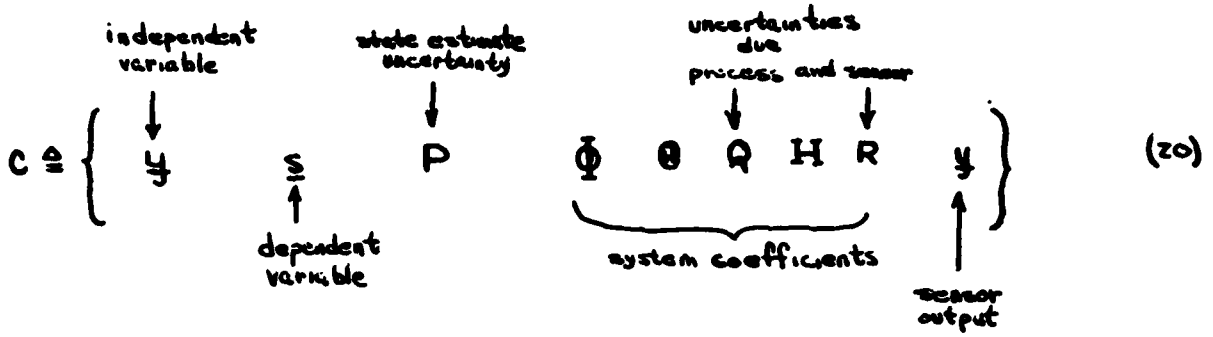
where

$$\underline{\Phi} \triangleq \left(\begin{array}{cc|cc} \phi_1 & \Theta_1 & 0 & 0 \\ 0 & \phi_3 & 0 & 0 \\ \hline 0 & 0 & \phi_2 & \Theta_2 \\ 0 & 0 & 0 & \phi_4 \end{array}\right); \qquad \underline{\Theta} \triangleq \left(\begin{array}{cc|cc} 0 & 0 & 0 & 0 \\ I_1 & M_1 - I_1 & 0 & 0 \\ \hline 0 & 0 & 0 & 0 \\ I_2 & M_2 - I_2 & 0 & 0 \end{array}\right)$$

$$\underline{z}' \triangleq (\underline{x}_1' \; \underline{v}_1' \; \underline{x}_2' \; \underline{v}_2'); \qquad \underline{y}' \triangleq (P_1' \; P_2' \; \underline{z}_1' \; \underline{z}_2')$$

$$\underline{W}' \triangleq (w_1' \; w_2' \; w_3' \; w_4'); \qquad \underline{V}' \triangleq (v_1 \; v_2 \; v_3' \; v_4')$$

Using Equations (18) and (19), the classification set can now be defined as



$$C \triangleq \left\{ \underline{y} \quad \underline{s} \quad P \quad \Phi \quad \Theta \quad Q \quad H \quad R \quad \underline{y} \right\} \qquad (20)$$

where

$$Q \triangleq E\{\underline{W}\underline{W}'\} \; ; \; P \triangleq E\{(\underline{s}-\hat{\underline{s}})(\underline{s}-\hat{\underline{s}})\} \; ; \; R \triangleq E\{\underline{v}\underline{v}'\}$$

and E is used as the expectation operator. The use of the superscript (^) is intended to signify an estimated value. Examination of the classification set by the friendly combatant reveals that sub-elements of all members of the classification s are unknown and hence the estimation and identification problems must be solved. Figure 9 illustrates the mechanization required to solve these problems.

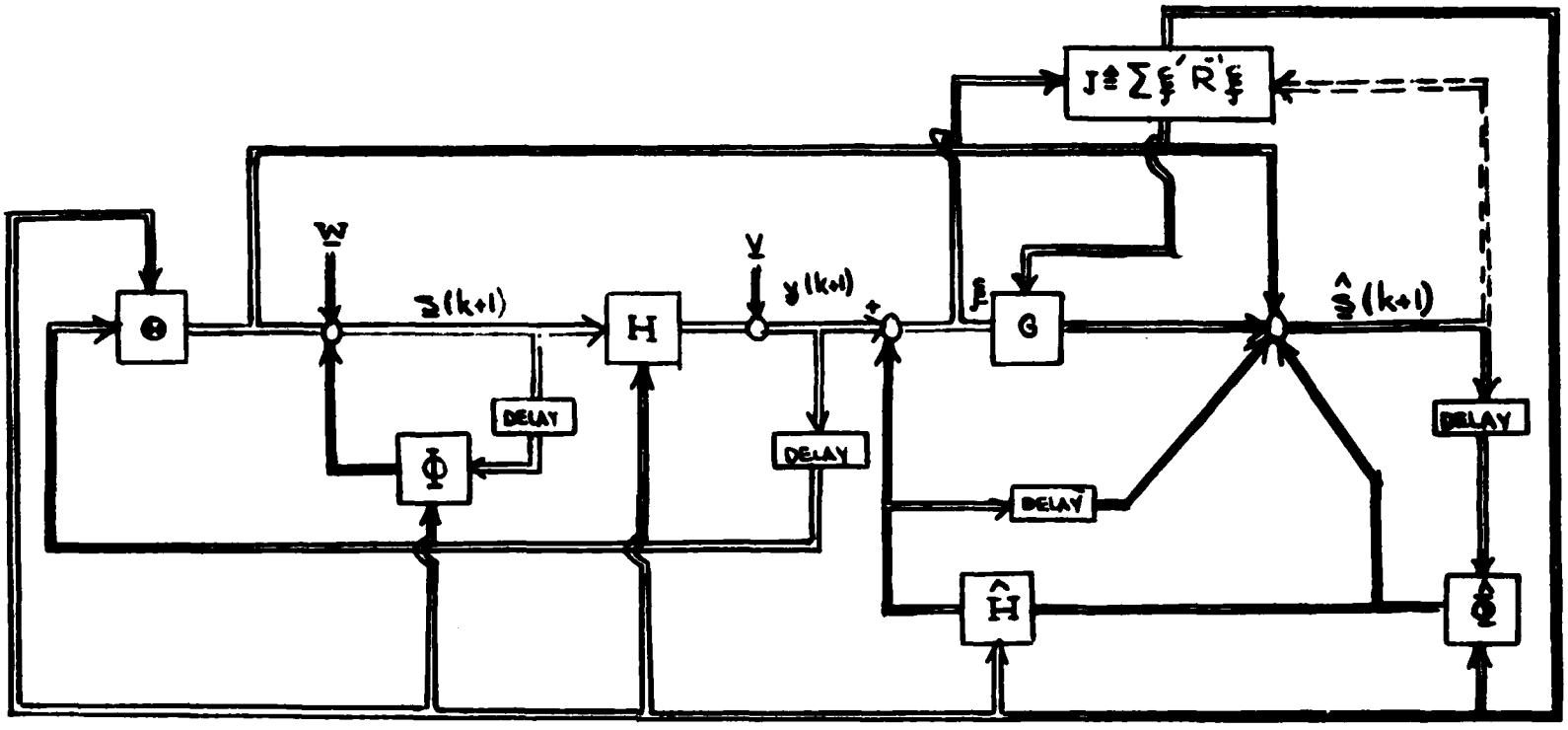


Figure 9. CLM Applied to CVSP

AD P001067

CONTROLLABILITY OF DISTURBED RETICLE TANK FIRE CONTROL SYSTEMS

P. G. Cushman
Consulting Systems Engineer
General Electric Company, Ordnance Systems
Pittsfield, Mass. 01201

INTRODUCTION

The history of U.S. Tank Gun Stabilization and Fire Control has been replete with evolutionary changes in response to updated requirements. For example, the M60A1 was originally equipped with non-stabilized gun drives, to which gyro stabilization was added to allow aiming and firing on the move. Also, the M60A1 had a sight with fixed reticles (elevation manually adjusted for range), so the gunner was required to estimate lead angle. The later M60 vehicles, M60A2 and M60A3, were equipped with sights with servo-driven reticles so that computed superelevation and deflection could be inserted automatically.

Presently, the Bradley Fighting Vehicle is equipped with a high-quality gun stabilization system which allows precision tracking for the TOW missile guidance with the vehicle stationary, and good gun aiming and firing accuracy with the vehicle on the move. No "fire control" in the form of automatic lead angle and super-elevation generation is included, but some such capability may be required as the missions for the BFV are extended. Any such upgrading of capability would logically build upon the existing system, and would thus most likely take the form of a disturbed reticle system. This study investigates the requirements and performance of such a disturbed reticle system, but it is not directed toward any particular system. Rather, it derives the necessary transfer function characteristics of the elements of such a system.

DISTURBED RETICLE SYSTEM ANALYSIS AND REQUIREMENTS

SYSTEM CONFIGURATION

Figure 1 shows a functional block diagram for one axis of the disturbed reticle system. (Figures 2 and 3 are modifications of Figure 1 that are useful for analysis purposes.) This representation follows quite closely that found in Reference 1. The primary tracking loop is closed by the gunner, who sees the error between target angular position and reticle angular position in his sight and corrects the observed error by commanding the gun turning rate by operating his hand station. For purposes of transfer function analysis, the gunner can be considered a quasi-linear transfer function of the form(2):

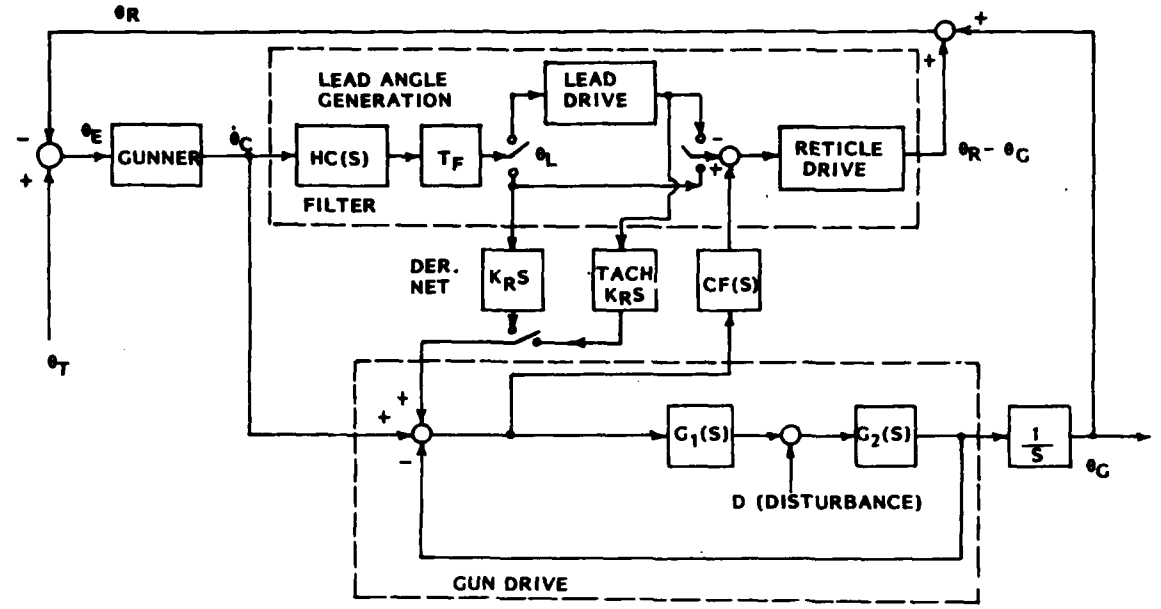


Figure 1. FUNCTIONAL BLOCK DIAGRAM–DISTURBED RETICLE SYSTEM

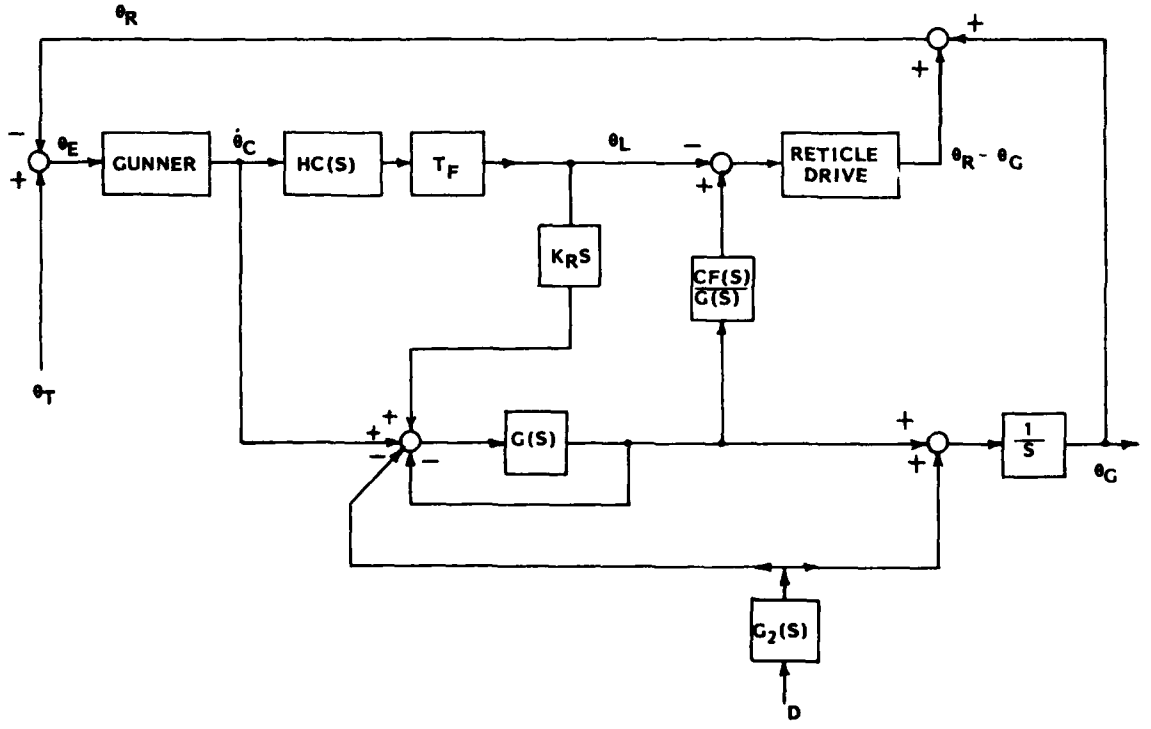


Figure 2. LINEAR TRANSFORMATION OF FIGURE 1 FOR USE IN GUN MOTION ANALYSIS

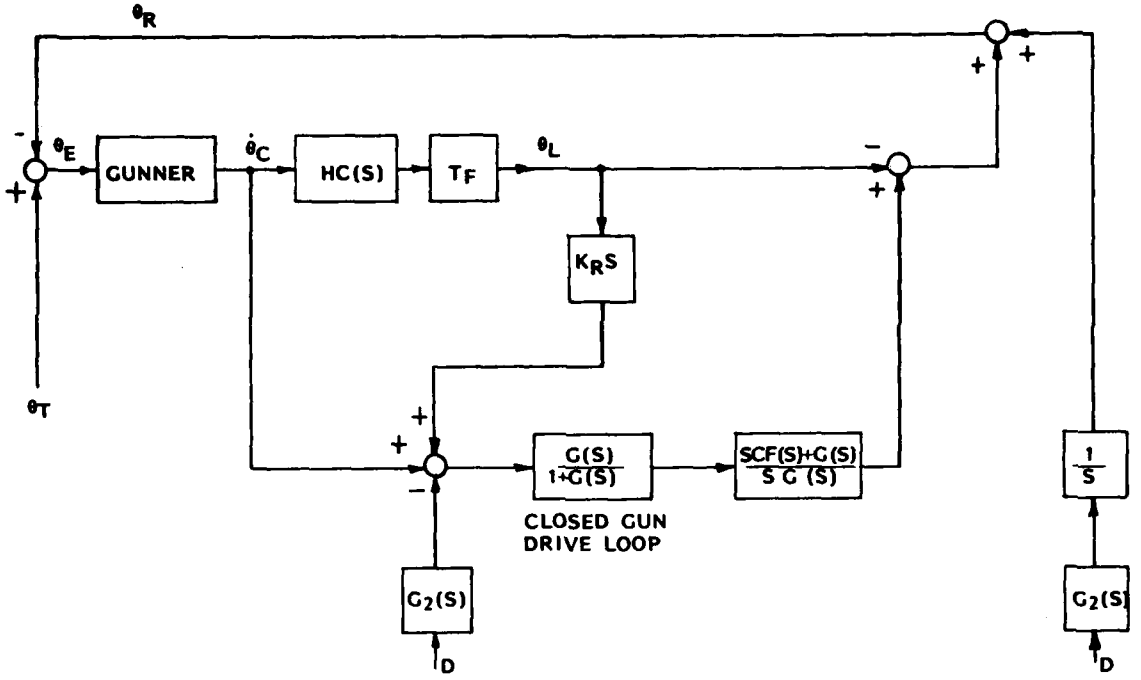


Figure 3. LINEAR TRANSFORMATION OF FIGURE 2 FOR USE IN RETICLE MOTION ANALYSIS (RETICLE DRIVE = 1)

$$\frac{\dot{\theta}_C}{\theta_E} = \frac{K\epsilon^{-\tau s}(1 + T_L s)}{(1 + T_1 s)(1 + T_N s)}$$

where K is the gain

T_1 is a lag time constant } Adjusted adaptively for the plant

T_L is a lead time constant }

τ is the visual delay

T_N is the neurological time constant, somewhat adjustable

The gunner adaptively adjusts his parameters to achieve a stable operation of his tracking loop at a crossover frequency, W_c. During tracking tests on the move on the M60A1E2[3] and the MICV-65[4] with electric gun stabilization drives, W_c was in the range 2 to 3 rad/sec. During stationary vehicle tracking tests,

W_c is 4 or more, and there is some tracking rate "feed forward." Functionally in Fig. 1, the gunner can be replaced with an automatic tracker, having a higher W_c and providing smoother tracking.

GUN STABILIZATION

When the system is using gun stabilization only, the lower half of Figure 1 applies. The gunner is working with a "load" or "plant" consisting of the gun drive, with rate gyro feedback, and the inherent integration to angle. That is, the plant is nearly a pure integrator, which is ideal for the gunner [1], with a high-frequency (relative to gunner responses) resonance and roll-off. The plant frequency characteristic, along with the overall open-loop characteristic achieved by the gunner, is shown in Figure 4. Note that for a well designed gun drive system, the bandwidth of the gun drive will be very much higher (an order of magnitude or more) than W_c. It should be mentioned in passing that functionally a stabilized sight system responds like a stabilized gun system, the only difference being the higher bandwidth achievable with the stabilized sight. From the considerations shown in Figure 4, this should make little difference as both bandwidths are well above W_c. The major advantage of a stabilized sight system lies in the reduced response to disturbances to the line of sight (LOS) caused by vehicle motions.

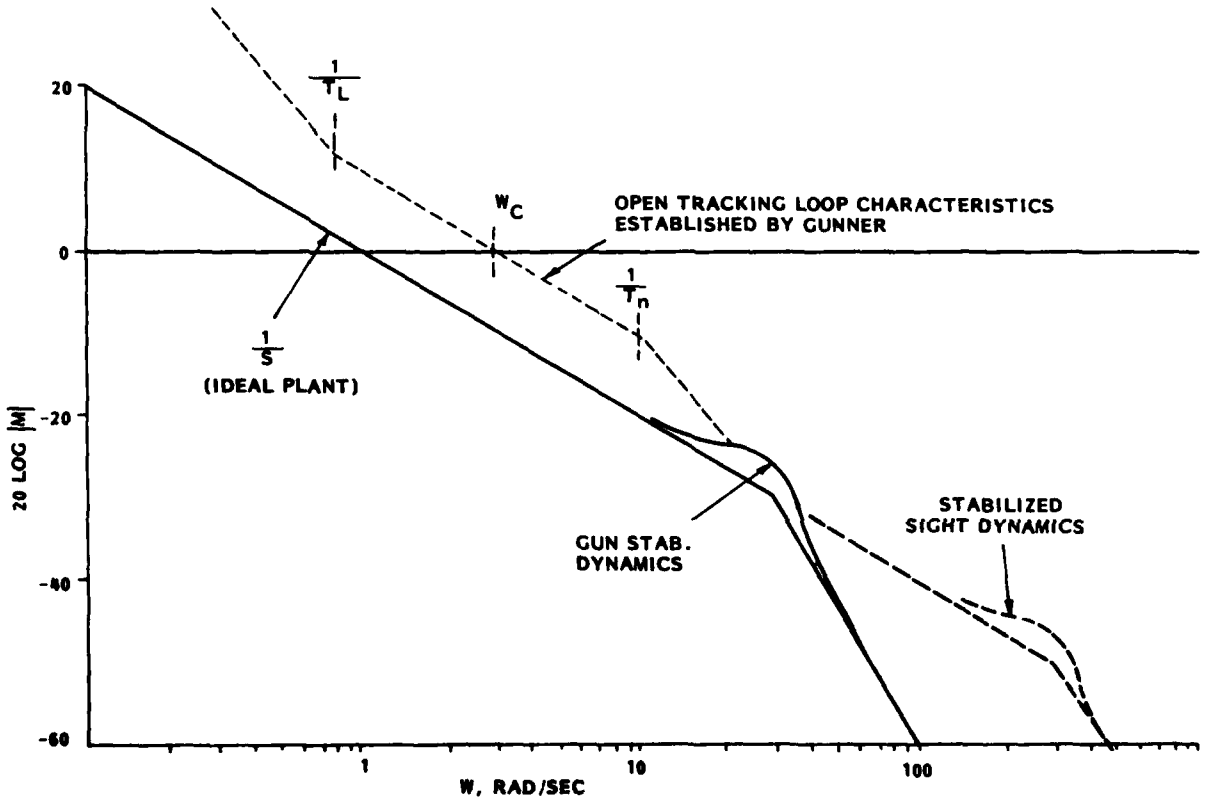


Figure 4. ELEMENTS OF TRACKING LOOP

LEAD ANGLE GENERATION

The lead angle generation is shown in the top half of Figure 1. The hand station rate signal is used as the measure of target angular velocity. This angular rate multiplied by the computed time of flight of the round, T_F, yields the lead angle. (This is a linear predicter, assuming straight-line, constant-speed target motion). At this stage the lead angle is in electrical signal form (either analog or digital) and must be converted to reticle and ultimately gun angular motion. Two alternate conversions are indicated in Figure 1. In one, the electrical signal drives a lead screw servo which is followed by the reticle (or mirror) servo. This system was described in detail in Reference 1 and is the system used in the traverse channel of the M-1 tank. It has the advantage that the target and reticle remain centered in the field of view of the sight as the lead angle is entered. In the second approach, which is representative of the M60A2 and A3 systems, the electrical signal feeds the reticle servo directly. In this approach, the reticle and target do not remain centered in the field of view as the lead is entered. From field tests on the M60A2, this characteristic does not seem to cause gunner performance degradation. Aside from this "human factors" difference, no functional difference exists between the two methods of entering lead angle, and this study will consider them to be the same.

It is seen in Figure 1 that the hand station command rate signal is filtered before lead angle is generated. This is necessary because the rate signal may be noisy (even when tracking angle error is being maintained at a low value), and this noise will result in erroneous lead angle values. Note that this filtering is required for either a stabilized sight or disturbed reticle system. Sometimes the filtering is greatly increased for a disturbed reticle system to compensate for an inadequate system configuration, as will be seen presently. However, such filtering presents an unnecessary penalty on the disturbed reticle system, if only the configuration of existing system elements is changed as indicated below.

CROSS CONNECTIONS BETWEEN GUN DRIVE AND LEAD GENERATION

Two cross connections are shown in Figure 1. The first is a derivative of lead signal that is fed into the input of the gun stabilization. This is necessary to move the gun by the amount of the lead angle, as the lead angle is being generated. If this is done properly, the motion is equal and opposite to the reticle presentation in the sight, and the gunner is unaware of lead angle insertion. To investigate this, refer to Figure 3; assume for the moment that there is no cross-feed, CF(s), and no hand station signal, θ_c. Apply θ_L and observe θ_R.

$$\left.\frac{\theta_R}{\theta_L}\right| = K_R \left[\begin{matrix}\text{Closed Gun}\\ \text{Drive Loop}\end{matrix}\right] - \left[\begin{matrix}\text{Reticle}\\ \text{Drive}\end{matrix}\right]$$

$$\left|\begin{matrix}\dot{\theta}_c = 0\\ CF(s) = 0\\ D = 0\end{matrix}\right.$$

Under steady-state conditions, presumably both the gun drive and reticle drive have unity gain. Thus, the steady-state error angle appearing in the sight is zero, if $K_R = 1$. Furthermore, if the dynamics of the reticle drive and gun drive are matched, no transient error would appear in the sight. However, this matching of dynamics would be difficult to achieve. Normally, the bandwidth of the reticle drive can easily be made higher than that of the gun drive, and in the presentation to come this is a desirable characteristic. Now to repeat the previous equation, assuming infinite reticle bandwidth (unity transfer function):

$$\left.\frac{\theta_R}{\theta_L}\right| = \left[\begin{matrix}\text{Closed Gun}\\ \text{Drive Loop}\end{matrix}\right] - 1 = \frac{G(s)}{1 + G(s)} - 1 = -\frac{1}{1 + G(s)}$$

$$\left|\begin{matrix}\theta_c = 0\\ CF(s) = 0\\ D = 0\\ K_R = 1\\ \text{Reticle Drive} = 1\end{matrix}\right.$$

This is an anomalous response that may be confusing to the gunner, if it is large enough. It can be used to determine the overall plant that the gunner perceives:

$$\frac{\theta_R}{\theta_c} = \frac{1}{s}\left[\begin{matrix}\text{Closed Gun}\\ \text{Drive Loop}\end{matrix}\right] - \frac{HC(s)\,T_F}{1 + G(s)}$$

$$= \frac{1}{s}\left[\frac{G(s)}{1 + G(s)}\right] - \frac{HC(s)T_F}{1 + G(s)}$$

These transfer function components are shown in Figure 5 for several values of T_F. It is seen that the "confusing" part of the response predominates at frequencies just above the frequency at which the gunner is attempting to establish tracking loop crossover. This is particularly confusing because it is a positive feedback type of response. Such a system would be impossible to stabilize at gains anywhere near the normal value. It is seen that the problem gets worse with increasing target range (T_F) and with decreasing gun drive bandwidth. The problem can be alleviated by adding a lot of filtering (HC(s)) in the hand station signal. To reduce the "confusing" response to the magnitude level of the "expected" response would require a single lag break at about W = 1 or a double break at about W = 3. This amount of filtering can degrade overall system performance appreciably(1).

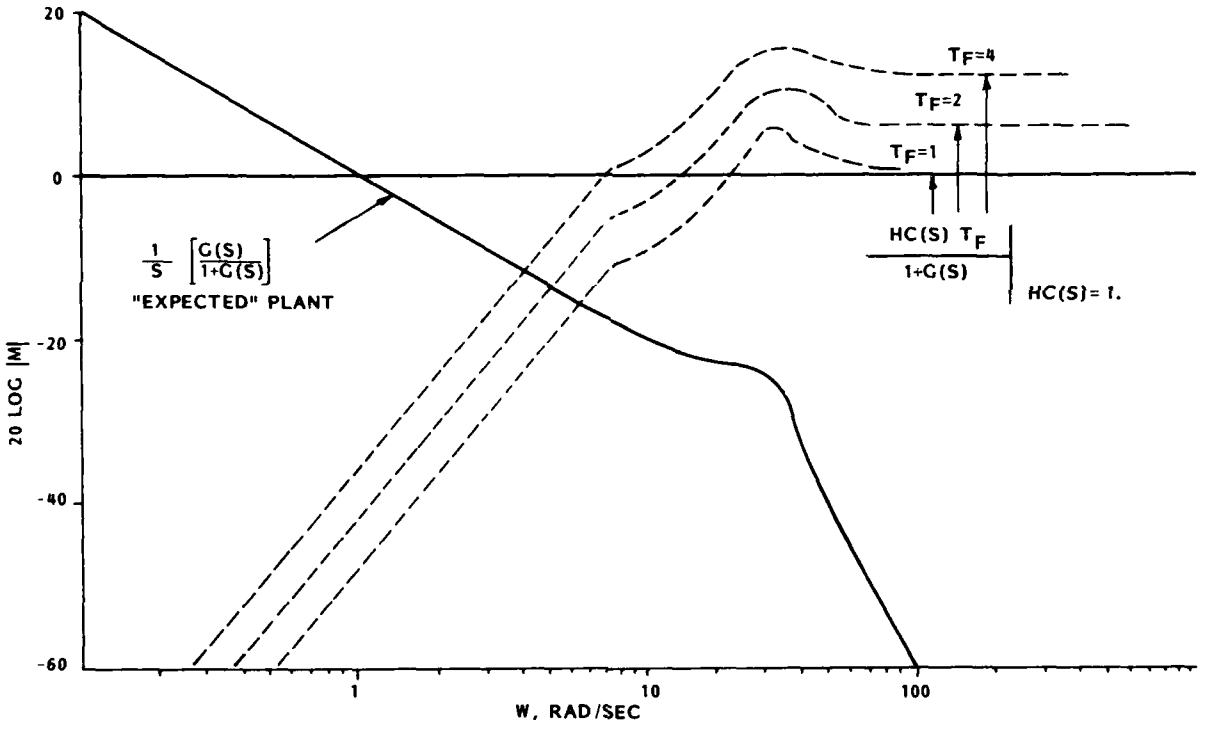


Figure 5. PLANT TRANSFER FUNCTIONS WITHOUT CROSS FEED OR HANDSTATION FILTER

The problem described above can be greatly relieved by the use of the cross-feed, CF (s), shown in Figure 1. Physically, the error of the gun drive is measured and applied to the reticle servo, so that the gunner is not bothered by the delays in the gun drive response. For successful application, the reticle drive bandwidth must be high, relative to the gun drive. The response of the reticle to lead angle generation can be easily determined from Figure 3.

$$\frac{\theta_R}{\theta_L} = K_R \; s \left[\frac{G(s)}{1 + G(s)}\right] \left[\frac{sCF(s) + G(s)}{s\,G(s)}\right] - 1$$

From this, an ideal cross-feed, CF(s), can be selected. If $K_R = 1$, as found above, and $CF(s) = 1/s$, then

$$\frac{\theta_R}{\theta_L} = 1 - 1 = 0$$

regardless of the gun drive response. This means that the implementation of lead angle in gun pointing is completely removed from the gunner's view, just as it is in the stabilized sight case.

It is, of course, necessary to explore the effect of this cross-feed on the normal tracking response of the plant and the disturbance response of the plant. The tracking response is

$$\frac{\theta_R}{\dot{\theta}_c} = \left[\frac{G(s)}{1 + G(s)}\right] \left[\frac{sCF(s) + G(s)}{sG(s)}\right] = \frac{1}{s} \quad \text{if}$$

$$CF(s) = \frac{1}{s}$$

Thus, the cross-feed has caused the plant response to approach the ideal of a simple integrator, just as the stabilized sight does.

The disturbance response of the plant, as it appears to the gunner, is

$$\frac{\theta_R}{D} = G_2(s) \left[\frac{1}{s} - \left[\frac{G(s)}{1 + G(s)}\right] \left[\frac{sCF(s) + G(s)}{sG(s)}\right]\right]$$

$$= G_2(s) \left[\frac{1}{s} - \frac{1}{s}\right] = 0 \quad \text{if } CF(s) = \frac{1}{s}$$

This is in contrast to the actual motion of the gun; see Figure 2:

$$\frac{\theta_G}{D} = G_2(s) \left[\frac{1}{s} - \frac{1}{s}\left[\frac{G(s)}{1 + G(s)}\right]\right] = G_2(s)\,\frac{1}{s}\left[\frac{1}{1 + G(s)}\right]$$

That is, the gun aim is being erroneously disturbed from the proper

position by the torque disturbances, but the gunner is completely unaware of these disturbances. This situation is desirable for the gun motions at suspension frequencies (and above) which are beyond the gunner's capability to correct. However, any low-frequency errors in gun pointing should not be shielded from the gunner's view, but should be presented to him so that he can correct for them. That is, instead of CF(s) = 1/s, the cross-feed should be of the form

$$CF(s) = \frac{1}{s + W_0} \quad \text{or possibly} \quad CF(s) = \frac{s}{(s + W_0)^2}$$

so that CF(s) performs an integration function above W_0, thus effectively removing high-frequency transients, which are beyond the range of the ability of the gunner to correct, from the gunner's view. However, at the low frequencies, below W_0, the gunner is aware of the gun pointing errors and can correct them. The value of W_0 can be found by substituting this CF(s) function into the pertinent transfer functions. That is,

$$\left.\frac{\theta_R}{\theta_L}\right|_{\dot{\theta}_c = 0} = K_R s \left[\frac{G(s)}{1 + G(s)}\right] \left[\frac{\frac{s}{s + W_0} + G(s)}{sG(s)}\right] - 1$$

$$= \left.\frac{-1}{(1 + s/W_0)\left[1 + G(s)\right]}\right|_{K_R = 1}$$

and the overall plant response is

$$\frac{\theta_R}{\dot{\theta}_c} = \frac{1}{s}\left[\frac{\frac{s}{s + W_0} + G(s)}{1 + G(s)}\right] - \frac{HC(s)\, T_F}{\left(1 + \frac{s}{W_0}\right)}\left[1 + G(s)\right]$$

The first term is very nearly the ideal integral response. The second term is the undesirable "confusing response", but now it is already filtered by the $1/(1 + s/W_0)$ term. In terms of the previous discussion, W_0 should be of the order of 1. The hand station signal can still be filtered in HC(s), but the filtering needs to be only that required to smooth gunner input noise, as it is in the stabilized sight case.

SIMULATION STUDY

HITPRO* MODEL

The derivations performed above have assumed linear and relatively simple transfer functions for the major system elements. Since the gun power drives and reticle servos may contain considerable nonlinearity, it seemed worthwhile to check some of the derived conclusions using a realistic simulation of the system. This simulation work employed HITPRO, [3][4] which was developed for the U.S. Army as a general purpose tool for studying the effect on gun firing accuracy of various elements of an armored vehicle - suspension, gun drives, fire control, etc. Various vehicles that have been modeled on HITPRO are MICV-65, M60A1/A0S, M60A3, M1, HIMAG and HSTVL. This study used a modified version of HITPRO that has been used for studying the Bradley Fighting Vehicle (BFV) gun stabilization drives. The modifications were associated with a larger gun (75 mm) than is used on BFV, and a somewhat lighter hull. This was done to include the possibility of a yaw suspension flexibility effect on tracking.

HITPRO uses a McRuer model for the gunner. (See Reference 2). Extensive tracking tests have been made with the BFV. These tests were made with three different individual gunners. The parameters of the McRuer model were selected so that the HITPRO tracking performance matches quite closely the poorest of the three gunners. This was done because the tracking tests were made without the gun gyro feedback, which helps the gunner performance slightly. These simulation runs were made with the gun gyros in place.

The scenario chosen for the study was the same as that used in Reference 1. Own vehicle was stationary. Target was initially approaching head-on at a speed of about 10 meters/sec. at a range of 750 meters. Thereafter it turns, performs a rather violent evasive maneuver, and ends up on a near crossing course. The target trajectory is shown in Figure 6, and the required tracking angle and rate are shown in Figure 7. The round time of flight of 2 seconds, as used in Reference 1, is unusually long for this relatively short range, but is useful in showing the difficulty of aiming correctly to hit a maneuvering target.

SIMULATION RESULTS

First, the system was run with hand station signal-filtering break set at W = 1. This amount of filtering was described previously as excessive. The results of this run are shown in Figure 8. Note that the tracking error (the error observed by the gunner) is small, generally well under 1 mr. However the ideal linear prediction

*Hit Probability

FIG 6

TARGET TRAJECTORY FOR STUDY
X DISTANCE VS Z DISTANCE, METERS

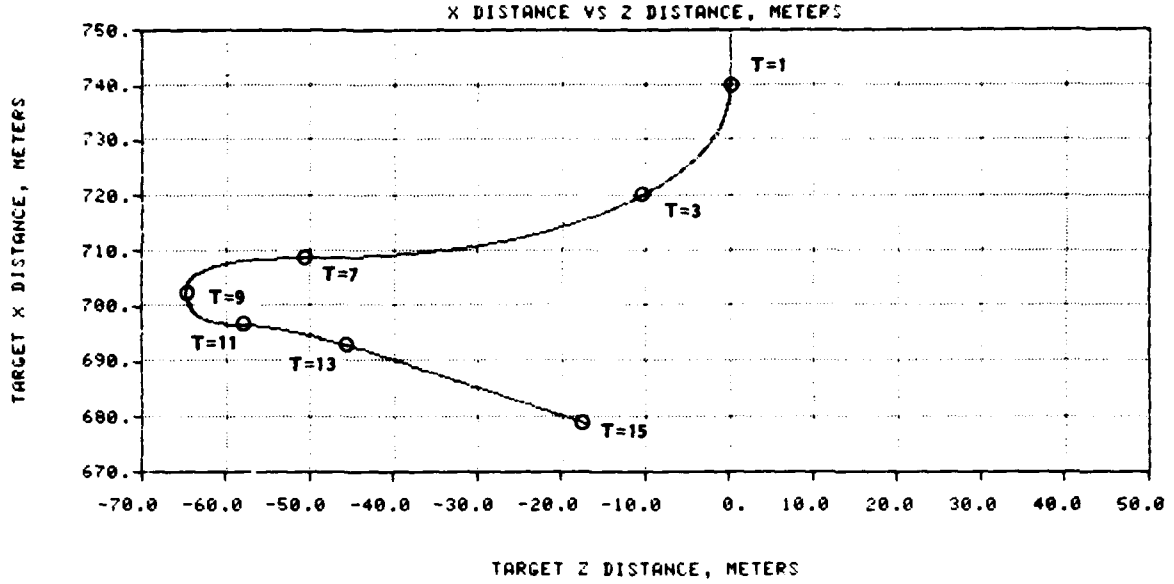
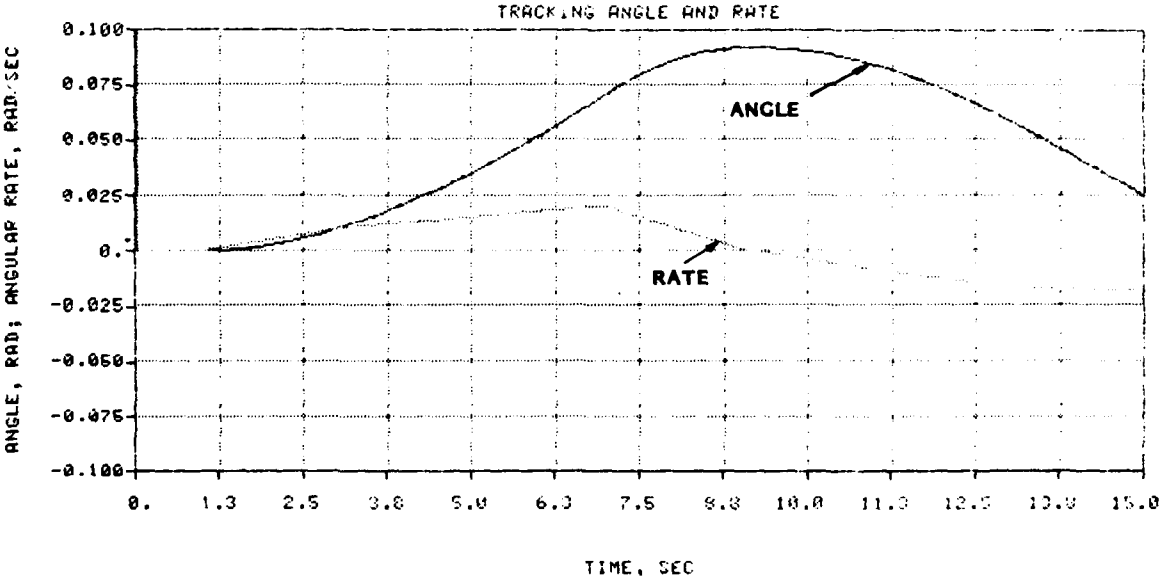


FIG 7

TARGET TRAJECTORY FOR STUDY
TRACKING ANGLE AND RATE



"gun pointing error" is quite large, reaching a peak of 19 mr. This error is large because the lead angle being generated from the filtered hand station signal is not "keeping up" with the lead that would be associated with the actual target angular rate.

FIG 8

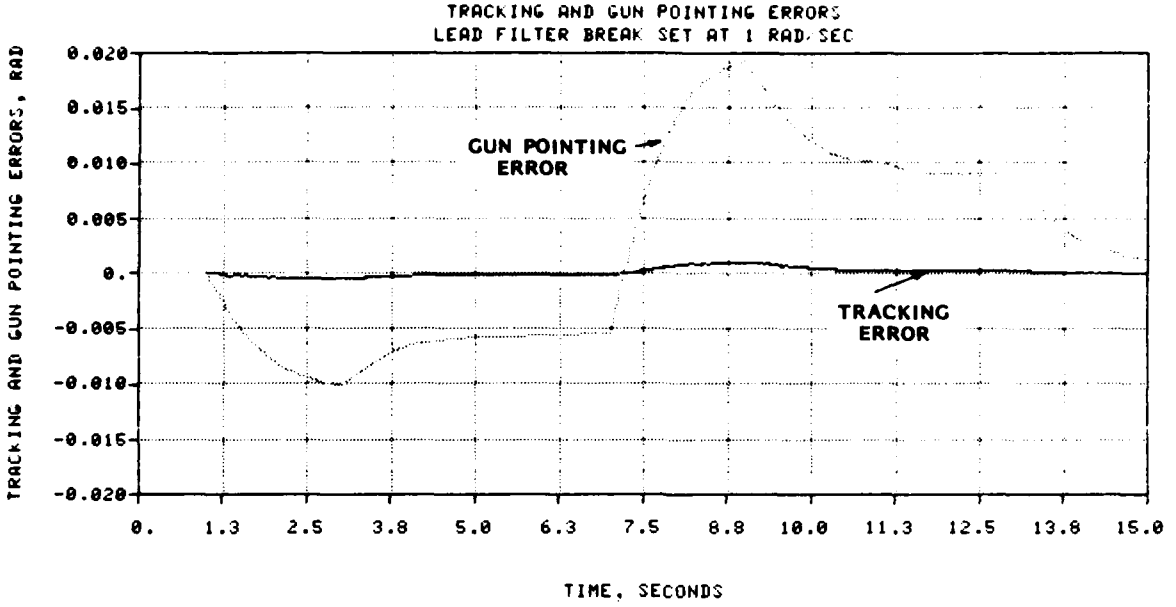
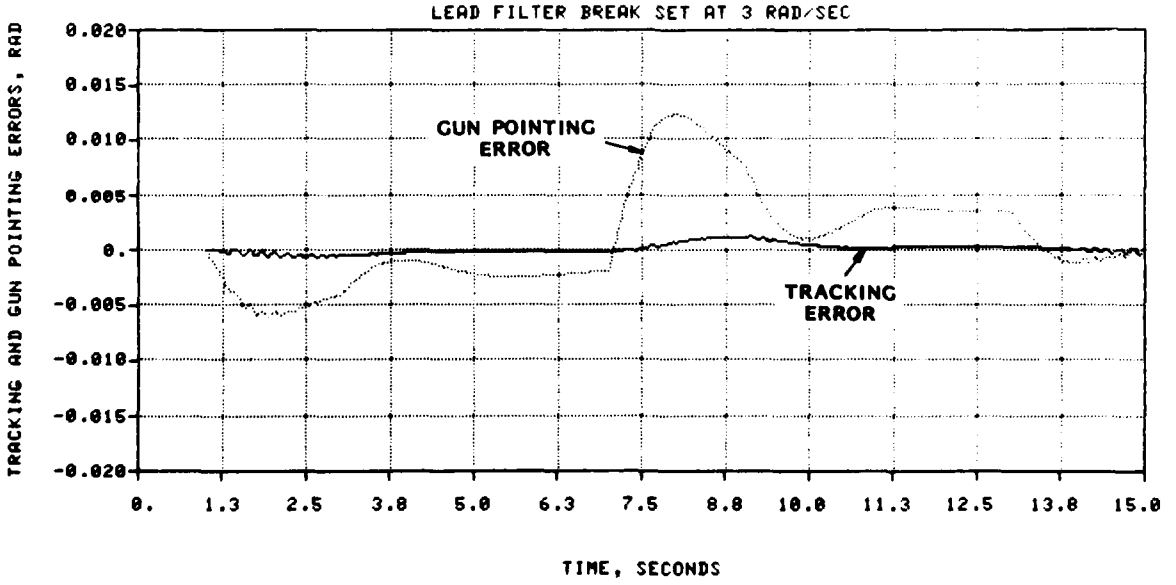


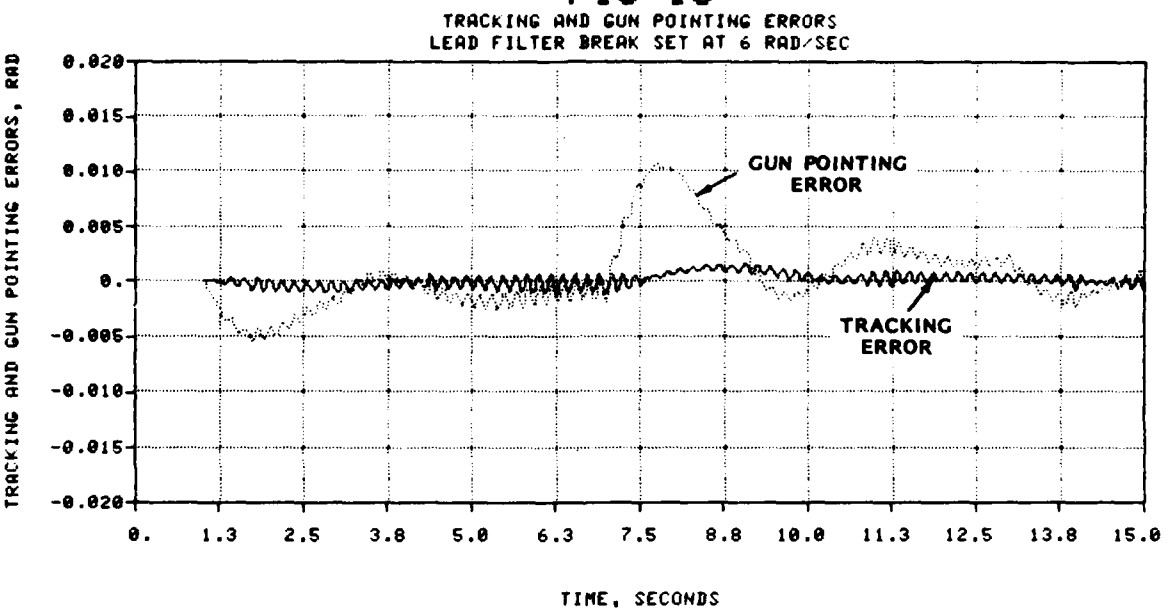
FIG 9



Second, the system was run with the hand station filter break set at W = 3, with the results of this run shown in Figure 9. The tracking error is about the same as before, but the gun pointing error is substantially reduced, having a peak of about 12 mr.

Figure 10 shows the results with the hand station filter break set at W = 6. The gun pointing error is reduced slightly to a peak of about 10.5 mr. Great improvement should not be expected as this filter break is already well above the gunner bandwidth. Note in Figure 10 the high frequency oscillation in the error response which is associated with suspension resonant frequency. It is expected that a "real" gunner would not excite this noise at all.

FIG 10



The large gun pointing errors presented above do not represent the whole story. These errors are simply those associated with failure to follow a lead angle based on a straight-line target course. For a maneuvering target, such as used here, the simple lead is far from correct. After the target trajectory has been completed, the correct lead angle at every point can be determined. Figure 11 shows the "gun pointing error" of Figure 9, and also the additional error associated with an incorrect lead solution. It is clear that the latter error is greater than the former during most of the trajectory. The true error is of course the sum of these components, and is shown in Figure 12.

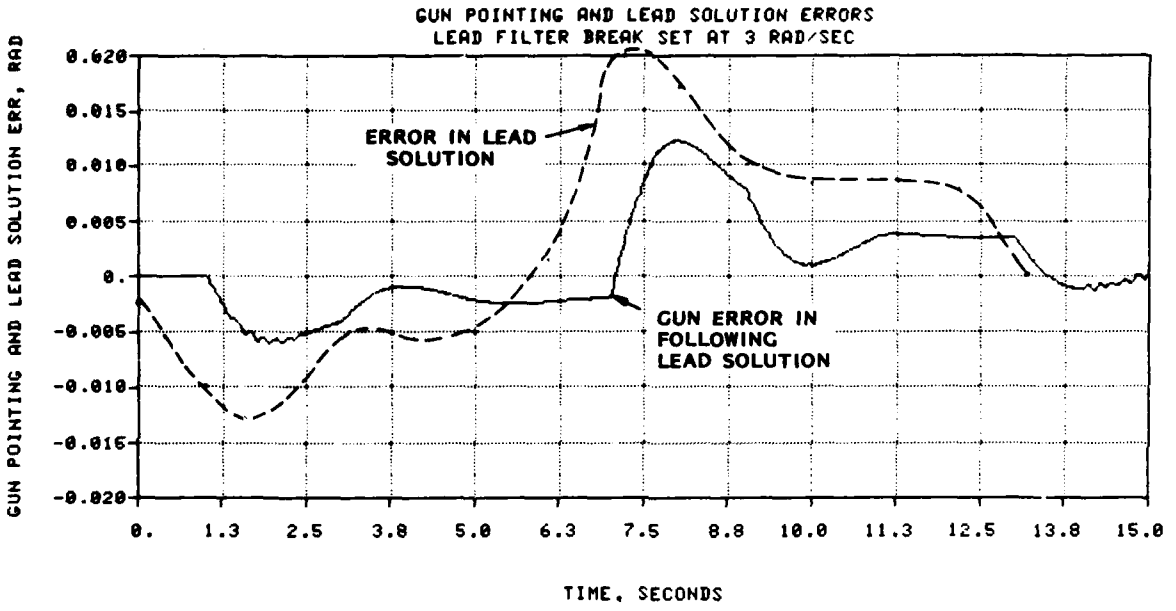
In view of the incorrect lead solution being a large part of the total error, a logical improvement would be to use a higher order lead predictor. That is, instead of

$$\text{Lead} = \dot{\theta} \; T_F$$

the following function was tried:

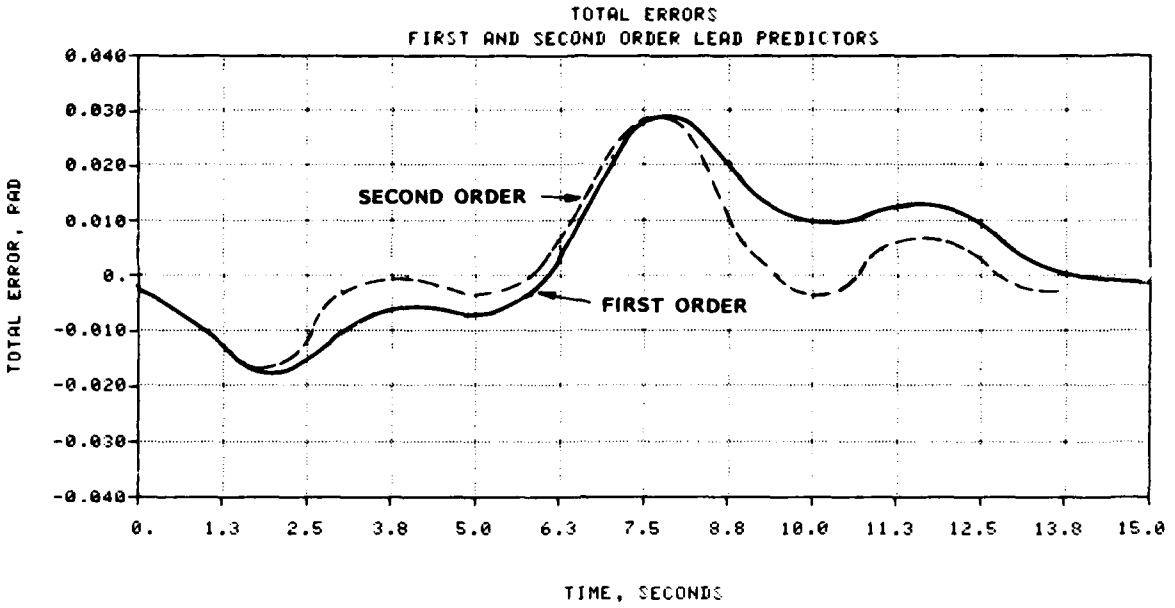
$$\text{Lead} = L = \dot{\theta} \; T_F + \ddot{\theta} \; \frac{T_F^2}{2}$$

FIG 11



The results of this are also shown in Figure 12. The accuracy is improved considerably during the "well behaved" portions of the trajectory, but not at all during the unpredictable portions of the trajectory. Obviously, large target maneuvers occurring within the time of flight of the round are going to cause large miss distances regardless of the sophistication of the fire control system.

FIG 12



CONCLUSIONS

Functional requirements for some of the elements of a disturbed reticle "add on" fire control system have been defined, particularly those that have an important effect on the plant that the gunner sees and feels. These requirements have been checked using a simulation of a real system. In particular, excessive filtering of the gunner's hand station rate signal for lead generation is not required, and the performance of a disturbed reticle system can be adequate relative to inherent overall errors in a fire control system.

This study has concentrated on target tracking from a stationary vehicle. The complete fire control system may include rate aided tracking, dynamic cant correction, and other features for aiding the gunner during own vehicle maneuvers.(5) The simulation results have shown the value of own vehicle maneuvers as a defensive measure.

REFERENCES

1. "Analysis of Tank Fire Control Systems by Optimal Control Theory" by H. Burke, et al.

   Proceedings of Third Meeting of the Coordinating Group on Modern Control Theory, Part I, 20 Oct. 1981.

2. "A Theory for Driver Steering Control of Motor Vehicles" by Wier and McRuer, Highway Research Record #247, 1968.

3. RE-TR-71-63
   HITPRO, Vol. I, "System Analysis of Hit Probability for Firing on the Move" (U)
   Confidential
   Nov. 1971

4. SWERR-TR-72-17
   HITPRO II, Vol. II, "System Analysis of Hit Probability for Firing on the Move for a Rapid Fire Weapon System" (U)
   Confidential
   April 1972

5. AD 772000
   "Study of Gunner Aids for Automatic Cannon Type Weapons" by P. G. Cushman, Dec. 1973.

SESSION II: MISSILE/AIR DEFENSE FIRE CONTROL

27 OCT 1982

(MORNING)

ROOM #2

FOURTH MEETING OF THE COORDINATING

GROUP ON MODERN CONTROL THEORY

HOSTED BY: OAKLAND UNIVERSITY
ROCHESTER, MICHIGAN

Next page is blank.

AD P001068

ENDGAME PERFORMANCE TRADEOFF STUDY OF A SPECIAL CLASS OF INTERCEPTORS

Dr. Jonathan Korn
ALPHATECH, Inc.
3 New England Executive Park
Burlington, Massachusetts 01803

INTRODUCTION

This study is concerned with investigating the endgame performance of a specific class of ballistic missile defense (BMD) interceptors: small, agile missiles configured to destroy reentry vehicles (RVs) by direct impact deep in the atmosphere. The endgame performance evaluation is carried out by analyzing the sensitivity of the miss distance statistics (mean and standard deviation) to various system parameters. The system parameters of interest are sensor accuracy, interceptor response time, physical dimensions (mass and shape), sensor aperture, and sensor carrier frequency. One fixed parameter is the interceptor guidance law; the one used is of the predictive proportional navigation type.

The analytical tools used in this effort are the Cramer-Rao lower bound technique and a nonlinear covariance analysis. The first provides a measure of the interceptor's tracking performance: a lower bound on the estimation error. Given the bound time history, the nonlinear covariance equations of the engagement are propagated from handover to intercept. This procedure results in the final miss distance statistics.

In this paper we will present partial results of the interception tradeoff analysis. A more detailed discussion can be found elsewhere [1]. The following tradeoff curves will be presented:

1. sensor accuracy versus missile response time for several values of equal-miss-distance (rms);
2. interceptor response time versus mass (during homing phase) parameterized by L/D (Length-to-Diameter);
3. missile mass versus sensor aperture parameterized by L/D; and
4. sensor aperture versus sensor accuracy parametrized by carrier frequency.

These four sets of curves are then integrated into a single figure (Fig. 1) such that an overall tradeoff analysis can be performed. In the following we develop the equations leading to Fig. 1.

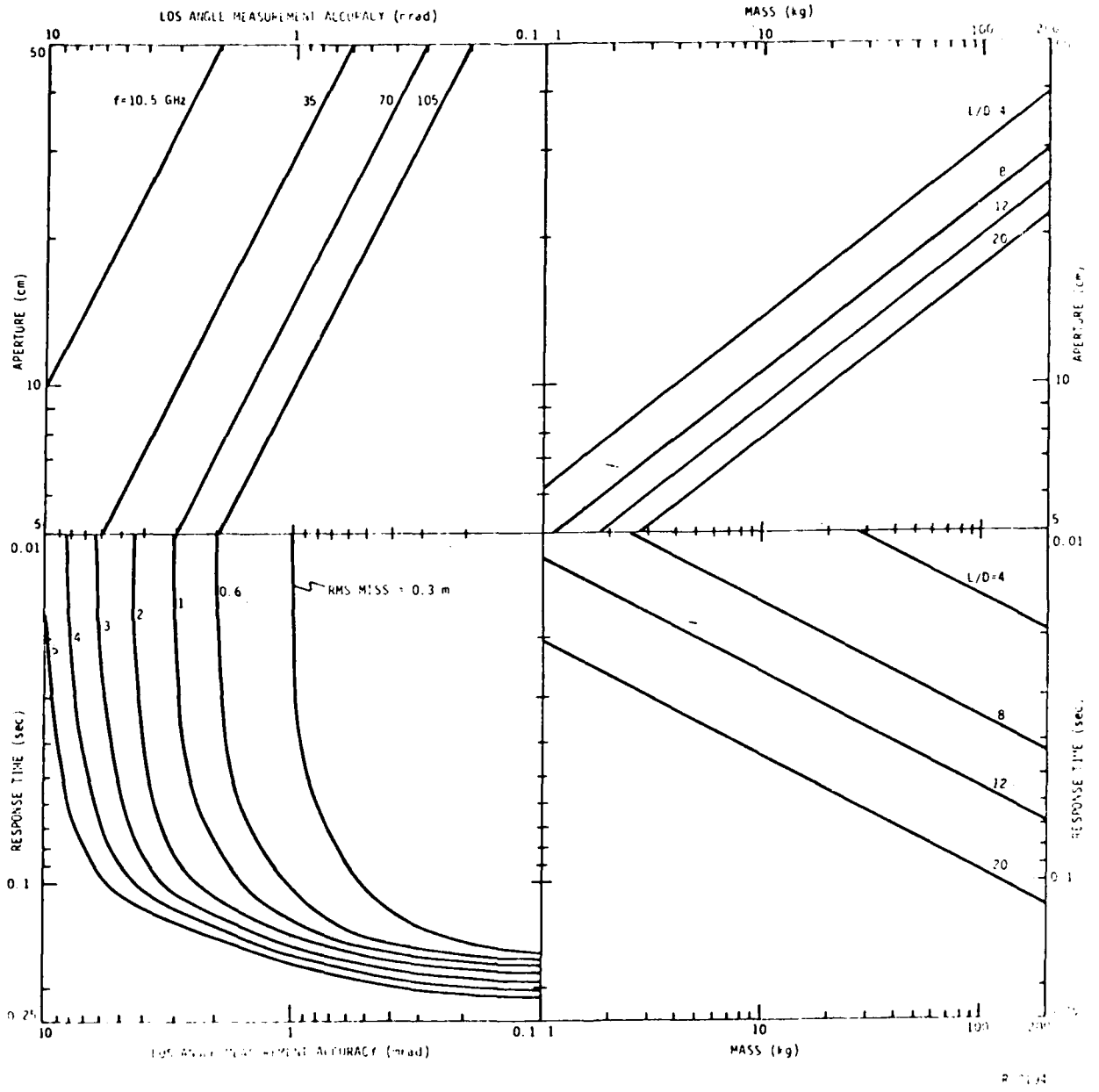


Figure 1. Overall Tradeoff Analysis Curves.

SENSOR ACCURACY/RESPONSE TIME TRADEOFF*

Clearly, if a specific miss-distance (rms) is to be achieved, several interceptor parameters must be traded off. We fix the handover volume, the interceptor acceleration limit, and the data rate at their nominal values [1], and trade off the LOS angle accuracy (σ_ϕ) versus the interceptor response time (τ_m) such that a particular rms miss value is attained. The equations leading to these curves are beyond the scope of this paper and can be found elsewhere. The curves are constructed in the lower-left quadrant of Fig. 1. Observe that, for a given miss distance, higher sensor accuracy permits larger time lags, and, on the other hand, higher sensor noise requires faster response times.

RESPONSE TIME/INTERCEPTOR MASS TRADEOFF

The dominant factors affecting the response time are the missile's mass and its aerodynamic properties. In this paper we consider a cylindrical and, typically, long missile, similar to the design of Vought Corporation. Such a missile is often characterized by its Length-to-Diameter ratio, or L/D. Given an L/D value, the single dominant parameter which determines the missile's response time is the mass, M.†

The response between the commanded and the attained lateral acceleration of a typical missile is dominated by its longitudinal axis short-period natural frequency ω_n. This frequency is given by [2].

$$\omega_n = \left[\frac{\frac{D}{2v_m} C_{M_q} C_{Z_\alpha} - \frac{Mv_m}{Sq} C_{M_\alpha}}{\frac{I_y}{SqD} \quad \frac{Mv_m}{Sq}} \right]^{1/2} \tag{1}$$

---

*Response time, as defined in this context, is equivalent to the airframe dynamic time lag τ_m. It should be interpreted as the time it takes to attain $a_L=(1-e^{-1})a^c=0.63a^c$, where a^c is an acceleration step command.

†Usually, the response time is linked to the missile's closed-loop control bandwidth. From discussions with Vought Corporation's technical staff, however, it has been established that the control loop is used mainly for stabilization, and that its contribution to the missile's response time can be neglected.

where

D = missile's diameter

S = characteristic area ($= \pi/4\ D^2$),

v_m = missile's velocity

q = dynamic pressure ($= 1/2\ \rho v_m$, ρ = air density),

M = missile's mass, and

I_y = pitch axis moment of inertia;

and C_{M_q}, C_{Z_α}, and C_{M_α} are the missile's longitudinal stability derivatives, defined as

C_{M_q} = damping in pitch,

C_{Z_α} = slope of the normal force curve, and

C_{M_α} = static longitudinal stability.

From discussions with Vought technical personnel it has been determined that the typical cylindrical missile design is characterized by stability derivative values such that

$$\frac{D}{2v_m} C_{M_q} C_{Z_\alpha} << - \frac{Mv_m}{Sq} C_{M_\alpha} \tag{2}$$

Thus, Eq. 1 can be simplified, viz.,

$$\omega_n = \left[\frac{-C_{M_\alpha} \cdot SqD}{I_y} \right]^{1/2} \tag{3}$$

This equation can be further simplified if we make use of the definition of C_{M_α} [2]

$$C_M = \frac{1}{SqD} M_\alpha \tag{4}$$

where M_α is the sensitivity of the pitch axis moment to the missile angle of attack. Now,

$$\omega_n^{-1} = \left[\frac{-M_\alpha}{I_y} \right]^{-1/2} \tag{5}$$

which, for the Vought design, is typically associated with the 90 percent value response time. Thus we may write

$$\tau_m = \frac{0.63}{0.9} \cdot \frac{1}{\omega_n} = 0.7 \left[\frac{I_y}{-M_\alpha} \right]^{1/2} \tag{6}$$

or

$$\tau_m = 0.7 \left[\frac{I_y}{-C_{M_\alpha} SqD} \right]^{1/2} \tag{7}$$

Note, the moment of inertia is given by

$$I_y = \frac{1}{12} M \left[3 \left(\frac{D}{2} \right)^2 + L^2 \right] \tag{8}$$

where L is the missile's length. Since we will consider L/D values in excess of 4 (a typical value is 12), Eq. 8 can be approximated by

$$I_y = \frac{1}{12} ML^2 \tag{9}$$

Substituting Eq. 9 and the equations for the characteristic area S, and the dynamic pressure q into Eq. 7, yields

$$\tau_m = 0.7 \left[\frac{\frac{1}{12} ML^2}{-C_{M_\alpha} \frac{\pi}{4} D^2 \cdot \frac{1}{2} \rho v_m^2 D} \right]^{1/2}$$

$$= 0.7 \left[\frac{2}{3\pi(-C_{M_\alpha})\rho v_m^2} \right]^{1/2} D^{-1/2} \cdot M^{1/2} \cdot (L/D) \tag{10}$$

In order to obtain τ_m in the requisite form the missile's diameter must be expressed in terms of its mass and its L/D ratio. Clearly,

$$M = \rho_m \cdot \frac{\pi}{4} D^2 \cdot L = \rho_m \cdot \frac{\pi}{4} \left(\frac{L}{D} \right) D^3 \quad , \tag{11}$$

where ρ_m is the missile average density; thus

$$D = \left(\frac{\pi}{4} \rho_m \right)^{-1/3} \left[\frac{M}{(L/D)} \right]^{1/3} \tag{12}$$

Substituting Eq. 12 into Eq. 10 results in

$$\tau_m = 0.7\left[\frac{2}{3\pi(-C_{M_\alpha})\rho v_m^2}\right]^{1/2}\left(\frac{\pi}{4}\rho_m\right)^{1/6}\cdot(L/D)^{7/6}\cdot M^{1/3} \tag{13}$$

We use the following typical values for the constants in Eq. 13:

ρ = 0.002 lb/ft^3 (note, the engagement is assumed to take place at a low altitude),

ρ_m = 0.4 gr/cm^3 (note missile's low mass during homing phase),*

C_{M_α} = -0.7,* and

v_m = 1500 m/sec (nominal value).

Therefore

$$\tau_m = 6.6 \cdot 10^{-4}(L/D)^{7/6}M^{1/3} \quad \text{(in sec; M in kg)} \tag{14}$$

One can plot now the desired equal L/D curves of τ_m versus M, as shown in the lower right quadrant of Fig. 1. The L/D values considered are 4, 8, 12, and 20.

INTERCEPTOR MASS/SENSOR APERTURE TRADEOFF

A typical sensor aperture has a diameter (P) which is approximately two-thirds of the interceptor's diameter (D). Thus,

$$M = \rho_m \frac{\pi}{4}\left(\frac{3}{2}P\right)^2 \cdot L = \rho_m \frac{\pi}{4}\cdot\left(\frac{3}{2}P\right)^3 (L/D) \tag{15}$$

$$P = \left(\frac{32}{27\pi\rho_m}\right)^{1/3}(L/D)^{-1/3}M^{1/3} \tag{16}$$

and with ρ_m = 0.4 gr/cm^3,

$$P = 9.8(L/D)^{-1/3}M^{1/3} \quad \text{(in cm; M in kg)} \tag{17}$$

*Numbers obtained from Vought Corporation.

This equation is illustrated in the upper-right quadrant of Fig. 1 for L/D = 4, 8, 12, and 20.

SENSOR APERTURE/LOS ANGLE ACCURACY TRADEOFF

A widely used empirical formula for the accuracy of a LOS angle measurement is

$$\sigma_\phi \simeq \frac{K}{f \cdot p} \quad , \tag{18}$$

where f is the carrier frequency, P is the sensor aperature, and K is a constant. From experience, a 15 cm aperture in conjunction with a frequency of 35 GHz will result in about 2 mrad sensor accuracy. Thus, we may assume that

$$K = \sigma_\phi \cdot f \cdot p$$

$$K = 2 \cdot 10^{-3} \cdot 35 \cdot 10^{9} \cdot 15 = 1.05 \cdot 10^{9} \cdot \text{rad} \cdot \text{Hz} \cdot \text{cm} \tag{19}$$

and

$$\sigma_\phi \simeq \frac{1.05 \cdot 10^{6}}{f \cdot p} \quad \text{(in mrad; f in Hz, and P in cm)} \tag{20}$$

This result is shown in the upper-left quadrant of Fig. 9-1, for f = 10.5, 35, 70, and 105 GHz.

OVERALL TRADEOFF ANALYSIS

A possible application of Fig. 1 to an overall tradeoff analysis is illustrated in Fig. 2. Suppose that it is desired to achieve a 0.3 m rms miss distance, and it is assumed that the interceptor will have a 50 msec response time. This design parameter is indicated by point 1 in the lower-left quadrant, and the resultant LOS angle measurement accuracy is ~0.85 mrad. Next, we choose a typical L/D value of 12, thus defining point 2 in the lower-right quadrant. By extending a straight line from point 2 to the upper-right quadrant we find that the missile's corresponding mass is ~75 kg. Point 3 is then defined, in the upper-right quadrant, by the intersection of this line with the L/D = 12 curve. Point 3 also corresponds to an aperture of about 18 cm. The final point (4) in the upper-left quadrant is obtained from points 1 and 3, as shown, and it determines the required carrier frequency. In the case at hand, point 4 defines a carrier frequency which is slightly lower than 70 GHz.

This example illustrates a possible application of this approach. Naturally, one may start at any quadrant and proceed in a similar

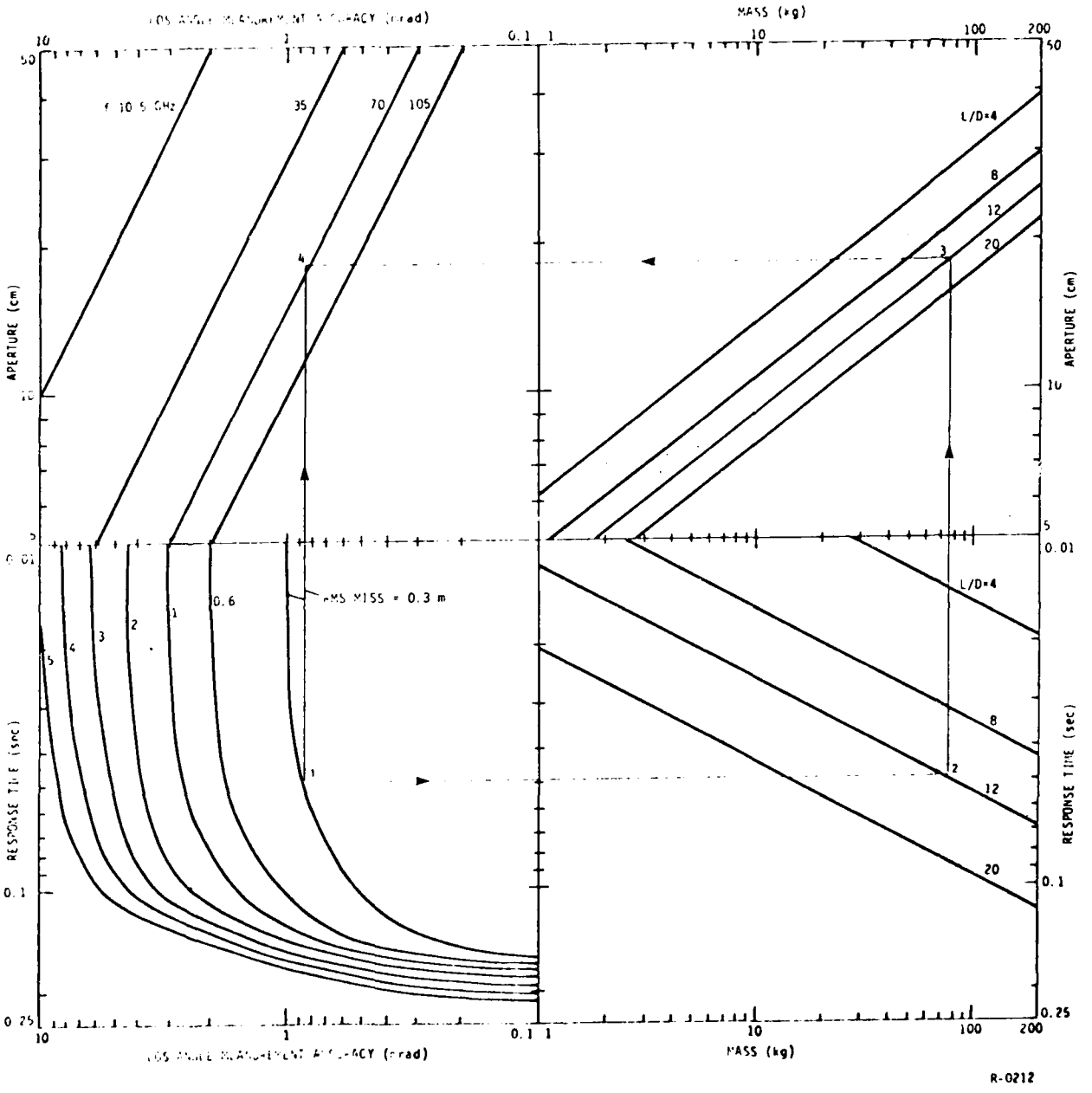


Figure 2. Tradeoff Analysis - A Representative Example.

manner through the remaining three. Note, however, that neither the lower-right nor the upper-right quadrants should be the last ones in such analysis, as both must assume the same L/D.

CONCLUSIONS

In reference [1], a comprehensive statistical technique for analysing the interception performance of a ballistic missile in an NNK engagement was developed. The method employs analytical tools such as Cramer-Rao lower bound and nonlinear covariance analysis of the engagement kinematics. Assuming a specific engagement geometry and guidance law, a sensitivity analysis of the miss distance statistics to various system parameters was performed.

In this paper, the endgame performance analysis has been extended to a more general tradeoff study. This extension addressed the tradeoffs associated with interceptor parameters such as mass, response time, physical dimensions (L/D), active sensor aperture, carrier frequency, and measurement accuracy. The tradeoff curves included:

1. sensor accuracy versus missile response time for several values of equal-miss-distance (rms),

2. interceptor response time versus mass (during homing phase) parametrized by L/D,

3. missile mass versus sensor aperture parametrized by L/D, and

4. sensor aperture versus sensor accuracy parametrized by carrier frequency.

REFERENCES

1. Korn, J., "Endgame Performance Tradeoff Analysis for NNK Interceptors", TR-132, ALPHATECH, Inc., 3 New England Executive Park, Burlington, Massachusetts 01803.

2. Blakelock, J.H., Automatic Control of Aircraft and Missiles, John Wiley and Sons, Inc., 1965.

Next page is blank.

AD P001069

APPLICATIONS OF HEURISTIC AND GAME-THEORETIC PARADIGMS TO FIRE CONTROL

Max Mintz[1] Terry L. Neighbor[2]

Walter Dziwak[3] Stephen S. Wolff[4]

ABSTRACT

This presentation illustrates two diverse applications of heuristic and game-theoretic decision models in air combat and air defense fire control.

Part I. THE DEVELOPMENT OF A REAL-TIME GLOBAL DECISION ALGORITHM FOR MULTIPLE MISSILE THREAT ASSESSMENT, THREAT PRIORITIZATION, AND EVASION: A Look-Up Table Concept Development Study

This look-up table concept development study examines the efficacy of new heuristic algorithms for single and multiple missile evasion. These new techniques are based on anti-proportional navigation (APN) and guidance plane normal (GPN) maneuvering, and exploit the geometric and physical characteristics of generic proportional navigation guidance laws.

Part II. DESIGNING ROBUST PREDICTORS AND FILTERS FOR AAA FIRE CONTROL SYSTEMS

This study addresses two primary questions: (i) the design of robust predictors for continuous state processes based on finite state markov chain approximations; and (ii) the design of robust recursive state estimators which may be subject to complexity constraints. The exposition of each design technique is illustrated with antiaircraft artillery (AAA) fire control system simulation results based on authentic flight test data.

---

[1]Dept. of Systems Engineering, University of Pennsylvania, Philadelphia, PA; and NRC-BRL Research Associate.

[2]Advanced Development Branch, Air Force Flight Dynamics Laboratory, Wright-Patterson AFB, OH.

[3]US Army Armament Research and Development Command, Fire Control and Small Caliber Weapon Systems Laboratory, Dover, NJ.

[4]US Army Armament Research and Development Command, Ballistic Research Laboratory, Aberdeen, MD.

PART I. THE DEVELOPMENT OF A REAL-TIME GLOBAL DECISION ALGORITHM FOR MISSILE THREAT ASSESSMENT, THREAT PRIORITIZATION, AND EVASION: A Look-Up Table Concept Development Study.

Introduction and Summary

Current projections of future air combat environments suggest the importance of developing effective techniques to evade multiple missile threats. Real-time algorithms for threat assessment, threat prioritization, and evasion should:

a). Be hierarchical in structure;

b). Be able to handle at least two simultaneous or closely time-sequenced missile threats;

c). Be able to account for a potential future threat from a second missile while coping with an initial single threat;

d). Generate dynamically acceptable evasion strategies.

This Look-Up Table Concept Development Study is based on an underlying simulation model which was used to investigate the effectiveness and parametric sensitivity of several real-time heuristic algorithms for missile evasion.

Background

The present study is an outgrowth of earlier research [1] performed by Dr. M. Mintz and his colleagues at the University of Pennsylvania. This earlier research demonstrated the potential of four real-time heuristic algorithms for multiple missile evasion. These original heuristic algorithms were based on myopic decision procedures which sought to exploit the geometric and physical characteristics of generic proportional navigation guidance laws by:

i). maximizing the instantaneous absolute value of the aircraft - missile line-of-sight rate, or

ii). introducing a transient into the missile guidance solution by continuously maximizing the absolute value of the projection of the aircraft acceleration normal to the missile's guidance or maneuver plane.

These heuristics are referred to respectively as Anti-proportional Navigation (APN), and Guidance Plane Normal (GPN) maneuvering. One undesirable characteristic of the original version of the GPN heuristic (and to a lesser degree its APN counterpart) was the tendency to generate evasive maneuvers which caused the aircraft to 'thrash', i.e., to command rapid oscillations in the aircraft's roll angle. The occurrence of these rapid oscillations depended on the engagement geometry which, in

the case of multiple missile evasion, could be quite complex. These erratic rolling motions were an artifact of the myopic algorithms and did not contribute to effective missile evasion; the joint aircraft - missile dynamics tended to average out this high frequency behavior.

One of the objectives of this present research effort was to develop effective heuristics for missile evasion based on the APN and GPN concepts. One of the requirements on these heuristics was that erratic rolling motions should not occur. This requirement suggested the investigation of heuristics based on the APN and GPN concepts which were defined by a single high g turn, or by a pair of synergic high g turns. The APN concept applies when the orientation of the aircraft acceleration vector lies in the guidance plane, and the GPN concept applies when the orientation of the aircraft acceleration vector is normal to the guidance plane. These maneuvers are parameterized by:

i). Maneuver Initiation Timing (for the single turn);

ii). Maneuver Initiation and Transition Timing (for dual synergic turns);

iii). Turning Away or Towards the LOS (relevant to the APN concept).

Other Parametric Considerations

In order to develop a maneuver effectiveness and sensitivity data base, the aircraft - missile engagements were further parameterized by:

Engagement Geometry - missile launch range, initial aircraft heading angle (aspect angle), initial missile heading angle,

Airspeeds - target aircraft airspeed, launch aircraft airspeed.

Salient Model Characteristics

Two baseline cases for the missile model were considered:

Case I. A 30 g missile, with a seeker/autopilot/airframe aggregate time constant of 0.4 sec., and a 65 deg. seeker look-angle limit;

Case II. A 15 g missile, with a seeker/autopilot/airframe aggregate time constant of 0.15 sec., and a 45 deg. seeker look-angle limit.

Although two baseline missile cases were considered in this study to address certain parametric sensitivity questions, we emphasize that the Case I baseline model (30 g missile) more closely represents the current and future threat situation.

The baseline aircraft for the study was assumed to have a maximum lateral acceleration capability of 8 g.

Results

The simulation model was exercised over a range of engagement geometries, airspeeds, and maneuver initiation and transition times.

Several Important Conclusions

a). Generally, the APN concept dominated (was as good as or better than) the GPN concept in terms of efficacy for evasion. This is not to say that the GPN concept should be avoided, but rather that, against a single missile threat it was generally found that: either a single APN turn or a pair of synergic APN turns was as good as or better than a single GPN maneuver or a pair of APN - GPN synergic maneuvers. However, in a multiple missile threat environment, the GPN technique provides an additional valuable degree of freedom which should not be ignored.

b). Over a wide range of engagement geometries, a substantial improvement in miss distance can be achieved by using a pair of synergic APN maneuvers as opposed to a single APN turn. We call this idea 'one good turn deserves another.'

c). The preferred direction (away from or towards the LOS) of the APN turns depends on engagement geometry and missile maximum g limit and seeker look-angle limit.

d). The seeker look-angle limit plays an important role in escapes against the "high g" missile at short time-to-go maneuver initiation times.

e). Initial aircraft - missile airspeeds can play a critical role in engagement outcomes.

f). The effectiveness of the APN and GPN maneuvers is not substantially sensitive to the choice of Maneuver Initiation Timing and (in the case of dual synergic turns) Transition Timing. This effective robustness is an important factor in the successful determination of a simplified look-up table method for missile evasion.

A Methodology for Multiple Missile Evasion

In order to blunt the effectiveness of a single missile threat, the combat pilot can clearly benefit from those decision aids which provide effective cues for initiating

and developing evasive maneuvers as a function of engagement geometry. The increased complexity of the multiple missile threat over the single threat environment suggests that the benefits from these decision aids will be even more substantial in this potentially far more critical environment. Next, we outline briefly an approach to the multiple missile evasion problem which can be implemented with a look-up table decision procedure.

The Single Missile Threat Function

Single missile threats (where the missile type is known a priori) will be ordered by the predicted value of a Single Threat Function (STF). The STF could depend on the aircraft - missile Distance of Closest Approach (DCA), as well as the Track Crossing Angle (TCA), and aircraft - missile Heading Angles (HA) at minimum range. (We remark parenthetically that DCA and relative aircraft - missile orientation angles have been incorporated in a vector scoring system which is intended to support the USAF AMRAAM development flight test program .) Since the predicted value of the STF depends on the choice of evasion strategy, the set of admissible strategies can be ordered (ranked) by their STF values. Against a single missile threat, it is reasonable to select an evasion strategy which minimizes the overall STF value.

Multiple Missile Threats

Against a simultaneous threat from two missiles, it is useful to consider the selection of an evasion strategy which minimizes the maximum value of the pair (STF1, STF2), where STFi denotes the value of the missile threat due to missile i, (i=1,2).

Against a current missile threat (say missile 1) and a potential future threat (say missile 2), it may be useful to consider the selection of an evasion strategy which again minimizes the maximum value of the pair (STF1, STF2), where STF2 denotes the threat value of a potential second missile. We remark that a related myopic max-min procedure was exploited successfully in [1] to blunt the effectiveness of a multiple missile threat.

Evasive Maneuvers

The class of evasive maneuvers will be based on those suggested by the APN - GPN concepts decribed heretofore, i.e.,

i). Single high g turns which are oriented approximately in the missile guidance plane, or normal to the guidance plane;

ii). Dual synergic turns which are oriented approximately in the missile guidance plane and/or normal to the guidance plane.

These ideas will apply most readily when the missile velocity vectors and aircraft velocity vector are approximately co-planar.

Decision Making

In the context of the multiple missile environment, we suggest the exploration of:

i). The Look-Up Table Concept, and

ii). Fast Flyout Simulation Techniques

to select an effective evasive maneuver.

In this present study we have focused on developing the look-up table concept against a single missile threat. However, it is very evident that the look-up table method can be applied successfully in the multiple missile environment when the missile threats have approximately co-planar velocity vectors, i.e., both missile velocity vectors lie in the plane defined by the LOS vectors defined by the aircraft and each missile.

The Look-Up Table Concept - A Summary of Results

In the remainder of this section we summarize the salient features and performance of our simplified look-up table decision model exercised against a single missile threat.

The Aircraft and Missile Models

The aircraft simulation model is intended to represent a generic F-16. The aircraft is assumed to have a maximum lateral acceleration capability of 8 g, and a roll rate limit of 300 deg./sec. A complete description of the aircraft simulation model is contained in Section 2 and Appendix A of [2].

The missile simulation model is intended to represent a generic small air-to-air missile, such as the AIM-9L. We have adopted the Case I baseline missile model in this look-up table decision model development. The Case I baseline refers to a generic 30 g missile, with a seeker/autopilot/airframe aggregate time constant of 0.4 sec., and a 65 deg. seeker look-angle limit. A complete description of the missile simulation model is contained in Section 2 and Appendix A of [2].

Nominal Engagement Envelope

In order to study the efficacy of a look-up table approach to missile evasion, we selected a nominal engagement envelope in which we focused our attention. This 'sectorial' approach to look-up table construction provides:

a). sensitivity information which characterizes the 'extent' or 'volume' of the engagement parameter space in which this prototype nominal look-up table is useful, and

b). valuable insight on the details of the structure of suitable simplifying approximations to make the look-up table 'robust' as well as 'simple.'

It should be emphasized that the 'product' to be described in this section is a piece or 'sector' of a 'global' look-up table whose 'remaining details' have been left for further exploration. It is our belief that the piece of the look-up table provided here is both substantial enough and useful enough to justify further efforts in this direction.

The nominal engagement envelope is characterized by the following initial engagement parameters:

Initial Altitudes - The aircraft and missile are initially at a co-altitude of 30 kft.

Initial Airspeeds - The target aircraft and missile launching aircraft have equal initial airspeeds, respectively VAI & VMI, of 1500 fps. (We address the results of varying the initial values, VAI & VMI, in [2].)

Initial Heading Angles - HA are measured with respect to the aircraft - missile LOS. The range of initial aircraft heading angles was 0 - 180 deg. The missile was launched in accordance with the following 'proportional navigation' heading angle algorithm:

$$TMI = \arcsin[(VAI/VMP)*\sin(TAI)]$$

where:

VAI - denotes the initial airspeed of the target aircraft;

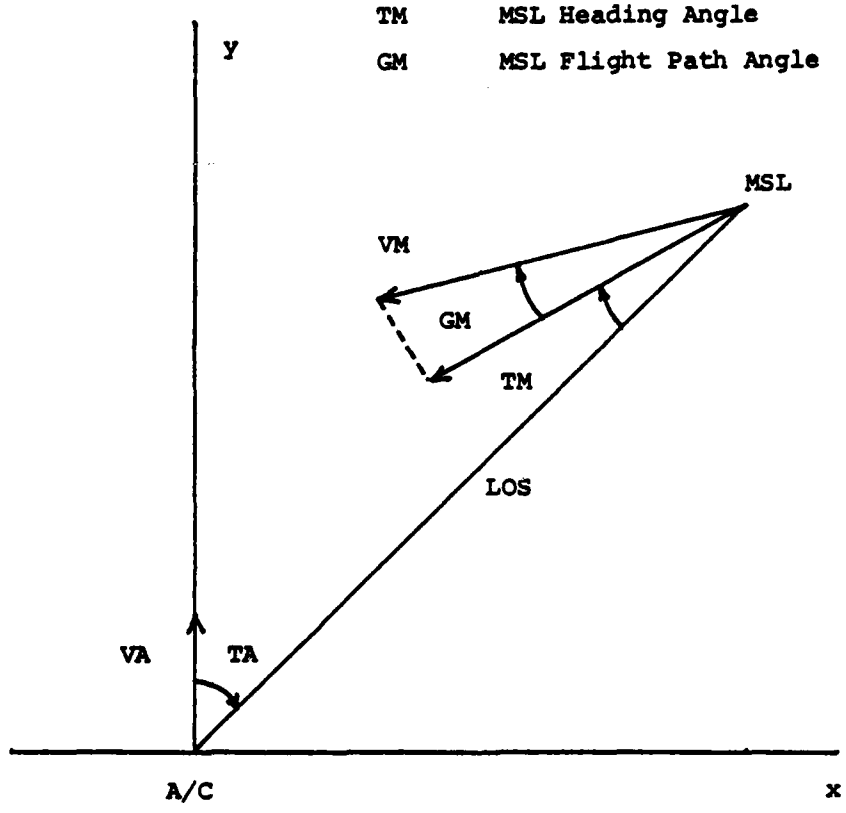
VMP - denotes the peak airspeed of the missile (attained just prior to engine burnout);

TAI - denotes the target aircraft initial heading angle measured with respect to the initial aircraft - missile LOS;

FIGURE 1.1

ENGAGEMENT GEOMETRY

LOS	A/C - MSL Line-of-Sight
VA	A/C Velocity Vector
TA	A/C Heading Angle
VM	MSL Velocity Vector
TM	MSL Heading Angle
GM	MSL Flight Path Angle



TMI - denotes the missile initial heading angle measured with respect to the initial aircraft - missile LOS.

These initial engagement variables are depicted in Figure 1.1. The missile was launched in the guidance plane. Hence, the initial value of the missile flight path angle, GMI, was 0 deg.

Initial Launch Range - The initial launch range RM was assumed to be limited to the interval 15 kft $\leq$ RM $\leq$ 25 kft. (We will address the results of extending RM outside this interval in the sequel.)

Summary of Results

Engagement Envelope Partitioning

In developing a look-up table decision model for the given nominal engagement envelope, it was useful to partition this envelope into four disjoint sets in the Initial Range - Initial Aircraft Heading Angle plane. This partition of the R - HA plane is depicted in Figure 1.2. In the R - HA plane, the nominal engagement envelope is defined by a semi-annular region. With reference to Figure 1.2, we note that the four partition sets, which we refer to as Regions 1-4, are displayed in Table 1.1.

TABLE 1.1

PARTITION OF NOMINAL ENGAGEMENT ENVELOPE IN R - HA PLANE

Region	R(kft)	HA(deg)
1	15 - 25	0 - 45
2	15 - 25	45 - 75
3	15 - 25	75 - 90
4	15 - 25	90 - 180

Evasive Maneuvers

The class of evasive maneuvers adopted in this look-up table study are of two types:

i). A maneuver consisting of a single 6 g APN turn (remember that an APN turn lies in the guidance plane);

ii). A maneuver consisting of a single pair of 8 g dual synergic APN turns.

In what follows, we shall refer to the maneuver consisting of a single turn as a 'Type 1' maneuver, and the maneuver consisting of the dual synergic turns as a 'Type 2' maneuver.

The Type 1 maneuver is parameterized by:

i). the direction of turn - towards or away from the LOS, and

ii) the maneuver initiation time.

The Type 2 maneuver is parameterized by:

i). the initial (first) direction of turn - towards or away from the LOS,

ii). the maneuver initiation time (for this first turn), and

iii). the maneuver transition time -- the time at which the aircraft rolls 180 degrees and executes a reverse turn away from or towards the LOS.

In this simulation study, the maneuver initiation time for both Type 1 and Type 2 maneuvers is measured in terms of simular ellapse time (in seconds) following the missile launch. The maneuver transition time for the initiation of the 180 degree aircraft roll in the Type 2 evasion strategy is measured in terms of time-to-go (TGO). The present value of TGO (expressed in seconds) is determined by the ratio RM/VREL, where RM denotes the current range between the aircraft and missile, and VREL denotes the current magnitude of the difference between the aircraft and missile vector velocities. A discussion of the relation between these two distinctly different time scales appears in Section 3 of [2]. In the sequel we use the abbreviation: MIT - Maneuver Initiation Time, and MTT - Maneuver Transition Time.

Manuever Duration

The Type 1 maneuver level was limited to 6 g, whereas, the Type 2 maneuver level was limited to 8 g. The reason for the g level difference is due to the expected and actual maneuver durations. The Type 1 maneuvers (6 g) could be up to 14 seconds in duration. The Type 2 maneuvers (8 g) were limited to a maximum duration of approximately 6 seconds. The ability of the pilot to withstand high g maneuvers clearly depends on the level and duration of the maneuver.

TABLE 1.2

LOOK-UP TABLE ALGORITHM SUMMARY

Region	Maneuver Type	Turn Direction (Init./Primary)	MIT	MTT	DCA Results
1	2	towards LOS	Fig. 1.4	Fig. 1.5	Fig. 1.3/ Table 1.3
2	2	towards LOS	Fig. 1.4	Fig. 1.5	Fig. 1.3/ Table 1.3
3	2	towards LOS	Fig. 1.4	Fig. 1.5	Fig. 1.3/ Table 1.3
3	1	away from LOS	Immed.	NA	Table 1.4
4	1	away from LOS	Immed.	NA	See Text

FIGURE 1.2

PARTITION OF NOMINAL ENGAGEMENT ENVELOPE
IN R - HA PLANE

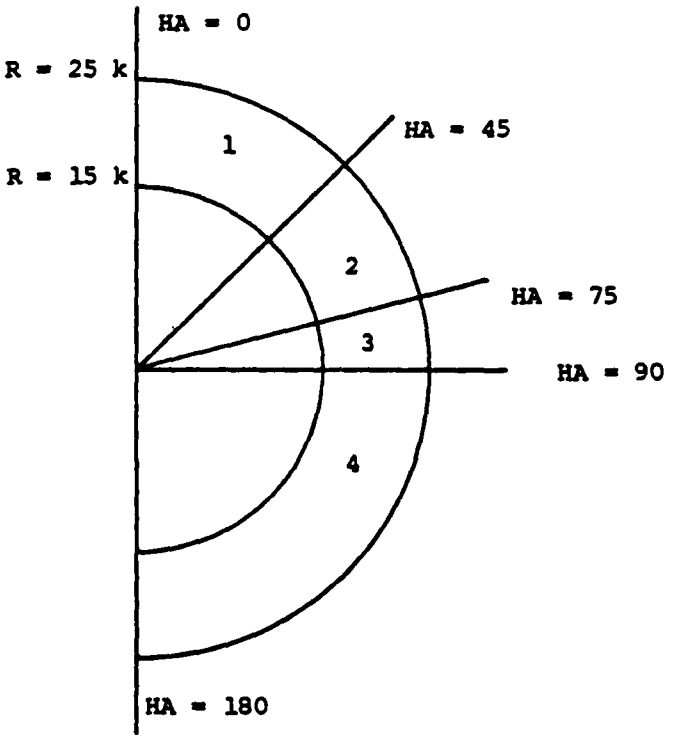


FIGURE 1.3

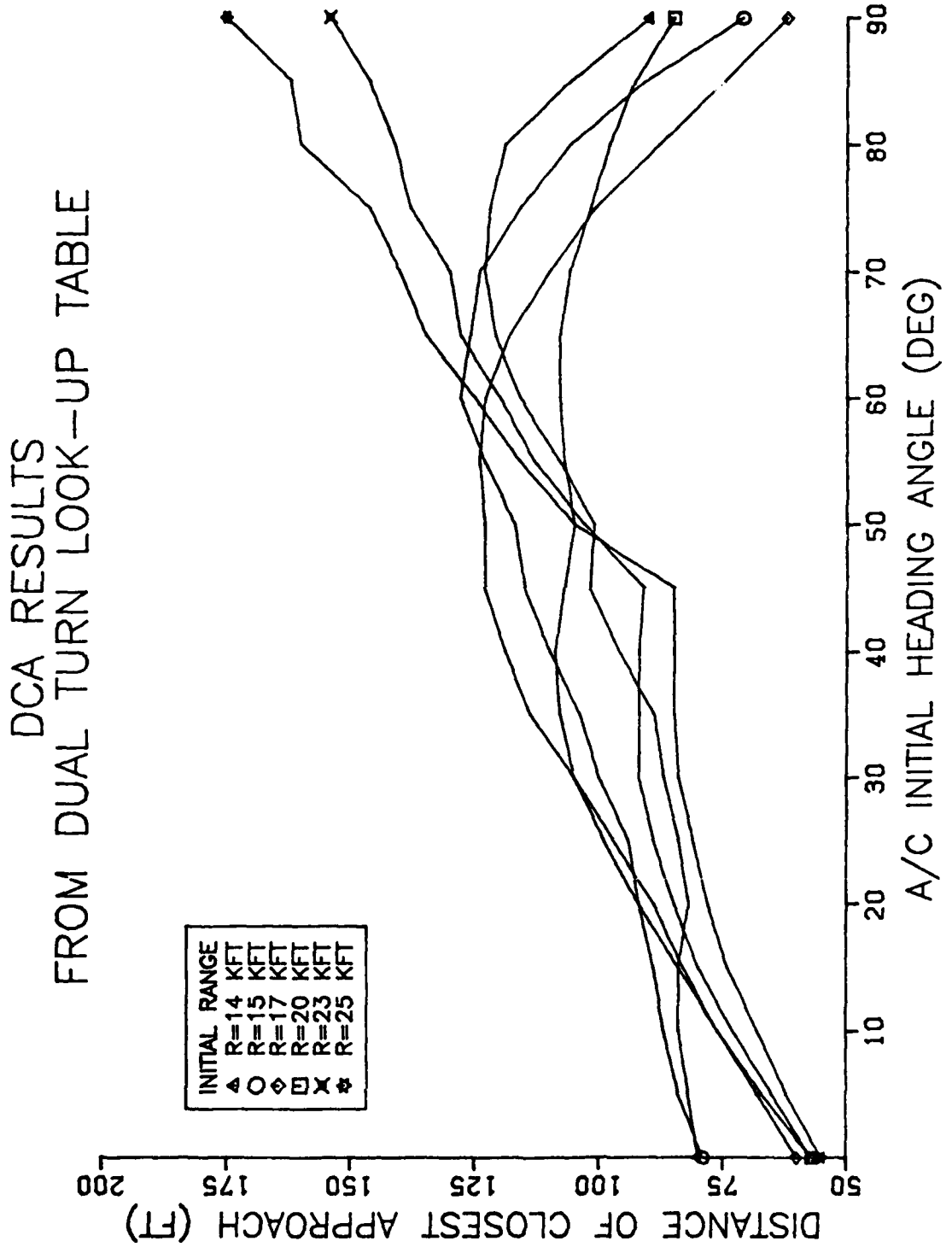

DCA RESULTS
FROM DUAL TURN LOOK-UP TABLE
INITIAL RANGE
R=14 KFT
R=15 KFT
R=17 KFT
R=20 KFT
R=23 KFT
R=25 KFT
DISTANCE OF CLOSEST APPROACH (FT)
50
75
100
125
150
175
200
A/C INITIAL HEADING ANGLE (DEG)
10
20
30
40
50
60
70
80
90

TABLE 1.3

DCA RESULTS
FROM DUAL TURN LOOK-UP TABLE
DISTANCE OF CLOSEST APPROACH (FT)

A/C HA	INITIAL RANGE (KFT)					
	R=14	R=15	R=17	R=20	R=23	R=25
0	80	79	60	57	57	55
5	82	84	68	67	65	62
10	84	87	76	76	73	68
15	84	89	83	84	80	74
20	82	92	89	92	85	78
25	84	94	97	99	89	81
30	87	100	105	105	92	84
35	89	104	114	108	92	85
40	96	110	119	109	92	85
45	102	115	123	107	91	85
50	101	117	123	105	103	105
55	108	123	124	107	113	116
60	116	128	123	108	120	125
65	121	126	118	108	128	135
70	123	124	110	106	130	140
75	122	116	101	102	138	146
80	119	106	88	98	141	160
85	106	91	75	93	146	162
90	90	71	62	85	154	175

TABLE 1.4

DCA RESULTS
FROM SINGLE 6 G APN MANEUVER
DISTANCE OF CLOSEST APPROACH (FT)

A/C HA	INITIAL RANGE (KFT)		
	R=15	R=20	R=25
75	113	4087	7870
80	1053	5103	8347
85	1900	5900	8791
90	2648	6402	9471

FIGURE 1.4

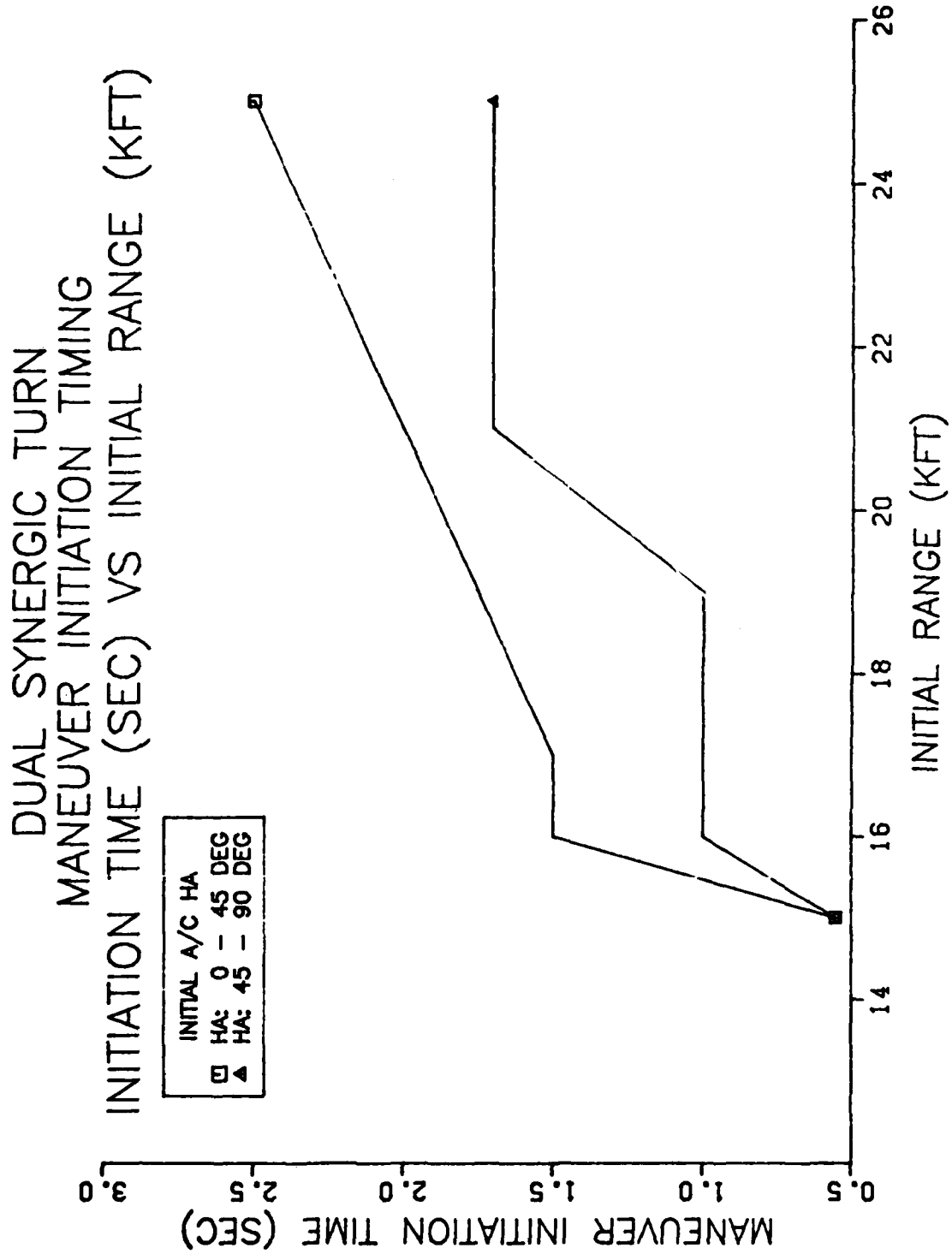
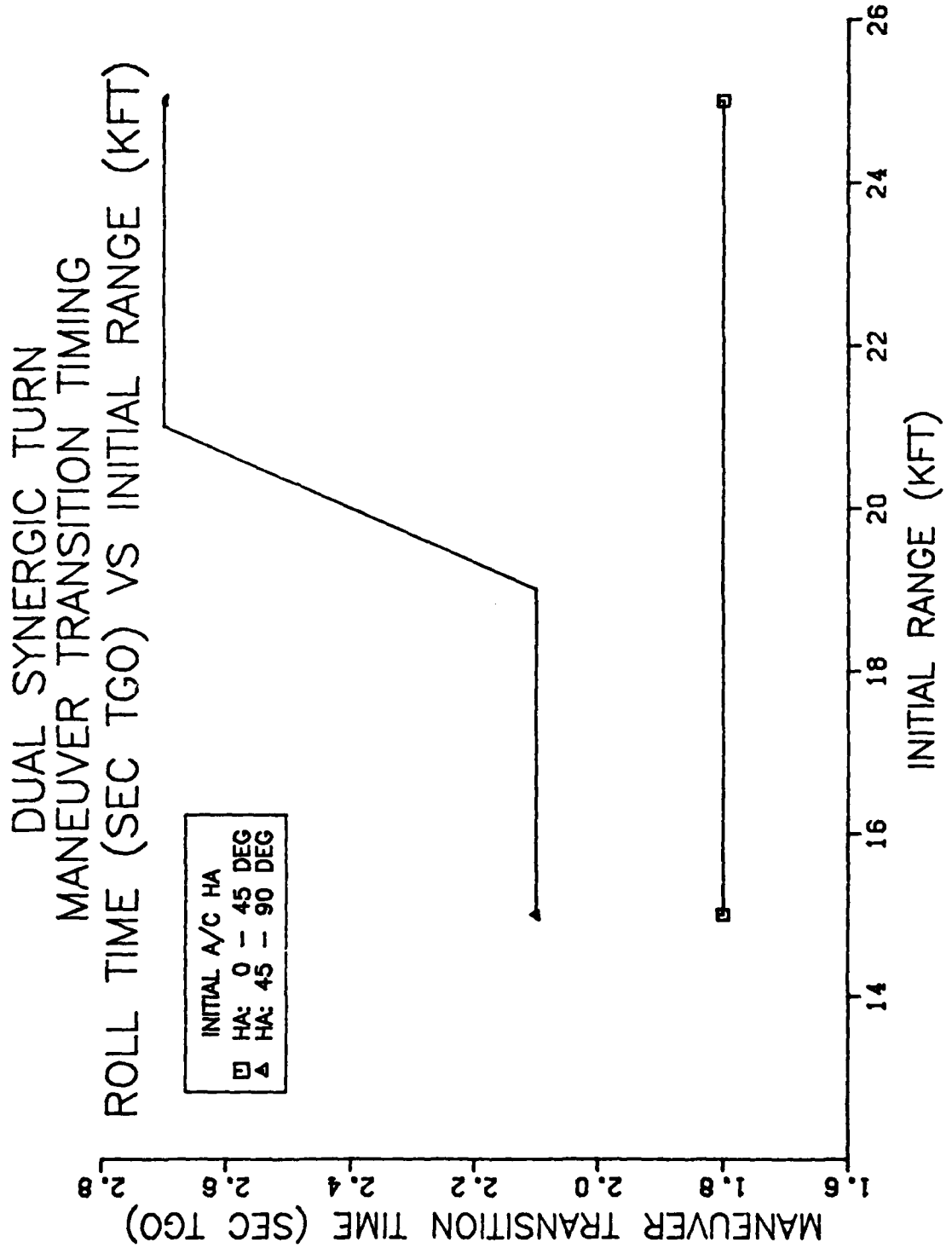

DUAL SYNERGIC TURN
MANEUVER INITIATION TIMING
INITIATION TIME (SEC) VS INITIAL RANGE (KFT)
INITIAL A/C HA
HA: 0 - 45 DEG
HA: 45 - 90 DEG
MANEUVER INITIATION TIME (SEC)
0.5
1.0
1.5
2.0
2.5
3.0
INITIAL RANGE (KFT)
14
16
18
20
22
24
26

FIGURE 1.5


DUAL SYNERGIC TURN
MANEUVER TRANSITION TIMING
ROLL TIME (SEC TGO) VS INITIAL RANGE (KFT)
INITIAL A/C HA
HA: 0 - 45 DEG
HA: 45 - 90 DEG
MANEUVER TRANSITION TIME (SEC TGO)
1.6
1.8
2.0
2.2
2.4
2.6
2.8
INITIAL RANGE (KFT)
14
16
18
20
22
24
26

The Look-Up Table Algorithm

The selection of a specific evasive maneuver strategy depends on the specific values of Initial Range and Initial Aircraft Heading Angle within the nominal engagement envelope. In Regions 1-2, the Type 2 maneuver is the suggested strategy type. In Region 3, both Type 1 and Type 2 maneuvers are suitable. In Region 4, the Type 1 maneuver is the suggested strategy type. In the context of this nominal engagement envelope, the suggested MIT parameter value for the Type 1 maneuver, which is applicable in Regions 3-4, is zero in all cases. This implies an evasive maneuver initiation immediately following the missile launch. As we shall see in the sequel, the DCA for the Type 1 maneuver in both Regions 3 and 4 is quite large, and hence, a nominal delay in the MIT is not critical. As we shall see, this robustness also extends to the MIT and MTT for the Type 2 maneuvers. The DCA results for Regions 1-3 are displayed in Figure 1.3 and Tables 1.3 and 1.4. The results for Region 4 are described in general terms in the text. We summarize the information in this subsection via Table 1.2.

Discussion of Results

a). Results for the Unaware Target

In order to judge the efficacy of this look-up table decision model (or any other evasive maneuver decision model), one must first establish the so-called Missile Launch Envelope (MLE) for the non-maneuvering or unaware target. An analysis of this simulation model which incorporates the Case I baseline (30 g) missile, has established that, in the context of the nominal engagement envelope, the non-maneuvering MLE includes all of Regions 1-2, and the bulk of Region 3. The approximate outer MLE boundary in Region 3 is delineated by a smooth curve in the R - HA plane connecting the (R, HA) points: (25 k, 80), (23 k, 85), and (20 k, 90). This same analysis also indicates that the bulk of Region 4 lies outside the non-maneuvering MLE. We shall therefore exclude Region 4 from further discussion, since it represents, for the most part, a region of 'out-of-bounds' launches.

b). Engagement Geometry and Maneuver Selection

Based on the DCA results as displayed in Figure 1.3 and Tables 1.3 - 1.4, it is evident that a successful choice of maneuver type and its associated parameter values are influenced by the engagement geometry. The results for Region 3 include both maneuver Types 1 and 2. A detailed study of the simulation output reveals that there is a very basic difference between the modalities of evasion associated with the Type 1 and Type 2 maneuvers in Region 3. Briefly stated, the evasion

modalities characterized by the Type 1 maneuver are based on the aircraft's ability to 'outrun' the missile in a 6 g single turn 'tail-chase' situation. In contrast, the evasion modalities characterized by the Type 2 maneuver are based on the aircraft's ability to 'out turn' the missile and exploit the missile's seeker look-angle limit in a 8 g dual turn 'head-chase' situation. We discuss these modalities, as well as others, in comprehensive detail in Section 3 of [2].

c). Robustness

The results of this study indicate that the choice of simplified MIT and MTT functions, which depend on Initial Range and Initial Aircraft Heading Angle, are not particularly sensitive in their R - HA structural characteristics. This is a very desirable result, if one envisions the eventual implementation of this look-up table concept in actual avionics. We have displayed the results of using this look-up table decision model, determined on the basis of the nominal engagement envelope, in a portion of the R - HA plane which lies outside the nominal engagement envelope. Namely, we have displayed the results for R = 14 kft with HA: 0 - 90 degrees, in Figure 1.3 and Table 1.3. These sensitivity results are quite encouraging. We have also examined the effect of altering the initial airspeeds of both the aircraft and missile. Briefly stated, the effect of initial airspeed is quite important. It was found, for example, that equal initial airspeeds, or an advantage in initial airspeed, generally favored the aircraft. We discuss these and other sensitivity results in Section 3 of [2].

d). Multiple Missile Evasion

While no totally comprehensive conclusions will be made here concerning the efficacy of this look-up table concept for multiple missile evasion, we must cite the following:

The current results provide an immediate possibility to evaluate certain multiple missile threats. For example, by referring to Figure 1.3 and Table 1.3, we see that an approximately co-planar multiple missile threat from approximately equal initial ranges, with different initial heading angles in Region 1, can be defeated by the indicated Type 2 maneuver. A similar statement holds for an approximately co-planar multiple missile threat from approximately equal initial ranges -- with different initial heading angles in the union of Regions 2 and 3. This multiple missile threat can also be defeated by the indicated Type 2 maneuver.

e). Concluding Remarks

All of these results are quite encouraging, and suggest worthwile directions for further research. We remind the

reader that the technqiues described in this section are not optimal in any specific sense, and that the focus in this study has been on the development of simplified robust techniques which lead to satisfactory results.

References

[1] Sheketoff, M. S., Huling, S. F., and Mintz, M., "A Simulation Study of Four Real-Time Heuristic Algorithms For Multiple Missile Evasion: A Game Theoretic Approach," Final Report on AFOSR Grant No. 77-3327, and CSDL Contract No. DL-H-139457, University of Pennsylvania, Philadelphia, PA, June 1979.

[2] Hudson, B., and Mintz, M., "DEVELOPMENT OF A REAL-TIME GLOBAL DECISION ALGORITHM FOR MISSILE THREAT ASSESSMENT, THREAT PRIORITIZATION, AND EVASION: Phase I -- A Look-Up Table Concept Development Study," Final Report submitted to USAF Flight Dynamics Laboratory on Contract No. F33615-81-K-3616, University of Pennsylvania, Philadelphia, PA, January 1982.

Part II. DESIGNING ROBUST PREDICTORS AND FILTERS FOR AAA FIRE CONTROL SYSTEMS

SUMMARY

Robust Prediction Via Finite State Markov Chain Approximations

Background

Time series predictors based on nominal autoregressive (AR) models may exhibit severe dichotomous behavior when operating on clean (noiseless) data versus data contaminated with additive noise. The degradation in predictor performance may be severe enough to warrant a reconsideration of the applicability of a nominal AR model. Here, a nominal AR model refers to a model obtained by a standard least squares identification procedure employed in conjunction with the usual goodness-of-fit tests [1,2,3]. The need to exercise caution when using least squares procedures to fit models to data has been well-documented in the literature. In particular, we cite [4] as an excellent collection of papers which examine robust statistical methods with attention to both theory and applications. Our motivation for and approach to the determination of robust procedures for time series prediction differs intrinsically from robustness studies which address: (i) departures from distributional assumptions, (ii) outliers, (iii) sample censoring, and (iv) large sample requirements. Our approach is probably best described by the terminology "model robustfication" [5]. Here, we focus on the delineation of a suitable class of models to represent the stochastic behavior of an uncertain dynamic system. We select a candidate class of models based on the performance of the underlying predictors which can be constructed on the basis of this given class. In this study, we consider prediction performance in the context of noisy data, where we make no a priori distributional assumptions about the clean data which we use to generate the model, nor about the additive observation (or filtration) noise which we must be able to cope with in virtually all applications. Our performance criterion is taken to be average hit probability, which is a natural measure of predictor performance in fire control applications.

Previous Research

In a previous study [6] we examined clean kinematic data from eleven attack profiles flown by A-7E aircraft during weapon delivery flight tests. A principal outcome of this study was the delineation of enhanced algorithms for prediction and filtering based on high-order AR models. This enhancement was gauged against a typical benchmark predictor/filter based on a first-order AR model of target acceleration. A central conclusion of this study was the recognition that high-order AR models could provide substantial improvements in average hit probability against evasive targets. The

choice of AR model adopted in this study was however, not the nominal AR model suggested by the clean data, but rather, a modified model which resulted from adjusting the overall predictor bandwidth and damping. The important point to emphasize here is that, in a noiseless environment, a predictor based on a nominal high-order AR model achieved excellent average hit probability against all eleven flight paths, and further, the specific choice of flight path which generated the nominal AR model did not appreciably affect the results. This latter result is consistent with the observation that the thirty-three acceleration-dot data sets exhibited very similar AR(5) spectra. The extreme sensitivity of the nominal predictor to additive filtration noise is explained by adopting a dynamic systems perspective and recognizing that the filtration noise effectively excited the dominant underdamped natural modes which characterize the predictor as a dynamic system, thus obscuring the desired predictions based on the true state of the target. The spectrum of the prediction noise contains significant energy in a range of frequencies which are equal to the reciprocal of the times-of-flight of the projectiles over the effective range of the gun system. If the prediction noise spectrum had relatively little energy content in this critical frequency range, i.e., it was characterized by a "notched" spectrum with spectral energy distributed above or below this critical region, the effect of the prediction noise would have tended to either average out or be less consequential due to its relatively slow growth.

The process of adjusting the bandwidth and damping characteristics of the nominal AR predictors to achieve good prediction in the presence of noise, required a degree of numerical experimentation [6]. This situation suggested that an alternative class of models should be sought to provide enhanced prediction capability in the presence of noise, with the added proviso that the resulting predictors be obtained with little or no reliance on numerical experimentation. Motivated by an extensive examination of this flight test data base resolved in aerodynamic coordinates (i.e., aircraft normal acceleration, tangential acceleration, etc.), we decided to investigate the suitability of finite state markov chain approximations to the acceleration-dot data resolved in a Cartesian coordinate system. The results of our preliminary investigation are reported in [7]. A primary outcome of this research is the demonstration that a finite state markov chain approximation to the acceleration-dot data in the flight test data base described in [6] leads to a robust predictor, i.e., a predictor which achieves high average hit probability in the presence of noise and performs well against each of the eleven evasive attack profiles in the data base. These results were obtained by first quantizing the acceleration-dot data to five equally spaced levels (a naive state assignment algorithm), and finally estimating the state transition matrices based on the method

of maximum likelihood [8]. Our prediction algorithm was defined by the evolution of the conditional mean of these numerically valued states. With the exception of the decision to use five levels of quantization, the method leading to the robust predictor is basically algorithmic and does not require numerical tuning. In carrying out these procedures, we found that: the thirty-three estimated state transition matrices are numerically rather similar, and the predictor performance was not sensitive to the choice of the specific flight path data which was used to generate the predictor (state transition matrix). Reference [7] also includes a game-theoretic technique for making a robust choice of state transition matrix, when the process is assumed to be described by a transition matrix which belongs to a known set of stochastic matrices.

Further Results

(i) These foregoing concepts and techniques are applied to other target data bases.

(ii) The impact of signal to noise ratio on robust predictor performance is examined. It is already evident from [7] that there is a definite threshold effect, since the robust markov chain approximations do not outperform the nominal AR models in a noiseless environment. This result is expected due to quantization effects.

Robust Recursive State Estimation

Our previous game-theoretic research [6, Section 3-D] has led to the delineation of recursive filters, which are resistant to the uncertainties in the AR dynamics of the underlying target truth models. Recently, these game-theoretic techniques have been extended in [9] to embrace the problem of robust recursive state estimation in the context of the uncertainty class of: linear, m^{th}-order, time-varying, discrete-time systems with uncertain dynamics; uncertain initial state covariance; and uncertain nonstationary input and observation noise covariance. The results in [6,9] indicate that a linear robust filter can always be realized recursively. However, based on the intrinsic aspects of the problem, the resulting robust procedure could have a state vector with dimension considerably greater than m, the dimension of the uncertain system. In this present paper, we examine techniques for approximating this globally robust procedure with a recursive decision rule, which is subject to a complexity constraint with respect to its dimension. These ideas and design techniques are illustrated with flight test data.

References

[1] Anderson, T. W., The Statistical Analysis of Time Series, New York: John Wiley & Sons, Inc., 1971.

[2] Box, George E. P., and Jenkins, Gwilym M., Time Series Analysis: Forecasting and Control, revised edition, San Francisco: Holden-Day, Inc., 1976.

[3] Kashyap, R. L., and Rao, A. Ramachandra, Dynamic Stochastic Models from Empirical Data, New York: Academic Press, Inc., 1976.

[4] Launer, Robert L., and Wilkinson, Graham N., Editors, Robustness in Statistics, New York: Academic Press, Inc., 1979.

[5] Box, George E. P., "Robustness in the Strategy of Scientific Model Building," appearing in: Robustness in Statistics, New York: Academic Press, Inc., 1979.

[6] Huling, S. F., and Mintz, M. "ENHANCED FILTERING & PREDICTION FOR AAA FIRE CONTROL: An Application of Game Theory and Time Series Analysis," Final Report on Contract Number DAAK10-78-C-1086, submitted to US Army ARRADCOM, May 1980. Published as Contractor Report ARSCD-CR-80015, AD-E400 507, November 1980.

[7] Pate, E. B., Mintz, M., Dziwak, W., and Goodman, S. A., "On Designing Robust Predictors Based on Finite State Markov Chains: A Game-Theoretic Approach," Proceedings of the Nineteenth Annual Allerton Conference On Communications, Control and Computing. University of Illinois, Urbana, IL, October 1981, pp. 688-696.

[8] Anderson, T. W., and Goodman, L. A., "Statistical Inference About Markov Chains," Annals of Mathematical Statistics, Vol. 28, 1957, pp. 89-110.

[9] Martin, C. J., and Mintz, M., "Robust Filtering and Prediction for Linear Systems with Uncertain Dynamics: A Game-Theoretic Approach". To appear in the Proceedings of the 21st IEEE Conference on Decision and Control, December 1982. Submitted for publication in the IEEE Transactions on Automatic Control.

AD P001070

APPLICATION OF MODERN CONTROL THEORY AND ADAPTIVE CONTROL CONCEPTS TO THE GUIDANCE AND CONTROL OF A TERMINALLY GUIDED ANTI-TANK WEAPON

R. D. Ehrich
Missile Systems Division
Rockwell International
Columbus, Ohio

INTRODUCTION AND SUMMARY

The advent of the microprocessor makes feasible the implementation of more complex guidance and control algorithms than were possible with analog autopilots. The purpose of this study was to demonstrate the increase in system performance possible through the application of such laws to an existing weapon system while requiring no changes to the airframe, sensor complement, actuation system, or rocket motor. The goal is to have the performance of the resulting system limited only by physical plant constraints such as seeker rate capability, gimbal limits, maximum fin deflection, total impulse of rocket motor, or structural strength. For this study, advanced control concepts were applied to four aspects of guidance and control: terminal guidance for large initial offsets, trajectory control for maximizing the vertical impact angle, airframe stabilization and actuator control. The weapon system considered was the laser-guided HELLFIRE missile, although the design concepts are applicable to other systems. The performance of the modern control system design is significantly different from that of HELLFIRE and therefore does not reveal its performance.

The general approach taken was to apply appropriate optimal control principles to a linearized system model. The resulting control law, as a function of system states, was then simplified and mechanized using a combination of measurement data and estimated states. To provide these state estimates, an estimation algorithm was developed using available sensors and apriori knowledge of vehicle mass, thrust, aerodynamics and launch platform constraints. The outputs are esimtates of missile speed, dynamic pressure, the altitude increment from launch, current and initial range and time-to-go until impact. The resulting control algorithms were integrated into a flight control system which was simulated in six degrees of freedom. Actuator adaptive control concepts were verified with a breadboard digital autopilot and actuator hardware. Duty cycle estimates for a digital processor were computed and found to be well within the capability of a low-cost, moderate speed, 16-bit microprocessor of the Zilog Z-8002 or Intel 8086 class. Performance in terms of stability criteria, off-boresight capability and impact angle are generally greater than a factor of two better than a system with conventional guidance implemented with an analog autopilot. The producibility of the actuator system was also increased by a reduction in the required bandwidth along with a reduction in its sensitivity to parameter and load variations.

SYSTEM DEFINITION

The HELLFIRE weapon system includes a laser-guided missile which is launched from a helicopter against ground targets, principally tanks. The seeker is of the semi-active type, tracking laser energy reflected from the target. The laser designator can be located in the launch helicopter, a scout helicopter, or mounted on a tripod on the ground. The major subsystems include the seeker, autopilot, attitude gyros, actuator and control surfaces and rocket motor. The configuration is shown graphically in Figure 1.

The all boost rocket motor burns for approximately 2.5 seconds at a relatively constant thrust level. The seeker is momentum stabilized with a two axis gimbal structure. Inertial line-of-sight (LOS) rates are generated for guidance purposes. The seeker gimbal angles are also available to the autopilot. Control of missile rotational motion is made possible by small control surfaces or fins which are moved by a pneumatic actuation system. The control fluid is compressed gas stored in a spherical bottle or pneumatic accumulator. A regulator drops the pressure to the desired level to move the pistons in the actuator. The guidance section contains autopilot electronics, two attitude gyros and a thermal battery. Each attitude gyro has two axes of information.

A number of the subsystem characteristics and operating limits affect or limit the performance of the system. For example, the control surfaces or fins are limited to +20 degrees. This limits the speed of response of vehicle rotational motion and maneuvering accelerations. Similar mechanical motion limits exist for the gyros and seeker. Addition limitations include the maximum torque and rate capabilities of the actuator, the maximum LOS rate of the seeker, and the noise characteristics of the seeker and gyros.

One objective of the study, as previously stated, is to have system performance constrained only by these component limitations and not by deficiencies in the control algorithms. One benefit of knowledge of the above limits and constraints on the system initial conditions is that many system states can easily be estimated or at least bounded. Limits on initial conditions, for example, are related to the launch aircraft flight envelope. Helicopters operate at relatively low altitude (less than 10,000 feet) and at speeds less than 150 to 200 knots. This altitude range represents a small spread of air densities. The effect of variations in launch velocity on the missile velocity profile is also minor. The following design approach takes advantage of these limits on subsystems and initial conditions.

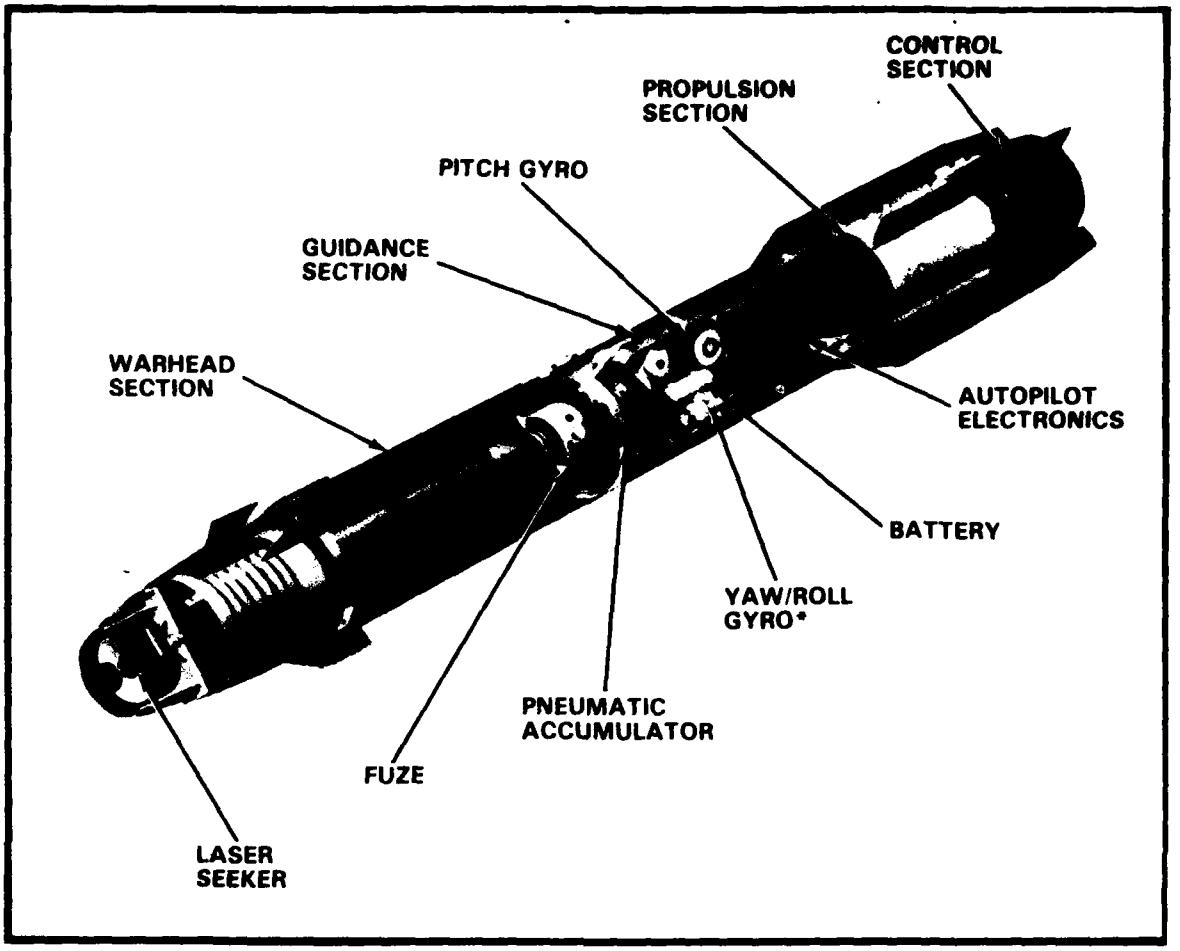


Figure 1. HELLFIRE Missile Configuration

ADAPTIVE AND MODERN CONTROL DESIGN

DESIGN APPROACH

The basic design approach applied to each of the four guidance and control functions consists of the following steps:

(1) establish requirements

(2) define and model system (use linear models where possible)

(3) select appropriate control strategy (and cost function)

(4) identify system states and parameters to be measured or estimated

(5) develop suboptimal law with estimated and measured states

(6) use non-linear simulation to "tune" and evaluate resultant control algorithms with respect to requirements and cost function.

The system model is typically defined in terms of system equations, transfer functions, non-linearities, and time variable functions. In addition, it is valuable to evaluate the expected value (μ) and uncertainty or variability (σ) for each significant parameter, system state or error source. Reducing the system to a linear model or to essential non-linearities is often useful in obtaining insight into the problem. This will also aid in the next step of applying optimal control principles such as the Pontryagin maximum principle. The selection of weighting factors for the cost functional involves some skill and trial and error. The resulting control law may require the identification of system states which are not directly measurable. The use of optimal estimation techniques such as Kalman filtering are available to obtain estimates of these states. Even if a full Kalman filter is not required, as was the case in this study, the basic concepts were employed. This involves identifying the process and measurement uncertainties or variances and the propagation of these errors in the estimates of system states. An error analysis based on covariance techniques is appropriate for this purpose. A suboptimal control law with estimated and measured states is then developed and evaluated. In this study is was discovered that optimal trajectory control for maximum impact angle also increased the observability of some states to be estimated. Therefore, the control and estimation problems are by no means independent. The use of a detailed, non-linear simulation of the total system is invaluable in both evaluating system performance, and in "tuning" the control law for optimum performance.

It was the conclusion of this study that modern control theory plus simple linear models can provide valuable insight for control law formulation and suboptimal implementations. It was also found that even without sophisticated implementation, the concepts of optimal estimation can provide a basis for the generation of state estimates from limited measurements and apriori knowledge of the system states, plant and measurement errors and initial conditions.

The following sections describe in some detail the application of these concepts to various guidance and control functions of the HELLFIRE missile. These functions are:

(1) terminal guidance

(2) trajectory control

(3) airframe stabilization

(4) actuator control

(5) state estimation

The objective of the terminal guidance study phase was to improve short range performance, particularly with large initial pointing errors. The resulting control law required the estimation of time-to-go before impact ($\hat{T_{GO}}$) for maximum performance. The objective of trajectory control was to maximize the vertical impact angle in order to improve the probability of kill of the warhead against armored targets. The derived control law has three distinct phases: climb, hold maximum altitude, and dive. The altitude hold phase is necessary due to the increasing probability of seeker loss of lock with increasing altitude under conditions of cloud cover. The mechanization of this law requires estimates of $\hat{T_{GO}}$ as well as the missiles altitude ($\hat{h}$) above the launch point. The generation of these state estimates yielded estimates of missile velocity ($\hat{V_m}$) and dynamic pressure ($\hat{q_o}$) as intermediate results. Under the airframe stabilization study phase, the stability and steady state error characteristics of the weapons three attitude control loops were improved dramatically using $\hat{V_m}$ and $\hat{q_o}$. The objective of the actuator control phase was to improve the producibility of the mechanical unit by reducing bandwidth requirements. A secondary objective was to improve uniformity of response. The unit is typically extremely nonlinear, with significant sensitivity to load (H_δ), direction of fin deflection (δ), solenoid supply voltage (V_D), and the pressure of the gas supply (P_S). Both measurements (δ,V_D) and parameter estimates ($\hat{H_\delta}$) were employed in the control law for the pulse width modulation commands. Finally, the state estimation algorithm is described. Currently, this is a straight forward integration of the state equations followed by a least squares filtering of raw range estimates. A Kalman filter is also under consideration.

TERMINAL GUIDANCE

Performance improvements for launches with large offsets were made possible by acknowledging the presence of a large axial missile acceleration for the first seconds of flight. Using linear optimal control theory, it was shown [Reference (1)] that a performance index was minimized by a control law of the form:

$$\dot{\theta}_C = K_{NAV}\,\dot{\lambda}_q + K_2(\dot{V}_m/V_m)\,\theta_g$$

The performance index was a weighted sum of terminal accuracy and control energy. For constant missile velocity, i.e., $\dot{V}_m = 0$, the law reduces to proportional navigation with navigation gain, K_{NAV}. The second term is a pursuit-type guidance, since it points the weapon directly at the target. Although $\dot{V}_m$ and V_m are available from the estimator, it was found through simulation that a simple linear approximation to $(\dot{V}_m/V_m)$ minimized miss distance. The chosen gain characteristic equals:

$$K_2(\dot{V}_m/V_m) = \begin{cases} 12(1 - t/t_{bo}) \text{ degrees/second} & \text{for } t \le t_{bo} \text{ seconds} \\ 0 & \text{for } t > t_{bo} \text{ seconds} \end{cases}$$

The large initial gain requires a lag compensator with corner frequencies of 2 and 10 radians/seconds to avoid instability. The maximum offset achievable was further increased by replacing " θ_g" in the law by:

$$\theta_g + (1 - t/\hat{T_f}) \dot{\lambda} q$$

where $\hat{T_f}$ = estimated time of flight = $t + \hat{T_{GO}}$

$\hat{T_{GO}}$ = estimated time to go before impact

This yields a temporary increase in the effective navigation gain which is phased out at impact. The resulting performance at launch ranges between 100 and 500 meters is shown in Figure 2. Even for zero yaw offset, the suboptimal law is superior to proportional navigation. The off-boresight capability is limited primarily by fin deflection and seeker gimbal freedom. The performance boundaries indicate comparable performance whether the initial range is estimated or known exactly.

An additional adaptive strategy was applied to the so-called "guidance filter" of the system. The purpose of the filter is two-fold. First it cancels the flight path pole or maneuvering time constant of the weapon with a first order lead. Second, it attenuates noise components of the seeker line-of-sight rate output with a second order lag. The adaptive feature relates to the fact that the flight path time constant of the vehicle is a function of missile speed. The corner frequency (ω_{fp}), in the absence of thrust, equals:

$$\omega_{f_p} = \left(\frac{q_o S_\pi}{m V_m}\right) C_{N_\alpha}(M_n, \alpha')$$

where q_o = dynamic pressure (lb/ft^2)

S_π = reference area (ft^2)

m = mass (slugs)

$C_{N_\alpha}(M_n, \alpha')$ = normal force coefficient (per radian)

V_m = missile speed (ft/sec)

This can be easily derived from the aerodynamic normal force equations. For transonic flight, the normal force coefficient ($C_{N\alpha}$) is relatively independent of Mach (M_n) and total angle-of-attack (α'). Since the mass is constant, and estimates of speed and dynamic pressure are available from the Estimation Algorithm, a reasonably accurate estimate of ω_{fp} can be derived. This value is used for the guidance filter lead network. Since dynamic pressure is proportional to velocity squared, the flight path pole is roughly proportional to velocity.

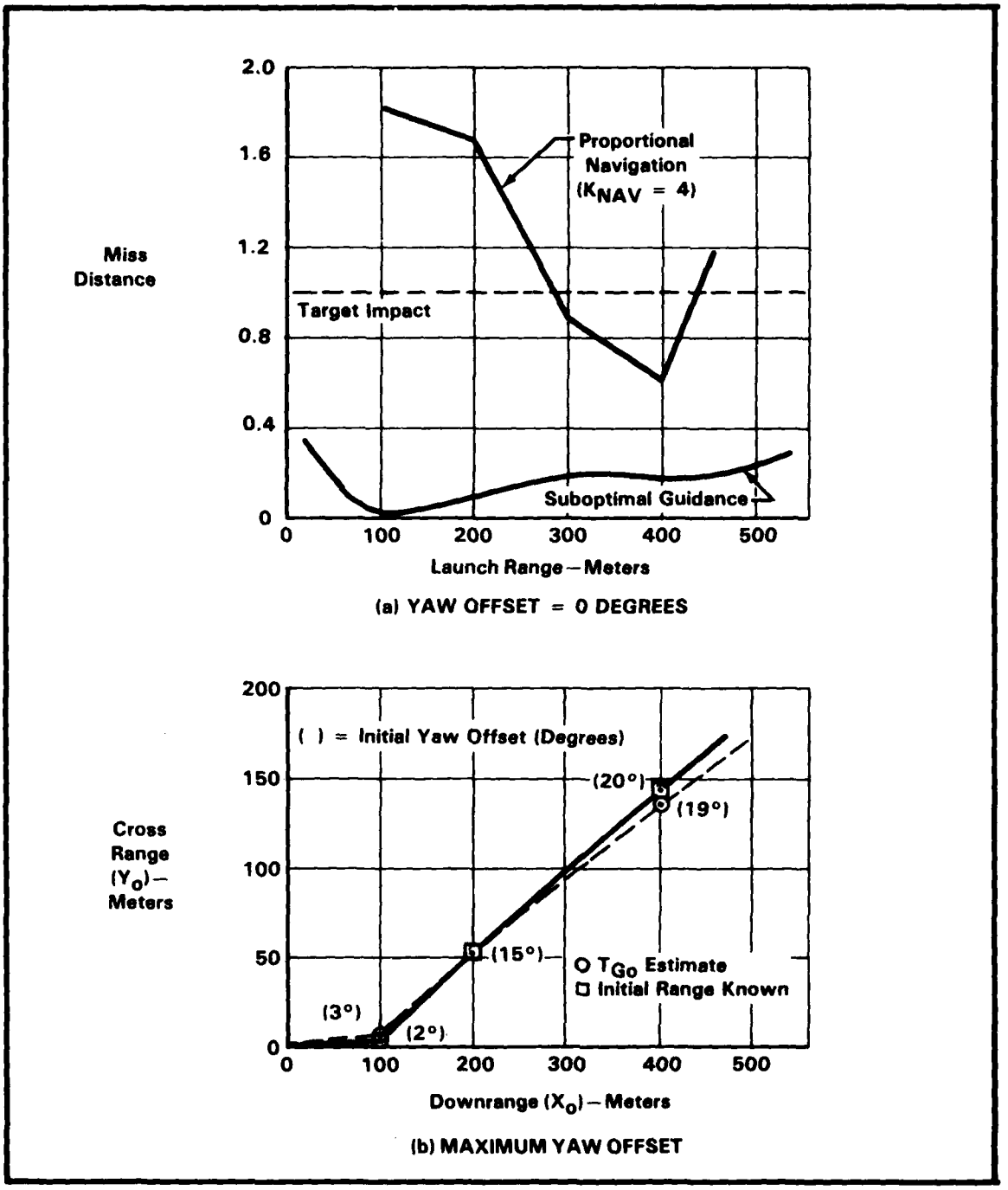


Figure 2. Short Range Performance Characteristics

For a terminal speed range of Mach 0.4 to 1.2, a constant guidance filter lead would have an error of 150 to 300 percent. For the adaptive system, this error is determined by the error in the velocity estimate, which is less than 20 percent (1σ). By making the guidance filter lag frequency proportional to the lead frequency, the noise gain of the filter is held to a constant value. The primary result of this adaptive guidance filter on system performance is improved terminal accuracy at long ranges and against maneuvering targets.

TRAJECTORY CONTROL

The probability of kill for typical warheads used against armored vehicles increases quickly for impact angles above 10 degrees from the horizontal. Achieving these angles through the use of a constant rate bias has several drawbacks. The impact angle is roughly proportional to time of flight. A bias suitable for short ranges must be relatively large, which yields high gimbal angles and high altitudes when used at long ranges. A bias chosen for long range flights will generate shallow impacts at short ranges. It is important to limit the altitude for laser guided weapons to avoid loss of lock by flight above clouds. Additional constraints are the seeker gimbal freedom and finite vehicle maneuverability.

Investigation of the optimal control law for a constant velocity system, subject to these constraints, yields a control law with three distinct phases: climb, hold altitude, and terminal. The switching times between phases are functions of initial range, maximum allowable altitude (h_m), and maximum weapon maneuverability ($\dot{\gamma}_{max}$). For the practical case of an accelerating weapon, a suboptimal control law is shown in Table 1. The estimates of altitude ($\hat{h}$), speed ($\hat{V_m}$), and time-to-go ($\hat{T_{GO}}$) are provided from the Estimation Algorithm. The gimbal angle commands used in the first two phases are applied to the gimbal angle control loop defined in the previous section. However, a fixed gain of 4.0 radians/second is used in the pitch channel, unless the estimated time of flight ($\hat{T_f}$) is less than motor burn-out. During each phase, the body rate commands ($\dot{\theta}_c$) are limited to 40 degrees/second to avoid excessive angles-of-attack. This corresponds to the maneuverability limits of $\pm \dot{\gamma}_{max}$ for the constant velocity model.

The terminal phase employs proportional navigation [$4G(S)\dot{\lambda}_q$], a pursuit term [$f(\theta_g)$] previously defined, plus a gravity compensation term which is a function of estimated speed ($\hat{V_m}$). The simulated vertical trajectory is shown in Figure 3 for a long range launch (Rx) and commanded cruise altitude (h_m) of 600 feet. The trajectory parameters from the Estimation Algorithm are also plotted, with a maximum altitude error of 50 feet before the terminal dive. The switch from the "hold altitude" phase to the terminal dive occurs at a nominal value (T_{SW}) of 3.5 seconds before impact. The terminal flight path angle (γ_f) is 21 degrees, and the miss distance is 150 millimeters. As expected, the impact angle is roughly proportional to cruise altitude (Figure 4). Cruise altitude selection involves factors such as seeker sensitivity and

Table 1. Control Law for Maximum Impact Angle

CLIMB PHASE

$(\hat{h} < h_m,\ \hat{T}_{Go} > T_{Sw})$

$\theta_{gc} = -20$ Degrees, $\dot{\theta}_{Max} = \pm 40$ Deg/Sec

HOLD ALTITUDE PHASE

$(\hat{h} \geq (h_m - h^*),$ Latched, $\hat{T}_{Go} > T_{Sw})$

(A) Hold h: $(|\theta_g| < 20°)$

$$\dot{\theta}_c = K_H\, G(s) \left[\left(\frac{-\hat{h}}{\omega_H}\right) + (h_m - \hat{h})\right]$$

Where $K_H = K_H' (57.3)/\hat{V}_m$

(B) Hold Max θ_g: $\theta_{gc} = -20$ Degrees $(|\theta_g| \geq 20°)$

TERMINAL PHASE

$(\hat{T}_{Go} \leq T_{Sw})$

$$\dot{\theta}_c = 4\, G(s)\, \dot{\lambda}_q + f(\theta_g) + \dot{\theta}_{Bias}$$

Where $\dot{\theta}_{Bias} = (1845/\hat{V}_m)$ Deg/Sec

NOMINAL PARAMETERS

$h_m = 600$ Feet, $h^* = 250$ Feet, $K_H' = 4.0$ Deg/Sec per Foot

$\omega_H = 1.0$ Rad/Sec

$$G(S) = \frac{(S/\omega_{fp} + 1)}{(S/\omega_n + 1)^2} \quad \text{Where} \quad \omega_{fp} = \begin{cases} 1.75 \text{ Rad/Sec}, & t \leq t_{bo} \text{ Sec} \\ \left[\dfrac{\hat{q}_o S_\pi C\hat{N}_\alpha}{m\hat{V}_m}\right], & t > t_{bo} \text{ Sec} \end{cases}$$

$$\omega_n = \begin{cases} 15\, \omega_{fp}, & \omega_{fp} \leq 1.33 \text{ Rad/Sec} \\ 20 \text{ Rad/Sec}, & \omega_{fp} > 1.33 \text{ Rad/Sec} \end{cases}$$

$$f(\theta_g) = \begin{cases} \left[12\,(1 - t/t_{bo})\,\dfrac{(S/10 + 1)}{(S/2 + 1)}\right] |\theta_g + (1 - t/T_f)\,\dot{\lambda}_q| & \text{for } t \leq t_{bo} \text{ Sec} \\ 0 & \text{for } t > t_{bo} \text{ Sec} \end{cases}$$

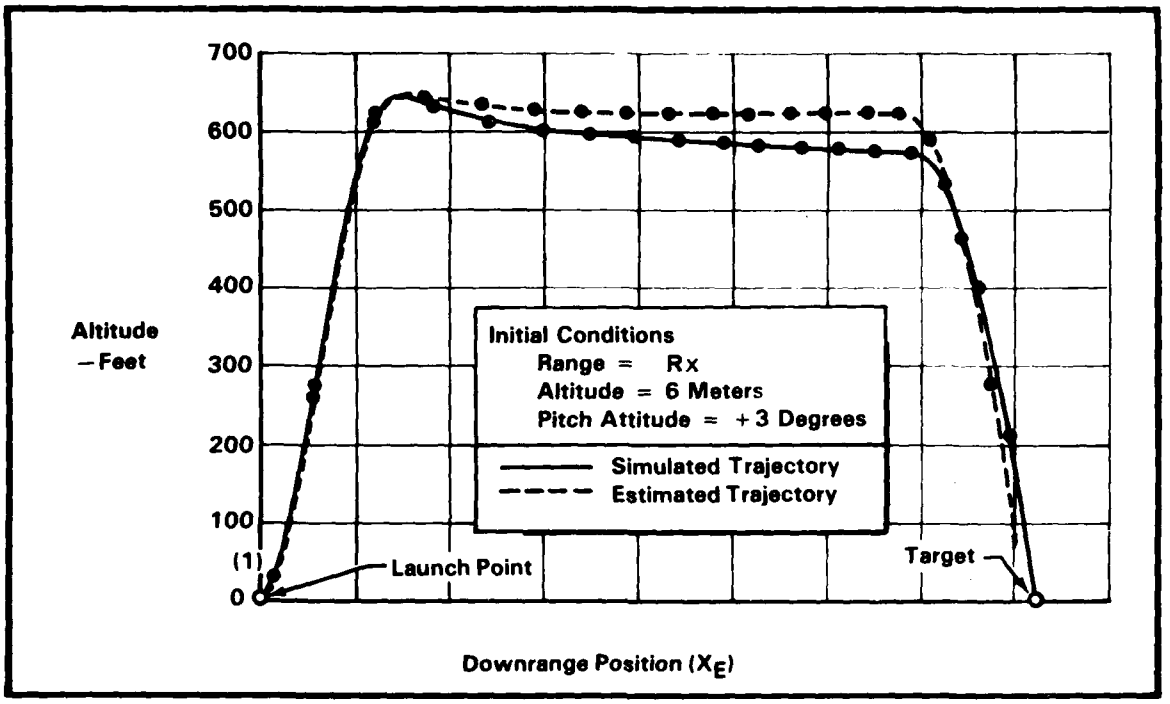


Figure 3. Simulated Missile Trajectory and Estimation Algorithm Output for Long Range Conditions

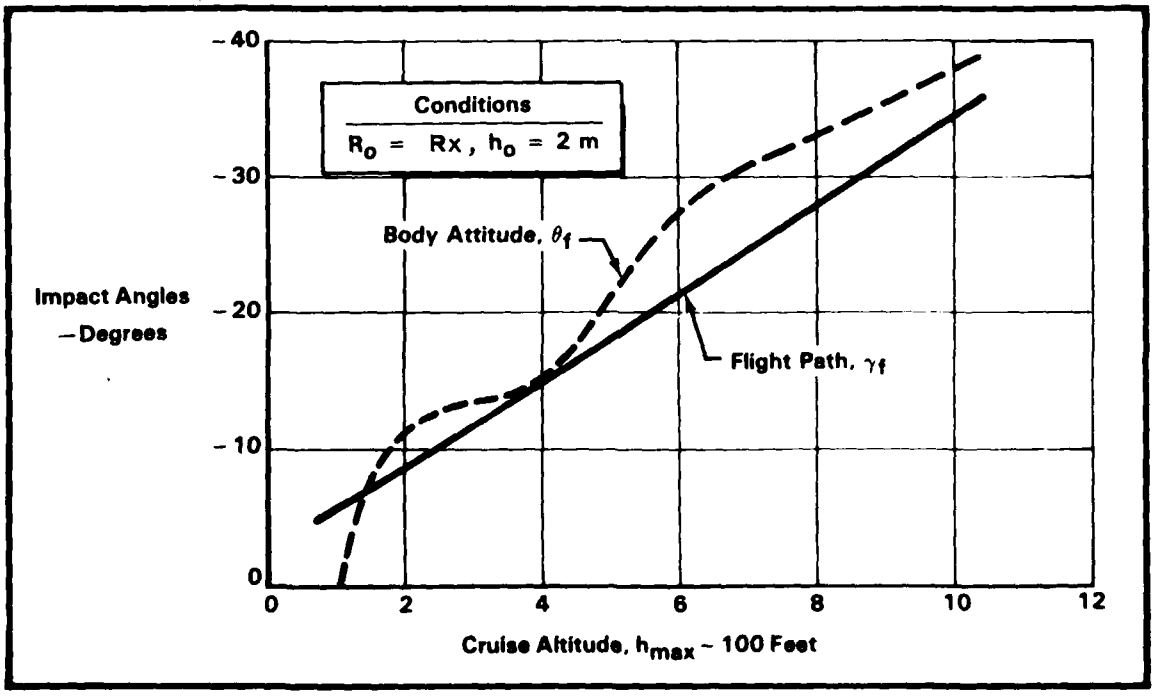


Figure 4. Impact Angle as a Function of Selected Cruise Altitude

cloud cover probabilities as a function of altitude and visibility. For the 600-foot cruise altitude, the average impact angle is -18.8 degrees for the full extent of launch ranges. The standard deviation is only 1.8 degrees or less than 10 percent of the mean, thus demonstrating very uniform performance. Miss distance over this range averages only 25 percent of the requirement as shown in Figure 5.

This uniformity of terminal impacts and low miss distances distinguishes this technique from earlier efforts in this area [Reference (2)]. These efforts were based on open-loop control in the form of climb commands as a function of time only, a hold attitude cruise phase, and terminal dive triggered by seeker gimbal angle. Since the Estimation Algorithm yields reasonable estimates of system states, uniform performance is assured, independent of launch range and offsets. Further refinements are being considered such as adding the yaw plane to the estimator, and employing a closed-loop estimation concept such as a Kalman filter to minimize errors in trajectory and velocity states.

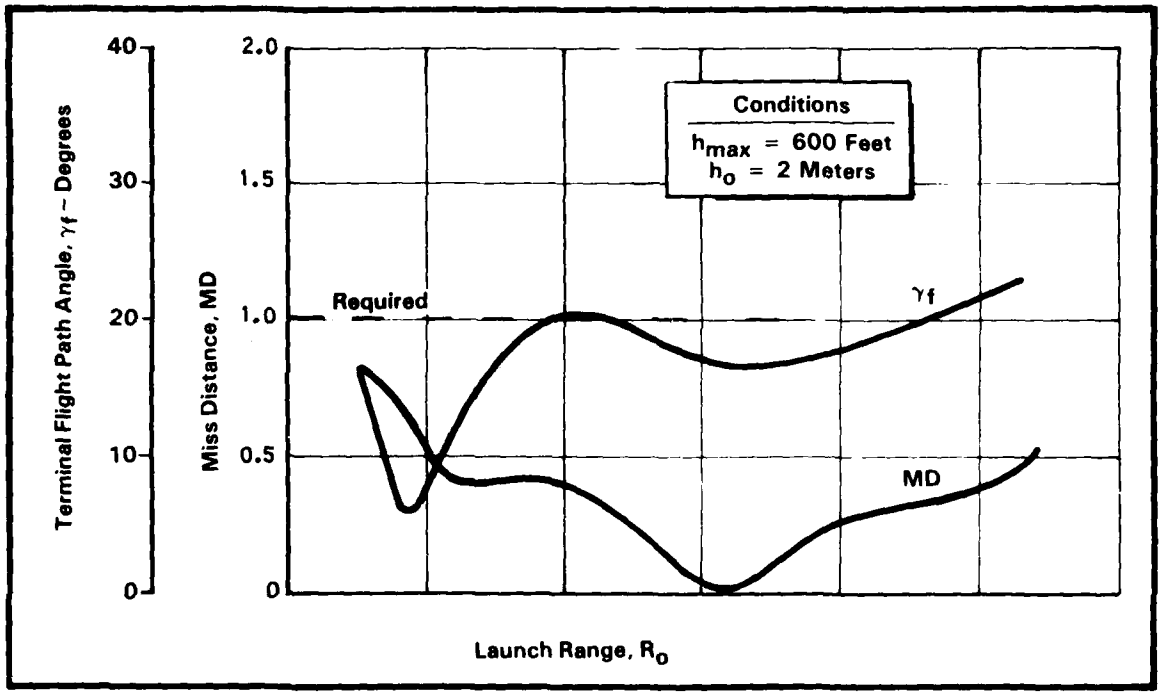


Figure 5. Terminal Flight Path Angle and Miss Distance for Various Launch Ranges

AIRFRAME STABILIZATION

The objectives of this phase of the design is to improve the stability and steady state error characteristics of the attitude control loops of the missile. The weapon employs attitude control loops for roll, pitch and yaw using the outputs of two gyroscopes. Each gyro has two orthogonal axes of sensitivity, yielding one redundant axis. The estimates of missile velocity ($\hat{V_m}$) and dynamic pressure ($\hat{q_o}$), available from the Estimation Algorithm, allow increases in system bandwidth and steady state gain at low speeds with respect to a fixed gain analog autopilot. This is achieved without increasing the maximum system bandwidth or actuator requirements. Therefore, the design philosophy is to employ the assets of the digital processor, i.e. the ability to vary gains and compensation, to improve system performance, while minimizing the costs associated with high bandwidths and high computational speeds.

The adaptive gain strategies for the stability loop are based on the premise that the velocity time history is a predictable function of time. Indeed, even when such factors as launch speed variations (0 to 165 knots), rocket motor tolerances ($3\sigma \leq 9$ percent), and temperature sensitivities (0.16 percent per ^{o}F) are analyzed, the maximum speed will be known to within about 17 percent (1σ). Fortunately, the dominant factor affecting missile aerodynamics is the missile speed with angle-of-attack and angle-of-side slip effects being secondary.

Consider, for example, the development of the adaptive gain strategy for the roll control loop. Neglecting aerodynamic coupling, i.e. $C_{\ell\beta} = 0$, the aerodynamic transfer function for the roll loop is a first order lag of the form:

$$\left(\frac{p}{\delta p}\right) = \frac{K_A}{\left(\frac{S}{\omega_A} + 1\right)}$$

where δ_p= effective roll fin deflection (deg)

p = roll rate (deg/sec)

The aerodynamic gain, K_A, and lag frequency, ω_A, are in turn functions of aerodynamic characteristics ($C_{\ell p}$, $C_{\ell \delta p}$), roll inertia (I_{xx}), speed (V_o), and dynamic pressure (q_o). The functional forms, with appropriate constants (S_π, ℓ), equal:

$$K_A = \left(\frac{2}{\ell}\right)\left(\frac{C_{\ell\delta_p}}{C_{\ell_p}}\right) V_o$$

$$\omega_A = \left[\frac{q_o S_\pi \ell^2 \, C_{\ell_p} \, (57.3)}{2V_o \, I_{xx}} \right]$$

The high frequenty gain of the transfer function, i.e. for $\omega >> \omega_A$, is approximately proportional to dynamic pressure, as shown below:

$$\left| \frac{p}{\delta p} \right| \approx \frac{K_A}{(\omega/\omega_A)} = \left[\frac{S_\pi \ell (57.3) C_{\ell_{\delta_p}}}{I_{xx}} \right] \left(\frac{1}{\omega} \right) q_o$$

Therefore, to maintain a constant roll bandwidth, the control gain ($K\phi$) must be inversely proportional to the estimated dynamic pressure ($\hat{q_o}$). The resulting roll gain can be expressed as:

$$K_\phi = \left(\frac{K_{\phi_o}}{\hat{q}_o} \right) \qquad \text{where } K_{\phi_o} = \text{constant}$$

The constant, $K\phi_o$, is selected to yield the desired roll bandwidth. The bandwidth is limited by the actuator bandwidth, and to a less extent by the computational and phase delays of the digital processor. The remainder of the roll compensation is a pair of lead/lag compensators of the form:

$$G(Z) = \frac{(1-A_\ell z^{-1})^2}{(1-A_n z^{-1})^2}$$

where A_n, $A\ell$ are fixed coefficients. The resulting system exhibited an order of magnitude improvement in steady state gain at flight conditions of low dynamic pressure over the fixed gain analog autopilot. At the same time the maximum actuator bandwidth was reduced as will be explained in the following section.

ACTUATOR CONTROL

Closing the actuator position loop through the digital autopilot by sensing fin position and generating pulse width modulation (PWM) commands has some clear advantages. The actuator, a highly nonlinear device, can be made to appear linear through adaptive digital control. However, to implement the digital control, the bandwidth of the actuator must be reduced to compensate for computational delays. This lower bandwidth and uniformity of performance using digital control permits a sizable relaxation of specifications for the actuator frequency response. This, in turn, will increase the producibility of the actuator subsystem.

Analytical Actuator Design

Requirements for the actuator were based on the given airframe and rocket motor. Using a high speed flight condition, which yields the highest aerodynamic short period mode, an actuator bandwidth requirement of 15 Hz was established. This assumed that an adaptive or programmable gain and compensation concept would be employed in the autopilot, so that no additional gain or bandwidth was needed to provide stiffness at low dynamic pressures. Since it was desirable to maintain the same basic mechanical actuator design, the only design freedom was in the compensation and PWM calculations. Due to the solenoid response time of 1 to 2 milliseconds, the PWM frequency was kept at 125 Hz or an 8-millisecond period. Pulse width modulation has an advantage of requiring only a discrete output to the solenoid driver electronics. This avoids a D/A converter.

A simulation block diagram of the actuator position loop with digital controller is shown in Figure 6. The "on" time of the solenoid is computed using an equation involving the position error (δ_ϵ), the fin position (δ'), and the estimated hinge moment ($H\hat{\delta}$). A predictor is used to compensate for the phase loss due to computational delays and the effective zero order hold in the system. Details of the PWM equations appear in Figure 7. The effective gain is inversely proportional to δ_{sat}, where δ_{sat} is nominally 8.81 degrees. This is a gain reduction of 65 percent or 9 dB from the analog actuator design.

The parameter δ_{sat} is made a function of fin position (δ') since the actuator had significantly different characteristics in the extend ($\delta' > 0$) and retract ($\delta' < 0$) directions. This effect of differing control volumes is moldeled in a digital simulation as $\omega_p = f(\delta')$ in Figure 6. Notice that the aerodynamic force on the fin, or hinge moment load, also effects performance. To obtain a speed of response independent of load, δ_{sat} is also a function of $H\hat{\delta}$. Although the hinge moment cannot be measured directly, it is a well defined function of Mach number (Figure 7). The simulation block diagram also indicates a number of nonlinear elements such as torque limits, static friction, and hysteresis which make such systems difficult to analyze and control. Another significant parameter is the pressure of the gas supply. Although nominally 600 psi, the pressure can drop to as low as 300 psi after the 46 seconds at a temperature of -45°F. Since no appreciable drop occurs at 70° to 145°F, and a temperature measurement is not available to the autopilot, this effect cannot be compensated. However, for the selected actuator gain schedule, the system is stable at 300 psi, even for the worst case of no load.

Hardware Tests

The hardware tests were considered necessary in view of the extensive nonlinearities of the hardware which are not readily analyzed by linear methods. The tests were conducted with the actuator mechanical structure controlled by a breadboard digital autopilot to confirm design analyses,

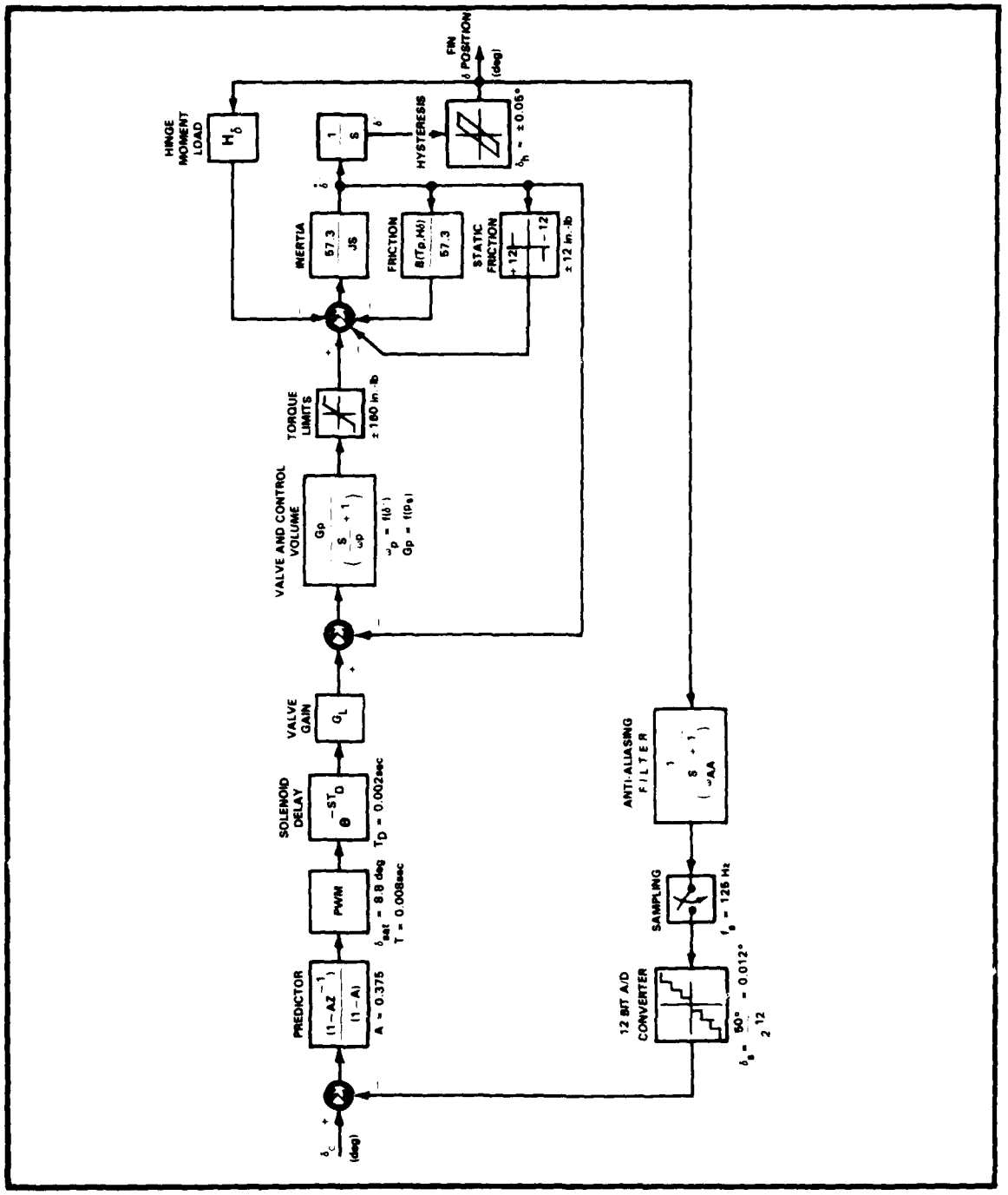


Figure 6. Actuator Simulation Block Diagram

PULSE WIDTH MODULATION EQUATIONS

(1) $t_{on} = \left(T/2\right) + \left(T/2\right) \left(\delta_\epsilon / \delta_{sat}\right) + K_{V_D} (24 - V_D)$

(2) $0 \leq t_{on} \leq T$

WHERE T = CARRIER PERIOD = 8 MS (125 Hz)

t_{on} = SOLENOID "ON" TIME INTERVAL

δ_{sat} = FIN SATURATION LEVEL

$\delta_{sat} = \left[\delta_{sat_o} + 0.735\,\bar{\delta}\right] \left[1 - 0.5\,(H_\delta / H_{\delta\,max})\right]$

V_D ≈ SOLENOID VOLTAGE = 24 – 32 VOLTS

K_{V_D} ≈ SOLENOID VOLTAGE SENSITIVITY IN MS/VOLT

where

δ_{sat_o} = 8.81 deg

$$\bar{\delta} = \begin{cases} 0 & \text{for } \delta \leq 0° \\ \delta & \text{for } \delta \leq 10° \\ 10° & \text{for } \delta > 10° \end{cases}$$

$H_\delta = f(M_n)$

$H_{\delta max}$ = 12 in.-lb/deg

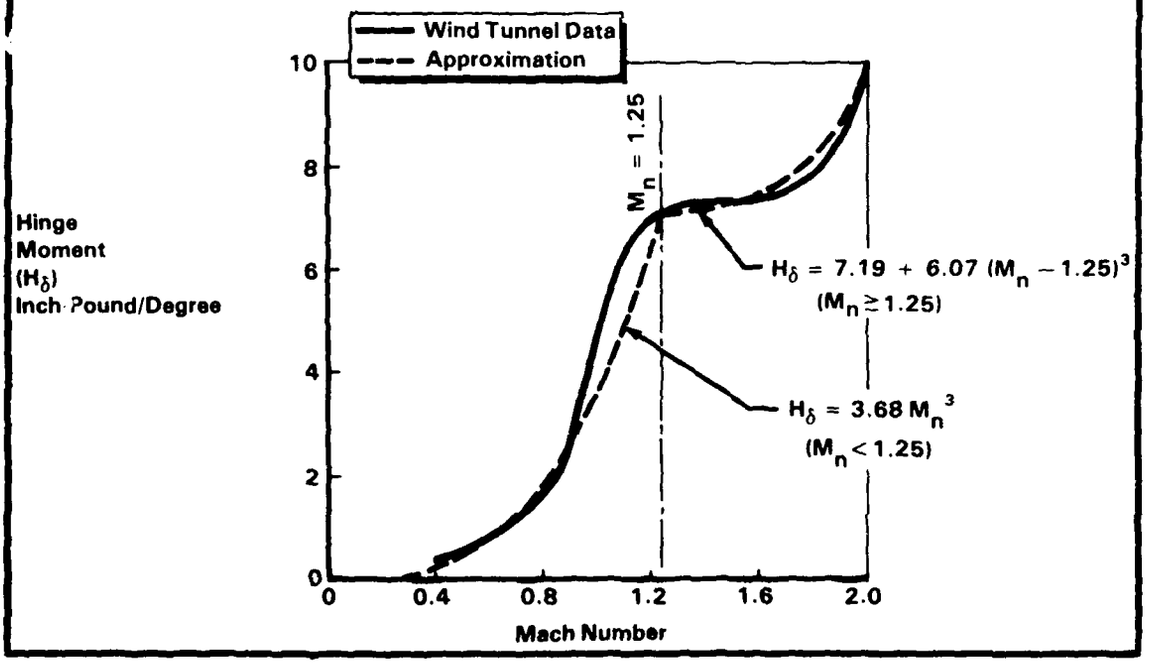


Figure 7. Pulse Width Modulation Equations

measure parameter sensitivities, and establish a performance baseline. A comparison of simulation and these hardware-in-the-loop results for step inputs is shown in Figure 8. Also notice the differences in the responses in the extend and retract directions, particularly for the constant gain (δ_{sat} = 8.81 degrees) system. For the adaptive gain case, the lightly damped response in the extend direction has been corrected, although the initial overshoot remains. This is due to the delays in the adaptive gain mechanization. However, step commands cannot be generated by the autopilot, since the commands are rate limited.

Frequency response test data (Figure 9) demonstrates the relatively uniform performance between no-load and a maximum load of 12 inch-pound/ degree. For example, at a frequency equal to the required bandwidth of 15 Hz, the overall gains vary from +1.5 dB to -2.3 dB for the no-load and maximum load cases respectively. At the same frequency, the phase ranges from -53 to -65 degrees. The simulation results, also given in Figure 9, indicate reasonable correlation with the hardware, particularly at lower frequencies.

Gain and phase margins were assessed with the actuator hardware to a limited degree. Gain margin is not easily defined, since this nonlinear system exhibits a stable limit cycle as the gain is increased. This limit cycle is undesirable, but the system is not unstable in the linear system sense. For the no-load and maximum load cases the gain can be increased by 3 dB and 6 dB respectively, before the limit cycle amplitude becomes significant (i.e. greater than 1.0 degree peak to peak).

Phase margins were determined by adding computational delays or pure lags of up to one period or 8 milliseconds. The system remained stable at all levels of phase delay, which represents up to 43 degrees of phase lag at the approximate gain crossover frequency of 15 Hz.

STATE ESTIMATION

This estimation concept uses existing seeker and gyro measurements as shown in Figure 10. The measurements are LOS rate ($\dot{\lambda}_q$), seeker gimbal angle (θ_g), and gyro angle (θ) for the pitch plane. The block labeled system equations is essentially a two-degree-of-freedom simulation of the weapon in the vertical plane. These equations are presented in Table 2.

The key assumption is that the longitudinal acceleration and velocity are predictable since the rocket motor has repeatable characteristics and the initial velocity is small (0 to 165 knots) compared with the maximum velocity. For accelerations normal to the missile centerline, the aerodynamic characteristics are known from wind tunnel tests. These accelerations are then integrated to yield velocities and positions. The seeker and gyro gimbal angles are used to transform velocities into line of sight (LOS) and inertial coordinates, respectively. The estimate of range rate ($\hat{\dot{R}}$) is then the velocity component along the LOS. Considering the speed of ground targets, this is a good approximation. The raw range estimate ($\hat{R}$) is formed as the ratio:

$$\hat{R} = \frac{(V_Z)_{LOS}}{\dot{\lambda}_q}$$

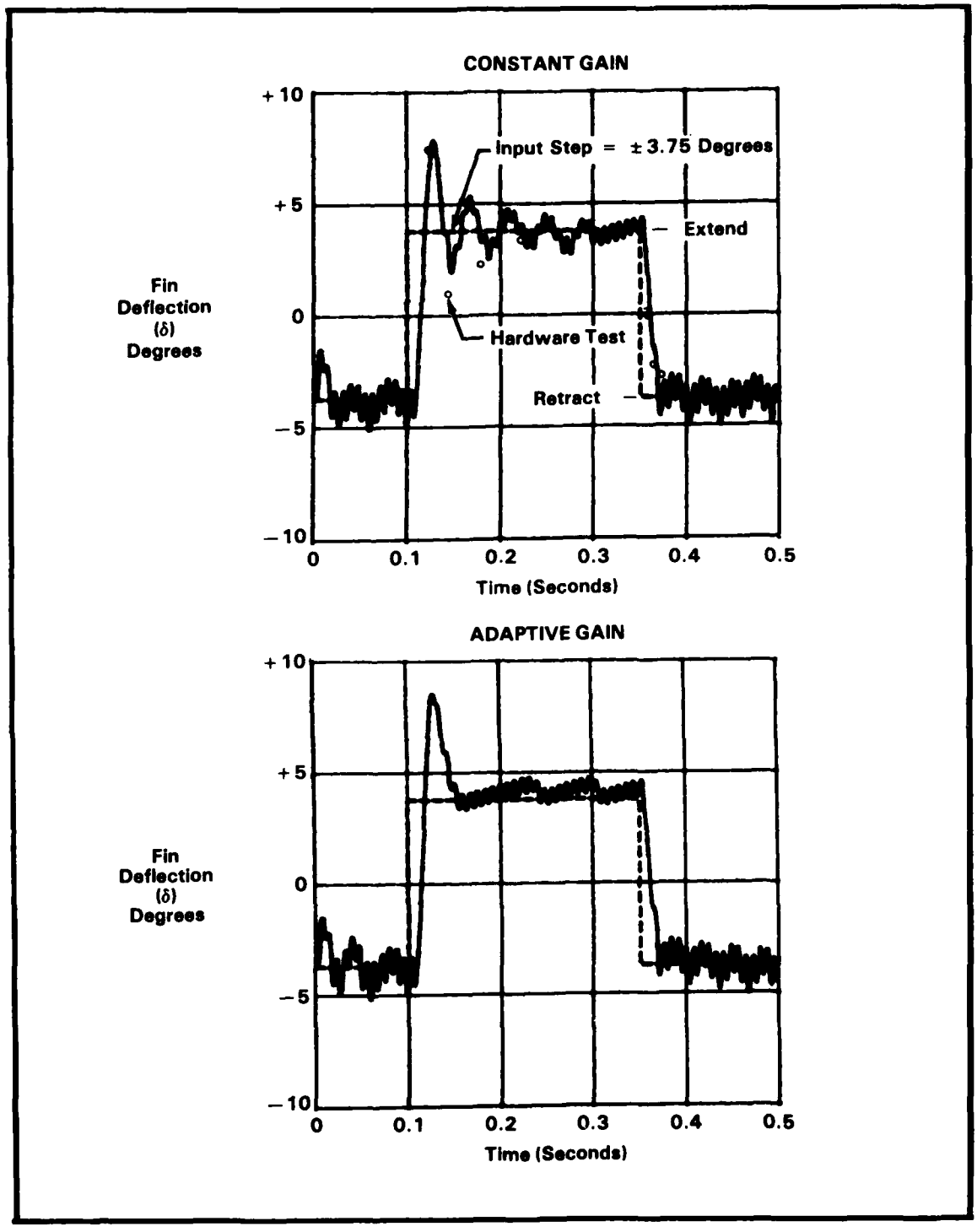


Figure 8. Simulation and Hardware Test Data for Unloaded Actuator

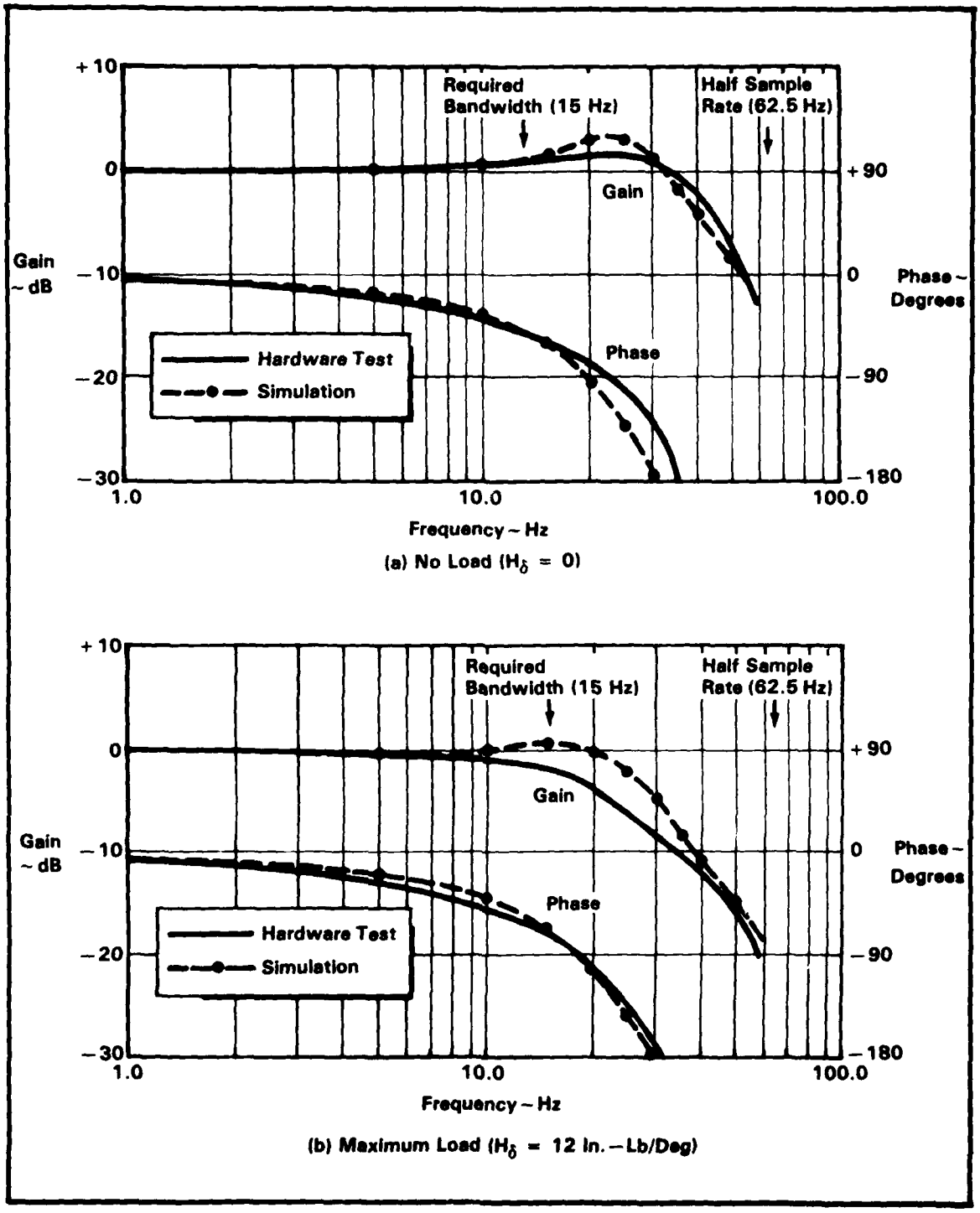


Figure 9. Actuator Frequency Response for Two Hinge Loads

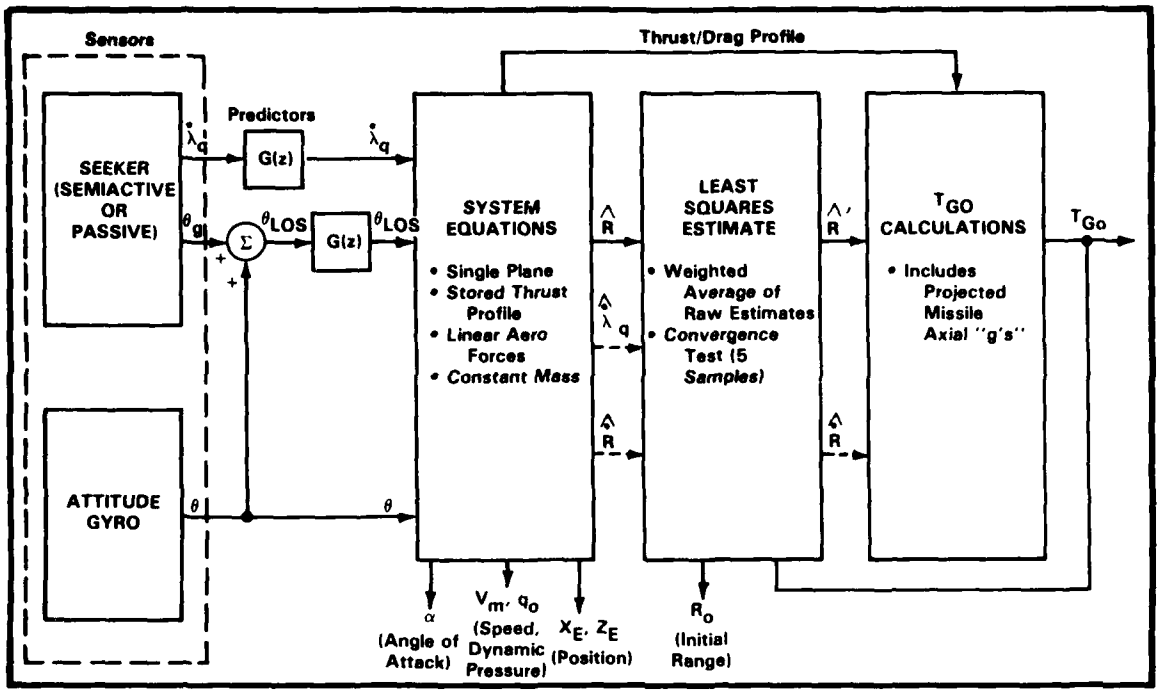


Figure 10. Block Diagram of Estimation Algorithm

where $(V_Z)_{LOS}$ = component of velocity normal to LOS

The raw estimates are subsequently smoothed by a least squares filter which minimizes the mean squared error between the raw estimates and the range function:

$$R = R_0 - 1/2\ a_X t^2$$

where R_0 = initial range (feet)

a_X = average thrust acceleration (feet/second^2)

t = time (seconds)

The computed time-to-go ($T_{\hat{GO}}$) before impact is a function of estimated range ($\hat{R}$) and range-rate ($\hat{\dot{R}}$) and assumed acceleration (a_X).

$$T_{\hat{GO}} = f\ [(\hat{R}/\hat{\dot{R}}),\ (\hat{\dot{R}}/a_X)]$$

The convergence of the $T_{\hat{GO}}$ estimate is shown in Figure 11. Notice that for this case, the error is essentially zero by 5 samples at a rate of 16 Hz. An alternate estimate (T^*_{GO}), neglecting the rocket thrust (a_X), shows considerable error until the range becomes small. Estimated missile trajectory parameters were shown earlier (Figure 3).

Table 2. System Equations (Pitch)

(1) ACCELERATIONS (BODY AXIS)

$A_X = A_{X_O}, t \leq t_{bo}$ sec

$= q_0 S_\pi C_{Do}, t > t_{bo}$ sec

$A_Z = q_0 S_\pi C_{N\alpha}$

(2) BODY-TO-EARTH TRANSFORM

$\theta' = \theta - \theta_{go}$

$CP = \cos\theta'$, $SP = \sin\theta'$

(3) ACCELERATIONS (EARTH)

$A_{XE} = CP \cdot A_X + SP \cdot A_Z$

$A_{ZE} = -SP \cdot A_X + CP \cdot A_Z$

(4) VELOCITY (EARTH)

$V_{XE}^{(+)} = A_{XE} \cdot \Delta T + V_{XE}^{(-)}$

$V_{ZE}^{(+)} = A_{ZE} \cdot \Delta T + V_{ZE}^{(-)}$

(5) POSITION (EARTH)

$X_E^{(+)} = V_{ZE}^{(+)} \cdot \Delta T + X_E^{(-)}$

$Z_E^{(+)} = V_{X_E}^{(+)} \cdot \Delta T + Z_E^{(-)}$

(6) VELOCITY (BODY)

$V_X = CP \cdot V_{XE} - SP\ V_{ZE}$

$V_Z = SP \cdot V_{XE} + CP\ V_{ZE}$

(7) TOTAL VELOCITY, α, q_0

$V_o^2 = V_{XE}^2 + V_{ZE}^2$

$\alpha = V_Z/V_X$

$q_0 = 1481. (V_o^2/V_s^2)$

(8) LOS AXIS SYSTEM

$\theta_{LOS} = \theta + \theta_g$

$CPL = \cos\theta_{LOS}$, $SPL = \sin\theta_{LOS}$

(9) VELOCITY (LOS)

$V_{XL} = CPL \cdot V_{XE} - SPL \cdot V_{ZE}$

$V_{ZL} = +SPL \cdot V_{XE} + CPL \cdot V_{ZE}$

(10) RANGE (R) AND RANGE RATE ($\dot{R}$) ESTIMATES (RAW)

$\dot{R} = -V_{XL}$

$R = +V_{ZL}/\dot{\lambda}_q$

DEFINITIONS

- α - Missile Angle-of-Attack
- θ - Gyro Pitch Angle
- θ_g - Seeker Pitch Gimbal Angle
- θ_{go} - Seeker Pitch Gimbal Angle at Launch
- S_π - Missile Reference Area (ft^2)
- ΔT - Integration Time Step (0.1 sec)
- q_o - Dynamic Pressure ($Lbs./Ft^2$)
- C_{Do} - Aerodynamic Drag Coefficient
- C_{No} - Aerodynamic Normal Force Coefficient

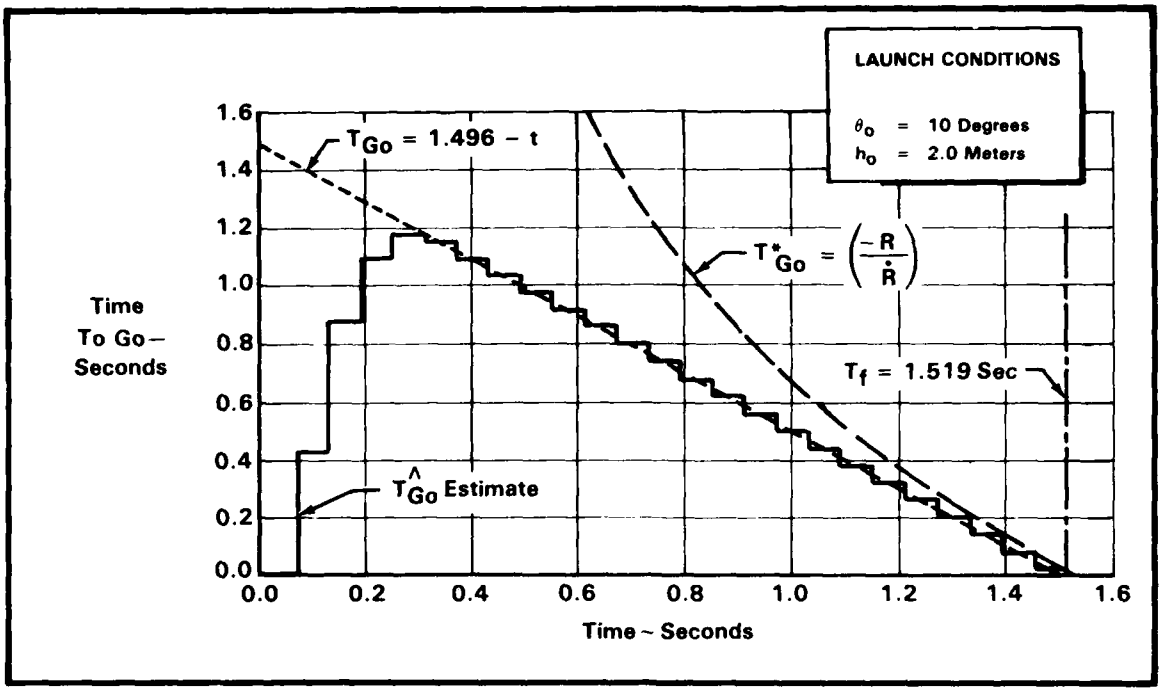


Figure 11. Comparison of Various Time-to-Go Estimates

The observability of system states is increased by the large vertical maneuver utilized to maximize the impact angle, thus avoiding a convengence problem for zero launch errors. The vertical plane has an additional advantage over the horizontal plane in that a potential error source, target velocity normal to the LOS, is nearly zero. In addition, the estimate of vertical displacement above the launch point has an application in altitude control, as explained in an earlier section. Estimates of missile velocity ($\hat{V_m}$) and dynamic pressure ($\hat{q_o}$), which are also produced, allow increases in system bandwidth and steady-state gain at low speeds. This was described in the section titled "Airframe Stabilization".

CONCLUSIONS

In general, optimal or suboptimal control laws require more information than is available to a tactical missile autopilot. For the system under study, measurements are limited to inertial LOS rates and gimbal angles from a semiactive laser seeker and body attitudes (three axes) with respect to an inertial reference from two attitude gyros. It is undesirable from cost, weight, and space requirements to increase the sensor complement. Therefore, either the desired system states must be estimated from existing measurements and apriori knowledge of the system or launch conditions, or the sensitivity of the control concept to the absence (or low accuracy) of the desired information must be reduced.

An estimation algorithm was developed to generate estimates of missile speed, dynamic pressure, the altitude increment from launch, current and initial range, and time-to-go until impact. These estimates were incorporated in adaptive control strategies to improve system performance and in suboptimal control laws to improve terminal guidance and maximize vertical impact angle.

The resulting control concepts were integrated into a flight control system which was simulated in six degrees of freedom. Performance in terms of stability criteria, off-boresight capability and impact angle is generally greater than a factor of two better than obtainable with classical control techniques implemented with an analog autopilot. In several cases, an order of magnitude improvement was obtained.

The producibility of the weapon system was also improved by reducing the actuator specifications and the sensitivity to rocket motor thrust-offsets.

System flexibility was enhanced by improved performance against maneuvering targets, thus allowing helicopter targets to be engaged. Launches from ground vehicles or fixed wing aircraft are also possible with simple software changes or selectable program options.

Requirements for the digital processor in terms of interfaces, conversion accuracy, and memory requirements appear in Table 3. Analog inputs include signals from the seeker, gyros, fins and fire control system. The analog outputs are for the seeker, BIT test, and telemetry. Discrete inputs and outputs control launch logic and BIT tests. The counters are used both as timers for controlling the sample period and time variable gains, and as output devices to the solenoid drive electronics. As the latter, the processor generates a data word representing the "on" time for a particular solenoid. The counter then sends an "on" voltage level to the solenoid until counting down to zero.

Table 3. Preliminary Digital Autopilot Requirements

PARAMETER	WORD LENGTH (BITS)	NUMBER REQUIRED	
		Total	Spares
ANALOG INPUT	12	16	1
ANALOG OUTPUT	8	6	3
DISCRETE INPUT	1	15	3
DISCRETE OUTPUT	1	12	2
ROM MEMORY	16	8k	3k
RAM MEMORY	16	1k	700
COUNTERS	8–16	8	0

The estimated duty cycle for a Zilog Z-8002 microprocessor with 4 MHz clock is only 36 percent. This is based on a 125 Hz sample frequency for body attitude control loops and actuator control, and a 25 Hz rate for guidance functions. These estimates include a 50 percent overhead for Higher Order Language programming.

The overall conclusion is that adaptive and modern control concepts can be applied to existing systems through the use of a low cost digital processor. The results of such an application is a dramatic improvement in weapon performance, producibility and flexibility.

REFERENCES

(1) "Optimal and Suboptimal Terminal Guidance Laws and Practical Considerations for a Short Range Missile Against an Accelerating Target", Dissertation, by Carlton J. Bates, Ohio State University, 1980.

(2) "The Development and Implementation of an Advanced Multimode Guidance Scheme in the Modular Guidance Digital Autopilot for the T6 Missile", CSC-TR-79-5582, by J. R. Kennamer and W. V. Albanes, Computer Sciences Corporation, 1979.

AD P001071

FREE-FLIGHT ROCKET GUIDANCE WITH THE SPINNING PLUG NOZZLE

W. E. Judnick and A. H. Samuel
Battelle-Columbus Laboratories
505 King Avenue
Columbus, Ohio 43201

INTRODUCTION

The spinning plug nozzle (SPN) has a direct effect on the flow of the rocket exhaust gases. It acts like a gyroscope to restore the angle between the rocket axis and the spinning plug axis to zero. Thus, when the rocket body axis becomes misaligned with the plug axis, due to external moments acting upon the rocket, leading to inaccuracy, the SPN restores the alignment and minimizes the flight path error.

The SPN concept was invented by Captain John E. Draim and was documented in his Massachusetts Institute of Technology thesis in 1969[1]. Missile Command (MICOM) later funded an exploratory prototype development with Booz/Allen to demonstrate hardware and the feasibility of using off-the-shelf materials such as standard bearings. Lockheed was MICOM's technical monitor/consultant on the program. Experiments by Draim[1] and Freeman[2] have shown that the theoretical SPN effect can be achieved in practice. The restoring moment on the rocket is sizable. In 1980, Battelle's Columbus Division completed a contract for Lockheed Missile and Space Company on the military applications of the SPN.[3] Battelle developed its SPIN (Spinning Plug In Nozzle) model to help evaluate the concept. The software was first applied to three different rocket types: the 2.75-in., the Multiple Launch Rocket System (MLRS), and the OATS. This paper summarizes this work at Battelle. In the authors' personal opinion, the concept shows considerable promise and merits wider exposure and consideration within the control theory community.

The remainder of the paper is organized into three additional sections. The SPIN model is briefly described in the next section. Highlights of the initial simulation results for the 2.75-in., MLRS, and OATS rockets are then presented. We end with some brief conclusions and recommendations of a more general nature.

The authors wish to gratefully acknowledge the participation of R. T. Batcher and J. H. Ott, both of Battelle's Washington Operations, in the described study. The advice and support of J. A. Freeman of the Lockheed Missile and Space Company were most valuable and are much appreciated. We also wish to thank Captain Draim for a copy of his thesis.

SPIN MODEL METHODOLOGY

Rockets destroy targets by hitting a vulnerable area, which may be smaller (High Energy Anti Tank, HEAT) or larger (Improved Conventional Munitions, ICM) than the physical area of the target. A rocket aimed at a point will miss it due to

the accumulation of errors. Let the miss distance be S. This value can be compared to the target vulnerable area dimensions. Military worth will generally increase as S decreases. The miss distance, S, is a good measure of effectiveness which can be related to kill probabilities or to numbers of rockets required in the case of area targets.

The SPN can correct only a portion of the errors of a rocket system. Our approach quantifies the degree to which SPN corrects the following errors:

(1) Initial error angle, ALPHAZ, the angle between the rocket's axis and the true aim vector as the rocket clears the launcher

(2) Initial angular velocity (pitch and yaw), DALFZ, the time derivative of the error angle at the same instant

(3) Externally imposed rotational moment, EMM, acting on the rocket axis, due to cross wind (surface wind, rotor wash, etc.).

The simplest model of the physical process is as follows. The SPN produces a restoring force proportional to the angle between the plug axis and the rocket axis. This force produces a torque that acts on the rocket. In the simplest representation, there are no out-of-plane forces, no damping, and the lever arm is constant. In these circumstances, the SPN would produce a simple harmonic oscillation of the rocket around the true direction, in the plane defined by the original rocket and plug axes.

However, we are not interested in the direction in which the rocket is pointing, as such, but rather in the miss distance. If it is valid to assume that the rocket moves in the direction of its axis, and that the plug axis is pointed at the target, then the increment to the miss distance in an infinitesimal time interval will be proportional to the sine of the angle between the axes and to the instantaneous rocket velocity. It is thus possible to cumulate the miss distance along the trajectory. In fact, there is a value of the miss distance S corresponding to each possible target distance, though, of course, one is primarily interested in the value corresponding to the actual distance.

For the simple case defined above, miss distance can be obtained in closed-form, which turns out to be sinusoidal. An integrated solution in series form has been obtained for the case in which the lever arm of the restoring force increases at a constant rate. This also is an oscillating function. However, in more general cases of military significance, an algebraic solution is not to be expected. The calculations described in this paper are therefore based on numerical integration.

The SPIN model essentially follows the rocket over its trajectory. At each time interval, the following operations are performed. In the notation a prime indicates a new value being computed from the old value and current values of other variables.

(1) The miss distance is incremented according to the formula

$$S' = \int_0^T \frac{V*SIN(ALPHA)}{SINB}\, dt$$

where V = rocket velocity

ALPHA = rocket pitch-yaw angle between rocket axis and plug axis (In the cylindrically symmetrical rocket we do not distinguish pitch and yaw.)

SINB = angle between trajectory plane and target plane, an input

In the numerical integration, the miss distance is cumulated over many small time intervals in accordance with the following algorithm

$$S' = S + V*SIN(ALPHA)*DT/SINB$$

$$S(0) = 0$$

where DT is the input time interval of integration.

(2) The distance X traveled by the rocket is also cumulated by

$$X' = X + V*DT$$

$$X(0) = 0$$

The calculation is terminated when X reaches XZERO, the input distance to the target.

(3) The rocket velocity is updated according to the formula

$$V' = V + (ACCEL + GRAV*SINB - QDRAG*V*V)*DT$$

$$V(0) = VZERO \text{ (an input)}$$

where ACCEL = acceleration due to rocket thrust, an input

GRAV = acceleration due to gravity, an input

QDRAG = drag coefficient of rocket for forward movement in units of 1/length, an input

This formula is appropriate if the target plane is horizontal, and must be modified if it is not.

(4) The rocket pitch-yaw angle ALPHA is updated by integrating its derivative DERALF, the corresponding angular velocity:

$$ALPHA' = ALPHA + DERALF*DT$$

$$ALPHA(0) = ALPHAZ \text{ (an input)}$$

(5) The angular velocity, in turn, is updated by accounting for three types of angular acceleration:

$$DERALF' = DERALF + (RESTOR + EMM - DPG)*DT$$

$$DERALF(0) = DALFZ \text{ (an input)}$$

where RESTOR = angular acceleration due to the SPN restoring force

EMM = angular acceleration due to externally imposed moments (e.g., surface wind)

DPG = angular deceleration due to damping.

(6) The calculation of RESTOR is given by the formulas:

$$RESTOR = RESMOM/ZI$$

$$RESMOM = RESFOR*ARM$$

$$RESFOR = ZKR*ALPHA$$

where RESMOM = restoring moment or torque

ZI = rocket moment of inertia in pitch-yaw dimension

RESFOR = restoring force

ARM = lever arm, distance from point of application of force to rocket center of gravity

ZKR = restoring force per unit angle, an input property depending only on the geometry of the SPN, an input

(7) The lever arm length varies with time because the rocket's center of gravity moves forward as fuel is consumed. It is updated by:

$$ARM' = ARM + DARM*DT$$

$$ARM(0) = ARMZ \text{ (an input)}$$

where DARM = velocity of rocket center of gravity relative to the rocket, an input.

(8) The externally imposed moment arises from the noncoincidence of the center of pressure from impinging wind with the center of gravity. The distance between them is EARM which, like

ARM, must be updated. EARM is the lever arm for the force coefficient ECONST, an input. Thus:

$$EMM = ECONST*EARM/ZI$$

$$EARM' = EARM + DARM*DT$$

$$EARM(0) = EARMZ \text{ (an input)}$$

(9) The deceleration due to damping is proportional to the angular velocity:

$$DPG = DAMP*DERALF$$

where DAMP is an input damping constant that is characteristic of the system.

(10) Finally, the moment of inertia also must be updated, because it is reduced by fuel consumption:

$$ZI' = ZI + DI*DT$$

$$ZI(0) = ZIZ \text{ (an input)}$$

where DI = rate of change of moment of inertia, an input.

These operations constitute the mathematical structure of the SPIN model, implemented on Battelle's Control Data Corporation 6500 computer. Figure 1 represents a rocket in flight with some of the more important relationships as defined as above. The SPIN model is a simplified representation in which the following processes are not represented: curvature of the trajectory; out-of-plane forces and motions; and components of the miss distance that cannot be affected. Thus, the SPIN model cannot be used for engineering calculations. It does indicate, however, with what is believed to be adequate accuracy, to what extent the SPN can correct the errors that it does affect, as a function of SPN design, rocket design, and environmental parameters.

Typical SPIN runs required less than three seconds of central processing unit time, thus permitting the extensive exploratory studies. Outputs of the SPIN program include:

(1) At frequent user-determined intervals, instantaneous values of X, S, T, ALPHA, V, and DERALF

(2) At the end of simulated flight:

a. Maximum S along the trajectory
b. Number of times S crosses zero
c. Maximum ALPHA along the trajectory
d. Number of times ALPHA crosses zero
e. "Probability of hit": the fraction of time intervals for which $S \leq R$, after traveling a minimum standoff distance (R is an input target dimension)

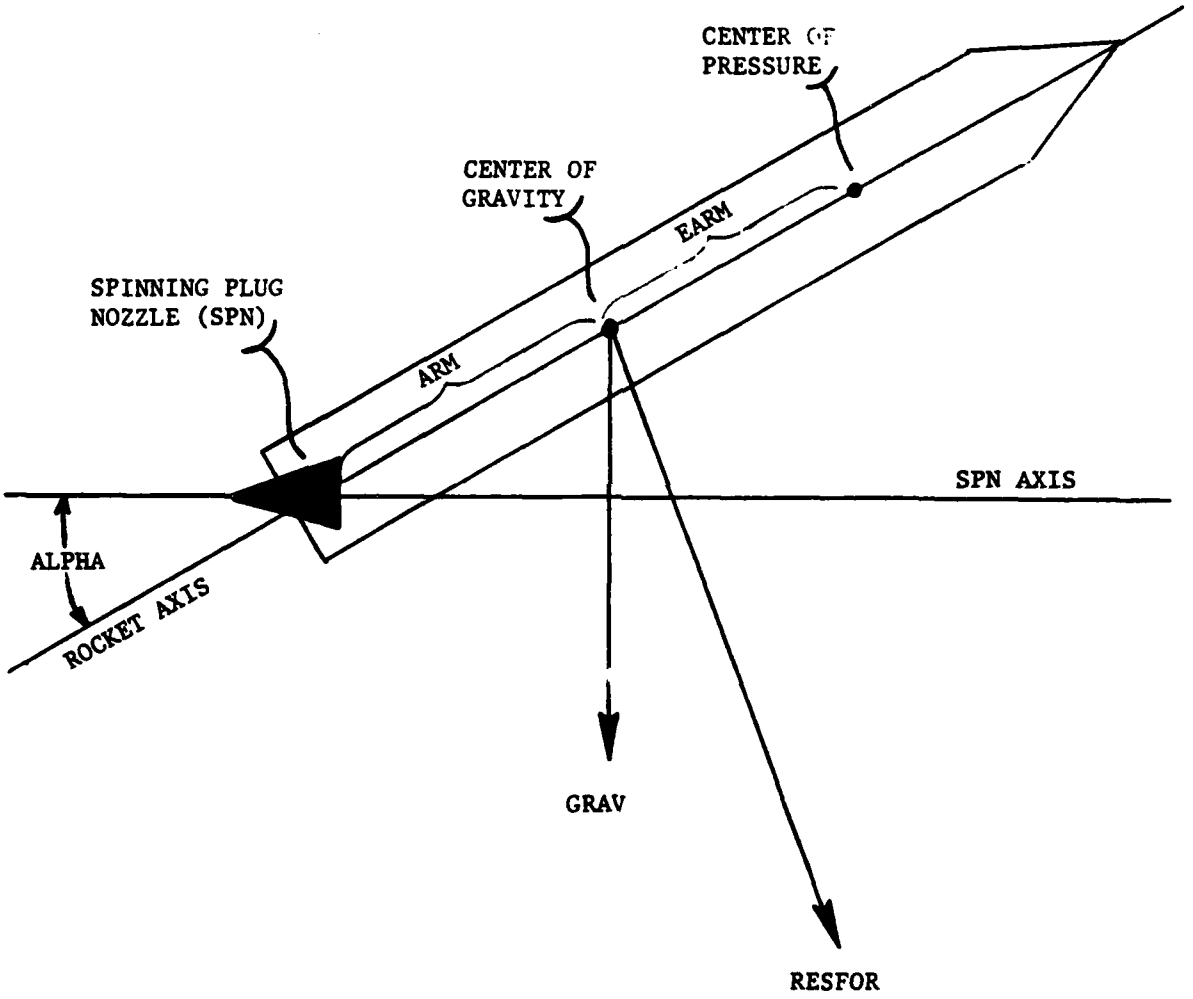


FIGURE 1. SPN SYSTEM TRANSIENT RESPONSE

Some distances and angles have been exaggerated from their more typical values for ease of illustration.

f. Final velocity V
g. Final miss distance S in meters
h. Final miss distance S in milliradians.

The most important outputs for the determination of military worth are 2g and 2h. The other outputs assist analysts in developing an understanding of the nonlinear processes involved, particularly the relative influences of design and environmental factors.

Table 1 summarizes SPIN model inputs representing the base cases for the conceptual rockets considered in this paper.

SELECTED SIMULATION RESULTS

To investigate the potential application of the SPN to the 2.75-in. Folding Fin Aircraft Rocket (FFAR), several runs of the SPIN (Spinning Plug In Nozzle) model were made. The primary figure of merit used for the conceptual system represented in these runs was the deflection error in meters, firing at a slant range of 4 km. Several early runs were devoted to the base case, with the primary conclusion being that performance is extremely sensitive to the factor DAMP, the damping of angular motion due to air.

The sensitivity to DAMP was confirmed in other SPIN runs in which the burn time of the rocket was extended from the usual 1.06 seconds to two and three times as long. The idea behind these runs was that the longer the SPN was working, the better the result might be. Of course, with a heavier rocket during the earlier part of the flight, the more difficult it would be for the SPN to influence its course. Therefore, there is an optimal burn time for any given plug and propellant quantity.

Extension of the burn time from 1.06 seconds to 2.12 seconds, and then to 3.18 seconds had a salutary effect on accuracy. For a graphical summary, see Figure 2. In essence, to get the most benefit from the plug and rocket, the whole rocket has to be redesigned. Of course, getting an SPN to fit within such a small diameter rocket is a noteworthy design problem.

As shown in Figure 3, miss distance is primarily in the negative direction, due to the prop wash external moment imposed during the first 5 meters of flight. The curve shown is sinusoidal with damped frequency and damped amplitude.

To investigate the potential application of the SPN to the MLRS system, the error budget published in the Special Study Group report[4] was examined. Each error source was classified as to whether or not the SPN could be expected to appreciably reduce that type of error. As shown in Table 2, this classification showed that several quantitatively important error sources fell into the "correctable" category. The contribution of these correctable error sources is about 6 mils. Because the total from all error sources is roughly 10, the estimated circular error probable (CEP) for a fully corrected MLRS is 8 mils.

TABLE 1. BASE CASE PARAMETER INPUTS

MK66 FFAR (2.75-In.)	MLRS	OATS
ACCEL = 0 to 67 g's in 0.04 sec, 67 to 97 g's in next 0.94 sec, drop to 0 in next 0.09 sec	ACCEL = 600 m/sec^2	ACCEL = 222.22 m/sec^2
ALPHAZ = 0.018 radians	ALPHAZ = 0.004 radians	ALPHAZ = 0.008 radians
ARMZ = 0.7 m	ARMZ = 1.6 m	ARMZ = 0.23 m
DALFZ = 0.0 radians/sec	DALFZ = 0.0 radians/sec	DALFZ = 0.0 radians/sec
$1.0 \leq DAMP \leq 14.0$ sec^{-1}	DAMP = 1.0 sec^{-1}	DAMP = 20 sec^{-1}
DARM = 0.127 m/sec	DARM = 0.305 m/sec	DARM = 0.0237 m/sec
DI = -1.5 kg-m^2/sec	DI = -95.56 kg-m^2/sec	DI = -0.05985 kg-m^2/sec
DT = 0.0004 or 0.0012 sec	DT = 0.001 sec	DT = 0.001 sec
EMM = 0.01158 radians/sec^2 during first 5 m, 0.0 otherwise	EMM = 0.01158 radians/sec^2	EMM = 1.603526*EARM/ZI radians/sec^2
GRAV = 9.81 m/sec^2	GRAV = 9.81 m/sec	GRAV = 0.0 m/sec
QDRAG = 0.000166 m^{-1}	QDRAG = 0.0004 m^{-1}	QDRAG = 0.00055 m^{-1}
SINB = 0.05	SINB = 0.7071	SINB = 1.0
VZERO = 63.84 m/sec	VZERO = 50 m/sec	VZERO = 23.1 m/sec
XZERO = 4000 m	XZERO = 675 m	XZERO = 1000 m
ZIZ = 3 kg-m^2	ZIZ = 280 kg-m^2	ZIZ = 0.4843 kg-m^2
ZKR = 1450 Newtons/radian	ZKR = 1500 Newtons/radian	ZKR = 400 Newtons/radian

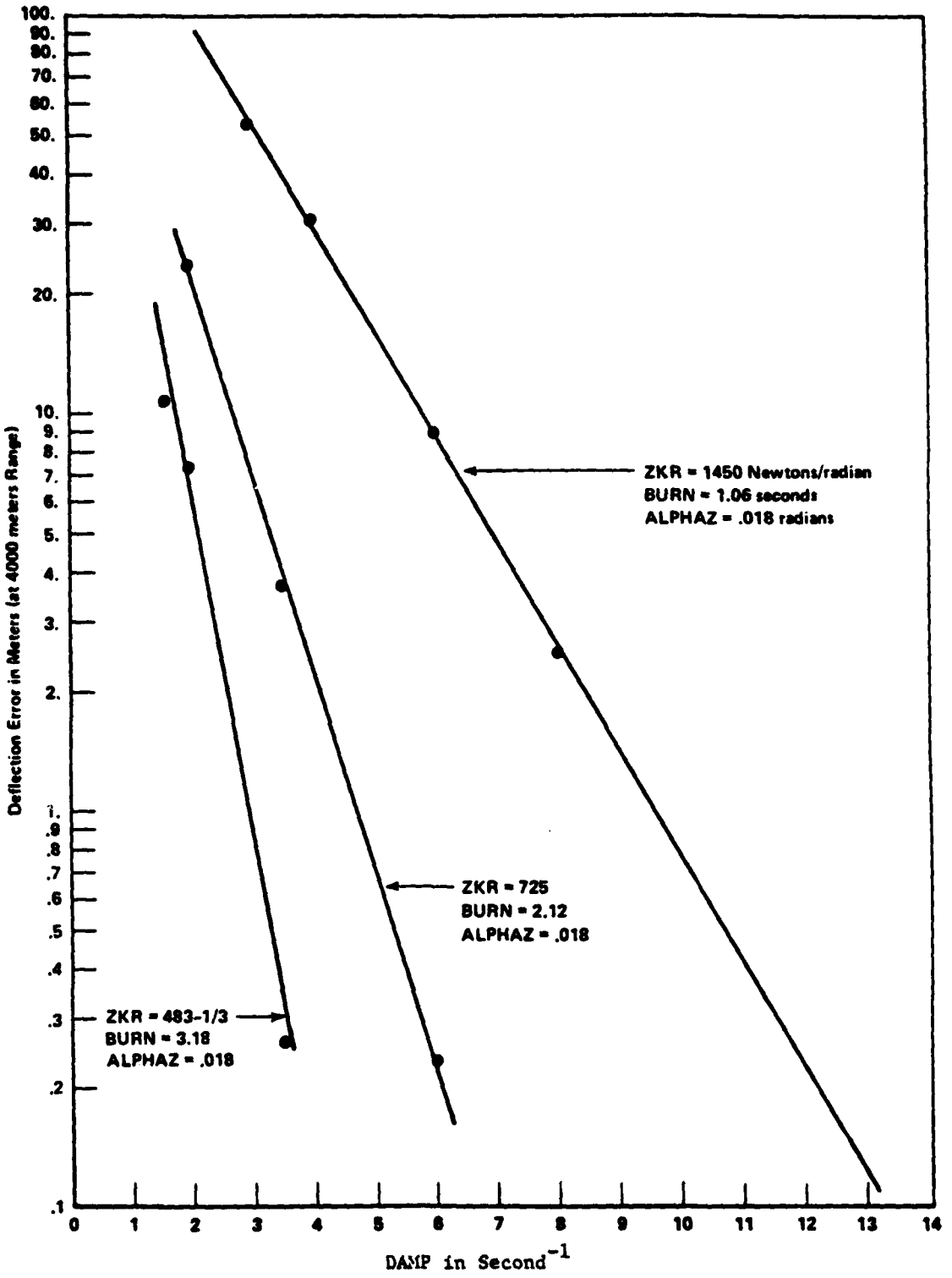


FIGURE 2. BURN TIME VARIATIONS FOR 2.75-IN. FFAR

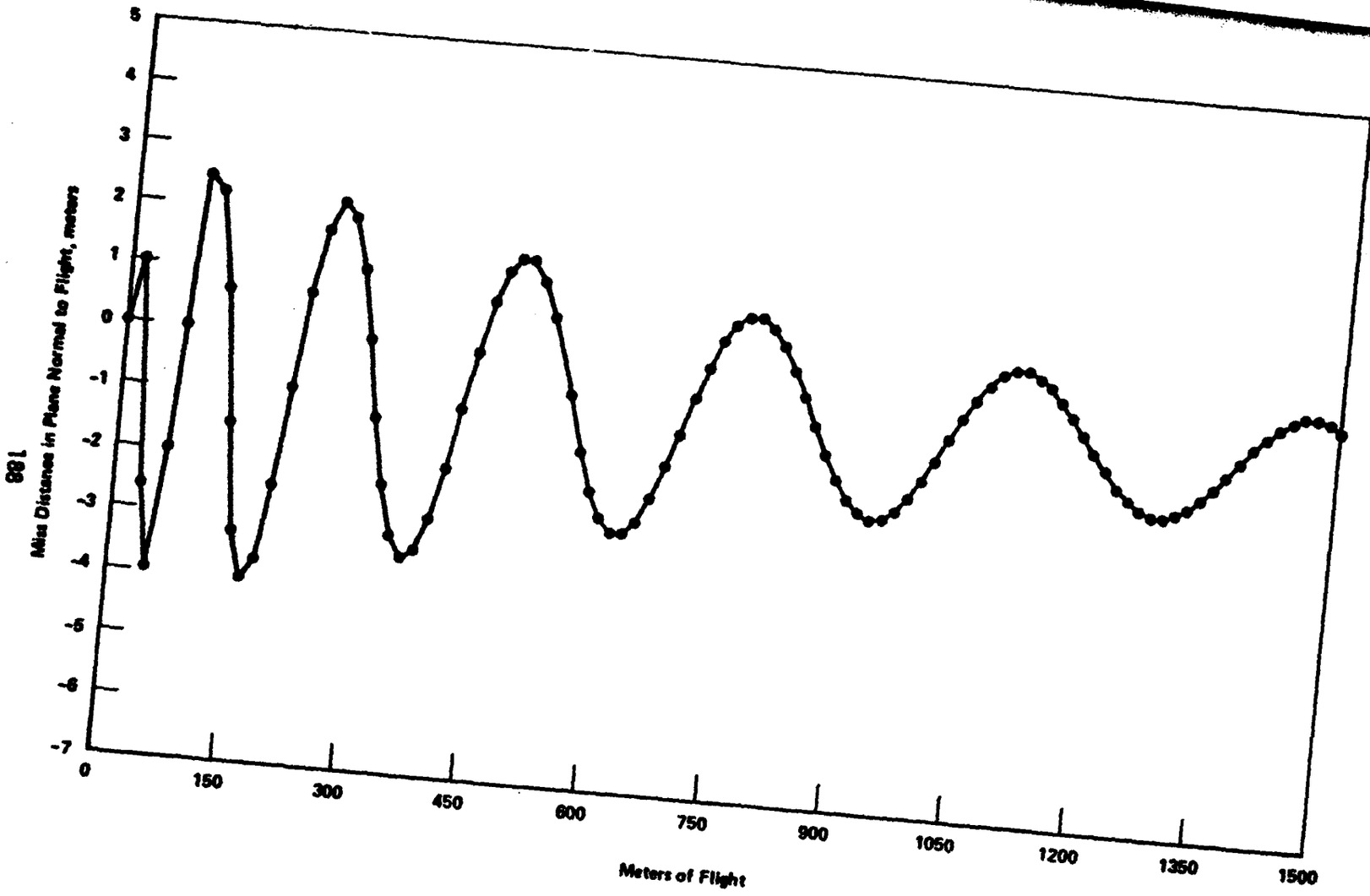


FIGURE 3. NON-BALLISTIC PORTION OF BASE CASE FLIGHT

TABLE 2. CLASSIFICATION OF MLRS ERROR SOURCES

Correctable or Partially Correctable		Not Correctable with SPN	
Source	Importance	Source	Importance
Mal-launch	Major	Total Impulse	Major
Thrust Misalignment	Major	Ballistic Wind	Major
Dynamic Unbalance	Major	Air Density	Medium
Ballistic Coefficient	Major	Time Fuze	Minor
Surface Wind	Medium	Munitions Drift	Minor
		Mal-aim	Medium

The military significance of improvement from 10- to 8-mil error for the MLRS system may be judged by considering Table 3. Suppose the target is self-propelled artillery--a prime MLRS target--at 35 km. The target location error (TLE) will be typically between 75 to 200 m depending on the acquiring assets. Suppose the objective is to kill 30 percent of the target elements--a value commonly used for destruction missions. The ICM pattern radius cited in the Special Study Group report[4] is 125 m, but it could in fact be as large as 200 m. Table 3 then shows the number of rockets which should be launched under various assumptions about the overall accuracy expressed in mils.

TABLE 3. MLRS ROCKETS TO COVER 30 PERCENT OF A SELF-PROPELLED ARTILLERY TARGET AT 35 KM

		TLE = 75 m		TLE = 250 m	
	Pattern Radius:	125 m	200 m	125 m	200 m
Overall MLRS Accuracy	10 mil	17	17	23	24
	8 mil	11	12	18	19
	6 mil	7	8	14	15

What is evident from the table is that an improvement from 10- to 8-mil error would significantly reduce the number of rockets required--whatever the acquiring asset or pattern size. While it is conceded that reductions in the number of fire-and-forget munitions to defeat similar targets would not be as dramatic, the cost savings in <u>either</u> case should be considerable.

The MLRS platform is relatively stable compared to the helicopter platform considered for the 2.75-in. rocket. Consequently, the initial error angle ALPHAZ was not varied over as wide a range in establishing an appropriate MLRS ZKR. It was considered that platform vibration was unlikely to produce an initial error angle greater than 15 mrad.

Similarly, it was considered that the external moment, EMM, would not be as large in the MLRS case as it was for the 2.75-in. FFAR. (The principal difference is the absence of prop wash.) Considering that a 6-mile per hour surface wind is roughly the equivalent of EMM = 0.012, the external moment was varied within the range 0 to 0.1 radians per second squared.

The initial SPIN model runs indicated that a restoring force ZKR in the 1240 to 1500 Newtons/radian range would largely compensate for initial angular errors and external moments as described above. In these runs, the rocket's flight is simulated through the thrust phase and the error values are shown at burnout. Converting this result to the K_r of Freeman[2], these values correspond to $378 \leq K_r \leq 457$ Newton-meters per radian.

In the base case, the correctable (with SPN) component of error is reduced from about 6 mils to 1.56 mils. This refers to range error measured in the plane normal to the trajectory. Consequently, overall system error is reduced from about $\sqrt{8^2 + 6^2} = 10$ mils to $\sqrt{8^2 + 1.56^2} = 8.15$ mils. Because 8 mils is the lower limit to overall error, ZKR = 1500 Newtons/radian achieves about 90 percent of the potential contribution.

Several runs of the SPIN model were then made for sensitivity analysis of this base case. Of particular interest was the variation of the input parameters whose values were not precisely determinable, due to the newness of the MLRS system and the lack of experimental data on the SPN.

Table 4 summarizes sensitivity runs on the MLRS base case. For comparative purposes, range error in mils on the ground plane is used as the figure of merit.

As shown in Table 4, range errors in the sensitivity runs were in the range 2.11 to 1.11 mils. The sole exception occurred when DALFZ was set to -0.025 radian per second. Initial rates of change in the error angle of this magnitude are not likely in the field. Consequently, we estimate that the spinning plug nozzle, if applied to the MLRS rocket, would achieve a range error (correctable component) of 1.6 ± 0.5 mils. The overall system error would thus be improved from approximately 10 mils, to 8.2 ± 0.1 mils. As explained above, such an improvement is of military significance.

To investigate the potential application of the SPN to the OATS conceptual system, several runs with the SPIN (Spinning Plug in Nozzle) model were obtained. The majority of the inputs to the SPIN model described the OATS concept as per information supplied by Mr. J. A. Freeman of Lockheed Missile and Space Company. Initially, it was to be determined if there were a feasible value of the restoring force ZKR attributed to the spinning plug that could produce satisfactory miss distances over a broad spectrum of initial error angles ALPHAZ and external moments EMM.

In the OATS concept, a free-flight rocket passes above the target, between 5 and 15 m above ground level. A sensor in the warhead detects the target and

TABLE 4. RANGE ERROR SENSITIVITY FOR MLRS WITH SPN

Sensitivity Run				Mils
Base Case				1.56
ZIZ	280	→	300	1.73
	280	→	320	1.90
DT	0.001	→	0.0002	1.56
ZKR	1500	→	1000	2.11
	1500	→	2000	1.18
DI	-95.56	→	-100.0	1.52
	-95.56	→	-90.0	1.61
SIN^{-1}	45^0	→	50^0	1.56
(SINB)	45^0	→	50^0	1.56
ACCEL	600	→	500	1.32
	600	→	700	1.78
VZERO	50	→	40	1.55
	40	→	60	1.56
XZERO	675	→	600	1.55
	675	→	750	
QDRAG	0.0004	→	0.0002	1.51
	0.0004	→	0.0006	1.49
GRAV	9.81	→	0.0	1.57
ALPHAZ	0.004	→	0.006	1.85
	0.004	→	0.008	2.14
ARMZ	1.6	→	1.8	1.41
	1.6	→	1.4	1.73
DAMP	1.0	→	2.0	1.11
	1.0	→	0.5	1.86
DARM	0.305	→	0.290	1.57
	0.305	→	0.320	1.54
DALFZ	0.0	→	-0.025	2.63
	0.0	→	+0.025	1.51

initiates a forged fragment warhead, which produces a slug that penetrates the target at high speed. The slug can be directed at the target if its course is not more than 20 degrees off the vertical (downward) direction. From this, one can derive the specifications for a kill of a Soviet T-62 tank. The rocket must hit a trapezoid in the vertical plane, centered on the target, whose height is from 5 to 15 m above the ground, whose bottom dimension is 6.9917 m, and whose top dimension is 14.2711 m. In our calculations, this trapezoid is replaced by a circle of equal area, with radius R = 5.81728 m. The miss distance S must be less than R.

Because the OATS rocket was yet to be built, there was no empirical evidence as to how the air would interact with the rocket to damp its angular motion. Therefore, the input DAMP was the subject of parametric variation. Also, a suitable value for the time interval between calculations had to be established on the basis of resultant accuracy.

The basic conclusion at the end of the preliminary runs of the SPIN (Spinning Plug In Nozzle) model was that OATS was a viable concept with the SPN, but not without it. Because of the conceptual nature of OATS, it was possible that one or more input parameters could be having an undue influence on that conclusion. Accordingly, a sensitivity analysis was performed. Each input parameter to the model was varied, up and down, by at least 25 percent from its "base case" value (Table 1). The choice of restoring force ZKR = 400 Newtons/radian in the base case is a conservative one. It is within experimentally observed values for spinning plugs, and it allows a margin for error. That is, future results tailored to more specific OATS concepts may well show that a lesser value for ZKR would suffice.

The OATS base case deflection error is 0.733 meter at 1 kilometer, which is well within the area needed to score a direct hit. In fact, it leaves room for about 5 mils of independent error from sources that are not correctable with the SPN. Generally speaking, deflection error stayed within 0.75 ± 0.16 meter as the base case parameters were varied individually by $\pm$ 25 percent. (Parameters with 0 value in the base case were varied as follows: GRAV to 9.81 m/sec^2; and DALFZ between -0.1 and +0.1 radians/second.) Simultaneous variations of ZIZ and DI were also attempted, as we simultaneous variations in ARM, DARM, and EARM, with concordant results.

The initial conditions of the base case have an 8 mil error angle into a 12 mph cross-wind. Because a wide continuum of other initial conditions is also of interest, a more detailed sensitivity analysis was performed on the initial error angle ALPHAZ and the external moment EMM due to surface wind. The initial error angle can be anywhere in the range 20 milliradians into 12 mph wind to 20 milliradians with such wind, and deflection error will still be 0.75 ± 0.09. Fixing the error angle at 8 mils, the surface wind can be anywhere from 15 miles per hour, roughly, with or into the error angle while deflection error stays within 1 meter (1 mil at this distance). We conclude that a ZKR of 400 Newtons/radian will be sufficient to produce good performance under a wide range of initial conditions.

The restoring force ZKR due to the plug is of central interest in the design of the OATS rocket. As shown in Figure 4, there is a log-log relationship between the deflection error SDEF and ZKR, provided $100 \leq$ ZKR ≤ 450 Newtons/radian. (The R^2 of the regression line fit is 0.99.) At lesser values, the relationship does not hold; other variables would be needed to explain OATS

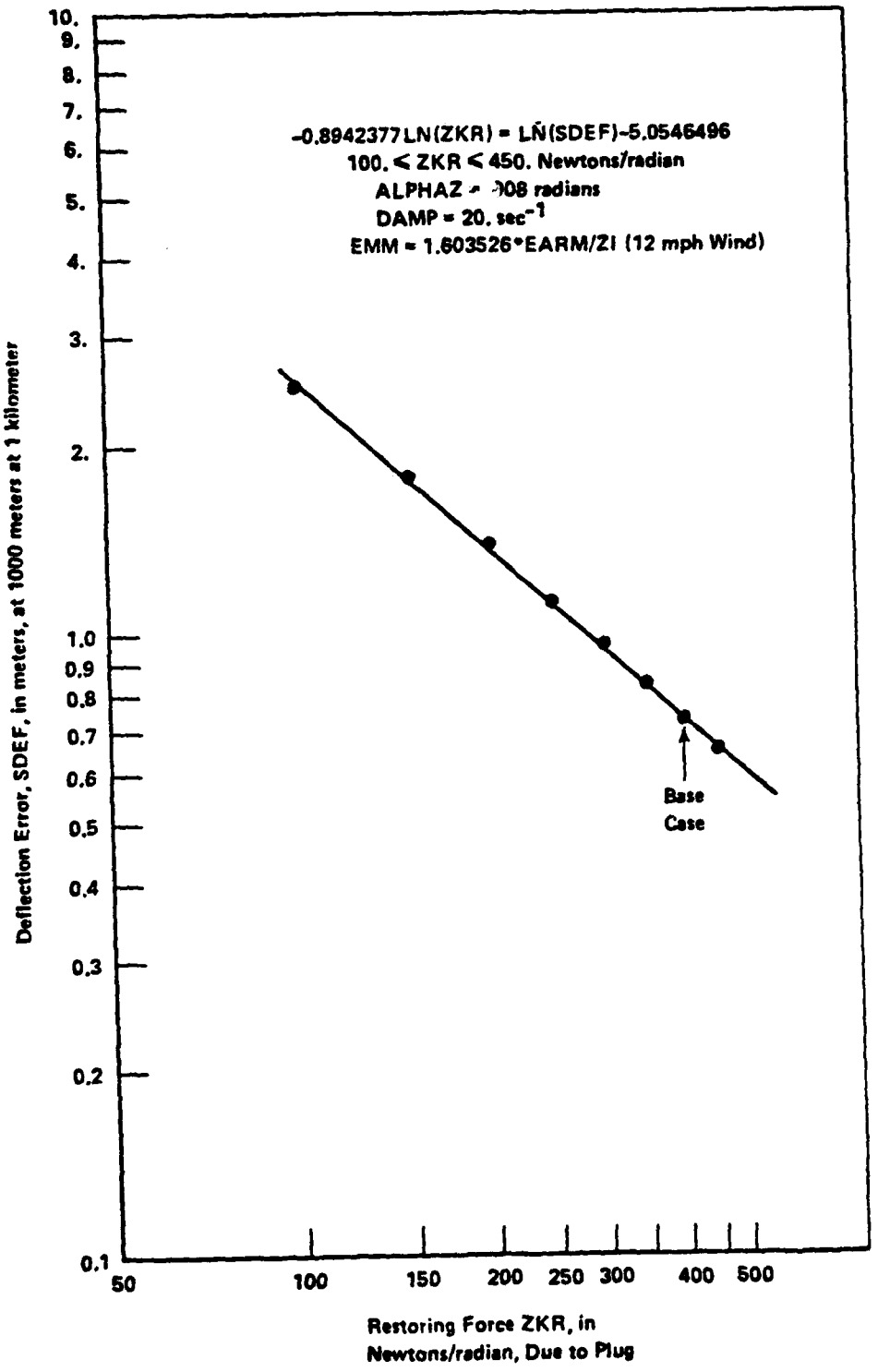


FIGURE 4. EFFECT OF VARYING RESTORING FORCE PER UNIT ANGLE

performance. Thus, the dominant variable determining OATS performance will be under our control provided ZKR is 100 Newtons/radian or greater. At 100, notice that we can still root-sum-of-square some 5 mils worth of independent error not under SPN influence and still hit the trapezoidal basket described earlier.

The miss distances calculated for the OATS base case and variations at a range of 1000 meters are, in general, less than 1 meter. It may be pointed out that these values are also appropriate for a direct-fire weapon with a HEAT warhead. This could be an even cheaper alternative for the medium-range, anti-armor weapon.

CONCLUSIONS AND RECOMMENDATIONS

The major conclusion to be drawn from the analysis is that miss distances can indeed be reduced by use of the SPN. The consequences of this finding, in terms of the gain in military worth and the desirability of adapting the SPN configuration, vary from system to system. In each system, the restoring force constant that will remove most of the correctable error has been estimated. In this section, we consider improved accuracy in terms of military worth, and also what system modifications are required to achieve the advantages of SPN.

It is our judgment that it would not be desirable to convert the 2.75-in. FFAR to an SPN configuration. It does not follow, however, that the SPN is useless for the air-to-ground mission. In fact, it is possible to generate an air-to-ground rocket concept that would be greatly enhanced by SPN. It would have the following properties:

(1) Diameter substantially greater than the 2.75-in. FFAR

(2) Burn time substantially longer than the 2.75-in. FFAR, preferably until the target is reached

(3) Average and final velocities would then also be greater, so that the trajectory would be more nearly rectilinear

(4) Spin-up while the pilot still has the target in his sights, possibly by an auxiliary motor

(5) Improved fire control.

The rocket described by these specifications would look very much like the Navy's ZUNI. Since this study has concentrated on Army weapon systems, it has not included a quantitative evaluation of SPN in ZUNI; but it seems this would be a promising subject for further investigation. An SPN rocket, resembling ZUNI and possible based on it, would be expected to have greater effectiveness than the 2.75-in. FFAR.

The MLRS system is a more favorable case. A ZKR value of 1450 Newtons/radian is sufficient to reduce the error by about 90 percent of the maximum that can be achieved by the SPN. This is a conservative estimate based on experimental results. It is concluded that a plug of this diameter would enable an SPN-equipped MLRS rocket to achieve a militarily significant improvement in accuracy.

Installation of an SPN of this size should require no other major modification in the design of the MLRS. The weight of the plug (approximated as a cone of height equal to its diameter, made of stainless steel having a density of 7.75 g/cm^3) would be about 11.5 pounds. This is less than 2 percent of the weight of the MLRS. There would be some leeway for reducing the plug's diameter before the upper limit of ZKR is encountered.

Rapid spin-up of the plug is not so important a consideration in the case of the MLRS, which is fired from a static platform. It, thus, appears that the SPN-modified MLRS would be more effective than the current model. The reduction in the number of rockets required to achieve a military objective would be about 30 percent while the weight increase of each rocket would only be 2 percent. Assuming that the number of rockets that can be used is limited by logistics, as is expected, the same supply line could achieve a target servicing rate that is increased by more than 25 percent. The ultimate desirability of making this change must be determined by a calculation that includes cost figures.

MLRS is a relatively unfavorable case for SPN application (indirect fire, long ballistic trajectory, curved trajectory). It is remarkable that even in this case the SPN provides a very palpable increase in effectiveness.

Among the competing concepts for a new generation infantry medium-range, anti-armor weapon, the OATS concept is the only one that does not rely on guidance. It is natural to ask whether it can meet the accuracy specifications that are required for an effective weapon. Our results give an unequivocal answer to this question: without an SPN it cannot; with an SPN it can.

OATS offers an opportunity to design a rocket system that is able to take full advantage of the SPN concept. The benefits of SPN would be greater in such a device than in one in which an SPN is merely retrofitted.

Since there is no experience with the OATS concept, it is hard to say anything about its uncorrectable errors. Again, it appears essential to remove one source of error by spinning up the plug as soon as the rocket has been aimed, but before it is fired. Other uncorrectable errors that are assessed as potentially significant are translation by cross-wind and gravitational drop. Both can be compensated for in the aiming process, and we recommend a fire control mechanism that incorporates cross-wind velocity and target distance data while still permitting the firers to aim visually. Marconi's Simplified Fire Control System (SFCS 600) is one such mechanism.[5]

REFERENCES

(1) Draim, John E., "Attitude Stabilization Using a Rotating Plug Nozzle", Technical Report 158, Aerophysics Laboratory, Massachusetts Institute of Technology, July 1969.

(2) Freeman, J. A., "Signature Characterization--Final Report. Volume II--Spinning Plug Nozzle (SPN) Feasibility Demonstration Program", Technical Report RK-CR-80-5, U. S. Army Missile Command, Redstone Arsenal, Alabama, September 1980.

(3) Judnick, W. E., and Samuel, A. H., "Military Applications of the Spinning Plug Nozzle", Battelle Final Technical Report to Lockheed Missile and Space Company, Huntsville, Alabama, October 31, 1980.

(4) "General Support Rocket System - Volume III: Cost and Operational Effectiveness Analysis (U)", Report ACN 20555, U. S. Army Field Artillery School, Special Study Group (SSG), Fort Sill, Oklahoma, November 1976, (CONFIDENTIAL).

(5) International Defense Review, Special Series, Volume 11, "Armoured Vehicles", pp. 79-81 (Figure 6).

AD P001072

BOOST-PHASE STEERING FOR SURFACE-LAUNCHED CRUISE MISSILES

D. J. FROMNES
GENERAL DYNAMICS CONVAIR DIVISION
P.O. BOX 80847 SAN DIEGO, CA 92138

INTRODUCTION

Implementation of boost-phase control for steering surface-launched cruise missiles to initiation of aerodynamic flight is presented. The algorithm is based on the solution of the Matrix Ricatti equation in a pseudo time domain in which the duration of booster burn is invariant. The resulting design achieves maximum launch performance in all expected environmental conditions with minimum impact on software requirements. Identification of coefficients requires little computational effort and time compared to alternative methods and is easily modified to accommodate alternate configurations and launchers.

BACKGROUND

Cruise missiles support a variety of operational scenarios from surface-launch platforms. This includes antiship autonomous search and strike as well as nuclear and conventional land attack. These roles are filled from sea- and land-based launchers. Land-based missiles are deployed from the Transporter Erector Launcher shown in Figure 1. Sea-based versions are fired from deck-mounted armored box launchers (also in Figure 1) or from the vertical launch system depicted in Figure 2.

Each launcher, launch platform, and missile configuration is unique in its relationship to launch performance and operational requirements. The generic launch sequence from booster ignition through transition to cruise flight is, however, identical in all missions. The major events in this sequence are illustrated in Figure 3.

Following booster ignition, pressure builds within the canister, causing forceful ejection of the vehicle through a frangible cover. Thrust vector control is initiated once the booster base clears the canister. Ejection of wing plugs and inlet cover, and fin erection follows. Aerodynamic roll control can be established when angle of attack is within appropriate limits and dynamic pressure is high enough to provide fin effectiveness. Once appropriate conditions of angle of attack, velocity, and flight path angle are achieved, wing deployment occurs and the shaped-trajectory autopilot assumes control. Following booster burnout, the sustainer engine is initiated and mission-dependent guidance laws take on steering functions, with the cruise autopilot providing stabilization while maximizing responsiveness.

Boost-phase steering is accomplished by indirect control of the direction of acceleration by control of pitch attitude. A number of options for boost-phase steering exist. The simplest is open-loop pitch attitude control as a function of time from launch. The design procedure is to develop a profile for nominal conditions. The profile is then altered until acceptable performance under dispersions (booster thrust, burn time, launch altitude, winds, temperature, etc.) is accomplished. A disadvantage of this approach is that these profile alterations compromise performance of the launches most likely to accommodate highly unlikely launch conditions. In principle, some form of closed-loop steering can eliminate this problem.

The specific problem which boost-phase steering must solve for the ground-launched cruise missile is maximization of downrange clearance. This provides launch site flexibility. The algorithm must also be reasonably insensitive to weight to allow flight tests with vehicles configured with recovery, telemetry, and exercise packages.

The performance of a particular missile in a particular environment for various pitch command histories is shown in Figure 4. Trajectories may be divided into two classes:

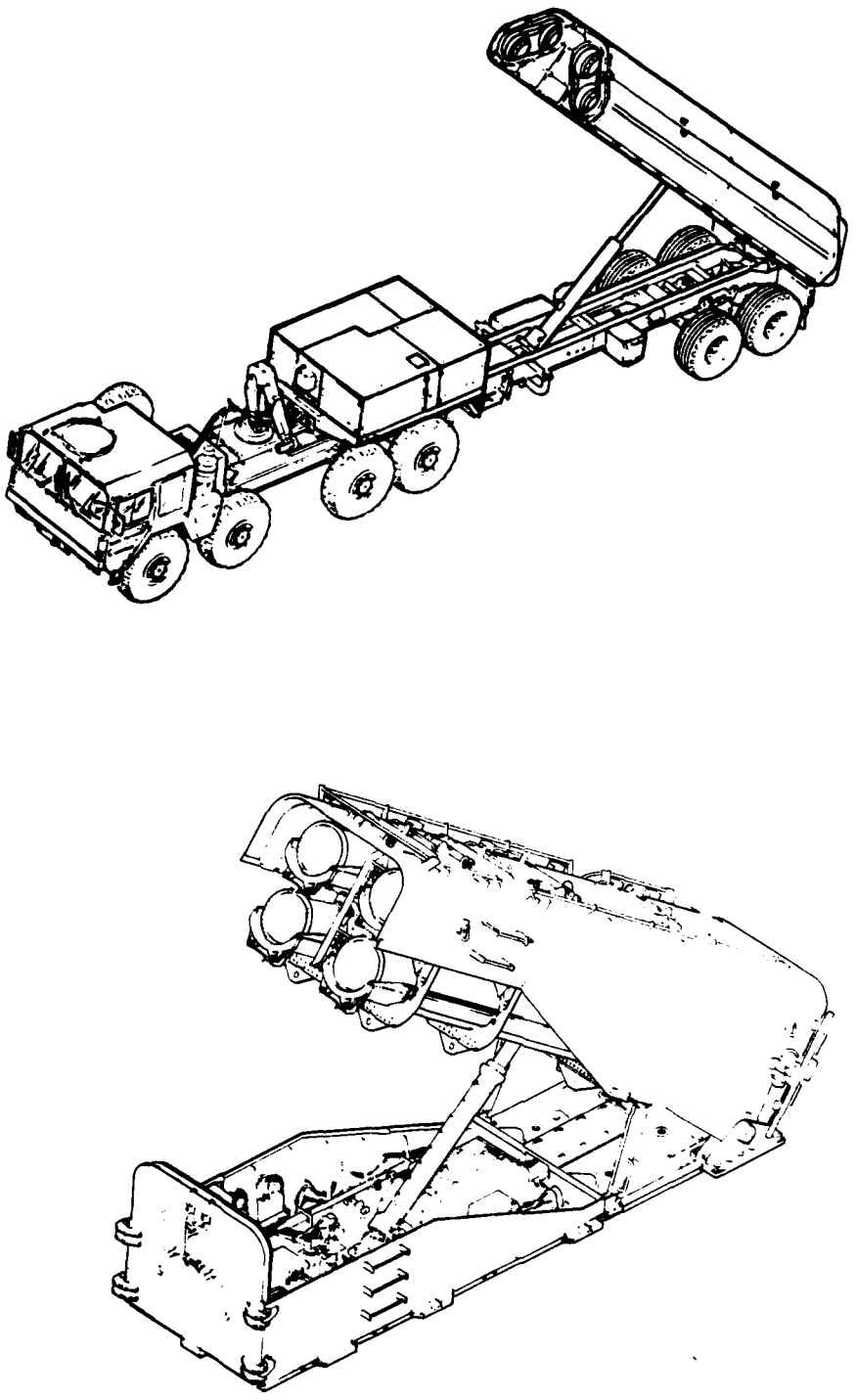


Figure 1. Transporter erector launcher and armored box launcher.

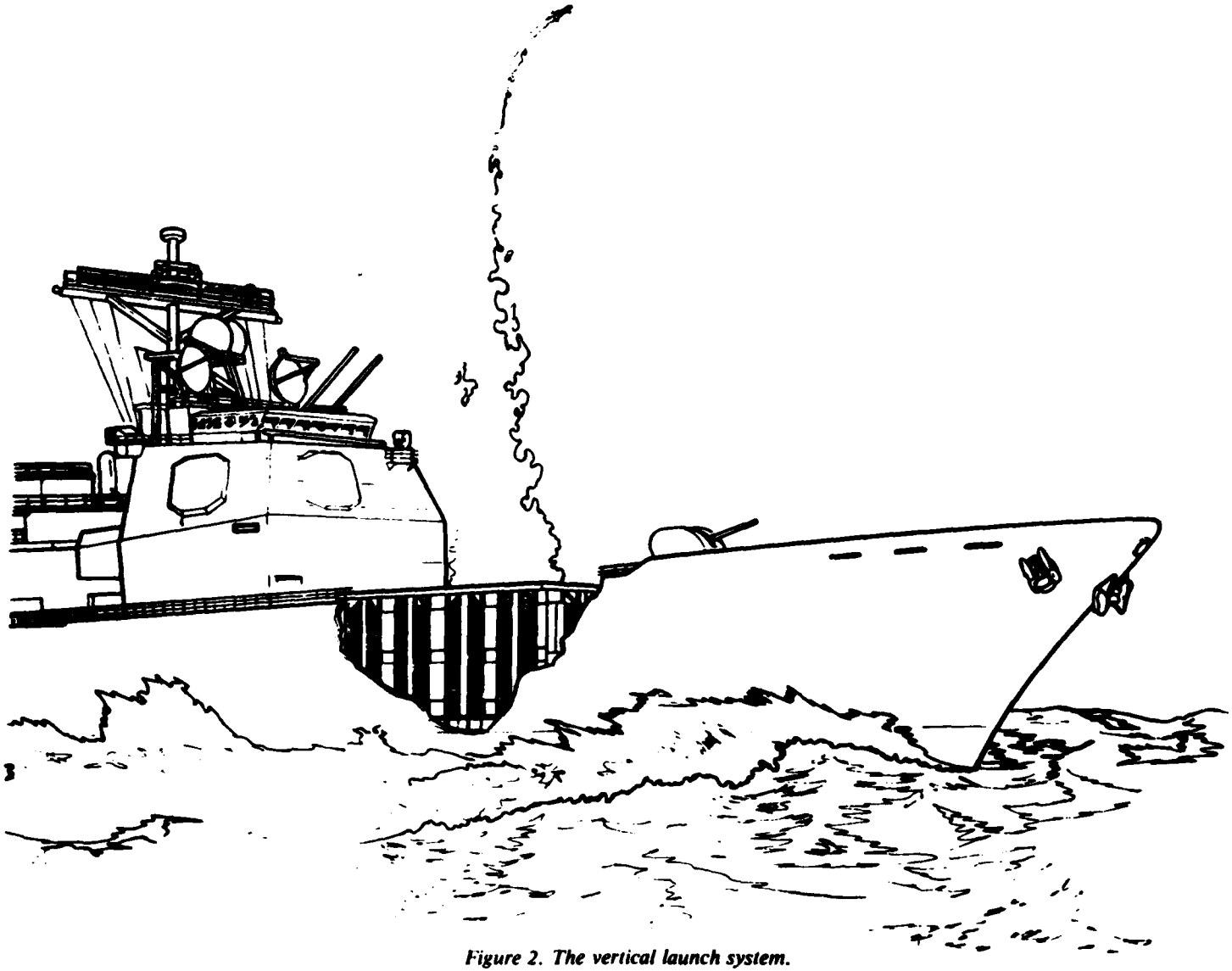


Figure 2. The vertical launch system.

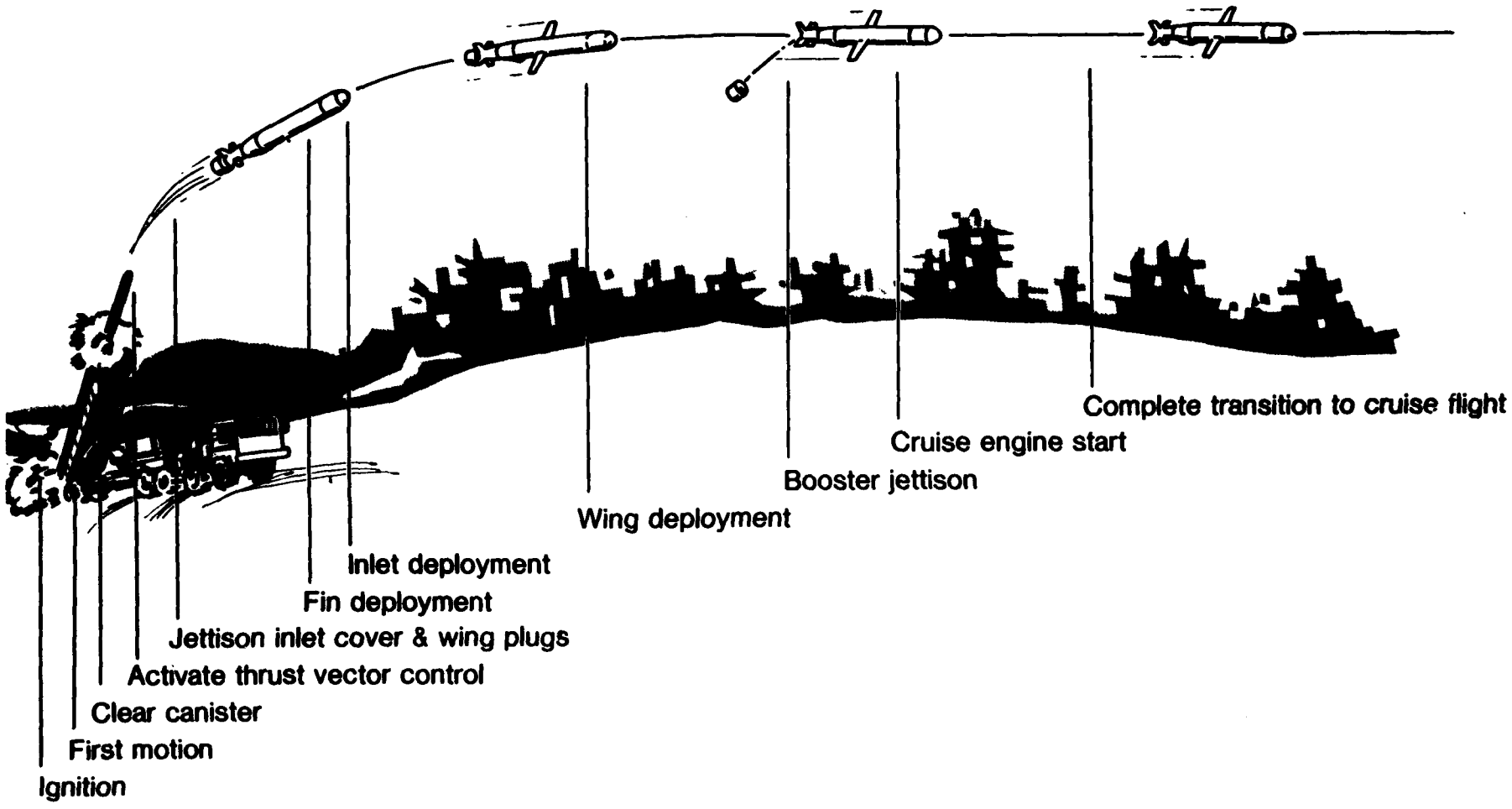


Figure 3. Generic launch sequence for surface-launched cruise missiles.

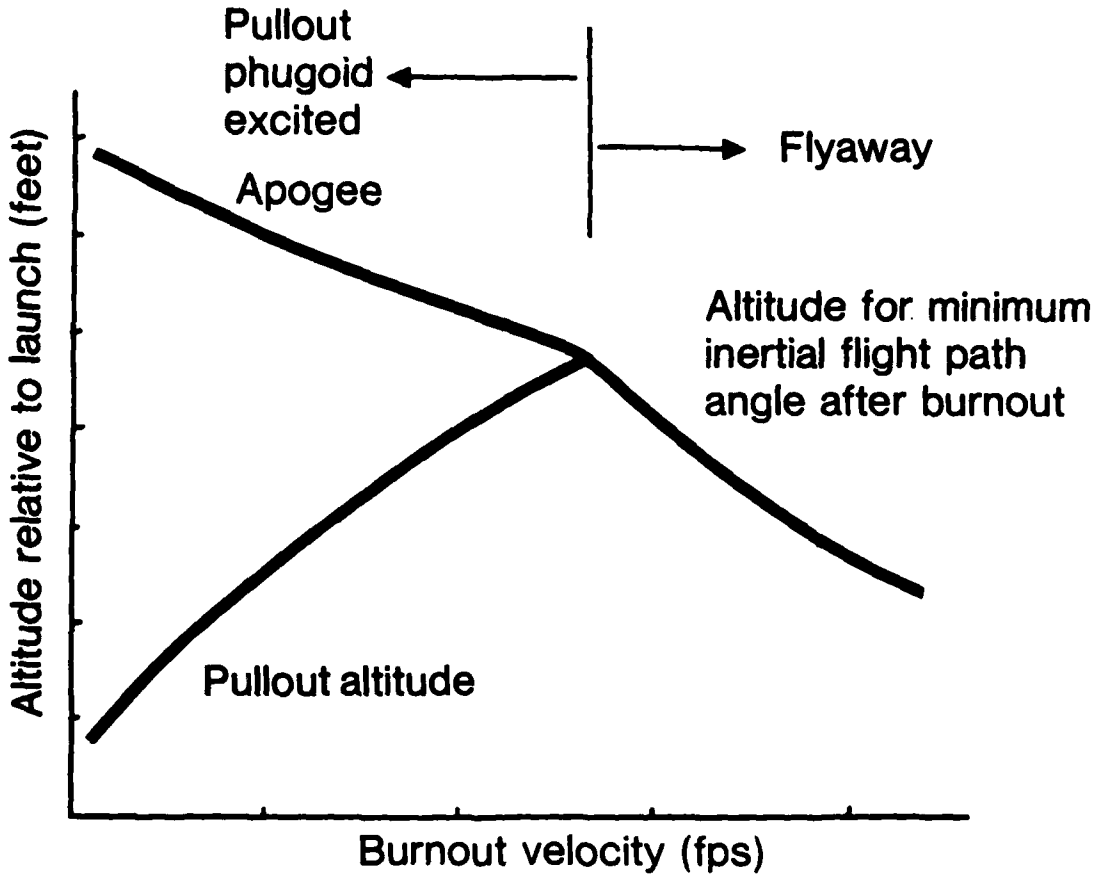


Figure 4. Maximum downrange clearance is obtained by operating as near the pullout flyaway boundary as possible.

Flyaway — Monotonically increasing altitude from launch, through transition, to cruise.

Phugoid — Climb to apogee followed by accelerating dive until pull-up velocity is obtained.

Maximum downrange clearance occurs for the pitch profile which gives performance just at the flyaway/phugoid boundary.

Figure 5 shows how velocity and inertial flight path angle can be traded over an ensemble of launch conditions to maintain this optimum flyaway condition.

Practical vehicle performance can be restricted from achieving this optimum condition in two ways. If no intersection of the apogee and pullout loci exists, then the vehicle has insufficient thrust or total impulse to achieve flyaway. As mentioned above, constraints exist on angle of attack at and following deployment of aerodynamic surfaces. These constraints restrict the set of pitch profiles available in practice.

The general character of the control system action is now clear. For any launch condition, the algorithm should adjust its trajectory to ensure burnout conditions as near as possible to the flyaway/phugoid boundary by trading velocity and flight path angle.

Many potential closed-loop steering algorithms can be identified. The best solution is one which requires minimal design effort and has the least impact on onboard computer requirements.

The classical solution for closed-loop control, compensating for vehicle and environmental dispersions, involves solution of a two-point boundary value problem. This would require computer resources in terms of both storage and duty cycle which are unacceptable for inflight implementation. In Reference (1) it was correctly concluded that a small perturbation approach would provide a solution requiring minimal computer resources and might produce a practical solution. The solution in Reference (1) experienced convergence problems when constraints on altitude and flight path angle were imposed. These convergence problems arise since the total system energy (kinetic plus potential), at some particular time from launch, varies from missile to missile. When terminal constraints are imposed on altitude, system potential energy is constrained. Terminal constraints on flight path angle constrain system kinetic energy. When dispersions are large, these constraints defeat the small perturbation assumption and make the problem ill-conditioned.

The approach take here utilizes a closed-loop steering law formulation via a small perturbation approach after the equations of motion are transformed into a pseudo-time, t^*, domain. The selection of the best nominal trajectory and best feedback are coupled. No analytical claim can be made for optimality of the overall design. However, given a feedback algorithm, evaluation of how loop closures readjust the trajectory to compensate for various dispersions allows relatively rapid determination of the nominal conditions which satisfy the objective of maximizing the launch envelope.

THE CONTROL LAW

To establish the control law, it is necessary to formulate a problem statment which can be both expressed and solved in terms of the variables available in the guidance set. The closed-loop steering problem is nonlinear. If the problem is linearized about a nominal trajectory, a linear control law can be established. The general form of such a control law is shown in Figure 6. The philosophy behind this approach is that a small variation in missile state from the nominal generates a compensating change in the command profile.

The solution procedure given such a structure is two-fold. The best combination of nominal trajectory parameters $u_o(t)$ and $x_o(t)$ must be selected, together with the best feedback, $K(t)$, to produce overall optimum performance. A linear control problem with fixed end-time constraints leads, via the Hamilton-Jacobi equations, to the Matrix Ricatti equation. This development for the time domain is well known and is described in Reference 2. If the problem is not a fixed end-time problem, variation in end time must be treated either as an additional dispersion (Reference 1) or a change of variable must be made (Reference 3).

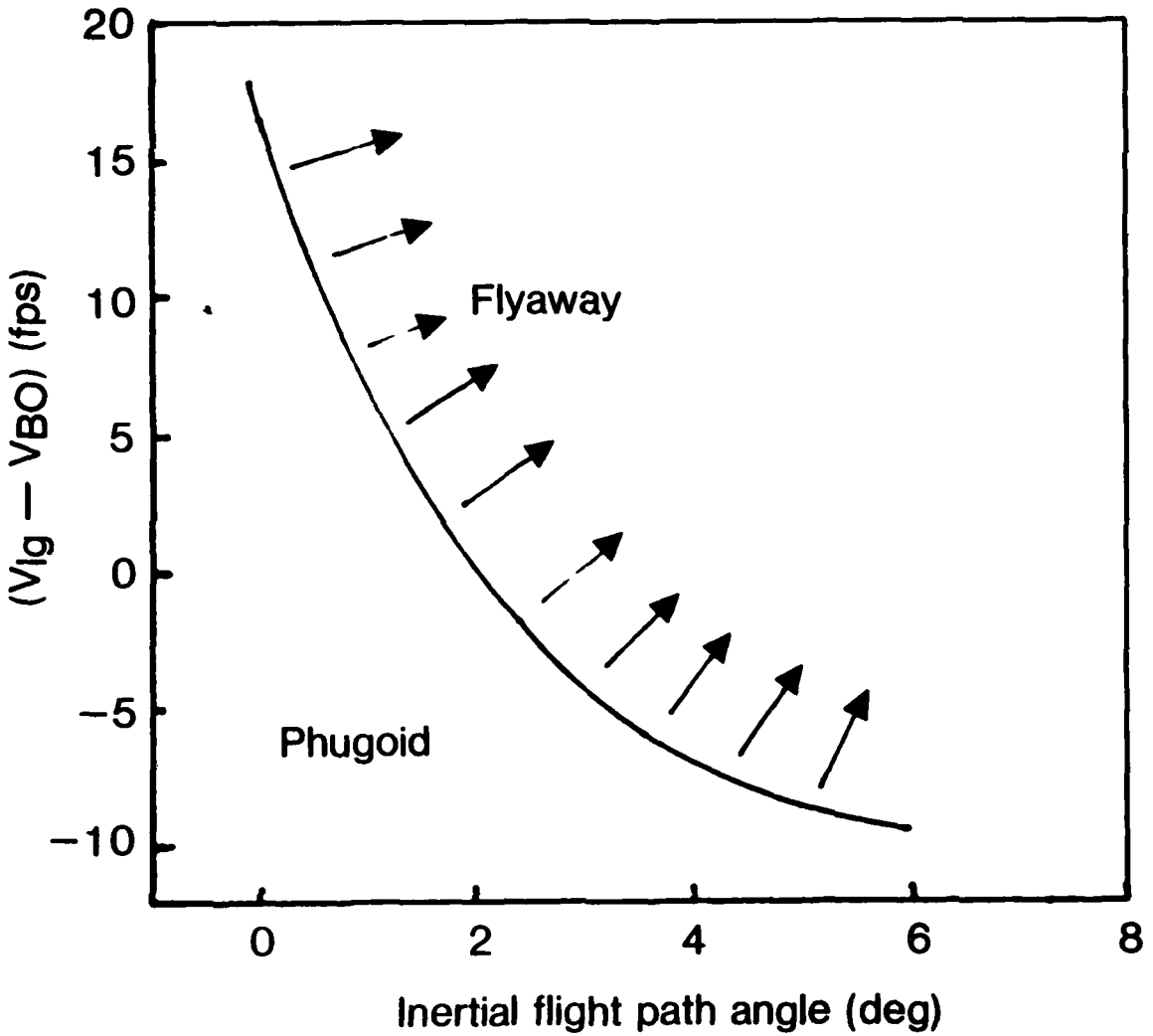
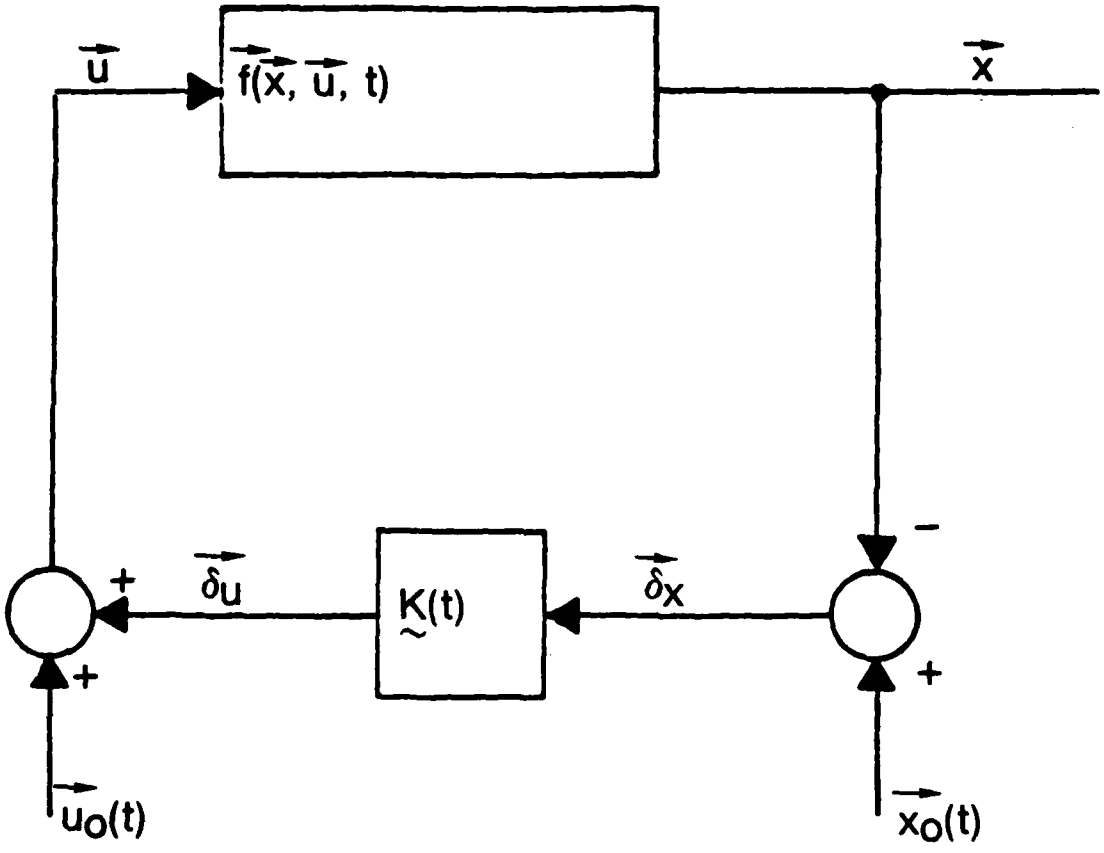


Figure 5. The relation of flight path angle and velocity at burnout to flyaway capability.



$\vec{x}$ System state

$\vec{x}_o$ Nominal state trajectory

$\vec{u}$ Control input

$\vec{u}_o$ Nominal control input

$\vec{\delta x}$ Difference between nominal and measured state

$\vec{\delta u}$ Compensatory adjustment to nominal input

$\underset{\sim}{K}(t)$ Feedback array

Figure 6. Closed-loop steering to a nominal trajectory.

A variable end-time control law might also be attempted. Here, a change of variable was made to transform the problem into a domain (t*) in which the end time was fixed. The linear control problem was solved in this domain.

SYSTEM EQUATIONS

Solution of the closed-loop feedback problem requires observability and controllability of the process. Practically, this means that it must be possible to measure all missile states as well as affect them through available inputs. The simplest equations which completely define the path of a missile in boosted flight have been used. It is assumed that the relevant motion of the vehicle is essentially planar. Figure 7 shows the pertinent geometry.

The axes u and w represent inertial (nonrotating) reference axes, with origin at the launch point. Axes x and z represent body axes fixed with respect to the vehicle. The vehicle pitch attitude is θ. Acceleration components directed along the x and z axes are a_X and a_Z, respectively. The acceleration in inertial coordinates is given by:

$$\dot{v}_u = a_X \cos\theta - a_Z \sin\theta \tag{1}$$

$$\dot{v}_w = a_X \sin\theta - a_Z \cos\theta \tag{2}$$

The altitude rate is:

$$\dot{h} = v_w \tag{3}$$

and the body axis accelerations are:

$$a_Z = g\cos\theta - (T/m)\sin\delta \tag{4}$$

$$a_X = (T/m)\cos\phi - g\sin\theta \tag{5}$$

where:

T = booster thrust
m = vehicle mass
g = gravitational acceleration
δ = thrust vector deflection angle
v_u, v_w = vehicle inertial velocity components in directions u, w

DISPERSIONS

Rather than proceeding directly to formulation of a control law, consider the effects and the form of dispersions.

BOOSTER DISPERSIONS

Solid rocket motor performance varies at a constant temperature as well as with the grain temperature of the booster. Figure 8 shows the range of variation of thrust time histories. Burn time varies by as much as three seconds and thrust magnitude by a factor of 1.8. Boosters which have higher soak temperature or are off-nominal "+2 sigma" have higher peak thrust and shorter burn time than cooler or off-nominal "−2 sigma" boosters.

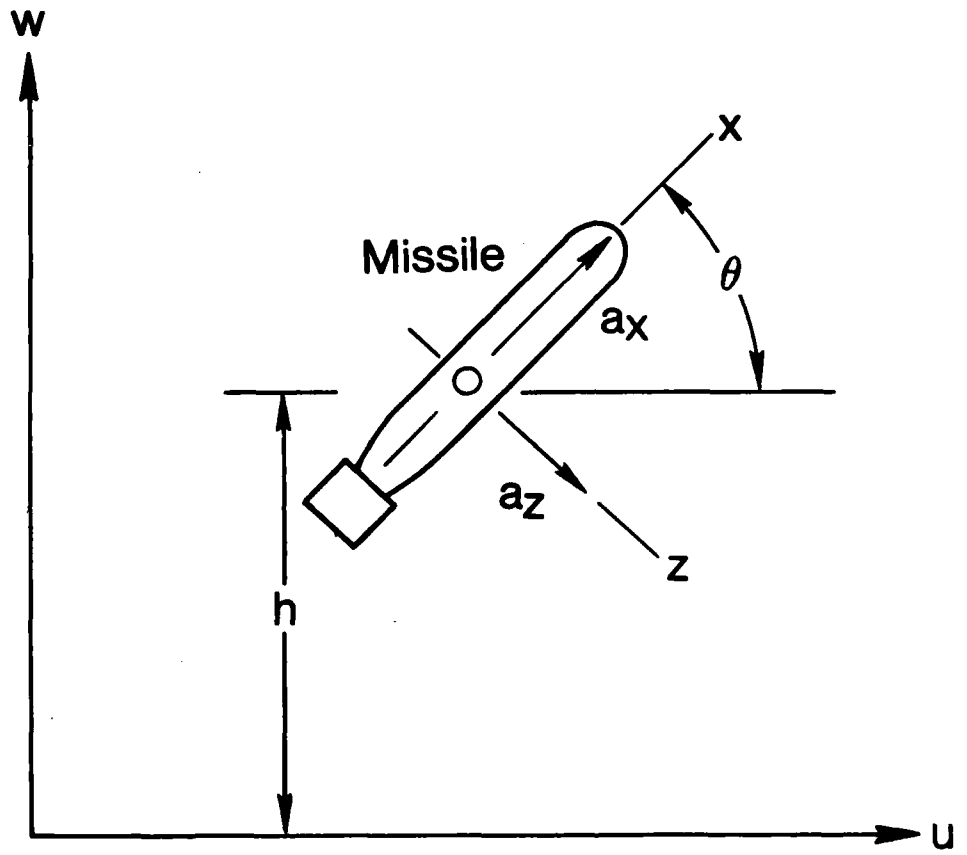


Figure 7. Geometry for vertical plane steering.

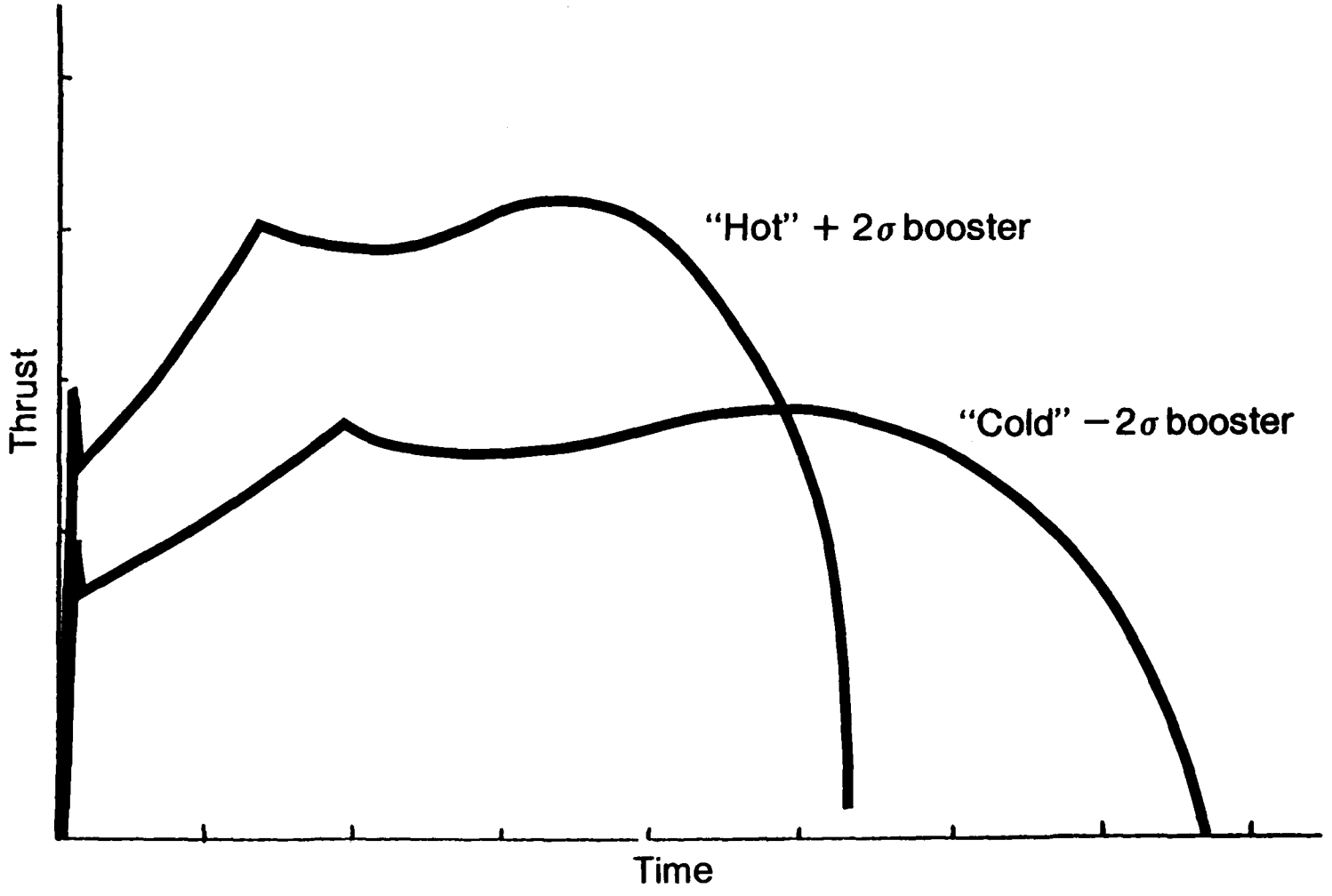


Figure 8. Variation in thrust time history.

Reference (3) identified a function: $t^* = v^{t^N}$ (6)

which could be computed from data available in the guidance set and which predicted the amplitude (to within a scale factor) and the duration of booster burn. This function was identified by regression against simulation results. Unfortunately, confidence in functions derived by regression against a limited number of simulations is low.

A physical basis for the existence of this invariant function can be identified by considering the equation which describes the velocity of a boosted vehicle.

$$v = v(o) - gI_{sp} \int_{W_o}^{W} \frac{dw}{w} - g \int_{t_o}^{t} \sin \gamma \, dt - g \int_{t_o}^{t} \frac{D}{w} \, dt \tag{7}$$

where:

v = inertial velocity, $v = v(t)$

I_{sp} = propellant specific impulse

w = vehicle weight

t = time

γ = inertial flight path angle

D = drag force

To see how equation (7) leads to an equation of the form given in equation (6), consider the ensemble of ground-launched missiles. For all ground-launched missiles $v(o) = 0$. Since all missiles will fly approximately the same flight path, the variation in the third term should be small. The aerodynamic drag integral is small compared to the second term and has restricted variation from launch to launch, so this might also be ignored.

Variations in the velocity of the missile will refelct the major launch-to-launch dispersion that is the variation in the rate of propellant consumption.

A function with small missile to missile variation should be a function of measured velocity and time from launch, such as t^*. The function t^* can now be used with a high level of confidence in the synthesis of a control system.

Thrust as a function of t^* from first motion for the extreme boosters is shown in Figure 9. Control of the vehicle as a function of t^* is a fixed end-time problem. The variation in burn time does not need to be incorporated as an unknown dispersion in performance which might defeat the small variation assumption, nor does it force the solution of a variable end-time problem.

Booster thrust, T, may now be described as:

$$T = K_b f_T(t^*) \tag{8}$$

where f_T is a nominal thrust profile and K_b is a variable peculiar to each booster. K_b is unknown but bounded by the expected range of thrust variations as seen in Figure 9.

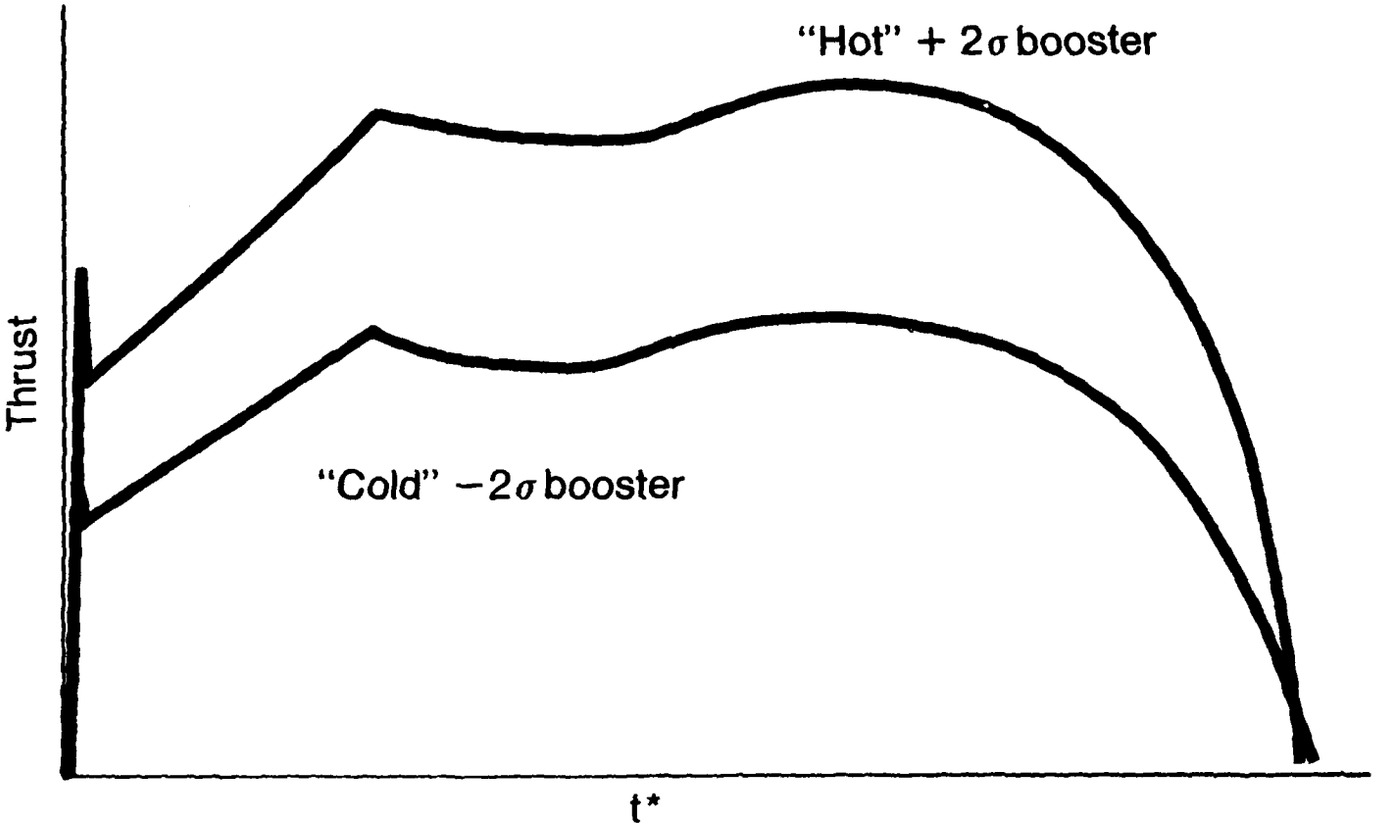


Figure 9. Thrust duration as a function of t.*

WIND DISPERSIONS

Next to variations in booster performance, the most powerful dispersion which acts to limit the operational envelope is wind. Winds act to limit the performance of a fixed-pitch profile through the variation in angle of attack at activation of fin roll control and wing deployment. In headwinds the angle of attack must be low enough to prevent a stall, while in tailwinds the angle of attack must be high enough to generate lift.

The vehicle should respond to off-nominal tailwinds by raising the pitch profile and to off-nominal headwinds by lowering the pitch profile. Pitch profiles for various wind conditions are shown in Figure 10. A closed-loop algorithm can compensate for wind dispersions and provide angle-of-attack control without attempting to measure or estimate wind explicitly. This is possible since a tailwind acts to increase downrange velocity, while a headwind, through body lift, increases vertical velocity. Thus, angle-of-attack control is accomplished without explicit inclusion of aerodynamic characteristics.

LAUNCH ANGLE DISPERSIONS

The missile must accommodate variations in launch angle in addition to all other variations. The impact of variation in launch angle on a fixed pitch profile is shown in Figure 11. The result is variation in altitude at wing deployment of approximately 200 feet and variation in inertial flight path angle of 5 deg. Since launch angle variations change the initial state without significantly varying available system energy, a closed-loop algorithm will steer to the same terminal condition from any launch angle. In fact, as will be seen, the optimal control solution is independent of initial state.

TEMPERATURE DISPERSION

As mentioned above, temperature affects the duration and thrust magnitude of the booster. At higher air temperatures atmospheric density is reduced so dynamic pressure, hence, g-capability and engine performance during shaped trajectory is reduced. For fixed-pitch profiles and some steering algorithms this means poorer performance at elevated temperatures (Reference 3).

Higher temperature boosters do have slighly more total specific impulse. Shorter burn time and higher thrust means lower gravity losses during boost. If used by a steering algorithm, these differences can compensate for performance losses due to reduced air density.

LAUNCH ALTITUDE DISPERSIONS

While launch altitude is coupled to temperature in the reference atmosphere, the primary impact on launch performance is through reduced air density at higher altitudes. There is no compensating change in booster performance. Because air data is not available during boost, closed-loop steering cannot change the performance sensitivity to launch altitude.

TRANSFORMATION OF THE SYSTEM EQUATIONS

To implement the optimal control law, the state variable form of the system equations is required. That is:

$$\frac{d}{dt}\vec{x}(t) = \vec{f}\,(\vec{x}(t),\ \vec{u}(t),\ t) \tag{9}$$

Further, the equations must be transformed to the t* domain in order to provide the fixed end-time solution. Equation (9) then becomes:

$$\frac{d}{dt^*}\vec{x}\,(t^*) = \vec{f}_2(\vec{x}\,(t^*),\quad \vec{u}\,(t^*),\ t^*) \tag{10}$$

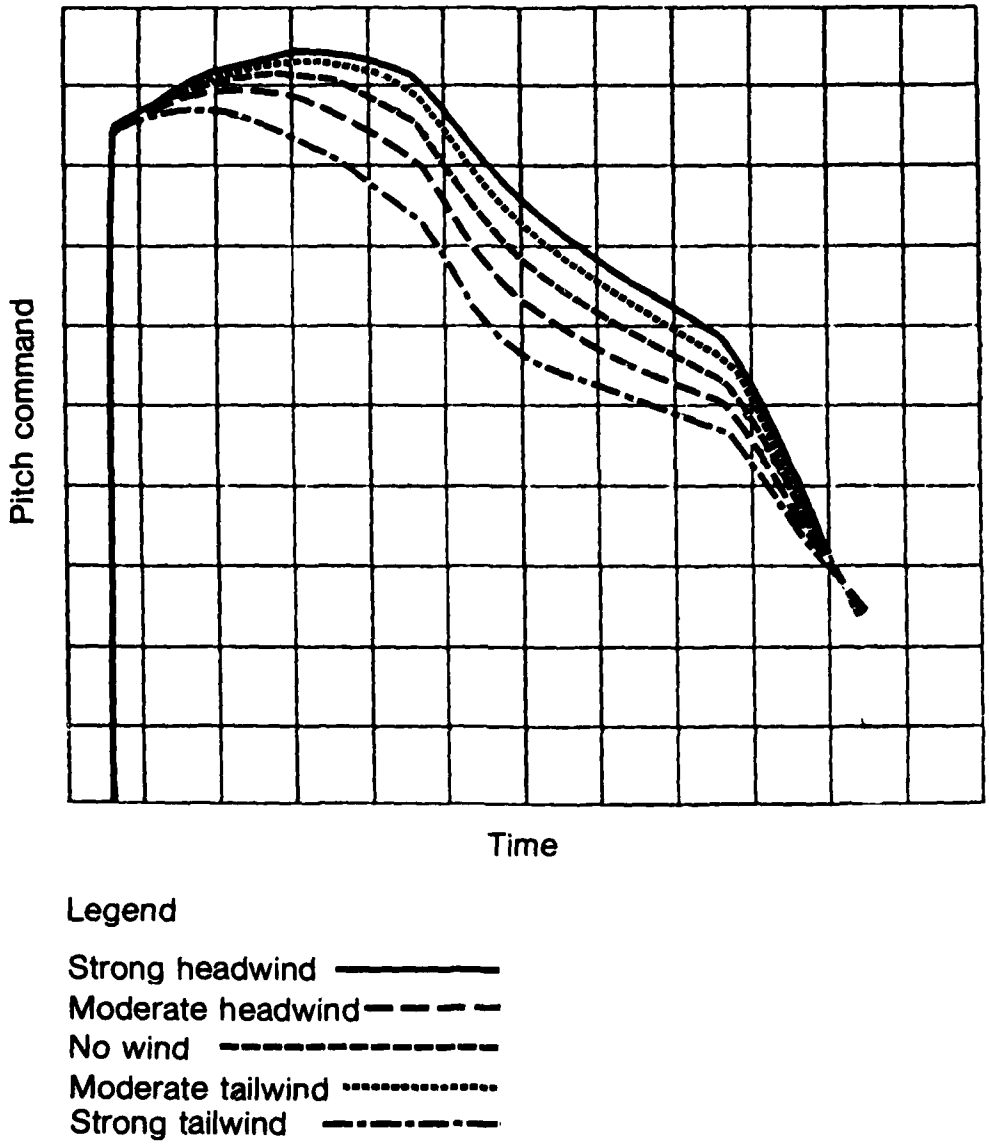


Figure 10. Pitch commands should be modified according to local wind conditions to reduce angle-of-attack variation at wing deployment.

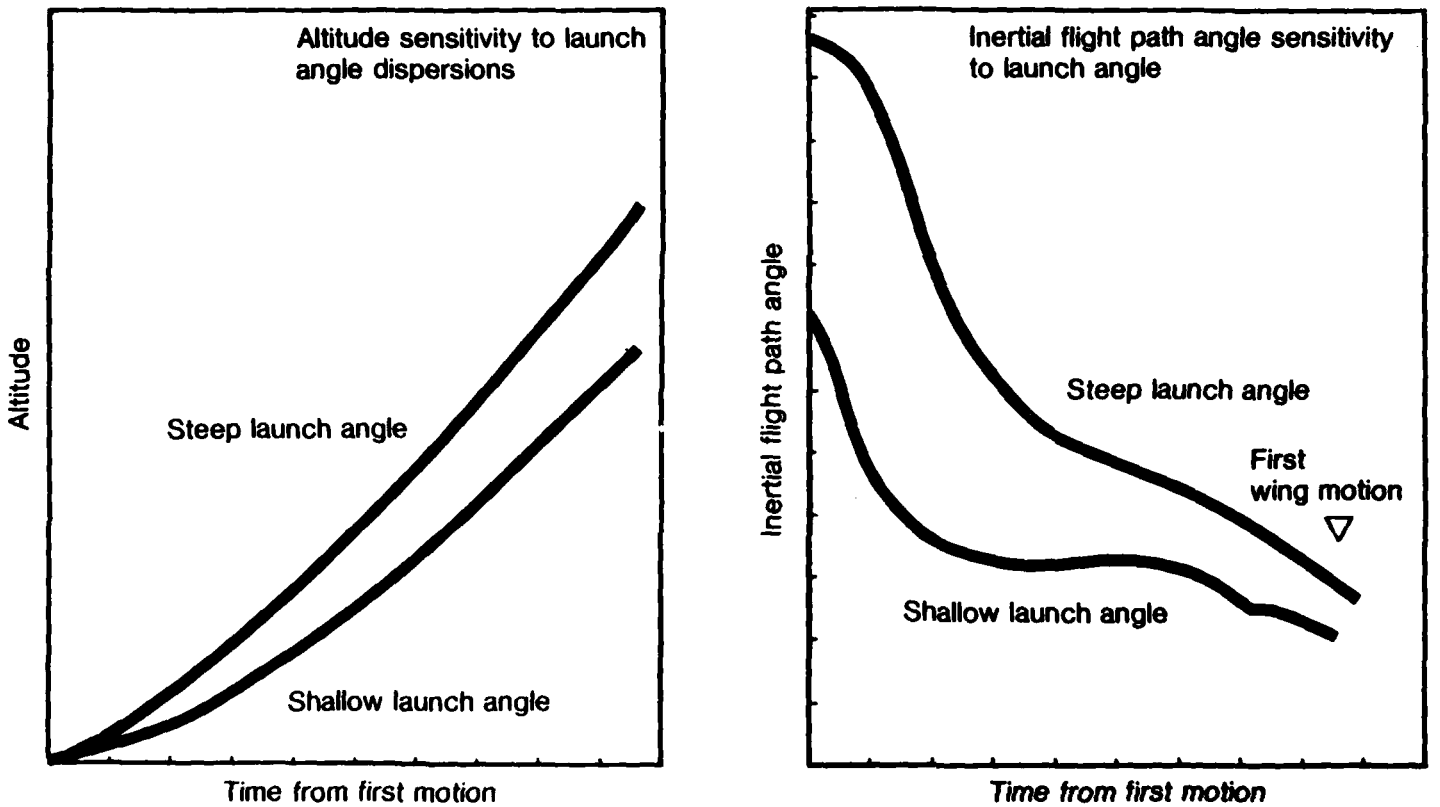


Figure 11. Launch angle sensitivity of open-loop profile.

The form of equation (9) can be obtained from equations (1) through (5) by substituting for a_x and a_z in (1), (2), and (3). The transformation to the t* domain starts with substitution for thrust, T, as defined in equation (8). Also, the variables δ, θ, and m are now functions of t* rather than t. Explicit time dependence has been removed except for the operator d( )/dt. The transformation is completed by using the fact that:

$$\frac{d(\ )}{dt}\ \frac{dt}{dt^*} = \frac{d(\ )}{dt^*} \tag{11}$$

Differentiating equation (6):

$$\frac{dt^*}{dt} = \frac{d}{dt}\ (vt^N) \tag{12}$$

$$= \frac{dv}{dt}\, t^N + N\, t^{(N-1)} \tag{13}$$

since:

$$\frac{(t^*)}{v} = t^N \tag{14}$$

$$\frac{(t^*)}{v}^{1/N} = t \tag{15}$$

and

$$t^{(N-1)} = \frac{t^N}{t} \tag{16}$$

Equation (13) can be rewritten:

$$\frac{dt^*}{dt} = \frac{dt^*}{dt}\ \frac{dv}{dt^*}\ \frac{t^*}{v} + N\, v\, \left(\frac{t^*}{v}\right)^{\left(1-1/N\right)} \tag{17}$$

Solving for (dt/dt*) gives:

$$\frac{dt}{dt^*} = \frac{1 - v'\ \left(\frac{t^*}{v}\right)}{N\, v\ \left(\frac{t^*}{v}\right)\ (1\text{-}1/N)} \tag{18}$$

where:

$$(\ )' = \frac{d(\ )}{dt^*}$$

Multiplying through the system equations by dt/dt* at this point gives:

$$v'_u = \left(\frac{dt}{dt^*}\right) \frac{K_b}{m} f_T(t^*) \cos\delta \cos\theta - \frac{K_b}{m} f_T(t^*) \sin\delta \sin\theta \tag{19}$$

$$v'_w = \left(\frac{dt}{dt^*}\right) \frac{K_b}{m} f_T(t^*) \cos\delta \sin\theta + \frac{K_b}{m} f_T(t^*) \sin\delta \cos\theta - g \tag{20}$$

$$h' = \left(\frac{dt}{dt^*}\right) v_w \tag{21}$$

The difference between the form of equations (19) through (21) and equation (10) is that derivatives of the states are on both sides of the equation because of the presence of v' in dt/dt*. This is corrected by the use of algebra only to give the state equations in the t* domain.

$$v'_u = \frac{1}{a_1}\left\{ A - \left(\frac{b_1}{b_2 - \frac{a_2}{a_1} b_1} \right)\left(B - \frac{a_2}{a_1} A \right) \right\} \tag{22}$$

$$v'_w = \left(\frac{1}{b_2 - \frac{a_2}{a_1} b_1} \right) \left(B - \frac{a_2}{a_1} A \right) \tag{23}$$

$$h' = \left\{ - \frac{a_3}{a_1} \left(A - \frac{b_1}{b_2 - \frac{a_2}{a_1} b_1} \right) - \frac{b_3}{b_2 - \frac{l_2}{a_1} b_1} \right\} \left(B - \frac{a_2}{a_1} A \right) + C \tag{24}$$

where:

$$a_1 = 1 + \left(\frac{K_1 K_b}{m} f_T \, t^{*(1/N-1)} \, V - (2+1/N) V_u \right) (\cos\delta \cos\theta - \sin\delta \sin\theta)$$

$$b_1 = \left(\frac{K_1 K_b}{m} f_T t^{*(1/N-1)} V - (2+1/N) V_w \right) (\cos\delta \cos\theta - \sin\delta \sin\theta)$$

$$A = \left(\frac{K_1 K_b}{m} f_T t^{*(1/N-1)} \, V(-1/N) \right) (\cos\delta \cos\theta - \sin\delta \sin\theta)$$

$$a_2 = \left(\frac{K_1 K_b}{m} f_T t^{*(1/N-1)} \, V - (2+1/N) \, V_u \right) (\cos\delta \sin\theta - \sin\delta \cos\theta - g)$$

$$b_2 = 1 + \left(\frac{K_1 K_b}{m} f_T t^{*(1/N-1)} \, V - (2+1/N) \, V_w \right) (\cos\delta \sin\theta + \sin\delta \cos\theta - g)$$

$$B = \left(\frac{K_1 K_b}{m} f_T t^{*(1/N-1)} \, V(-1/N) \right) (\cos\delta \sin\theta + \sin\delta \cos\theta + g)$$

$$a_3 = -K_1\, t^{*(1/N-1)}\, V^{-(2+1/N)}\, V_u\, V_w$$

$$b_3 = -K_1\, t^{*(1/N-1)}\, V^{-(2+1/N)} V_w^2$$

$$C = K_1\, t^{*(1/N-1)}\, V^{(1/N)}\, V_w$$

$$K_1 = (1/N)$$

Clearly, acquiring the fixed end-time problem, as well as the desired form of the system equations, has greatly complicated the system equations. As will be shown, it is only required that this form of the equations exist. Implementation proceeds via a numerical approach.

THE CONTROL LAW

Implementation of the control law as two components. The analytical effort demonstrates that a control law of the type proposed (t^* based) can be synthesized. This is of more than academic interest. It makes possible validation of the control law without such extensive simulation analysis as would otherwise be required. It also identifies the structure of the control law. The second part of implementation is determination of the actual coefficients. It is inappropriate to determine the actual coefficients from the simplified analytical model.

ANALYTICAL CONSIDERATIONS

The classical method for optimal control uses the Lagrange multiplier-Pontryagin method for solving the basic optimal control problem. In that case the system is described by equations of the form of equation (9) with performance index

$$G = \int_{t_o}^{t_f} L(\vec{x}, \vec{u}, t)\, dt \tag{25}$$

The computational problem is the two-point boundary value problem and only open-loop control is obtained. The method can be used to obtain closed-loop control if this problem can be solved repeatedly in real time readjusting t_o forward. This is infeasible with present flight computers.

The use of the Hamilton-Jacobi approach admits solution in a straightforward manner and the resulting control law is a function of the state variables which implies closed-loop control (Reference 2).

The solution is begun by assuming that the input, $\vec{u}$, is given by an optimal control law $\vec{u}^{\,o}(\vec{x}, t^*)$. Next, define a scalar function $V(\vec{x}, t^*)$ which is the value of the performance index when evaluated along the optimal trajectory beginning at $\vec{x}\,(t^*_o)$.

$$V(\vec{x}, t^*) = \int_{t^*_o}^{t^*_f} L(\vec{x}, \vec{u}^{\,o}(\vec{x}, \tau), \tau)\, d\tau \tag{26}$$

The derivative of $V(\vec{x}, t^*)$ with respect to t^* evaluated at the lower limit can be written as:

$$V'(\vec{x}, t^*) = -L(\vec{x}, \vec{u}^{\,o}(\vec{x}, t^*), t^*) \tag{27}$$

Alternatively, using the chain rule:

$$V'(\vec{x}, t^*) \times \nabla^{-} V^T(\vec{x}, t^*) \vec{f}(\vec{x}, \vec{u}^o(\vec{x}, t^*), t^*) + \frac{\partial V(\vec{x}, t^*)}{\partial t^*} \tag{28}$$

where ∇ denotes gradient and $(\ )^T$ transpose. These two equations can be combined to provide:

$$\vec{\nabla} V^T(\vec{x}, t^*) \vec{f}(\vec{x}, \vec{u}^o(\vec{x}, t^*), t^*) + \frac{\partial V(\vec{x}, t^*)}{\partial t^*} + L(\vec{x}, \vec{u}^o(\vec{x}, t^*), t^*) = 0 \tag{29}$$

The next step is to find $\vec{u}^o(\vec{x}, t)$ as a function of $\vec{\nabla} V$, x and t^*. Substituting this in equation (29) results in a partial differential which is soluble for $V(\vec{x}, t^*)$. With $V(\vec{x}, t^*)$ known, $\vec{u}^o(\vec{x}, t^*)$ can be found. Without going into all the details, this procedure is accomplished by forming the Pontryagin state function, H, with the adjoining variables replaced by $\vec{\nabla} V$. That is:

$$H(\vec{x}, \vec{u}, \vec{\nabla} V, t^*) = \nabla V^T \vec{f}(\vec{x}, \vec{u}, t^*) + L(\vec{x}, \vec{u}, t^*) \tag{30}$$

Then minimize $H(\vec{x}, \vec{u}, \vec{\nabla} V, t^*)$ with respect to u to obtain $\vec{u}^o(\vec{x}, \vec{\nabla} V, t^*)$. Find the optimal H, H^o, by substituting u^o just computed into equation (30). If the partial differential equation:

$$H^o(\vec{x}, \vec{\nabla} V, t^*) + \frac{\partial V}{\partial t^*} = 0 \tag{31}$$

with appropriate boundary conditions is solved, $V(\vec{x}, t^*)$ is obtained. The resulting $V(\vec{x}, t^*)$ determines $\vec{u}^o$ as a function of $\vec{x}$ and t^* only.

Clearly, given the complexity of the state equations, this procedure could not be carried out analytically in any reasonable time frame. It has been shown by repeating the development to this point that an analagous form of the Hamilton-Jacobi procedure for computing an optimal control law exists in the t^* domain.

If the state equations are linearized about some nominal flight path, and a performance index of the form

$$PI = \int_{t^*_o}^{t^*_f} \vec{x}^T \underline{Q} \vec{x} + \vec{u}^T \underline{P} \vec{u} \, d\tau \tag{32}$$

is used, then, applying the Hamilton-Jacobi procedure results in a control input which is a linear combination of vehicle state. The linearized state equations are of the form

$$\frac{d}{dt^*} \vec{x} = \underline{A} \vec{x} + \underline{B} \vec{u} \tag{33}$$

where $\vec{x}$, the state vector is physically the variation of the missile from the nominal trajectory, $\vec{u}$ is the variation of the input from the nominal input. The problem which must be solved is a form (in the t^* domain) of the familiar matrix Ricatti equation.

$$\underline{R}'(t^*) - \underline{Q} - \underline{R}(t^*) \underline{B} \underline{P}^{-1} \underline{B}^T \underline{R}(t^*) + \underline{R}(t^*) \underline{A} + \underline{A}^T \underline{R}(t^*) = 0 \tag{34}^*$$

with boundary condition $R(t^*_f) = 0$.

Once R(t*) is known, the optimal control law is

$$\vec{u}^{\,o}(x, t^*) = -\underset{\sim}{P}^{-1}\,\underset{\sim}{B}^{T}\,\underset{\sim}{R}(t^*)\,\vec{x}$$

The analytical work to this point has demonstrated that closed-loop control in the t* domain is reasonable. It also has identified the procedures which can be used to generate a practical solution.

IMPLEMENTATION CONSIDERATIONS

It has been shown that a controller can be formulated in the t* domain and that a system of equations which could, at least in principle, be solved is available. The simplest structure for such a controller (assuming off-diagonal elements of $\underset{\sim}{K}$ are zero) is shown in Figure 12. There are several approaches available for determining the elements of the $\underset{\sim}{K}$ matrix.

If many optimal trajectories were available, a nominal trajectory could be selected; then, the $\Delta\theta$ and state variations between these optimal trajectories would also be available and all elements of $\underset{\sim}{K}$, $\underset{\sim}{R}$, $\underset{\sim}{P}$, and Q could be computed algebraically. The time and expense of such a procedure is prohibitive. In any event, the $\underset{\sim}{P}$, Q, and $\underset{\sim}{R}$ arrays are of little practical significance.

The approach used here was selection of the simplest form of the optimal control structure. Selection of the nominal trajectory was based on an intuitive understanding of how the pitch profile should be modified under various dispersions. It was previously described, qualitatively, how compensation should act. The next section discusses selection of the nominal trajectory and feedback exclusively in terms of system requirements.

The decision was made to begin with the most reduced form of the optimal control structure because it was essential to minimize the number of inflight computations and the duty cycle of the onboard computer. It was also necessary to meet the original performance specification. The minimal implementation would only be upgraded if it became necessary to enlarge the launch envelope.

SELECTION AND GENERATION OF NOMINALS AND COEFFICIENTS

A restricted number of optimal trajectories for specific flight conditions can be generated automatically by trajectory optimization programs. The requirement in the GLCM program for boost phase steering is to maximize downrange clearance for the specified range of variations in launch conditions.

Since the nominal trajectory is optimum for the specified conditions in all situations where total available energy is the same, the vehicle should steer to the nominal terminal state. When the nominal trajectory is the minimum energy case, higher energy situations can steer to conditions which provide minimum excitation of the pullout phugoid, while "disposing" of excess energy by increasing altitude. The optimum nominal trajectory is, therefore, the minimum energy case.

Figure 5 shows how velocity and flight path angle at burnout can be traded to maintain a flyaway condition for the vehicle studied. Figure 4 shows that maximum downrange clearance is obtained by operating as near as possible to the boundary between flyaway and excitation of the pullout phugoid.

Rough calculation of a $\underset{\sim}{K}$ array and some experimentation resulted in fixed-feedback coefficients which satisfied the condition that for the same available energy the vehicle steers to the same terminal condition (Figure 13). Figure 10 showed pitch command modification with wind variation which allowed angle-of-attack constraints to be met.

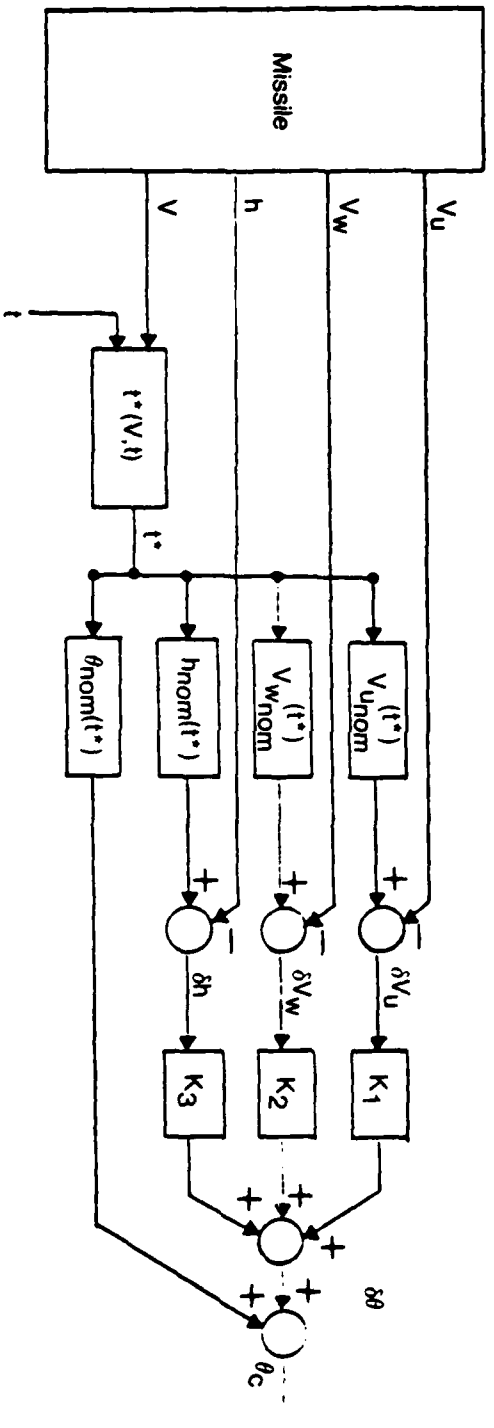
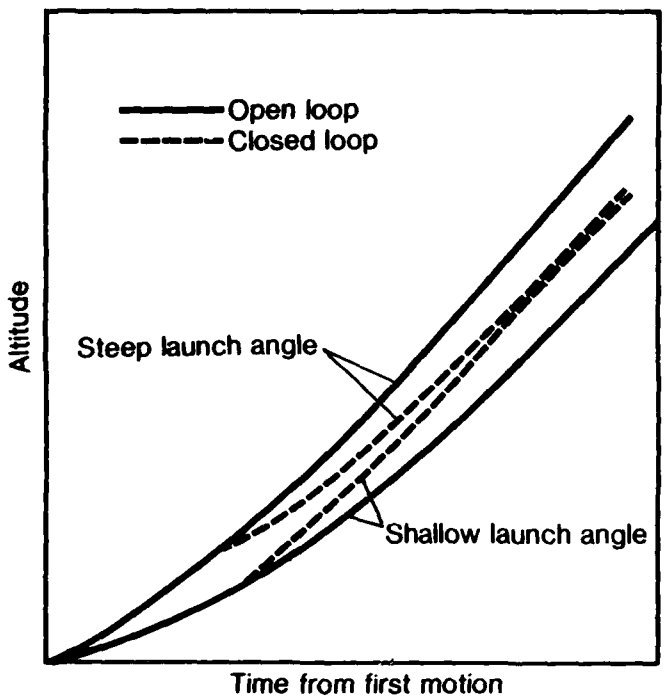


Figure 12. Explicit structure of the control law.



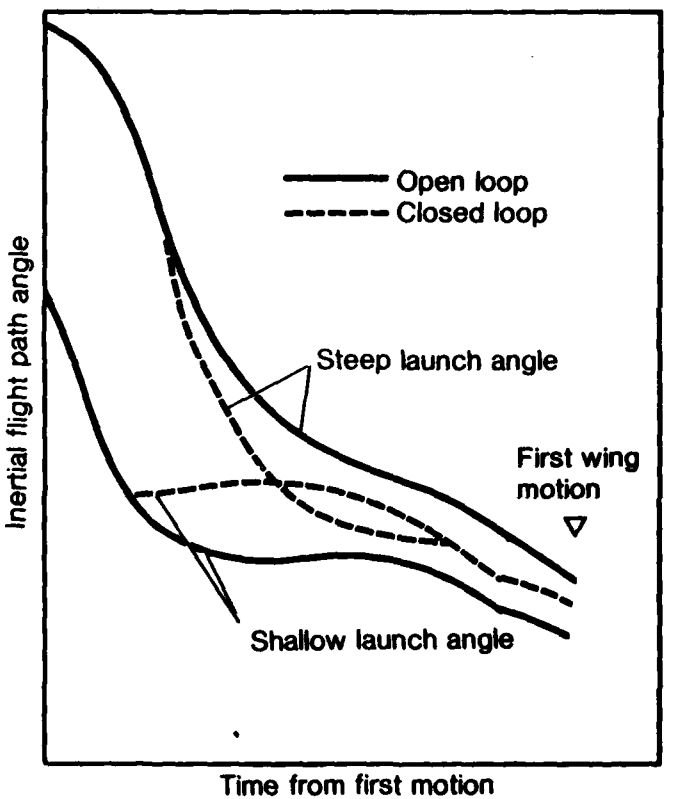


Figure 13. Closed-loop sensitivity to ***launch angle dispersions.***

It is desirable to meet the specified performance in terms of tailwinds, temperature, and altitude while at the same time maximizing downrange clearance in the anticipated launch envelope. Maximizing tailwind capability is synonymous with suppressing the nominal trajectory. For this reason the nominal trajectory, just meeting the performance spec, was chosen. This minimizes suppression of downrange clearance in the expected launch envelope.

Figure 14 shows vehicle performance under variation in wind speed. The nominal is a trajectory which maximizes altitude for a strong tailwind constrained to a velocity at burnout of Vl_g plus 20 feet per second. The performance, given temperature, altitude, and wind variations, verifies the approach to selecting the nominal.

SOFTWARE IMPLEMENTATIONS

As mentioned above, for implementation in the onboard computer it is desirable to minimize duty cycle and core requirements. It is also desirable to minimize the impact on existing software. The simplest and most compact means of storing the nominal trajectory parameters is as single polynomials. The coefficients of this polynomial are obtained by generating a sequence of orthogonal polynomials using a weight least-squares algorithm (Reference 4). The orthogonal polynomials can then be combined algebraically (by collecting terms of like power) to form a single polynomial.

Adjustment of the weighting function and experimentation with polynomials of various order leads to the conclusion that a fourth-order fit will provide errors of less than 2% in the interval of interest. It was further determined (by simulation) that errors of this magnitude do not significantly deteriorate performance of the steering loop.

Implementing the polynomials in nested form minimizes the impact on duty cycle. In the absence of exponentiation and logarithmic functions in the autopilot, t^* is also implemented as a polynomial.

The nominal pitch profile is not implemented as a polynomial; but, it is a pair of tables of pitch attitudes and "times" (t^*). This is to minimize impact on existing boost-phase software.

Boost-phase steering is terminated by ramping the $\delta\theta_c$ value to zero over one second following passage of the normalized velocity test ($t^* \geq t^*_{NVT}$) which initiates wing deployment. Ramping the algorithm out in this way was found to reduce the pitch rate just prior to wing deployment.

The philosophy of the normalized velocity test is to provide the fixed end-time problem required for boost-phase steering. Practically, it means that wing deployment occurs for all launches with the same fraction of booster mass expended, hence, identical cg position.

The use of t^* continues in the shaped-trajectory autopilot. It replaces a time scheduling of gains which was intended as an approximate schedule with cg location. Scheduling with t^* reduces the uncertainty in cg location.

The nominal pitch command is computer at 64 Hz to maintain consistency with existing software. Adjustments, $\delta\theta_c$, are computed at 16 Hz. Simulations have been done as slowly as 8 Hz with no degradation in performance. The cycle-to-cycle variation in $\delta\theta_c$ between successive cycles is typically less than 0.05 degrees.

FLIGHT TEST RESULTS

Two flight tests of the ground-launched cruise missile which included boost-phase steering have been conducted. Flight test telemetry and simulation data are shown in Figure 15. Differences can be attributed largely to differences between simulated and actual environmental conditions (such as winds aloft).

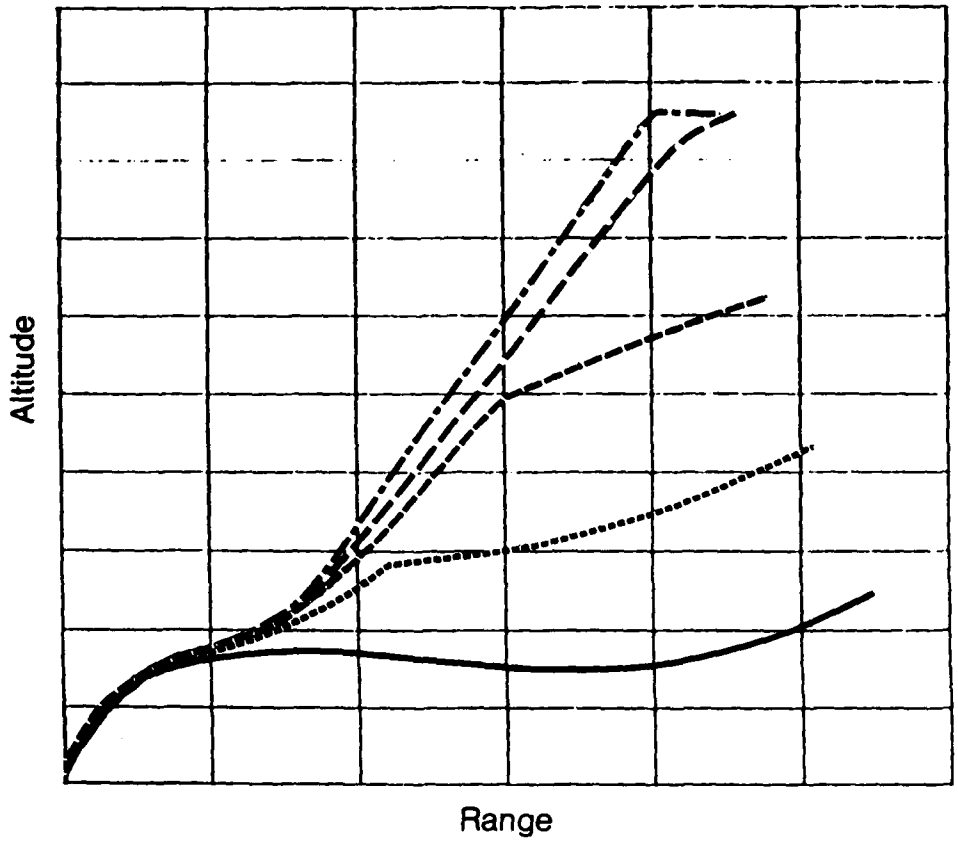
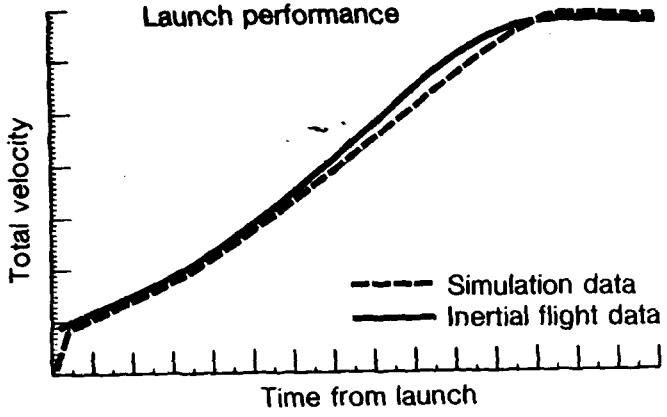
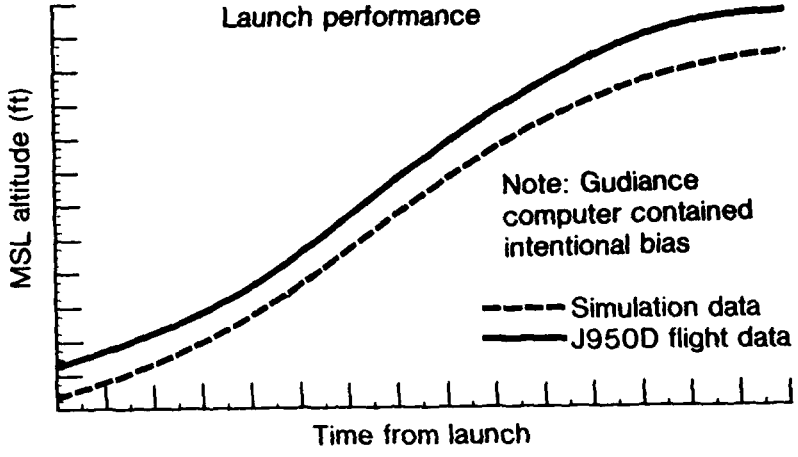
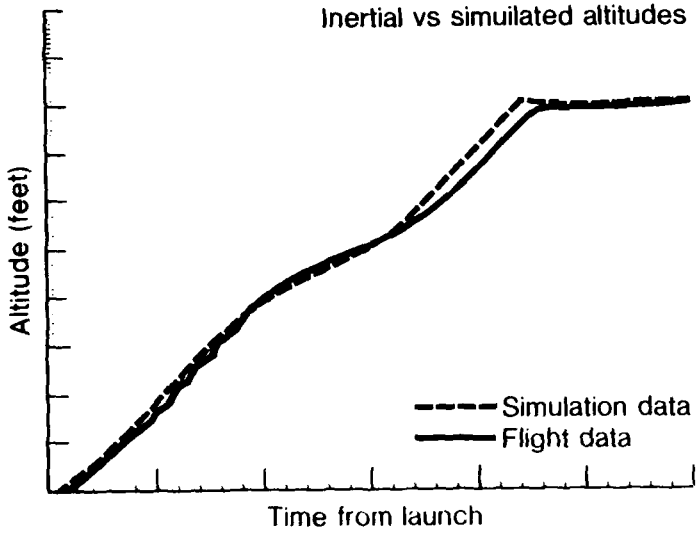


Figure 14. Boost-phase steering uses available resources to maximize downrange clearance.







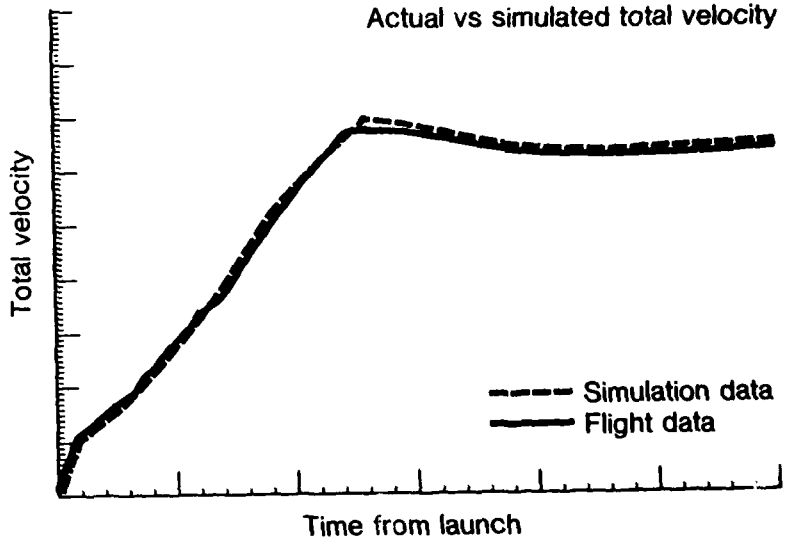


Figure 15. Comparison of flight test data with predicted flight.

In addition to validation of performance and onboard software testing, these flight test results validate simulation software. The ability to synthesize a controller using this approach requires *a-priori* existence of a highly detailed, validated simulation.

MODIFICATION OF THE ALGORITHM

Other launch platforms and vehicle configurations are easily accommodated by this design approach once the trajectory optimization and verified six-degree-of-freedom simulation program are available. Moving launch platforms such as surface ships use a pseudo time domain in which velocity relative to launch velocity is measured.

The exponent of time is dependent, as can be seen from equation (7), on mass and flight path. Vehicles with highly different flight paths such as exist between the vertical launch system and the armored box launcher can be expected to have different coefficients for t^*. Optimization for criteria other than maximizing downrange clearance is also possible.

REFERENCES

(1) Backus, F. I., "Closed-Loop Booster Guidance," NCM-7369, 18 May 1977.

(2) Bryson, A. E. and Ho, Y. C. "Applied Optimal Control," Hemisphere Publishing Corporation, 1975.

(3) Wright, W. N., "An Approach to Optimum Launch Performance for the GLCM Launch Vehicle," DN #1265, 17 July 1979.

(4) Conte, S. D. and deBoor, C., "Elementary Numerical Analysis: An Algorithmic Approach," McGraw-Hill, 1972.



Next page is blank.

AD P001073

CLOSED-LOOP BULLET TRACKING ALGORITHMS FOR DIGITAL FIRE CONTROL SYSTEMS

Radhakisan S. Baheti
Corporate Research and Development
General Electric Company
Schenectady, New York 12345
Tel. 518-385-5629

ABSTRACT

A new concept in closed-loop digital control for rapid fire gun defense system is proposed. It assumes that a phased-array radar tracks both the enemy targets and the bullets fired by a defensive gun system. The paper describes an adaptive algorithm developed for processing the large number of radar measurements.

A flyby subsonic target under an attack mission is considered. The ballistic estimation algorithm consists of three parts. First, the radar observations on each bullet in flight are compensated for different gun angles. Second, an averaging algorithm is used to filter the radar noise and round dispersions. Finally, a recursive estimator updates the parameters of the bullet trajectory model in real time. The gun-order computation is enhanced by feedback from the ballistic estimator.

A computer simulation model of the closed-loop fire control system has been developed. It is seen that the closed-loop system reduces the target miss distance by a factor of five compared with an open-loop system. The response time of the closed-loop system is less than one second.On the other hand, the first bullet has a time of flight of five seconds to reach the target range.

The approach has the following significant features:

a. The adaptive model compensates for inaccurate apriori information of the muzzle velocity, gun azimuth and elevation biases and the drag coefficient.

b. The response time of the closed-loop system is significantly less compared to an alternative design. Therefore, a precalibration fire is not crucial for success.

c. Wind effects can be easily compensated by suitable estimators.

d. The proposed approach makes use of the information gathering ability of the phased-array radar.

I. INTRODUCTION

Advancements in radar technology and computational power of microprocessors have significantly influenced modern digital fire control systems. The present level of technology in phased-array radar allows tracking of target and bullet trajectories with high accuracy. This has opened up a new dimension to gun fire systems. One possible approach to improve gun aiming accuracy is to utilize all the available information about the fired bullets and correct the gun-orders in a closed-loop manner. This calls for development of new algorithms to process the large number of radar measurements. In this paper, a closed-loop bullet tracking approach is developed to improve the gun aiming accuracy. The method is based on estimation algorithm to update parameters of the bullet trajectory model in real time.

A block diagram of the fire control concept with closed-loop bullet tracking is presented in Figure 1. A phased-array radar is used for measurement of the target position $\underline{X}_T(t)$ and each bullet position $\underline{X}_n(t)$ in flight. A recursive algorithm estimates the unknown parameters $\underline{\theta}$ of the bullet trajectory model based on the radar measurements. The estimated parameters are input to the ballistic predictor. A target tracking filter provides input to the target predictor. The outputs of the ballistic predictor and the target predictor are used to solve for the time-of-flight and the future target state. Finally, a gun-order estimator computes the desired gun angles. The algorithm to track bullets using radar data is briefly presented in the following:

A ballistic trajectory model is represented by nonlinear coupled differential equations. Approximate closed-form solution (algebraic model) is derived by treating drag as the dominant forcing term in the direction of initial bullet velocity. The algebraic model represents the bullet motion in the XL-coordinate fired with a fixed gun elevation angle. The XL-coordinate is in the direction of the gun aim vector. The YL-coordinate is defined in a vertical plane formed by the reference gun aim vector and the gravity. The YL and ZL axes are chosen to form an orthogonal right-handed coordinate system. It is assumed that during an engagement period the radar can track all the bullets fired. In general, the bullet motion will be affected by the gun angle, wind, air density, muzzle velocity and the bullet characteristics. The gun angle effect on the XL-coordinate is modeled with a polynomial function, and a precomputed correction is applied to radar data. The YL-coordinate of the bullet is modeled as a ratio of two polynomials. Both of these are functions of the gun elevation angle and time-of-flight. The ZL-coordinate of the bullet is affected by the cross component of the wind. The wind

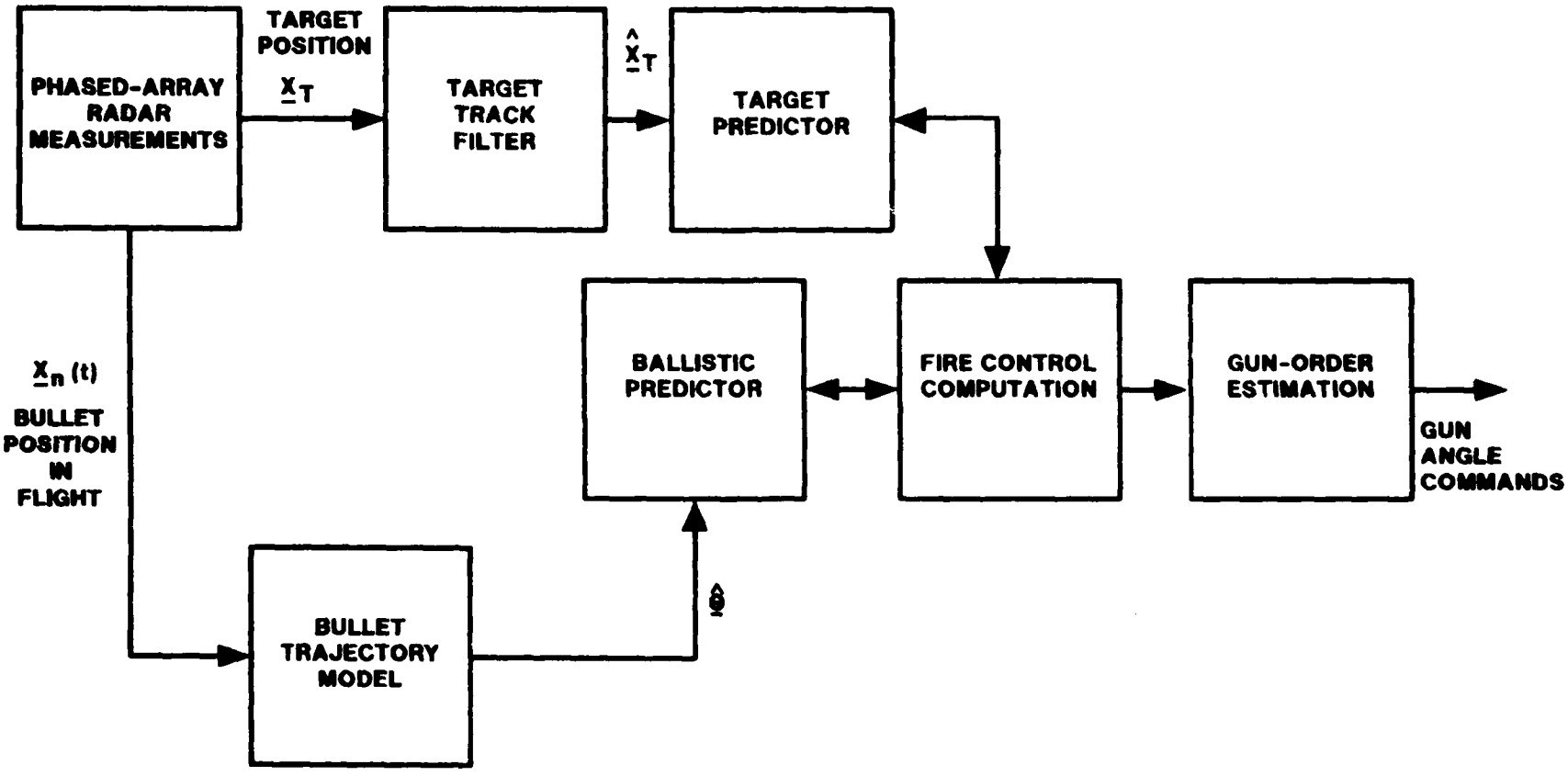


FIGURE 1.
CLOSED-LOOP BULLET TRACKING FOR DIGITAL FIRE CONTROL SYSTEM

speed and direction are estimated from YL and ZL-coordinates. The XL-coordinate of the bullet motion is affected by the range component of the wind, air density, muzzle velocity and bullet characteristics.

In a hypothetical situation, assume that there is no radar noise, no wind and all bullets are identical. For this case, each bullet fired at a fixed gun elevation angle will have almost the same XL-coordinate at flight time T_f. Thus, the first bullet and the second bullet, even though apart in real time, will have the same time-of-flight to reach a distance XL. If radar noise and round-to-round variations are considered, then, mathematically, the bullet motion can be represented by a stochastic process added to the original trajectory. If each bullet trajectory observed by the radar is averaged, then the radar noise and round-to-round variations can be easily filtered. After this, a recursive least-squares estimator (Kalman filter) can be used on the average trajectory data to estimate unknown coefficients in the algebraic model for XL-direction. The update of the model coefficients can be done at a slower rate than data observed by radar. The tracking algorithm is summarized in the following.

1. Observe a bullet position denoted by Range R, elevation θ_E, azimuth angle θ_T, and the corresponding gun angles ω_E and ω_T.

2. Transform the radar measurements to the line-of-sight gun coordinates XL, YL, ZL.

3. Select a fixed line-of-sight XL-axis. In this work, it is assumed 30 degrees elevation angle. Correct the XL-coordinate of a bullet to account for the gun elevation angle.

$$XL(T_f, 30^o) = XL\ (T_f, \omega_E) - \Delta X(T_f, \omega_E) \qquad (1.1)$$

   ΔX is a precomputed correction term.

4. Average XL $(T_f, 30^o)$ on the observed bullets to filter the random noise. This will generate a relation between average bullet position and time-of-flight from the data obtained in step 3.

5. Estimate parameters in the algebraic model for XL-axis.

6. Estimate wind velocity and direction from YL and ZL averages on multiple bullets.

7. Use updated parameters to bullet trajectory prediction.

The organization of the paper is as follows.

In Section II, an estimator is developed to track a single bullet fired with a fixed gun elevation and azimuth angle. The algorithm is generalized in Section III to track multiple bullets and estimate the trajectory model parameters. A simulation of closed-loop bullet tracking approach for a flyby target is presented in Section IV.

II. SINGLE BULLET TRACKING ALGORITHM

An algebraic model to represent a bullet motion in XL-axis fired with a fixed gun elevation angle is developed. A recursive algorithm is derived to estimate parameters of the model from the measurements of the bullet position.

A line-of-sight coordinate system for a bullet fired at gun azimuth angle ω_T and ω_E is shown in Figure 2. The line-of-sight and the inertial coordinate system are related by:

$$\begin{bmatrix} XL \\ YL \\ ZL \end{bmatrix} = \left[\begin{array}{c|c|c} \text{COS } \omega_T \text{ COS } \omega_E & \text{SIN } \omega_T \text{ COS } \omega_E & \text{SIN } \omega_E \\ -\text{COS } \omega_T \text{ SIN } \omega_E & -\text{SIN } \omega_T \text{ SIN } \omega_E & \text{COS } \omega_E \\ \text{SIN } \omega_T & -\text{COS } \omega_T & 0 \end{array}\right] \begin{bmatrix} XB \\ YB \\ ZB \end{bmatrix} \qquad (2.1)$$

Where XB, YB, ZB denote the inertial bullet coordinates and XL, YL, ZL are the line-of-sight coordinates. If there is no wind, then the bullet motion will be in the line-of-sight plane. A closed-form approximation for a bullet motion in XL-axis is given by

$$XL\ (T_f) = \frac{V_M T_f}{1+K_D (V_M)^{1/2} T_f} \qquad (2.2)$$

where T_f denotes the time-of-flight. V_M is the muzzle velocity. K_D is a constant dependent on the atmospheric temperature, pressure and the bullet characteristics. $XL(T_f)$ denotes the bullet XL-coordinate at flight time T_f. The derivation of equation (2.2) is presented in Appendix A. The algebraic model has been widely used in open-loop fire control systems [1].

For notational convenience, rewrite equation (2.2) as

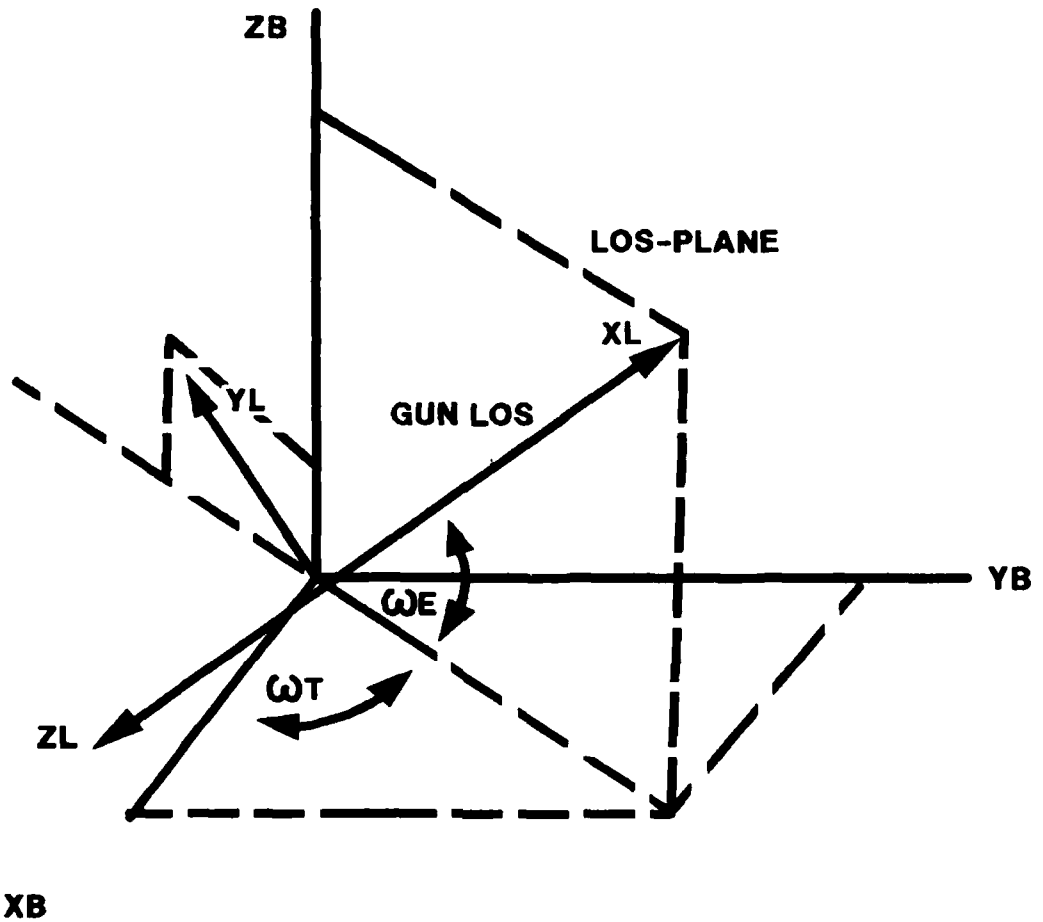


FIGURE 2.
LINE-OF-SIGHT COORDINATE SYSTEM

$$XL(T_f) = \frac{aT_f}{1 + bT_f} \tag{2.3}$$

Define a state vector $\underline{\theta}^T = [a, b]$. T is a transpose operation. Equation (2.3) with parameter uncertainty and measurement noise can be represented by

$$\underline{\theta}(k+1) = \underline{\theta}(k) + \underline{\omega}(k)$$

$$XL(k) = \underline{H}(k)\ \underline{\theta}(k) + \nu(k) \tag{2.4}$$

where k denotes the discretized time-of-flight of a bullet. Let ΔT_f denote the discretizing interval; for the first bullet $t = T_f = k\Delta T_f$ and for the nth bullet $t = T_f + (n-1)\Delta t = k \cdot \Delta T_f + (n-1)\Delta t$; where Δt is the time interval between bullet firing.

The vector $\underline{H}(k)$ is given by

$$\underline{H}(k) = [T_f, -XL(k)T_f] \tag{2.5}$$

$\nu(k)$ and $\underline{\omega}(k)$ denote measurement and modeling errors. It is assumed that $\nu(k)$ and $\underline{\omega}(k)$ are zero-mean normal random sequences such that

$$E[\nu^2(k)] = R$$

$$E[\underline{\omega}(k)\underline{\omega}^T(k)] = Q \tag{2.6}$$

When $\underline{\theta}(k)$ is interpreted as state vector and $\underline{H}$, Q, R are given, the problem can be solved by the Kalman filter [2].

The parameters can be updated by the following equations:

$$\hat{\underline{\theta}}(k) = \hat{\underline{\theta}}(k-1) + \underline{K}(k)$$

$$[XL(k) - \underline{H}(k)\ \hat{\underline{\theta}}(k-1)] \tag{2.7}$$

where $\hat{\underline{\theta}}(k)$ denotes the optimal estimate of parameter $\underline{\theta}$ based on measurements XL(k) up to k. The vector $\underline{K}(k)$ is the filter gain given by

$$\underline{K}(k) = P(k|k-1)\ \underline{H}^T\ [HP(k|k-1)\underline{H}^T + R]^{-1}$$

$$P(k|k-1) = P(k-1|k-1) + Q$$

$$P(k|k) = [I-K(k)H]\ P(k|k-1) \tag{2.8}$$

The Riccati equation (2.8) depends on the input and output data, via H, and the gain vector K has to be evaluated in real time.

III. MULTIPLE BULLET TRACKING ALGORITHM

An algorithm is presented to process radar measurements on multiple bullets in a closed-loop fire control system. The objective is to utilize on-line bullet position measurements to generate an input sequence to the ballistic parameter estimator. The wind effects are neglected in the present development and can be considered separately. Let $X_n(k)$ denote a position vector of bullet number n at time-of-flight k. Then

$$X_n(k) \triangleq [R_n(k),\ \theta_{T_n}(k),\ \theta_{E_n}(k)] \tag{3.1}$$

where $R_n(k), \theta_{T_n}(k), \theta_{E_n}(k)$ denote the bullet range, azimuth angle and elevation angle respectively. k denotes the discretized time-of-flight.

Let Δt denote the time interval between two successive bullets fired and let ΔT_f denote the time interval between two successive radar measurements of each bullet. The radar observations can be synchronized with the gun fire and, therefore, can have an integral number of bullet measurements in the interval Δt. To keep notation simple and to present the concept, it is assumed that $\Delta t = \Delta T_f$. However, in general, $\Delta t = m\ \Delta T_f$, where m is an integer. Further, it is assumed that at each time interval ΔT_f radar can measure all the bullets in the air up to the target range.

Step 1

The radar measurements on the bullets and the gun angles as a function of time, are shown in Table 1. It is assumed that at time t only the first bullet is in the air, while at time $n\Delta t$, radar measurements include n bullets in the air.

TABLE 1

Time	Gun Angles	Radar Measurements
Δt	$\omega_E(1)$, $\omega_T(1)$	$X_1(1)$
$2\Delta t$	$\omega_E(2)$, $\omega_T(2)$	$X_1(2)$, $X_2(1)$
$3\Delta t$	$\omega_E(3)$, $\omega_T(3)$	$X_1(3)$, $X_2(2)$, $X_3(1)$
.	.	.
.	.	.
.	.	.
$n\Delta t$	$\omega_E(n)$, $\omega_T(n)$	$X_1(n)$, $X_2(n-1)$,..., $X_n(1)$

Step 2

Transform the radar measurements to line-of-sight coordinate for each bullet.

For notational convenience, let R, Θ_T, Θ_E denote the range, azimuth angle and elevation angle of a bullet. Let ω_E denote the gun elevation angle at firing time. In the initial part of the trajectory $\omega_E = \Theta_E$. However, due to the gravity drop $\omega_E > \Theta_E$.

Let

$$RG = R \cos \Theta_E$$

$$ZB = R \sin \Theta_E \tag{3.2}$$

Then

$$XL = RG \cos \omega_E + ZB \sin \omega_E$$

$$YL = RG \sin \omega_E - ZB \cos \omega_E \tag{3.3}$$

Where RG is the projection of bullet range vector on the horizontal XB-YB plane. It is assumed that there is no cross wind, and the bullet will stay in the line-of-sight plane.

Step 3

Transform X_L to the reference line-of-sight axis

$$XL(k, 30^o) = XL(k, \omega_E) - \Delta X(k, \omega_E) \tag{3.4}$$

The correction term $\Delta X(k, \omega_E)$ is a precomputed algebraic model to account for the gun elevation angle ω_E being different from 30^o.

The correction term is computed by solving equation (A-1) for different gun angles. Regression analysis is used to determine the coefficients in the precomputed correction model.

Step 4

Averaging filter for XL-coordinate.

For notational convenience, XL (k, 30^{o}) is denoted by XL (k). For bullet number n, the notation used is $XL_n(k)$. Note that if all bullets are identical and there is no radar noise, then

$$XL_n(k) = XL_{n-1}(k) = \ldots XL_2(k) = XL_1(k) \tag{3.5}$$

Further, in real time, the data $XL_n(k)$ arrives last and $XL_1(k)$ arrives first. Since we are interested in real time processing, an exponential averaging filter is designed as shown in the following.

Define a recursive algorithm

$$AXL^{(n)}(k) = P*AXL^{(n-1)}(k) + (1-P)\ XL_n(k) \tag{3.6}$$

where $AXL^{(n)}(k)$ denotes the average measurement on n bullets at flight time k. The parameter P can be chosen to adjust the filter gain.

Step 5

The outputs of averaging filters consist of AXL(1), AXL(2),... AXL(n). If there is no noise, this sequence should coincide with XL(1), XL(2),..., XL (n) of a 30^{o} reference XL-coordinate. The equations (3.5) and (3.6) are valid for $n\Delta t \leq T_f$. A simple modification is required for largervalues of n. The output of the averaging filter is the input to the parameter estimator presented in Section II. The data processing algorithm is summarized in Figure 3.

IV. SIMULATION RESULTS

The simulation model of the proposed closed-loop fire control system is presented in the following. The objective is to determine the open-loop and the closed-loop performance of the fire control system with inaccurate a priori information of the muzzle velocity, drag coefficient, air density, wind velocity and random errors affecting the bullet flight path. The radar data is generated by numerical integration of nonlinear differential equations (A-1) to represent each bullet motion. A constant velocity target under attack mission is considered. The recursive estimator (2.4) updates the parameters of the bullet trajectory model

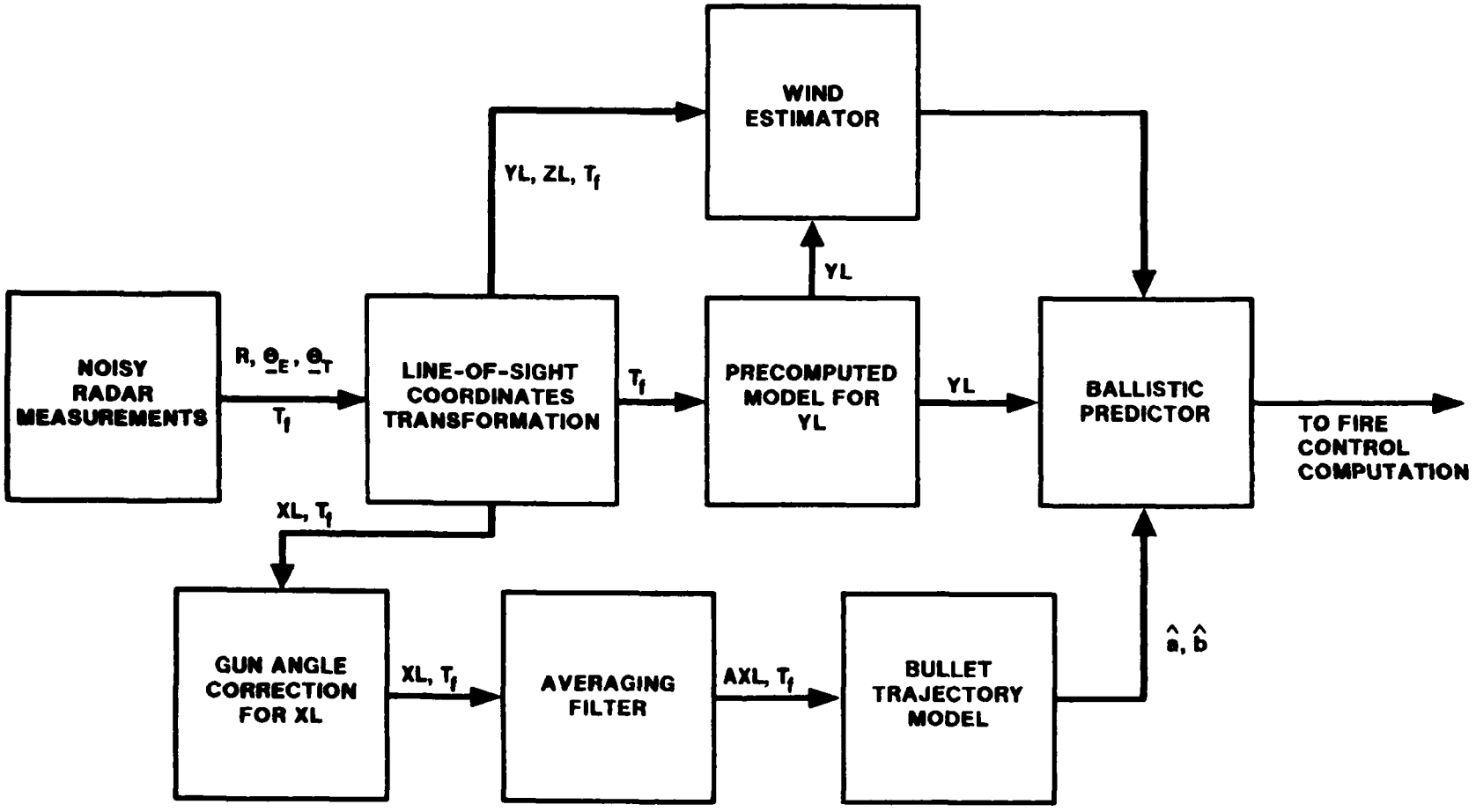


FIGURE 3.
BLOCK DIAGRAM FOR MULTIPLE-BULLET PROCESSING ALGORITHM

based on radar observations. A Newton-Raphson type gradient algorithm is used in the fire control computations to estimate the gun angle commands. The wind effects, muzzle velocity variations, azimuth and elevation biases and ballistic dispersions are included in the simulation. The major sources of errors and statistical error models are presented in Appendix B.

Consider a flyby target with an initial range of 3800 meters, slant crossover range of 200 meters, 50 meters altitude and 450 knots speed. The radar measurement and gun fire rate is synchronized at 64 per second. A miss distance is the distance of closest approach of the target and a bullet.

A competing system, "closed-loop range gate", is considered to compare the system performance. In the competing system, aim correction is based on the ability of the radar to track both the incoming target and the outgoing projectiles in the vicinity of the target and to reduce the miss distance. The competing system differs from the bullet tracking approach, in that the projectile spotting is limited to the vicinity of the target. Further, a more complex logic is required to separate the gun error and the miss distance due to the target maneuver during the bullet flight time.

A typical simulation result of miss distance as a function of firing time is shown in Figure 4. It is seen that the closed-loop bullet tracking algorithm converges within one second. On the other hand, the first bullet fired reaches near the vicinity of the target in 5.6 seconds. Therefore, the closed-loop range gate method cannot reduce miss distance until 384 bullets are fired. The simulation results indicate a convergence of the closed-loop bullet tracking fire control system under noisy radar measurements.

V. CONCLUSIONS

A closed-loop bullet tracking approach for a digital gun fire control system has been developed. The results indicate a substantially better performance of the proposed method because of its ability to quickly estimate parameter corrections needed in the gun-order computations. The bullet tracking algorithm is independent of the target motion and can be easily implemented on a microprocessor for real-time fire control computations. It is expected that the results of this paper will provide a basis for further studies on closed-loop bullet tracking in gun fire control systems.

ACKNOWLEDGEMENTS

The author gratefully acknowledges the valuable help in the simulation of the proposed concept by Dr. E. G. Holzmann, General Electric Co., Schenectady, NY.

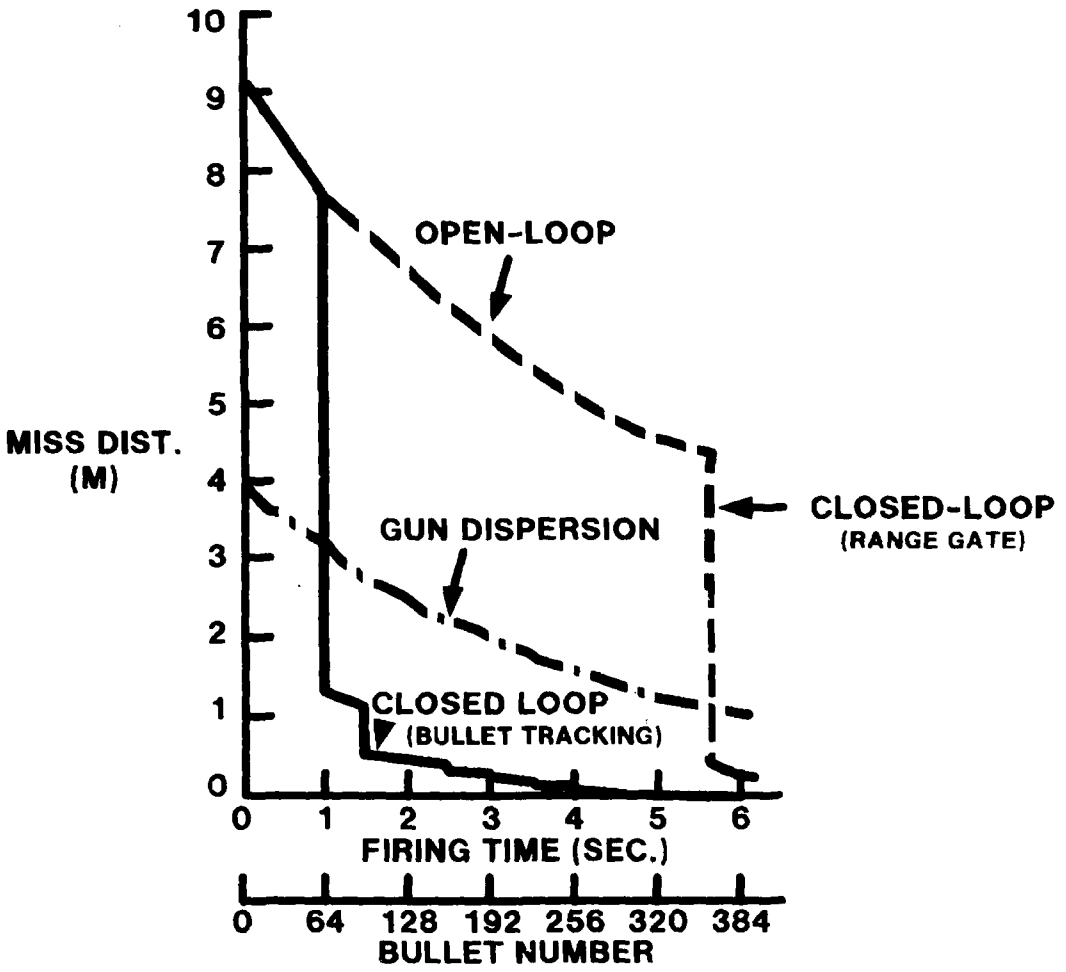


FIGURE 4.
BULLET TRACKING FOR DIGITAL FIRE CONTROL SYSTEM

The constant encouragement and financial support from Armament Systems Department, General Electric Company, Burlington, VT is gratefully acknowledged.

REFERENCES

[1] Windhalm, J. W., "An Analytical Ballistic Trajectory Model for Digital Fire Control", NAECON '76 Record, pp. 616-622.

[2] Mehra, R. K. and Lainiotis, D. G., "System Identification: Advances and Case Studies", Academic Press, New York, 1976.

APPENDIX A

DERIVATION OF BULLET TRAJECTORY MODE

A nonlinear differential equation to represent a bullet trajectory as a function of the time-of-flight is considered. The equation can handle relatively long time-of-flight and the projectile may pass from supersonic to subsonic [1].

The motion of a bullet is considered in a vertical plane formed by the direction of initial bullet velocity vector and the gravity. Out of plane dynamics are attributed to wind errors and are neglected in the present derivation. A correction factor may be applied for this error. The equation of motion for the ballistic projectile may be written as

$$\begin{aligned} \dot{x}(t) &= V_x(t) \\ \dot{y}(t) &= V_y(t) \\ \dot{V}_x(t) &= -D(t)\, V_x(t) - g \sin \theta_E \\ \dot{V}_y(t) &= -D(t)\, V_y(t) - g \cos \theta_E \end{aligned} \qquad \text{(A-1)}$$

where

$$D(t) = \frac{C_D(M,\delta)\ \rho(h)\ S\ V(t)}{2m}$$

$$M = \frac{V(t)}{V_s(t)};\quad v(t) = [v_x^2 + v_y^2]^{1/2}$$

The initial conditions are given by

$x(0) = y(0) = V_y(0) = 0$

$V_x(0) = V_M$

x	Coordinate in the direction of initial bullet velocity
y	Orthogonal to x in vertical plane
θ_E	Angle of x axis above local horizontal
V_x, V_y	Projectile velocities in x an y directions
g	Gravity acceleration
C_D	Aerodynamic coefficient of drag
M	Mach number
δ	Yaw angle of the bullet

ρ Air density function of altitude h

S Reference area of bullet

V_s Speed of sound

m Mass of the bullet

The equation (A-1) with a second-order Runge-Kutta numerical integration has been used for numerous air-ground weapon delivery algorithms.

The following approximations are made to derive a closed-form solution:

1. The speed of the bullet is approximated by

$$V(t) = [V_x^2 + V_y^2]^{1/2} \simeq V_x$$

This is a good approximation because the speed in x-direction is much large than in y-direction.

2. Air density if assumed constant. Changes in density with altitude can be considered as a perturbational correction.

3. The dominant forcing term in x-direction is assumed to be drag. The gravity influence can be added as a perturbational correction.

4. Yaw effect and dependence of velocity of sound on altitude is neglected. Equation (A-1) can be written as

$$\begin{aligned} \dot{x}(t) &= V_x(t) \\ \dot{y}(t) &= V_y(t) \\ \dot{V}_x(t) &= -KC_D(V_x)V_x^2(t) \\ \dot{V}_y(t) &= -g \cos \theta_E \end{aligned} \qquad \text{(A-2)}$$

where

$$K = \frac{\rho S}{2m}$$

In the supersonic flight of a bullet, the drag coefficient may be approximated by

$$C_D(V_x) = \frac{q}{(V_x)^{1/2}} \qquad \text{(A-3)}$$

where q is a constant.

Equation (A-2) has a closed-form solution given by

$$x(t) = \frac{V_M\, t}{1 + \frac{Kq}{2}(V_M)^{1/2} t} \qquad \text{(A-4)}$$

In a subsonic flight path, the drag coefficient may be assumed constant and the appropriate closed-form solution with initial conditions can be derived.

APPENDIX B

STATISTICAL ERROR MODEL

The major sources of errors in the estimation of bullet trajectories are considered in the following.

1. Wind

The wind effect can be modeled as velocity component imparted to shell during flight. The resulting equations are given by

$$\Delta E = \frac{1-K_B}{K_B} \frac{W}{V_M} \sin \omega_E \cos(\omega_T - \theta_W)$$

$$\Delta T = \frac{1-K_B}{K_B} \frac{W}{V_M} \sin (\omega_T - \theta_W)$$

$$\Delta R_f = \frac{-(1-K_B)}{\cos \lambda} T_f W \cos \omega_E \cos(\omega_T - \theta_W) \qquad \text{(B-1)}$$

where

W	-	Wind speed
V_M	-	Muzzle velocity
ω_E	-	Present elevation angle
ω_T	-	Present azimuth angle
θ_W	-	Wind azimuth angle
λ	-	Lead angle
T_f	-	Time of flight
K_B	-	Ballistic coefficient
R_f	-	Future range
Δ_E	-	Deviation in elevation angle
Δ_T	-	Deviation in azimuth angle
ΔR_f	-	Deviation in range

The ballistic coefficient is given by

$$K_B = \frac{V_{AV}}{V_M} = \frac{R_f}{V_M T_f} \qquad \text{(B-2)}$$

The effect of altitude on wind speed is neglected in the model. V_{AV} is the average wind speed.

Equation (B-1) can be used to model wind effect on each bullet. ΔE and ΔA can be estimated from radar data. The range component of the wind will affect the estimate of the muzzle velocity.

2. Muzzle Velocity

The rounds can be identified by a designated nominal value, V_{MO}, of muzzle velocity. For a given nominal value, the bias can change between -120 meters per second to 60 meters per second about the nominal value. Round to round standard deviation is assumed as 10 meters per second. The barrel characteristics of the gun may change as fire proceeds, due to increased temperature and will affect the muzzle velocity. The error can be modeled as

$$V_M(t) = V_{MO} + B(t) + W_1(t) \qquad \text{(B-3)}$$

where $V_M(t)$ denotes muzzle velocity of the bullet fired at time t. $B(t)$ is a time-varying bias; $w_1(t)$ is a zero-mean stochastic process with $E[w_1^2(t)] = 100$ meters/sec. E denotes the expected value.

3. Azimuth and Elevation Offsets

The gun azimuth and elevation angles may be different from their nominal values at the bullet firing. This may be due to a variety of error sources beyond control. For example, errors in the ship motion estimator, servo and synchro errors, and mechanical alignment errors may contribute to the offsets. The errors are not constants in the engagement period and can be assumed as time-varying.

4. Radar Measurement Noise

The minimum range is 100 meters, and the resolving ability of radar is 5 feet (1.524 meters). The standard deviation of the measurement noise for the range is assumed to be 6 feet (1.829 meters). For the azimuth and elevation angles $\sigma_T = \sigma_E = 1$ mills.

5. Ballistic Dispersion

The is a random error. An RMS value of 1.9 mills is assumed for the simulation.



SESSION III: ROBOTICS

27 OCT 1982

(AFTERNOON)

ROOM #1

FOURTH MEETING OF THE COORDINATING

GROUP ON MODERN CONTROL THEORY

HOSTED BY: OAKLAND UNIVERSITY
ROCHESTER, MICHIGAN

Next page is blank.

AD P001074

DARPA PROGRAM INTELLIGENT TASK AUTOMATION (ITA)*

Dr. Edward C. van Reuth
Director
Materials Sciences Division
Defense Advanced Research Projects Agency
1400 Wilson Boulevard
Arlington, Virginia 22209

Dr. Elliott C. Levinthal
Director
Defense Sciences Office
Defense Advanced Research Projects Agency
1400 Wilson Boulevard
Arlington, Virginia 22209

ABSTRACT

The establishment of a science and technology base for many aspects of defense manufacturing and for adapting intelligent systems for complex military operational tasks is a cornerstone effort of advanced research with great national significance. This presentation provides an overview of the efforts of the Defense Advanced Research Projects Agency (DARPA) and the Air Force Wright Aeronautical Laboratories (AFWAL) to plan and fund technology development for a substantial leap in Intelligent Task Automation (ITA). In addressing the needs for high productivity in manufacturing and robust applications to complex military tasks, the ITA program develops and integrates the generic technologies impacting, gripping, sensing, viewing, recognizing and understanding the environment, controlling manipulation, and intelligently providing command of the task.

INTRODUCTION

Automation and automatic control of industrial processes has been permeated by robotic concepts, with the intent of providing greater industrial productivity for a "reindustrialization in America." Flamboyant feature articles in the popular press and some technical literature raise the expectation that future robots will be sophisticated, dexterous, adaptable and intelligence for a wide gamut of industrial, military and community operations -- on Earth and in space. Some caution is needed in estimating the time scale for those events. It is necessary to take into account the inertial forces that resist change in production methods, military

---

*This paper is also presented at IVth IFAC/IFIP Symposium on Information Control Problems in Manufacturing Technology held at the National Bureau of Standards, Gaithersburg, MD, October 26-28, 1982, by Dr. E. C. Levinthal.

operations and social behavior. These conservative forces limit the considerable support that is necessary to transfer what is possible in the laboratory into actual practice. DARPA's role is to remove some of the constraints so that these promises of the future are realized sooner and more fully.

Forecasts of unfolding robot technology were brought under rational considerations in a recent "Overview" of robotics prepared by the National Bureau of Standards in conjunction with the National Aeronautics and Space Administration (Gervater, 1982). In this report, the industrial needs and expectations are compared with directions being taken in research and development. Emerging in the foreseen evolution are hands with improved dexterity, the advanced control systems to support them, the vision and touch sensors to support the programmed control, and (later) a self-planning for intelligently supporting more general commands.

There are various tasks being considered for application of the expected intelligent capabilities in automation. In manufacturing they range from providing speed and economy in mass production assembly tasks to totally automating inventory and tool management in manufacturing. In military operations they include handling such complex tasks as reconnaissance and sweeping mine fields.

Getting the technology trends to provide the anticipated payoffs in automation of intelligent tasks is not straightforward. In terms of R&D economics, there are strenuous issues as to whether the advanced concepts and developments providing economical soundness of approach for manufacturing industries will sufficiently support a robust realization of the possibilities. For instance, re-engineering the production methods within existing plants presents considerable economic competition for the robotic alternatives of installing flexible automation that copes with the unstructured environment. Manufacturing, for some time to come, may in the large remain permissive enough to support vision with structured light or to take advantage of 2-D images at fixed range -- in spite of the significant efforts in laboratories to secure the necessary technologies for understanding 3-D images with grey scale.

DARPA'S ROLE

As the central research organization for the Department of Defense, DARPA has a primary responsibility to support advanced research bearing on manufacturing because of the significant military value of the industrial base to military force structure. The present joint project linking DARPA with the Air Force Wright Aeronautical Laboratories (AFWAL) at Wright-Patterson Air Force Base is in large part due to the challenge of meeting our nation's defense readiness goals through integrated computer-aided manufacturing (ICAM). Solving problems in the production base and developing tomorrow's new, more efficient manufacturing processes for the military hardware that will be required at the turn of the century is a vital support activity for DARPA.

In addition, the military services look to DARPA for the kinds of technological advances that will extend and enhance operational capabilities in the combat environment. Presently, the military is looking into the implications of robotic technology and recognizes that today's technology, except for a few innovations in space, is dedicated to the assembly line and will remain there unless military needs are defined and developments funded.

For the near term, the military is expected to adopt the industrial robotic technologies for the same advantages found in manufacturing -- relieving personnel from hazardous tasks that demand time-critical effort. Handling ammunition resupply for self-propelled artillery or tanks has been considered as a direct application of the industrial robots. The continuous-path capabilities currently available appear suited to transferring ammunition from armored resupply vehicles to armored combat vehicles in the battlefield environment under possible threat of nuclear, biological, or chemical (NBC) actions. Essentially, these tasks call for the mobile mounting of an industrial robot for forward operations with the combat support forces.

But the military is especially interested in such broader applications of automation technologies as providing intelligent solutions to the Army's countermine problem. Concepts for solving this problem will go beyond the physical handling of material and tools to include the Army's thinking about automating the "land rover." Where initially, remotely controlled mine clearing may be obtained by outfitting armored vehicles with a roller or mine plow and dispensing mine-clearing line charges, the eventual concepts will be intelligent about the overall countermine objective of establishing passage through a mined area. Instead of blindly clearing an intended area, many mines could be located by detecting the mine "footprint" with appropriate sensors and then marking the mine for avoidance. This intelligent approach would be based on an integrated automation of the roving vehicle, information handling, and physical handling of markers and cover material at a mine location.

In pointing out the enormous possible breadth of applications, it is intended not to thoroughly define the scope for using DARPA's resources, but rather to provide some insight to the range of choice being addressed. The Defense Sciences Office (DSO) has arrived at a focus in terms of the following concept for Intelligent Task Automation (ITA). While not excluding other interests, this focus is usefully providing a point of departure for prioritizing technologies opportunities. The DSO program is coordinated with the efforts of the Information Processing Techniques Office (IPTO) of DARPA. IPTO's programs in artificial intelligence, information processing and computer technologies have an important impact on the ITA goals. The emphasis of DSO is presently on device subsystems with ITA capabilities and, in the future, on complete systems.

THE CONCEPT OF INTELLIGENT TASK AUTOMATION

Among the technological advances in automation promising operational payoffs in either defense manufacturing or military operations are some potential advances that may not get bridged "naturally" by industrial support and incentives. As pointed out above, such tradeoffs in the industrial environment as using advanced robotic sensing versus engineering the robot's environment are not likely to arrive at the same critical demand that the military has for sensor driven control. Without the means to structure its environment, the military robot is confronted with obstacles, clutter, or unknown conditions; and its target will have highly variable character. Exploitation of the kinds of sensory controls outlined by D. Nitzan (1981) will be a military necessity; and it can be anticipated that the economic tradeoffs for industry will also eventually prove out the advantages of gaining flexibility with extensive sensing.

Simply, DARPA is recognizing that some technological opportunities are apparently missing investments because of the competition of attention to nearterm engineering "problems." Technologies suitable for military operations and the longer term goals for flexible manufacturing should not take advantage of structures for the environment. For example, the "bowl" feeder used in partsorting in industrial assembly is unlikely to work out for an ammunition handler in the combat arena.

To obviate structured solutions, the research program places an emphasis on integrating vision, touch, and proximity sensing in process control. Sensor integration is apparently a prime target in the generally held concensus about gaining flexibility. For instance, the NBS/NASA report (Gevarter, 1982) notes such aims in its synthesis of needed research that drew on surveys and recommendations of conferences and workshops during the previous three years. The implied emphasis is on the integration as well as the generation of sensory data that is, on linking the computation of an understanding of the environment to the mechanical function.

In summary, the DARPA program in intelligent task automation seeks technology development representing a substantial leap forward from current capabilities with a focus on realizing automation in unstructured environment. The necessary intelligence to deal with both uncertainty of the environment and sophistication of the intended task is specifically sought; and, the technological opportunities are expected in linking computation to mechanical function. The choice of scope in carrying out this objective is depicted in Figure 1 below and described in the following sections of this paper.

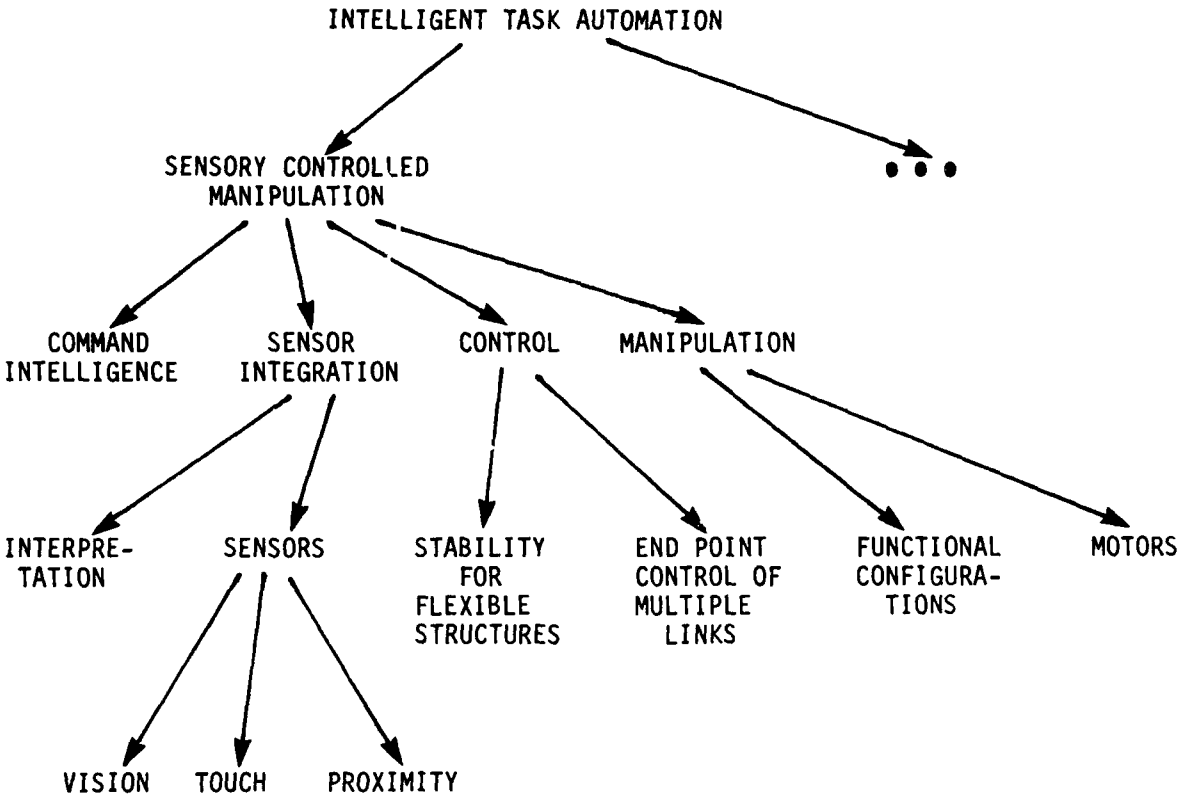


Figure 1. Couplings in DARPA Program

END MANIPULATOR CONTROL

Available technologies present a broad gamut of limitations to achieving the "smart hands" called for in intelligent task automation. The needed dexterity entails rapid movement within the context of the work space, sensitive force control and fine movement enabling the "give" needed for inserting or mating parts, and a secure grasp that accomodates irregular objects. In contract to these needs, manipulators now primarily respond to position control, requiring that the robot's environment be engineered to the same high accuracy as the robot. Large and heavy structures are used to provide stiffness so that end point locations can be accurately inferred from joint angles. Thus, movements are slow and clumsy; and position accuracy is only as good as the accumulation of errors and the stiffness of the members. Designs for multifinger hands, suitable for grasping, have only progressed to the ability to impart some limited motion by a heuristic combination of position and force-controlled fingers.

End point control of the manipulator and the individual fingers is the key to quick and precise actuation with lightweight structures. It is not yet available because robust (stable) control of the flexible structures has not been possible. When torque at one end of a series of links is based on feedback at the other end, any flexibility in the series makes the system inherently unstable. The techniques for stable control using end-point sensing are difficult to perfect. DARPA is now sponsoring research to directly address the integration of end point sensing with efficient stable control.

Specific attention is being turned to developing minimum time algorithms for slewing a flexible robotic arm through a large angle and then touching an object softly. That is, large impulsive "crashes" are to be avoided at the contact. To handle uncertainty in the target object's location, the research will incorporate end-point sensors such as optics, simple range finders, strain-gauge-equipped fingers and proximity sensors. New design concepts for arms are expected that will enable controlling higher terminal speeds without large impact forces even when there is uncertainty in the target's location. For example, mass distributions and flexibility will be varied in design trade-off studies.

Since a number of control modes must be involved, beginning with a large positional slew and ending with force control, methods are under investigation for smooth switching between control regimes while the mechanism is in motion. Initial objectives are to obtain the minimum-time algorithm for the "slew and touch" task. Further investigation of new arm designs will then take advantage of flexibility and distribution of arm control to best accomplish specific tasks.

As control techniques are developed that are tolerant of flexibility in a manipulator's mechanical structure, manipulators can be lightened and made faster. They will be safer to use, less prone to damage from collisions, require less power to run, and cost less to fabricate.

Control of force sensing fingers is also being explored under the current DARPA sponsorship. The control theory for coordinated motion of complex hands developed by Salisbury and Craig (1982) at Stanford University is being pursued. The theory specifies position and force control for the coordinated motions desired in such tasks as insertion where the goal is to minimize transverse forces while exerting a force in the intended direction of the insertion. Such tasks require force control throughout the relative motion and necessitate sensing force and contact for feedback. Several architectures for position and force control of the multiloop mechanisms are being investigated. Preliminary results are appearing for the joint's torque subsystem. The physical dimensions of multi-fingered hands can be optimized on the basis of kinematic performance and the volume of grasp.

END SENSING

Force and contact sensing are also being explored for perceptual information. Components for force sensing are now being perfected that provide force measurements without friction and with little mass between sensor and load. At the command or strategy level in automation for a task, contact sensing provides the information for inference and estimation of geometric and dynamic properties of loads and the environment. Contact of individual fingers provides an estimate of local surface curvature and orientation, while several point contacts on several fingers provide gross orientation and curvature, e.g. fingers wrapped around a cylinder. Integrated data from fingers moving over a surface should reveal surface shape and dynamic properties of objects. As this research progresses, it is expected that strategies in hand control will evolve from experiements. Manipulation rules for re-orientation of grasped objects within the hand is one of the goals.

Integrating vision, range sensing and proximity sensing with the force and contact sensing is also being addressed. There are two levels of intended integration in the hierarchy of command and control -- at the command level for intelligent planning of the task actions, and at the control level for tracking.

Vision and image analysis are major research areas of the same magnitude as the intended focus on ITA (see, for instance, the survey by T. Binford, 1982). Results from vision research at leading institutions will be extensively drawn into the investigations of the command and control processes for ITA. Understanding how vision integrates with other sensors is the major objective, rather than the vision science per se. In particular, the research foundations for the use of models in sensory processing and interpretation are being explored in relation to representations of sensor estimates as geometric constraints.

RANGING AND 3-D SENSING

The practical benefits of ranging systems are beginning to be recognized. The data so gathered may be organized in depth maps, range images or like forms of 3-D "vision." Three-dimensional sensing has the same aim as other forms of computer vision -- the higher level representation of the scene for purposes of comparison or recognition.

When a manipulator is on the move in dealing with a dynamic situation, it is necessary that it work with shape in its three dimensional space. The system should be capable of dealing with information acquired piecemeal from different vantage points. In fact, arrangements as have been tried by G. Agin (1979), among others, have shown the advantages of moving the sensors for the express purpose of obtaining more detailed information about the environment, such as seeing around occluding objects.

In research receiving support by DSO and IPTO jointly, a goal is set on classifying objects and determining their position and orientation with a ranging system. The activity is constructing a sensing system for generating light-stripe range data from multiple points of view and exploring concepts for gaining speed and accuracy in its operation. The data analysis developments are devising advantageous data structures for indexing the data and controlling image scanning. Generalized cylinders make up the low-level primitives in range data.

Identification of objects is sought on the basis of a preponderance of evidence from a matching process.

PROXIMITY SENSING IN ASSEMBLY

Of special interest is the role of proximity sensing in relation to the vision perspective at relatively long ranges and the perspective of touch sensors at contact. Short-range proximity and part-presence sensors can possibly overcome finger shadowing of a vision sensor and may enhance the ability to cope with unstructured or cluttered fields of view as occur with some assembly tasks. Operations involving the important assembly tasks of mating shafts into holes and bearings onto shafts without jamming can benefit from improvements in accuracy and speed. Current capabilities for such automation of assembly particularly lack ability to detect whether the assembly has proceeded properly.

A current objective of DARPA supported research is to demonstrate the capabilities of an acoustic sensing method based on phase monitoring as a means of detecting and controlling the performance of robotic assembly. Demonstration of shaft and bearing mating is intended. The research extends the technology of an automated positioning system based on phase monitoring of an array of acoustic sensors (microphones) as developed earlier by J. Tavormina (1978) and S. Buckley at MIT. A manipulator was positioned by phase measurements from the acoustic sensor array, locking onto an objects position. All the necessary elements of a robot for assembly were demonstrated and later work at MIT showed that the sensor system could provide sufficient accuracy for commercial robots.

Now software is under development for detailed processing of the sensor data and for integrated control of a commercial robot. The software development is including the development of various algorithms to interpret phase information and couple control to the robot. The investigations are addressing "matrix" algorithms for interpreting phase information, and "proximity" algorithms to detect range and direction data in less structured environments. The goal of the proposed work is to demonstrate assembly of mating parts with response sufficiently rapid for industrial application (typically one second for shaft or bearing assembly).

MICRO-MINIATURE MOTORS

Mechanical concepts for the dexterous hand have made extensive progress. The jointly conceived "Stanford-JPL hand" has appeared prominently in the popular press, presumably by virtue of appearing to borrow heavily from nature by using tendon-like cables to actuate its fingers. Motors are mounted on the forearm to avoid encumbering the fingers. The tendon-like design allows three joints, on each of three fingers, with an overall geometry similar to that of a human hand. The nine degrees of freedom provide a firm basis for dexterity.

The "tendons" are cables and the electromechanical devices are conventional motors, nonetheless. Electric motors have a number of inherent problems which limit their effectiveness in application to fine-motion manipulators. Such limitations are addressed by another research effort currently supported by DARPA aimed at capitalizing on the lessons from biology about the structure and scale of natural muscle.

While electric motors are well suited for applications such as fans, disc drives, pumps, etc., their relatively low output torques require use of transmission systems for the high-torque and low-speed operation in a servosystem or robotic application. Transmission systems introduce a number of serious limitations on electric motors by compromizing the dynamic performance. Dynamic characteristics of the motor such as armature inertia and damping are affected by the square of the transmission ratio. Transmissions also impact efficiency. For example, high performance planetary transmission, utilized extensively in today's aircraft industry, drop efficiencies into the range of only 50%.

A more desirable option for an electric actuator in a manipulator of the size of the human hand would be a motor which itself produces high torque at lower speed and eliminates the need for transmission systems altogether. However, even without transmissions, the high mass density of most magnetic materials and electric conductors, makes the power-to-weight ratio of electric motor systems extremely poor. When compared to hydraulic, pneumatic, and combustion based systems, electric motors are inferior by a full two orders of magnitude.

The lessons from biology are that natural muscles are fast, efficient, develop large forces (60 pounds per square inch), can be configured in a variety of sizes, and operate with an extremely low output impedance. Muscle has: (1) a large number of small force-generating elements mechanically connected in parallel; and (2) close proximity between force-generating elements (charges), taking advantage of inverse square laws to produce high local field strengths which increase the force generated per charge. Muscle thereby avoids the use of gross fields and employs instead a fine tapestry of field interactions locally commutated for the production of smooth output forces.

It is expected that the feasibility of field actuation systems with microgeometric structure can take advantage of the understanding of muscle. Already, the understanding of sensor based manipulation benefits from developments in institutions engaged in biomedical design. Artificial hand and hook designs are providing insight about grasping functions and structural configurations. Also, sensory feedback systems developed for prosthesis, including touch sensing and slip detection in multi-axis control, provide methodologies for complex geometry manipulators.

The goal of investigation into field actuation systems of the nature of a volumetric array of charges is to produce contractile or repulsive forces in high density systems matching biological muscle in efficiency, speed, specific force, packaging flexibility and low output impedance. Manufacturing is also being addressed, including the possibilities of adopting the precision techniques of the microcircuit industry. This research is anticipated to offer the possibility of order-of-magnitude improvements over today's electric, hydraulic and pneumatic devices in efficiency, power-to-weight ratio, and combined high-torque/low-speed characteristics.

THE INTEGRATION TECHNOLOGY

In addition to supporting the technology developments described above, DARPA has also linked with AFWAL in a substantial single program to push the state-of-the-arts and force the technology breakthroughs so that a significant demonstration is conducted in intelligent task automation. The objective includes building individual components of the ITA subsystem, integrating the subsystem, and demonstrating applicability to defense manufacturing and flexibility for application to other military applications.

The Air Force context for the program is described by W. Kessler (1982) in terms of the Air Force's new initiatives in manufacturing sciences. The existing materials research and development, manufacturing technology programs, and ICAM activities are augmented by the initiatives. And, the emerging science related to manufacturing is substantially enhanced in order to provide the manufacturing technology base for the defense-related factory of the future. The ITA activity is envisioned as providing the cornerstone for payoffs in intelligent tasks of factories-of-the-future and military operations.

It is intended that the individual ITA technology R&D and the joint DARPA-AF ITA program be complementary. The ITA subsystem demonstration (being specifically defined in the first phase of the investigations) is intended to provide the focal point for developing the requisite integration of technologies. Pragmatic emphasis is placed on the technology to integrate advanced concepts, thereby complementing the attention to concept formulation in the individual areas of related technology. Advancing the technical means (gripping, sensing, viewing, recognizing and understanding the environment, controlling manipulation, and intelligently providing command of the task) within the same time frame as concept

formulations means that the job of integration remains highly unknown with persistently uncertain requirements. All-in-all, the technological opportunity to integrate advanced technologies provides considerable leverage for the individual technical means.

SUMMARY

Specific opportunities for substantial technical advance and breakthrough are presented in a somewhat narrow field of automation pertaining to the higher order linkage of computation to mechanical function. The payoffs of pursuit of these opportunities are expected to amplify the ultimate operational applications of intelligent task automation at large.

REFERENCES

Agin, G. (1979). Time control of a robot with a hand-held camera. Proc. 2nd USA-Japan Computer Conference, Tokyo, Japan, August 1975, p. 233.

Binford, Thomas O. (1982). Survey of model-based image analysis systems. The International Journal of Robotics Research, Vol. 1, No. 1, Spring 1982, p. 18.

Gevarter, William B. (1982). An Overview of Artificial Intelligence and Robotics, Volume II - Robotics, NBSIR 82-2479, National Bureau of Standards, March 1982.

Kessler, William C. (1982). AFWAL-Manufacturing science program. IVth IFAC/IFIP Symposium on Information Control Problems in Manufacturing Technology, held at National Bureau of Standards, Gaithersburg, MD, October 1982.

Nitzan, David (1981). Assessment of robotic sensors. Proc. 1st International Conference on Robot Vision and Sensory Controls, held at Stratford-upon-Avon, UK, April 1981, p. 1.

Salisbury, Kenneth J., and John J. Craig (1982). Articulated hands: force control and kinematic issues. The International Journal of Robotics Research, Vol. 1, No. 1, Spring 1982, p. 4.

Tavormina, Joseph and Shawn Buckley (1978). Automatic positioning and assembly under microcomputer control via acoustic phase monitoring. Transactions of the Society of Manufacturing Engineers, Vol. 6, 1978, p. 448.

AD P001075

VISION SYSTEMS FOR INTELLIGENT TASK AUTOMATION

Dr. C. Paul Christensen
Dr. Roger A. Geesey
Dr. C. Martin Stickley
7915 Jones Branch Drive
McLean, Virginia 22102

Robot vision systems have undergone rapid evolution over the past several years. Several review articles have recently appeared which discuss various aspects of robot vision including industrial needs and applications (1),(2), model-based image analysis (3), and image understanding (4). These serve as a useful introduction to the robot vision area, and are recommended to the reader. The vision problem, however, is an extremely complex one, and much research and development work remains to be done. The BDM Corporation has overviewed the state-of-the-art of robot vision with emphasis on identification of generic problems and research and development needs. In this paper we review the results of this short study and discuss a pervasive problem in the robot vision area--high speed data processing.

Current robot vision systems typically are comprised of a sensor, an illuminator, and an image processing unit. CCD, CID, or photodiode one- or two-dimensional arrays are currently employed for image sensing. Detector array technology is sufficiently well developed that appropriate arrays are usually available as standard OEM products.

A variety of techniques for scene illumination have been explored. Laser illuminators, various types of noncoherent structured light sources, backlighting, and a variety of other approaches to scene illumination have been investigated. Many vision systems are sensitive to fluctuations in ambient light levels so that well controlled illumination is necessary for their operation. Special lighting techniques are also used to simplify image understanding or to extract additional information about position, range, or shape of objects in the scene.

Although both sensing and illuminating devices need additional refinement, the processing of images acquired by these devices poses a much more difficult problem. Image processing in current systems often begins by "thresholding" the required scene at a suitable grey level to produce binary black and white images which can be digitally processed at useful frame rates. Edge finding and region growing algorithms can then be applied to locate objects of interest. Object recognition is frequently carried out using a feature analysis approach in which features like moments of inertia, area/perimeter ratios, number of holes, etc. are used for identification of unknown structures in the scene. Interpretation of complex scenes which may contain background clutter, occluded or moving objects, variations in illumination, and other complicating factors leading to extensive image manipulation or analysis can require long periods of computation or may not be possible at all.

Although available vision systems are limited in capability, they have found a large number of applications in manufacturing, automated assembly, and inspection. More advanced vision modules, when coupled with improved mechanical and control systems, would allow construction of sensor robots of impressive sophistication. The nature of the potential application will strongly influence the specific characteristics desired in advanced vision systems. Extensive conversations with robotics researchers revealed that one or more of the following features is usually desirable in most applications:

Feature	Impact
3-D Sensing	Better object recognization and localization
Grey Scale Image Operations	Reduced scene illumination requirements; better resolution
High Speed	Integration with control systems; higher productivity
Easy Teaching/ Programming	Reduced operator involvement; simple adaption to new tasks
Low Cost	Minimum capital outlay

The first three of the above features directly involve high speed processing of massive volumes of data. The adage that every picture is worth a thousand words is a severe understatement when one deals with television quality images. Current vision systems operate with microcomputers and/or array processors on binary images at frame rates which are barely adequate. Achievement of higher operating speeds or addition of 3-D and/or grey scale capabilities can increase data rates by one to four orders of magnitude. New approaches to high speed data processing are required to meet this challenge, and the solution to this problem should also be characterized by relatively low cost and easy programmability.

Many, if not most, image processing operations encountered in scene analysis are compatible with parallel processing techniques which allow a large number of operations to be carried out simultaneously. For example, edge finding, linear transformation, convolution, and many other operations can be accomplished with parallel data processing architectures. The use of highly concurrent processors can allow dramatic increases in image processing rates. Improvements of several orders of magnitude are achieveable in situations in which all image manipulation can be accomplished with parallel data processing architecture.

The hardware configuration best suited to robot vision applications will reflect speed, programmability, and cost tradeoffs. In general, the lowest-cost and highest-speed circuitry exhibits the least programmability. It seems likely that hardwired systems will be used as extensively as possible as a result of this consideration. Many of the operations required in

image manipulation can be accomplished using a small set of processors which are hardwired to perform fundamental operations like, for example, matrix multiplication or Fourier transformation. Higher order operations (for example, correlation) can then be achieved through a sequence of fundamental operations.

Advanced digital devices utilizing VLSI and VHSIC technology and optical processors incorporating improved spatial light modulators and source and detector arrays will soon be available for implementation of hardwired parallel processing schemes. Relative advantages of electronic and optical approaches can be discussed but the type of technology that will ultimately dominate in this area is difficult to identify. It seems likely that both electronic and optical systems as well as electro-optical hybrids will find a variety of applications.

References

1. R. P. Kruger and W. B. Thompson, Proc. IEEE 69, 1524 (1981).

2. R. Allan, Elect. Design, April 29, 1982, p. 87.

3. T. O. Binford, Int. J. of Robotics Res. 1, 18 (1982).

4. M. Brady, Computing Surveys 14, 3 (1982).

Next page is blank.

A ROBOTIC TANK GUN AUTOLOADER

S. J. Derby
Benet Weapons Laboratory, LCWSL
US Army Armament Research and Development Command
Watervliet Arsenal, Watervliet, NY 12189

AD P001076

ABSTRACT

The use of a robotic arm to load rounds in a tank gun has been considered for the Improved Conventional Armament System (ICAS). Such a device will be able to both transfer the ready rounds located in the turret basket to the rear of the breech and resupply the turret with rounds stored in the hull. The present preliminary design has been modeled on a robot computer graphics simulation program (GRASP). To assist the robot controller, the GRASP program will provide a trajectory that is computed to minimize unnecessary joint motion. A mini computer will operate the robot's servo controlled hydraulic actuators.

INTRODUCTION

The formation of the Improved Conventional Armament System (ICAS) program in 1981 was a result of the ARRADCOM Future Vehicle Armament Technology (FVAT) study (1). The ICAS program consists of the development of a complete armament system, including an effective main gun, with sufficient lethality to defeat the projected threat main battle tank.

A major goal is to achieve the overall objective with what will be the state-of-the-art technologies available in the near future. An attractive technology to use is the area of robotics. Existing industrial use has shown the merits of material handling in a computer controlled environment. The programming flexibility and dexterity of one mechanical unit can replace human and/or "hard" automation.

DESIGN CONSIDERATIONS

Why an Autoloader? The ICAS tank armament study has envisioned two candidate ammunition configurations which must be handled. The first is a fixed (one piece round), and the second a separated (two piece round). Additional handling considerations are the weight and degree of ruggedness of the round when subjected to the induced loads of autoloading. Along with desire to reduce the overall area and volume of a tank, the function of the human loader becomes more difficult and perhaps impossible. Thus some form of autoloader may be a necessity.

There are various design parameters that tend to define the working envelope of an autoloader. The ready rounds are to be stored in the turret basket for protection. The rear end of the gun tube and the associated breech block, recoil mechanisms, etc. must have space to move up and down corresponding to the gun elevation and depression. Large recoil strokes must also be accommodated at all angles of gun elevation. (Variations of concepts have a manned and unmanned turret.) The large gun tube and hardware must also be not too far out of balance in order to keep reasonable tracking speeds and with the trunnion location in the turret somewhat constrained, even more space may be needed as the gun might be pushed farther back into the turret. Also, secondary stored rounds in the hull must be reachable and reloaded into the turret basket.

All of these parameters helped to define the autoloader concepts, both "hard" automation or mechanical and robotic.

MECHANICAL VS ROBOTIC LOADER

Some of the details of each loader system will now be discussed. A "hard" automation mechanical loader must consist of several devices. The first device must transfer the round from a pickup location in the turret basket to the breech. The viable paths are constrained by selecting either a fixed or separated round. A second device must index the ready rounds to the pickup location. This can be a carrousel (a merry-go-round) or a set of cams, levers or screw threads that move the rounds as if they were cans in a soda machine. Autoloaders of this nature have been constructed and do function in the T64 and T72 tanks. The T72 has a carrousel to index its separated rounds. Other mechanical devices needed are a means of ramming the round into the gun and a device to remove the stub cartridge case for convenient disposal. If the space claims do not allow a desired number of ready rounds to be stored in the turret basket, then another device would be needed to reload the basket from a tank hull storage area. This concern also overlaps with the desire to rapidly reload the tank.

A robotic loader can function for several of these tasks. The ready rounds stored in the basket can be anchored to the basket floor and side wall. The robot can pivot independently and access the round type desired. After grabbing the round, the robot can transfer it to the breech for loading. The same robot can reach in to the hull storage area for reloading the basket. The ramming mechanism and the stub cartridge case removal device are still needed. The robot arm must also fold itself out of the way of the breech recoil motion.

The advantages of a robotic loader are several. The flexibility to accommodate different round types and locations by means of reprogramming and not by hardware modification is desirable. Equipment changes within the work environment can be handled within reason. Only one

mechanism is needed to handle three tasks. The disadvantages are the need for better control, since three simple machines may be easier to run, repair and maintain. The controlled motion of the robot must have limited overshoot and deflections due to the dynamic g-loads of the tank. Physical stops may be needed to aid with accuracy. The cost may be unaffordable.

COMPUTER MODEL

Many concepts of both mechanical and robotic loaders were developed by the ICAS group. A robot loader was chosen as one of the viable choices and was explored in some detail. Initial thoughts were to use an existing manipulator if possible, but the rounds weight and the space limitations eliminated all known robots. Existing design geometry was modified to create a new robot concept capable of both loading the separated rounds to the gun and reloading from the hull. The breech was oriented so that the breech block would move away from the robot. An unmanned turret was selected for initial analysis.

A robot concept was then modeled on the General Robot Arm Simulation Program (GRASP) (2-7). GRASP was developed to design new robots, modify existing robots and evaluate robots in their working environment. GRASP prompts the user for all the geometric dimensions and parameters and visually confirms them on the vector refresh computer graphics screen. A gripper was selected from a family of available models and the round cartridges, breech block and rammer mechanism simulated. Figure 1 shows a top view of the layout. The arm is gripping one of the cartridges in the basket. The path of the robot is determined from the user selected boundary conditions. Figure 2 shows the front half of the round in position to be rammed into the gun. The model of the robot, though shown as consisting of only box like primitives, is made up of various selectable cross sections. Material properties, joint limits, actuator specifications and member weights are also needed from the user of the program.

Figure 3 shows a reloading sequence from the hull to the basket. These stored rounds could have been loaded through the top of the tank hull and would have been previously palletized in groups of 10 in reusable containers. All of the programed motions can be investigated by replaying the animated display from different views to inspect for collisions, and they can be evaluated numerically. Instead of printing out reams of paper, GRASP will plot the displacement, velocity acceleration and joint actuator torques. Figure 4 shows the 3rd joint displacement for loading and Figure 5 the velocity and acceleration. Also available are plots of power requirements, member bending percent and hand deflections. The latter two are helpful to evaluate the design for rigidity purposes. The cycle time is also calculated.

DESIGN MODEL

After evaluating and redesigning of a robot concept, a designer can take the loader and place it in a tank body. Figure 6 shows the top and front view of the turret, robot loader, cannon, recoil mechanism, etc. The concept shown is still not designed with any great detail. Figure 7 shows an overall possible tank view. The crew is located in the front third while the power plant is in the rear. This is as far as the autoloader feasibility study is taken.

FUTURE PLANS

The anticipated mode of design construction and operation of a selected robot autoloader is now discussed. It is here that the challenge of fast, economical control methods need to be met.

The robot loader would be built with as many off the shelf components as possible. This is now practical since robotic components are becoming quite reliable and readily available. The members would be welded to create the working mockup. The design need not be ready for mass production at the time its built. A mini computer similar in power to a DEC PDP 11/34 would be used. There are existing DEC compatible controller cards available for servo actuator control with position and velocity feedback. But these standard units may not include the ability to feed forward all the potentially available information.

Instead of teaching the robot loader a path to follow and living with its possible unnecessary high accelerations and joint torques, the GRASP program can be used. By optimizing the motion on an off line mainframe computer, a set of desired paths can be generated. This should help with the overall control scheme. By means of a floppy disk, the path data information can be transferred to the robot's minicomputer controller.

The first control method will probably use the position and velocity information, and hopefully will use feed forwarding. The driving parameter is the need for a small cycle time. After selecting a round from the video terminal display, the robot is to move at the state-of-the-art speeds with very little overshoot. As mentioned earlier, physical stops may be needed to assist the arm, and other sensors' inputs feed into the control loop. The "real world" application will also be much rougher with its many directional g-loads produced while loading on the move. A modified version at GRASP will be used to simulate the sample terrain test data. Strain gauges may also be incorporated to assist with the analysis.

Other future steps may require using the GRASP produced joint torques, work by Wu and Paul (8) has shown the feasibility of dynamically handling manipulators with their Resolved Motion Force Control (RMFC). Compensation will be done initially in software and later in hardware. Deflections of the robot may also be able to be compensated in real time as well as offline in GRASP (7).

CONCLUSION

A viable answer to tank autoloading is a custom designed robot. By using GRASP in the design stage, more confidence in the operation can be given. But by using GRASP for offline programming, higher levels of control may be attempted with less real time computing power.

Upon funding, the ICAS concept will aid in the nations defense needs. The leading edge of technologies brings exciting new answers to existing problems.

ACKNOWLEDGEMENT

The author would like to thank Doug Olcott for the tank concept drawings and the entire ICAS group for their friendly assistance.

REFERENCES

1. Warshall, Theodore, Firepower Action Team Report Future Vehicle Armament Technology(s) ARRADCOM, Nov 1981

2. Derby, S. J., Kinematic Elasto-Dynamic Analysis and Computer Graphics Simulation of General Purpose Robot Manipulators, PhD Thesis, Rensselaer Polytechnic Institute, 1981

3. Derby, S. J., Computer Graphics Simulation of Robot Arms Using the GRASP program, MIT, CAD/CAM Conference, March 1982

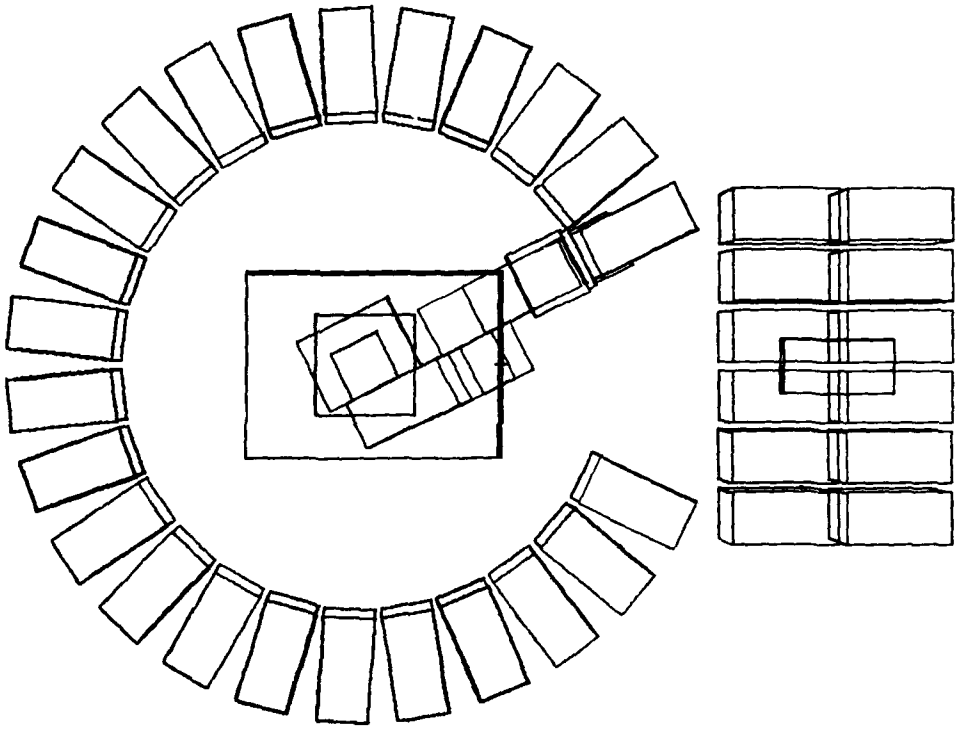
4. Derby, S. J., General Robot Arm Simulation Program (GRASP): Part 1, A Program to Evaluate the Performance of Industrial Robots in Their Working Environment, ASME Computer Eng. Conference, Aug 1982, San Diego

5. Derby, S. J., General Robot Arm Simulation Program (GRASP): Part 2, Methods of Joint Solutions and The Reachable Volume, ASME Computer Eng. Conference, Aug 1982, San Diego

6. Derby, S. J., Motion Characteristics of General Purpose Robot Arms. ASME Mechanisms Conference, Sept 1982, Wash, DC

7. Derby, S. J., The Deflection and Compensation of General Purpose Robot Arms. Submitted to Mechanisms and Machine Theory Journal, April 1982

8. Wu, C. H., Paul, R. P., Resolved Motion Force Control of Robot Manipulator, IEEE Trans Vol SMC-12 No. 3, May/June 1982



USING			STORED	LOG.101481.0 10/07/81			
H0007	A0008	W0008	P0011	H0001	A0001	W0001	P0001
NEW LOG		RECALL		REVIEW		RETURN	
RESTORE		SIMULATE		VIEW			

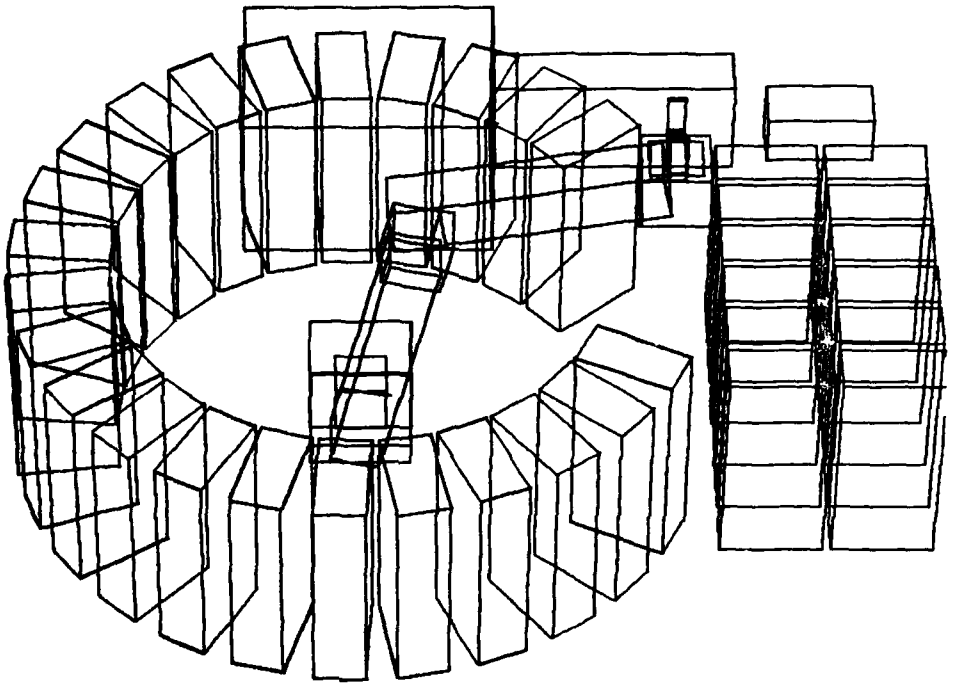
SESSION
NO LIMITS

NO MINMAX

NO DEFORMATION
NO HAND TRACE
NO INTERFER CHK
NOT SHOW ATTEMPTS

FIGURE 1

TOP VIEW - GRASP SIMULATION



USING			STORED	LOG.101481.0			10/07/81
H0007	A0008	W0008	P0011	H0001	A0001	W0001	P0001
NEW LOG	RECALL		REVIEW	RETURN			
RESTORE	SIMULATE		VIEW				

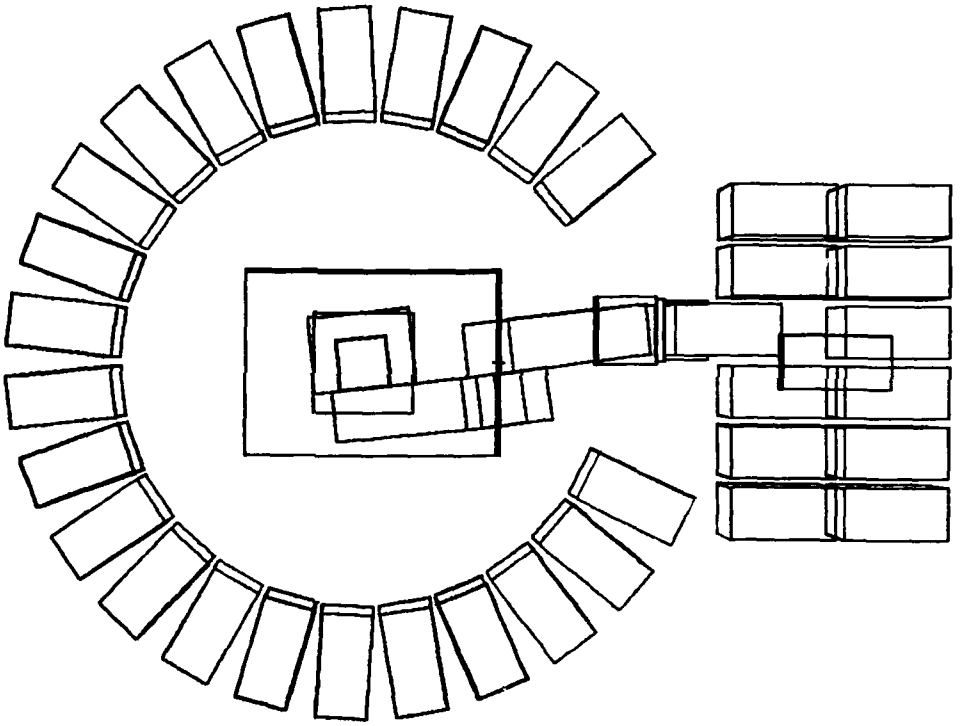
SESSION
NO LIMITS

NO MINMAX

NO DEFORMATION
NO HAND TRACE
NO INTERFER CHK
NOT SHOW ATTEMPTS

FIGURE 2

GRASP SIMULATION - PATH OF CARTRIDGE



USING		STORED	LOG.I02881.I 10/28/81		
A0007 A0008 W0008		P0011	A0001 A0001 W0006 P0006		
NEW LOG	RECALL		REVIEW	RETURN	
RESTORE	SIMULATE		VIEW		

SESSION
NO LIMITS

NO MINMAX

NO DEFORMATION
NO HAND TRACE
NO INTERFER CHK
NOT SHOW ATTEMPTS

FIGURE 3

GRASP SIMULATION - REPLENISHING READY ROUNDS

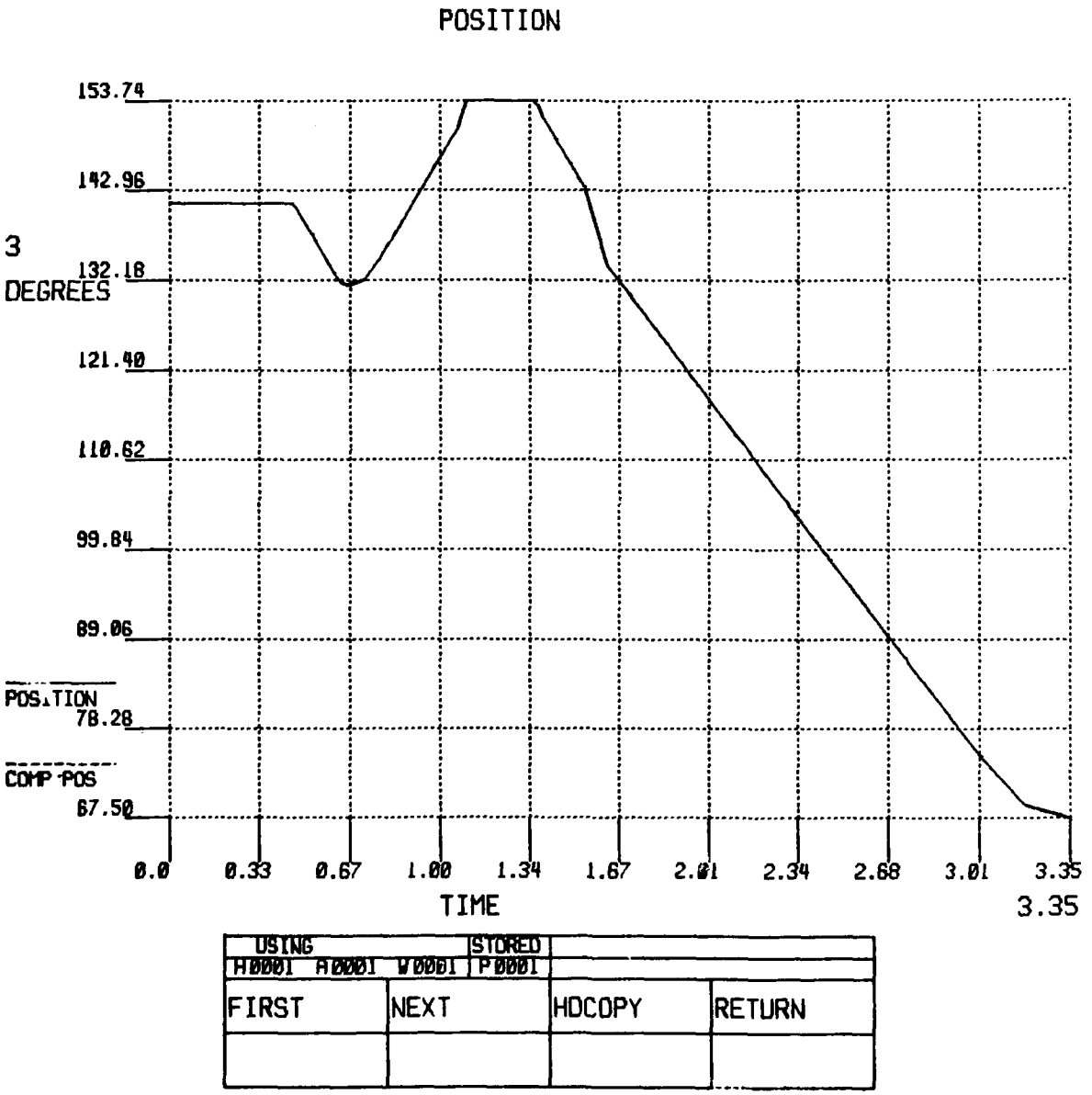


FIGURE 4

GRASP OUTPUT - DISPLACEMENT OF JOINT 3

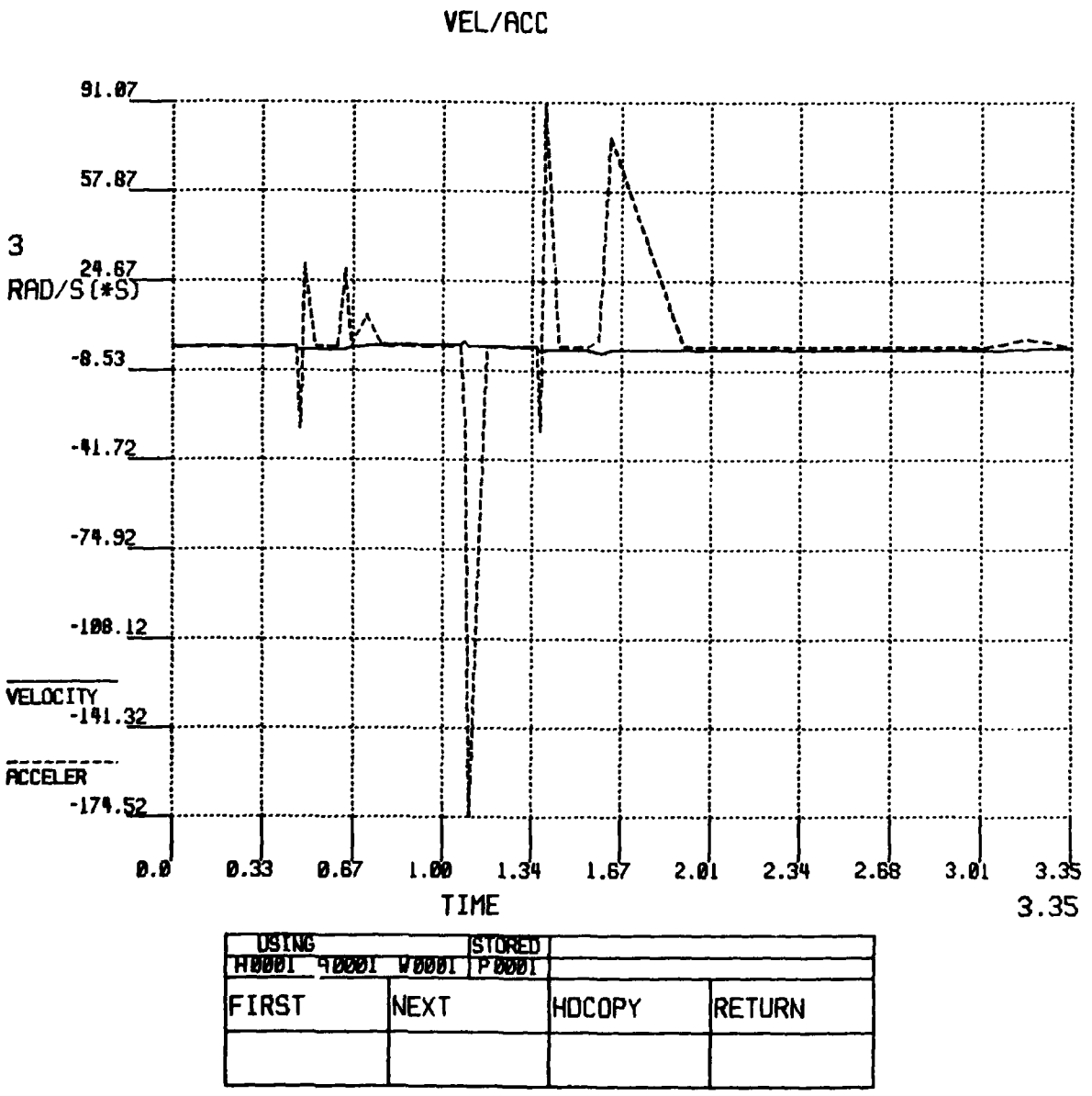


FIGURE 5

GRASP OUTPUT - VELOCITY AND ACCELERATION OF JOINT 3

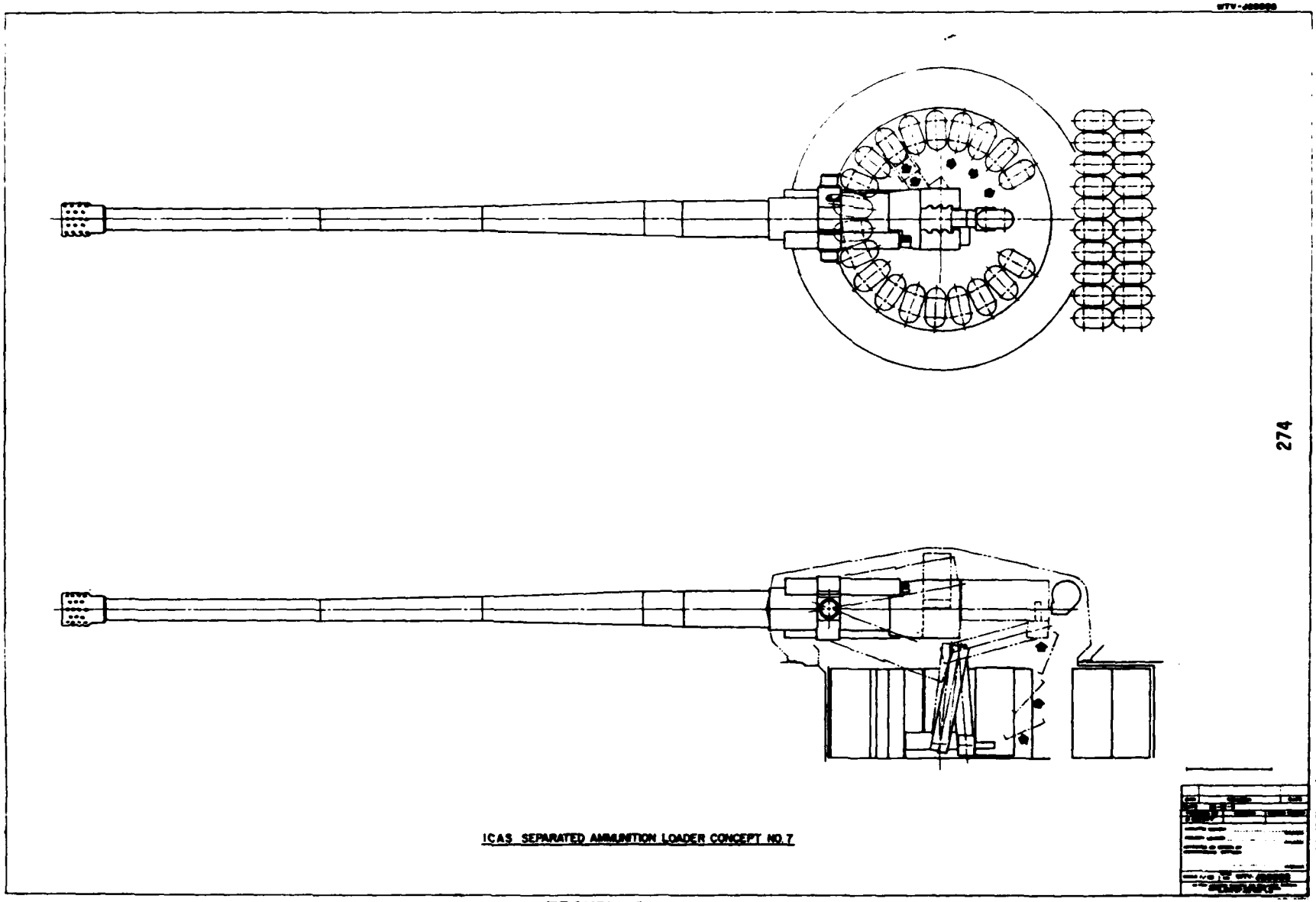


FIGURE 6
CONCEPT DRAWING - TOP AND FRONT OF TURRET BASKET

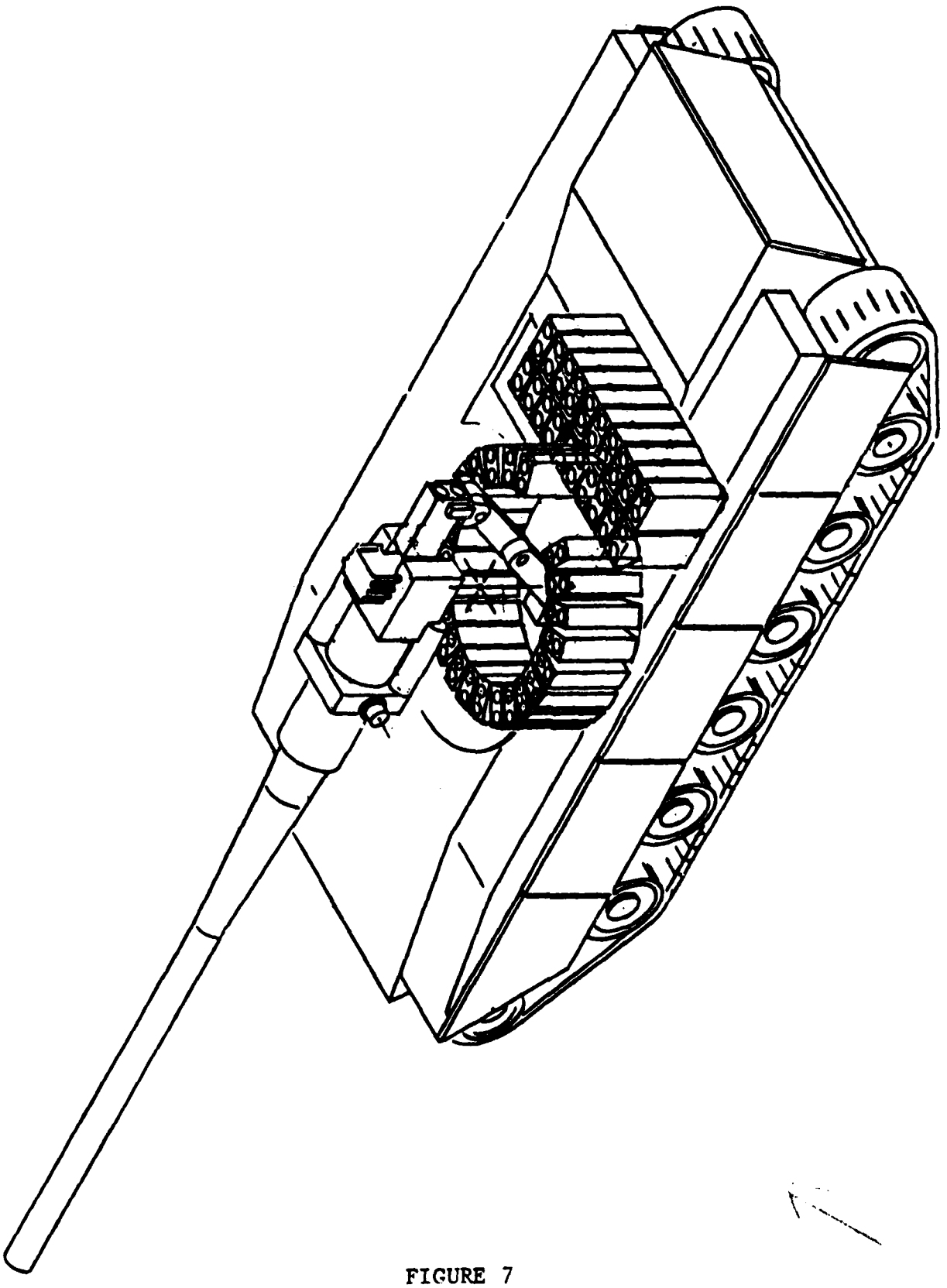


FIGURE 7

CONCEPT DRAWING - LOADER AND ROUNDS RELATIVE TO THE TANK

Next page is blank.

AD P001077

EXPERIMENTS IN NONLINEAR ADAPTIVE CONTROL OF MECHANICAL LINKAGE SYSTEMS

T. Depkovich
Advanced Automation Technology Section
Martin Marietta Corporation
P.O. Box 179, Denver, CO 80201

H. Elliott
Department of Electrical and Computer Engineering
University of Massachusetts
Amherst, MA 01003

I. INTRODUCTION

With the growing interest in robotics, the problem of controlling mechanical linkage systems, such as manipulators, has recieved considerable attention in the literature [1]-[6]. This problem is difficult for a number of reasons. First, by applying either Newtonian or Lagrangian mechanics, it is easily shown that such linkages are characterized by nonlinear dynamics. Second, while positioning and control of the end point of the linkage in terms of room (or workspace) coordinates is the ultimate goal in robotics applications, motor control commands are most naturally specified in terms of controlling joint angles. Again the nonlinear transformation relating joint angle coordinates to end point room coordinates complicates the problem. In this report, we address the first problem--namely, control of the nonlinear dynamics relating joint angles to motor torques. Although some reports, using optimal control theory, have presented complex nonlinear control strategies [3],[4], for the most part, simpler linear strategies have been suggested [1], [2]. Furthermore, because of the nonlinearities and the dependence of control parameters on time-varying system parameters (in particular, changing loads), adaptive control has been proposed to make these algorithms robust [5],[6]. In both of these reports, adaptive controllers were designed by neglecting the nonlinear dynamics and assuming a link to be characterized by second-order linear dynamics.

By simulating a single link under the influence of gravity, it will be shown that while adaptive control using the linear modeling approach can work for certain geometries and loading, it performs very poorly for others. The single link system is relevant as a test case since the equations of motion contain a trigonometric nonlinearity similar to a more complex system. It is then shown that this problem can be overcome by using a nonlinear adaptive control scheme proposed in [7]. Although nonlinear, the control is simple and its complexity is of the same order as the linear adaptive scheme. It is demontrated, via

simulation, that this approach also has the advantage over the linear formulation of not requiring control parameter variation to adapt to different set points. Simulations showing the performance of both the linear and nonlinear adaptive control under changing loads are also presented. Finally, we briefly discuss the extension of the approach from the single link to higher-degree-of-freedom cases.

The report is organized as follows. Section II formulates the control problem for the single link case, and Section III discusses both linear and nonlinear fixed control strategies which could be implemented if the system parameters were known. The strategy applied is deadbeat or minimum variance tracking. Section IV presents the adaptive formulation; Section V gives our simulation results. Finally, Section VI discusses the extension of this approach to higher-degree-of-freedom cases and gives some concluding remarks.

II. PROBLEM FORMULATION

Consider the problem of controlling a hinged rod of length, ℓ, and mass m using a torque, u(t), as shown in Figure 1.

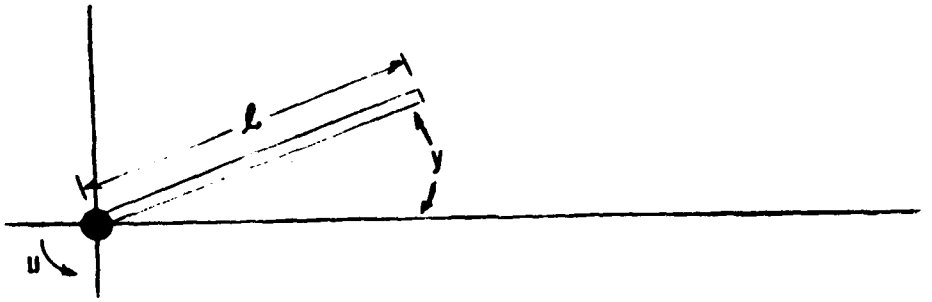


Figure 1. A Single Hinged Link

If the rod rotates in the vertical plane so that it is under the influence of gravity and if the hinge has a coefficient of friction F, then this system is characterized by the nonlinear differential equation

$$\frac{m\ell^3}{3}\ddot{y}(t) + F\dot{y}(t) + mg\,\ell\cos y(t) = u(t) \qquad (1a)$$

Defining $J = m\ell^3/3$, and $G = mg\ell$ we can rewrite this as

$$J\ddot{y} + F\dot{y} + G\cos y = u \qquad (1b)$$

One control problem involves design of a feedback signal $u(t)$ which causes $y(t)$ to follow a desired trajectory $y^*(t)$. In order to use a digital computer for control in the next section, we solve this problem using classical sample data methodologies.

III. A FIXED DIGITAL CONTROL STRATEGY

To design a digital control for (1), we assume that $u(t)$ is generated by a computer and output through a zero order hold so that

$$u(t) = u_k \qquad t\varepsilon[kT,(k+1)T]$$

where T is the sampling period. We will choose u_k so that

$$\begin{aligned} y(kT) &= y_k \\ &= y^*_k \\ &= y^*(kT) \end{aligned}$$

In the deterministic, noise-free case, this is called deadbeat control, while in the noisey case, it is referred to as minimum variance control. Although for simplicity, we will use this strategy. Since it is well known that this can sometimes lead to large control signals, we point out that one can also derive a model reference version. In order to derive the control sequence (u_k), we must first derive a discrete approximation to 1. The simplest approach is to approximate

$$\dot{y}(kT) \cong (y_k - y_{k-1})/T$$

$$\ddot{y}(kT) \cong (y_{k+1} - 2y_k + y_{k-1})/T^2$$

In this case, one obtains

$$\frac{J}{T^2}(y_{k+1}-2y_k+y_{k-1}) + \frac{F}{T}(y_k-y_{k-1}) + G\cos\theta_k = u_k \qquad (2)$$

Note that by using different approximations to $\dot{y}(kT)$ and $\ddot{y}(kT)$, slightly different models can be obtained. Thus, a fairly general model might take the form

$$\phi_k^T\theta = u_k \qquad (3a)$$

where

$$\phi_k^T = [y_{k+1}, y_k, y_{k-1}, u_{k-1}, \cos(y_k), \cos(y_{k-1})] \qquad (3b)$$

and

$$\theta^T = [\ _1,\ _2, \ldots,\ _6] \tag{3c}$$

is a parameter vector. Assuming (3) to be correct and θ known, one can assure deadbeat control for $k \geq 1$, i.e.,

$$y_k = y^*_k\ ,\ k \geq 1$$

provided u_k is chosen so that $y_{k+1} = y^*_{k+1}$,

$$u_k = \phi_k^{-T}\theta\ ,\ k \geq 0 \tag{4a}$$

where

$$\phi^{-T} = [y^*_{k+1}, y_k, y_{k-1}, \cos(y_k), \cos(y_{k-1})] \tag{4b}$$

That is, $\bar{\phi}_k$ is obtained from ϕ_k by replacing y_{k+1} by y^*_{k+1}.

To linearize this control, one would neglect the $\cos(y_k)$ and $\cos(y_{k-1})$ terms in (4) and simply use

$$u_k = \tilde{\phi}_k^T\tilde{\theta}_k \tag{5a}$$

where

$$\tilde{\phi}_k^T = [y^*_{k+1}, y_k, y_{k-1}, u_{k-1}] \tag{5b}$$

and

$$\theta^T = [\ _1,\ _2,\ _3,\ _4] \tag{5c}$$

As will be seen in the simulations, if G is small by comparison to J, then this control performs adequately. On the other hand, if $G/J > 30$, the nonlinear control performs significantly better. This is certainly possible since when m = 2kg and ℓ = 1/2 meter, we have

$$J/G = 9.8/8.33 \times 10^{-2}$$

$$= 117.65$$

For the case of linear models, it is known that this control only remains bounded if the plant is "minimum phase", that is, all its zeros are inside the unit circle. Since no formal analogous condition has been developed for nonlinear deadbeat control of the boundedness of the control must be determined by simulation. Our simulation studies thus far, in which the sampling period ranged between 0.1 and 0.01 seconds, have shown that control boundedness is not a problem. It might also be pointed out that this system does not exhibit certain physical characteristics of nonminimum phase systems such as an initially-decreasing unit step response.

IV. ADAPTIVE CONTROL

To implement nonlinear adaptive control, we simply replace the fixed parameter vector θ in (3) by an estimate θ_k. Using sequential least squares for parameter estimation, the complete control law is

$$u_k = \bar{\phi}_k^T \theta_k \tag{6a}$$

$$\theta_k = \theta_{k-1} + \frac{P_{k-2}\phi_{k-1}e_{k-1}}{1 + \phi_{k-1}^T P_{k-2}\phi_{k-1}} \tag{6b}$$

$$P_{k-1} = P_{k-2} + \frac{P_{k-2}\phi_{k-1}\phi_{k-1}^T P_{k-2}}{1 + \phi_{k-1}^T P_{k-2}\phi_{k-1}} \tag{6c}$$

$$P_{-1} = \gamma I \quad \gamma > 0 \tag{6d}$$

$$e_{k-1} = u_{k-1} - \phi_{k-1}^T \theta_{k-1} \tag{6e}$$

Note that although the control is nonlinear because of the trigonometric terms, it is linear in the unknown parameters so that standard sequential linear parameter estimation procedures can be applied. It should also be pointed out that technical aspects of stability analysis require that θ_{1k}, the first entry in θ_k, be restricted from converging to zero. In [7] and [8], modifications to (6) have been developed to assure this. However, in our simulations to date, we have not found it necessary to implement such modifications.

The linear approximation to adaptive control (6), as used in [6] and as used in our simulations below, can be obtained from (6) by simply replacing $\bar{\phi}_k$ by $\tilde{\phi}_k$ as defined in (5) and ϕ_k by ϕ'_k defined as

$$\phi'_k = [y_{k+1}, y_k, y_{k-1}, u_{k-1}]$$

That is, one neglects the trigonometric terms for control and parameter estimation.

V. SIMULATIONS

In this section, a number of simulations are presented to demonstrate the potential improved performance which can be obtained by using the nonlinear strategy.

COMPARISON OF LINEAR AND NONLINEAR CONTROL FOR DIFFERENT GEOMETRIES

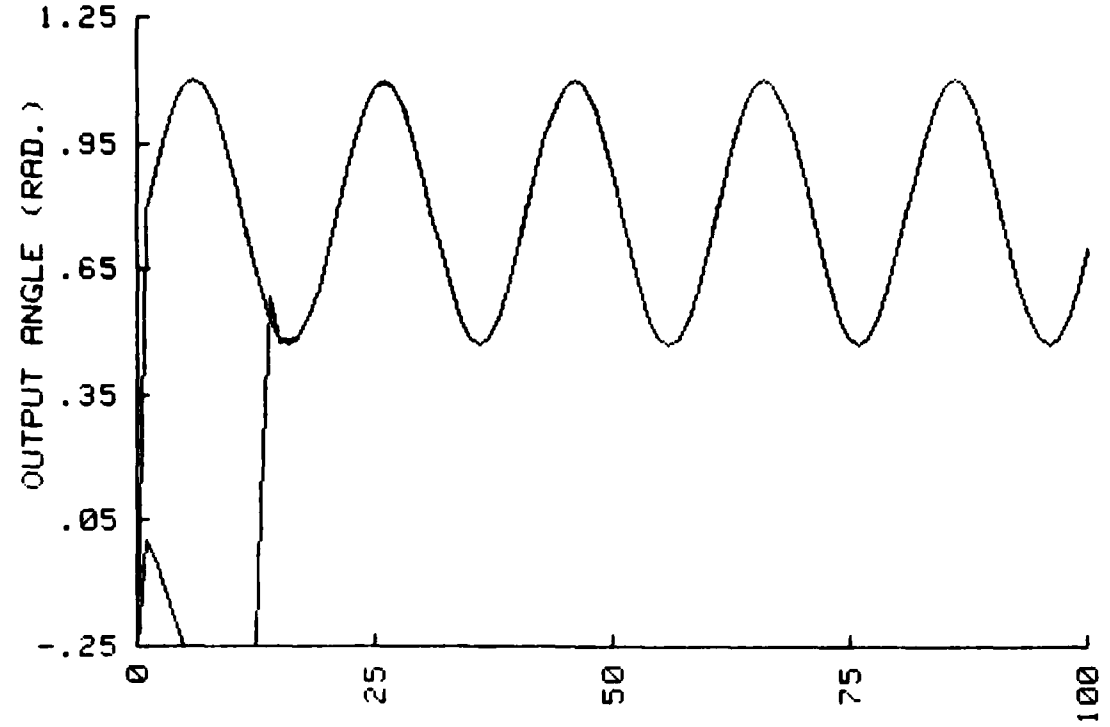
In this experiment, we compared the linear and nonlinear controls for the cases m = 2kg and ℓ = 2, 1 and 1/2 meters. As is seen by comparing Figures 2-4, as the rod length ℓ decreases, there is considerable degradation in the performance of the

linear controller while the nonlinear controller suffers only from a slight decrease in convergence rate. As previously pointed out, these values of ℓ correspond to successfully larger relative weights of the nonlinear term in (1). In particular, $G/J = 14.7$, 26.4, and 117.6. For these simulations, all entries in θ_0 were arbitrarily initialized to one, the sampling period $T = .1$, $F = 20$, $P_{-1} = 10^{20}I$, and

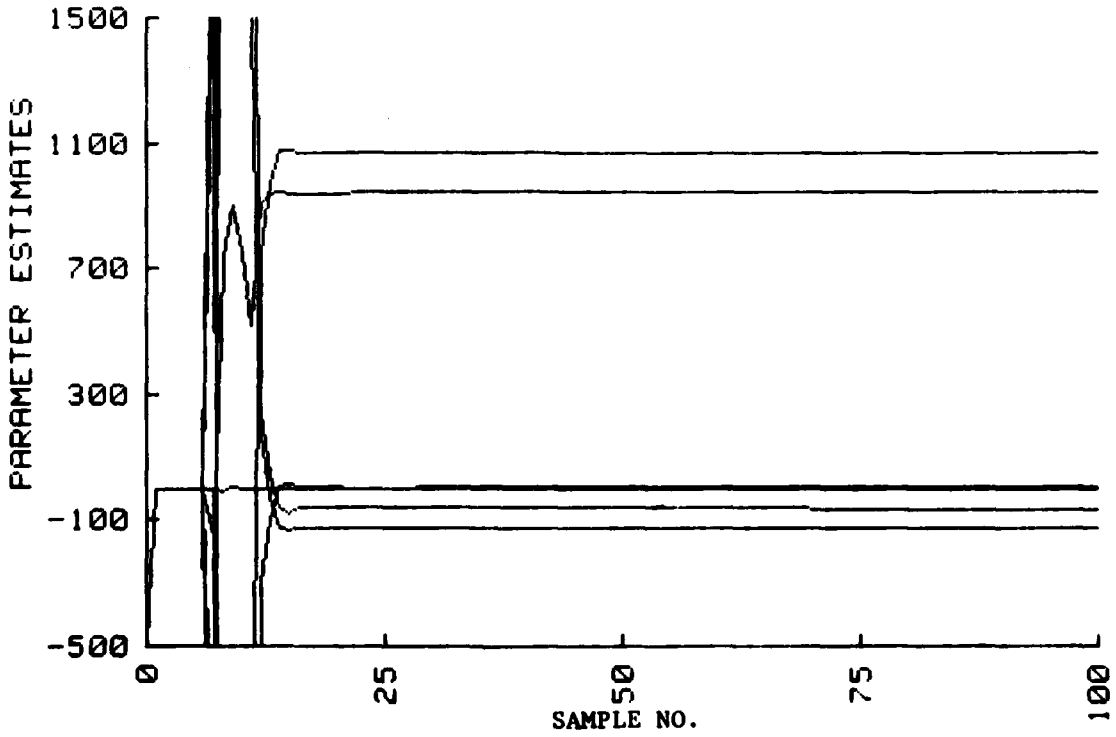
$$y^*(t) = \pi/4 + \pi/10 \sin(\pi t)$$

Figure 5 shows the results of a change in set point during operation. At $k = 50$(t=5 sec.), $y^*(t)$ was incremented by an angle $\pi/4$. In order that the least squares scheme track time-varying phenomena, it is necessary that P_k be kept from going to zero. There are many approaches which can be used such as exponentially-weighted sequential least squares. Here we chose to periodically reinitialize P_k every 30 samples. This approach does not affect the global stability properties of the scheme in the deterministic noise-free case [9]. However, since the simulation of (1) was done using a simple fourth-order Runge-Kutta algorithm on a desktop computer, simulation inaccuracies appear as noise on the system. Because P_k was reset to a very large value, $10^{20}I$, the noise tends to cause some parameter drift at the reset instants. This can be seen in Figures 5c and 5d. In theory, a set point change should only affect the linear controller. The improved performance of the nonlinear controller is apparent in the output plots 5a and 5c. For this simulation, all other parameters were as in the first experiment, in particular, $m = \ell = 2$.

In the final set of plots (Figure 6), m was increased from 2kg to 4kg at $k = 50$ (t=5 sec.). This should affect the parameters of both the linear and nonlinear controller. Although, because of the resetting of P_k to $10^{20}I$, the parameters are slow to settle the improved performance of the nonlinear controller can be seen by looking at the output plots 6a and 6c.

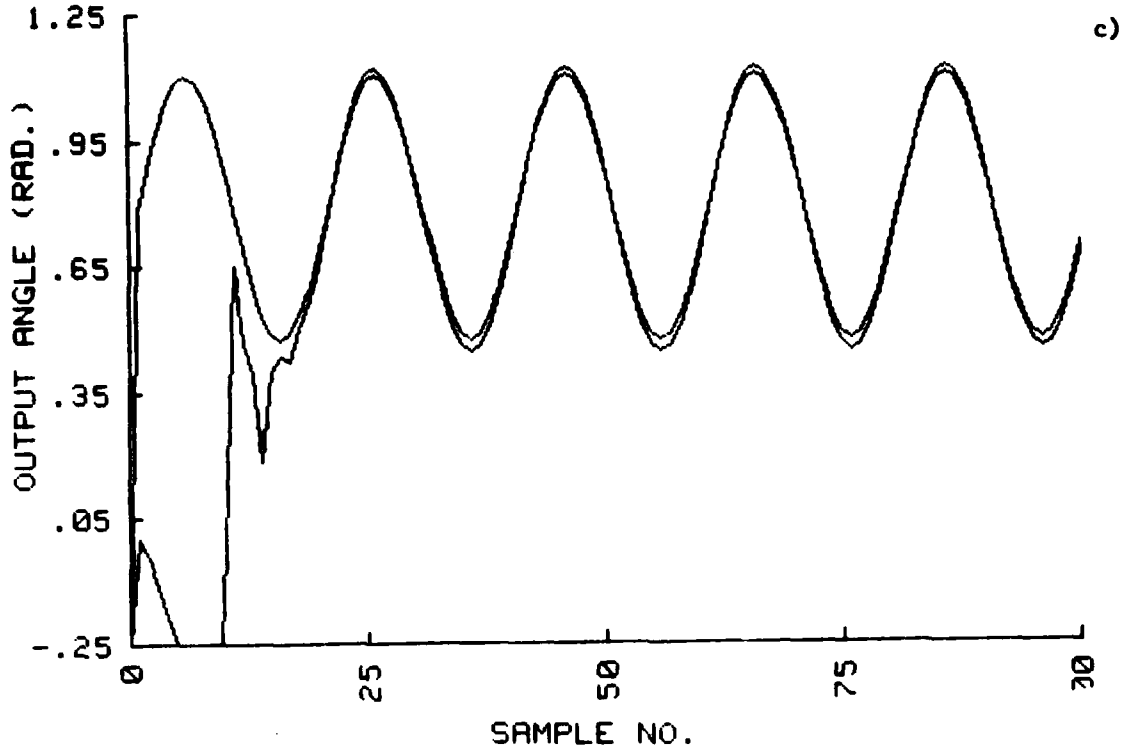


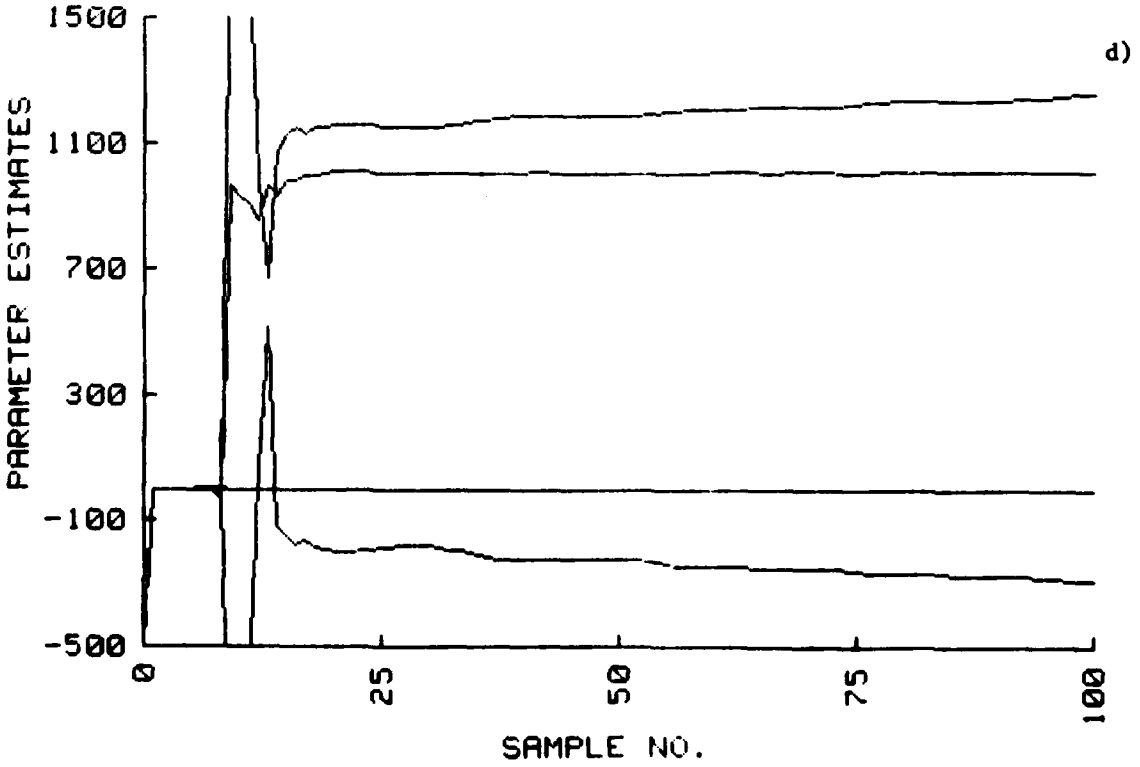
a)

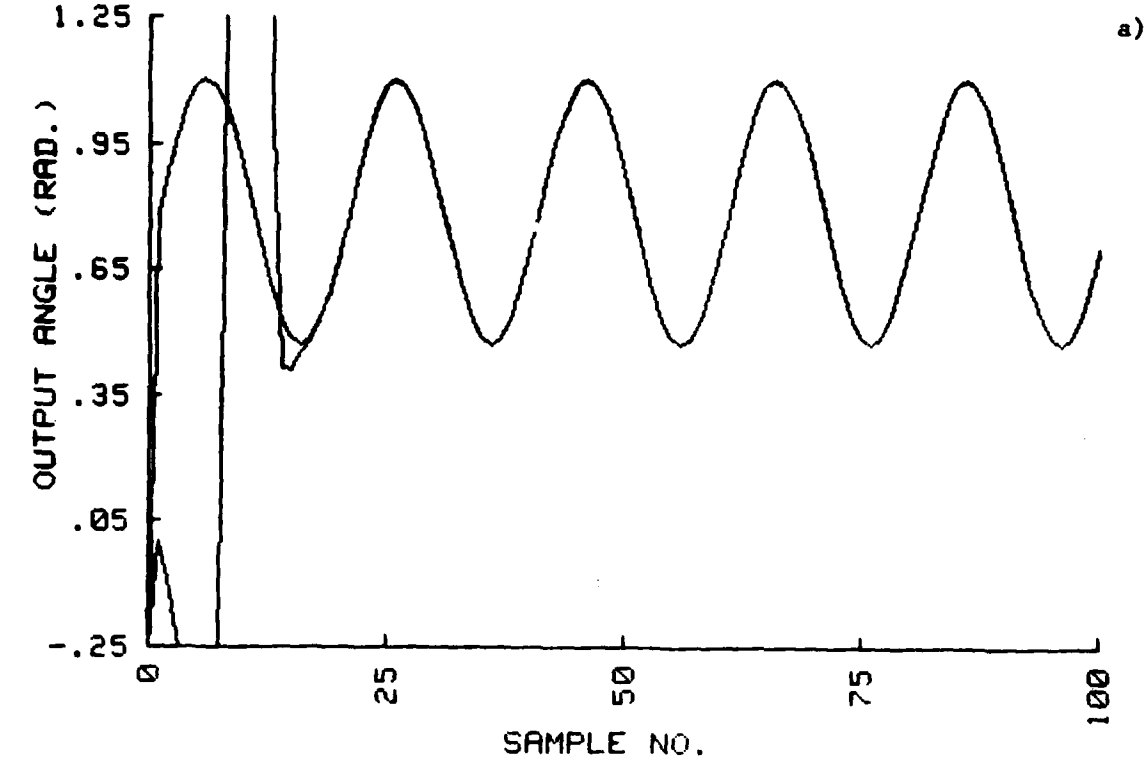


b)

Figure 2. Response of nonlinear, a), b), and linear c), d) when $n=2$, $\ell=2$.


c)
1.25
.95
.65
.35
.05
-.25
OUTPUT ANGLE (RAD.)
0
25
50
75
100
SAMPLE NO.


d)
1500
1100
700
300
-100
-500
PARAMETER ESTIMATES
0
25
50
75
100
SAMPLE NO.



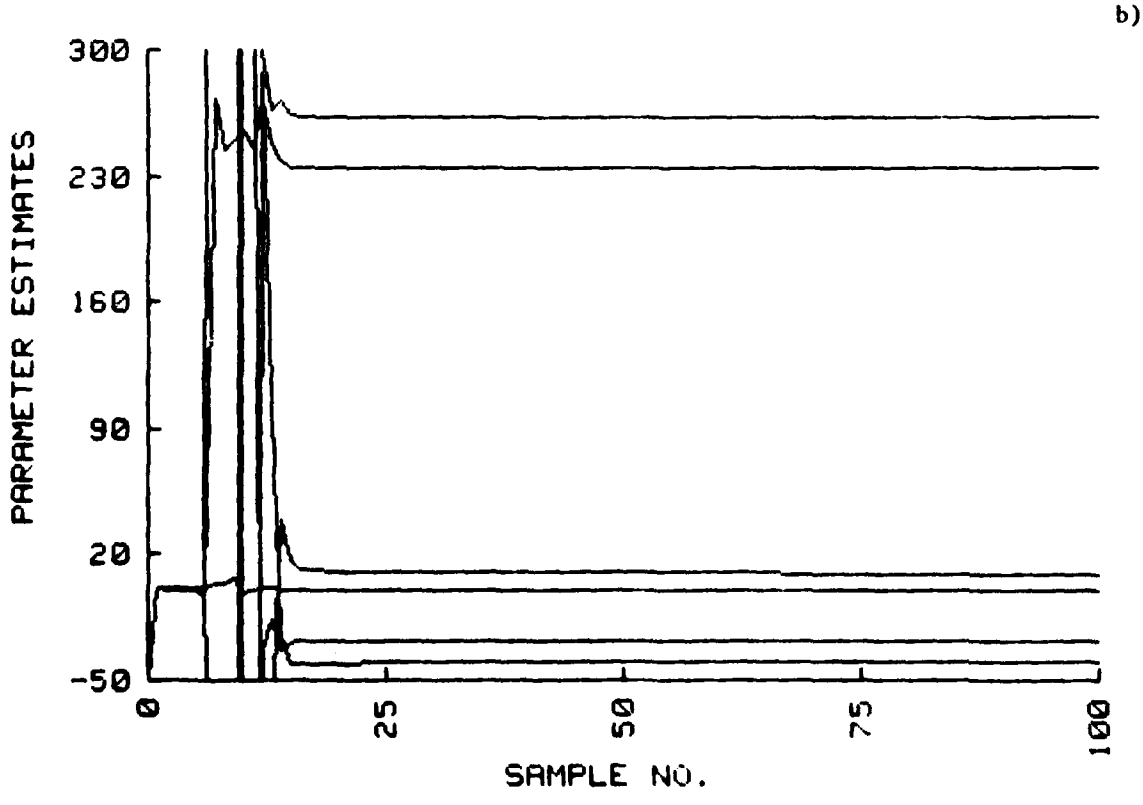
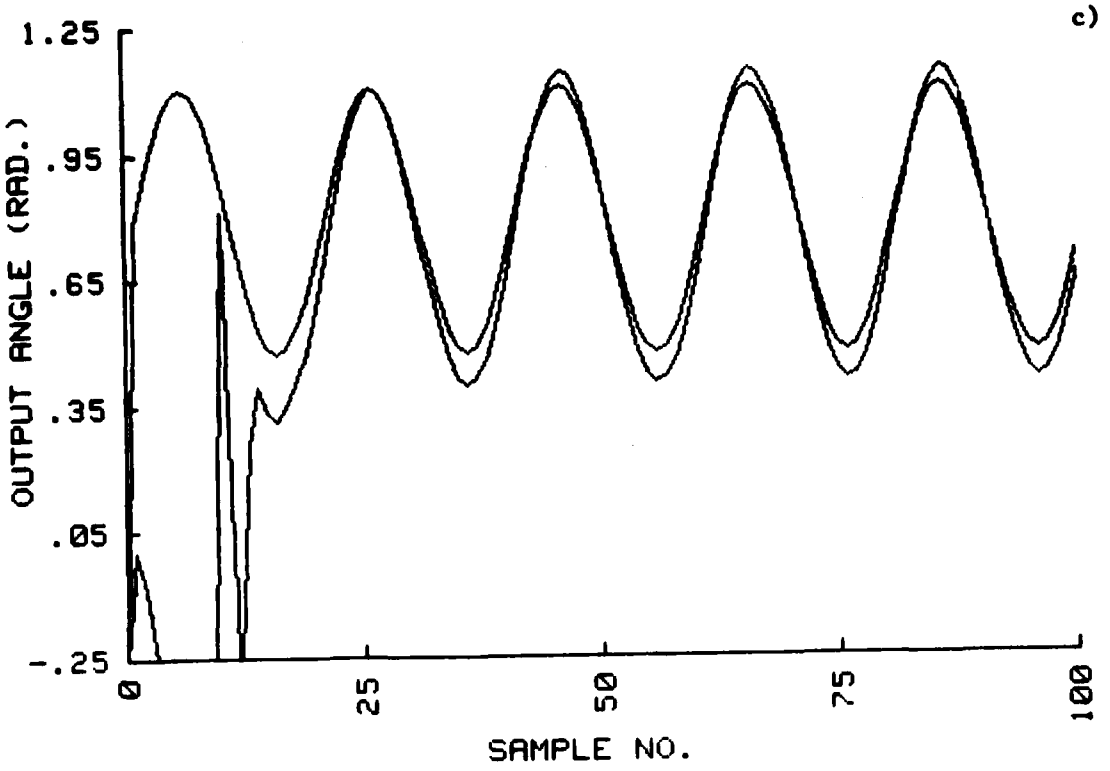
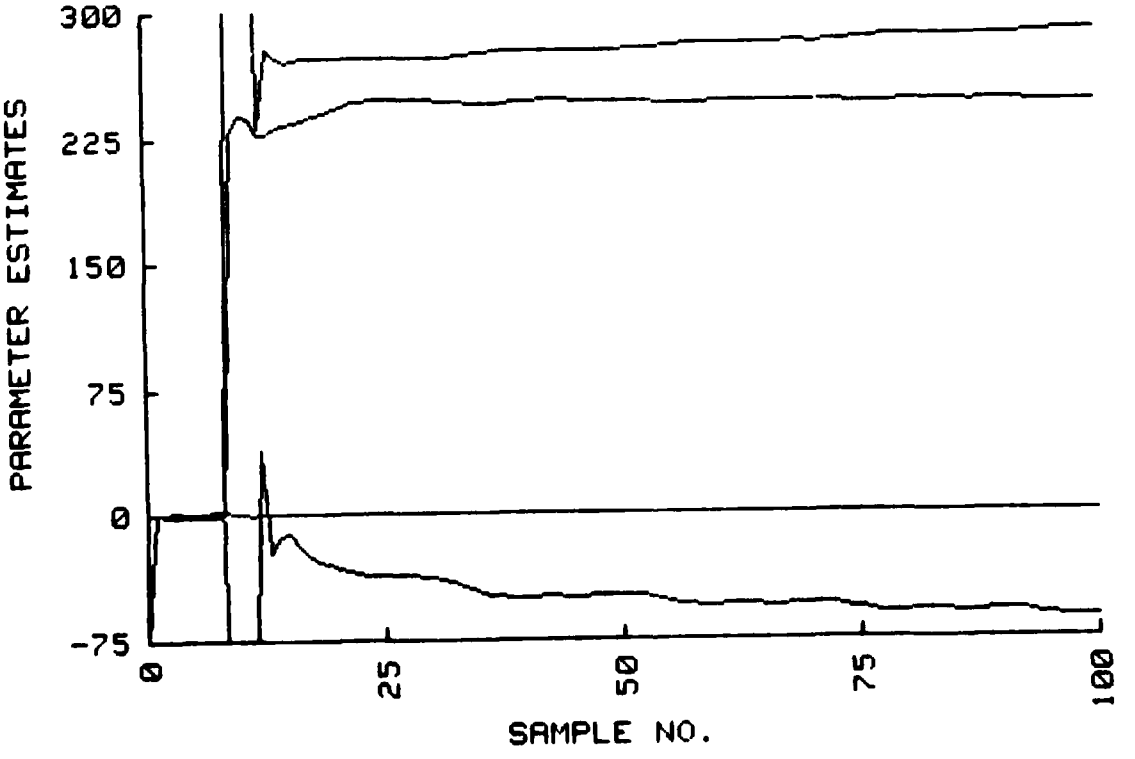


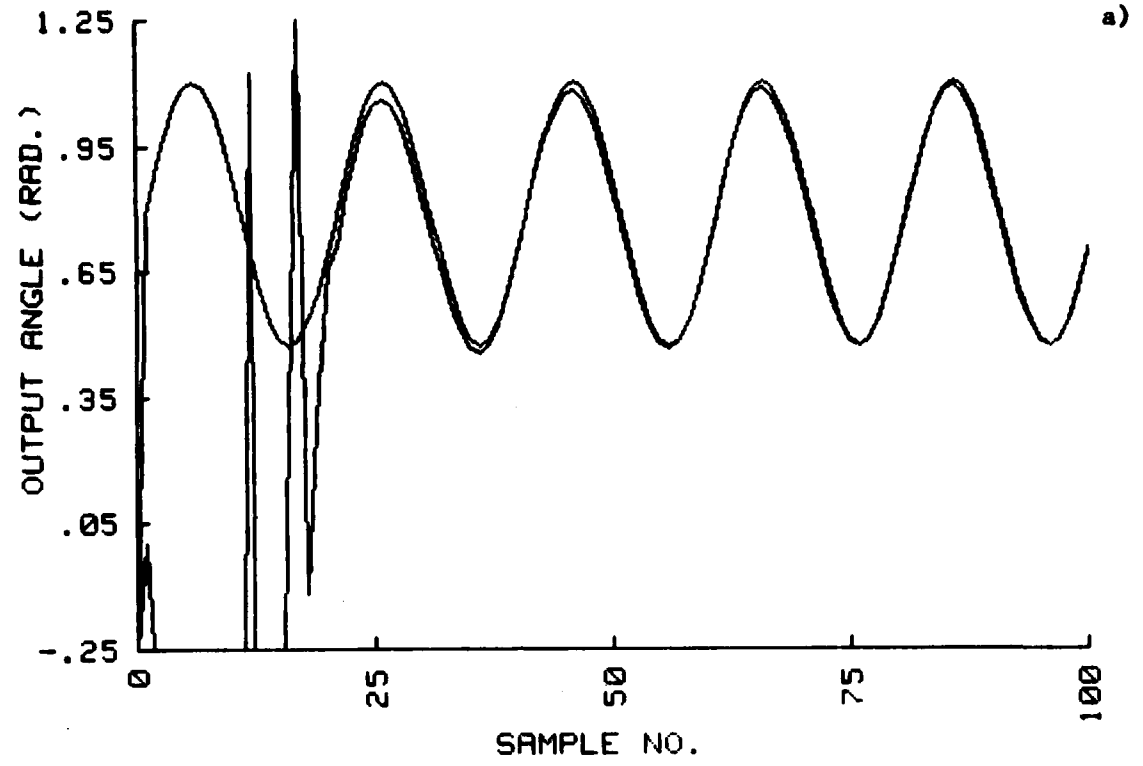
Figure 3. Response of nonlinear a), b), and linear c), d) when m=2, ℓ=1.

c)


1.25
.95
.65
.35
.05
-.25
OUTPUT ANGLE (RAD.)
0
25
50
75
100
SAMPLE NO.

d)


300
225
150
75
0
-75
PARAMETER ESTIMATES
0
25
50
75
100
SAMPLE NO.



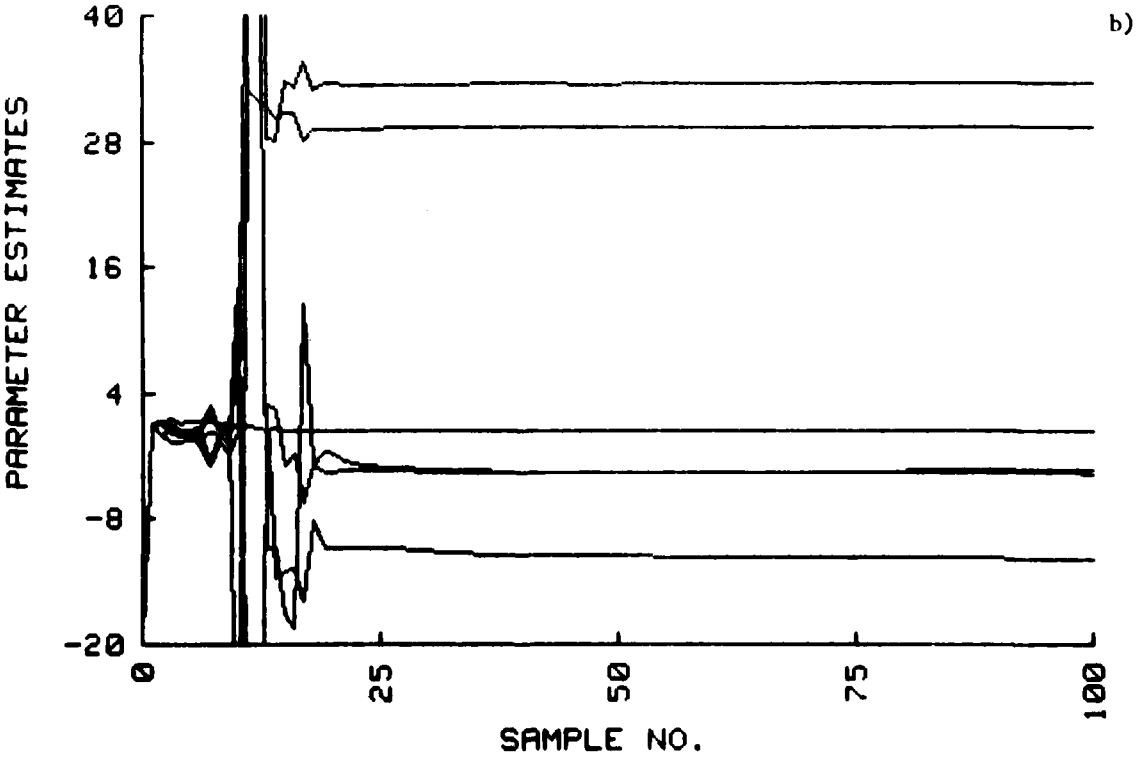
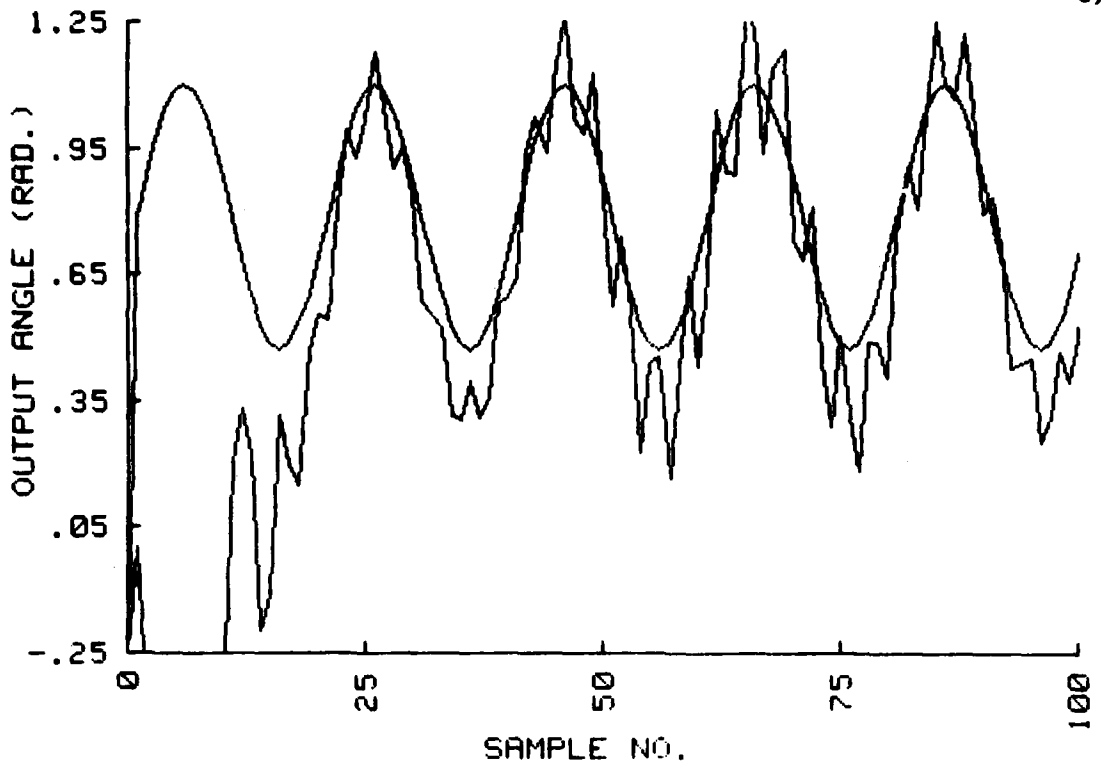
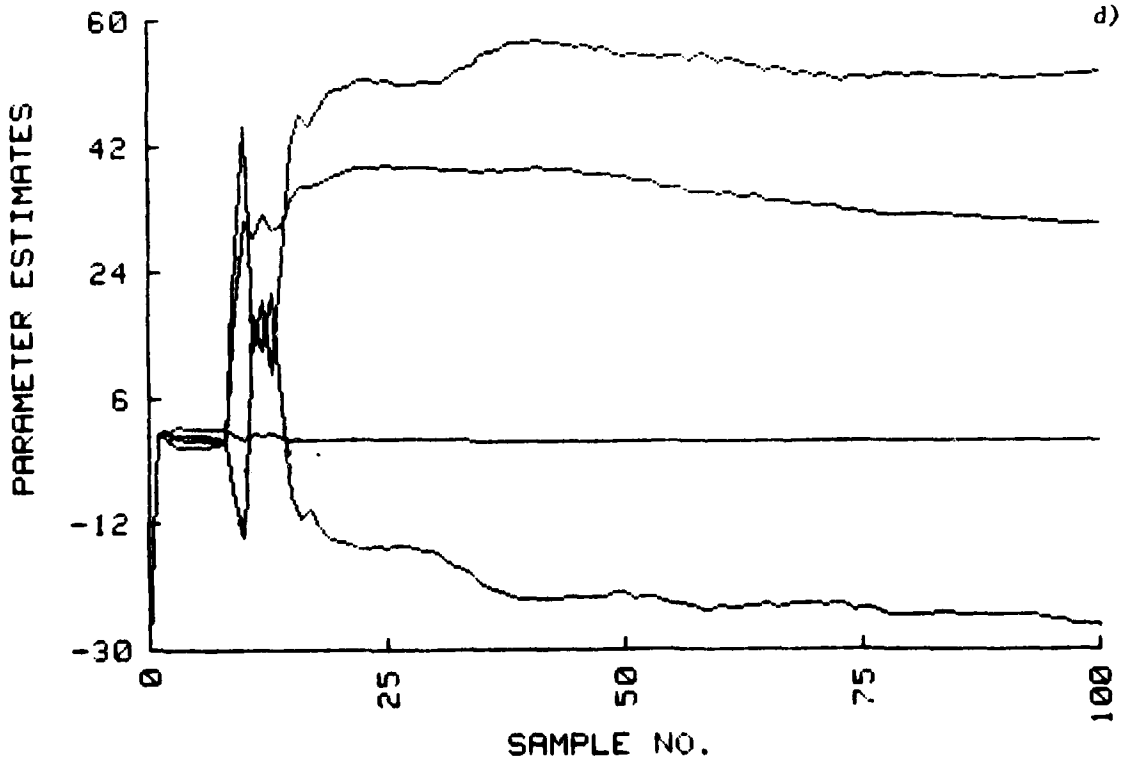


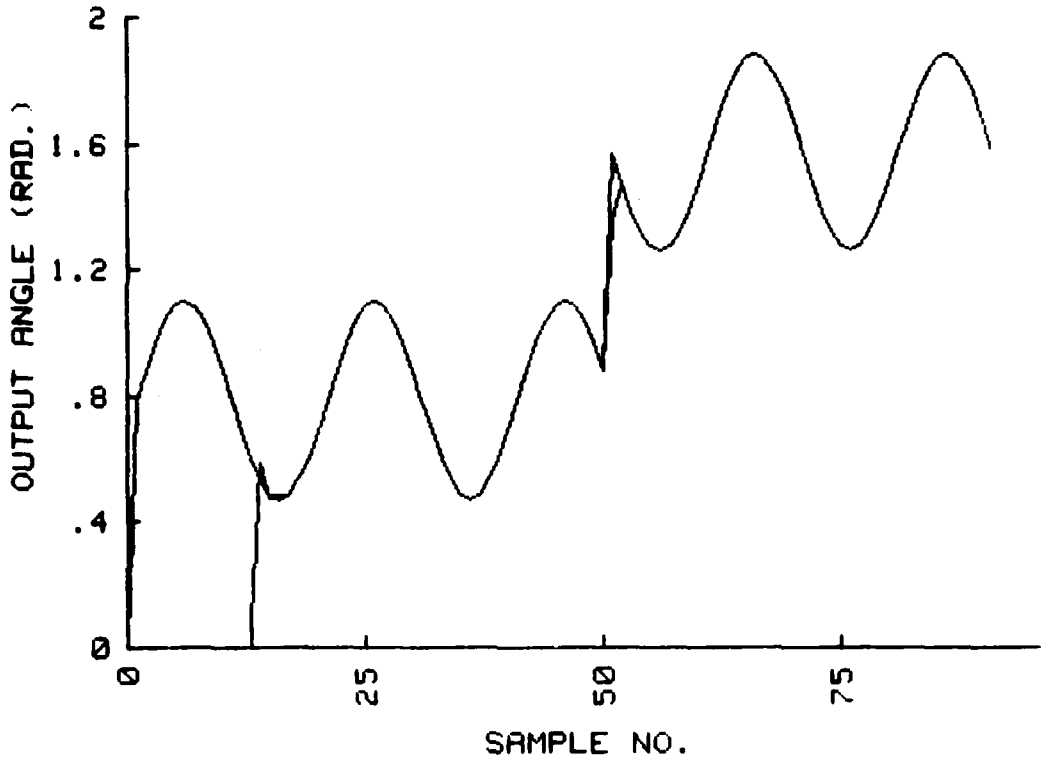
Figure 4. Response of nonlinear a), b) and linear c), d) when m=2, $\ell = \frac{1}{2}$.

c)


1.25
.95
.65
.35
.05
-.25
OUTPUT ANGLE (RAD.)
0
25
50
75
100
SAMPLE NO.

d)


60
42
24
6
-12
-30
PARAMETER ESTIMATES
0
25
50
75
100
SAMPLE NO.



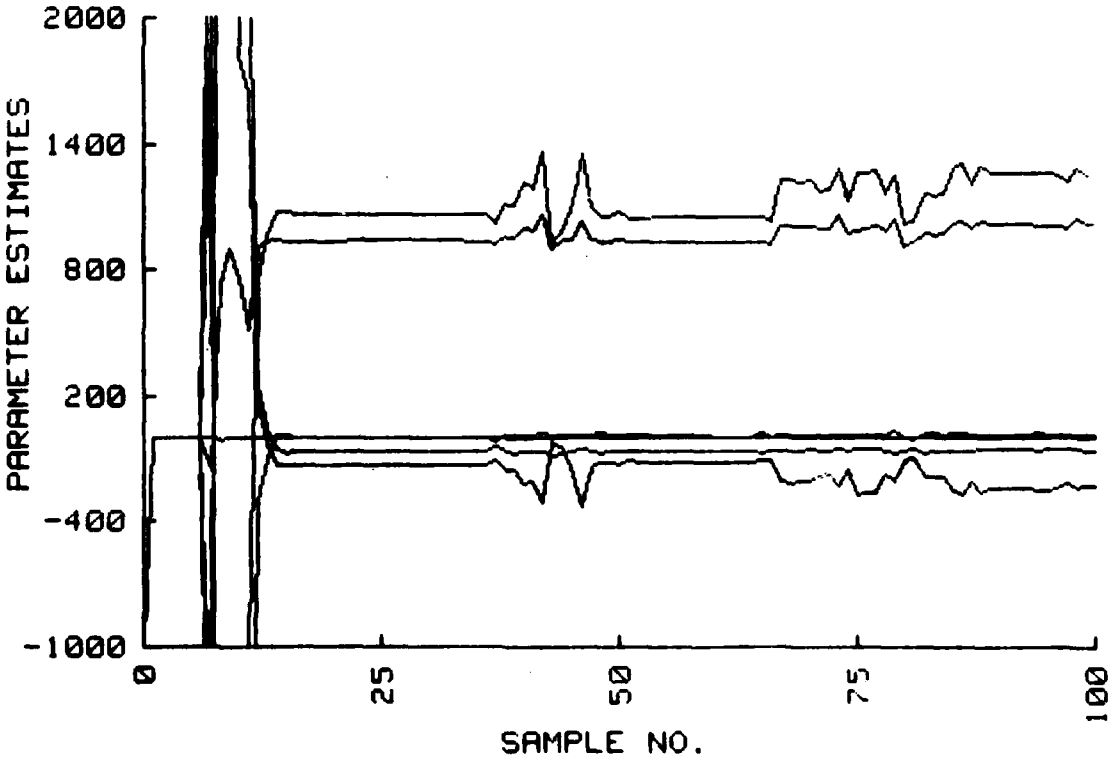
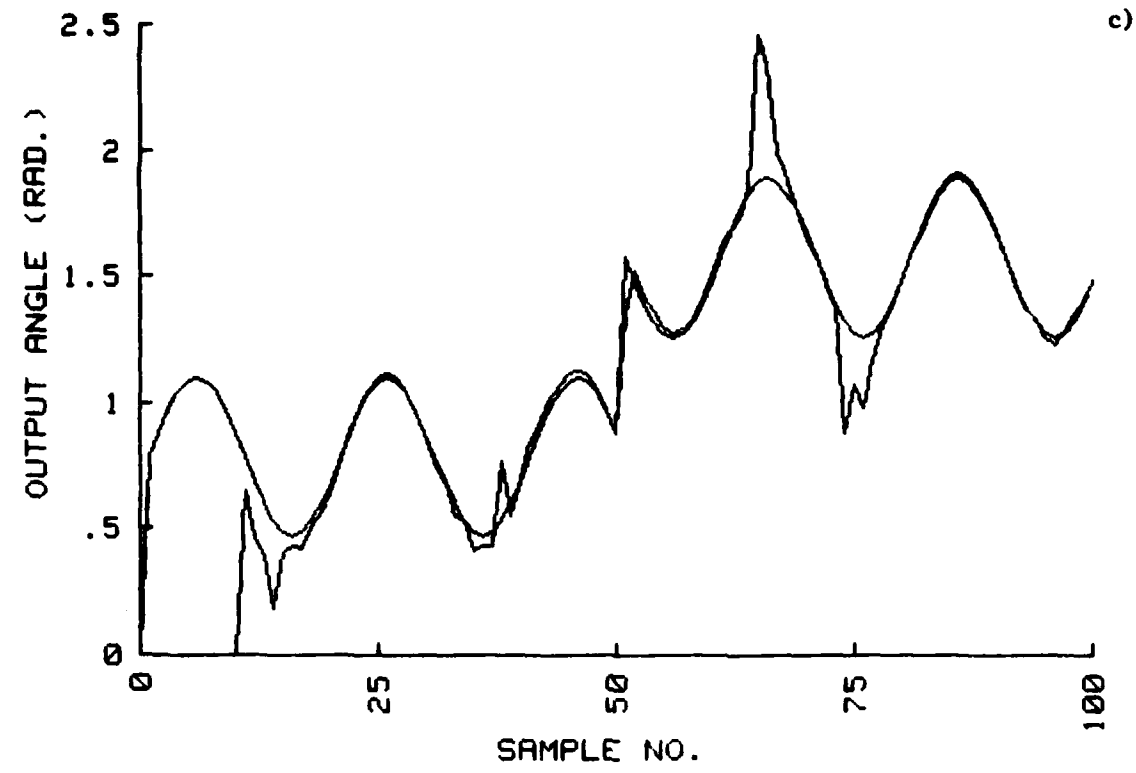
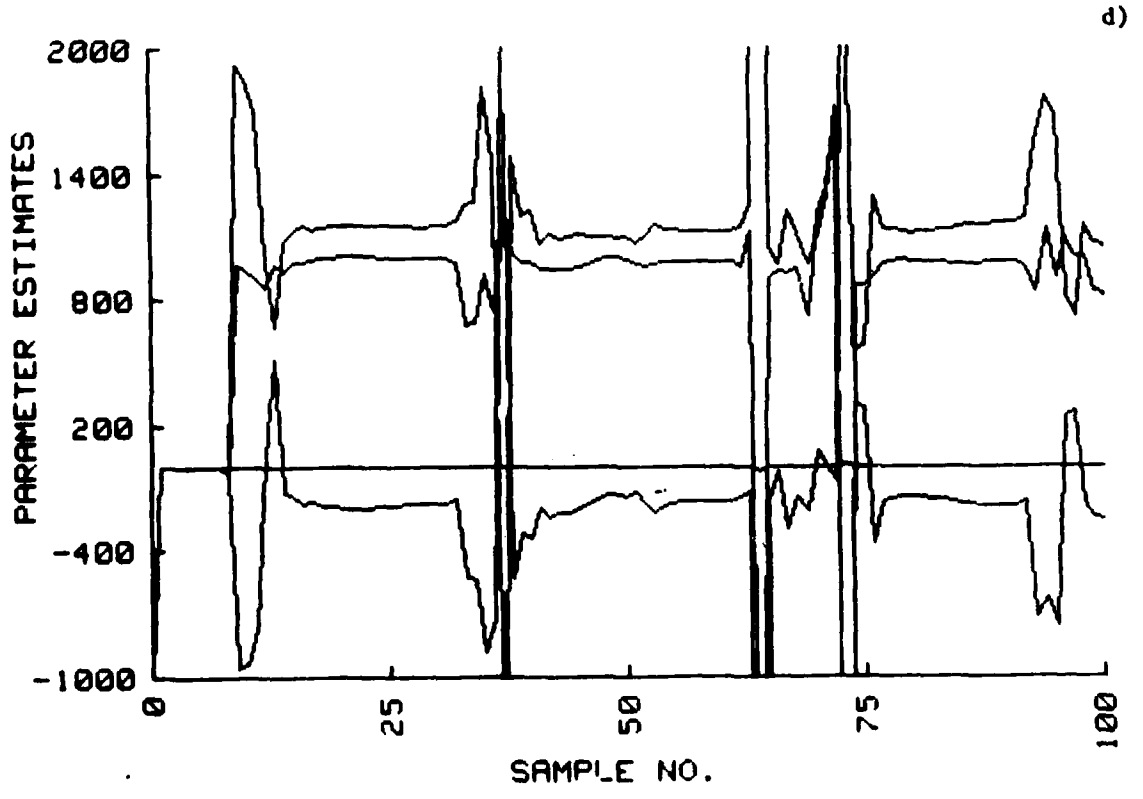
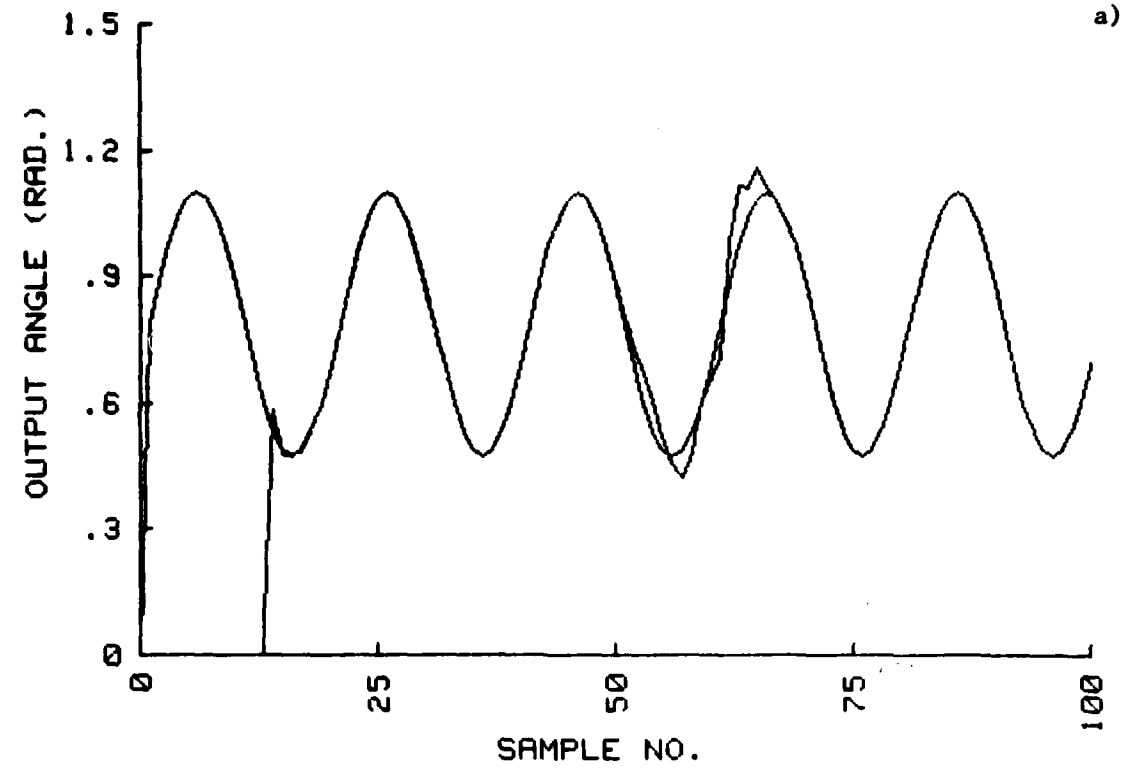


Figure 5. Response of nonlinear a), b) and linear c), d) when m=2, ℓ=2 but a change in set point occurs.


c)
OUTPUT ANGLE (RAD.)
2.5
2
1.5
1
.5
0
0
25
50
75
100
SAMPLE NO.


d)
PARAMETER ESTIMATES
2000
1400
800
200
-400
-1000
0
25
50
75
100
SAMPLE NO.



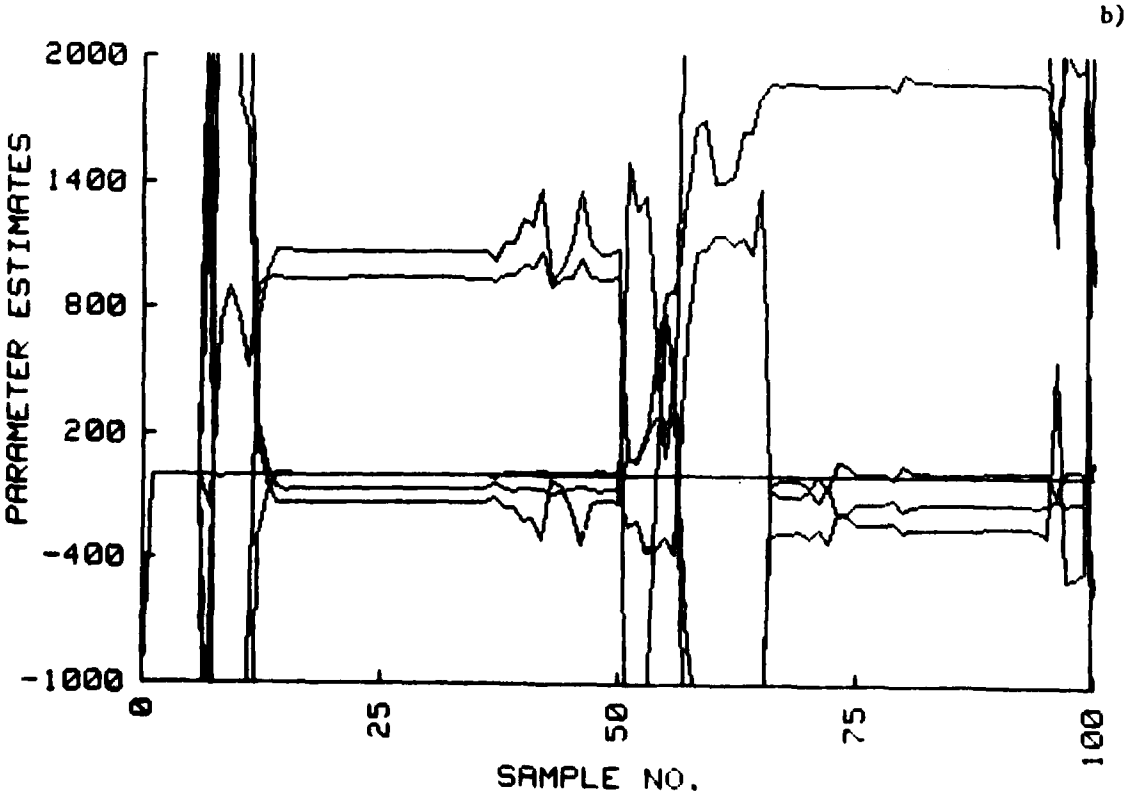
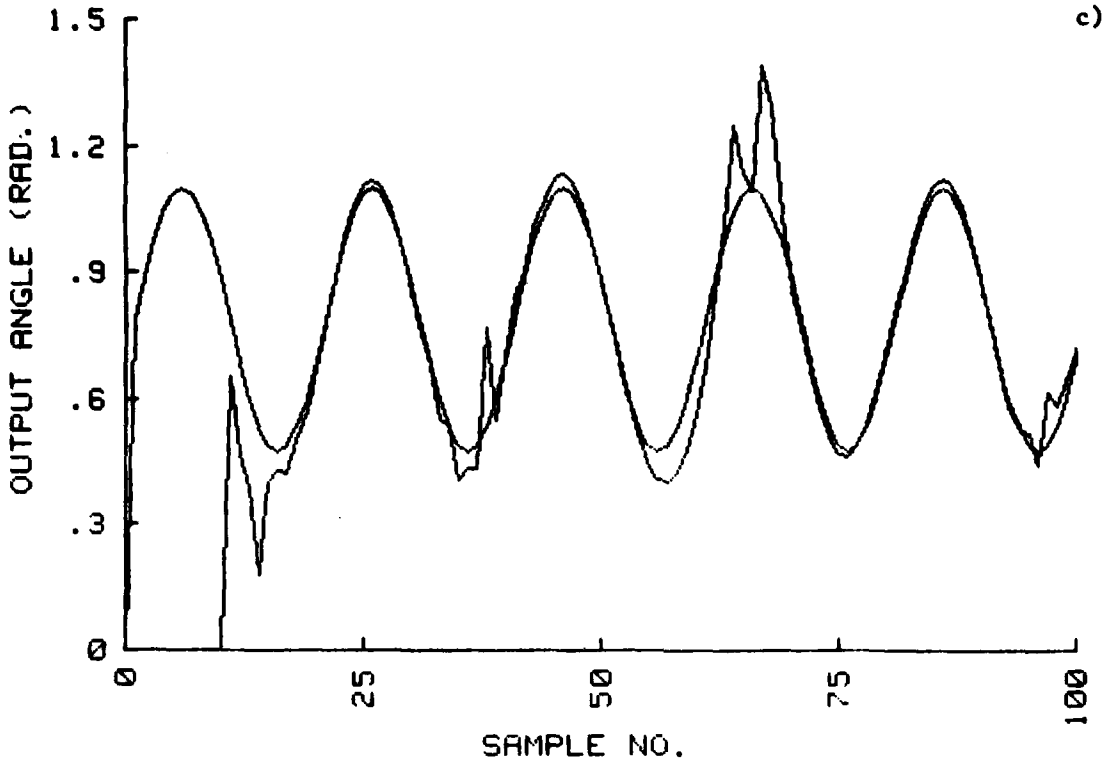
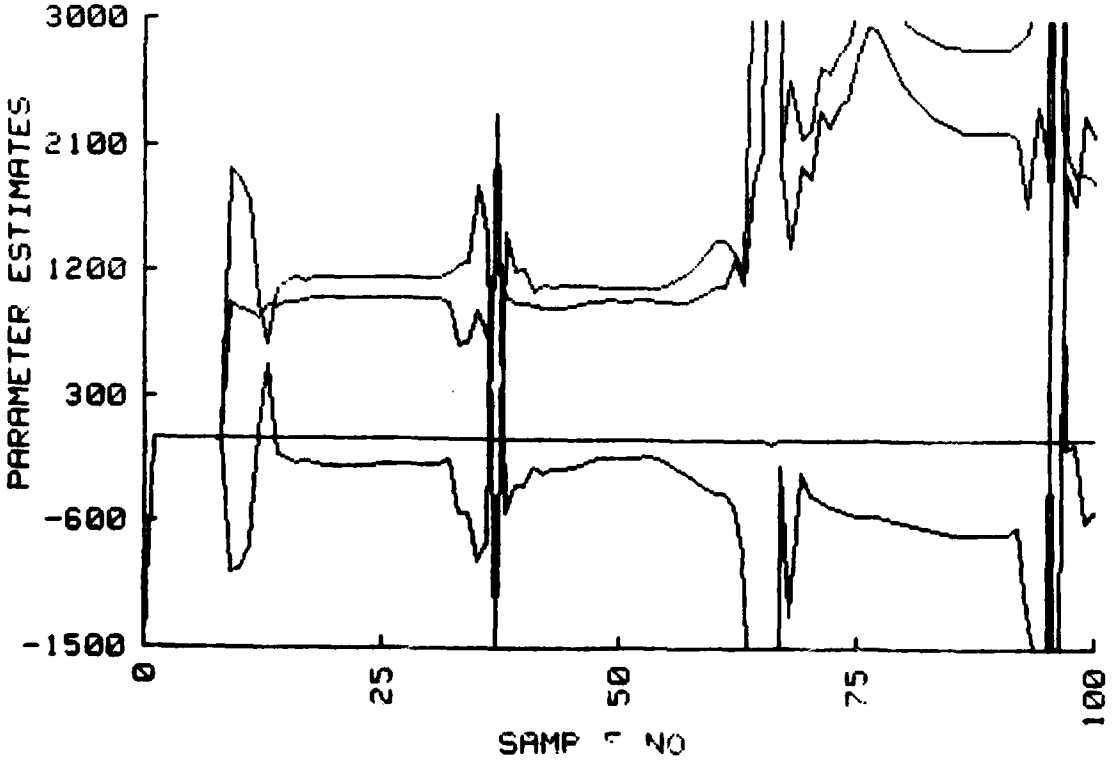


Figure 6. Response of nonlinear a), b) and linear c), d) when m=2, ℓ=2 initially but m changes to 4.

c)

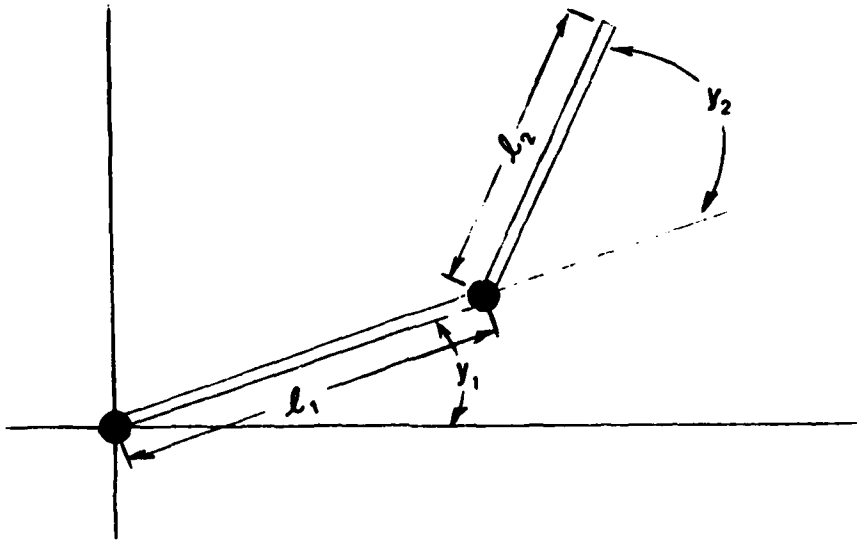

1.5
1.2
.9
.6
.3
0
OUTPUT ANGLE (RAD.)
0
25
50
75
100
SAMPLE NO.

d)


3000
2100
1200
300
-600
-1500
PARAMETER ESTIMATES
0
25
50
75
100
SAMP

VI. EXTENSIONS AND CONCLUSIONS

In this section, as an example of how the procedure discussed in the previous section extends to more complex cases, we consider the 2-link configuration shown in Figure 7.



This system is characterized by the simultaneous nonlinear differential equations:

$$\begin{bmatrix} J_1 + J_2(1+\alpha^2) + 2J_2\alpha\cos y_2 & J_2(1+\alpha\cos y_2) \\ J_2(1+\alpha\cos y_2) & J_2 \end{bmatrix} \begin{bmatrix} \ddot{y}_1 \\ \ddot{y}_2 \end{bmatrix} +$$

$$\begin{bmatrix} -J_2\alpha\sin y_2(2\dot{y}_1+\dot{y}_2)\dot{y}_2 \\ J_2\alpha\sin\dot{y}_2\dot{y}_1^2 \end{bmatrix} + \begin{bmatrix} F_1\dot{y}_1 \\ F_2\dot{y}_2 \end{bmatrix} +$$

$$\begin{bmatrix} (m_1+m_2)g\ell_1\cos y_1 + m_2g\ell_2\cos(y_1+y_2) \\ mg\ell_2\cos y_2 \end{bmatrix} = \begin{bmatrix} u_1 \\ u_2 \end{bmatrix}$$

In these equations,

m_i = mass of link i

ℓ_i = length of link i

J_i = moment of inertial of link i

$\alpha = \ell_1/\ell_2$

F_i = friction coefficient of link i

Discretizing by defining

$$\ddot{y}_i(kT) = (y_{ik+1}-2y_{ik}+y_{ik-1})/T^2 \triangleq x_{ik}/T^2$$

$$\dot{y}_i(kT) = (y_{ik}-y_{ik-1})/T \triangleq z_{ik}/T^2$$

yields equations in the form

$$\phi_{1k}^T\theta_1 = u_{1k}$$

$$\phi_{2k}^T\theta_2 = u_{2k}$$

where

$$\phi_{1k}^T = [x_{1k}, x_{1k}\cos y_{2k}, x_{2k}\cos y_{2k}, z_{2k}z_{2k}\cos_{2k},$$
$$z_{2k}^2 \sin y_{2k}, z_{1k}, \cos y_{1k}, \cos(y_{ik}+y_{2k})]$$

$$\phi_{2k}^T = [x_{1k}, x_{1k}\cos y_{2k}, x_{2k}, z_{1k}\sin y_{2k}, z_{2k}, \cos y_{2k}]$$

and θ_1 (9x1) and θ_2 (6x1) are unknown parameter vectors. Note that is the linkage moves in the horizontal plane, and if friction is neglected, θ_1 will contain only 6 parameters and θ_2 only 4 parameters.

For adaptive control, one would determine estimates θ_{1k} and θ_{2k} for θ_1 and θ_2 using two sequential least squares algorithms to minimize the errors

$$e_{1k} = u_{1k} - \phi_{1k}^T\theta_{1k}$$

$$e_{2k} = u_{2k} - \phi_{2k}^T\theta_{1k}$$

Similar to before, the control signals u_{1k} and u_{2k} can then be generated as

$$u_{1k} = \phi^{*T}_{1k}\theta_{1k}$$

$$u_{2k} = \phi^{*T}_{2k}\theta_{2k}$$

where ϕ^*_{1k} and ϕ^*_{2k} are defined analogously to ϕ_{1k} and ϕ_{2k} but with x_{1k} and x_{2k} replaced by

$$x^*_{1k} = (y^*_{1k+1} - 2y_{1k} + y_{1k-1})$$

$$x^*_{2k} = (y^*_{2k+1} - 2y_{2k} + y_{2k-1})$$

Note that the key difference between this formulation and that used in the single-link case involves formation of the regression vectors. To reduce the number of terms in the regression vectors ϕ_{1k} and ϕ_{2k} and hence the dimension of the parameter vectors θ_1 and θ_2, we have fixed the derivative approximations. For the single link case, these derivative approximations were implicitly estimated.

In conclusion, in this report we have shown that a combination of simple nonlinear and adaptive control strategies has the potential of improving the performance of mechanical linkage control systems for robotic manipulators. We are presently studying the extension of this idea to higher-degree-of-freedom cases. In addition, we plan to look at this approach for rate and acceleration as well as position control.

REFERENCES

[1] J. Y. S. Luh, M. W. Walker, and R. P. C. Paul, "Resolved Acceleration Control of Mechanical Manipulators," IEEE Transactions on AC, June 1980.

[2] J. Y. S. Luh, M. W. Walker, and R. P. C. Paul, "Online Computational Scheme for Mechanical Manipulators," Journal of Dynamic System Meas. and Control, June 1980.

[3] M. E. Kahn and B. Roth, "Near Minimum Time Control of Open Loop Articulated Kinematic Chains," Journal of Dynamic System Meas. and Control, September 1971, pp. 164-172.

[4] M. A. Townsend and T. C. Tsai, "On Optimal Control Laws for a Class of Constrained Dynamical Systems," Journal of Dynamic System Meas. and Control, June 1977, pp. 98-102.

[5] S. Dubowsky and D. T. DesForges, "The Application of Model Reference Adaptive Control to Robotic Manipulators," Journal of Dynamic System Meas. and Control, September 1979, pp. 193-200.

[6] A. J. Koivo and T. H. Guo, "Control of Robotic Manipulator with Adaptive Control," Proceedings of 1981 CDC, San Diego.

[7] G. C. Goodwin and K. S. Sin, Adaptive Filtering Prediction and Control, to appear from Prentice Hall in 1982.

[8] H. Elliott, "Hybrid Adaptive Control of Continuous Time Systems," IEEE Transactions on AC, April 1982.

[9] G. C. Goodwin, H. Elliott, and E. K. Teoh, "Deterministic Convergence of a Self-Tuning Regulator with Covariance Resetting," Colorado State University Tech. Report No. MY82-DELENG-1, May 1982 (submitted to IEEE Proceedings).

THE FOLLOWING PAGES ARE INTENTIONALLY DELETED

297 - 332

Copy available to DTIC does not permit fully legible reproduction

AD P001078

MULTI-RESOLUTION CLUTTER REJECTION

Dr. Allen Gorin
Image Processing Lab
Lockheed Electronics Company
Plainfield, New Jersey

INTRODUCTION

This paper presents preliminary results on a new clutter rejection algorithm for computer vision systems. It yields a real-time procedure for segmenting objects on the basis of size in a cluttered scene.

In computer vision applications it is necessary to break a scene into identifiable objects. For example, in Figure 1, there are several objects, all easily identifiable by a human observer. To a computer, however, the image is represented as a matrix of grey-level intensity measurements. Each dot in the matrix is a picture element (pixel). The goal of scene anaysis algorithms is to identify the objects in the image from the matrix of numbers. The first step in scene analysis is segmentation, which identifies the "blobs" in the image. The second step is to identify each blob. We concentrate here on the segmentation step.

Many segmentation algorithms, see [1] and [2], perform a thresholding operation in which all pixels of a given intensity range are highlighted. These highlighted pixels form a binary image, as shown in overlay in Figure 2. These must then be clustered into blobs, and the characteristics of each blob examined to determine if it is an object of interest. In Figure 2, the only object of interest highlighted at that threshold is the tank, the rest is clutter. To analyze and reject all the small clutter segments in that image using clustering techniques [1], is very time consuming.

This paper presents a novel method of rejecting clutter segments on the basis of size, without requiring the time-consuming clustering step described above.

DESCRIPTION OF SMALL REGION REJECTION

We now describe an algorithm which rejects small blobs in an image. Figure 1 shows a cluttered image. Figure 2 shows, highlighted in white, the results of thresholding that image to retain only dark objects. The objects highlighted are the tank plus pieces of the other objects which are characterized as clutter.

The original image is 512x512 pixel resolution. Figure 3 shows

Copy available to DTIC does not permit fully legible reproduction /

the result of creating a low resolution image of the thresholded data, using size 16x16 superpixels. The superpixels covering the threshold data is seen as a set of squares overlaid on the image. A filter which removes isolated points in the superpixel representation is applied. This removes all clutter silhouettes which have dimensions of 1 or 2 superpixels. An expand filter is then applied to the remaining superpixels, yielding the low-resolution mask overlaying the tank in Figure 4. This mask is then combined with the original thresholded silhouette to reject the small clutter, as shown in Figure 5. Figure 6 shows the calculation of the centroid of the detected object.

To discuss the transfer properties of the above algorithm, we first name it REJECT(N), where in the above case N=16. We perform the analysis for the x-dimension of an object, but the same results apply in the y-dimension. It is assumed that objects are well separated, so that there are no proximity effects.

If the x-dimension of an object is <N, then it can exist in at most 1 or 2 superpixels, and will be rejected by REJECT(N). If the x-dimension is >N, it will exist in 3 or more superpixels and thus be retained. For the x-dimension between N and 2N, assuming that the pdf of actual position is uniformly distributed, there will be a uniform transition in probability of rejection as size increases. This is shown in Figure 7. Two such "filters" can be subtracted to yield a probability transfer function of REJECT(n)-REJECT(n), as shown in Figure 8.

REAL-TIME CONSIDERATIONS

The above algorithm utilizes 3 major operations: resolution lowering, spatial filtering, and the Boolean 'AND'. Resolution lowering can be accomplished by a smooth and subsample operation, which is implementable at high speed using analog techniques. Spatial filtering for large images is often slow, but this filtering is done here on a low-resolution image with little data. The Boolean 'AND' is performed on only a small image segment.

This operation for small blob rejection can be considered to clustering techniques, such as in [1], which require much logic and iteration.

REFERENCES

1. W.K. Pratt, Digital Image Processing, Wiley-Interscience, (1978).

2. D.L. Milgram, Region Extraction Using Convergent Evidence, Computer Graphics and Image Processing, (1979).



Figure 1
Cluttered Scene



Figure 2
Thresholded Scene

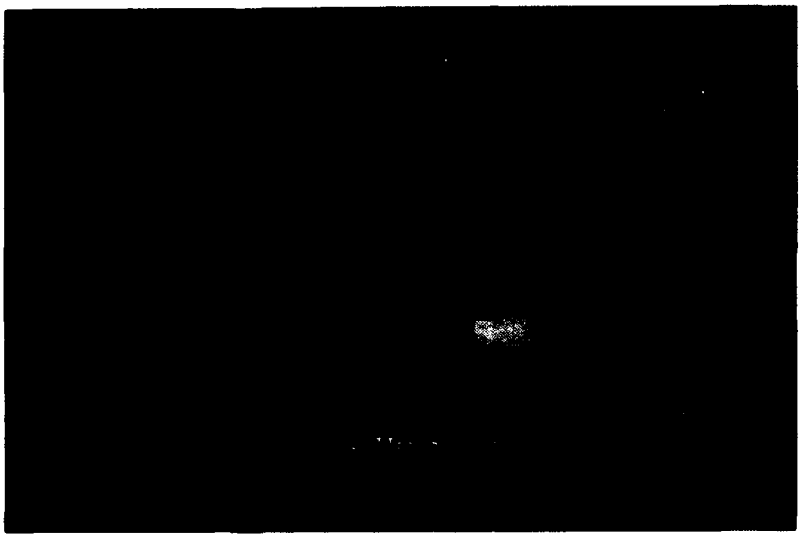


Figure 3
Superpixel Overlay



Figure 4
Superpixel Mask



Figure 5
Clutter Rejection



Figure 6
Centroid Calculation

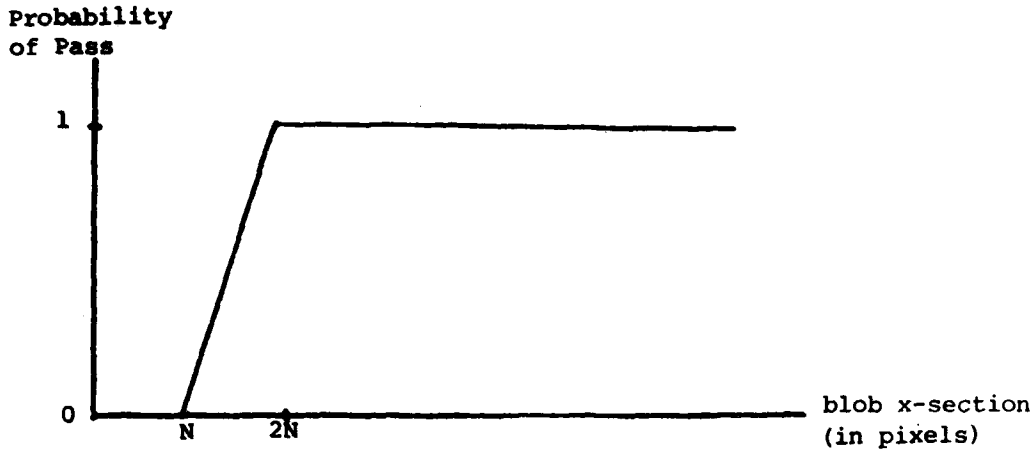


Figure 7
Transfer Function for REJECT(N)

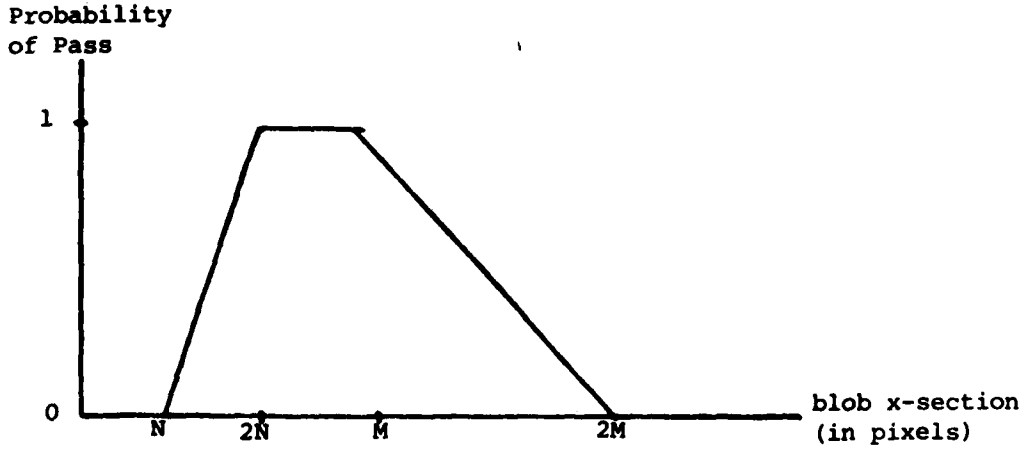


Figure 8
Bandpass Transfer Function

SESSION IV: CONTROL THEORY & APPLICATIONS

27 OCT 1982

(AFTERNOON)

ROOM #2

FOURTH MEETING OF THE COORDINATING

GROUP ON MODERN CONTROL THEORY

HOSTED BY: OAKLAND UNIVERSITY
ROCHESTER, MICHIGAN

Next page is blank.

AD P001079

AN OPTIMAL INTEGRAL SUBMARINE DEPTH CONTROLLER

M. J. Dundics
Director of Program Development
Tracor Incorporated
19 Thames St., Groton, Connecticut

INTRODUCTION

Since the initial inception of the Gaussian Quadratic Regulator using the state variable formulation of dynamic systems, numerous application have shown the viability of its utilization in concert with digital hardware. Optimal trajectory searches of differing types have also been pursued with varying results. All formulations rely on the minimization of some non-unique objective function. Some approach the subject, taking into account the constraints as penalty functions, either as a sequential unconstrained minimization or as a direct minimization.

The design algorithm presented herein is a mathematical programming approach using a nested minimization of a constrained function. The internal optimization is a closed form solution of the optimal output controller problem. As can be readily shown, there is a unique optimal set of system feedback and feedforward integral error gains for every relative set of weighting matrix elements. The system and control dynamics are formulated into the familiar adjoint form

$$\begin{bmatrix} \dot{\bar{x}} \\ \hline \dot{\bar{p}} \end{bmatrix} = W \begin{bmatrix} \bar{x} \\ \hline \bar{p} \end{bmatrix}$$

where

$$W = \left[\begin{array}{c|c} A^* & -B^* R^{-1} B^{*T} \\ \hline -C^{*T} Q C^* & -A^{*T} \end{array}\right]$$

Now, $\bar{P}$, being related to the adjoint variable by $\bar{p}(t) = \bar{P}\bar{x}_{op}(t)$, satisfies the steady-state Ricatti equation

$$0 = C^{*T} Q C^* - \bar{P} B^* R^{-1} B^{*T} \bar{P} + \bar{P} A^* + A^{*T} \bar{P}$$

The solution of the previous formulation is given by

$$\bar{P} = -V_{12}^{-1} V_{11}$$

where

$$V = \left[\begin{array}{c|c} V_{11} & V_{12} \\ \hline V_{21} & V_{22} \end{array}\right]$$

is the inverse of the modal matrix of W. The optimal feedback gain matrix for the system is then readily given as

$$\bar{G} = -R^{-1}B^{*}\bar{P}$$

and the optimal system input vector as

$$\underset{\sim}{u} = -\bar{G}\,\bar{\underset{\sim}{x}}$$

This control law is based on the specific assumptions that:

1. The system is defined (at least in piecewise sense) as

$$\dot{\underset{\sim}{x}} = A\underset{\sim}{x} + B\underset{\sim}{u}$$

$$\underset{\sim}{y} = C\underset{\sim}{x} + D\underset{\sim}{u}$$

2. The system performance index is of the form

$$J = \int_{0}^{\infty} [\,(\underset{\sim}{y}^{T}Q\underset{\sim}{y}) + (\underset{\sim}{u}^{T}R\underset{\sim}{u})\,]\;dt$$

3. The input available is unconstrained.

4. The matrix Q is positive semi-definite and R is positive definite.

Because the theory applies to regulation with unlimited input, the resultant control laws are all lacking in a guarantee of optimal response with avoidance of control saturation or system parameter overshoots during large excursions. The major difficulty facing the design engineer is the iterative selection of the relative weighting matrix elements, especially for higher order systems, to satisfy a required response within physical limitations. Therefore, the external optimization algorithm utilizes the relative values of the weighting matrix elements as the design variables.

The technique utilized in the external optimization loop is referred to as a method of feasible direction and is, in fact, a generalization of the method first developed by Zoutendijk.

MATHEMATICAL FORMULATIONS

FEASIBLE DIRECTION ALGORITHM

The general design problem may be stated as a constrained minimization problem of the form

$$\text{MINIMIZE } F(Z) \tag{1}$$

subject to

$$G_j(Z) = 0 \qquad j = 1, NIC \tag{2}$$

Where Z is a vector of design variables and NIC is the number of inequality constraints. In the case where the elements of the weighting matrices are the variables,

$$Z = \begin{bmatrix} Q_{ii} \\ \hline R_{kk} \end{bmatrix} \tag{3}$$

Q_{ii} are the diagonal elements of the system output weighting matrix elements and the R_{kk} are the diagonal elements of the system input rate weighting matrix. The optimization operates on the relative values of the above matrix elements, thus the elements are first normalized and the search is over a design space composed of (nn + m - 1) elements where

nn - output vector size ($nn \geq n$)

m - input vector size

(Note: It is not required that the matrices be diagonal, however, cross coupling weighting values were not considered).

F(Z) is referred to as the objective function and $G_j(Z)$ are inequality constraint functions. If equations (2) are satisfied, the design is said to be 'feasible.' For the control system design algorithm, the inequality constraints (equations 2) include allowable limits on parameter peak values, system roots, component maximum and minimum input or input rate values, etc. Required settling time can also be formulated as an inequality constraint as will be shown later.

The design process proceeds iteratively by defining the design vector, Z, at the q + 1st iteration as

$$Z^{q+1} = Z^q + \alpha^* S^q \tag{4}$$

where S^q is a vector move direction in the design space and α^* is a scalar mulitplier. At the qth iteration it is then necessary to determine the direction of travel, S^q, such that for some small move distance, αS^q, the objective function is decreased (usable direction) and no constraints are violated (feasible direction). Once S^q is known, equation (4) becomes a one dimensional search problem. The scalar, α^*, must then be found such that the objective is minimized, some new constraint is encountered or some currently active constraint ($G_j(Z^q) = 0$) is encountered again (owing to curvature of $G_j(Z^q)$).

The design problem at the q + 1st iteration now becomes one of finding a usable-feasible direction, S^q, and the move parameter, α^*. The requirement that S^q be usable is stated mathematically as

$$VF(Z^q) \cdot S^q \leq 0 \tag{5}$$

where $VF(Z^q)$ is the gradient of the objective function with respect to the independent design variables. Equation (5) defines a half-space bounded by the hyperplane $VF(Z^q) \cdot S^q = 0$. The requirement that S^q be feasible is given as

$$\nabla G_j(Z^q) \cdot S^q \leq 0 \qquad j = 1, NAC \tag{6}$$

(NAC = number of active constraints)

$\nabla G_j(Z^q)$ is the gradient of the jth active constraint ($G_j(Z^q) = 0$. Equation (6) defines a half-space bounded by the hyperplane $\nabla G_j(Z^q) S^q = 0$. A usable-feasible direction is one which satisfies both equations (5 and 6). Because of numerical imprecision as well as various approximations in the design process, the constraint functions ($G_j(Z^q)$) will seldom be precisely satisfied ($G_j(Z^q) = 0$. Therefore, constraint $G_j(Z^q)$ is defined as active if its value is within the range

$$-\delta \leq G_j(Z^q) \leq \delta min \qquad j = 1, NIC \tag{7}$$

and is violated if

$$G_j(Z^q) > \delta min \qquad J = 1, NIC \tag{8}$$

So that the same constraint tolerance, δ, may apply uniformly to all design constraints, it is important that the constraint functions be normalized. For example, if the peak value of one of the outputs is required not to exceed a specified value, $\bar{\sigma}$, the corresponding constraint function would be

$$G_j(Z^q) = \frac{\sigma}{\bar{\sigma}} - 1 \leq 0 \tag{9}$$

where σ is the calculated peak value for the output at the given iteration. In this manner, the constraint functions will have values between -1 and 0 for all strictly feasible designs ($G_j(Z^q) \leq 0$).

Zoutendijk has shown that the direction, S^q (Eqs.5 and 6) may be found by solving the following problem:

$$\text{MAXIMIZE} \quad \beta \quad \text{SUBJECT TO} \tag{10}$$

$$\nabla F(Z^q) \cdot S^q + \beta \leq 0 \tag{11}$$

$$\nabla G_j(Z^q) \cdot S^q + \theta_j \beta \leq 0 \qquad j = 1, \text{NAC} \tag{12}$$

$$S \text{ BOUNDED} \tag{13}$$

The scalars, θ_j, in Equations (12) are referred to as 'push-off' factors which effectively 'push' the design away from the active constraints. It is necessary to impose bounds on the direction vector, S^q (Eq. 13) so that the solution of Equations (10,11, and 12) will be finite. The choice of θ_j and the method of imposing bounds on S^q have significant affect on the efficiency of the method.

INTERNAL OPTIMIZATION

The internal optimal solution is obtained by the commonly known eigenvector method applied to a properly defined system, in the form

$$\dot{\underset{\sim}{x}} = A\underset{\sim}{x} + B\underset{\sim}{u} \tag{14}$$

$$\underset{\sim}{y} = C\underset{\sim}{x} + D\underset{\sim}{u} \tag{15}$$

$$\underset{\sim}{y}_c = E\underset{\sim}{y}$$

where

$\underset{\sim}{x}$ - vector of state variables

$\underset{\sim}{u}$ - vector of manipulatable input variables

$\underset{\sim}{y}$ - vector of system output variables used in the quadratic performance integral

$\underset{\sim}{y}$ - vector of controlled output variables

To achieve tight output tracking, an output feedback configuration is first constructed using the method derived in Michael (1973).

With the addition of m integrators, the augmented system dynamics become

$$\dot{\bar{x}} = \left[\begin{array}{c|c} A & B \\ \hline 0 & 0 \end{array}\right] x + \left[\begin{array}{c} 0 \\ \hline I_m \end{array}\right] \bar{u} \qquad (16)$$

where

$$\bar{x} = \left[\begin{array}{c} x \\ \hline u \end{array}\right] \qquad (17)$$

$$\bar{u} = \dot{u}$$

Likewise

$$\bar{y} = [C \mid D]\, \bar{x} \qquad (18)$$

The control scheme for the optimal output integral controller is represented in Figure 1. The quadratic performance index

$$J_1 = \int y^T Q y + \dot{u}^T R \dot{u}$$

was used as the initial objective function. Final gain element tuning was done using

$$J_2 = \int t^n \, [y^T Q y + \dot{u}^T R \dot{u}]$$

as the performance index.

If it is assumed that $t_o = 0$ and that the contribution of the system dynamics beyond $t = t_f$ is small, then the limits of integration can be changed to

$$J = \int_{t_o}^{t_f} (y^T Q y + \dot{u}^T R \dot{u})\, dt$$

The solution to the optimal state feedback gain matrix is given by

$$\dot{u}_{op} = -\bar{G}\, \bar{x}, \text{ or}$$

$$u_{op} = \left[\begin{array}{c|c} -G_1 & G_2 \end{array}\right] \left[\begin{array}{c} x \\ \hline u \end{array}\right]$$

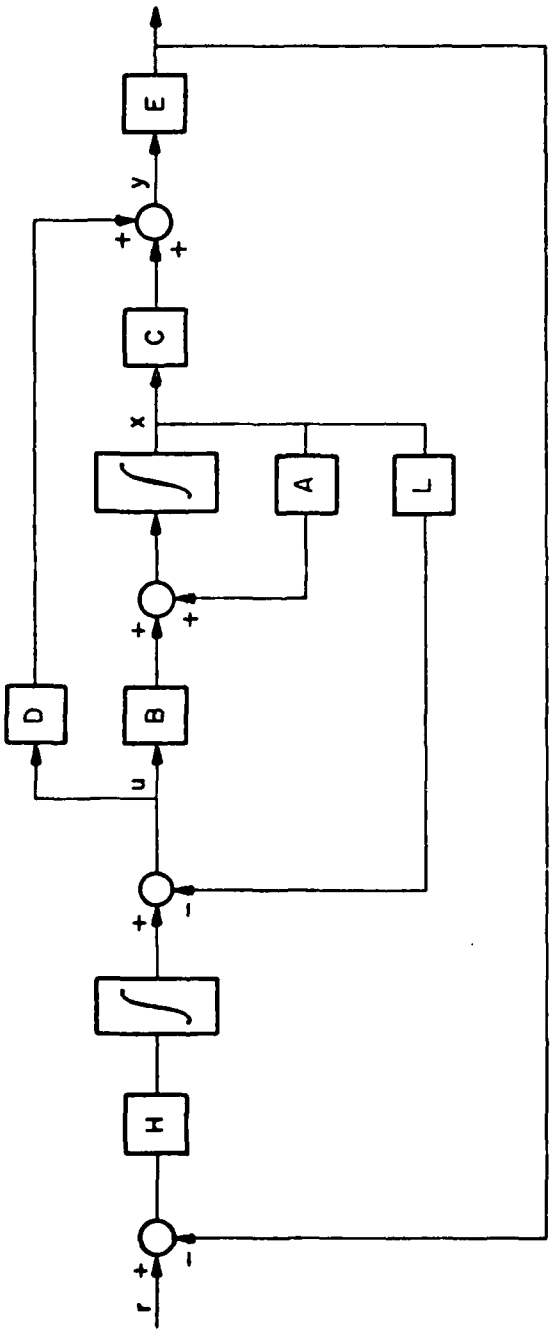


Fig 1. Optimal Integral Output Controller

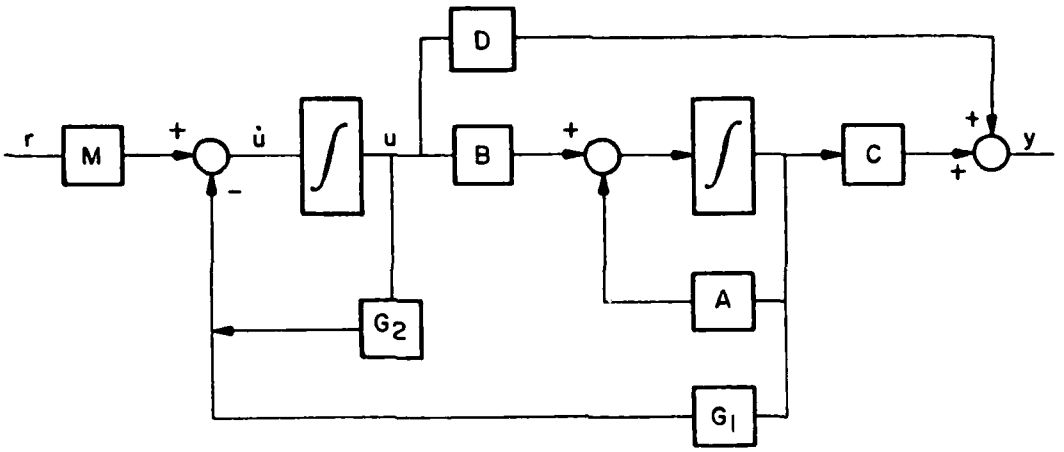


Fig 2. Optimal Controller-Augmented System

The system dynamics are defined as

$$\dot{\underset{\sim}{x}} = \left[\begin{array}{c|c} A & B \\ \hline 0 & 0 \end{array}\right] \underset{\sim}{x} - \left[\begin{array}{c} 0 \\ \hline I_m \end{array}\right] \left[\begin{array}{c|c} G_1 & G_2 \end{array}\right] \underset{\sim}{x}$$

$$\dot{\underset{\sim}{x}} = \left\{\left[\begin{array}{c|c} A & B \\ \hline 0 & 0 \end{array}\right] - \left[\begin{array}{c} 0 \\ \hline I_m \end{array}\right] \left[\begin{array}{c|c} G_1 & G_2 \end{array}\right]\right\} \underset{\sim}{x}$$

This can be rewritten as

$$\dot{\underset{\sim}{x}} = (A^* - B^*\bar{G})\ \underset{\sim}{x} \tag{19}$$

where

$$A^* = \left[\begin{array}{c|c} A & B \\ \hline 0 & 0 \end{array}\right]$$

$$B^* = \left[\begin{array}{c} 0 \\ \hline I \end{array}\right]$$

The solution of Equation (19) is given as

$$\underset{\sim}{x} = \exp\left\{Ft\right\}\ \underset{\sim}{x}(0)$$

where

$$F = (A^* - B^*\bar{G}).$$

Likewise

$$\underset{\sim}{y} = C^*\ \exp\left\{Ft\right\}\ \underset{\sim}{x}(0),\ C^* - [C\ D]$$

$$\underset{\sim}{u} = [G_1\ \ G_2]\ \exp\left\{Ft\right\}\ \underset{\sim}{x}(0)$$

To establish the equivalence between the systems in Figures 1 and 2, the systems are expanded in Laplace form. From Figure 1

$$\underset{\sim}{U}(S) = \frac{1}{S}H\ (\underset{\sim}{R}(S) - \underset{\sim}{Y}_c(S)) - L\underset{\sim}{X}(S)$$

$$S\underset{\sim}{U}(S) = H\ (\underset{\sim}{R}(S) - \underset{\sim}{Y}_c(S)) - LS\underset{\sim}{X}(S) \tag{20}$$

since

$$\underset{\sim}{SX}(S) = A\underset{\sim}{X}(S) + B\underset{\sim}{U}(S)$$

$$\underset{\sim}{Y}_c(S) = E\underset{\sim}{Y}(S) = E\,(C\underset{\sim}{X}(S) + D\underset{\sim}{U}(S))$$

and

$$\underset{\sim}{Y}_c(S) = EC\ \underset{\sim}{X}(s) + ED\ \underset{\sim}{U}(S)$$

Substitution into Equation (20) yields

$$S\underset{\sim}{U}(S) = H(\underset{\sim}{R}(S) - EC\underset{\sim}{X}(S) - ED\underset{\sim}{U}(S))$$

$$- LA\underset{\sim}{X}(S) - LB\underset{\sim}{U}(S)$$

Collecting coefficients

$$S\underset{\sim}{U}(S) = (-HEC - LA)\underset{\sim}{X}(S) + (-HED - LB)\underset{\sim}{U}(S)$$

$$+ H\underset{\sim}{R}(S)$$

Expanding the relations portrayed in Figure 1 in the same manner yields

$$S\underset{\sim}{U}(S) = M\underset{\sim}{R}(S) - G_1\underset{\sim}{X}(S) - G_2\ \underset{\sim}{U}(S)$$

where M is the matrix that generated optimal tracking. The time response of the two systems will be identical to any command R(s), if the coefficients of R(s), X(s) and U(s) are equivalent. Thus, it follows that

$$G_1 = HEC + LA$$

$$M = H$$

$$G_2 = HED + LB$$

When reconstructed in partitioned form

$$[G_1 \mid G_2] = [L \mid H] \begin{bmatrix} A & B \\ \hline EC & ED \end{bmatrix}$$

and matrices L and H are found as

$$[L \mid H] = [G_1 \mid G_2] \begin{bmatrix} A & B \\ \hline EC & ED \end{bmatrix}^{-1}$$

If matrix S is defined as

$$S = \left[\begin{array}{c|c} S_{11} & S_{12} \\ \hline S_{21} & S_{22} \end{array}\right] = \left[\begin{array}{c|c} A & B \\ \hline EC & ED \end{array}\right]^{-1}$$

then

$$[L \mid H] = [G_1 \mid G_2] \left[\begin{array}{c|c} S_{11} & S_{12} \\ \hline S_{21} & S_{22} \end{array}\right]$$

and finally

$$L = G_1S_{11} + G_2S_{21}$$

$$H = G_1S_{12} + G_2S_{22}$$

Having calculated the feedback and feedforward gains L & H, the closed loop characteristics can be numerically simulated by an expansion series of exp [Ft] and matched to describe design constraints and specification. The results of the comparisons as well as the value of the objective function will drive the optimization routine to select the next proposed set of design variables.

As can be seen from the foregoing equations, the objective function and the system dynamic values are dependent on initial conditions. The intent of the algorithm is to generate an optimal feedback gain matrix for a set of initial condition vectors and then through a scheduling logic that maps gain element against system error, generate gains that prevent input saturation for large system errors and yet ensure tight regulating gains about set point.

DESIGN ALGORITHM

The design algorithm in general terms may now be written for solving the general constrained minimization problem as applied to control system design.

1. Choose an initial design vector Z, where $Z = [\frac{Q_{11}}{R_{kk}}]$. the system weighting matrix elements. It is desirable, but not essential, that this initial design be feasible. Choose an initial constrain tolerance (say $\delta = 0.15$).

2. The value of the objective function, $(F(Z^q))$, which in this case is the value of J, is evaluated. System dynamic variables which are to be constrained are evaluated over a prescribed transient (viz. maximum values of states, inputs, input rates, outputs, settling times, etc).

3. The analytic gradients of the objective function and all active (and violated) constrained functions are evaluated and normalized.

4. If no constraints are active or violated, $S^q = \nabla F(Z^q)$, (direction of steepest descent) and logic goes on to step 9.

5. The push-off factors, θ_j, are determined.

6. The objective of the direction finding problem is found.

7. The constraints on the direction finding problem are defined by Equations (11 and 12) if no design constraints are violated, and by Equation (12) alone if one or more design constraints are violated.

8. A usable-feasible or modified-usable-feasible direction is obtained. If no constraints are violated and $\beta = 0$ logic goes to step 10.

9. The one-dimensional search problem is solved by Equation (4).

10. Convergence criterion is checked; if not satisfied or if current design is infeasible a return to step 3 is initiated. Otherwise termination of the problem occurs.

The choice of convergence criterion in step 10 is dependent on the nature of the design problem and the required precision to which the optimum must be found. The reason for choosing a rather wide constraint tolerance, δ is taken too small, these constraints sometimes cease to be active (due to the push-off factor, θ_j), only to become active again on the next iteration. The choice of an initially wide constraint tolerance coupled with the quadratic form of the push-off factor, θ_j, reduces this 'zig-zag' problem.

Since the closed form eignvector solution applies to the quadratic performance index J_1, performance tuning by individual gain adjustments was accomplished by the utilization of the contrained minimization algorithm with the gain matrix elements as the design variables, J_2 as the cost function, and the previous constraint vector. This index generated a more time optimal response without constraint violation. This same approach was used to generate a suboptional control gain matrix set by the elimination of the rate feedbacks $\dot{z}$ and ϕ, and the readjustment of the remaining elements of H and L to satisfy all of the constraints. Both response curves are represented in Figure 3.

OPTIMAL SUBMARINE DEPTH CHANGER/REGULATOR SYSTEM

The algorithms described in the previous sections were used to design an Optimal Integral Output Control logic to affect a 150 foot depth change of a submarine at 12 knots without plane or plane rate saturation. The actual system hardware constraints and the required system response specification comprise the contraint vector ($G(Z^1)$). The ship dynamics were linearized about 12 kts forward speed. Roll dynamics were not considered since the planes are symmetric about the longitudinal axis.

The system dynamic equations for depth and pitch can be described by

$$\begin{vmatrix} \dot{Z} \\ \ddot{Z} \\ \dot{\phi} \\ \ddot{\phi} \end{vmatrix} = A \begin{vmatrix} Z \\ \dot{Z} \\ \phi \\ \dot{\phi} \end{vmatrix} + B \begin{vmatrix} \delta 1 \\ \\ \delta 2 \end{vmatrix}$$

Z = vertical displacement

$\dot{Z}$ = vertical velocity

ϕ = pitch

$\dot{\phi}$ = pitch rate

δ_1 = stern plane position in radians

δ_2 = fairwater position in radians

The controlled outputs in a depth maneuver were defined as

$y_1 = Z$

$y_2 = \phi$

To minimize the activity of the planes during the maneuver, two additional outputs were defined to be included in the Performance Index

$y_3 = \delta 1$

$y_4 = \delta 2$

The system constraints and required performance specifications are given as:

Plane Position Limits:

Stern Plane (δ_1) ~ ±25° (.4363 radians)

Fairwater Plane (δ_2) ~ ±20° (.3491 radians)

Plane Rate Limits:

Stern Plane (δ_1) ~ 7°/sec (.1222 radians/sec)

Fairwater Plane (δ_2) ~ 7°/sec (.1222 radians/sec)

Response Requirements

For 150 foot depth change:

Settling Time (Depth within 5% of final value, i.e., 7.5 ft)	- 70 secs.
Depth Error (at $t = \infty$)	- 1 foot
Pitch (before and after excursion)	- 0%
Depth Overshoot	- 2 feet
Max Pitch (during excursion)	- 10° (0.174 rad)

To insure system stability during design, one of the elements of the constraint vector was chosen to be the largest real root. Requiring that this real root be less than zero by a specified amount guarantees that the search will always be in the stable region. The design, as such, contains 12 constraints and 5 design variables.

The initial Q and R matrices were obtained from an unconstrained optimization trial run. Arbitrary values can be used; however, more time for convergence would be required.

Q(1,1) was left alone and only the other 4 elements of Q and the two diagonal elements of R were designated as the design variables. In essence all the elements were normalized to Q(1,1).

SIMULATION INPUT INFORMATION

The simulation for each proposed design was 100 seconds in duration and accomplished in 0.1 second increments. Therefore, 1000 increments were required. From initial trial runs, it was found that 10 terms would converge exp [Ft] to an acceptable accuracy.

The initial condition vector used in the constraint evaluation is

$$\begin{vmatrix} Z(0) \\ \dot{Z}(0) \\ \phi(0) \\ \dot{\phi}(0) \\ \delta 1(0) \\ \delta_2(0) \end{vmatrix} = \begin{vmatrix} -150.0 \\ 0.0 \\ 0.0 \\ 0.0 \\ 0.0 \\ 0.0 \end{vmatrix}$$

(for the augmented state vector)

DESIGN RESULTS

OPTIMAL DESIGN

Initial set of Q and R matrices generated a response which violated 4 of the 12 constraints. Within three iterations there were no constraint violations and feasible optimum was reached in 9 iterations. Run time required for the augmented sixth order system was just under four minutes CPU and six minutes wall clock.

SUBOPTIMAL DESIGN

Unavailability of rate feedback was established by zeroing the equivalent column of the state feedback matrix. Initial values of the remaining matrix elements were those developed through the optional run. The constrained minimization algorithm took 5 iterations to realign the available feedback matrix element to achieve minimum performance index value for J_2 without constraint violation. A composite graphical representation of the depth change with and without full state feedback is represented in Figure 3.

CONCLUSIONS

The constrained minimization program, CONMIN, developed by G. Vanderplaats (1973) utilized in conjunction with the linear quadratic approach to control synthesis can be a powerful tool in the hands of a design engineer who has tight physical constraints to work with. Model following and robustness factor constraints have been also tried in the design process with excellent results. Present efforts in the expansion of the program capabilities is centered around a user interactive design process and an on-line constrained optimization routine.

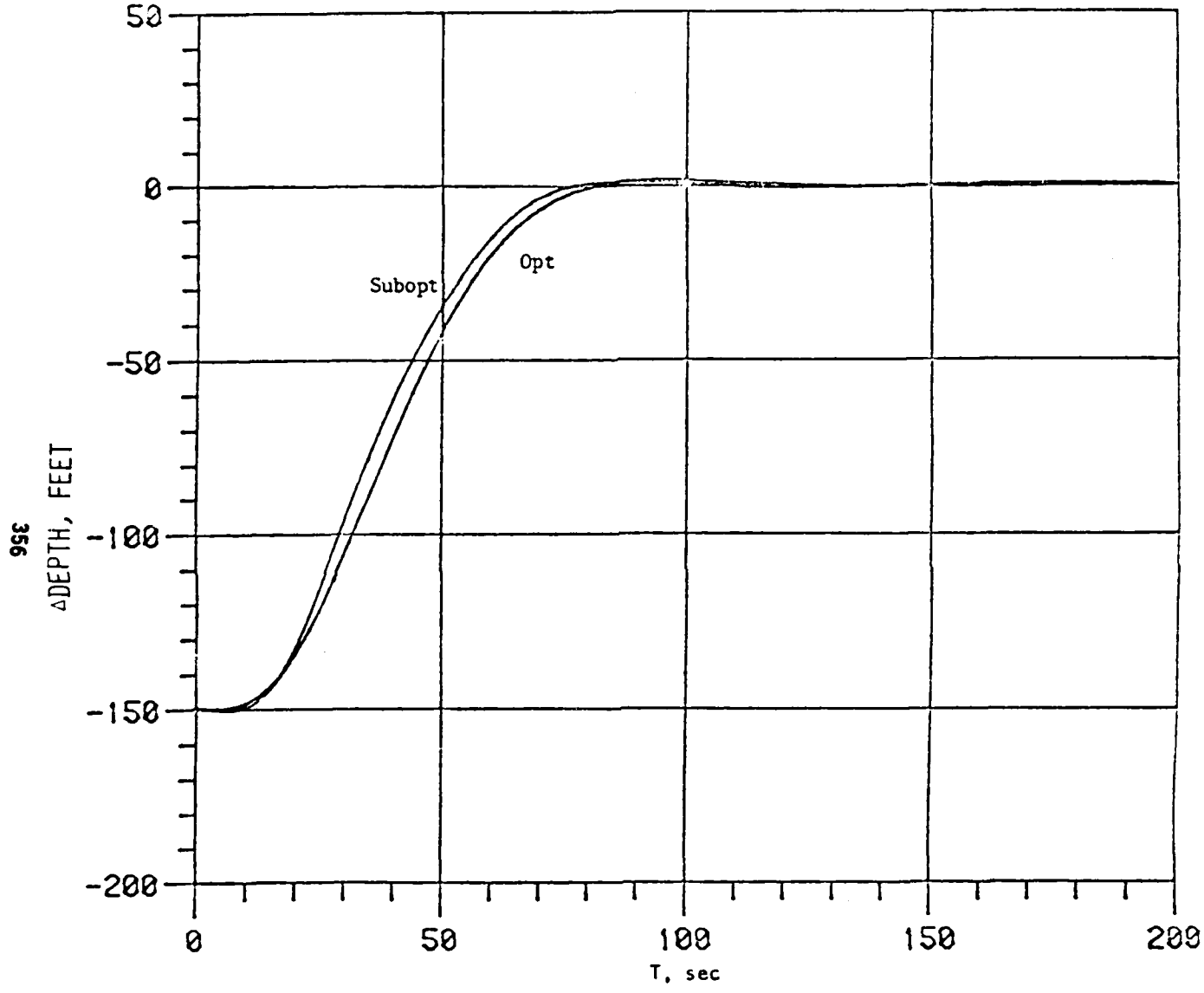


FIG. 3. 12 KNOT/150 FOOT DEPTH CHANGE, DEPTH RESPONSE

ACKNOWLEDGEMENT

The interaction of Dr. Garret Vanderplaats, Naval Post Graduate School, Monterey California in meshing optimal control design methods with his numerical optimization algorithms was invaluable.

REFERENCES

1. Michael, G.J. and Farrar, F.A., "An Analytic Method for the Synthesis of Nonlinear Multivariable Feedback Control" ONR, Dept of the Navy, AD-762-797, June 1973

2. G. Vanderplaats, CONMIN - A Fortran Program for Constrained Function Minimization User's Manual, NASA TMX-62.282, 1973

Next page is blank.

AD P001080

REGULATOR DESIGN FOR LINEAR SYSTEMS WHOSE COEFFICIENTS DEPEND ON PARAMETERS*

E. W. Kamen and P. P. Khargonekar
Center for Mathematical System Theory
Department of Electrical Engineering
University of Florida
Gainesville, Florida 32611

I. INTRODUCTION

In control system design, it is often the case that the structure of the system is known, but some of the coefficients of the system equations are functions of parameters that cannot be determined until the system is in operation. For example, the system coefficients may depend on the state of the system or on operating conditions such as temperature. In addition, the exogenous (external) signals which are applied to the system, such as disturbance or reference signals, may also depend on parameters. An example is a sinusoidal disturbance whose frequency varies while the system is in operation.

For systems whose coefficients depend on parameters, a major problem of interest is the design of controllers or regulators which satisfy a given set of performance specifications for all possible values of the parameters. In this paper we shall concentrate on the design of regulators to achieve tracking and/or disturbance rejection for all possible values of the parameters. The gains in the regulators will be functions of the parameters. To be able to implement the gains for real-time operation, they must be "nice" functions of the parameters, such as polynomial functions. We shall give conditions which insure that tracking and disturbance rejection can be accomplished using polynomial gains, and then indicate how the polynomial gains can be computed off-line.

II. SELF-TUNING REGULATORS FOR TRACKING AND DISTURBANCE REJECTION

We shall consider linear continuous-time systems whose coefficients are continuous functions of N parameters $\omega_1, \omega_2, \ldots, \omega_N$. We assume that parameter ω_i takes its values from a closed interval $[a_i, b_i]$. These intervals may be bounded or unbounded, but as will be seen later, the unbounded case is much more difficult to handle in terms of solving the problem posed in this paper. In the following development, we shall let Ω denote the set of all parameter values given by the Cartesian product

$$\Omega = [a_1, b_1] \times [a_2, b_2] \times \ldots \times [a_N, b_N].$$

An element $(\omega_1, \omega_2, \ldots, \omega_N)$ of Ω will be denoted by ω.

The system to be controlled is a m-input n-dimensional (n-state) p-output linear continuous-time system given by the state model

*This work was supported in part by US Army Research Contract DAAG29-81-K-0166.

$$\dot{x}(t) = \bar{F}(\omega)x(t) + \bar{G}(\omega)u(t) + \bar{D}(\omega)w(t). \tag{1a}$$

$$y(t) = H(\omega)x(t) + E(\omega)w(t), \ \omega \in \Omega. \tag{1b}$$

In (1a,b), $x(t)$ is an n-vector equal to the state at time t, $u(t)$ is a m-vector equal to the control at time t. $y(t)$ is a p-vector equal to the output at time t, and $w(t)$ is a q-vector which represents the state of an exogenous disturbance and/or exogenous reference. The entries of the coefficient matrices $\bar{F}(\omega)$, $\bar{G}(\omega)$, $\bar{D}(\omega)$, $H(\omega)$, $E(\omega)$ are assumed to be continuous functions of $\omega = (\omega_1, \omega_2, \ldots, \omega_N)$.

We shall also assume that the coefficients of the model for the state $w(t)$ of the exogenous signals are continuous functions of $\bar{N}$ parameters $\psi_1, \psi_2, \ldots, \psi_{\bar{N}}$, with $\psi_i \in [c_i, d_i]$. More precisely, letting Ψ denote the Cartesian product of the intervals $[c_i, d_i]$, we shall assume that the model for $w(t)$ is given by

$$\dot{w}(t) = \bar{A}(\psi)w(t), \ \psi \in \Psi, \tag{2}$$

where $\bar{A}(\psi)$ is a $q \times q$ matrix whose entries are continuous functions of $\psi = (\psi_1, \psi_2, \ldots, \psi_{\bar{N}})$.

Finally, we also suppose that we have a p-vector output reference signal $y_r(t)$ given by

$$y_r(t) = Cw(t), \tag{3}$$

where C is a $p \times q$ matrix over the reals. (The matrix C could depend on the parameters ω_i or ψ_i.) The matrix C may be zero so that $y_r(t) = 0$, in which case we would be considering disturbance rejection only (no tracking).

We want to consider digital control for the system (1a,b), so we shall first derive a sampled-data model. Letting T denote the sampling interval and discretizing (1a,b), (2), and (3), we get

$$x(kT + T) = F(\omega)x(kT) + G(\omega)u(kT) + D(\omega)w(kT) \tag{4a}$$

$$y(kT) = H(\omega)x(kT) + E(\omega)w(kT) \tag{4b}$$

$$w(kT + T) = A(\psi)w(kT) \tag{4c}$$

$$y_r(kT) = Cw(kT) \tag{4d}$$

where

$$F(\omega) = \exp\,[\bar{F}(\omega)T]$$

$$A(\psi) = \exp\,[\bar{A}(\psi)T]$$

$$G(\omega) = \int_0^T \exp\,[\bar{F}(\omega)t]\bar{G}(\omega)\,dt$$

$$D(\omega) = \int_0^T \exp\,[\bar{F}(\omega)t]\bar{D}(\omega)\,dt.$$

Let's now consider the closed-loop system shown in Figure 1 below.

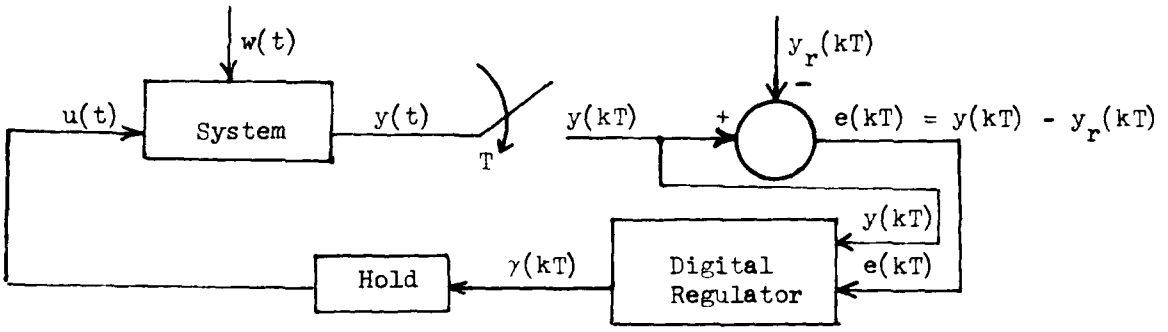


Figure 1. System with digital regulator

The regulator in the feedback loop is given by the state equations

$$\xi(kT + T) = F_c(\omega, \psi)\xi(kT) + G_c(\omega, \psi)e(kT) + B_c(\omega, \psi)y(kT) \qquad (5a)$$

$$\gamma(kT) = H_c(\omega, \gamma)\xi(kT), \qquad (5b)$$

where the regulator coefficient matrices $F_c(\omega, \psi)$, $G_c(\omega, \psi)$, $B_c(\omega, \psi)$ and $H_c(\omega, \psi)$ may depend on <u>both</u> sets of parameters.

The objective is to compute (off-line) closed-form expressions for the coefficient gain matrices of the regulator so that for each parameter value $\omega \in \Omega$, $\psi \in \Psi$,

(1) the closed-loop system is asymptotically stable (not including the state $w(t)$ of the exogenous signals);

(2) the error $e(t) = y(t) - y_r(t)$ converges to zero as $t \to \infty$ for any initial states $x(0)$, $w(0)$, and $^r\xi(0)$.

The above specification of performance in terms of point-by-point evaluations of the parameters is reasonable if the parameter variations are "slow" with respect to the time constants of the system. If this is not the case, a point-by-point specification of performance may not suffice. For instance, pointwise asymptotic stability (i.e., asymptotic stability for each value of the parameters) may not be sufficient to insure that the closed-loop system has desirable stability properties. Such complications will not be considered here.

To operate the closed-loop system given in Figure 1, it of course will be necessary to estimate (on-line) the parameters $\omega = (\omega_1, \omega_2, \ldots, \omega_N)$ and $\psi = (\psi_1, \psi_2, \ldots, \psi_N)$. Various parameter-estimation techniques exist for doing this, so we will not consider this aspect of the problem.

The regulator design problem posed above can be approached in several ways. We shall restrict our attention to a method based on an "internal model" of the exogenous signals which will be driven by the error signal $e(kT)$. Another

class of methods is based on an observer for the disturbance states. A concise survey of some of these design techniques for systems with constant coefficients can be found in the paper by KWATNY and KALNITSKY [1978].

Define the q-dimensional error-driven system

$$\eta(kT + T) = A(\psi)\eta(kT) + Be(kT), \tag{6}$$

where B is chosen so that the pair $(A(\psi), B)$ is reachable for all $\psi \in \Psi$. The system (6) is said to be an internal model for the exogenous signals.

Now consider the discretized augmented system shown in Figure 2 below.

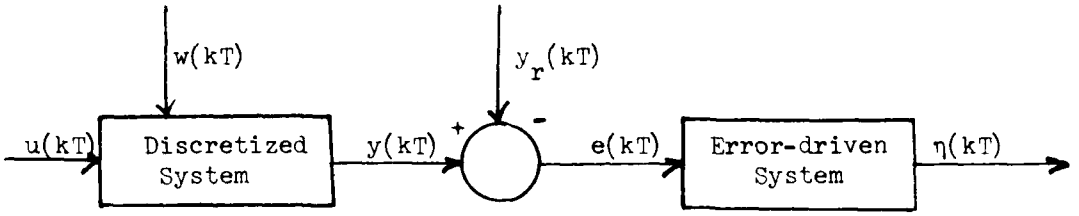


Figure 2. Discretized Augmented System.

The state equation for the augmented system shown in Figure 2 is given by

$$\begin{bmatrix} x(kT + T) \\ \eta(kT + T) \end{bmatrix} = \left[\begin{array}{c|c} F(\omega) & 0 \\ \hline BH(\omega) & A(\psi) \end{array}\right] \begin{bmatrix} x(kT) \\ \eta(kT) \end{bmatrix} + \begin{bmatrix} G(\omega) \\ \hline 0 \end{bmatrix} u(kT) + \begin{bmatrix} D(\omega) \\ \hline B(E(\omega) - C) \end{bmatrix} w(kT). \tag{7}$$

The augmented system (7) is said to be pointwise stabilizable if for each $\omega \in \Omega$, $\psi \in \Psi$, there exist feedback gains $K_1(\omega, \psi)$ and $K_2(\omega, \psi)$ over the reals, such that with the feedback

$$u(kT) = - K_1(\omega, \psi)x(kT) - K_2(\omega, \psi)\eta(kT) \tag{8}$$

the resulting closed-loop system is asymptotically stable; i.e., all eigenvalues of the closed-loop system matrix

$$\left[\begin{array}{c|c} F(\omega) - G(\omega)K_1(\omega, \psi) & - G(\omega)K_2(\omega, \psi) \\ \hline BH(\omega) & A(\psi) \end{array}\right] \tag{9}$$

are inside the unit disc of the complex plane. It follows from known results that the system (7) is pointwise stabilizable if and only if

$$\text{rank}\left[\begin{array}{c|c|c} zI_n - F(\omega) & 0 & G(\omega) \\ \hline - BH(\omega) & zI_q - A(\psi) & 0 \end{array}\right] = n + q, \quad |z| \geq 1, \quad \text{all} \quad \omega \in \Omega, \quad \psi \in \Psi.$$

For this condition to hold, it is necessary (but not sufficient in general) that the pair $(F(\omega), G(\omega))$ be pointwise stabilizable; i.e.,

$$\text{rank}\,[\, zI_n - F(\omega) \quad G(\omega)\,] = n, \quad |z| \geq 1, \quad \text{all} \quad \omega \in \Omega.$$

Assuming that the augmented system (7) is pointwise stabilizable, the question then arises as to whether or not the stabilizing feedback gain matrices $K_1(\omega, \psi)$ and $K_2(\omega, \psi)$ can be selected so that their entries are continuous functions of the parameters ω and ψ. The answer is in the affirmative if the parameter sets Ω and Ψ are bounded. This result was first proved by GREEN and KAMEN [1981]. Another proof is given in KAMEN and KHARGONEKAR [1982].

If the parameter set Ω or Ψ is not bounded, it is an open question as to whether or not pointwise stabilizability implies that stabilization can be achieved using nondynamic feedback with continuous gains. For systems depending on a single parameter with unbounded variation, it is known that pointwise stabilizable systems can be stabilized using dynamic feedback. For details, see the paper by KHARGONEKAR and SONTAG [1982].

It follows from the (real) Weierstrass approximation theorem that if the augmented system (7) is stabilizable using continuous gains, then the system can be stabilized using gains that are polynomial functions of the parameters. Here we are again assuming that the parameter sets Ω and Ψ are bounded. Polynomial stabilizing gains can be computed by applying existing procedures for stabilizing linear systems with constant coefficients. Such an approach has already been utilized by COLEMAN [1982]. We shall briefly describe a stepwise method for computing polynomial stabilizing gains.

For each interval $[a_i, b_i]$ comprising the parameter set Ω and for each interval $[c_i, d_i]$ comprising the parameter set Ψ, construct a grid consisting of r points. We could start with $r = 1$ and take the single grid point to be the middle point of each interval. For all parameter values $\omega^i \in \Omega$, $\psi^j \in \Psi$ with components equal to grid points, compute stabilizing gain matrices $K_1(\omega^i, \psi^j)$ and $K_2(\omega^i, \psi^j)$ using any of the existing methods for stabilizing a constant linear discrete-time system. For example, the stabilizing gains could be computed by solving an algebraic Riccati equation associated with a quadratic performance criterion. Using polynomial interpolation, we can then compute polynomial matrices $K_1(\omega, \psi)$ and $K_2(\omega, \psi)$ such that

$$K_1(\omega, \psi)\Big|_{\substack{\omega = \omega^i \\ \psi = \psi^j}} = K_1(\omega^i, \psi^j)$$

$$K_2(\omega, \psi)\Big|_{\substack{\omega = \omega^i \\ \psi = \psi^j}} = K_2(\omega^i, \psi^j) \qquad \text{for all } i, j.$$

With the feedback matrices in (8) equal to these polynomial matrices, it follows from continuity of the system coefficient matrices that the closed-loop system with system matrix (9) will be asymptotically stable in an open neighborhood of each of the parameter values ω^i, ψ^j. However, the closed-loop system may not be asymptotically stable for every $\omega \in \Omega$, $\psi \in \Psi$. To check whether or not this is the case, it is necessary to test for asymptotic stability of the closed-loop system for values of ω and ψ in a suitably fine grid for Ω and Ψ. If the closed-loop system is not stable for all $\omega \in \Omega$, $\psi \in \Psi$, it is necessary to refine the original grid for Ω and Ψ and repeat the above process.

Whether or not the above step wise procedure converges to a solution depends on how the grid is selected. It is not clear if it is possible to guarantee that this procedure will always yield a solution, even though the theory tells us that a polynomial solution must exist if the augmented system is pointwise stabilizable. Nevertheless, preliminary results indicate that the process does work well.

If polynomial stabilizing gains $K_1(\omega, \psi)$ and $K_2(\omega, \psi)$ can be computed and the state $x(kT)$ of the system (4a) is accessible, then with the feedback (8), the closed-loop system will have both properties (1) and (2) in the above regulator-design problem. If $x(kT)$ not accessible, then as discussed in the next section, we must build an observer for $x(kT)$

III. REGULATOR DESIGN USING AN OBSERVER

In designing an observer for $x(kT)$, it turns out that we can ignore the input term $D(\omega)w(kT)$ in the discretized system equation (4a), since this term will be "rejected" as a result of the error-driven system (6). Hence we can consider using a n-dimensional Luenberger observer given by the state equation

$$\hat{x}(kT + T) = F(\omega)\hat{x}(kT) + G(\omega)u(kT) + L(\omega)(y(kT) - H(\omega)\hat{x}(kT)), \quad (10)$$

where $\hat{x}(kT)$ is the state of the observer and $L(\omega)$ is the $n \times p$ observer gain matrix. The system (10) is an observer for $x(kT)$ (assuming $w(kT) = 0$) if $x(kT) - \hat{x}(kT) \to 0$ as $k \to \infty$ for any initial states $x(0)$, $\hat{x}(0)$ and any $\omega \in \Omega$. This is equivalent to requiring that the pair $(F(\omega), H(\omega))$ be detectable for all $\omega \in \Omega$; that is,

$$\text{rank} \begin{bmatrix} zI_n - F(\omega) \\ H(\omega) \end{bmatrix} = n, \quad |z| \geq 1, \quad \text{all} \quad \omega \in \Omega.$$

By "dualizing" the results on stabilization discussed in the previous section, it follows that if the parameter set Ω is bounded and if $(F(\omega), H(\omega))$ is detectable for all $\omega \in \Omega$, then there is an observer of the form (10) with the entries of the gain matrix $L(\omega)$ equal to polynomials in ω. Further, a polynomial gain matrix $L(\omega)$ can be computed by interpolating values of $L(\omega)$ computed at points in a suitably fine grid for Ω.

With polynomial stabilizing gains $K_1(\omega, \psi)$ and $K_2(\omega, \psi)$ as computed in the previous section and with a Luenberger observer (10) with a polynomial gain matrix $L(\omega)$, we can then feed back the state estimate $\hat{x}(kT)$ and the state $\eta(kT)$ of the error-driven system (6), in other words, we can set

$$u(kT) = - K_1(\omega, \psi)\hat{x}(kT) - K_2(\omega, \psi)\eta(kT).$$

The resulting closed-loop system can be expressed in the form shown in Figure 1 with the digital regulator given by

$$\begin{bmatrix} \hat{x}(kT + T) \\ \eta(kT + T) \end{bmatrix} = \left[\begin{array}{c:c} F(\omega) - L(\omega)H(\omega) - G(\omega)K_1(\omega,\psi) & - G(\omega)K_2(\omega,\psi) \\ \hdashline 0 & A(\psi) \end{array}\right] \begin{bmatrix} \hat{x}(kT) \\ \eta(kT) \end{bmatrix} + \left[\begin{array}{c:c} L(\omega) & 0 \\ \hdashline 0 & B \end{array}\right] \begin{bmatrix} y(kT) \\ e(kT) \end{bmatrix}$$

By construction, the closed-loop system (not including $w(t)$) is asymptotically stable for all $\omega \in \Omega$, $\psi \in \Psi$. In addition, it follows from the results of DAVISON [1976] that $e(t) \to 0$ for any initial states $x(0)$, $\hat{x}(0)$, $\eta(0)$, and $w(0)$. Hence with this regulator, the closed-loop system satisfies both properties (1) and (2) of our design problem.

The regulator given above has dimension $n + q$, where n is the dimension of the observer and q is the dimension of the model for the exogenous signals. We could build a lower-order regulator if it is possible to build a lower-order observer. It is not clear if this is always possible since the system coefficient matrices depend in general on the parameter ω. But if the output matrix $H(\omega) = H$ is constant (does not depend on ω), then there does exist a lower-order observer. In fact, if rank $H = p$, we can follow the construction of GOPINATH [1971] to obtain an observer of dimension $n - p$. A brief sketch of the procedure is given below.

Without loss of generality, we may assume that $H = [0 \quad I_p]$. We can then partition the system matrices $F(\omega)$ and $G(\omega)$ so that the system equation becomes

$$\begin{bmatrix} x_1(kT + T) \\ x_2(kT + T) \end{bmatrix} = \begin{bmatrix} F_1(\omega) & F_2(\omega) \\ F_3(\omega) & F_4(\omega) \end{bmatrix} \begin{bmatrix} x_1(kT) \\ x_2(kT) \end{bmatrix} + \begin{bmatrix} G_1(\omega) \\ G_2(\omega) \end{bmatrix} u(kT)$$

$$y(kT) = [0 \quad I_p] \begin{bmatrix} x_1(kT) \\ x_2(kT) \end{bmatrix} = x_2(kT).$$

Here we are again ignoring the term involving $w(kT)$. Now we need to construct an observer for $x_1(kT)$ alone, as $x_2(kT)$ is directly accessible. Note that the dimension of $x_1(kT)$ is $n - p$ and that the state equation for $x_1(kT)$ is given by

$$x_1(kT + T) = F_1(\omega)x_1(kT) + F_2(\omega)y(kT) + G_1(\omega)u(kT).$$

Let $y_1(kT) = y(kT + T) - F_4(\omega)y(kT) - G_2(\omega)u(kT)$, so that

$$y_1(kT) = F_3(\omega)x_1(kT).$$

It is not difficult to show that if $(F(\omega), H(\omega))$ is detectable for all $\omega \in \Omega$, then $(F_1(\omega), F_3(\omega))$ is detectable for all $\omega \in \Omega$. Thus, assuming that Ω is bounded, by dualizing the results of the previous section we have that there exists a $(n - p) \times p$ polynomial matrix $L_1(\omega)$ such that $F_1(\omega) - L_1(\omega)F_3(\omega)$ is asymptotically stable for all $\omega \in \Omega$. Using the techniques of GOPINATH [1971], it can be shown that the system

$$\mu_1(kT + T) = (F_1(\omega) - L_1(\omega)F_3(\omega))\mu_1(kT) + (F_2(\omega) - L_1(\omega)F_4(\omega)$$
$$+ F_1(\omega)L_1(\omega) - L_1(\omega)F_3(\omega)L_1(\omega))y(kT)$$
$$+ (G_1(\omega) - L_1(\omega)G_2(\omega))u(kT)$$
$$\mu(kT) = \begin{bmatrix} \mu_1(kT) + L_1(\omega)y(kT) \\ y(kT) \end{bmatrix}$$

is an observer for $x(kT)$; i.e., $\mu(kT) \to x(kT)$ as $k \to \infty$. Finally, the control law

$$u(kT) = - K_1(\omega, \psi)\mu(kT) - K_2(\omega, \psi)\eta(kT)$$

will solve the regulator design problem posed in the previous section.

REFERENCES

N. P. COLEMAN, Jr.

[1982] Private Communication.

E. J. DAVISON

[1976] "The robust control of a servomechanism problem for linear time-invariant multivariable systems", IEEE Trans. Automatic Control, AC-21: 25-34.

B. GOPINATH

[1971] "On the control of linear multiple input-output systems", Bell Syst. Technical Journal, 50: 1063-1081.

W. L. GREEN and E. W. KAMEN

[1981] "Necessary and sufficient conditions for stabilizability of a linear discrete-time system defined over a *-subalgebra of a C*-algebra", submitted for publication.

E. W. KAMEN and P. P. KHARGONEKAR

[1982] "On the control of linear systems depending on parameters", submitted for publication.

P. P. KHARGONEKAR and E. D. SONTAG

[1982] "On the relation between stable matrix fraction factorizations and regulable realizations of linear systems over rings", IEEE Trans. Automatic Control, AC-27: 627-638.

H. G. KWATNY and K. C. KALNITSKY

[1978] "On alternative methodologies for the design of robust linear multivariable regulators", IEEE Trans. Automatic Control, AC-23: 930-933.

A NONLINEAR LIAPUNOV INEQUALITY*

Leon Kotin
Center for Tactical Computer Systems
U. S. Army Communications-Electronics Command
Fort Monmouth, NJ 07703

AD P001081

INTRODUCTION

Liapunov's classical inequality applies to the boundary value problem

$$x'' + q(t)x = 0, \quad x(0) = x(a) = 0, \quad x \not\equiv 0 \tag{1}$$

and gives the following best possible bound

$$\int_0^a |q(t)|\, dt > 4/a, \tag{2}$$

in the sense that the constant 4 cannot be increased [4, p. 451].

In the context of control theory, the control variable $q(t)$ takes a solution initially at the origin in the (t,x)-plane to the point $(a,0)$ while meeting the lower bound in (2) arbitrarily closely. We extend this inequality in two directions. First, we generalize the boundary value problem (1) itself to certain nonlinear equations. Secondly, we minimize more general integrals than the one in (2). Among other things, these results permit us to obtain new sufficiency criteria for the stability of Hill's equation.

Much of the material in this paper has already appeared in [6] and [7].

A SPECIAL CASE

Ordinary differential equations have been studied for centuries, so it is surprising that elementary techniques can still yield new and interesting results. Such a technique is a scaling technique suggested by Garrett Birkhoff (private communication) which leads to the following special case of our principal result.

THEOREM 1. Consider the boundary value problem (1). Then for any $\gamma > 1$, there is a k_γ independent of a such that

$$\inf \int_0^a |q(t)|^\gamma dt = k_\gamma / a^{2\gamma - 1}, \tag{3}$$

where the infimum is taken over all piecewise continuous q for which Eq. (1) is satisfied.

---

* The material in this paper which has appeared in [6] has been copyrighted by Academic Press.

This document has been approved for public release and sale; its distribution is unlimited.

PROOF. Define

$$I_\gamma(a) \equiv \inf\{\int_0^a |q(t)|^\gamma dt\}$$

over all piecewise continuous q(t) satisfying (1). With t = as, this becomes

$$I_\gamma(a) = a \inf\{\int_0^1 |q(as)|^\gamma ds\}$$

over the same set of q's. However, under the same substitution t = as, with $y(s) \equiv x(as) = x(t)$, Eq. (1) becomes

$$y'' + a^2 q(cs)y = 0, \quad y(0) = y(1) = 0. \tag{4}$$

Then

$$I_\gamma(1) = a^{2\gamma} \inf\{\int_0^1 |q(as)|^\gamma ds\}$$

over all q(as) satisfying (4). But the conditions (4) are satisfied if and only if (1) is satisfied. Then

$$I_\gamma(1) = a^{2\gamma-1} I_\gamma(a),$$

whence

$$I_\gamma(a) = k_\gamma / a^{2\gamma-1}, \text{ where } k_\gamma \equiv I_\gamma(1).$$

This result would be almost worthless unless it can be shown that $k_\gamma > 0$. However from Hölder's inequality and (2), it is easily shown that

$$k_\gamma \geq 4^\gamma. \tag{5}$$

One can show even more. McShane [8] proved that when $\gamma > 1$, there is a q for which the infimum in (3) is assumed. In [7] we obtained the optimal q's, the corresponding constants k_γ, and the corresponding solutions x(t) of Eq. (1) for the special cases γ = 3/2, 2 and 3. The value of k_2 had already been found earlier (cf. [3, pp. 60-61]) in another form by Borg.

Theorem 1 leads to the following obvious Corollary, in which a nontrivial solution x(t) of a differential equation is said to be *oscillatory* if it has an infinite sequence of zeros $t_0, t_1, t_2, \ldots$ with $t_n \to \infty$. Then the differential equation below is also said to be oscillatory. (Note that, by the Sturm separation theorem, all solutions are then oscillatory.)

COROLLARY. Consider the oscillatory equation

$$x'' + q(t)x = 0$$

where q(t) is piecewise continuous and

$$\int_0^\infty |q|^\gamma dt < \infty$$

for some $\gamma > 1$. Then

$$\sum_{n=0}^{\infty} (t_{n+1}-t_n)^{1-2\gamma} \leq (1/k_\gamma) \int_0^\infty |q|^\gamma dt.$$

THE PRINCIPAL RESULT

The same technique can be applied to obtain our principal result.

THEOREM 2. Let $x(t)$ be a (nontrivial) solution of the boundary value problem

$$x'' + q(t)t^\lambda f(x,tx') + t^{-2} g(x,tx') = 0, \quad x(0) = b_0, \; x(a) = b_1 \tag{6}$$

with $q(t) \in C^n[0,a]$ for some integer $n \geq 0$, $t^\lambda f(x,tx') \in C'$ and $t^{-2} g(x,tx') \in C'$, both for $t \in [0,a]$, as functions of t, x, x'. Suppose that, for some real constant α, the function

$$t^\alpha \phi \equiv t^\alpha \phi(t^{\lambda+2} q, \; t^{\lambda+3} q', \ldots, t^{\lambda+n+2} q^{(n)}) \tag{7}$$

is nonnegative and integrable as a function of t over $[0,a]$. Then

$$\int_0^a t^\alpha \phi \, dt \geq k a^{\alpha+1} \tag{8}$$

where k is independent of $q(t)$ and a, and is the best possible constant for fixed f, g, λ, b_0, and b_1.

The proof is similar to that of Theorem 1 except for obvious modifications and we omit it. The interested reader may derive it himself or look it up in [6].

The same technique can be used in the following examples.

EXAMPLES

The examples in this section include specializations of Theorem 2 and offer other applications of the same technique.

EXAMPLE 1. Suppose $q(t)$ satisfies Eq. (1) and $c = \text{const.} \geq 0$. Then

$$\int_0^a t^c |q|^\gamma dt \geq k a^{c-2\gamma+1},$$

since Theorem 2 can be applied to the integrand expressed as $t^{c-2\gamma}|t^2 q|^\gamma$. In particular, if $c = 0$, then we obtain Theorem 1. On the other hand, if $c = 1$, then we can obtain a result due to Hartman and Wintner [5],

who show further that $k = 0$, 1 or $(2-c)^{2-c}/(1-c)^{1-c}$ according as $c > 1$, $c = 1$ or $c < 1$ respectively.

EXAMPLE 2. The function ϕ can be generalized to include arguments involving integrals. For example, the same scaling technique used for Theorem 2 yields

$$\inf_q \int_0^a \left(\int_c^t |q(s)|ds \right)^2 dt = c/a$$

for some c independent of q and a. Moreover, $c \geq 1$, for

$$\begin{aligned} \int_0^a \left(\int_0^t |q(s)|ds \right)^2 dt &\geq \left(\int_0^a \int_0^t |q(s)|ds\, dt \right)^2 /a \\ &= \left(\int_0^a (a-t)|q(t)|dt \right)^2 /a \\ &\geq 1/a \end{aligned}$$

from Example 1 by a change in variable. More generally,

$$\inf_q \int_0^a \left(\int_c^t |q|ds \right)^\gamma dt = c_\gamma a^{1-\gamma}$$

with $c_\gamma \geq 1$ for $\gamma \geq 2$, from Hölder's inequality and the preceding result.

EXAMPLE 3. The boundary values in (1) may include values of the derivative. Consider the boundary value problem

$$x'' + q(t)x = 0, \quad x'(0) = x(a) = 0.$$

As in Example 1, we have

$$\int_0^a |q|^{-1/2} dt \geq ka^2$$

for some suitable k which cannot be decreased. This appears in Tadjbakhsh and Keller's investigation [10] of the shape of strongest columns with given length and volume. They show that $k = \sqrt{3}/\pi$.

EXAMPLE 4. The differential equation in (1) may be the general second order linear homogeneous differential equation, say in self-adjoint form. Consider the boundary value problem

$$(px')' + qx = 0, \quad p > 0, \quad x(0) = x(a) = 0. \qquad (9)$$

Introducing the standard substitution

$$s = \int_0^t du/p(u)$$

and letting $y(s) \equiv x(t(s))$, we obtain

$$y'' + pqy = 0, \quad y(0) = y(s(a)) = 0.$$

From (3), with a change in the resulting variable of integration we obtain

$$\int_0^a p^{\gamma-1}|q|^\gamma dt \cdot \left(\int_0^a dt/p \right)^{2\gamma-1} \geq k_\gamma.$$

In the particular case that $\gamma = 1$, Liapunov's inequality yields

$$\int_0^a |q|dt \cdot \int_0^a dt/p > 4.$$

EXAMPLE 5. We may also treat higher-order equations and certain nonhomogeneous boundary values, for instance

$$x^{iv} + q(t)x = 0, \quad x(0) = b_0, \; x'(0) = 0, \; x(a) = b_1, \; x'(a) = 0.$$

Then the same technique can be used to show that

$$\int_0^a |q|^\gamma dt \geq k_\gamma / a^{4\gamma-1}$$

where k_γ is independent of a and is best possible.

STABILITY OF HILL'S EQUATION

Using an argument due to G. Borg [2] (cf. [3, pp. 60-61]) we can apply the previous generalizations of Liapunov's inequality to obtain stability conditions for Hill's equation. We say that Hill's equation is stable if each solution is stable, i. e., if each solution is bounded in the t-interval $(-\infty, \infty)$.

THEOREM 3. Consider Hill's equation

$$x'' + q(t)x = 0, \quad q(t+a) = q(t) \not\equiv 0, \tag{10}$$

where the coefficient q(t) satisfies the following conditions in the notation of Theorem 1:

(i) q(t) is piecewise continuous;

(ii) $\int_0^a q(t)\, dt > 0$;

(iii) $\int_0^a |q(t)|^\gamma dt < k_\gamma / a^{2\gamma-1}$ for some $\gamma > 1$.

Then (10) is stable.

PROOF [G. Borg]. We know from Floquet's theory that there is a distinguished solution x(t) and a constant λ such that $x(t+a) = \lambda x(t) \not\equiv 0$. Moreover, λ is one of the two characteristic factors which are either both real or complex conjugates and whose product is unity. Now assume that (10) is not stable. Then the λ's are real and there is a real solution x(t) such that $x(t+a) = \lambda x(t) \not\equiv 0$. Thus x(t) either has no zeros or an infinite number of zeros.

In the latter case, the distance between successive zeros is less than or equal to a; i. e., if t_0 and $t_1 > t_0$ are consecutive zeros of x(t), we have $0 < t_1 - t_0 \leq a$. Therefore, by Theorem 1,

$$\int_0^a |q|^\gamma dt \geq \int_{t_0}^{t_1} |q|^\gamma dt \geq k_\gamma / (t_1 - t_0)^{2\gamma-1} \geq k_\gamma / a^{2\gamma-1}.$$

But this contradicts (iii).

Suppose then that x(t) has no zeros. Then from (10),

$$\int_0^a (x''/x)dt + \int_0^a q\,dt = 0.$$

Integrating by parts gives us

$$x'/x\Big|_0^a + \int_0^a (x'/x)^2\,dt + \int_0^a q\,dt = 0.$$

Since $x(t+a) = x(t)$, the first term vanishes, whence

$$\int_0^a q\,dt < 0 \quad \text{or} \quad x' \equiv 0.$$

Either of these conclusions contradicts the hypotheses. Consequently, our assumption that (10) is not stable is untenable. This completes the proof.

Applying the inequality (5) to this Theorem, we obtain the following stability criterion.

COROLLARY 1. If there is a $\gamma \geq 1$ such that the coefficient in Hill's equation (10) satisfies

$$\int_0^a |q(t)|^\gamma dt < 4^\gamma/a^{2\gamma-1} \quad \text{and} \quad \int_0^a q(t)dt \geq 0, \qquad (11)$$

then (10) is stable.

The upper bound in (11) is very crude and can be greatly increased. In proving the Corollaries 2 and 3, we borrow the following results from [6] for the cases $\gamma = 3$ and $3/2$ respectively. For the boundary value problem (1),

$$\int_0^a |q(t)|^3 dt \geq \Gamma^{18}(1/3)/(2^4\cdot 5\pi^6 a^5) = (656.6\ldots)/a^5 \qquad (12)$$

and

$$\int_0^a |q(t)|^{\frac{3}{2}} dt \geq 3^{3/2}\Gamma^9(1/3)/(2^6\pi^3 a^2) = (18.608\ldots)/a^2. \qquad (13)$$

COROLLARY 2. If

$$\int_0^a |q(t)|^3 dt \leq 656.6/a^5 \quad \text{and} \quad \int_0^a q(t)dt \geq 0,$$

then (10) is stable.

COROLLARY 3. If

$$\int_0^a |q(t)|^{3/2} dt \leq 18.6/a^2 \quad \text{and} \quad \int_0^a q(t)dt \geq 0,$$

then (10) is stable.

The corresponding result for the case $\gamma = 2$ is due to Borg and is included here for completeness and comparison. (Cf. [3, pp. 60-61] and [7].) The analytical expression for the upper bound was derived in [7].

COROLLARY 4 [Borg]. If

$$\int_0^a [q(t)]\, dt < \Gamma^{18}(1/4)/(2^4 \cdot 3\pi^2 a^3) = (63.024\ldots)/a^3$$

and

$$\int_0^a q(t)dt \geq 0,$$

then (10) is stable.

The same argument can be applied to the case where ϕ in Theorem 2 involves integrals. From Example 2, we can show that if

$$\int_0^a \left(\int_0^t |q(t)|ds\right)^{\gamma} dt < a^{1-\gamma} \quad \text{and} \quad \int_0^a q\, dt = 0,$$

for some $\gamma > 2$, then all solutions of (10) are bounded. (Cf. synopsis of article by T. M. Karaseva in Math. Rev. 18, p. 306.)

REFERENCES

[1] G. Borg, Uber die Stabilitat gewisser Klassen von linearen Differentialgleichungen, Ark. Mat. Astr. Fys., 31A, no. 1 (1944), 1-39.
[2] G. Borg, On a Liapounoff criterion of stability, Amer. J. Math., 71 (1949), 67-70.
[3] L. Cesari, "Asymptotic Behavior and Stability Problems in Ordinary Differential Equations," Springer, Berlin, 1959.
[4] P. Hartman, "Ordinary Differential Equations," John Wiley & Sons, New York, 1964.
[5] P. Hartman and A. Wintner, On an oscillation criterion of Liapounoff, Amer. J. Math., 73 (1951), 885-890.
[6] L. Kotin, A Liapunov inequality for nonlinear systems, "International Conference on Differential Equations," Academic Press, New York, 1975, 449-458.
[7] L. Kotin, A generalization of Liapunov's inequality, submitted for publication.
[8] E.J. McShane, personal communication.
[9] Z. Nehari, some eigenvalue estimates, J. d'Anal. Math., 7 (1959), 79-88.
[10] L. Tadjbakhsh and J. B. Keller, Strongest columns and isoperimetric inequalities for eigenvalues, J. Appl. Mech. (March 1962), 159-164.

Next page is blank.

AD P001082

NONLINEAR CONTROL FOR ROBOTIC APPLICATIONS

William H. Boykin
Allon Guez
SYSTEM DYNAMICS INCORPORATED
1219 N. W. 10th Avenue
Gainesville, FL 32601

ABSTRACT

State feedback regulation of a general class of nonlinear systems is considered. The control scheme presented here uses a nonlinear compensator and linear (static and dynamic state feedback. It is shown that, despite the presence of inaccuracies in modeling, precision control is attained without degradation of other specifications.

INTRODUCTION

State feedback regulation of a general class of nonlinear systems is considered in this report. The class includes general lumped mechanical systems with the number of control terminals (or actuators) equal to the number of degrees of freedom in motion, in particular robotic manipulators.

More precisely, the system treated here is given by the mathematical model

$$\dot{x} = Fx + Gu \tag{1a}$$

$$u = f_N(x) + G_N(x)\, v \tag{1b}$$

where $x \in R^n =: X$ is called the state (or phase), and $v \in R^m$ is the input. F, G are constant matrices of appropriate sizes and we assume that the pair (F, G) is reachable with rank G = m. $f_N : R^n \to R^m$ and $G_N : R^n \to R^m$ are constant nonlinear maps where $G_N(x)$ is assumed to be a nonsingular matrix for each $x \in R^n$ and G_N, G_N^{-1} are smooth. The intermediate vector u is introduced for convenience.

In most practical applications it is important that control systems satisfy criteria in addition to the main control purpose of positioning. Such criteria include:

a. precision;
b. robustness;
   1. for deviations in the control law;
   2. for system parameter variations;

3. for undesired time delays;
4. for external disturbances;
5. for saturation nonlinearities;

c. ease of implementation (including speed of computation);
d. smoothness of the output trajectory;
e. speed of response.

It is apparent that simple open loop control will not suffice for these purpose since the method does not involve any adjusting (adaptive) procedures. Therefore, it is natural to think that feedback control will be a desired control scheme.

One of the standard ways to approach the control problems of nonlinear systems is by decomposition into a number of simpler systems (Brockett [1]). Young [2] treated a control problem for a robotic manipulator by first decomposing it into the second order linear systems and then applying linear optimal feedback laws. However, it is known that slight modelling inaccuracies may destroy the utility of the system decomposition.

In this paper we make the realistic assumption that the modelling of a physical system is inaccurate, and we focus attention on the stabilization of the system about the origin of the state space (rather than decomposition of the system). We then provide a simple new approach to a precision nonlinear control problem.

In the following sections we will discuss: two basic control schemes; the limitations of these schemes; a control scheme for precision control, which is used in the neighborhood of the origin of the state space; control on a larger scale. Our control strategy is either single mode with dynamic state feedback or simi-dual mode in which an additional dynamic compensator is activated when the trajectory reaches near the origin.

NOTATION AND TERMINOLOGY

In addition to the notation standardized above, the following will be used. An $n \times n$ matrix A is stable iff the real parts of all the eigenvalues are negative. $\|.\|$ denotes the euclidian norm, ''' designates 'the transpose of', and ':=' means 'is defined to be'. I_n is the $n \times n$ identity matrix. If $x \in R^n$ and A is an $n \times n$ matrix, then $\|x\|_A^2 := x'Ax$. Unless otherwise stated all the matrices and the vectors are over the reals (which is denoted by R).

BASIC CONTROL SCHEMES

Consider the system described in (1a and 1b). It is desired to control any initial state $x(0)$ to the origin of X. Let the control law be

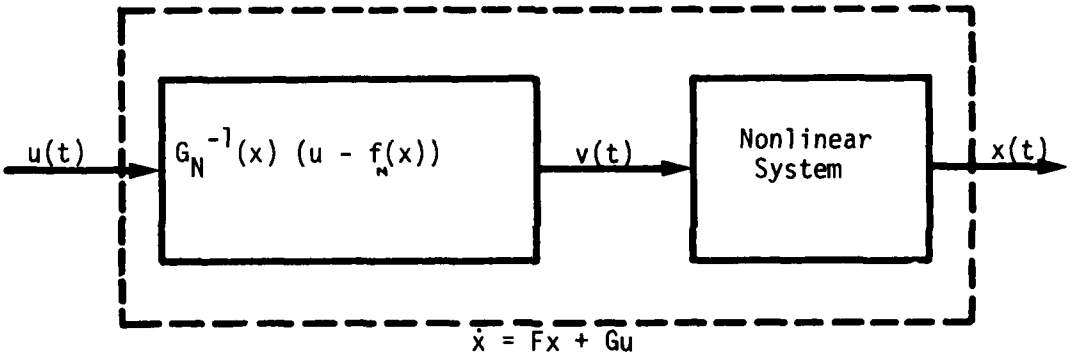


FIGURE 1

$$v = G_N^{-1}(x)\ (\hat{u} - f_N(x)) \tag{2.1}$$

for some continuous function $\hat{u}$, $t \geq 0$.

Then we have

$$\begin{aligned} \dot{x} &= Fx + G(f_N(x) + G_N(x)\ v) \\ &= Fx + G(f_N(x)) + G_N(x)\ G_N^{-1}(x)\ (\hat{u} - f(x)) \\ &= Fx + G\ \hat{u} \end{aligned} \tag{2.2}$$

i.e., the resulting system appears to be a linear system. (See Figure 1.) Therefore, straightforward application of linear control theory yield the desired results. As basic control laws we employ the following two schemes.

1ST SCHEME

The first scheme uses

$$\hat{u} = K\ x \tag{2.3}$$

as a control law where K is an $n \times m$ matrix such that $F + GK$ is stable. In particular, we shall choose K that is a solution of the following well-known linear optimal control problem. (There are some important reasons for its use, which will be discussed in the section discussing control on a larger scale.

Consider the linear system described by (2.2). Let α be a nonnegative constant, and let Q be an $n \times m$ symmetric positive semidefinite matrix. Write $Q = \tilde{Q}'\tilde{Q}$ for some matrix of an appropriate size, and assume that $(F, \tilde{Q})$ is observab le. A control law which minimizes the cost function

$$J[\hat{u}(.),\ x(0)] = \int_0^\infty e^{2\alpha t}\ (||x||_Q^2 + ||\hat{u}||^2)\ dt \tag{2.4}$$

is given by

$$\hat{u} = K_\alpha\ x,\ t \geq 0 \qquad K_\alpha = G'P_\alpha \tag{2.3}'$$

where P_α is the unique positive definite solution of the Ricatti equation

$$(F + \alpha I)'\ P_\alpha + P_\alpha(F + \alpha I) - P_\alpha G'GP_\alpha + Q = 0 \tag{2.5}$$

When the control law (2.4) is applied to (2.2), the resulting closed loop system has the representation

$$\dot{x} = (F + GK\alpha)\ x \tag{2.6}$$

where all the eigenvalues of $F + GK_\alpha$ are known to have real parts less than α. Thus there exists a positive constant c satisfying

$$||x|| \geq ce^{-\alpha t} \tag{2.7}$$

for all $t \geq 0$ and for all $x(0) \in X$, i.e., the closed loop system is asymptotically stable in the large (Kalman and Bertrum [4]) with the degree of stability α. (Anderson and Moore [5].)

The above control law would cause a sudden jump of the input v at $t = 0$. However, it is often preferable to have smooth (at least continuous) input everywhere. The following scheme eliminates the discontinuity at the outset.

2ND SCHEME

The second type of control law has the form

$$\hat{u} = \hat{u}(0) + K_S x + \int_0^t K_D x(\tau)\, d\tau \tag{2.8}$$

Here $\hat{u}(0)$ can be arbitrarily chosen. Thus, if $v_o \in R^m$ is the input value just before $t = 0$, by choosing $\hat{u}(0) = f_N(x(0)) + G_N(x(0))v_o$ (see Equation (1b)) v becomes continuous. The matrices K_S and K_D are chosen based on the following lemma.

Lemma 2.1. By suitable choices of K_S and K_D the closed loop system described by (2.2) and (2.8) can be made asymptotically stable in the large.

Proof: Define $u_A := \dot{\hat{u}}$, $t \geq 0$. Then by (2.2) we have

$$\begin{bmatrix} \dot{x} \\ \dot{\hat{u}} \end{bmatrix} = \begin{bmatrix} F & G \\ 0 & 0 \end{bmatrix} \begin{bmatrix} x \\ \hat{u} \end{bmatrix} + \begin{bmatrix} 0 \\ I_m \end{bmatrix} u_A \tag{2.9}$$

Since (F, G) is reachable, so is the pair

$$\begin{bmatrix} F & G \\ 0 & 0 \end{bmatrix}, \begin{bmatrix} 0 \\ I_m \end{bmatrix}. \tag{2.10}$$

Therefore by pole assignment theorem (see Wonham [6], Theorem 2.1) there exists $m \times n$ and $m \times m$ matrices K_1 and K_2 and a corresponding control law

$$u_A = [K_1 \; K_2] \begin{bmatrix} x \\ \hat{u} \end{bmatrix} \tag{2.11}$$

such that the closed loop system

$$\begin{bmatrix} \dot{x} \\ \dot{\hat{u}} \end{bmatrix} = \begin{bmatrix} F & G \\ K_1 & K_2 \end{bmatrix} \begin{bmatrix} x \\ \hat{u} \end{bmatrix} \tag{2.12}$$

is asymptotically stable.

From (2.11) it is easy to see that

$$\dot{\hat{u}} = K_1 x + K_2 G^+ (\dot{x} - F x).$$

Therefore,

$$\hat{u} = \hat{u}(0) + K_2 G^+ x + \int_0^t (K_1 - K_2 G^+ F) x(\tau) \, d\tau. \tag{2.8}'$$

and we may define

$$K_S := K_2 G^+ \quad \text{and} \quad K_D := K_1 - K_2 G^+ F \qquad \text{Q.E.D.}$$

In particular, we may choose $[K_1 \; K_2]$ so that (2.11) minimizes the cost function (2.4) where $\hat{u}$ is replaced by u_A, x is replaced by $[x' \; \hat{u}']'$ and the $n \times n$ matrix Q is replaced by an $(n + m) \times (n + m)$ matrix $\bar{Q}$ (symmetric, positive semidefinite). We denote this optimal gain by $[k_{\alpha 1} \; K_{\alpha 2}]$ where $k_{\alpha 1}$ and $K_{\alpha 2}$ are $m \times n$ and $m \times m$ matrices, respectively, and we designate the corresponding K_S and K_D by $K_{S\alpha}$ and $K_{D\alpha}$. Clearly, (2.5) holds and the previous stability arguments are also true with suitable replacements.

SHORTCOMINGS OF THE PREVIOUS CONTROL SCHEMES

The discussion of the previous section was based on the assumption that the modeling is accurate. However, if inaccuracies exist (as is always the case in practice), we no longer have the linear equation as (2.2).

More precisely, suppose that instead of (2.1) we have

$$v = \hat{G}_N^{-1}(x) \, (\hat{u} - \hat{f}_N(x)) \tag{3.1}$$

where $\hat{f}_N(.)$ and $\hat{G}_N(.)$ satisfy the same defining properties

as $f_N(.)$ and $G_N(.)$, except that the former pair is 'slightly different' from the latter. Then from (1a and 1b) and (3.1)'

$$\dot{x} = F\,x + G(f_N(x) + G_N(x)\,v)$$

$$= F\,x + G(f_N(x) + G_N(x)\,\hat{G}_N^{-1}(x)\,(\hat{u} - \hat{f}_N(x))$$

$$= F\,x + G(G_N(x)\,\hat{G}_N^{-1}(x)\,\hat{u} + f_N(x) -$$

$$G_N(x)\,\hat{G}_N^{-1}(x)\,\hat{f}_N(x) \qquad (3.2)$$

Since

$G_N(x)$, $\hat{G}_N(x)$ are invertible for all $x \in X$, we write

$$f_o(x) = G_N^{-1}(x)\,f_N(x),\ x \in X \qquad (3.3a)$$

$$\hat{f}_o(x) = \hat{G}_N^{-1}(x)\,\hat{f}_N(x),\ x \in X \qquad (3.3b)$$

Also let

$$\Delta G_N^{-1}(x) := \hat{G}_N^{-1}(x) - G_N^{-1}(x)\ ,\ x \in X \qquad (3.4a)$$

$$\Delta f_N(x) := \hat{f}(x) - f(x)\ ,\ x \in X \qquad (3.4b)$$

Then it is straightforward to show that (3.2) can be rewritten as

$$\dot{x} = F\,x + G(\hat{u} + w(x)) \qquad (3.5a)$$

where

$$w(x) = G_N(x)\,(\Delta G_N^{-1}(x)\,\hat{u} - \Delta f_N(x)) \qquad (3.5b)$$

Notice that $\hat{u}$ is the control of choice already obtained but that $w(x)$ is unknown since the true matrix and vector $G_N(x)$, $f_N(x)$, $x \in X$ are unknown. Furthermore $w(0)$ may not be zero.

Now the question arises whether the system can still be stabilized precisely at the origin of X. It is clear that the control law of the type $\hat{u} = Kx$ (1st scheme) will not work since the resulting closed loop system does not have an equilibrium at the origin. By the same token (in regard to (2.9) and (2.11) with addition of the disturbance term $w(x)$) the second scheme in the last section obviously fails as well. It is known that a slight modification of the second scheme will yield asymptotic stability at the origin if $w(x)$ is a constant. (Johnson [7]) This

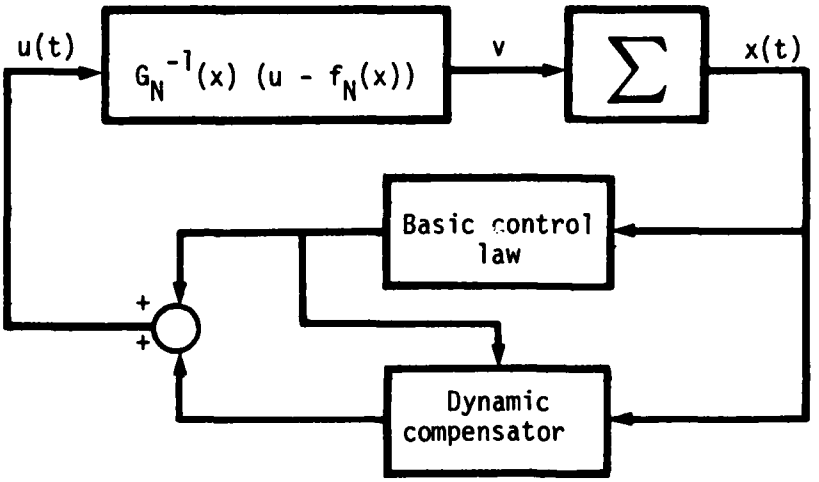

u(t)
$G_N^{-1}(x)\ (u - f_N(x))$
v
Σ
x(t)
Basic control law
+
+
Dynamic compensator

FIGURE 2

method has been extended to the case where $w(x)$ is a polynomial of t [7], but not a polynomial of x. Of course, the case when $w(x)$ is a general nonlinear term with $w(o) \neq 0$ has not been previously treated.

PRECISION CONTROL

In the previous section it was found that in the presence of modeling inaccuracies the equilibrium under consideration deviates from the origin if the basic schemes are used. In this section we discuss the method to avoid this deflection, and we stabilize the system at the origin.

We are now concerned with the system described by (3.5). We adopt a dual mode control consisting of far field control and near field control. The far field control is applied when x is 'distant' from the origin. For this we use either the first or the second control scheme in BASIC CONTROL SCHEMES section. The near field control is applied when x is within some 'distance' from the origin. For this the method introduced by the authors in [3] will be used.

The two basic schemes in BASIC CONTROL SCHEMES section are based on accurate modeling. Therefore, it may not seem logical to use them in the presence of modeling inaccuracies. However, the justification for such use will be given in the next section. Here we summarize the method for near field control.

This method is a combination of the first basic scheme and a dynamic compensator, which is drawn schematically in Figure 2. We select the control law $\hat{u}$ according to

$$\hat{u} = K x + \tilde{x}_c + F_c G^+ x \tag{4.1a}$$

$$\dot{\tilde{x}}_c = - F_c G^+ F x - F_c K x \tag{4.1b}$$

where K and F_c are not yet specified.

Then the subsequent theorem states that $x, \dot{x} \to 0$ as $t \to \infty$ in the neighborhood of $0 \in X$. Define

$$x_c := \tilde{x}_c + F_c G^+ x \ , \ t \geq 0 \tag{4.2}$$

and further let

$$x_{cw_o} := x_c + w(0) \ , \ t \geq 0 \tag{4.3}$$

Denote by X_{cw_o} the space in which x_{cw_o} is defined.

Also write

$$x_e := \begin{bmatrix} x \\ \\ x_{cw_o} \end{bmatrix} \tag{4.4}$$

Now consider the system jointly described by (3.5) and (4.1). Then we obtain Theorem 4.1 (Hamano, Warren and Boykin [3]). There exists $n \times n$ and $m \times m$ matrices K and F_c, respectively, and a neighborhood N_e of 0 in $X \oplus X_{cw_o}$ such that $x_e(0) \in N_e$ implies

$$\text{(i)} \quad x_e \in N_e \quad \text{for all} \quad t \geq 0,$$

$$\text{(ii)} \quad ||x_e|| \leq ce^{-\alpha_o t} ||x_e(0)||. \tag{4.5}$$

for some constants $\alpha_o > 0$ and $c > 0$.

Remark. In practice, the degree of stability α_o in the far field control mode should be chosen relatively small to prevent saturation of the actuators (although limited saturation could be tolerated. See the following section.). On the other hand K and F_c in the above theorem can be and should be chosen so that α_o is relatively large.

STABILITY BASIN AND GLOBAL STABILITY

In choosing the gains in the basic control laws it is preferable to choose $[K_{\alpha 1}, K_{\alpha 2}]$ as in the optimal control problem discussed in the BASIC CONTROL SCHEMES section. Consider the system described by (3.5), and recall the notation used in BASIC CONTROL SCHEMES section. Then as an immediate consequence of the criterion for stability given in [5], we have the following theorem corresponding to two schemes in the above referenced section. Denote by $\bar{x}$ either the vector $x \in R^n$ or the extension $\begin{bmatrix} x \\ y \end{bmatrix}$ of x for some $y \in R^m$. Let $\bar{K}$ be either K or $[K_1 \; K_2]$, respectively. Also let $\bar{w}(x)$ be either $w(x)$ or

$\begin{bmatrix} w(x) \\ 0 \end{bmatrix}$, respectively. Then

Theorem 5.1. (Anderson and Moore, [5]. If there is an (arbitrary small) $\varepsilon > 0$ such that

$$(1/2 + \varepsilon) \|\bar{K}_\alpha \bar{x}\|^2 \geq (\bar{K}_\alpha \bar{x})' (\bar{K}_\alpha + 2\bar{w}(x) \qquad (5.6)$$

for all $x \in X$, then the closed loop system (3.5) and (2.3)' (or, respectively, (3.5) and (2.8) with K_s and K_D replaced by $K_{S\alpha}$ and $K_{D\alpha}$) is asymptotically stable in the large with the degree of stability α.

If (4.7) does not hold, our next concern is whether the closed loop system can be asymptotically stable. A stright forward application of Lyapunov's theorem yields

Theorem 5.2. If there exists a positive definite function $V(x)$ such that for the use of the first control scheme

$$\dot{V}(x) := -2\alpha \|x\|^2_{p_\alpha} - \|x\|_Q - (K_\alpha x)' x$$

$$(K_\alpha x + 2w(x)) < 0 \qquad (5.7)$$

for all $x \in R^n$, then the system (3.5) with (2.3)' is asymptotically stable in the large. A similar result holds for the second control scheme with appropriate substitutions for x, P_α, Q, $w(.)$.

Proof: Let $V(x) := \|x\|^2_{p_\alpha}$, and take the time derivative along the trajectory, i.e., $\dot{V}(x) := \frac{d}{dt} V(x)$ (along the trajectory of (3.5) and (2.3)'). Then

$$\dot{V}(x) = \dot{x}' P_\alpha x + x' P_\alpha \dot{x} \qquad (5.8)$$

It can be shown easily that this is equal to

$$-2\alpha \|x\|^2_{P_\alpha} - \|x\|^2_Q - (Kz)' (Kz) + 2w(x)). \qquad (5.9)$$

The result then follows by Lyapunov's theorem. (See Kalman and Bertram [4].)

Remark. Very often it is not necessary to require global stability and it would satisfy to find a sufficiently large neighborhood of the equilibrium point in which stability is guaranteed. Neglecting the close vicinity of the origin (see section on BASIC CONTROL SCHEMES and [4]), such a neighborhood N_{st} can be simply given.

CONCLUSION

We have shown how to design simple controllers for a class of nonlinear systems assuming that the modeling may not be accurate. We have seen that when some very mild conditions are met our performance criteria are satisfied, (preceeding section, Theorems and Remark).

REFERENCES

[1] R. W. Brockett, "Algebraic Decomposition Methods for Nonlinear Systems".

[2] K. D. Young, "Control and Trajectory Optimization of a Robot Arm", Army Electronics Command, Report AD-A023 669, 1975.

[3] F. Hamano, M. E. Warren, and W. H. Boykin, Jr., "Stabilization of a System with Unknown Nonlinearity", to appear.

[4] R. E. Kalman and J. E. Bertram, "Control System Analysis and Design via the 'second method' of Lyapunov - I Continuous Time Systems", ASME Journal of Basic Engineering.

[5] B. D. O. Anderson and J. B. Moore, Linear Optimal Control, Prentice-Hall, N.J., 1971.

[6] W. M. Wonham, Linear Multivariable Control - A Geometric Approach.

[7] C. D. Johnson, "Optimal Control fo the Linear Regulator with Constant Distrubances", IEEE Trans. on Auto. Contr., pp. 416-421, 1968.

AD P001083

INTEGRATED SIMULATION OF VEHICULAR SYSTEMS WITH STABILIZATION[1]

George M. Lance, Cwo-Gee Liang and Mark A. McCleary
Center for Computer Aided Design, College of Engineering
The University of Iowa, Iowa City, Iowa 52242

ABSTRACT

The feasibility of the use of overall simulation for the purpose of investigating response characteristics of systems which are influenced by interaction between the vehicle structure and the line of sight control subsystem is demonstrated. The effect of tube flexibility on pointing accuracy is demonstrated by inclusion of a flexible tube model. The model includes active control, but with the flexible element outside the control loop.

A simplified model of the controlled system is used to identify proper actuation parameters required to maintain comparable control performance for different mass loads. The results are verified by simulation of the complete system. The model points out the relative importance of disturbance inputs resulting from vertical motion and pitch motion to line of sight control of systems with mass unbalance. It is shown that for certain classes of vehicles, mass balancing requires greater power input without significant improvement in pointing accuracy.

INTRODUCTION

Requirements for modern vehicular systems include the capability of stabilized weapon operation while the vehicle is moving over terrain. Performance in this mode implies that the weapon system must be able to maintain a fixed inertial orientation in the presence of significant disturbance inputs arising from interaction with the vehicle structure. One disturbance input of interest is the torque generated due to vertical accelerations when the weapon is not mass balanced about the trunnion axis.

The time and cost associated with experimental programs and the difficulty in analytical approaches makes computer simulation the only feasible method of investigating complete system behavior in an exploratory way. The development of the Dynamic Analysis and Design Systems (DADS) code has provided the basis for carrying out systematic investigations of the behavior of complex interacting systems prior to the fabrication and testing phases.

[1]This work was supported by the U.S. Army Tank-Automotive Command under contract DAAE07-81-C-4031.

The primary objectives of this study were to:

1. Demonstrate the feasibility of developing dynamic simulation models of vehicular systems which include the vehicle structure, weapon drives in both elevation and azimuth directions and control loops operating as a single interconnected system.

2. Utilize these models to investigate the behavior of systems which include weapons having significant mass unbalance.

The models developed utilize the DADS code in both the 2-D and 3-D forms and demonstrate the feasibility of including the effects of flexibility of the gun tube.

Dynamic performance was evaluated for operation over terrain profiles having roughness levels of 1, 1.5, and 2 inches RMS at speeds which would result in Vertical Absorbed Power Levels (VAPL) of 2, 4 and 6 watts at the gunner's station.

SYSTEM MODEL

The vehicle used in this study is a tracked armored concept vehicle in the 20 ton class. The system model consists of a rigid body representation of the vehicle, rigid body and flexible element models of the weapon and a control loop for stabilization of the weapon line of sight. The rigid body model includes the turret, chassis, and roadwheels with the roadwheels connected to the chassis by roadarms and spring-damper suspension elements. The final control element in the stabilization loop is an electrohydraulic servoactuator. Both two and three degree-of-freedom models are developed and provision is made to simulate operation over terrain.

A block diagram of the control system which was used as the basic configuration for this study is shown in Figure 1. The block diagram has been drawn in conventional control system form and assumes ideal measurement of inertial motion. The simplified form for the control loop was adopted for two reasons. First, so that the basic behavior pattern relative to the magnitude of gun mass unbalance could be studied with the minimum feasible complexity and second, to establish the feasibility of including the control function in the overall model. Both objectives are served very adequately by the model chosen.

The final control element consists of an electrohydraulic servovalve driving a piston actuator. The model of this segment was developed as basically an ideal drive, including only those characteristics which were considered to be of first order importance to the system behavior.

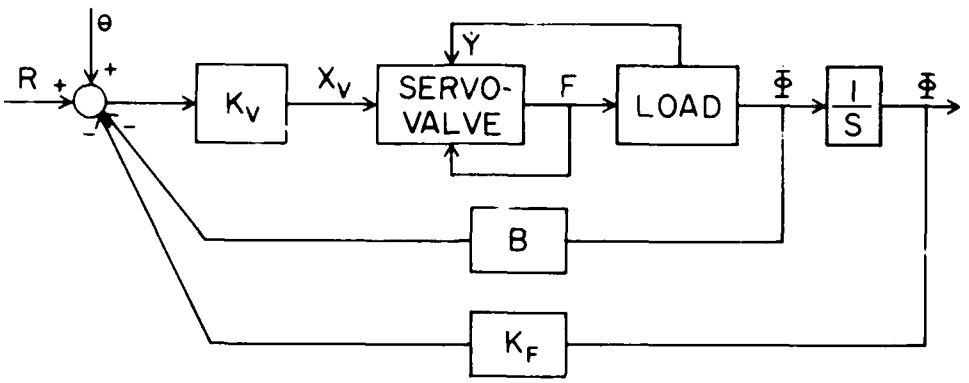


Figure 1. Control System Block Diagram

The first stage of the servovalve is in itself a closed loop system which positions the second stage valve spool in response to an electrical current input. The response of the first stage is normally very much faster than the overall system response and consequently the model used assumes a simple proportionality between current input and second stage valve spool position over the normal operating range. Ideal saturation occurs for larger input signals.

An ideal spool valve would have zero radial clearance and zero lap, resulting in no leakage flow and no flow at null position. The result would be very high pressure gain near null with corresponding stability problems in this range. To avoid these problems, an underlapped model was used to reduce the effective gain near the null position.

Overpressures which can occur due to sudden changes in valve position while driving a mass load were avoided by providing for bypass flow across the piston when the differential pressure became greater than supply pressure.

The piston actuator was modeled as having negligible rod end area and no friction.

The equations relating force output of the servoactuator, load velocity and second stage spool valve position can be written based upon the equations for flow through the spool valve. (See Figure 2).

Flows through the spool ports are assumed to be described by orifice equations with constant coefficients. A typical flow equation is

$$\begin{aligned} q_1 &= CX_1\sqrt{P_s - P_1}, \quad P_1 < P_s, \quad X_1 > 0 \\ &= -CX_1\sqrt{P_1 - P_s}, \quad P_1 > P_s, \quad X_1 > 0 \end{aligned} \tag{1}$$

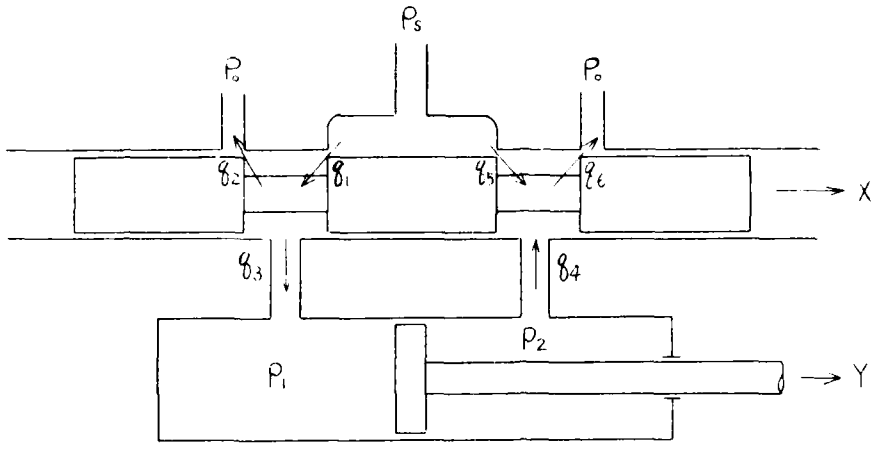


Figure 2. Servoactuator Schematic Diagram

Similar equations apply for all other orifice flows shown. For convenience, all pressures are taken relative to the drain pressure, P_0, which is set equal to zero. The overall flow constant is given by:

$$C = C_v \quad \pi D \sqrt{\frac{2g}{\gamma}} \tag{2}$$

where C_v = orifice flow coefficient

D = value spool diameter

γ = fluid specific weight.

Rewriting equation (1) in general form:

$$q_1 = CX_1 \sqrt{|P_s - P_1|}\ \mathrm{Sgn}(P_s - P_1)\ ; \quad X_1 > 0 \tag{3}$$

From continuity it is seen that:

$$q_1 = q_2 + q_3 \tag{4}$$

$$q_3 = A\dot{y} = q_4 \tag{5}$$

$$q_6 = q_4 + q_5 \tag{6}$$

The force applied to the load is:

$$F = (P_1 - P_2)A \tag{7}$$

This driving force is therefore a function of the system pressures which are in turn functions of both valve spool position and load velocity. The resultant equations must therefore be solved implicitly. Solving for P_1 and P_2 as functions of the X_i and load velocity:

$$P_1 = P_s - \left(\frac{A\dot{y} + CX_2 \sqrt{|P_1|}\ \mathrm{Sgn}\ (P_1)}{CX_1} \right)^2 \mathrm{Sgn}(P_s - P_1) \qquad (8)$$

$$P_2 = \left(\frac{A\dot{y} + CX_5 \sqrt{|P_s - P_2|}\ \mathrm{Sgn}(P_s - P_2)}{CX_6} \right)^2 \mathrm{Sgn}\ (P_2) \qquad (9)$$

Equations 7, 8 and 9 were used to represent the valve-load interaction over the normal operating range of valve displacements and pressures. If the pressure difference across the piston becomes greater than P_s, flow is bypassed around the piston according to:

$$q_{B1} = C_F A_B \sqrt{P_1 - P_2 - P_s}\ ; \quad P_1 - P_2 > P_s \qquad (10)$$

$$q_{B2} = C_F A_B \sqrt{P_2 - P_1 - P_s}\ ; \quad P_2 - P_1 > P_s \qquad (11)$$

$$q_{B1} = q_{B2} = 0\ ; \quad |P_1 - P_2| < P_s$$

where $$C_F = C_v \sqrt{\frac{2g}{\gamma}}$$

In the above, the X_i represent the valve port openings at the flow points shown as q_i in Figure 2. A valve underlap of amount d_o was assumed, leading to:

$$X_1 = X_0 + X = X_6$$

$$X_2 = X_0 - X = X_5$$

As seen from equations 8 and 9, the solution will be very sensitive to values of X_1 or X_6 near zero. To avoid this problem, X_1 and X_6 were given lower limits of Xmin. This is not an unrealistic condition since the effect is essentially the same as including a leakage coefficient.

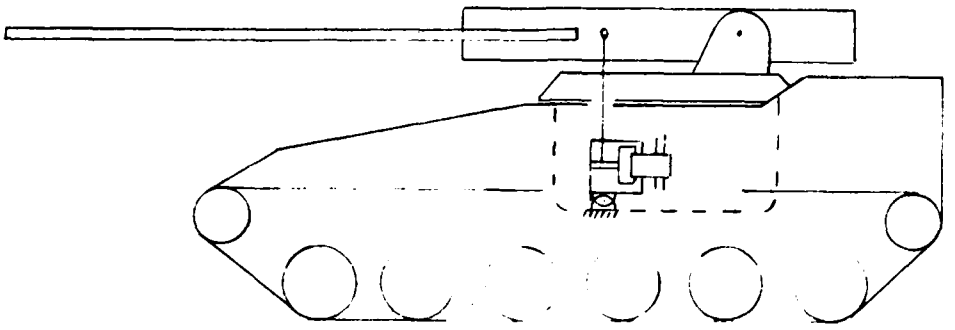


Figure 3. Concept Vehicle Outline Drawing

An outline drawing of the concept vehicle, as simulated for this study, is given in Figure 3. The DADS code was used as the basic simulation formulation. The underlying theory associated with the code has been reported previously (1,2,3).

The vehicle model treats the chassis and turret as rigid bodies. In the 2-D model, motion of the vehicle is in the pitch plane only and the chassis and turret are constrained to move as a single rigid body. The 3-D model has full three degree-of-freedom motion with the turret having rotational motion relative to the chassis. There are twelve roadwheels, treated as rigid bodies, which are mounted to the chassis through spring-damper suspension elements. The weapon is driven in elevation relative to the turret in both versions. Azimuth motion in the 3-D version is achieved by driving the turret relative to the chassis.

Vehicle travel is simulated by moving the desired terrain profile past the vehicle, imparting vertical motion to the wheel centers by a point following procedure. Track characteristics were not included in this model.

The use of a rigid body model for the gun tube is adequate for investigation of the basic system response. However, it is recognized that flexibility of the tube results in the centerline angle at the tube end being different from that at the breech. The flexibility effects under dynamic conditions are of particular interest since errors due to flexibility can be expected to be of the order of the desired pointing accuracy and they are not easily controlled.

A method of modeling flexible elements in a form which is compatible with the DADS 2-D code has been developed (4,5,6). The extension to the 3-D code is under development.

The flexible element model is developed by first modeling the tube using finite element techniques. The finite element model

is then used in a preprocessor program to generate the modal characteristics of the tube which are used as the input to the DADS program.

The accuracy of the model will depend upon both the number of finite elements used and the number of modes retained. In both cases, the choice depends upon the relative importance of computation time and accuracy and will usually require some exploratory work to determine the best values for a given application.

The terrain profiles used were developed at the Aberdeen Proving Grounds and are accepted as standards for comparison of off-the-road vehicle operation. The three terrain models used were the APG9, APG12 and APG29, having course lengths of 301 feet and RMS amplitude levels of 1.04, 1.70 and 2.17 inches respectively.

SIMPLIFIED MODEL

In order to conveniently define system parameter relationships on an analytic basis, a simplified two-body representation of the turret and gun as shown in Figure 4 was used. The equations of motion were linearized using small angle assumptions to permit development of the basic relationships between parameters and system response.

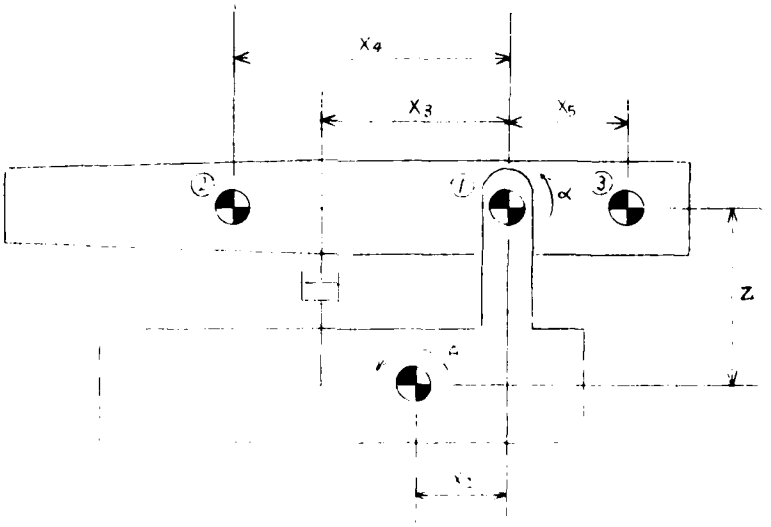


Figure 4. Simplified Turret-Gun Model

Referring to Figure 4, body 0 represents the turret, bodies 1 and 2 represent the nonrecoiling and recoiling parts of the gun, and body 3 the balancing mass, when used. In this study, the recoiling and nonrecoiling parts were considered to be a single rigid body, i.e. no firing capability was included.

For the balanced system, m_3 and X_5 are chosen so that

$$m_3 X_5 = m_2 X_4 \tag{15}$$

It is assumed that the center of mass for body 1 lies at the pivot.

Assuming small angular displacements the equation of motion can be derived as:

$$\ddot{\alpha} = -\frac{X_3}{J_B} F_a - \ddot{\theta} \tag{16}$$

Therefore, if an input motion to body 0 is given, and a control system providing a driving force, F, is defined, the angular motion of the gun can be determined. F and α will of course, not be independent.

For the unbalanced case, mass m_3 is zero resulting in a mass center for the gun at

$$X_c = \frac{m_2 X_4}{m_1 + m_2} \tag{17}$$

The equation of motion for this case is:

$$\ddot{\alpha} = \frac{m_T X_c}{J_u + m_T X_c^2} \ddot{y}_1 + \frac{m_T X_c X_2 - J_u}{J_u + m_T X_c^2} \ddot{\theta} - \frac{X_3}{J_u + m_T X_c^2} F \tag{18}$$

Thus the vertical acceleration of the turret, $\ddot{y}_1$ introduces an input to the unbalanced system while it does not in the balanced system (See Equation 16). Figure 5 is a block diagram of the control loop with the simplified model.

From equations 16 and 18, the force balance for the system with no disturbance input can be written as:

$$FX_3 = - J_{eq} \ddot{\alpha} \tag{19}$$

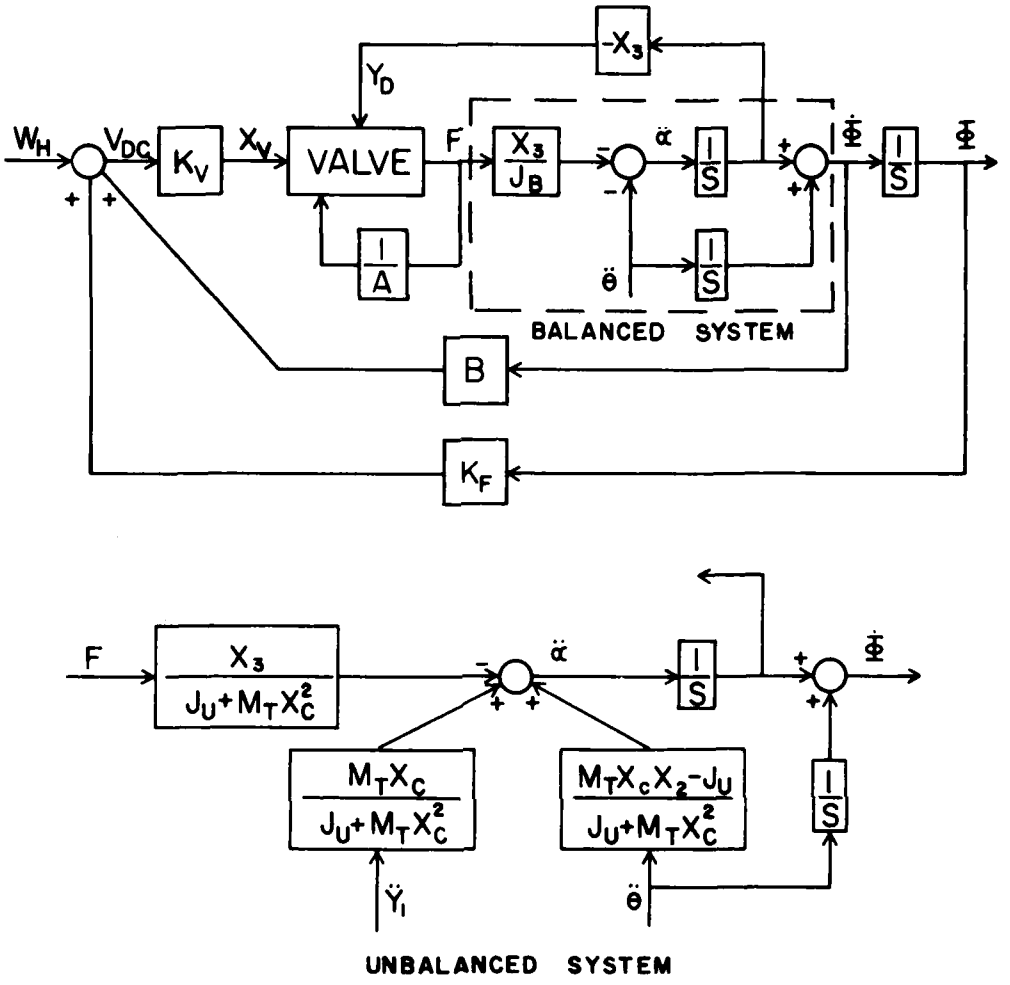


Figure 5. Simplified Control Loop

where:

$$J_{eq} = J_B \text{ (balanced case)}$$
$$= J_u + M_T X_c^2 \text{ (unbalanced case)} \quad (19)$$

The force in terms of the pressure difference and actuator area is:

$$F = P_L A \quad (20)$$

where

$$P_L = \text{Load pressure} = P_1 - P_2$$

The piston area can now be defined in terms of the desired acceleration, $\ddot{\alpha}_m$ resulting from the maximum pressure differential available, P_s.

$$A = \frac{J_{eq}\ \ddot{\alpha}_m}{P_s\ X_3} \tag{21}$$

Another performance criterion which might be used is the maximum angular velocity which can be achieved. This would occur when the valve was fully open and the load pressure was zero.

The velocity is governed by the valve flow rate and can be obtained from:

$$q = CX\ \sqrt{P_s - P_1} \tag{1}$$

$$\dot{y} = X_3\ \dot{\alpha} \tag{22}$$

$$q = A\ \dot{y} \tag{5}$$

Combining with equation 21 and using maximum values resulting from $P_1 = 0$,

$$C = \frac{J_{eq}\ \ddot{\alpha}_m\ \dot{\alpha}_m}{X_m\ P_s^{3/2}} \tag{23}$$

where the subscript m refers to maximum values.

Therefore, specifying maximum angular velocity, $\dot{\alpha}_m$, and angular acceleration, $\ddot{\alpha}_m$, permits the value of C to be determined. Note that from

$$C = C_v \pi D\ \sqrt{\frac{2g}{\gamma}}$$

this is equivalent to defining the valve spool diameter.

Equations 21 and 23 can be used to define the ratios between piston areas and flow constants (valve spool diameters) for two similar systems which have the same maximum angular velocity, angular acceleration and spool displacement.

$$\frac{A_2}{A_1} = \frac{J_2}{J_1} \frac{P_{s1}}{P_{s2}} \tag{25}$$

$$\frac{C_2}{C_1} = \frac{J_2}{J_1} \left(\frac{P_{s1}}{P_{s2}}\right)^{3/2} \tag{26}$$

If the servoactuator parameters are chosen according to these relationships, the system responses will be the same. This then provides a convenient guide for choosing system parameters for various amounts of unbalance so that the system performance can be evaluated on an equal basis.

The relationship of system power requirement as a function of supply pressure will also be of interest. The piston velocity can be written as:

$$V = q/A \tag{27}$$

Since the flow rate, q, must be delivered from the pump at a pressure of P_s, the instantaneous power delivered is given by:

$$P_H = P_s\ q = P_s\ VA$$

The ratio of power required for two systems is then:

$$\frac{P_{H2}}{P_{H1}} = \frac{P_{s2}\ V_2\ A_2}{P_{s1}\ V_1\ A_1}$$

For equal system responses, as assumed above, this reduces to:

$$\frac{P_{H2}}{P_{H1}} = \frac{P_{s2}\ A_2}{P_{s1}\ A_1}$$

and, choosing the area ratio as in Equation 25,

$$\frac{P_{H2}}{P_{H1}} = \frac{J_2}{J_1} \tag{31}$$

Therefore, under the stated assumptions, the power required will be directly proportional to the load inertia and independent of hydraulic supply pressure.

RESULTS

The investigation of system behavior for various amounts of gun mass unbalance required that system parameters be chosen for each case so that a meaningful comparison could be made. This was accomplished by choosing values which would provide approximately the same system response in every case. The criteria used to set the desired response behavior were: reasonable values of maximum angular acceleration and velocity and a transient response which was slightly underdamped. These criteria were not intended to represent an optimal system but rather to define a reasonable response and to provide a common base from which to evaluate the effects of changes in load conditions.

The parameters to be used in the control system were chosen so that a transient response with an input of sufficient magnitude to initially saturate the servovalve displacement would result in a slightly underdamped response. Table 1 contains a complete listing of the significant system parameter values.

Evaluation of system performance requires that a meaningful error criterion be established. The objective of the system is to maintain weapon line of sight during operation over terrain. Consequently, a measure of performance would be the deviation of the weapon centerline from horizontal during operation with zero command input. The specific error measure chosen was the percent of the time during which the error remained within a specified error range. This gives not only a measure of the peak errors encountered but also a clear indication of the error distribution. Due to the nature of the application, the percent time on target will be of greater significance than the maximum instantaneous error.

The hydraulic power and total energy requirements are of interest since the power to drive the hydraulic pump must be supplied by the engine and heat generated by internal losses must be removed through a heat exchanger.

The flow supplied to the servovalve from the hydraulic pump is the sum of q_1 and q_5 (See Figure 2). Assuming a constant supply pressure, P_s, the instantaneous power is given by:

$$P_H = P_s(q_1 + q_5) \tag{32}$$

The item of interest in this study is the comparison of the total energy required in runs of equal time duration. Therefore the parameter used is:

$$E_H = \int_0^t P_s(q_1+q_5)dt \qquad (33)$$

Peak power can, of course, be computed from the previously defined maximum flow rate and average power if desired can be found from total energy divided by run time.

The maximum speed at which the vehicle should operate over terrain will be dependent upon the ability of the gunner to function effectively. Vertical Absorbed Power Level (VAPL) has been developed as a measure of the severity of the ride (8) and is used in this study as the criterion for choosing vehicle speed.

Operating speeds were chosen for each of the three terrains used to result in VAPL's of 2, 4 and 6 watts at the gunner's station. Thus the comparison of system operation over various terrains was made based upon comparable ride characteristics experienced by the gunner.

A modal analysis technique described in reference 4 was used to obtain the modes associated with the flexible weapon model. The first four modal frequencies of 11.77, 26.91, 56.15, and 61.83 hertz were used as input to the DADS program.

The DADS 3-D code permits modeling of the vehicle in three dimensions, allowing interaction between elevation and azimuth motion of the weapon to be studied. Similar control loop models were used for the elevation and azimuth drive systems, with parameters chosen to be compatible with the different moments of inertia about the two axes.

A transient response of the weapon angle with the vehicle stationary is shown in Figure 6 to illustrate the general behavior of the unforced system. Figures 7 to 9 show the vehicle and weapon responses for a typical simulation run over terrain.

The dynamic pointing error behavior for a planar model of the concept vehicle operating over terrain is shown in Figures 10 to 15. The results shown were obtained from simulation runs using the DADS-2D code and the simulation model developed above.

Figures 10 to 12 show the effect of varying the speed over a fixed terrain to obtain desired values of Vertical Absorbed Power Level (VAPL). The ordinate is the percent of time during which the pointing error falls within the band given on the abscissa. In general three terrains were used with three

VAPL's for each. No data are shown for the 6 watt VAPL with the APG9 terrain since the vehicle speed required to reach this condition was beyound the feasible range.

Figures 13 to 15 present the same data replotted to show the effect of operating over the different terrains at a fixed VAPL.

It is seen that neither a fixed profile nor a fixed VAPL results in a consistent correlation with the error profile. For example, from Figure 11 it can be seen that increasing the speed over the APG-12 terrain results in reduced dynamic pointing errors over the entire range covered. However, Figure 12 shows that the worst results are obtained at the intermediate speed (VAPL = 4 watts) with better performance at both lower and higher speeds. These results clearly indicate that , while VAPL is an excellent criterion for determining a feasible environment for a human operator, it is not by itself adequate for use as a correlation parameter for weapon dynamic pointing error performance. This result can be explained by refering to the simplified model developed above. The effects of vertical and pitch motions of the chassis were shown as separate disturbance inputs to the control loop. Therefore, the specification of VAPL, which is a measure of the vertical motion, directly influences only one component of the disturbance input. Furthermore, inspection of the given terms associated with these signals (Equations 16 and 18) shows that the effect of pitch motion is much greater than that of vertical motion. (Using approximate maximum values of vertical and pitch accelerations and typical values for other terms, it can easily be verified that for the class of vehicles being considered, the pitch motion will dominate). This observation leads to the conclusion that gun mass unbalance will not by itself significantly alter the system behavior. It was shown that by proper choice of servoactuator parameters, inertia loads of different magnitudes could be controlled with the same dynamic behavior. Figures 16 and 17 show the responses obtained for a fully balanced and an unbalanced gun when the system parameters are set according to the criteria developed above. Conditions chosen represent the extremes in VAPL and terrain roughness levels used in this study and the essentially equivalent responses demonstrate the validity of the assumptions.

The system behavior is seen to be determined by the behavior obtainable with a given control configuration on a general system. Any degree of unbalance is accommodated by proper adjustment of system parameters. The control loop itself is therefore not of primary importance in a study of the effect of gun mass unbalance unless the system involved is one in which the vertical motion input is of primary significance.

The effect of modeling the gun tube as a flexible body rather than as a rigid body is shown in Figures 18 and 19.

Figure 18 shows the difference between the angular response of the two end elements using a model consisting of the first four flexible tube bending modes. A typical gun tube slope profile at a fixed time is shown in Figure 19.

The response of the three dimensional system is shown in Figures 20 to 23. This data was obtained using the DADS-3D code with active control of both elevation and azimuth axes. The terrain input was introduced by delaying the left hand side terrain profile by 5 feet in order to introduce a yaw angle input.

CONCLUSIONS AND RECOMMENDATIONS

A review of the results of this study shows that the feasibility of identifying system response characteristics through the use of an overall system simulation has been established. The simplified control model used permitted the basic system behavior to be studied without unnecessary complication. Modification of the basic system to include more sophisticated models is a matter of extension, based more on the ability to satisfactorily deal with questions of accuracy, convergence and scale than on the question of basic feasibility.

The mass unbalance problem is shown to be influenced very strongly by the relative sensitivities of the system to pitch inputs and to vertical inputs. For the class of vehicle considered, it appears that the disturbance input to the control loop due to vertical accelerations in the presence of mass unbalance is essentially negligible. This changes the entire complexion of the problem from one of concern for compensating for inertially induced disturbances to one of treating systems which differ significantly only in the magnitude of the mass loading. Under these conditions, it is shown that proper choice of servoactuator parameters will result in the system responses being the same for both balanced and unbalanced systems. However, the system which is mass balanced will require a greater power input for operation. Therefore the results indicate that the unbalanced system will be preferable from both the weight and energy consumption points of view with no additional control problems introduced.

An analysis of the error performance as a function of VAPL shows that the same phenomenon that influenced the mass unbalance problem is also important in this context. Since VAPL is a measure of vertical motion, the relative importance of pitch motion as a disturbance input means that if pitch motion and vertical motion are not directly related, VAPL and error will not be correlated. Considering the motion of a tracked vehicle over terrain, it is reasonable to expect that at higher speeds much of the terrain irregularity will be filtered out by the vehicle mass and suspension characteristics. This will be especially true of the pitch motion.

The above conclusions demonstrate the effectiveness of the overall simulation in bringing out performance characteristics which are strongly influenced by interaction between subsystems. While most of these effects could be discovered by careful analysis of the separate subsystems, this procedure is neither as efficient nor as reliable as a combined treatment.

The models used in this study were designed to allow certain characteristics and trends to be investigated and not to represent a final design configuration. Future efforts should be directed toward improvement in the overall models and development of effective design procedures based on overall system simulation. The success of efforts in this direction is very much dependent upon the adequacy of the models and the accuracy of the simulation results. This requires a well designed program of validation of results with experimental data. Only when the accuracy of the results has been conclusively demonstrated will sufficient confidence be generated to undertake serious design based upon simulation. The establishment of such confidence should be the next step toward the goal of computer aided design of integrated vehicle systems and ultimately of the inclusion of optimal criteria in the design process.

REFERENCES

1 Wehage R.A. and Haug, E.J., "Generalized Coordinate Partitioning for Dimension Reduction in Analysis of Constrained Dynamic Systems," Journal of Mechanical Design, Vol. 104, 1981, pp. 247-255.

2 Nikravesh, P.E. and Chung, I.S., "Application of Euler Parameters to the Dynamic Analysis of Three Dimensional Constrained Mechanical Systems," Journal of Mechanical Design, to appear July 1982.

3 Chung, I.S. Chang, C.O., Haug, E.J. and Wehage, R.A., "Dynamic Analysis of Three Dimensional Constrained Mechanical Systems Using Euler Parameters," Technical Report No. 81-11, CCAD, The University of Iowa, October 1981.

4 Shabana, Ahmed and Wehage, R.A., "Variable Degree-of-Freedom Component Mode Analysis of Inertia Variant Flexible Mechanical Systems," Technical Report No. 81-12, CCAD, The University of Iowa, December 1981.

5 Saifer, M.T. and Becher, R.S., "Dynamic Analysis of the 75 mm ADMAG Gun System," TR#81-02, S & D Dynamics, Inc., April 1981.

6 Shabana, A., Wehage, R.A., "A Coordinate Reduction Technique for Substructures with Large Angular Rotations," to appear in the Journal of Structural Mechanics.

7 Lance, G.M., "Control of Systems with Mass Unbalance," Technical Report No. 81-8, CCAD, The University of Iowa, September 1981.

8 Lins, W.F., "Human Vibration Response Measurement," Technical Report No. 11551, Mobility Systems Laboratory, Mobility Systems Laboratoy, TACOM, June 1972.

TABLE 1

Control Parameter Values

	2-D Model		3-D Model	
	Balanced	Unbalanced	Elevation	Azimuth
A	13.6	12	12	14.9 (effective
C	83.9	74	74	91.8
AF	0.133	0.117	0.117	0.145
CF	100			
KV	15			
B	0.0187			
KF	1.0			

$A = in^2$, $C = \frac{in^3}{sec\ \sqrt{T6}}$, $AF = in^2$, $CF = \frac{in^3}{sec\ \sqrt{T6}}$, $KV = {}^{in}/_{v}$,

$B = {}^{v\text{-}sec}/_{rad}$, and $KF = {}^{v}/_{rad}$

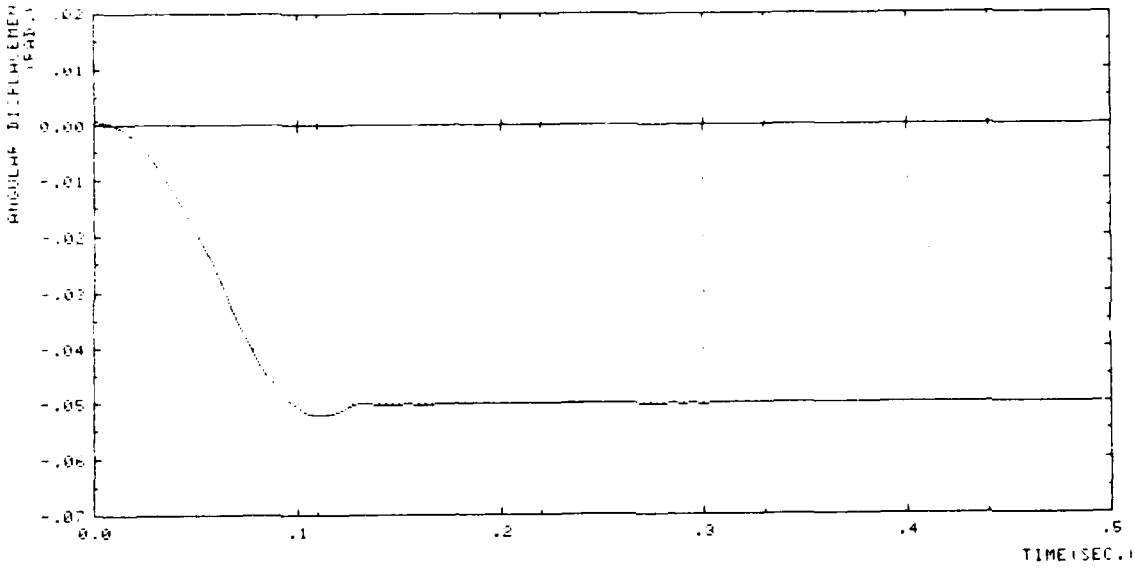


Figure 6. Transient Response of Gun Angle

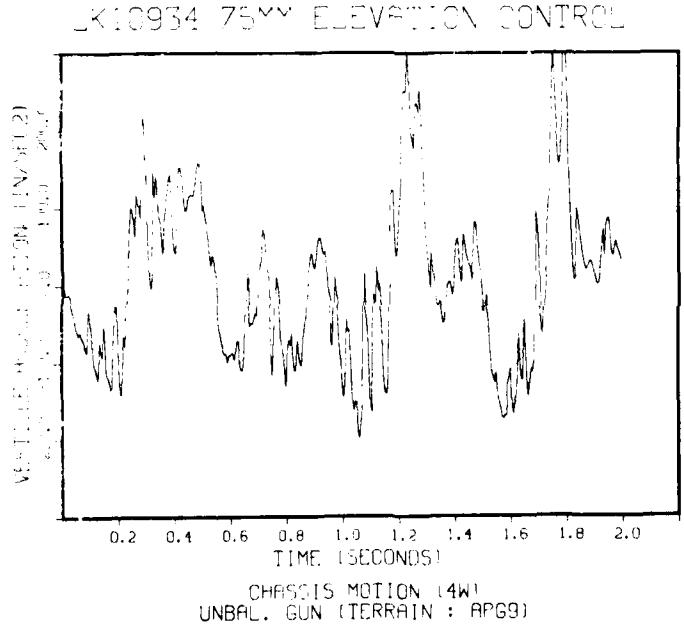


Figure 7. Chassis Vertical Acceleration

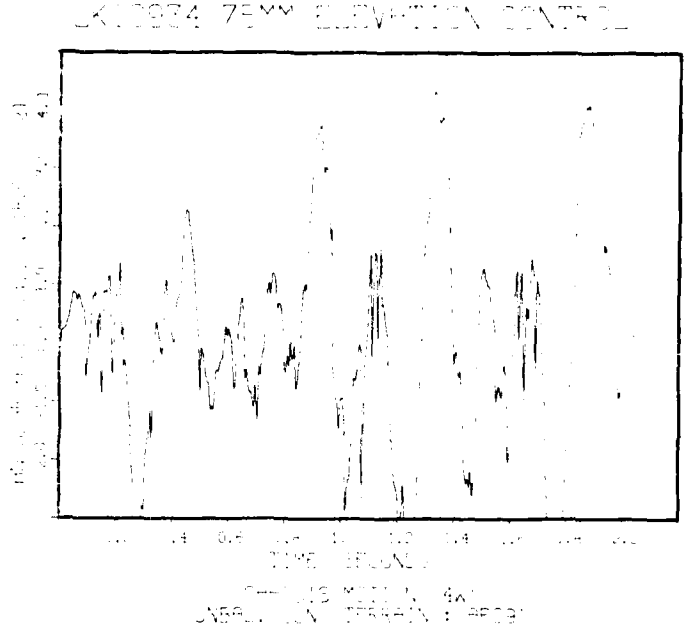


Figure 8. Chassis Angular Acceleration

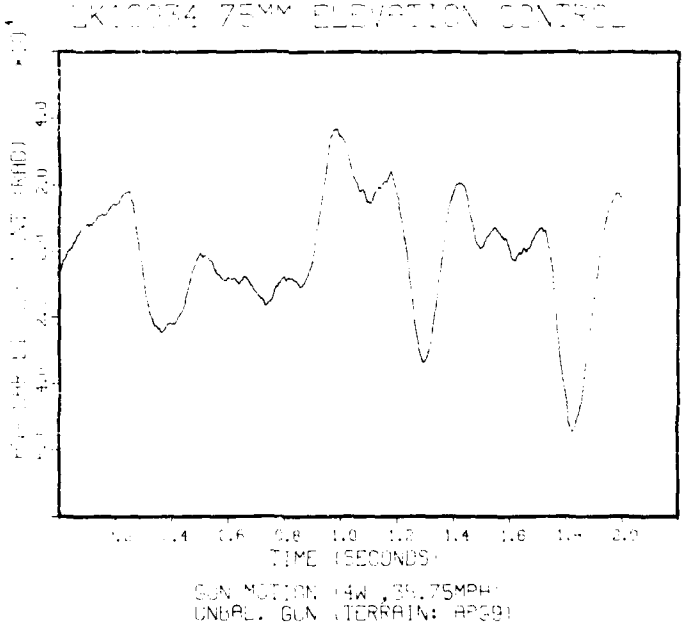


Figure 9. Weapon Angular Displacement

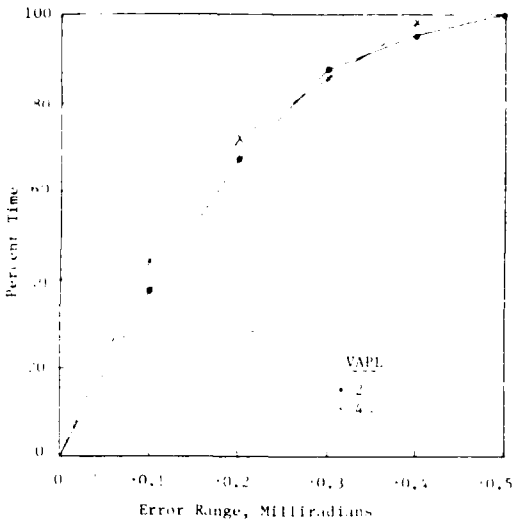


Figure 10. Error Distribution - APG9

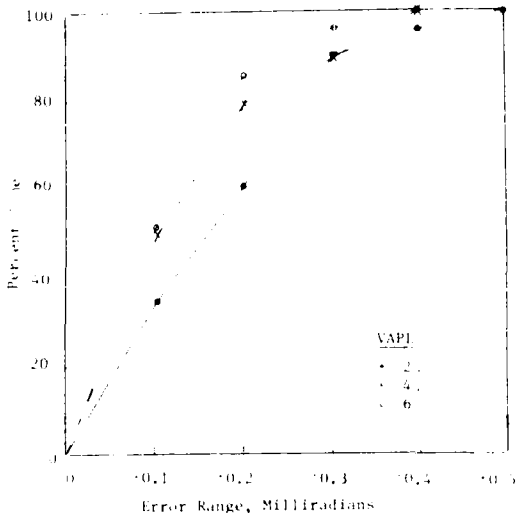


Figure 11. Error Distribution - APG12

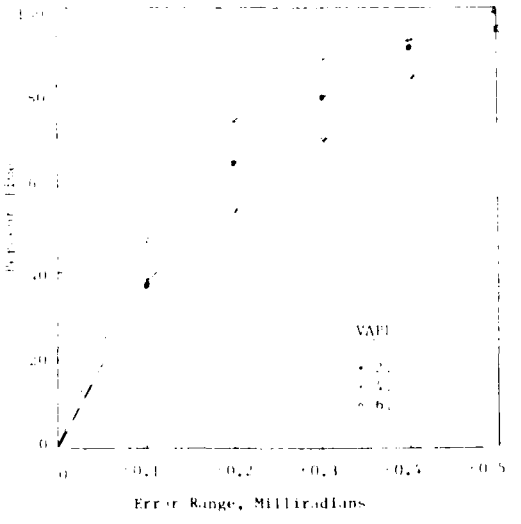


Figure 12. Error Distribution - APG29

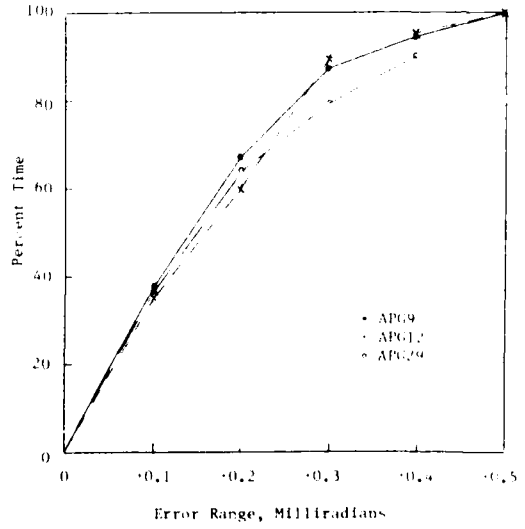


Figure 13. Error Distribution - VAPL=2

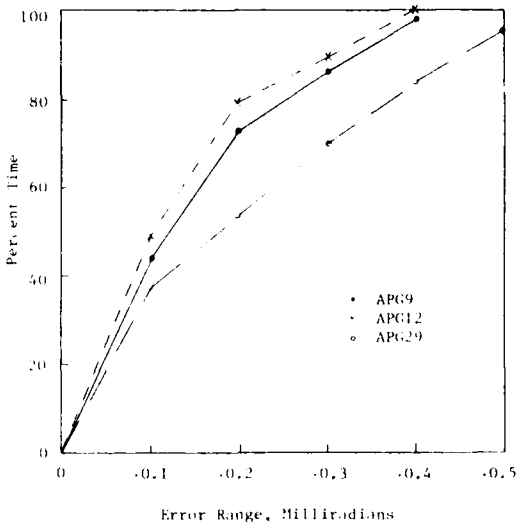


Figure 14. Error Distribution - VAPL=4

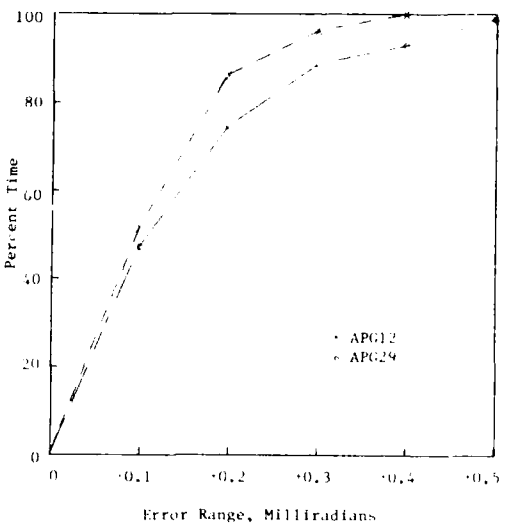


Figure 15. Error Distribution - VAPL=6

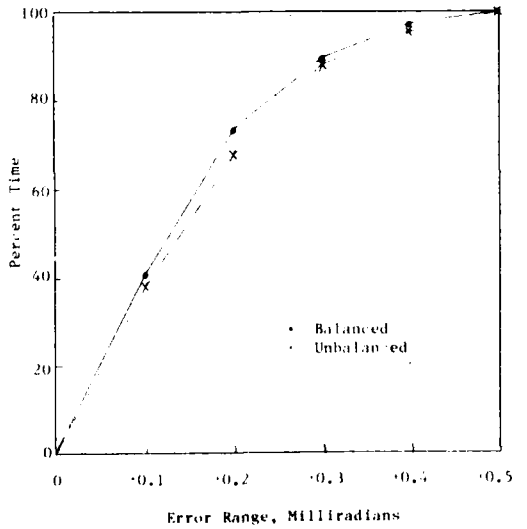


Figure 16. Error Comparison - APG9, VAPL=2

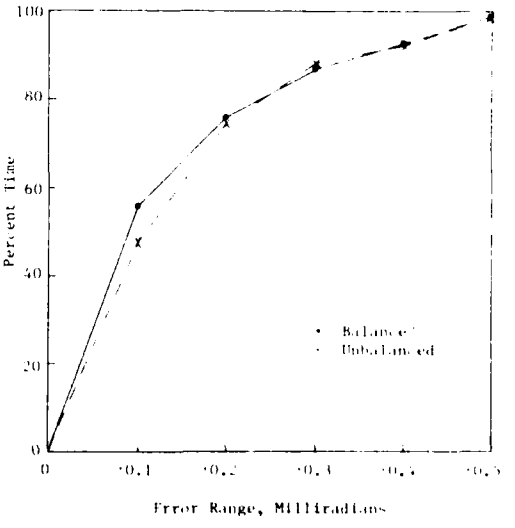


Figure 17. Error Comparison - APG29, VAPL=6

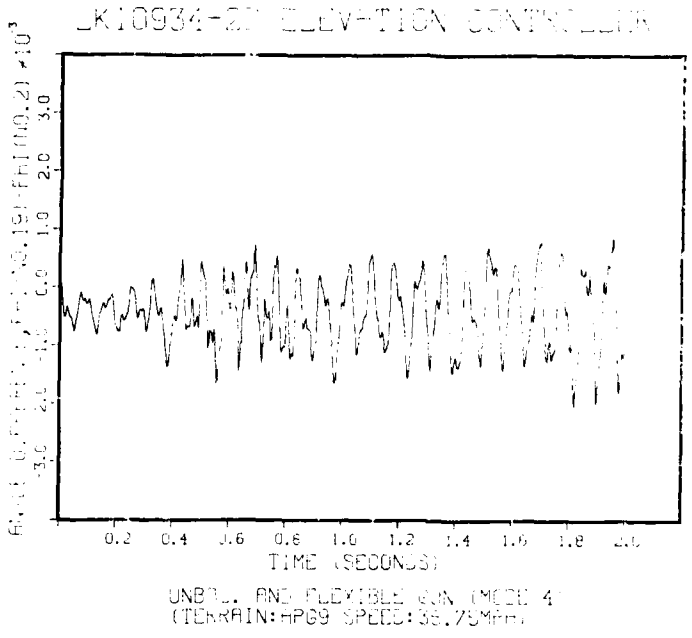


Figure 18. Flexible Tube Response-Difference

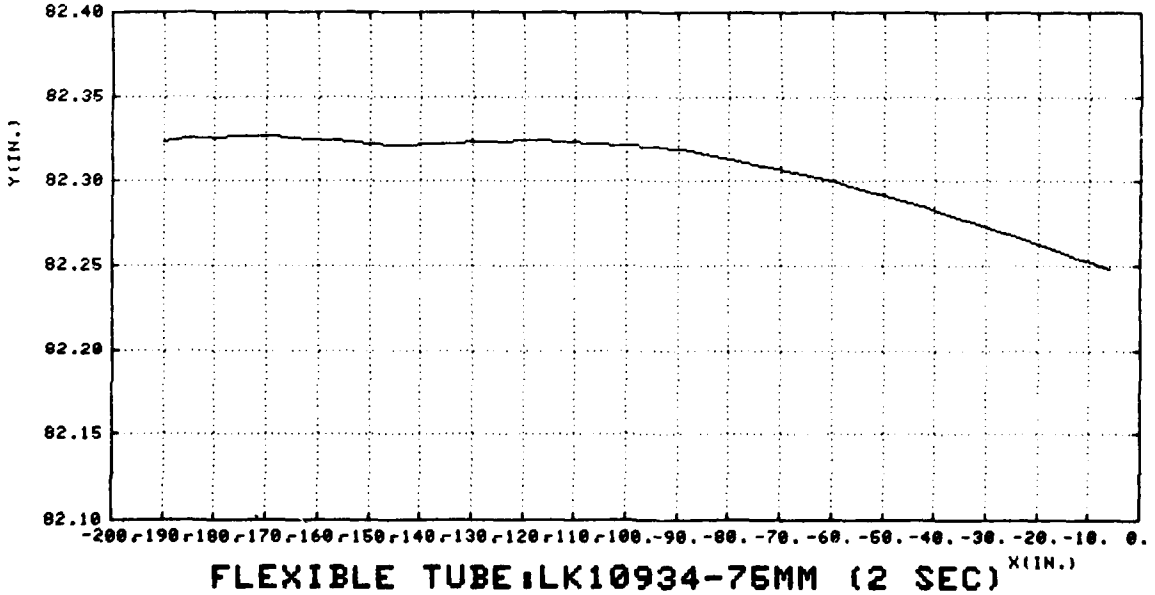


Figure 19. Typical Tube Profile

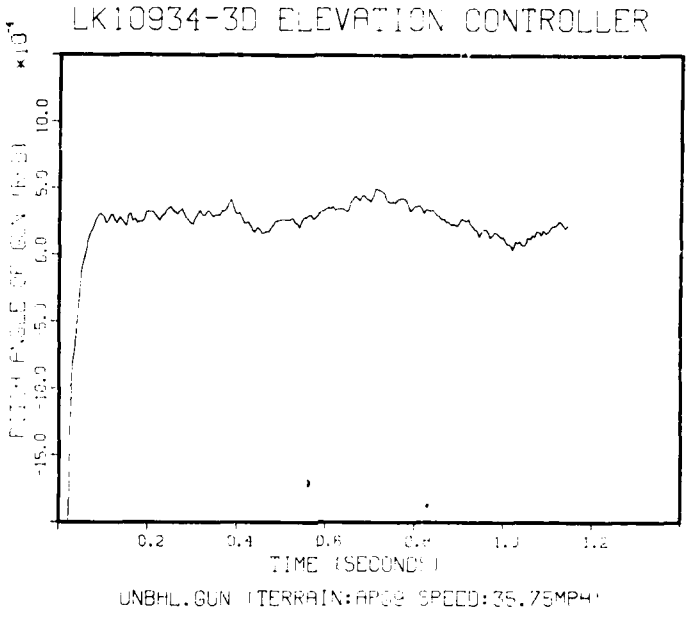


Figure 20. 3-D Model - Gun Pitch Angle

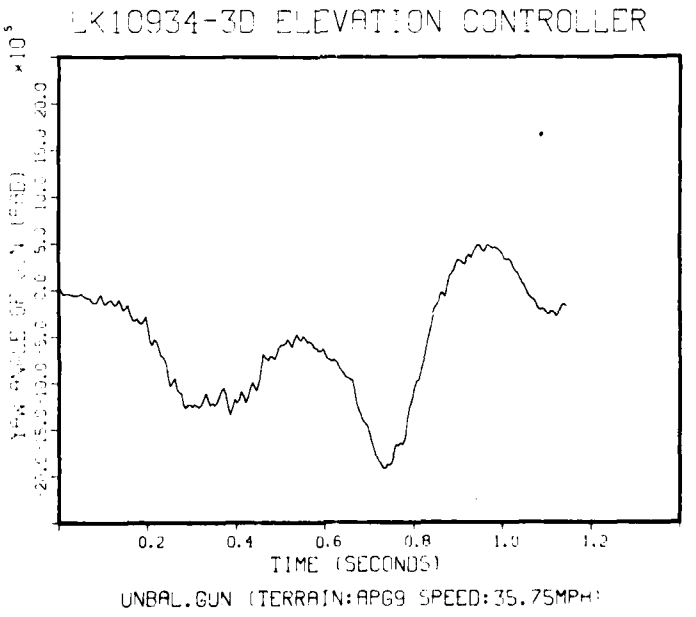


Figure 21. 3-D Model - Gun Yaw Angle

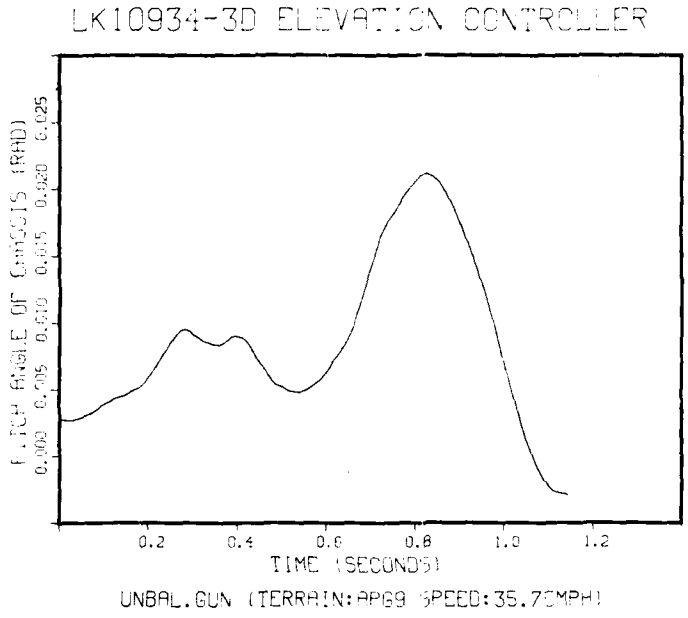


Figure 22. 3-D Model - Chassis Pitch Angle

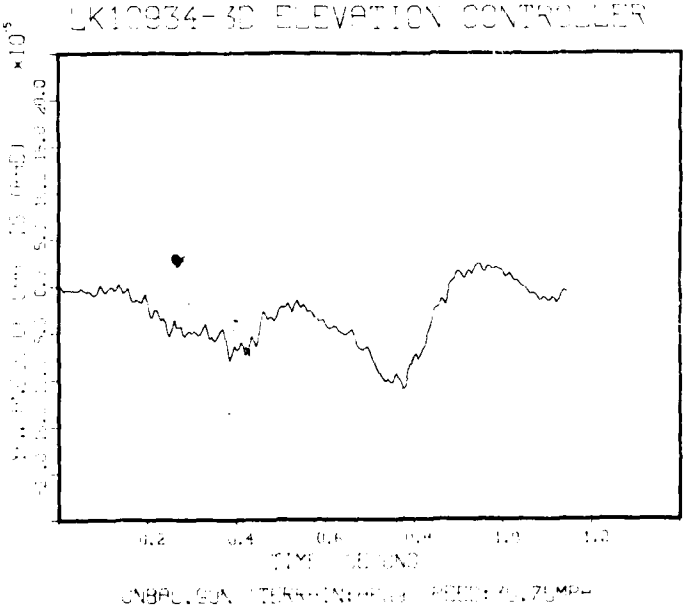


Figure 23. 3-D Model - Chassis Yaw Angle

AD P001084

FULL SCALE SIMULATION OF LARGE SCALE MECHANICAL SYSTEMS

Edward J. Haug and Gerald Jackson
Center for Computer Aided Design,
College of Engineering, The University of Iowa,
Iowa City, Iowa 52242 Phone: (319) 353-3820
and
Ronald Beck
U.S. Army Tank-Automotive Command
Warren, Michigan 48090

1. SUMMARY

This paper presents a computer-based method for formulation and solution of coupled differential and algebraic equations describing large scale mechanical systems, including feedback control, aerodynamic forces, and other multidisciplinary effects that interact with the mechanical system. An Euler parameter representation of the configuration of the mechanical system is employed to obtain singularity free solution for generalized coordinates and a much simplified algebraic formulation of the governing system of equations, compared with the more classical Euler angle generalized coordinate formulation. A generalized coordinate partitioning algorithm is employed to automatically identify independent generalized coordinates and reduce the dimension of the numerical integration problem. Animated graphics output is employed to assist in visualization of dynamic performance of several systems, including an aerobalistic device and wheeled and tracked vehicles.

2. INTRODUCTION

The field of computer aided dynamic analysis of mechanisms and machines has seen substantial development during the past decade, with introduction of planar system dynamic codes (Chace and Smith, 1971; Paul and Krajcinovic, 1970) and more recently general purpose spatial system dynamic simulations (Sheth and Uicker, 1972; Orlandea, Chace and Calahan, 1977). These codes treat rigid body mechanism and machine dynamics and have not been extended to incorporate interdiciplinary aspects of large scale dynamic systems. In this respect, the field of mechanical system dynamics lags substantially behind the better developed fields of electrical circuit analysis and especially the well developed field of finite element structural analysis.

The computer based system dynamic analysis technique presented in this paper has been developed (Wehage and Haug, 1982b; Nikravesh and Chung, 1982) with the objective of automated

generation of the governing equations for constrained dynamic systems and coupled with differential and algebraic equations representing feedback control subsystems, hydraulic subsystems, vehicle power plants, aerodynamic forces, and other interacting subsystems that make up modern automotive and industrial equipment. While the development here is limited to mechanical systems composed of rigid bodies, a recent development allows for direct extension of the technique and computer code to incorporate effects of flexibility of elastic bodies, making up the mechanical systems (Song and Haug 1980; Shabana and Wehage, 1981).

3. MECHANICAL SYSTEM REPRESENTATION

In order to specify the position of a rigid body in an inertial (global) xyz coordinate system, it is sufficient to specify the spatial location of the origin and the angular orientation of a $\xi\eta\zeta$ coordinate system that is rigidly attached to the body. In this paper, coordinate rotations are defined by Euler parameter generalized coordinates (Nikravesh and Chung, 1982; Wittenburg, 1977).

3.1 EULER PARAMETER GENERALIZED COORDINATES

Let the $\xi_i\eta_i\zeta_i$ axes be attached to the ith body of the system, as shown in Fig. 3.1, where the origin O_i is located at the center of mass of the body. A point P_i on body i is located in the inertial coordinate system by

$$\underline{r}^{P_i} = \underline{r}^i + A^i \underline{s}'^{P_i} \tag{3.1}$$

where $\underline{s}'^{P_i} \equiv [\xi^P, \eta^P, \zeta^P]_i^T$ are the coordinates of in the $\xi_i\eta_i\zeta_i$ coordinate system, $\underline{r}^i \equiv [x,y,z]_i^T$ are the coordinates of O_i in the xyz coordinate system, and Ai is the rotational transformation matrix of body i. Matrix Ai, expressed in terms of Euler parameters e_0^i, e_1^i, e_2^i, and e_3^i, is (Nikravesh and Chung, 1982)

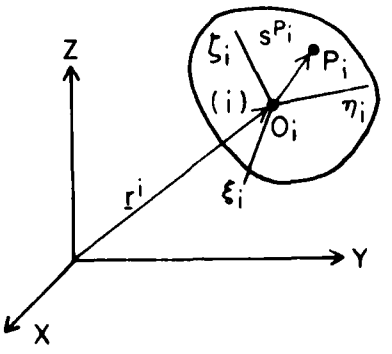


Fig. 3.1 Body-Fixed $\xi_i\eta_i\zeta_i$ and Global xyz Coordinate Systems

$$A^i = 2 \begin{bmatrix} e_0^2+e_1^2-1/2 & e_1e_2-e_0e_3 & e_1e_3+e_0e_2 \\ e_1e_2+e_0e_3 & e_0^2+e_2^2-1/2 & e_2e_3-e_0e_1 \\ e_1e_3-e_0e_2 & e_2e_3+e_0e_1 & e_0^2+e_3^2-1/2 \end{bmatrix}_i \qquad (3.2)$$

where the four Euler parameters are required to satisfy the equation

$$e_0^2 + \underline{e}^T\underline{e} = e_0^2 + e_1^2 + e_2^2 + e_3^2 = 1 \qquad (3.3)$$

The vector of parameters $\underline{e} \equiv [e_1,e_2,e_3]^T$ are the xyz components of a vector lying on the axis of rotation about which the body can be rotated from a reference position (in which the xyz and $\xi\eta\zeta$ axes are parallel) to the current position, as shown in Fig. 3.2. The vector $\underline{e}$ is defined by

$$\underline{e} = \underline{u} \sin \frac{\chi}{2} \qquad (3.4)$$

where $\underline{u}$ is a unit vector on the axis of rotation and χ is the angle of rotation. Existence of the axis is assured by Euler's theorem (Wittenberg, 1977). The fourth parameter e_0 is defined as

$$e_0 = \cos \frac{\chi}{2} \qquad (3.5)$$

Since $\underline{u}$ is a unit vector and $\sin^2(\chi/2)+\cos^2(\chi/2)=1$, Eq. 3.3 follows from Eqs. 3.4 and 3.5.

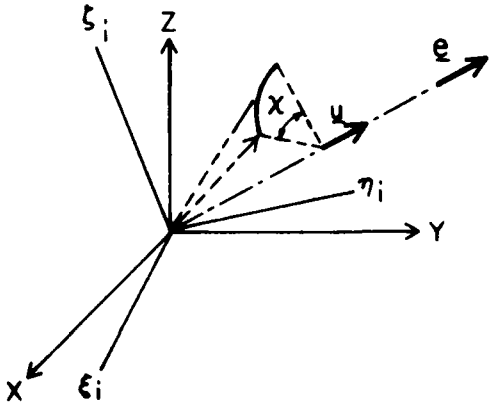


Fig. 3.2 Angular Rotation of $\xi_i\eta_i\zeta_i$ Coordinate System about $\underline{u}$ Axis

3.2 CONSTRAINT EQUATIONS

Standard constraints between rigid bodies are taken as friction free (workless) joints. Formulations for three constraints are pesented here as follows:

Spherical Joint: Figure 3.3 shows two adjacent bodies i and j connected by a spherical joint (ball joint). A vector loop equation can be written as

$$\underline{r}^i + \underline{s}^i - \underline{s}^j - \underline{r}^j = \underline{0} \tag{3.6}$$

Using Eq. 3.1, this equation can be rewritten as

$$\underline{r}^i + A^i \underline{s}'^{P_i} - \underline{r}^j - A^j \underline{s}'^{P_j} = \underline{0} \tag{3.7}$$

where the center P of the ball joint is located by the body-fixed vectors $\underline{s}'^{P_i}$ and $\underline{s}'^{P_j}$ in bodies i and j, respectively.

Revolute Joint: Figure 3.4 depicts a revolute joint between bodies i and j. Point P is common to both bodies and points Q_i and Q_j are located on bodies i and j, respectively, defining the axis of rotation of the joint. Equation 3.7 also holds for this joint. Additional constraints are obtained by requiring the cross product of vectors $\underline{g}i$ and $\underline{g}j$ to be zero, which forces the points P, Q_i, and Q_j to lie on a common line. Vectors $\underline{g}i$ and $\underline{g}j$ can be expressed in component form as

$$\underline{g}^k \equiv A_k(\underline{s}'^{Q_k} - \underline{s}'^{P_k}) \quad , \qquad k = i,j \tag{3.8}$$

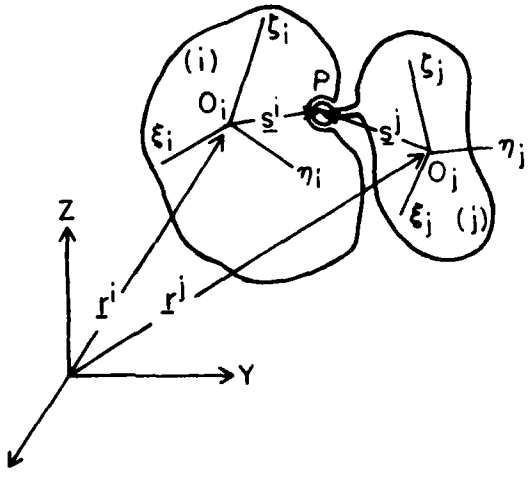


Fig. 3.3 Spherical Joint

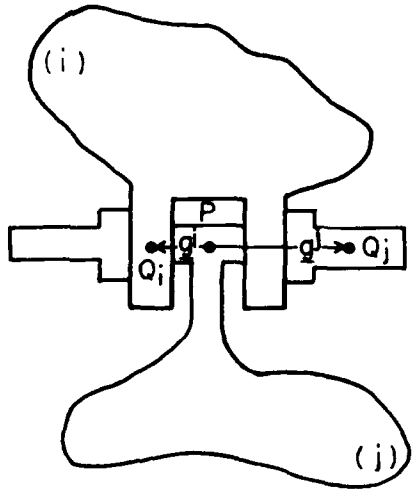


Fig. 3.4 Revolute Joint

Then, the cross product of $\underline{g}^i$ and $\underline{g}^j$, set equal to zero, yields three scalar equations

$$\tilde{\underline{g}}^i \, \underline{g}^j = \underline{0} \tag{3.9}$$

where $\underline{g}^i = [u,v,w]_i^T$, and $\tilde{\underline{g}}^i$ is a skew-symmetric matrix containing the components of $\underline{g}^i$, defined as

$$\tilde{\underline{g}}^i \equiv \begin{bmatrix} 0 & -w & v \\ w & 0 & -u \\ -v & u & 0 \end{bmatrix}_i$$

From the three scalar equations of Eq. 3.9, only two are independent. The best two should be selected, along with Eq. 3.7, to form five constraint equations for the revolute joint. To avoid numerical difficulties, proper selection of equations from Eq. 3.9 is important, particularly when the joint axis is parallel to one of the global axes. For example, when the joint axis is parallel to the z axis, the first equation of Eq. 3.9 yields singular equations. The second and third equations would be selected in this case. The technique used here for selection of the proper equations is to compare the absolute values of u_i, v_i, and w_i (or u_j, v_j, and w_j) and select the two equations having the largest terms.

Translational Joint: A translational joint forces two bodies i and j to move along a common axis without relative rotation about that axis. Four points, P_i and Q_i on body i and P_j and Q_j on body j, are selected to lie on the same axis, as shown in Fig. 3.5. The vectors $\underline{g}^i$, $\underline{g}^j$, and $\underline{g}^{ij}$ are required to remain colinear. Therefore, it is required that

$$\tilde{\underline{g}}^i \, \underline{g}^j = \underline{0} \tag{3.10}$$

$$\tilde{\underline{g}}^i \, \underline{g}^{ij} = \underline{0} \tag{3.11}$$

where two equations from Eq. 3.10 and two from Eq. 3.11 should be selected, based on the technique described for the revolute joint. To assure that the two bodies cannot rotate relative to each other, one additional equation is required. Two vectors, $\underline{h}^i$ and $\underline{h}^j$ on bodies i and j, shown in Fig. 3.5, are selected to be perpendicular, so it is required that

$$\underline{h}^{iT} \, \underline{h}^j = 0 \tag{3.12}$$

The four independent equations from Eqs. 3.10 and 3.11 and the scalar equation of Eq. 3.12 constitute the five equations of the translational joint.

Numerous other standard joints may be formulated in the same way (Nikravesh and Chung, 1982), including cylindrical, universal and composite joints. Once each of the standard joints is defined algebraically, the composite set of joint equations of a large scale system can be automatically assembled. This approach is analogous to assembling a finite element model of a structure from element stiffness and mass matrices.

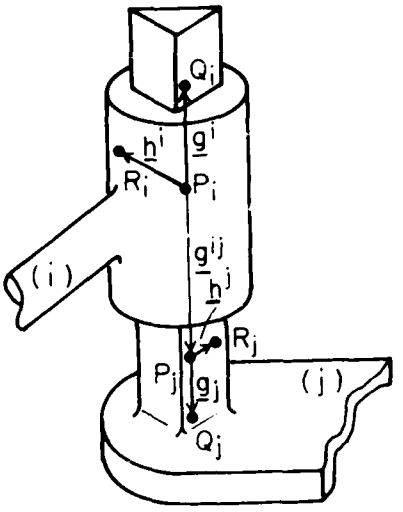


Fig. 3.5 Translational Joint

3.3 EQUATIONS OF RIGID BODY DYNAMICS

For body i, let $\underline{\omega}'^i = [\omega_\xi, \omega_\eta, \omega_\zeta]_i^T$ be the projection of the angular velocity vector onto the local coordinate axes, $\underline{r}_i = [x,y,z]_i^T$ be the global location of the center of mass, m_i be the mass and $I_{\xi\xi}$, $I_{\eta\eta}$, $I_{\zeta\zeta}$, $I_{\xi\eta}$, $I_{\eta\zeta}$, and $I_{\zeta\xi}$ be the moments and products of inertia about the ξ_i, η_i, and ζ_i axes. The kinetic energy of the ith body can be written as (Goldstein, 1980)

$$T_i = \frac{1}{2} \dot{\underline{r}}^{iT} J^i \dot{\underline{r}}^i + \frac{1}{2} \underline{\omega}'^{iT} I^i \underline{\omega}'^i \qquad (3.13)$$

where

$$J^i = \begin{bmatrix} m & 0 & 0 \\ 0 & m & 0 \\ 0 & 0 & m \end{bmatrix}_i , \quad I^i = \begin{bmatrix} I_{\xi\xi} & I_{\xi\eta} & I_{\xi\zeta} \\ I_{\eta\xi} & I_{\eta\eta} & I_{\eta\zeta} \\ I_{\zeta\xi} & I_{\zeta\eta} & I_{\zeta\zeta} \end{bmatrix}_i$$

Angular velocity $\underline{\omega}'^i$, in terms of Euler parameters, can be expressed as (Nikravesh and Chung, 1982)

$$\underline{\omega}'^i = 2B^i \dot{\underline{p}}^i$$

where $\underline{p}^i \equiv [e_0, e_1, e_2, e_3]_i^T$ and

$$B^i = \begin{bmatrix} -e_1 & e_0 & e_3 & -e_2 \\ -e_2 & -e_3 & e_0 & e_1 \\ -e_3 & e_2 & -e_1 & e_0 \end{bmatrix}_i \tag{3.15}$$

To simplify notation, let the kinematic constraint equations of all joints in the system, defined in Section 3.2, be written in the form

$$\underline{\Phi}(\underline{r}^1, \underline{p}^1, \underline{r}^2, \underline{p}^2, \ldots, \underline{r}^n, \underline{p}^n) = \underline{0} \tag{3.16}$$

where Φ is an m-vector of functions of the generalized coordinates of the n bodies making up the system.

Lagrange's equations of motion for the ith body may now be written as (Goldstein, 1980)

$$\frac{d}{dt}(T_{\cdot i})^T_{\underline{r}} + \underline{\Phi}^T_{\underline{r}\,i}\,\underline{\lambda} - \underline{f}^i = \underline{0} \qquad \text{(3 equations)} \tag{3.17}$$

$$\frac{d}{dt}(T_{\cdot i})^T_{\underline{p}} - T^T_{\underline{p}\,i} + \underline{\Phi}^T_{\underline{p}\,i}\,\underline{\lambda} - \underline{b}^i = \underline{0} \qquad \text{(4 equations)} \tag{3.18}$$

where $\underline{f}^i$ and $\underline{b}^i$ are the vectors of generalized forces and torques corresponding to generalized coordinates $\underline{r}^i$ and $\underline{p}^i$, respectively. Subscripts denote partial differentiation and $\underline{\lambda}$ is a vector of Lagrange multipliers corresponding to the constraints. It is well known (Goldstein, 1980) that the Lagrange multipliers define the joint reaction forces. Thus they provide an important output of the analysis.

Substitution of Eq. 3.13, with $T = \sum_{i=1}^{n} T_i$, into Eqs. 3.17 and 3.18 yields

$$J^i\,\ddot{\underline{r}}^i + \underline{\Phi}^T_{\underline{r}\,i}\,\underline{\lambda} = \underline{f}^i \tag{3.19}$$

$$4B^{iT}\,I^i\,B^i\,\ddot{\underline{p}}^i + \underline{\Phi}^T_{\underline{p}^i}\,\underline{\lambda} = \underline{b}^i + 8\dot{B}^{iT}\,I^i\,\dot{B}^i\,\underline{p}^i \tag{3.20}$$

Defining $\underline{G}^i = [\underline{f}^T,\ \underline{b}^T + 8\underline{p}^T \dot{B}^T I \dot{B}]_i^T$ and

$$M^i = \begin{bmatrix} J & 0 \\ 0 & 4B^T IB \end{bmatrix}_i \tag{3.21}$$

Equations 3.19 and 3.20 can be written as

$$M^i \ddot{\underline{q}}^i = \underline{G}^i - \underline{\Phi}_{\underline{q}^i}^T \underline{\lambda}\ ,\ i = 1,\ldots,n \tag{3.22}$$

where $\underline{q}^i = [\underline{r}^T,\underline{p}^T]_i^T \equiv [x,y,z,e_0,e_1,e_2,e_3]_i^T$. The total system equations of motion for n rigid bodies is then

$$M\ddot{\underline{q}} = \underline{G} - \underline{\Phi}_{\underline{q}}^T \underline{\lambda} \tag{3.23}$$

and the algebraic equations of Eqs. 3.3 and 3.16, where $M \equiv \text{diag.}\ [M^1,M^2,\ldots,M^n]$, $\underline{G} \equiv [\underline{G}^{1T},\underline{G}^{2T},\ldots,\underline{G}^{nT}]^T$, and $\underline{q} \equiv [\underline{q}^{1T},\underline{q}^{2T},\ldots,\underline{q}^{nT}]^T$. This is a nonlinear system of differential-algebraic equations.

3.4 FORCES OF SPRING-DAMPER-ACTUATORS

Internal forces acting between bodies due to the action of springs, dampers, and actuators may be obtained by a process similar to the constraint equation development of Section 3.2. For example, since springs, dampers, and actuators generally appear together, as shown in Fig. 3.6, they are incorporated into a single set of equations. Let the global coordinates of the attachment points be $\underline{r} = [u,v,w]_s$, s = i,j. The length of the spring-damper-actuator is thus

$$\ell = [(u_j - u_i)^2 + (v_j - v_i)^2 + (w_j - w_i)^2]^{1/2} \tag{3.24}$$

and the time rate of change of length is

$$\dot{\ell} = [(u_j - u_i)(\dot{u}_j - \dot{u}_i) + (v_j - v_i)(\dot{v}_j - \dot{v}_i) + (w_j - w_i)(\dot{w}_j - \dot{w}_i)]/\ell \tag{3.25}$$

The magnitude of the spring-damper-actuator force is

$$f = k(\ell - \ell^0) + c\dot{\ell} + a \tag{3.26}$$

where ℓ^0 is the undeformed length of the spring and k, c, and a are the spring rate, damping coefficient, and actuator force, respectively. The components of spring-damper-actuator force in the global coordinate system can be written

$$\underline{f}^s = f(\underline{r}^s - \underline{r}^m)/\ell \ , \ s,m = i,j \text{ and } s \neq m \tag{3.27}$$

Similar to the translational spring-damper-actuator, torsional spring-damper-actuator elements may be defined between adjacent bodies i and j that are connected by a revolute joint, as shown in Fig. 3.7. Two vectors $\underline{s}^i$ and $\underline{s}^j$, embedded in bodies i and j respectively, define a plane perpendicular to the revolute joint axis. In addition, the two vectors define the torsional spring attachment points on the two bodies. The angle between $\underline{s}^i$ and $\underline{s}^j$ is denoted by θ and is initially assumed to be $0 < \theta < \pi$. The angle θ can be calculated from the equation

$$\theta = \cos^{-1}\left[\underline{s}_i^T \underline{s}_j / |\vec{s}_i| \cdot |\vec{s}_j|\right], \quad 0 < \theta < \pi \tag{3.28}$$

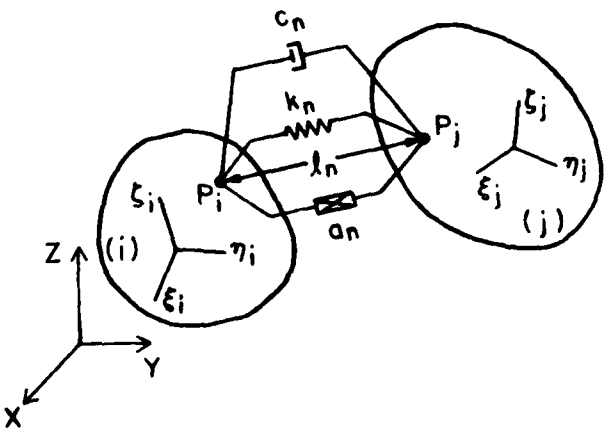


Fig. 3.6 Translational Spring-Damper-Actuator Element

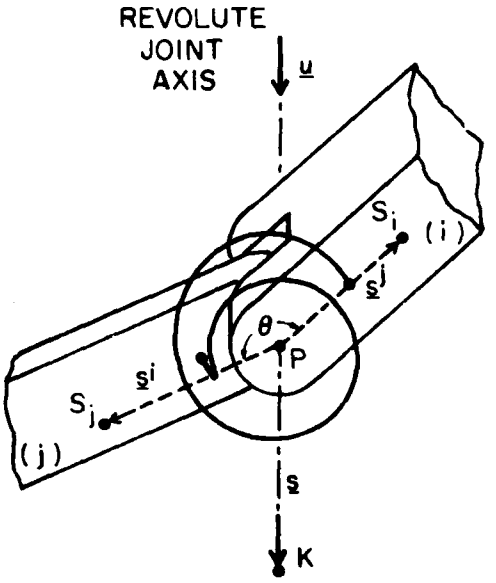


Fig. 3.7 Torsional Spring-Damper-Actuator Element

To determine all possible values of θ, a point K is initially defined on the revolute joint axis such that the direction of vector $\underline{s}$ is determined by the right-hand screw rule, rotating from $\underline{s}^i$ to $\underline{s}^j$ and sweeping through an angle θ (initially $0 \leq \theta \leq \pi$). During dynamic analysis, the cross product of $\underline{s}^i$ and $\underline{s}^j$ yields a vector parallel to $\underline{s}$, having the same direction if $0 \leq \theta \leq \pi$, and opposite direction if $\pi \leq \theta \leq 2\pi$, i.e.;

$$\underline{s}^T \underline{\tilde{s}}^i \underline{s}^j \begin{cases} > 0 \; ; & 0 \leq \theta \leq \pi \\ \\ < 0 \; ; & \pi \leq \theta \leq 2\pi \end{cases} \tag{3.29}$$

The torque of a torsional spring-damper-actuator element can now be written as

$$b = k_t(\theta - \theta^0) + c_t\dot{\theta} + a_t \tag{3.30}$$

where k_t, c_t, a_t, and θ^0 are the torsional spring stiffness, damping coefficient, actuator torque and undeformed angle of the element, respectively.

The translational and torsional spring-damper-actuator forces of Eqs. 3.27 and 3.28 are now transformed to generalized forces $\underline{f}^i$ and b^i in Eqs. 3.19 and 3.20, using the principle of virtual work. For details of this reduction, the reader is referred to Nikravesh and Chung (1982). While the default values of the parameters k, c, ℓ^0, a, k_t, c_t, θ^0, and a_t in Eqs. 3.26 and 3.30 are constants, these parameters can be prescribed as general nonlinear functions of the generalized coordinates $\underline{q}$, $\dot{\underline{q}}$, and the Lagrange multipliers $\underline{\lambda}$. This generality allows for representation of friction in joints, since $\underline{\lambda}$ defines the normal load $N(\underline{\lambda})$ in a joint and a friction force $\mu N(\underline{\lambda})$ may be represented. Further, general nonlinear springs and dampers can be represented and actuator forces can be used to represent control inputs.

4. INCORPORATION OF CONTROL AND OTHER EFFECTS

Virtually all modern large scale mechanical systems involve feedback controllers, hydraulic or electrical actuators, and other interdisciplinary subsystems that interact to influence the dynamics of the system. It is thus important that a usable computer aided analysis formulation explicitly include such effects.

Consider first a feedback control subsystem or a hydraulic subsystem that is described by a set of differential equations of the form

$$\dot{\underline{r}} = \underline{F}(\underline{q},\dot{\underline{q}},\underline{r},t) \tag{4.1}$$

where $\underline{r}$ is a vector state variable of the controller. The output of the controller is a set of driving forces that can be written as generalized forces contributing to the equations of motion of Eq. 3.23; i.e,

$$\underline{G}^c = \underline{G}^c(\underline{q},\dot{\underline{q}},\underline{r},t) \tag{4.2}$$

The form of the force input to the system will, of course, be dependent on the nature of the controller. In particular cases, one may be able to input the control driving effect explicitly as an actuator force or torque in a translational or torsional spring-damper-actuator. This is true for hydraulic rams, hydraulic motors, and electric motors. In such cases, the control actuator force is automatically incorporated into the the generalized force vector $\underline{G}$ by the spring-damper-actuator equations of Section 3.4.

Similarly, aerodynamic forces, ground-vehicle interface forces, metal cutting forces on machine tools, and other forces that depend in a complex way on the kinematic state $\underline{q}$ and $\dot{\underline{q}}$ may be incorporated into the model. It is clear that such effects can be routinely incorporated into the formulation, provided that the engineer can write expressions for the forces in terms of $\underline{q}$ and $\dot{\underline{q}}$. Examples of such effects are discussed in Section 6, where references are given to more detailed literature on the subject.

It is important to note that force input to the mechanical system from interdisciplinary effects, represented by Eq. 4.2, couple the differential equations of motion of Eq. 3.23 and control equations of Eq. 4.1. Thus, the system state equations of motion to be integrated include the differential equations of Eqs. 3.23 and 4.1, with the control force $\underline{G}_c$ of Eq. 4.2 included in $\underline{G}$ of Eq. 3.23, the algebraic equations of kinematic constraint of Eq. 3.16, and a set of initial conditions on $\underline{q}$, $\dot{\underline{q}}$, and $\underline{r}$. This is, at best, a complex set of differential-algebraic equations.

5. NUMERICAL INTEGRATION OF SYSTEM EQUATIONS OF MOTION

Presuming that the kinematic constraint equations of Eq. 3.16 written here in the form

$$\underline{\Phi}(\underline{q}) = \underline{0} \tag{5.1}$$

are independent, one can use a Gauss-Jordan reduction algorithm with double pivoting (Wehage and Haug, 1982b) on the Jacobian matrix

$$\underline{\Phi}_{\underline{q}} \equiv \left[\frac{\partial \Phi_i}{\partial q_j}\right] \tag{5.2}$$

to partition the vector $\underline{q}$ into $\underline{q} = [\underline{u}^T, \underline{v}^T]^T$, where $\underline{u}$ are dependent and $\underline{v}$ are independent generalized coordinates. The implicit function theorem of calculus (Hildebrand, 1976) guarantees that it is theoretically possible to solve Eq. 5.1 for $\underline{v} = f(\underline{u})$. In practice, however, this is impossible. To overcome this practical difficulty, an implicit elimination process is used here; i.e., when $\underline{v}$ is fixed, $\underline{u}$ is determined by Newton-Raphson iteration to solve Eq. 5.1 for $\underline{u}$. For details, see Wehage and Haug (1982b).

Differentiating Eq. 5.1 with respect to time, one has the velocity equation

$$\underline{\Phi}_{\underline{u}}\, \dot{\underline{u}} + \underline{\Phi}_{\underline{v}}\, \dot{\underline{v}} = \underline{0} \tag{5.3}$$

which can be solved for $\dot{\underline{u}}$, once $\dot{\underline{v}}$ is known, since $\underline{\Phi}_{\underline{u}}$ is non-singular. Differentiating Eq. 5.3 with respect to time yields the acceleration equation

$$\underline{\Phi}_{\underline{u}}\, \ddot{\underline{u}} + \underline{\Phi}_{\underline{v}}\, \ddot{\underline{v}} + (\underline{\Phi}_{\underline{u}}\, \dot{\underline{u}})_{\underline{u}}\dot{\underline{u}} + (\underline{\Phi}_{\underline{v}}\, \dot{\underline{v}})_{\underline{u}}\dot{\underline{u}}$$

$$+ (\underline{\Phi}_{\underline{u}}\, \dot{\underline{u}})_{\underline{v}}\dot{\underline{v}} + (\underline{\Phi}_{\underline{v}}\, \dot{\underline{v}})_{\underline{v}}\dot{\underline{v}} = \underline{0} \tag{5.4}$$

which can be solved for $\ddot{\underline{u}}$, once $\ddot{\underline{v}}$ and the velocities are known.

The system dynamic equations may now be solved by applying a predictor-corrector algorithm (Shampine and Gordon, 1975) to $\underline{v}$, $\dot{\underline{v}}$, and $\underline{r}$ as follows:

(1) Given $\underline{v}^i$ and $\dot{\underline{v}}^i$ at time step i (or t=0), solve Eqs. 5.1 and 5.3 for $\underline{u}^i$ and $\dot{\underline{u}}^i$.

(2) Having $\underline{u}^i, \underline{v}^i, \dot{\underline{u}}^i, \dot{\underline{v}}^i$, and $\underline{r}$, solve Eqs. 3.23, 4.1, and 5.4 for $\ddot{\underline{u}}^i, \ddot{\underline{v}}^i, \underline{\lambda}^i$, and $\ddot{\underline{r}}^i$.

(3) Having $\dot{\underline{v}}^i, \ddot{\underline{v}}^i$, and $\dot{\underline{r}}^i$, use a predictor-corrector algorithm to obtain $\underline{v}^{i+1}$, $\dot{\underline{v}}^{i+1}$, and $\underline{r}^{i+1}$ at time step i+1.

(4) Return to step (1) until the desired terminal time is reached.

The use of Cartesian and Euler parameter generalized coordinates yields a maximal set of loosely coupled nonlinear holonomic constraints and differential equations of motion. A Gaussian elimination algorithm with full pivoting (Duff, 1977) decomposes the constraint Jacobian matrix and automatically identifies dependent and independent generalized coordinates. The constraint Jacobian matrix is sparse, thus the algorithm provides the necessary information to establish a modified sparse matrix relating variations in dependent and independent variables. Sparse matrix algorithms (Duff, 1977) with symbolic factorization are used to efficiently carry out the repetitive numerical solution of matrix equations required in the algorithm. For more detail on this numerical algorithm and its implementation, the reader is referred to Wehage and Haug (1982b) and Nikravesh and Chung (1982). General-purpose computer programs, called the Dynamic Analysis and Design System (DADS) have been developed to implement the foregoing algorithm for planar (DADS-2D) and spatial systems (DADS-3D). All of the algebraic and differential equations are automatically assembled by the programs from input data describing the system. Additional nonstandard constraints, interdisciplinary force inputs, and control differential equations can be provided through user supplied subroutines. Since interpretation of Euler parameters may be difficult, input data can be expressed in terms of Euler angles or direction cosines.

6. ANIMATION OF DYNAMIC RESPONSE

A graphical snapshot can be created to represent the mechanical system at any specified time of the simulation. To obtain this a series of data files are first created, each containing data that describes the geometric characteristics of each of the rigid bodies in the system. Each of these geometry files is created with respect to a specified set of body-fixed coordinates.

In the next step, the position data of the rigid bodies for the specified time is stripped out of the computer simulation output. This position data is now used to translate and rotate each of the geometry files into a global coordinate system position. These transformed geometry files are combined into one frame file, representing the system at a particular time.

The frame file is now given to a graphics software package for processing. This package has the capability of handling both 2-dimensional and 3-dimensional frame files. It further allows for choice of viewing angle and removal of hidden lines in the 3-dimensional frame files. After being read into the graphics package, the frame files are transformed into a picture that is projected onto a graphics computer device.

Creation of an animation is very similar to the creation of the single frame graphical snapshots. First of all, the position data is stripped from the simulation output. An interpolation process allows the data to be rewritten so that it represents a frame rate of 24 to 30 time intervals per second of simulation (24 to 30 frames per second is the rate used to sustain the animation effect).

The position data of the first time interval is used to transform the rigid body geometry files into one frame file, representing the first time interval. This process is repeated until all of the frame files are created for each of the time intervals.

Now each of the frame files is read into the graphics software package. After the selection of viewing angle and removal of hidden lines, each frame file is transformed to a picture. Because of the amount of time involved for the computer to remove the hidden lines, the pictures are not immediately displayed on a graphics device. Instead they are written to an animation file as they are produced. The animation file, when completed, contains all of the picture data sets for all of the time intervals of the simulation. This animation file can then be projected on the high speed graphics terminal at a rate of 24 to 30 frames per second, thus creating the animation.

Many high speed graphics terminals are becoming available on the market. By coupling one of the devices to a host computer, through a high speed parallel interphase, it is possible to obtain a projection rate of 24 to 30 pictures per second on the high speed graphics device. This allows the ability for taking many graphical snapshots that represent a series of specified times and projecting them fast enough to create an animation.

Animation is extremely helpful in interpreting and understanding results of mechanical system simulations. Whereas "a picture is worth a thousand words," one could say that an animation is worth a thousand pages of computer print-out. Results are apparent and quickly analyzed when they are graphically animated.

7. EXAMPLES

Three examples of mechanical systems incorporating interdisciplinary effects are presented here, in summary form. Reference is given to papers and reports in which more detailed treatments can be found. Dynamic response of each system studied is illustrated through use of a sequence of graphical snapshots that provide a crude animation of system dynamics. To illustrate practicality of the techniques presented here, all calculations were performed on a minicomputer.

7.1 RING-VORTEX PARACHUTE LINKAGE

As a first illustration, consider the parachute-linkage system shown in Fig. 7.1. A relatively heavy package is attached to a circular disk by two small links. Three revolute joints connect the disk, links, and the package. The canopy is modeled as a circular panel of 0.508 m diameter. The strings connecting the canopy and the disk are modeled as three massless links, as shown in Fig. 7.1.

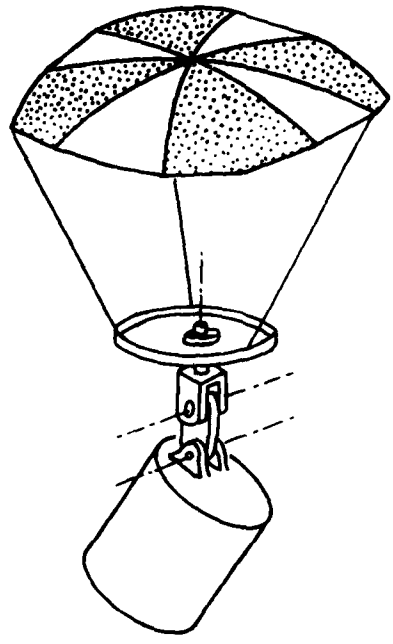


Fig. 7.1 Parachute Supported Linkage

Aerodynamic forces acting on the canopy are given in terms of generalized coordinates and velocities as follows:

$$F_\xi = QAC_1$$

$$F_\eta = QA(C_2 + C_3)\frac{v_\eta}{v_\xi} + C_4\beta$$

$$F_\zeta = QA\ C_2\frac{v_\zeta}{v_\xi} + C_4\beta$$

$$\tau_\xi = QAD\ C_5 + \frac{\omega_\xi D}{2v}C_6$$

$$\tau_\eta = QAD(C_1 + C_8)\frac{v_\zeta}{v_\xi} + C_9\beta + C_{10}\frac{\omega_\eta D}{2v}$$

$$\tau_\zeta = QAD\ C_7\frac{v_\eta}{v_\xi} + C_9\beta + C_{10}\frac{\omega_\zeta D}{2v}$$

where

$$\beta = \frac{(v_\eta^2 + v_\zeta^2)^{1/2}}{v_\xi} \cos(4\phi)$$

ξ, η, ζ = coordinate system in each canopy panel, where ξ is perpendicular to the panel

v_ξ, v_η, v_ζ = velocity components

$\omega_\xi, \omega_\eta, \omega_\zeta$ = angular velocities

z = altitude of the parachute

A = cross-sectional area

D = average diameter

ϕ = aerodynamic roll angle

ρ = air density

C_1 = axial force coefficient

C_2 = normal force slope coefficient

C_3 = normal force slope asymmetry coefficient (one panel different)

C_4 = normal force slope asymmetry coefficient (between panels)

C_5 = spin acceleration moment coefficient

C_6 = spin damping moment coefficient

C_7 = pitching moment coefficient slope

C_8 = pitching moment slope asymmetry coefficient (one panel different)

C_9 = pitching moment slope asymmetry coefficient (between panels)

C_{10} = drag coefficient

$$v = (v_\xi^2 + v_\eta^2 + v_\zeta^2)^{1/2}$$

$$\rho = 1.225(1 - 2.25 \times 10^{-5} z)^{4.2561} \text{ kg/m}^3$$

$$Q = 1/2\ \rho v^2$$

$$\tan \phi = v_\zeta / v_\xi$$

User-supplied subroutines are provided in the DADS-3D code to compute the aerodynamic forces and torques defined relative to the panel coordinate systems. The aerodynamic forces are then converted to the global coordinate system and are added to the vector of generalized forces. The simulation demonstrates that the aerodynamic forces impart spin and precession action to the canopy. The spin rate is 4.7 rad/s at an altitude of 2000 m. When friction is included between the circular plate and the attached link, the rest of the model follows the spin action of the canopy and the plate.

An animation of the dynamic response of the system is given in Fig. 7.2.

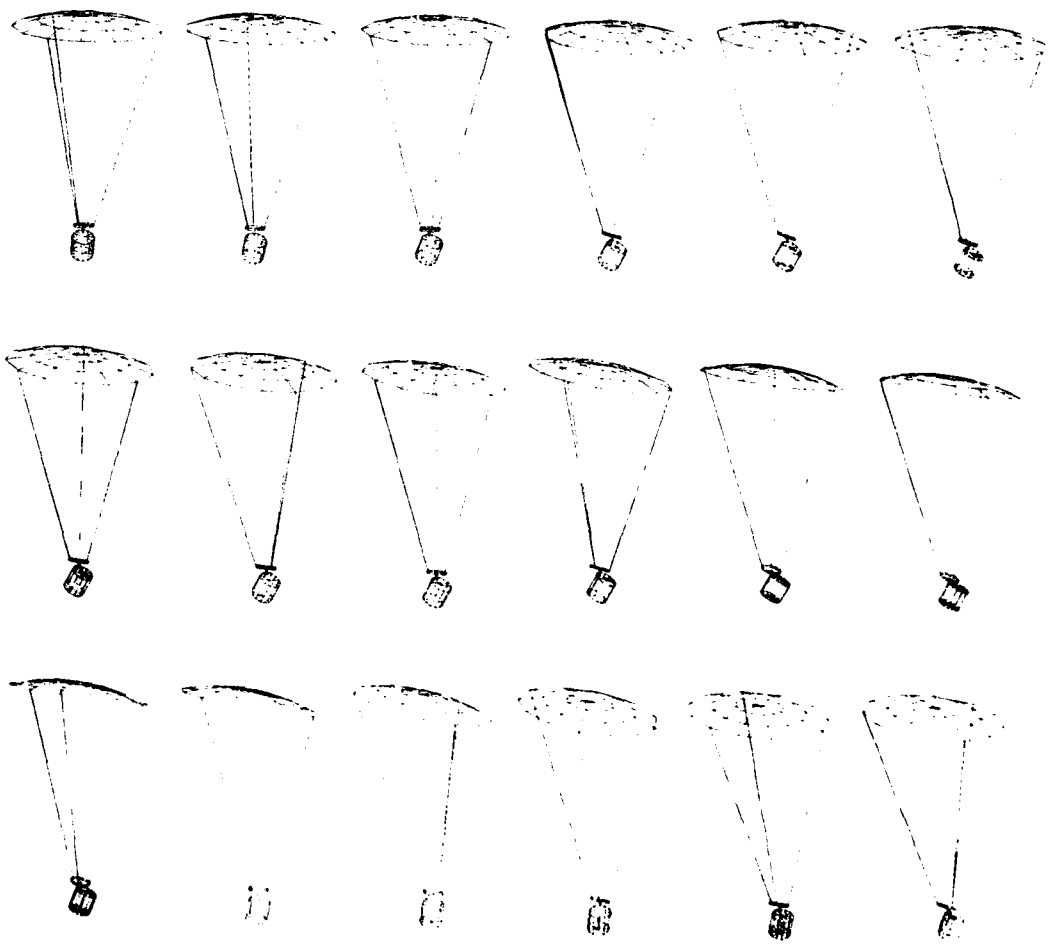


Fig. 7.2 Animation of Parachute Dynamics

7.2 TRACTOR-TRAILER

Dynamics of a tractor-trailer system shown in Fig. 7.3 over a rough road is analyzed with the aid of the DADS-3D code. Loads at the coupling between the tractor and trailer and stability of the system in traversing the depression in a road surface shown in Fig. 7.4 are analyzed in detail in Sohoni, Haug, Agrawal and Murthy (1982).

The front suspension of the tractor is a solid axle, supported from the chassis by two leaf springs. Two shock absorbers are attached between the chassis and front axle. As shown in Fig. 7.5, the front axle is modeled as a single body, body 1, connected to an intermediate body, body 5, by a revolute joint. A translational joint connects the intermediate body to the chassis. This kinematic configuration allows the axle to roll and move in a plane relative to the chassis. The suspension leaf springs and shock absorbers are modeled by spring-damper elements on each side of the chassis.

The rear suspension of the tractor consists of two driven tandem axles. This suspension is modeled by considering each of the axles to be separate bodies, bodies 3 and 4 shown in Fig. 7.5. An intermediate body is connected to each of the axles by a revolute joint. A translational joint then connects an intermediate body to the chassis. Leaf springs supporting the axles are pivoted about the chassis on each, side. The ends of the leaf spring rest in slippers on each of two tandem axles. This arrangement is modeled by introducing bodies 8 and 9, which are connected to the chassis by revolute joints. Each end of these pivoting bars is connected by a translational spring to the axle directly below. Since leaf springs have substantial coulomb friction, this damping effect is introduced into the springs connecting the pivoting bar to the tandem axles. Kinematics of the trailer bogie suspension are essentially the same as the tandem axles of the tractor, as shown in Fig. 7.5.

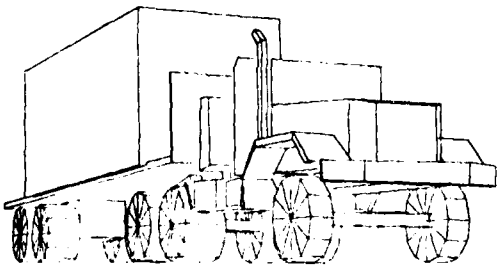


Fig. 7.3 Tractor-Trailer

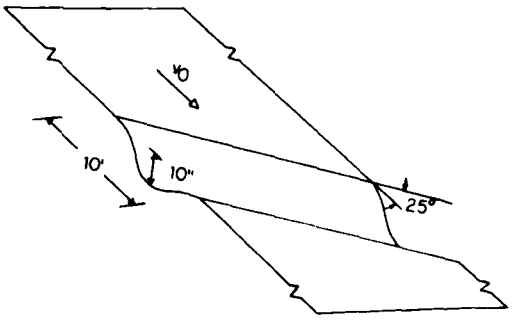


Fig. 7.4 Depression in Road

The fifth wheel hardware coupling the tractor and trailer is configured to provide articulation between the tractor and trailer, thus allowing the two to pitch, yaw, and roll relative to one another. To provide these 3 degrees of freedom, the fifth wheel is modeled by a spherical joint. While the fifth wheel does not restrict the relative yaw or pitch of tractor-trailer, there are two modes of operation with regard to the relative roll. The first mode, called the locked mode, occurs when the fifth wheel is locked, thus inhibiting any relative roll. The second mode of operation is called the unlocked mode. In this mode, the tractor and trailer are allowed to have a relative roll of ±7° before mechanical stops on the fifth wheel are encountered. Since the tractor chassis and the trailer are flexible, a torsional spring about the axis of relative roll is introduced at the fifth wheel.

Vertical and lateral tire flexibility effects are modeled, including a feature that allows the tires to slip laterally if the lateral tire force developed exceeds an allowable friction force. The tire generalized forces and tire slip logic are incorporated into the DADS-3D code through user supplied subroutines. Data approximating a tractor-cargo trailer are given in Sohoni, et al. (1982) together with an analysis of the

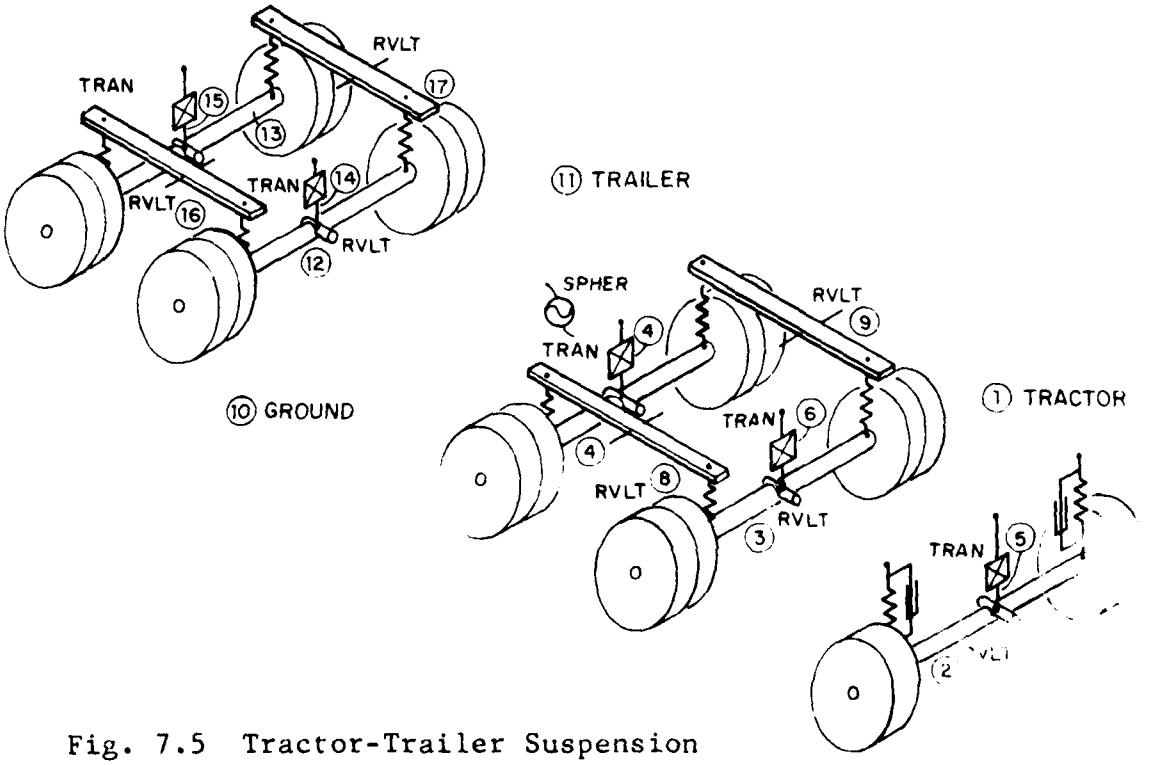


Fig. 7.5 Tractor-Trailer Suspension

vehicle traversing the road depression of Fig. 7.4 and off-road terrain at a variety of speeds.

An animation of the dynamic reponse of the vehicle, with the fifth wheel locked, traversing the road of Fig. 7.4 is given in Fig. 7.6.

7.3 ARTICULATED TRACKED VEHICLES

An articulated pair of tracked personnel carriers is shown in Fig. 7.7. The vehicles are coupled by a spherical joint and by hydraulic actuators (denoted by S23 in Fig. 7.7), to provide for relative pitch and yaw. A planar model of this system is treated here, for analysis of the vehicles as they traverse an obstacle.

Each vehicle is modeled with 6 rigid bodies. Bodies 1 to 10 represent roadwheels, where mass and inertia characteristics of roadwheels on opposite sides of the vehicle are combined. Bodies 11 and 12 include the chassis mass and inertia. The roadwheels are attached to the chassis using massless link constraints.

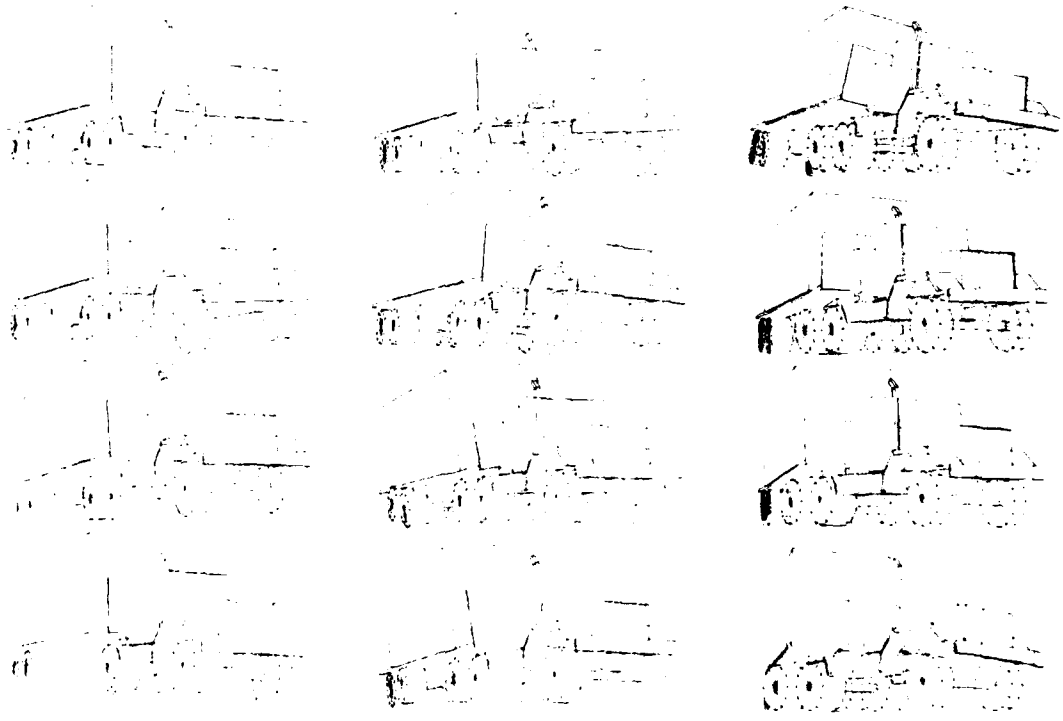


Fig. 7.6 Animation of Tractor-Trailer over Depression in Road

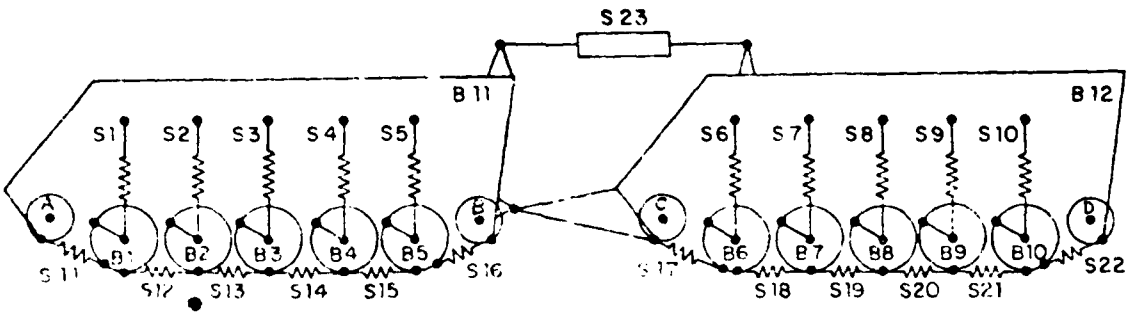


Fig. 7.7 Articulated Tracked Vehicles

Each vehicle has a torsion bar suspension. Spring-damper-actuators 1 to 10 are employed to incorporate the nonlinear suspension characteristics, including jounce stops and damping. Figure 7.8 illustrates typical force-displacement-velocity suspension characteristics. These relations, as well as other nonlinear functions, are incorporated into the model from discrete data points, using a cubic spline curve fitting algorithm. Springs 11 to 22 shown in Fig. 7.7 simulate pre-tensioned tracks connecting the drive sprockets and roadwheels. These nonlinear springs do not support compression.

The planar model of the 24 degree of freedom system of two vehicles shown in Fig. 7.7 has the tracked vehicles connected by a rotational joint and a hydraulic actuator. A nonlinear electro-mechanical-hydraulic system with positional feedback control, shown schematically in Fig. 7.9, controls the relative angular pitch rate between the two vehicles through the hydraulic actuator.

A set of differential equations, formulated for the electro-mechanical-hydraulic control system, are solved, along with the mechanical system differential equations. The two systems are coupled together by spring-damper-actuator number 23, as illustrated in Fig. 7.7. Hydraulic pressure is converted to force that is transmitted to the vehicles by the actuator. Positional and force feedback is provided by monitoring actuator length ℓ_{23} and pressure and hydraulic fluid flow rate is determined by monitoring v_{23}, the time rate of change of the actuator length.

The pitching motion of the vehicles is controlled as the driver moves a joy stick forward or rearward. Positional feedback

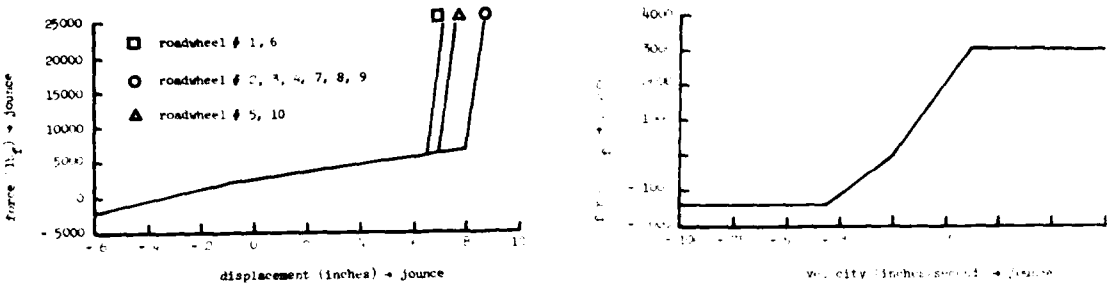


Fig. 7.8 Suspension Characteristics

allows proportional pitch control. A 100 percent pitch down command amounts to the driver pushing the stick forward to a mechanical stop and a full rearward displacement gives a 100 percent pitch up command. In hands-off operation, the joy stick is controlled by force feedback to maintain minimum pressure in the hydraulic system and allow the coupled vehicles to conform to the terrain.

Using data given in Wehage and Beck (1980) the coupled vehicles are analyzed as they traverse a three foot step obstacle in hands-off operation. The articulation provided by the hydraulic coupling allows the vehicles to successfully traverse the obstacle, whereas a single vehicle may not do so. An animation of the vehicles going over the obstacle is shown in Fig. 7.10.

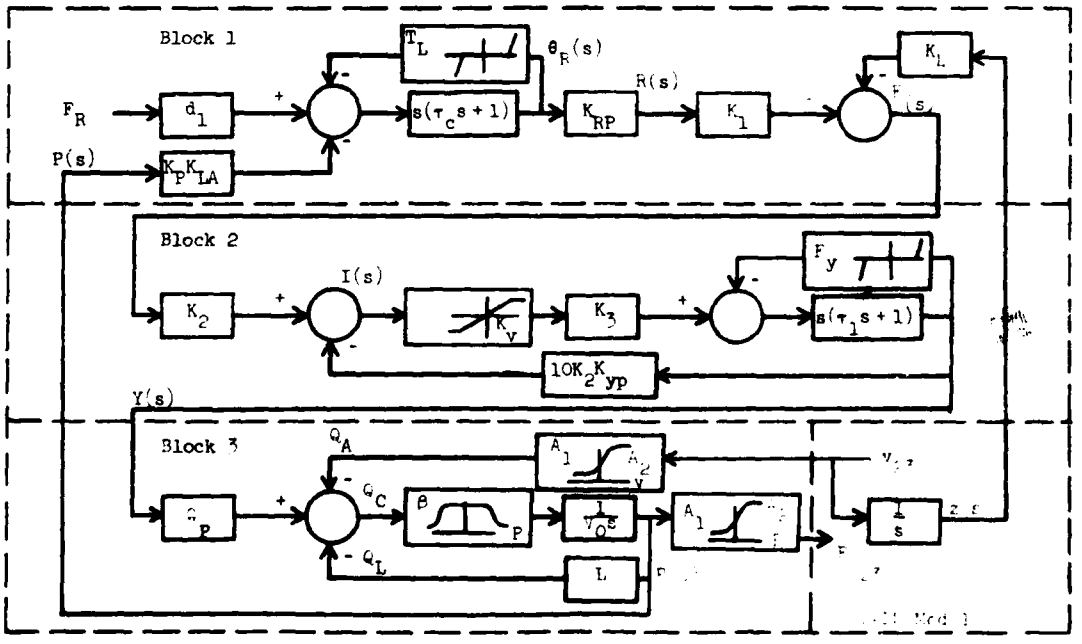


Fig. 7.9 Feedback Control Schematic

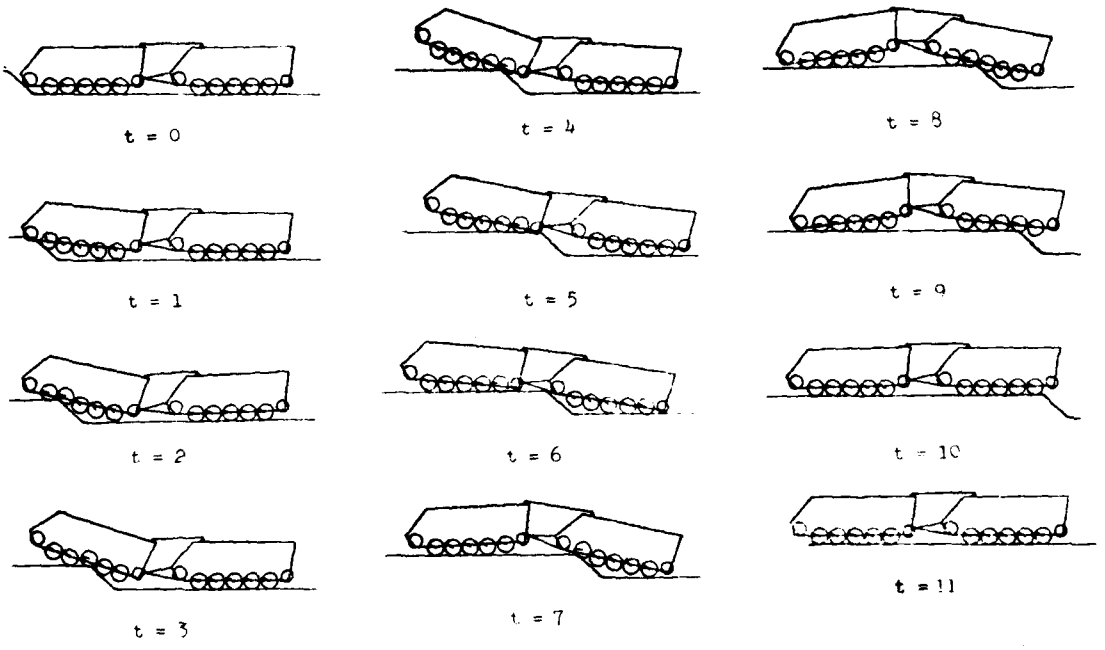


Fig. 7.10 Animation of Tracked Vehicle over Obstacle

8. ACKNOWLEDGMENTS

Research reported was supported by the U.S. Army Tank Automotive Command, Project No. DAAK 30-80-C-0042.

8. REFERENCES

CHACE, M.A. and SMITH, D.A. (1971): "DAMN-A Digital Computer Progam for the Dynamic Analysis of Generalized Mechanical Systems," SAE paper 710244.

DUFF, I.S. (1977): MA28-A Set of FORTRAN Subroutines for Sparse Unsymmetric Linear Equations, Rept. No. AERE-R.8730, Computer Science & Systems Div., AERE Harwell, Oxfordshire. GOLDSTEIN, H. (1980): Classical Mechanics, Addison-Wesley, Reading, Massachusetts.

HILDEBRAND, F.B. (1976): Advanced Calculus for Applications, Prentice-Hall, Englewood Cliffs, N.J.

NIKRAVESH, P.E. and CHUNG, I.S. (1982): "Application of Euler Parameters to the Dynamic Analysis of Three Dimensional Constrained Mechanical Systems," Journal of Mechanical Design, to appear July, 1982.

ORLANDEA, N., CHACE, M.A., and CALAHAN, D.A., (1977): "A Sparsity-Oriented Approach to the Dynamic Analysis and Design of Mechanical Systems, Parts I and II," Journal of Engineering for Industry, Vol. 99, p. 773.

PAUL, B. and KRAJCINOVIC, D. (1970): "Computer Analysis of Machines with Planar Motion - Part I: Kinematics; Part II: Dynamics," Journal of Applied Mechanics,Vol. 37,p. 697.
SHABANA A. and WEHAGE, R.A. (1981): "Variable Degree-of-Freedom Component Mode Analysis of Inertia Variant Mechanical Systems," Report No. 81-12, Center for Computer Aided Design, College of Engineering, The University of Iowa, Iowa City, Iowa.
SHAMPINE, L.F. and GORDON, M.K. (1975): Computer Solution of Ordinary Differential Equations: The Initial Value Problem, W.J. Freeman, San Francisco, California.
SHETH, P.N. and UICKER, J.J., JR. (1972): "IMP (Integrated Mechanisms Program), A Computer Aided Design Analysis System for Mechanisms and Linkages," Journal of Engineering for Industry, Vol. 94, p. 454.
SOHONI, V.N., HAUG, E.J., AGRAWAL, O.P. and MURTHY, A.P. (1982): "Spatial Dynamic Analysis of Tractor-Trailer Roll Stability," Report No. 81-17, Center for Computer Aided Design, University of Iowa, Iowa City, Ia. SONG, J.O. and HAUG, E.J. (1980): "Dynamic Analysis of Flexible Mechanisms," Computer Methods in Applied Mechanics and Engineering, Vol. 24, p. 359.
WEHAGE, R.A. and HAUG, E.J. (1982a): "Dynamic Analysis of Mechanical Systems with Intermittent Motion," Journal of Mechanical Design, to appear.
WEHAGE, R.A. and HAUG, E.J. (1982b): "Generalized Coordinate Partitioning for Dimension Reduction in Analysis of Constrained Dynamic Systems," Journal of Mechanical Design, Vol. 104, No. 1, p. 247.
WEHAGE, R.A. and BECK, R.R. (1980): "Dynamic Analysis of Articulated M-113 APC's with Position and Force Feedback Control," Modeling and Simulation, Proceedings of the Eleventh Annual Pittsburgh Conference, Vol. 11, part 3, p. 953.
WITTENBURG, J. (1977): Dynamics of Systems of Rigid Bodies, Teubner, Stuttgart.

SESSION V: GUN FIRE CONTROL

28 OCT 1982

(MORNING)

ROOM #1

FOURTH MEETING OF THE COORDINATING

GROUP ON MODERN CONTROL THEORY

HOSTED BY: OAKLAND UNIVERSITY
ROCHESTER, MICHIGAN

Next page is blank.

AD P001085

VATT - THE GUNNER'S "INVISIBLE" AID

J. A. Wes
Engineering Specialist
Northrop Corporation, Electro-Mechanical Division
Anaheim, California 92801

ABSTRACT

The Video Automatic Target Tracker (VATT) is a research and development program (DAAK10-81-C-0081) sponsored by the U.S. Army Armament Research and Development Command (ARRADCOM, Dover, N.J.) being conducted by Northrop Corporation's Electro-Mechanical Division. VATT integrates with modern vehicular fire control systems to aid the tank gunner in achieving improved accuracy with reduced workload. It is a digital edge-based-correlation tracker that automatically drives a stabilized line of sight to follow an operator selected target. The acquisition and tracking modes have been carefully matched to current M1 fire control procedures, utilizing the existing gunner's switches. Thus, manual operations with the tracker are identical to existing manual procedures, which allows the tracker to appear "invisible" to the gunner.

VATT is currently undergoing integration and test with ARRADCOM's fire control test bed tank. It will have been laboratory tested in June 1982, with tank field tests scheduled to commence in late summer of 1982. The modular VATT is based on the same day television (TV) or FLIR compatible design as systems in engineering development for the helicopter application (NTSH - MMS) and entering production for fixed-wing aircraft (F-4, F-111 - PAVETACK).

Discussion on tracker design, fire control system integration and operation, and laboratory and field test results is presented, including video tape excerpts from testing.

INTRODUCTION

Acquiring, tracking, and engaging targets under severe modern battlefield conditions at extended ranges has led combat vehicle designers and developers to employ fire control systems of

increasing complexity and sophistication. This has placed a heavy workload burden on the gunner whose basic tracking task is made even more difficult by the fire-on-the-move doctrine.

In order to reduce the burden of tracking-on-the-move, an automatic tracker is being considered. Additional benefits, such as increased accuracy and reduced line-of-sight jitter (which will lead to improved fire control solutions and ultimately higher hit probabilities) may also accrue through the use of automatic tracking aids. However, additional operational complexity for the overloaded gunner cannot be tolerated. For such a system to be viable, it must not only track well but must be operationally invisible to the gunner. Specifically,

- Command to start tracking must be initiated by an EXISTING switch, when the gunner is conducting a CURRENTLY MANDATED task. (No new lock-on command may be issued).

- Given the above one-time "start tracking" command, the tracker must acquire the same target the gunner is tracking, lock-on, verify that it is tracking the same target the gunner is, and then smoothly take control of the line of sight.

- The gunner must always be able to adjust the line of sight relative to the tracker without a new switch action. This is critical for sense and adjust aiming corrections (second round).

- The gunner's ability to adjust, without new switch action, must automatically grow to total control of the line of sight in case a change of target or an erred lock-on occurs.

- Should the tracker break lock, line-of-sight control must smoothly revert to the gunner until the tracker can automatically reacquire.

- Command to cease tracking must also be linked to an EXISTING switch, again only when the gunner is conducting a CURRENTLY MANDATED task.

- Should the tracker malfunction, it must self-evaluate and shut down, restoring normal manual operation. This also applies to the intentional or unintentional condition of tracker power OFF.

These stringent operational requirements matched to a history of fielded tenacious autotrackers are the basis for Northrop Corporation's VATT. VATT is being developed under contract to the Fire Control and Small Caliber Weapon Systems Laboratory at the U.S. Army Armament Research and Development Command (ARRADCOM), Picatinny Arsenal, Dover, New Jersey. It has been integrated with a two-axis, government furnished Stabilized Head Mirror Unit (SHMU) and demonstrated in Northrop's Optical Simulation Facility in Anaheim, June of 1982.

During the late summer of 1982, VATT will have been integrated with ARRADCOM's Fire Control Test Bed Tank (a modified M60 A1 RISE) and field tested. The VATT is being developed for eventual use in both the M1 and M60 series tanks and will be adaptable for use with any stabilized sight or stabilized turret system.

FIRE CONTROL SYSTEM INTEGRATION

FUNCTIONAL INTEGRATION

To reduce the complexity of a Product Improvement Program (PIP) and to be consistent with gunner's aid concept, VATT is installed (electrically) between the gunner's yoke and the remainder of the existing fire control system as indicated in Figure 1. Eventually, VATT will operate on the image stream output from the Tank Thermal Sight (M60 A3) or Thermal Imaging Sight (M1). Currently, however, a day TV camera installed in the SHMU provides the required input. In either case, the gunner views the target through his existing direct view optics or thermal sight, at his discretion. No TV viewer or monitor is required.

Yoke azimuth and elevation signals, as well as the palm switch (brake) and lase button are routed into the VATT, modified (if tracking), then returned to the fire control system and stabilization electronics as if they were the gunner inputs. All remaining fire control functions are unaffected.

OPERATIONAL INTEGRATION

The lase and palm (brake) switches were identified to be the "EXISTING" switches with associated "CURRENTLY MANDATED" tasks which best lend themselves to the tracking start/stop functions. Under standard procedures, the commander selects a target and informs the gunner. The gunner activates the palm switches and slews the turret to the target area, then adjusts the crosshairs onto the target. The range to the target is determined by lasing, then the target is engaged. This lase action implies that the gunner has found his target, has the crosshairs on it, and is ready to engage. The Lase Command is therefore also used as the command to VATT to initiate tracking. Table 1 shows the operation/control/function relationships.

The tracker assumes the gunner is keeping the reticle on the target. Once the tracker has acquired something at the center of the scene, it compares target motion with the gunner's continued tracking inputs. If they match (within limits), the tracker concludes it is tracking the desired target and smoothly takes control of the line of sight. Since the tracker is following the target, gunner inputs are now interpreted as corrections relative to the track point. This allows manual aimpoint selection as well as fire adjust after sensing first round impact.

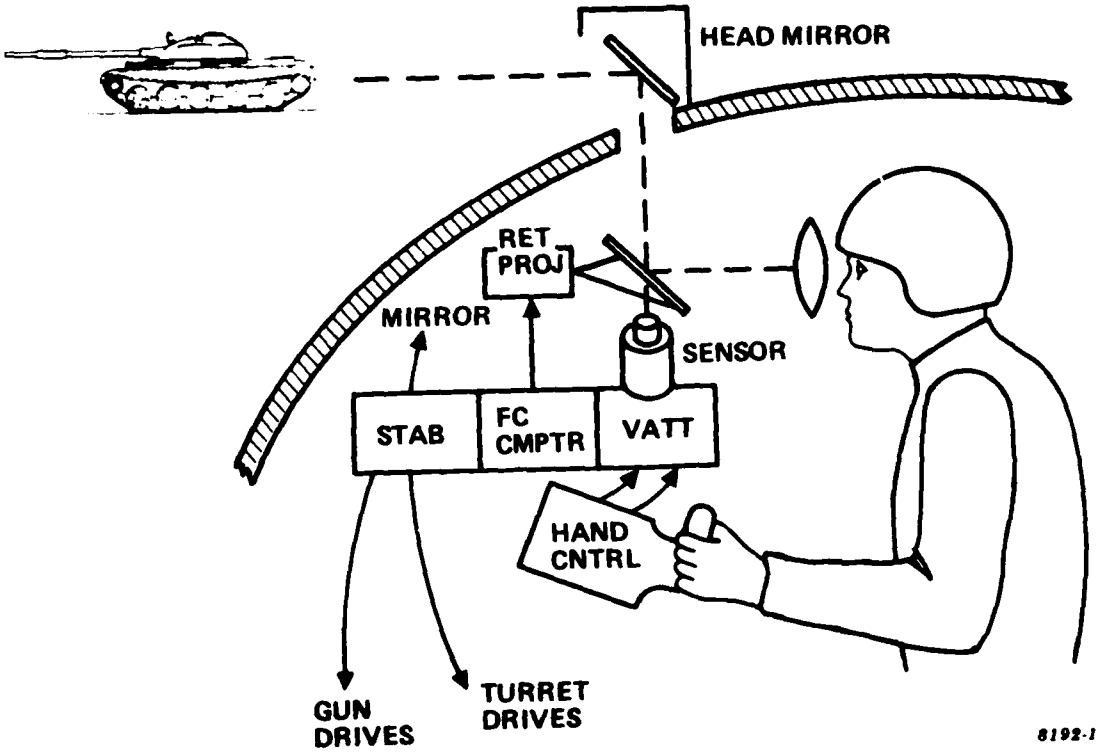


Figure 1. VATT Integrated With Tank Fire Control System

Table I. VATT Operation/Control/Function Relationships

Step	Operation	Control	System Function
1	Engage palm switch. Adjust Line of Sight (LOS) in AZ and EL so that reticle (cross-hairs) coincides with target	Gunner's "Yoke" hand control (Note: If target is moving, deflection of yoke must be maintained)	Turret, gun, and LOS follow target based on manual inputs
2	As crosshair is maintained on target, engage lase button to *command* autotrack	Lase button on either hand grip of gunner's "Yoke"	Turret, gun, and LOS follow target based on autotrack
3	Only if reticle is not on aim point: adjust AZ and EL to place crosshair on aim point	Maintain palm switch active adjust "Yoke" AZ and EL to adjust LOS	Hit point on target is adjusted
4	Fire	"FIRE" trigger on either grip	Round is launched
5	If reticle moves off of target, adjust LOS with yoke to desired target, then lase	Yoke, palm switch and lase button	Breaklock occurs Target is reacquired using operator inputs
6	Release Palm Switch	Palm Switch	Reverts to normal control

Standard procedure finds the gunner either slewing to a new target or releasing the palm switch at the end of the engagement. In the latter case, the tracker interprets the palm switch OFF as the end of the engagement. It automatically switches to a Standby Mode and allows standard manual operation until a Lase Command reactivates it. In the case of slewing to a new target without braking, the tracker senses an inordinately large adjustment, and assumes the operator is switching to a new target. When the gunner again holds the crosshairs on a target, the tracker automatically initiates track. (A Lase Command may also be used to reinitiate track.)

If the tracker determines that it has broken lock (an assessment that it evaluates at a 60 Hz rate), the last line-of-sight rate is held constant and gunner yoke inputs are used to adjust the line-of-sight rate relative to the "coast" rate. This ensures a smooth transition to manual control. If the gunner relocates the target, the tracker will automatically reinitiate track as it did after the line-of-sight adjustment. The tracker does, however, also attempt to reacquire automatically and will automatically take control in such a case.

Since the tracker controls the line of sight only when it has a target, but transitions into and out of control smoothly, the gunner need not worry whether VATT is tracking or not. A single Light Emitting Diode (LED) in the corner of the gunner's field of view is being evaluated as a track indicator (light on - auto-track aiding; light off - acquisition, coast, or manual track). This simple indicator will be the only indication to the gunner that the tracker is assisting him in his task. During the full test program, the determination of whether this feedback is actually required will be made. In any event, the real evidence of VATT operation will be the improved tank system performance.

TRACKER DESIGN

The VATT consists of four major functional blocks and three support blocks as shown in Figure 2. The TV, FLIR, or internal calibration video is selected and shaped in the analog preprocessor under computer control. The filtered video falling within an area around the target (called the Track Gate) is digitally encoded at discrete timing intervals. The shape and position of the Track Gate is continuously modified by the computer and implemented through the timing generator. The encoded video is then passed to the computer as a matrix of digital values once each video field (nominally 60 times per second). Correlation with a "stretchable" rectangular (target shaped) template provides the desired target position signals as well as the Track Gate size and position corrections mentioned above.

The tracker is controlled by the palm and lase switches. The yoke azimuth and elevation signals are also routed through VATT, with a special bypass circuit implemented to allow standard

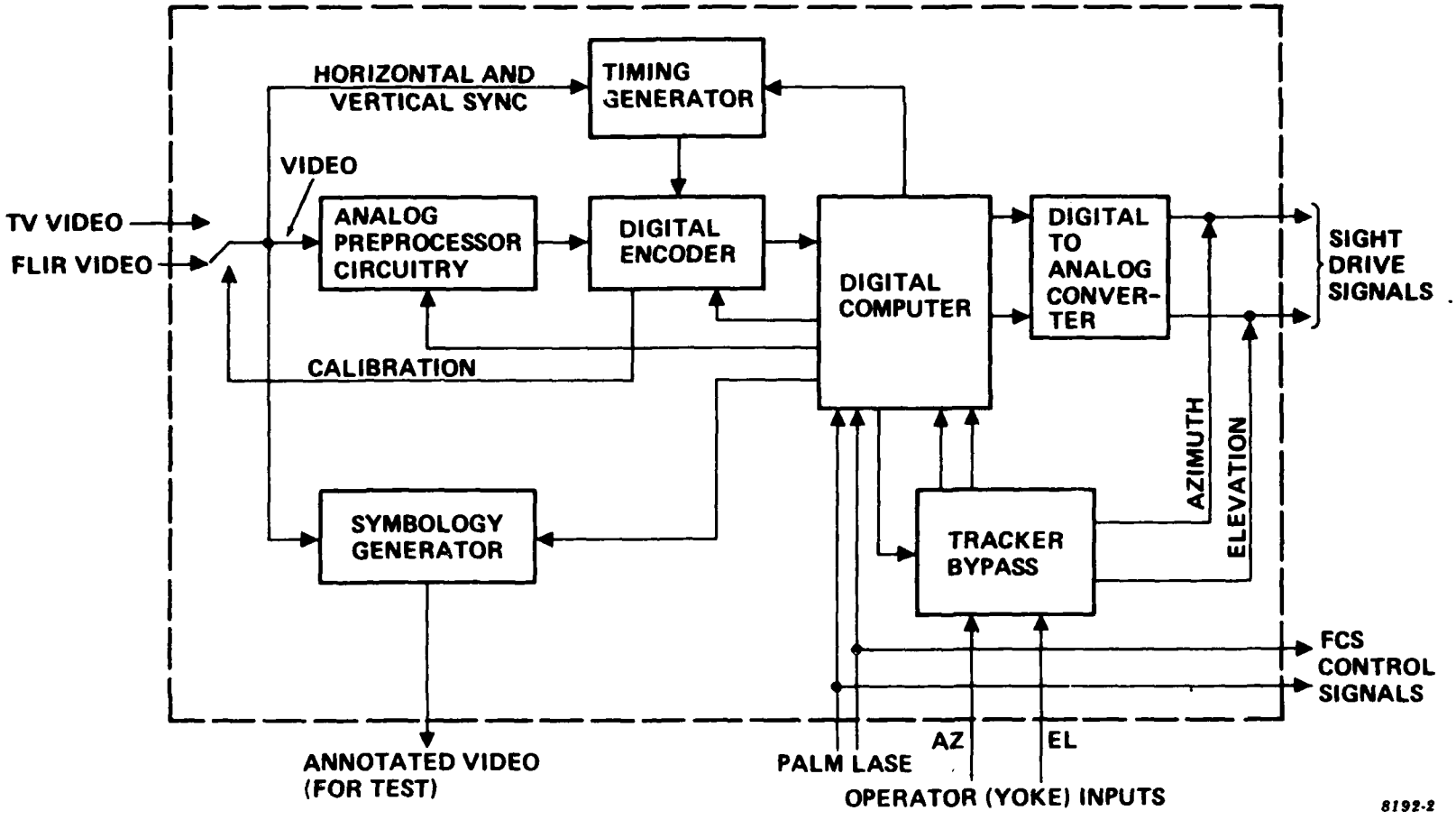


Figure 2. Simplified VATT Block Diagram

manual operation in case of power down or self-detected fault. The tracker outputs are scaled and converted to analog voltages, then routed to the fire control/stabilization electronics input, which normally accepts the yoke outputs.

Computer controlled symbology is added to the input video stream for engineering evaluation. In addition, a number of system diagnostics and track function internal parameters are displayed and updated each field.

TEST RESULTS

HISTORIC BACKGROUND

The modular VATT is based on the same day TV or FLIR, 525- or 875-line compatible design as systems in engineering development for helicopters (Near-Term Scout Helicopter, Mast Mounted Sight (NTSH-MMS)), and entering production for fixed-wing aircraft (F-4, F-111 - PAVETACK/VATS). All systems were derived from a basic prototype developed under Independent Research and Development (IR&D) at Northrop, Anaheim. The IR&D tracker has undergone the most extensive testing.

The tracker has the demonstrated ability to acquire and track targets that range in size from less than 1 percent of the Field of View (FOV) to greater than 50 percent. For the tank application with a 2° FOV (approximately, X 10 magnification), this equates to a capability of tracking tank-type targets at ranges well inside 500 meters to beyond 3 kilometers.

Tracking with day TV contrast as low as 1 percent relative has been demonstrated, as has tracking with a minimum FLIR ΔT of less than 1/4°C. Such reduced peak Signal-to-rms-Noise Ratios (SNR) do degrade tracking accuracy, but even a minimum SNR of 1 still provides "subresolution" tracking as indicated in Figure 3. The figure shows field-to-field tracker noise against a stationary closed contour target with the indicated size and SNR. A "TRU" is a Tracker Raster Unit or approximately a TV line. Thus, the figure indicates raw tracking jitter at less than 1/2 TV line for virtually any trackable target. For the VATT application (again 2° FOV), this equates to autotracker induced tracking jitter of less than 0.05 mil.

SYSTEM TEST

The PAVETACK/VATS (air-to-ground version of VATT) has undergone extensive Development Test and Evaluation (DT&E) and Initial Operational Test and Evaluation (IOT&E) at Eglin Air Force Base. After development and system integration were completed, VATS was enthusiastically recommended by test engineers and weapon systems operators alike. The most significant features were the greater than 50 percent reduction in workload, reduced training time for operators unfamiliar with PAVETACK operation, and improved system

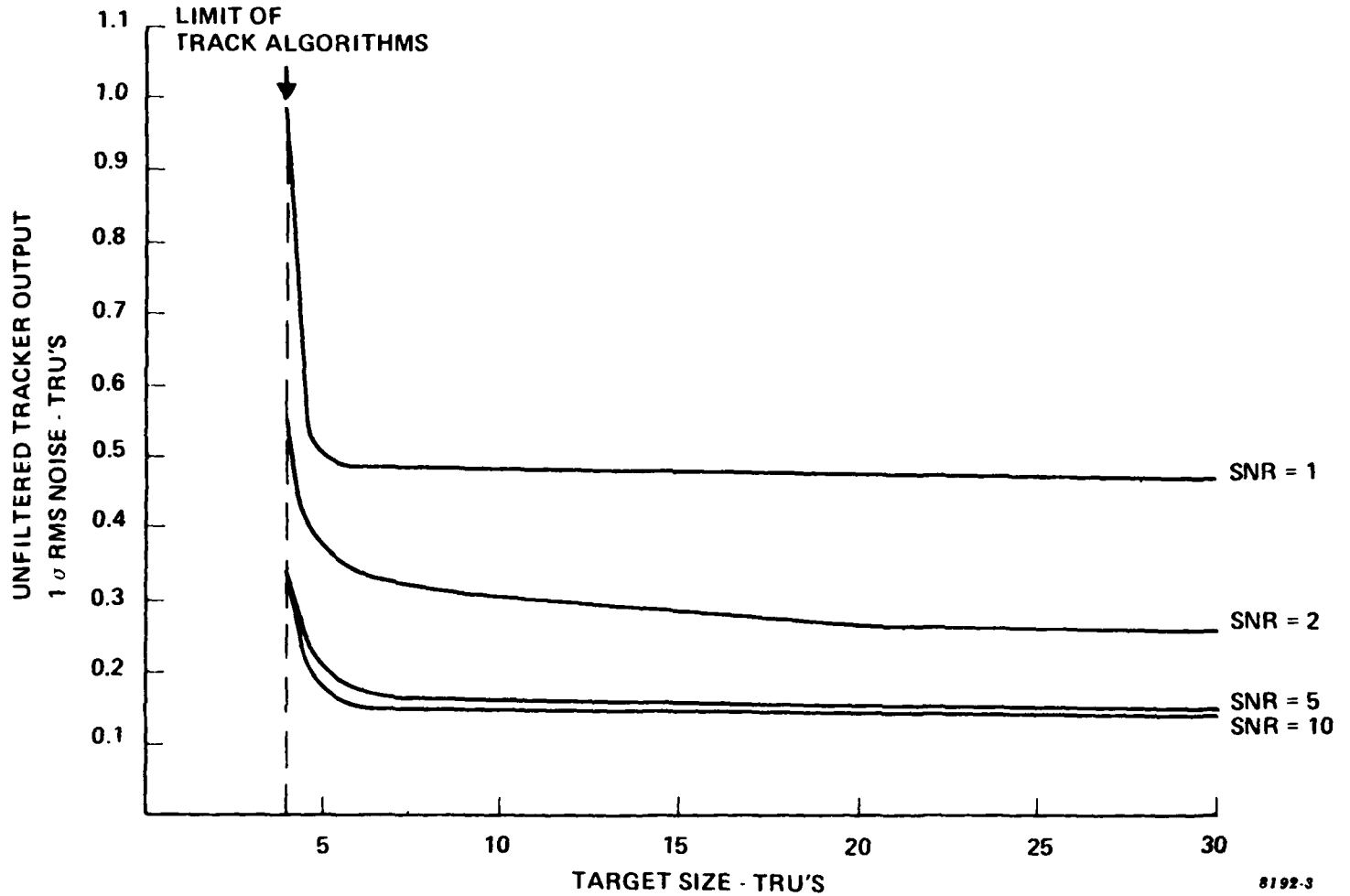


Figure 3 Tracker Induced Jitter

accuracy. Tracking accuracies in most engagements improved by a factor of two (0.18 mil to 0.09 mil), yielding an improved probability of mission effectiveness. (P_K = 0.73 to P_K = 0.95 at 60,000 ft. slant range)

The VATT laboratory integration tests have proceeded well, with noticeably improved tracking against maneuvering model targets. The "invisible" aid matched moding, and smooth transitions of line-of-sight control have also been demonstrated. Stable tracking-on-the-move will have been demonstrated in September of 1982. Operational evaluation and actual numeric testing, using fully qualified gunners from Ft. Knox, will begin in October 1982. Video tape excerpts from lab and field testing will be shown at the symposium.

SUMMARY - THE "INVISIBLE" AID

VATT is a gunner's automatic tracking aid developed for ARRADCOM by Northrop Corporation's Electro-Mechanical Division. Careful matching of VATT moding to EXISTING switches and CURRENTLY MANDATED tasks allows it to be invoked with no new gunner actions. Continual self-assessment and smooth automatic transition of line-of-sight control (both to and from the gunner) coupled with an unobstructed gunner ability to adjust the line of sight (at will), provides a virtually invisible aid.

Northrop's tenacious tracker design provides significantly reduced gunner workload, and lower induced noise (especially in fire-on-the-move engagements) will provide overall system performance improvements. The mature hardware is essentially the same as systems that have already been fielded. The tracker aid is currently undergoing field test and will soon be ready to aid gunners of M1, M60, and any other stabilized sight or stabilized turret armoured vehicle fire control systems.

AD P001086

A MODERN CONTROL APPROACH TO GUN FIRING ACCURACY IMPROVEMENTS

Robert J. Talir, Donald L. Ringkamp, and Fred W. Stein
EMERSON ELECTRIC COMPANY
Electronics and Space Division
8100 W. Florissant Avenue
St. Louis, Missouri 63136

ABSTRACT

The accuracy of firing a gun from a moving combat vehicle is affected significantly by the accuracy with which the gun muzzle is positioned to fire the projectile along a predicted path. Traditionally the problem of accuracy improvement has been addressed through gun mount stabilization while the motion of the barrel is treated as an uncontrolled additional dispersion in the trajectory of the projectile. Modern control technology provides a means of stabilizing the unmeasured gun muzzle. Minimization of a quadratic cost function coupled with estimation of unmeasured states ensure accurate muzzle response to command inputs as well as minimize reaction to base motion and external firing disturbances.

INTRODUCTION

Future fire control systems will be required to exploit the mobility of high performance weapons platforms. The accuracy with which the projectile can be launched along a predicted path must be improved or the demands placed on the gun by modern fire control systems will far exceed its capabilities. Traditionally, weapon control has been accomplished by directing the axis of the gun support gimbal. The gun barrel and therefore the absolute round exit angle is open loop with respect to the axis of rotation. Errors due to barrel bending and induced oscillation are accepted and included in the total firing accuracy budget. The motion of the barrel tip relative to the support gimbal is treated as an uncontrolled additional dispersion in the trajectory of the projectile. It would be desirable to remove most of this dispersion so that each round may be fired in the predicted direction.

Therefore, a need exists to stabilize and control the barrel tip in the presence of external turret motion or firing disturbances. Since useful muzzle position and rate information is difficult to obtain, conventional feedback techniques

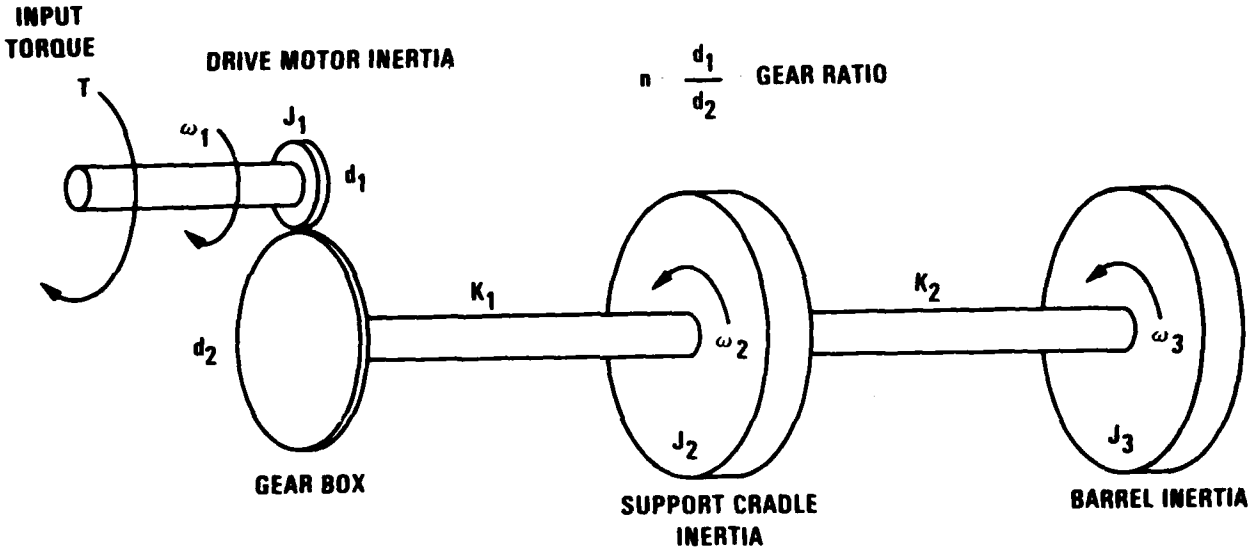
cannot be employed to control the barrel tip. The problem, then, is to use modern control theory employing state variable feedback and to supply the necessary parameter information through state estimation. In the approach presented here, the control emphasis has been placed on the barrel tip angular rate rather than position to ease the demands on the state estimator and provide the fastest command response and disturbance rejection. An optimal control technique with control tuning is employed to achieve the best response while maintaining adequate margins for model imperfections and estimator lag.

Effective state estimation depends on the degree of model fidelity and a model definition which allows the observation of every state via available measurements. Therefore, to impose a practical challenge to an otherwise academic approach, an Emerlec-30 (a twin 30 mm naval gun mount produced by Emerson Electric Co.) was chosen as the control test bed for the barrel tip optimal control and estimation technique. The only practical implementation of this technique, which requires the execution of numerous recursive equations in real time, demands the speed, memory, and flexibility of a digital processor. Therefore, the technique is configured such that all processing can be executed in a standard micro or minicomputer with serial or parallel I/O.

This paper presents the results of applying an optimal control and state estimation technique to achieve control over the barrel tip angular rate of a 30 mm gimballed gun mount. Simulation results are derived from a model of the test mount with all of its parameter characteristics and limitations.

TECHNICAL APPROACH

The general approach to this project has been to use optimal control and estimation techniques to achieve muzzle stabilization and control of a test bed gimballed gun mount (an Emerlec-30). Since a good optimal controller and an effective state estimator depend on model fidelity, the first step was to develop a representative math model of the gun mount plant using test data. The Emerlec-30 contains an electric motor drive geared to each control axis of the gun barrel. Frequency response data was obtained between various points from motor command to barrel tip by using a dual channel spectrum analyzer and rate gyros. Since high order estimators result in unwieldy algorithms for microprocessor implementation, a practical goal in model development was to restrict the order to as low as practical and still model the dominant characteristics. The frequency response data suggested that a series three body, fifth order model, such as shown in Figure 1, was adequate.



$$\omega_1/T = [J_2J_3S^4 + (K_1J_3 + K_2J_2 + K_2J_3)S^2 + K_1K_2]/\Delta$$

$$\omega_2/T = (n\,J_3K_1S^2 + n\,K_1K_2)/\Delta$$

$$\omega_3/T = n\,K_1K_2/\Delta$$

$$\Delta = J_1J_2J_3S^5 + (K_1J_1J_3 + n^2K_1J_2J_3 + K_2J_1J_3 + K_2J_1J_2)S^3 + K_1K_2(J_1+n^2J_2+n^2J_3)S$$

4529-1

Figure 1 Series Three-Body Plant Model

Using this basic model, parameters were calculated and adjusted, and damping terms were added until a very good frequency response match was obtained. Because the math model is fundamental to the real time estimator and is a key element in the development of the optimal control gains, its fidelity as a model of the actual plant is important. The more model imperfections allowed, the greater the control margins necessary for successful performance and a more suboptimal controller results. In addition, modeling imperfections cause unwanted estimator error dynamics that usually add more phase shift to the controller loop.

After defining the math model of the plant, a suitable sampling frequency is chosen to adequately control the highest frequency of interest through a digital computer. A sampling rate of 100 Hertz was chosen for good control out to the firing frequency of 10 Hertz. The continuous plant frequency domain definition was then transformed to the digital time domain for use in the control and estimation algorithms. This transformation was accomplished on a computer by a truncated series expansion of the system state transition matrix.

OPTIMAL CONTROL DEVELOPMENT

The word "optimal" in its general sense means "best" or "most desirable." In controls, as in other endeavors, the engineer is always searching for the best solution to the problem at hand. Via classical techniques (Nyquist, Nichols, Bode, root locus, etc.) the control problem concerns itself with finding "optimum controller settings", which is a process of parameter optimization. In optimal control techniques, the problem is concerned with finding the best control strategy for a given system and cost function. In determining an optimal control strategy, no prior assumptions or commitments are made that would fix the controller structure; on the other hand, in parameter optimization, the problem is to first fix the structure of the controller (e.g., a proportional-plus-integral controller, etc.) and then attempt to determine the optimum parameters. The aim of optimal control is to find some policy, which, when applied to the system input, will optimize the system's performance with respect to some cost function.

Although the variational viewpoint is the basis from which the engineer seeks an optimal strategy, its mathematical difficulty and computational complexity are so great that real progress in the field started only after major breakthroughs by Bellman (dynamic programming, 1960) and Pontryagin (maximum principle, 1962). Since then, the problem has attracted the attention of

many control mathematicians who have offered formal, rigorous, and general, but often very abstract, contributions. Even though engineers can often obtain solutions only by using simplified system models and simple performance indices, the optimal control approach has been an important tool, for example, by pointing the way to better controller structures, or by providing a measure of performance so that a designer can determine whether there is any sizable room for improvement in his design.

The approach taken to achieve control over virtually an unmeasurable entity, the barrel tip of a gimballed 30 mm gun mount, was to employ optimal control theory to define the control strategy and then identify and circumvent the problem areas with classical techniques. A parameter optimization of the resulting hybrid system then results in the best solution that can be practically implemented.

The control scheme chosen was a variation on R. Bellman's dynamic programming with modifications suggested by various standard control textbooks. The scheme is based on the principle of optimality, which states that an optimal policy (best system input sequence) has the property that whatever the initial state and initial decision are, the remaining decisions must constitute an optimal policy with regard to the state resulting from the first decision. The criterion for optimality was the minimization of a quadratic cost function. This function combines the sum of the squares of the errors between the actual system states and desired states plus the sum of the squares of system input values. The latter term keeps the control policy feasible by penalizing excessively large input values (i.e., infinite energy cannot be supplied to the system via the controller). As with most criteria, they are not all-encompassing. Achieving a minimum error in a certain desired state may not assure good step responses, frequency responses, or system disturbance immunity. Therefore, the cost function is adjusted through the values of an error state weighting matrix until the optimal policy derived from cost function minimization results in desired system response.

To illustrate the technique, consider the continuous system described by the differential equation:

$$\dot{x}(t)] = [A]x(t)] + B]u(t)$$

where $x(t)]$ is the system state column vector, $u(t)$ is the

input, [A] and B] are coefficient matrices. The z-transform of this system results in the state transition equation:

$$x(n+1)] = [\Phi(T)]x(n)] + \Theta(T)]u(n)$$

where T is the sample interval and

$$[\Phi(T)] = e^{[A]T},$$

$$\Theta(T)] = \int_0^T [\Phi(T-\lambda)]B]d\lambda.$$

Then, if the desired states of the system can be described by

$$x_d(n+1)] = [\Psi(T)]x_d(n)],$$

error states can be defined by

$$y(n)] = x_d(n)] - x(n)].$$

An error state transition equation can then be defined by

$$y(n+1)] = [\Gamma(T)]y(n)] + \Omega(T)]u(n)$$

where $[\Gamma(T)]$ is a function of $[\Phi(T)]$ and $[\Psi(T)]$, and $\Omega(T)]$ is a function of $\Theta(T)]$. An optimal control policy would then be a set of input commands, u(n), that drive the error states in such a way that a certain performance criterion is exactly satisfied. This optimal policy should have the form

$$u(n) = H(T)]'y(n)]$$

where $H(T)]'$ is the transpose of the optimum gain column vector, H(T)]. This equation suggests that control can be achieved through state variable feedback.

To continue the design, a suitable performance criterion must be selected. Since the system is defined with error states, initially the best policy would be that which drives the errors to zero. In essence, the minimization of the sum of the square of the errors should suffice. Therefore, a quadratic performance index (or cost function) was defined by

$$I = \sum_{n=1}^{N} y(n)]'[S]y(n)] + \lambda u^2(n-1)$$

where [S] is the error weighting matrix, λ is an input penalty factor, and N is the last stage of an N-stage process. Using the principle of optimality, and working from the Nth stage backward to the start of the process, the optimum gain vector is developed:

$$H(NT-jT)]' = - \frac{\Omega(T)]'\{[S] + [P(NT-jT-T)]\}[\Gamma(T)]}{\Omega(T)]'\{[S] + [P(NT-jT-T)]\}\Omega(T)] + \lambda}$$

where j = 0, 1, 2, ..., N-1, and

$$[P(NT-jT)] = [\Gamma(T)]'\{[S] + [P(NT-jT-T)]\} * \{[\Gamma(T)] + \Omega(T)]\ H(NT-jT)]'\}$$

These equations are solved recursively starting with j=N-1 and

$$[P(NT-jT-T)] = [P(0)] = 0.0$$

For an infinite stage process, the indicated iteratious can be carried until the optimum gain vector values $H(NT-jT)]'$, reach a steady state. These steady state values are then used in a fixed-gain feedback control configuration in which the only variables affecting the optimal policy are the error states. Since the optimal control policy will always result in the minimization of the cost function, changes in system performance can be effected by changing the cost function. This is accomplished by adjusting the error weighting matrix [S], and the input penalty factor, λ. Adjustments are made until the desired performance is achieved.

While the optimal control technique is an excellent way of handling a multiple feedback control law design, it does not automatically build in stability margins to allow for model imperfections or estimator lag. Therefore, using the results of the optimal control law development as a base system, each subloop was analyzed and tuned as necessary to provide adequate stability margin. Additional dynamics were included as necessary when the best control could not be achieved with a simple gain feedback. A block diagram of the resulting system is shown in Figure 2. This control law tuning is an exercise in classical control law design but retains the optimal control configuration. Optimal control tuning is the key to reliable and accurate pointing of the barrel tip. The best performance characteristics of the optimal controller ar retained, as evidenced in the Figure 3 frequency respons of barrel tip versus input command, while added stability rgin assures successful implementation.

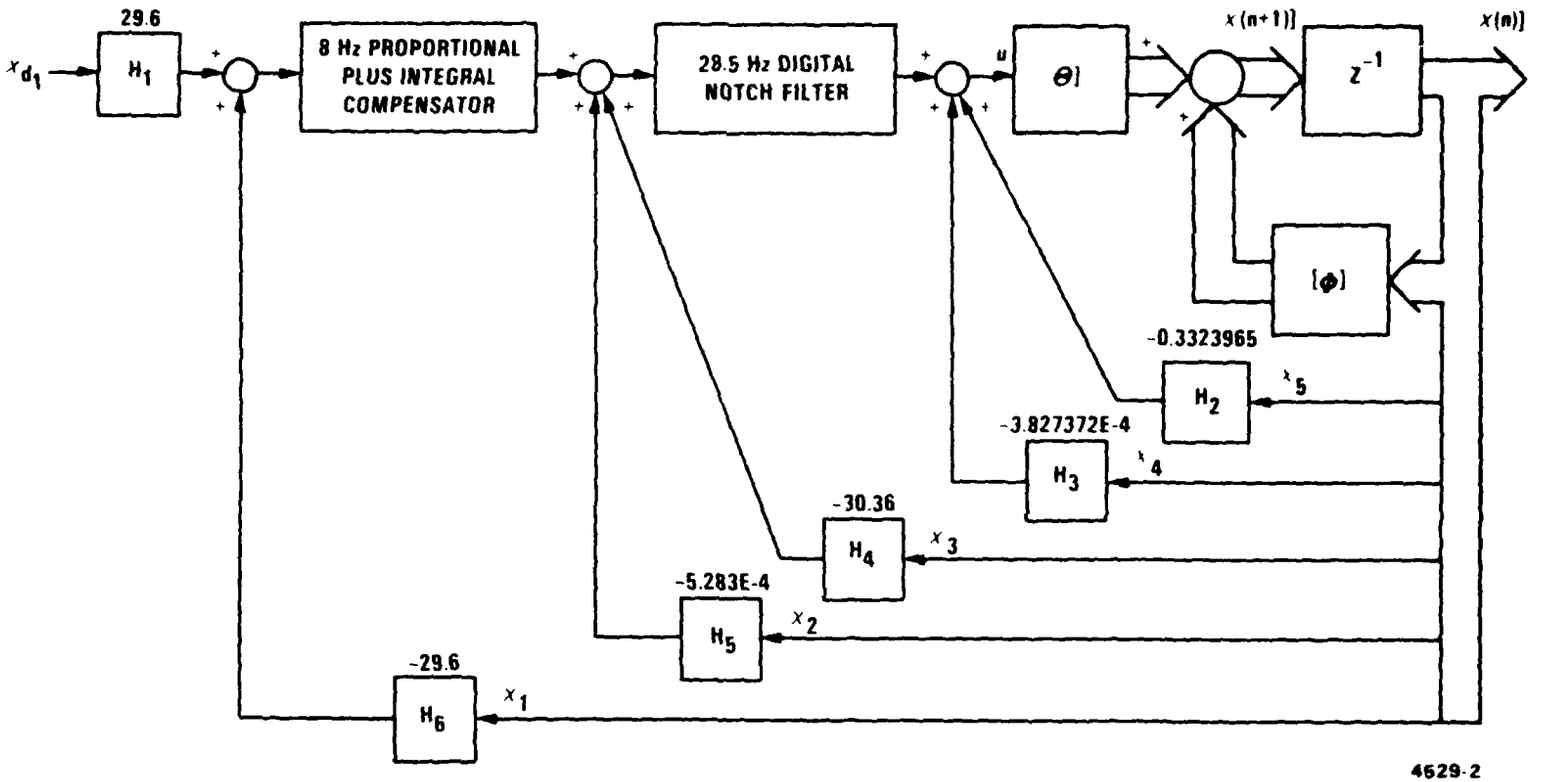


Figure 2 Block Diagram of Optimal Controller

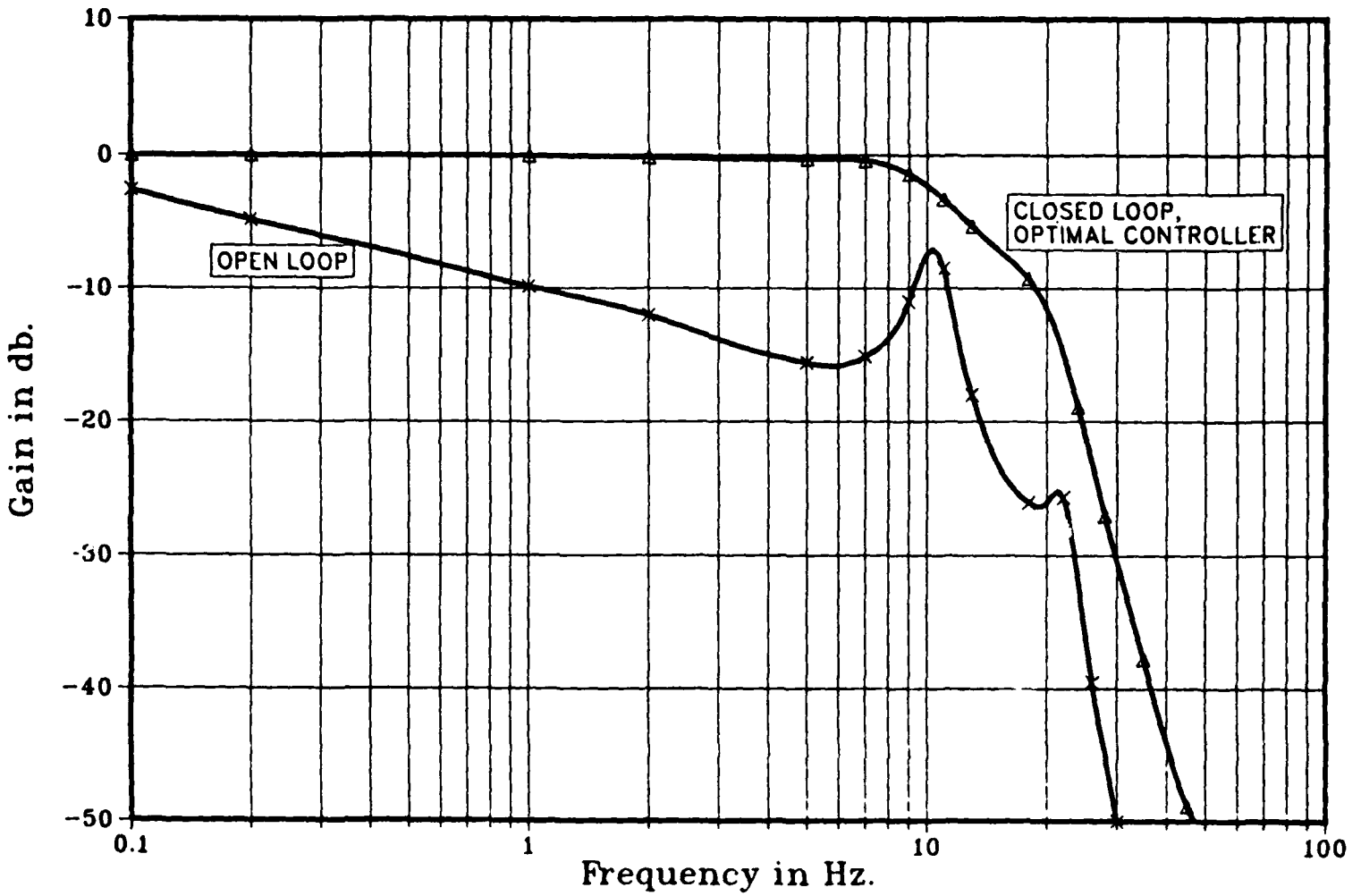


Figure 3 Muzzle Rate vs. Input Command

Besides a performance goal of good input command response out to the 10 Hertz firing frequency, an essential goal for stabilization is good rejection of vehicle disturbances. The highest dominant rate disturbance frequency expected from the vehicle in typical applications is 1 Hertz. Therefore, at least 90% attenuation of all disturbances up to 1 Hertz was a primary consideration during control law development. As shown in Figure 4, this goal, and more (greater than 20 db attenuation below 1 Hertz), was achieved. A time history of the barrel tip response to a 1 Hertz, 10 deg/sec vehicle rate disturbance is shown in Figure 5.

ESTIMATOR DEVELOPMENT

With an approach directed at control over an unmeasured system state, a state estimator is not only necessary but becomes the fundamental backbone of the control law. The accuracy with which the barrel tip can be pointed by the controller depends primarily upon the accuracy with which the barrel tip state variable can be estimated. A simple predictor type estimator, based solely on the propagation of plant input commands through a math model, derives its accuracy from the fidelity of the model. However, perfection is seldom achieved. A typical gun mount is difficult to precisely model due to complex structural interaction, mount-to-mount production variations, and day-to-day environmental changes resulting in friction and gear backlash variations. Therefore, in a practical application, the predictor type estimator will usually fail.

A predictor-corrector type estimator, based on feedback control concepts, offers a viable solution to the estimation problem. Although this type estimator is not without its problems, it is more immune to modeling imperfections than the essentially open loop predictor. The predictor-corrector propagates all inputs and disturbances through a math model the same as a simple predictor. A correction to the predicted states is then made based on the error between measurements of actual states and their estimated counterparts. Modeling imperfections, instead of causing estimate divergence as encountered in the predictor, results in varying degrees of underdamped estimate performance depending on the degree of imperfection and the gains associated with the correction. Therefore, the choice of a correction gain vector, $L]$, must be matched to the expected modeling imperfection and plant dynamics.

A somewhat painless approach to determining $L]$ is to employ Ackermann's formula. This formula allows the placement of estimator characteristic roots anywhere in the z-plane unit

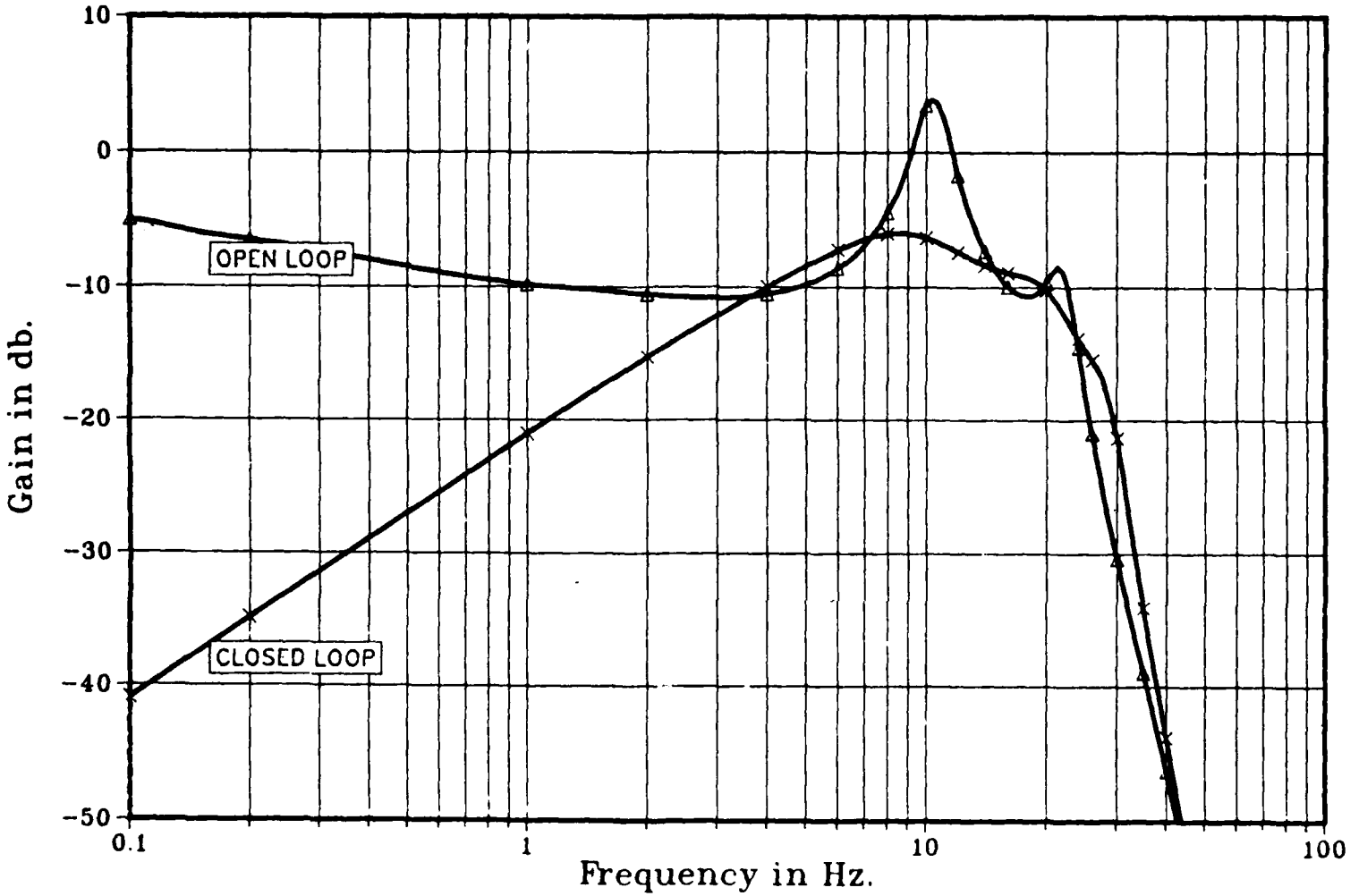


Figure 4 Muzzle Rate vs. Vehicle Disturbance

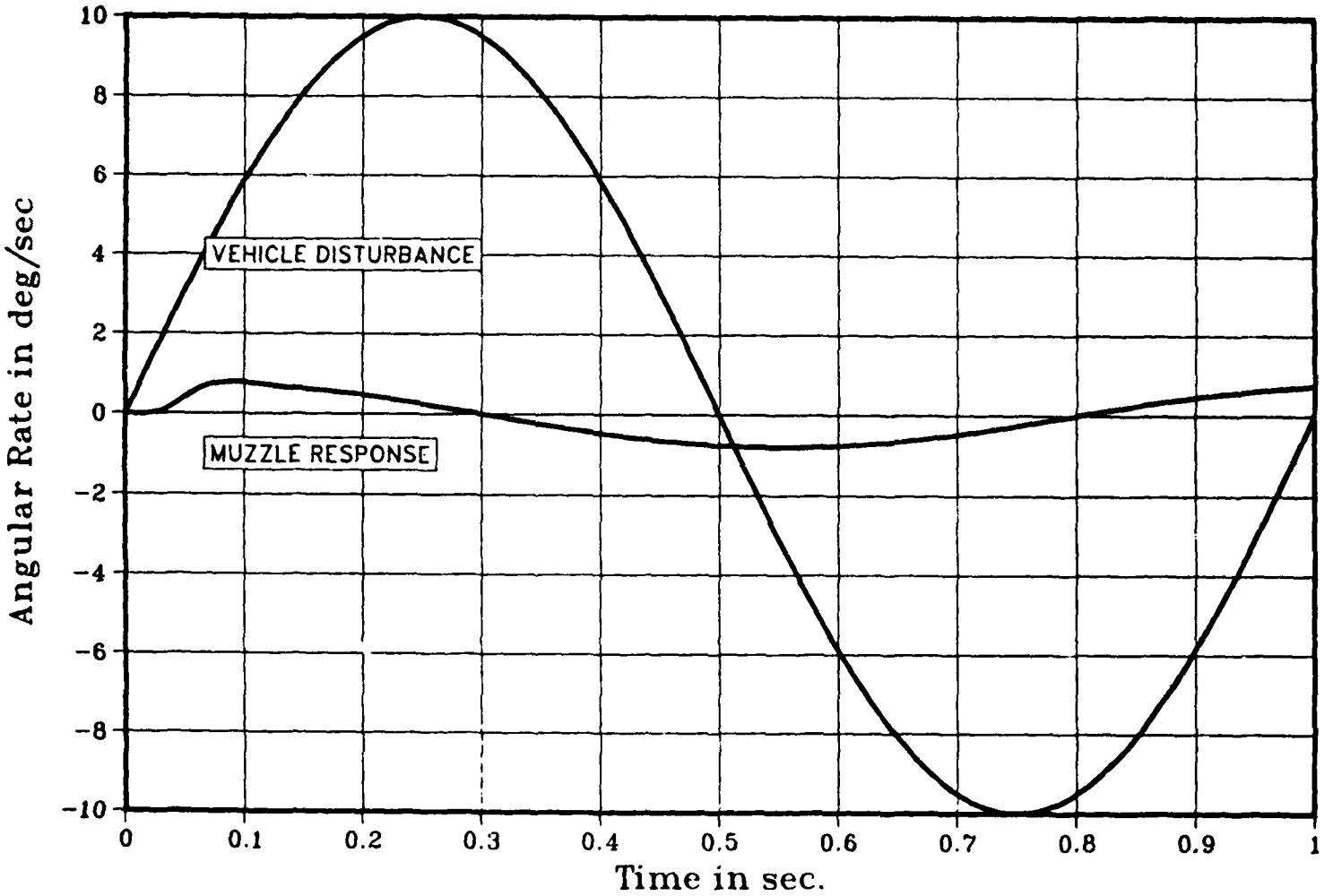


Figure 5 1 Hz. Disturbance Response

circle. By placing estimator poles in desired locations, a desired characteristic equation will result. This equation can be represented by:

$$\alpha_e(z) = z^k + \alpha_1 z^{k-1} + \alpha_2 z^{k-2} + \ldots + \alpha_k,$$

where k is the order of the system. Then, using the state transition matrix of the system model, $[\Phi(T)]$, a matrix characteristic equation can be constructed:

$$\alpha_e([\Phi(T)]) = [\Phi(T)]^k + \alpha_1[\Phi(T)]^{k-1} + \ldots . \alpha_k \quad .$$

This equation is dual with $\alpha_e(z)$. Finally, with a vector relating the measurement to the measured states, $D]'$, the Ackermann formula allows $L]$ to be determined by:

$$L] = \alpha_e([\Phi(T)]) \begin{bmatrix} D]'[\Phi(T)] \\ D]'[\Phi(T)]^2 \\ \vdots \\ D]'[\Phi(T)]^k \end{bmatrix}^{-1} \begin{bmatrix} 0 \\ 0 \\ \vdots \\ 1 \end{bmatrix}$$

Although painless, this approach allows pole-zero cancellation to obtain the desired characteristics. As such, the resulting estimator feedback system is very sensitive to a mismatch between the actual plant and the math model. This sensitivity is manifest in undesired estimated state dynamics. To avoid the difficulties, the correction gain vector, $L]$, is adjusted via classical techniques so that each estimate displays a fast, damped response to system measurement.

In order to finish the fine tuning of $L]$, the complete estimator must be considered. A block diagram of the estimator, and its relationship to the entire system, is shown in Figure 6. Since measured states include anti-aliasing filter and sensor dynamics, they are somewhat different from the plant states that are to be controlled. These differences must be accounted for in the estimator definition.

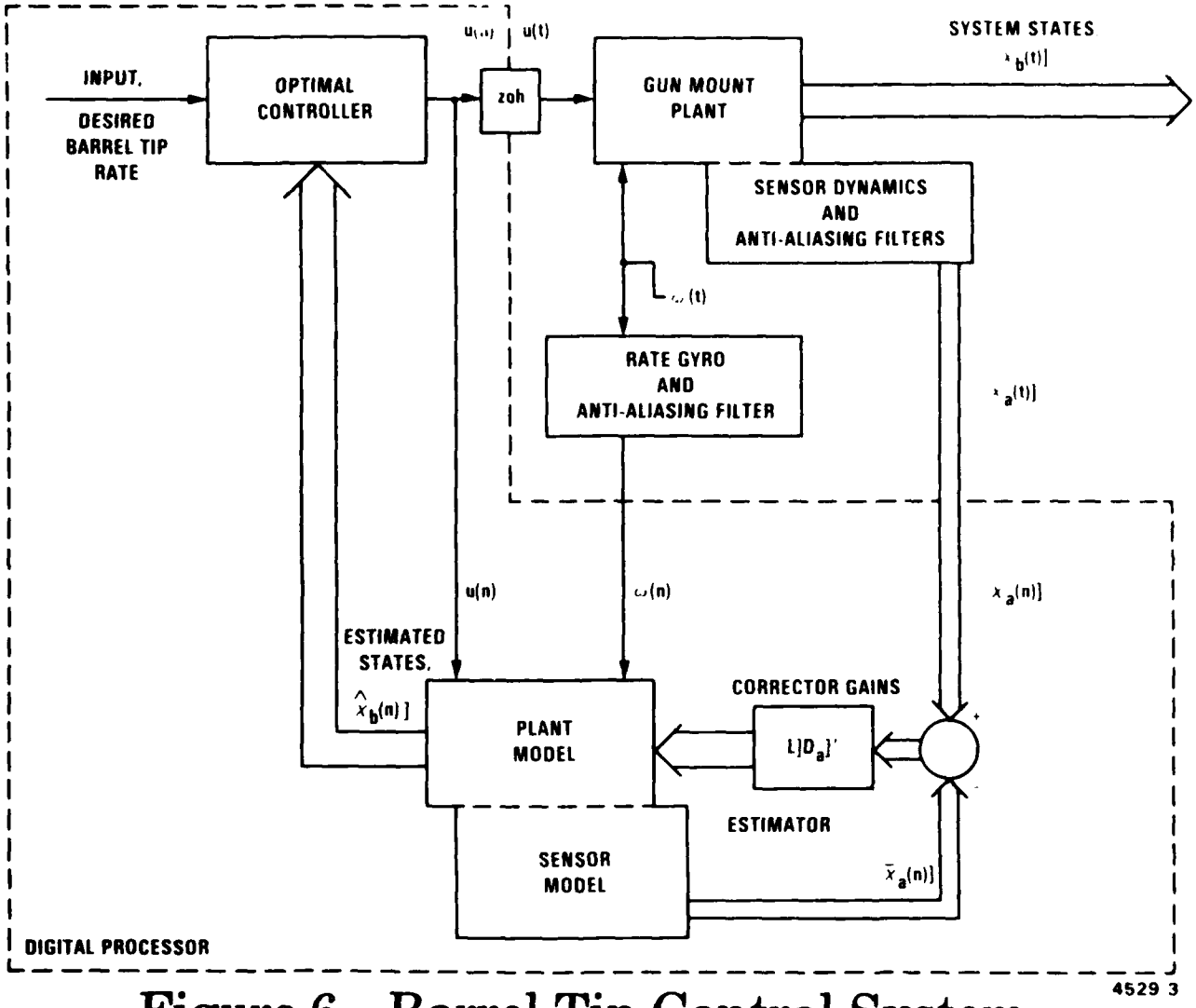


Figure 6 Barrel Tip Control System

Since the measured states are adequately filtered for anti-aliasing and do not need to be estimated, a reduced-order estimator can be constructed by partitioning the state transition equation into measured and unmeasured states:

$$\begin{bmatrix} x_a(n+1)] \\ x_b(n+1)] \end{bmatrix} = \begin{bmatrix} [\Phi_{aa}] & [\Phi_{ab}] \\ [\Phi_{ba}] & [\Phi_{bb}] \end{bmatrix} \begin{bmatrix} x_a(n)] \\ x_b(n)] \end{bmatrix} + \begin{bmatrix} \Theta_a] \\ \Theta_b] \end{bmatrix} u(n) + \begin{bmatrix} \Psi_a] \\ \Psi_b] \end{bmatrix} w(n)$$

where $x_a(n)]$ is the measured states, $x_b(n)]$ the unmeasured states, $u(n)$ the plant input, and $w(n)$ is the vehicle disturbance. An associated measurement equation can be described by:

$$y(n)] = \begin{bmatrix} D_a]' & x_a(n)] \\ 0 & x_b(n)] \end{bmatrix}$$

Using the partitioned definition of the system, the estimator algorithm is described by the following three equations:

$$\bar{x}_b(n+1)] = [\Phi_{bb}]\hat{x}_b(n)] + [\Phi_{ba}]x_a(n)] + \Theta_b]u(n) + \Psi_b]w(n) ,$$

$$\bar{x}_a(n+1) = [\Phi_{aa}]x_a(n)] + [\Phi_{ab}]\bar{x}_b(n+1)] + \Theta_a]u(n) + \Psi_a]w(n) ,$$

$$\hat{x}_b(n+1)] = \bar{x}_b(n+1)] + L]D_a]'\{x_a(n+1)] - \bar{x}_a(n+1)]\},$$

where $\bar{x}]$ is an intermediate prediction of the measured and unmeasured states and $\hat{x}]$ is the corrected estimate. The esti-

mator equations are executed in the order given above. The first equation is simply a propagation of the unmeasured estimator forward in time through the state transition matrix (model of the plant). Included in the equation are the inputs, u(n), the vehicle disturbance, w(n), and the measured states, $x_a(n)$]. The second equation is similar to the first, but predicts the future measured states. Finally, the third equation is calculated at the time N-1 so that a comparison between the predicted measured states and actual measured states can be made to determine the error in the estimate. This error, through the gain vectors L] and D_a], is used to correct the prediction resulting in the best estimate of unmeasured states, $\hat{x}_b$].

Although the estimator can be expected to add some phase lag to the optimal control feedback states, a well designed estimator will cause minimal degradation to the overall performance. A simulation step response of the Emerlec-30 test gun mount is shown in Figure 7. The excellent performance displayed by the tuned optimal controller was only slightly modified by the addition of the estimator. More importantly, control over a critical unmeasured system state, the barrel tip rate, was achieved.

SUMMARY

A modern control approach to firing accuracy improvements has been developed for a 30 mm naval gun mount. Optimal control techniques were applied to achieve the best control over the barrel tip while meeting the desired performance criteria of quick, damped response to system rate inputs and attenuation of system disturbances. The practical application of the optimal controller to a 30 mm test bed gun mount was made feasible by employing control tuning based on classical control techniques. Without tuning, the stability margins obtained through optimal control design would be inadequate for any imperfections in state estimation or plant modeling.

The key to achieving control over the barrel tip rate, since the useful measurement of tip rate information for feedback control is not only difficult but expensive, lies in the successful estimation of this system state. Using feedback control techniques, a predictor-corrector type state estimator was developed with minimal (no more than 15 deg) phase lag added to each state control loop.

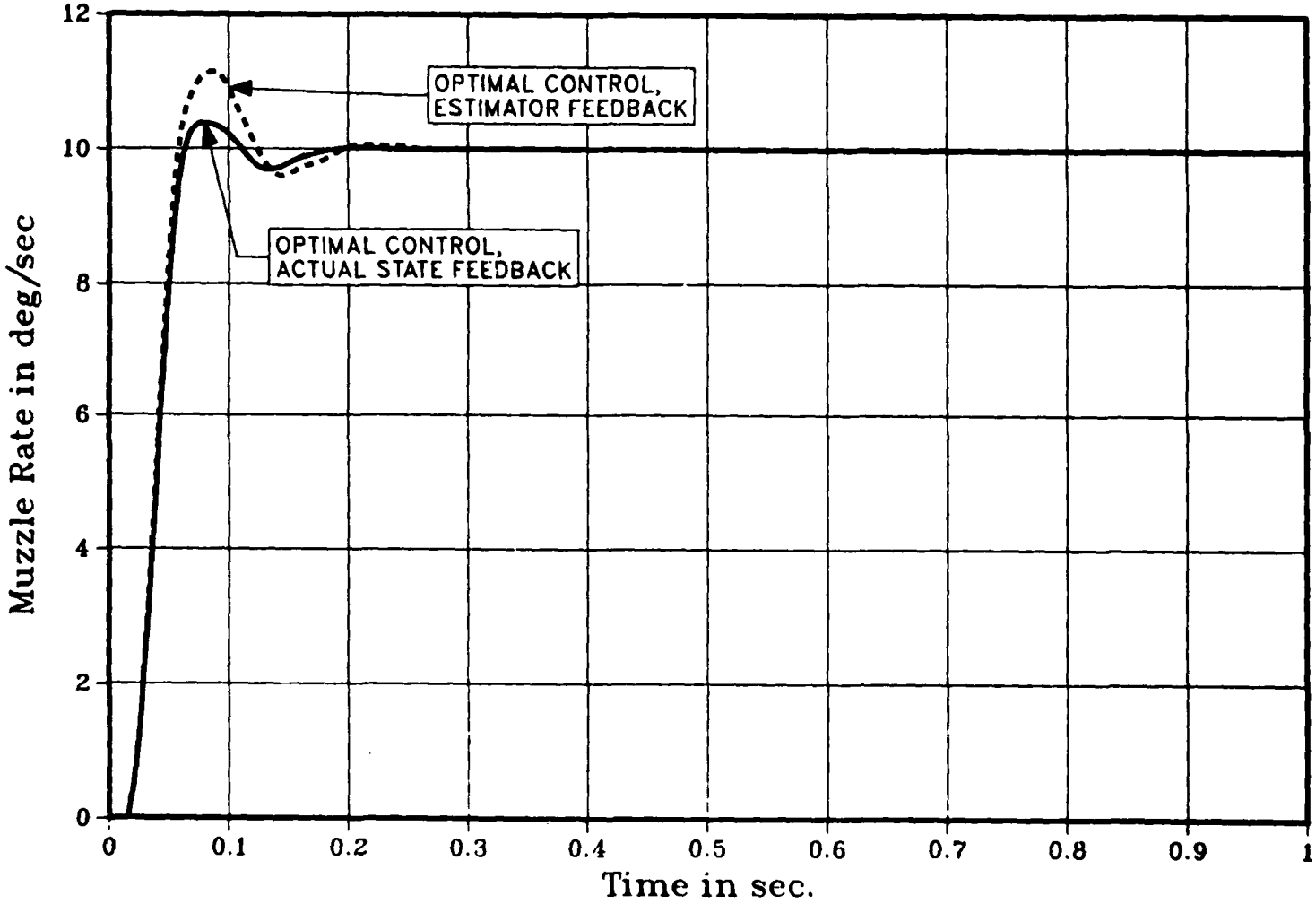


Figure 7 System Step Response

Together the tuned optimal controller and the predictor-corrector state estimator embody a modern state variable control technique to stabilize and drive the gun barrel tip. Control over the tip (or muzzle) rate greatly improves the pointing accuracy thereby decreasing the dispersion encountered when a gun is fired from a moving vehicle. By including higher order modes of the barrel and gun mount, the same technique could be extended to control virtually any point along the barrel. Thus, future firing accuracy may only be limited by the projectile itself.

The next phase of this endeavor will be to code the optimal controller and estimator for microprocessor control of the test gun barrel tip. Pointing accuracy will be assessed during various laboratory controlled disturbances. Also, a test firing should provide a real disturbance environment and penultimate proof of concept. The final proof should be in the field in battle conditions.

REFERENCES

Bellman, R., and Dreyfus, S.E. Applied Dynamic Programming. Princeton: Princeton University Press, 1962.

Franklin, G., and Powell, J.D. Digital Control of Dynamic Systems. Reading: Addison-Wesley, 1980.

Kuo, B.C. Discrete-Data Control Systems. Englewood Cliffs: Prentice-Hall, 1970.

Shinners, S. Modern Control System Theory and Application. Reading: Addison-Wesley, 1978.

Takahashi, Y. and others. Control and Dynamic Systems. Reading: Addison-Wesley, 1970.

Talir, R.J. "Optimal Control of a Digital System with Time Delay" (M.S. Thesis, University of Missouri - Rolla, 1977).



Next page is blank.

AD P001087

A MODERN CONTROL THEORY VIEW OF HIMAG TEST DATA

R.A. Scheder
A.T. Green
B.C. Culver
Delco Electronics Division
General Motors Corporation
Goleta, California 93117

ABSTRACT

Post-test analysis of the HIMAG moving target simulator (MTS) data shows that significant improvements in hit probability can be achieved through the use of modern control theory. The paper traces the evolution of the HIMAG estimator-sight controller from its early classical to its later quasi-optimal mechanization. The full solution, adaptive estimator, predictor, and nominal controller that subsequently emerged is presented and evaluated using MTS data.

INTRODUCTION

The intermittent and evasive targets of the modern battlefield seriously challenge classical fire control. The difficulty in hitting intermittent targets is due to:

- Step-like tracking commands and the resulting rapid and large change in sight rates during track initialization. These produce "transients" in the classical fire control that require a relatively long time to settle out.
- The necessity to extrapolate target motion through obscuration. The greater the capability of the algorithms to predict (without measurement) future target motion, the smaller the transients introduced when measurements are again available and reacquisition begins.

The problem of hitting evasive targets is tied to the ever changing character of their underlying motion:

- Since classical fire controls have no means of adapting to these changes, they are prevented from accurately estimating target acceleration and, therefore, are limited to first order target prediction schemes. These, in turn, result in large target-induced errors.
- Even in cases where target-induced error is small, the target velocity estimates will often contain lags that, in turn, result in large weapon pointing system bias errors.

A series of tests and analyses were conducted to determine the extent of these problems and if modern control theory could be used to solve them. The results of that study are presented in the following paragraphs.

STUDY OBJECTIVES

The objectives of the study were to develop a set of fire control algorithms based on modern control theory, to compare their performance with classical algorithms in the realistic environment provided by HIMAG, and to evaluate their military worth for the 1985-1990 time frame. The fire control measures of military worth selected are:

1. Fire Control Settling Time. This measures time to first fire and target servicing rate.

2. Estimator and Predictor Accuracy Against Evasive Targets. This measures hit probability and ability to extrapolate target motion through obscuration.

3. Hit Probability. This measures the effects of estimator/predictor performance within the context of the entire weapon-pointing error budget. (That is, effects that are large in themselves may or may not be the primary hit probability drivers.)

TEST SETUP

The moving target simulator (MTS) test setup consisted of a "cinerama" screen and a "spot generator" that projected a laser spot on the screen. The spot generator, under computer control, caused the laser spot to move back and forth on the screen simulating various types of target paths. The HIMAG autotracker tracked the laser spot as if it were the target vehicle aimpoint. This setup is illustrated in Figures 1, 2, and 3.

APPROACH

The study plan contained three steps:

1. Reconfigure HIMAG's classical sight control loop with a modern control loop.

2. Replace HIMAG's classical constant-gain estimator/sight controller and first order predictor with a modern time varying, self-adaptive gain estimator/controller and higher order predictor.

3. Reduce the MTS data, and evaluate the fire control measures for both the original, classical, and modern fire control algorithms.

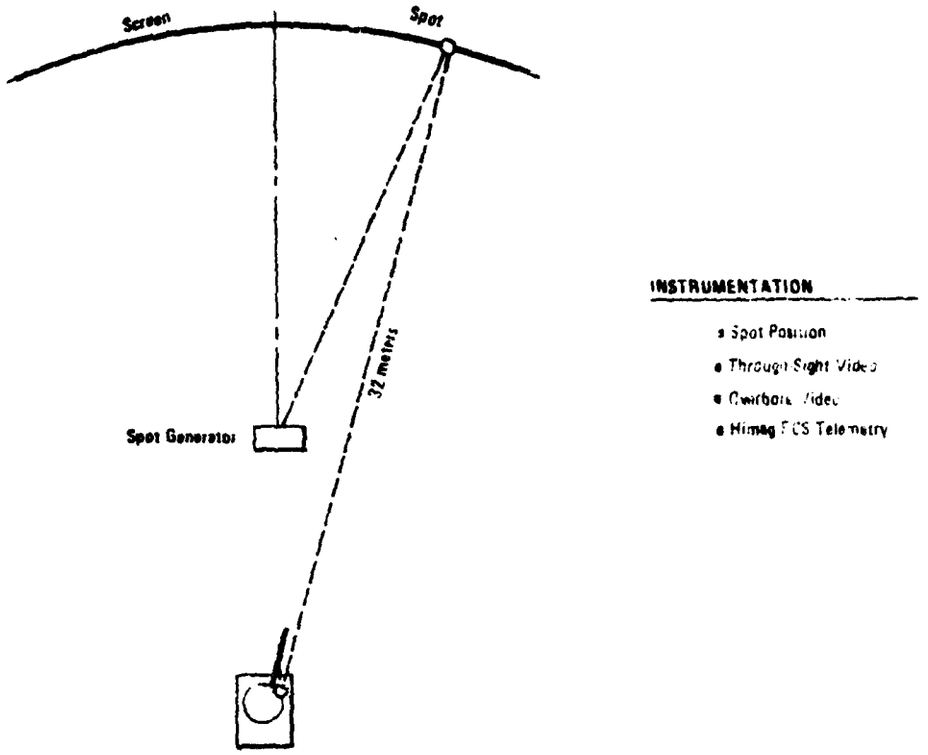


Figure 1. MTS Test Setup

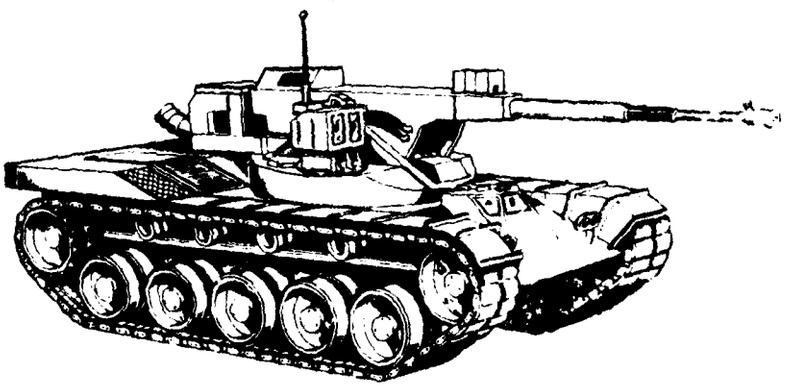


Figure 2. HIMAG Test Bed

S82-99

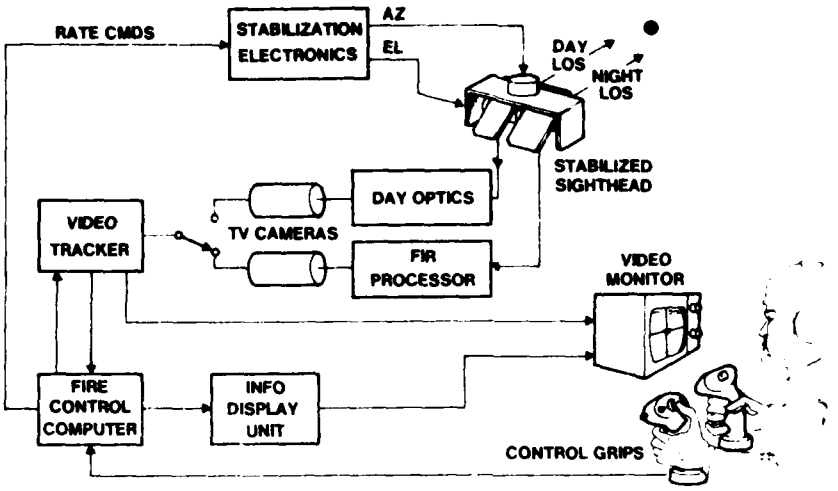


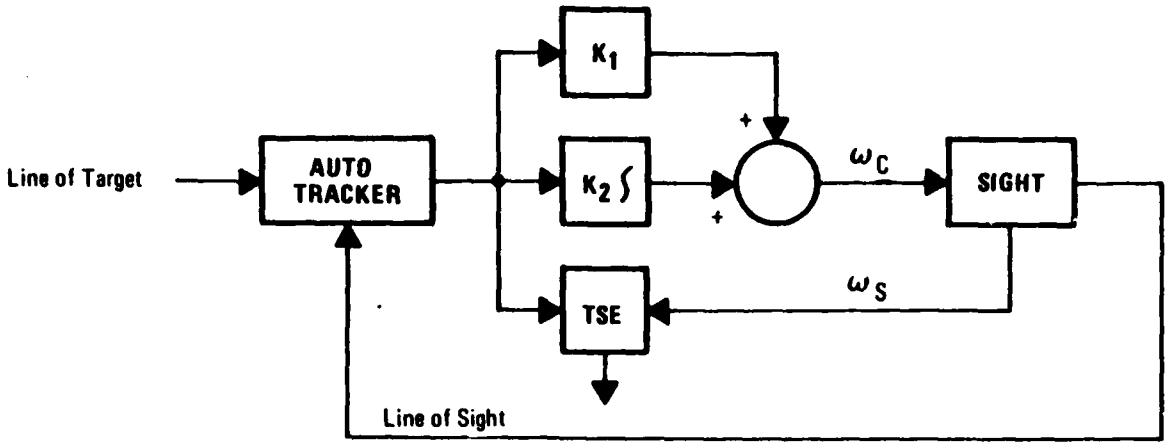
Figure 3. HIMAG Autotracking System

CONTROL LOOP RECONFIGURATION

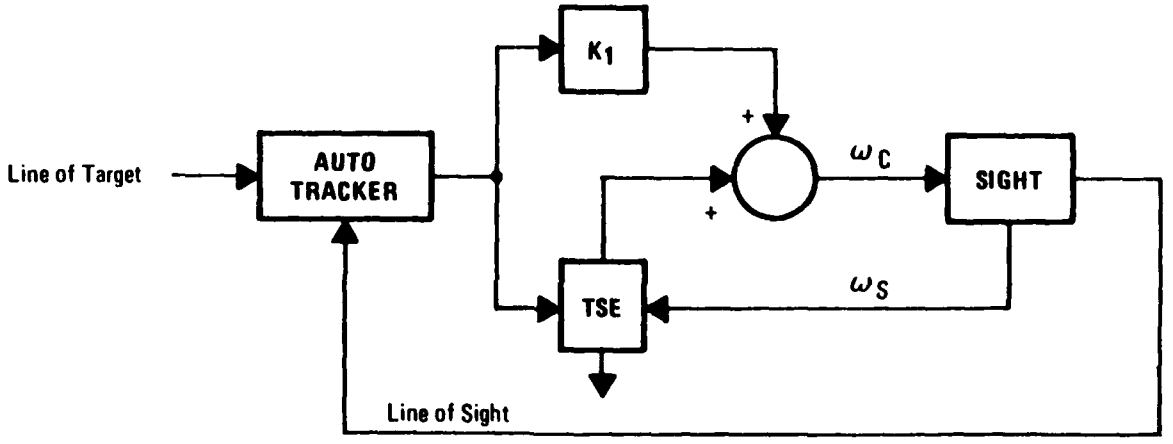
In 1979, video autotracking underwent extensive field testing against realistic military targets at the Yuma Proving Ground. Although the system tracked well under high mobility conditions, the target state estimates and estimator settling times were thought to be inadequate for an operational system of the 1985-1990 time frame.

An improved configuration (Figure 4) integrated a scheduled gain target state estimator into the control loop while retaining a direct proportional control path. When the improved configuration was mechanized into the Delco simulation facility, it showed promise for providing considerable improvement. The design was subsequently implemented into the HIMAG system and field tested.

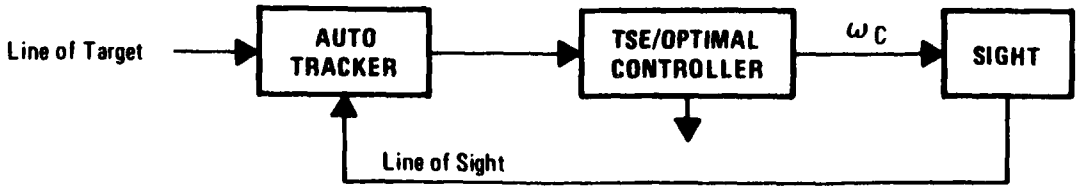
Development work continued on a modern optimal controller/target state estimator with full on-line gain computation (via the discrete Riccati equation). With the full optimal control configuration, there is no direct control link between the tracker and the sight. When this configuration was simulated, the results indicated considerably improved performance. The loop configuration without the modern estimator was mechanized into HIMAG in time for the MTS tests.



a. Original Autotrack Configuration (1979)



b. Improved Operational Autotrack Configuration (1980)



c. Full Optimal Control Configuration Used For MTS Testing (1980)

Figure 4. Chronology of HIMAG Autotrack Control Loop

Tabulated below are performance results for the three configurations across the range of scenarios from stationary firer/stationary target (S/S) to moving firer/moving target (M/M) with evasive maneuvers (E).

PARAMETER	FIELD TEST — ORIGINAL CONFIGURATION S/S-M/M-E	FIELD TEST — IMPROVED CONFIGURATION S/S-M/M-E	SIMULATION FULL OPTIMAL CONTROL S/S-M/M-E
Tracking Error (mrad rms)	0.2 - 0.7	0.2 - 0.5	0.2 - 0.4
Target Position Estimate Error (mrad rms)	0.2 - 0.3	0.1 - 0.2	0.1 - 0.2
Velocity Estimate Error (mrad/s rms)	0.3 - 1.5	0.2 - 1.0	0.2 - 0.5
Position Loop Settling Time (s)	2.0 - 3.0	1.0 - 2.0	0.2 - 0.5

MATHEMATICAL FORMULATION

The original HIMAG fire control algorithms consisted of a fixed-gain target state estimator, an integral plus proportional, fixed gain controller, and a first-order predictor. The modern control algorithms presented below feature time varying and self-adaptive gains for the estimator and sight controller, modern control loop configuration, and a higher order predictor containing a correction for target jerk.

DEFINITION OF TERMS

s Inertial target minus vehicle position vector expressed in the instantaneous line of sight frame (LOS frame).

v Inertial target minus vehicle velocity vector expressed in the LOS frame.

a Inertial target acceleration vector expressed in the LOS frame.

w Inertial sight angular rate vector expressed in the LOS frame.

v^v Inertial vehicle velocity expressed in the LOS frame.

a^v Inertial vehicle acceleration, as measured by the vehicle-mounted accelerometers, expressed in the LOS frame.

a^b Inertial target acceleration vector expressed in the instantantous target body frame.

w^b Inertial target body angular rate vector expressed in the LOS frame.

P^o Initial target state error covariance matrix expressed in the LOS frame.

R^a The error covariance matrix of the autotracker's measurement vector expressed in the LOS frame.

Q^b The *a priori* covariance matrix of the error in the target acceleration extrapolation equation expressed in the instantaneous target body frame.

u^m Inertial rate command vector to sight motors expressed in the LOS frame.

z The measurement vector (range, autotrack azimuth error, autotrack elevation error).

r Target range (first component of s)

t_f Bullet time of flight to predicted target position.

$s/r \equiv (1, x_1, -y_1)$

$v/r \equiv (v_{1/r}, x_2, -y_2)$

$a/r \equiv (a_{1/r}, x_3, -y_3)$

ASSUMPTIONS

The following assumptions were made in developing the modern control algorithms:

1. Slow moving distant target: v/r, a/r are small.
2. Sight roll rate nearly zero: w_1 is small.
3. Good target tracking: x_1, y_1, w_2-y_2, w_3-x_2 are small.
4. Time rate of change of target body frame acceleration is zero mean white noise: $\dot{a}^b = 0$.
5. Target and sight vertical axes are nearly parallel: w_1^b, w_2^b are small.
6. Negligible sight servo loop time constant: $u^m \equiv (w_3, w_2)$.

The first two assumptions are straightforward. The sight control performance criterion (in each axis) is chosen to assure the validity of Assumption 3;

$$J = x_1^2/P_{11} + (w_3 - x_2)^2/P_{22}.$$

P_{11} and P_{22} reflect the confidence in the estimates of x_1 and x_2. Assumption 4 implies that the driver of the target vehicle can be expected to hold his controls nearly constant over the estimator time step, dt. This assumption really has three parts:

1. The time derivative of target body frame translation acceleration is zero.

2. The target rotates only about the axis formed by the cross product of target translational velocity and acceleration.

3. The target is aligned with its velocity vector.

Assumption 5 implies that the earth is flat to within about 7 degrees. This assumption can be removed easily by adding the term, $-w_1^b\, x_3 dt$, in the extrapolation equation for x_3. Assumption 6 implies that the inertial rate of the line of sight instantaneously takes on the values of the inertial rate commands sent to the sight drives. In other words, the sight transfer function is one.

The algorithms presented below are a first order Taylor expansion in time, with terms that are second order in small quantities neglected. For brevity, only the azimuth equations are shown.

Initialize Estimator:

$$\bar{x}_1 = \bar{x}_2 = \bar{x}_3 = 0$$

$$\bar{P}_{11} = P_{11}^0,\ \bar{P}_{22} = P_{22}^0,\ \bar{P}_{33} = P_{33}^0$$

$$\bar{P}_{12} = \bar{P}_{13} = \bar{P}_{23} = 0$$

Correct Estimator:

$$R = [1.0 + C_1(r - c_2)^2]R^a \qquad (1)$$

$$D = \bar{P}_{11} + R$$

$$K_1 = \bar{P}_{11}/D; \quad K_2 = \bar{P}_{12}/D; \quad K_3 = \bar{P}_{13}/D$$

$$E = z - \bar{x}_1$$

$$x_1 = \bar{x}_1 + K_1E; \quad x_2 = \bar{x}_2 + K_2E; \quad x_3 = \bar{x}_3 + K_3E$$

$$F = 1.0 - K_1$$

$$P_{11} = F\bar{P}_{11}F + K_1RK_1$$

$$P_{12} = F\bar{P}_{12}F + K_1RK_2$$

$$P_{13} = F\bar{P}_{13}F + K_1RK_3$$

$$P_{22} = \bar{P}_{22} - 2\bar{P}_{12}K_2 + K_2\bar{P}_{11}K_2 + K_2RK_2$$

$$P_{23} = \bar{P}_{23} - 2\bar{P}_{12}K_3 + K_2\bar{P}_{11}K_3 + K_2RK_3$$

$$P_{33} = \bar{P}_{33} - 2\bar{P}_{13}K_3 + K_3\bar{P}_{11}K_3 + K_3RK_3$$

Command Sight:

$$G = P_{11} + P_{22}dt^2$$

$$u_1^m = (P_{22}dt/G)x_1 + x_2 + (1.5P_{11}dt/G)x_3 \qquad (2)$$

Extrapolate Estimator:

$$V = [v_1^2 + (rx_2)^2 + (rx_3)^2]^{1/2}$$

$$Q = (1.0 + c_2x_1^2)[Q_{11}^b(rx_2/V)^2 + Q_{22}^b(v_1/V)^2] \qquad (3)$$

$$w_b = (v_1x_3 - a_1x_2)r/V^2$$

$$j = w_ba_1/r \qquad (4)$$

$$\bar{x}_1 = x_1 + x_2 dt - u_1^m dt$$

$$\bar{x}_2 = x_2 + x_3 dt - a_2^v dt/r$$

$$\bar{x}_3 = x_3 + j\,dt$$

$$\bar{P}_{11} = P_{11} + 2dtP_{12} + dt^2 P_{13} + dt^2 P_{22}$$

$$\bar{P}_{12} = P_{12} + dtP_{13} + dtP_{22} + 1.5dt^2 P_{23}$$

$$\bar{P}_{13} = P_{13} + dtP_{23} + 0.5dt^2 P_{33}$$

$$\bar{P}_{22} = P_{22} + 2dtP_{23} + dt^2 P_{33}$$

$$\bar{P}_{23} = P_{23} + dtP_{33}$$

$$\bar{P}_{33} = P_{33} + Q$$

Predict Target Future State:

$$x_2^v = v_2^v/r$$

$$s_2^p = r[x_1 + (x_2 + x_2^v)t_f + x_3 t_f^2/2 + jt_f^3/6]$$

$$v_2^p = r[(x_2 + x_2^v) + x_3 t_f + jt_f^2/2](1 + t_f)$$

$$a_2^p = r(x_3 + jt_f)(1 + t_f)$$

The most interesting features of the algorithms are the nonlinear adaptations expressed in equations 1, 2, 3, and 4:

$$R = [1 + c_1(r - 1{,}250)^2]R^a$$

$$u_1^m = (P_{22}dt/G)x_1 + x_2 + (1.5P_{11}dt/G)x_3$$

$$Q = (1.0 + c_2 x_1^2)[Q_{11}^b (r x_2/V)^2 + Q_{22}^b (V_1/V)^2]$$

$$j = w_b a_1 / r$$

The expression for measurement error covariance, R, accounts for the fact that the autotracker has the smallest measurement error against tank size targets at about 1,250 meters. R^a is closely tied to the resolution limit of the autotracker.

The expression for the sight motor command, u_1^m, accounts for the varying uncertainties in the estimated values of x_1, x_2, and x_3. For example, when target tracking is first initialized, the estimate for x_1 is nearly equal to the measured tracking error, and the values for x_2 and x_3 are nearly zero,

$$P_{22} dt/G \cong 1/dt = 100 \text{ (for HIMAG)}$$

$$1.5 P_{11} dt/G \cong 0.$$

Hence, $u_1^m \cong 100\ x_1$ during initialization, which results in rapid loop closure. During steady state, the sight motor drives are rate aided by x_2 and perturbed by x_1 and x_3 according to the relative uncertainty in their estimated values.

The first factor in the expression for Q, $1 + c_2 x_1^2$, evolved during the initial MTS testing. Three simple (but different) target models were alternately programmed into the HIMAG fire control software. The first was tuned for steady state (constant acceleration) targets, the second for moderately evasive targets, and the third for highly evasive targets. Three results are notable:

1. In terms of weapon pointing accuracy, the third model was dramatically superior to the first and second models, against highly evasive targets. A 50 percent improvement in weapon pointing was observed.

2. For constant acceleration targets, the first model was dramatically superior to the third. Estimated acceleration was virtually identical to actual laser accelerations when the first model was used.

3. When the first model was used against highly evasive targets, tracking lags were large during periods of changing target acceleration.

These results suggest that a self-adapting target state estimator would significantly improve fire control effectiveness and that estimated tracking lag, x_1, can provide the necessary adapation by increasing the size of Q. The second factor in the expression for Q is just the target's body frame acceleration uncertainty rotated into the computational frame of the estimator, that is, the LOS frame.

Basically, the target jerk term, j, is the mathematical result of Assumption 4, $\dot{a}^b = 0$:

$$a = T^{bl} a^b$$

$$\dot{a} = T^{bl} \dot{a}^b - (w^b - w) \times a$$

$$\dot{a} \cong - w^b \times a$$

where T^{bl} is the coordinate transformation from target body frame to LOS frame. The j term is particularly important to the predictor equations because it results in substantially improve hit probability against long range rapidly accelerating targets in coordinated maneuvers.

DATA REDUCTION METHODOLOGY

The data available for analysis from MTS instrumentation consisted of laser spot position, HIMAG fire control telemetry, and video camera data. The reduction process and the major elements of the MTS data are listed below and are depicted in Figure 5.

1. The target state estimator error, particularly rate estimation error, is derived as the difference between HIMAG estimates and the corresponding estimates of the optimal smoother. The optimal smoother (also referred to as a double-sweep smoother) consists of two passes over the spot position data. The first pass, or forward sweep, is an adaptive Kalman filter. The second pass, or backward sweep, optimally corrects the target state estimates derived by the filter in the forward sweep. The double-sweep smoother approach was selected since its implementation is straightforward while yielding highly accurate results.

2. Lay error is derived from the through-sight video as the angular difference between the sight reticle and the desired tracking point on the target.

3. Target-induced error was computed as the miss distance due to target acceleration effects. In a linear lead system, no attempt is made to compensate for target

acceleration; thus, even in the absence of system errors (lay, rate, gun position), there will be a difference between the actual round impact point and the desired impact point due to target acceleration during projectile time of flight. Target-induced error was computed for this analysis by simulating the flight of a 75mm AP round under conditions free of system error and computing the miss distance at the point where target range and projectile range were equal.

4. Gun positioning error is obtained directly from HIMAG telemetry as the weapon control loop error signal (gun servo error). An external measure of gun/LOS offset is derived from through-sight video, overbore video, and tank geometry as a check on the commanded gun/LOS offsets. Gun positioning error was not found to be a significant contributor to weapon pointing error.

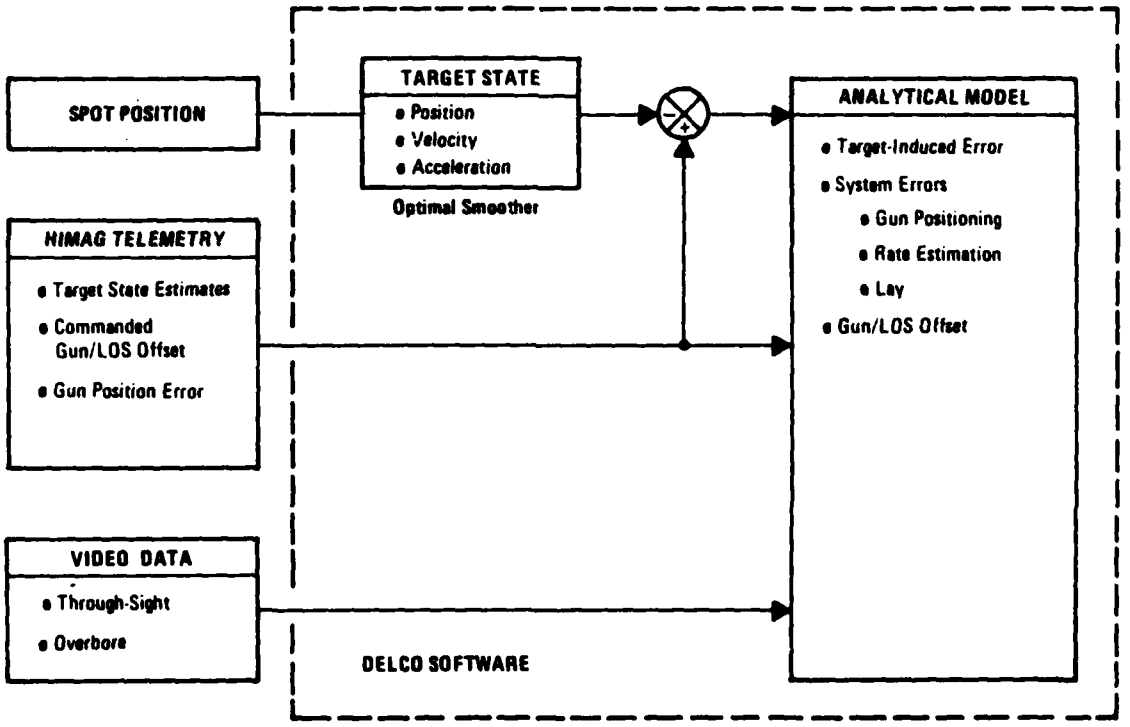


Figure 5. Analysis Data Flow

Time histories of the target state showed that each combat path time segment examined was composed of subintervals of varying levels of target maneuver, as measured by target lateral acceleration. Consequently, the test segments were subdivided according to target acceleration level and, the key parameters (target induced error, lay error, rate estimation error, and gun

position error) were evaluated over each subinterval for influences of target maneuver. The accompanying graphs make reference to data from the 1,500-meter simulations only; however, no significant difference exists between the 1,500-meter data and the 2,500-meter data.

RESULTS

The original plan called for programming the modern control equations into the HIMAG computer before MTS testing. Unfortunately, time constraints allowed only the programming of Configuration 3 with the steady state values of the Kalman gains and control coefficients. Hence, the actual MTS data represents the best possible performance of classical fire control. The modern fire control algorithms presented in the previous sections were evaluated by programming them into Delco's fire control effectiveness simulation and exercising them over the same MTS paths. (See Figure 6.)

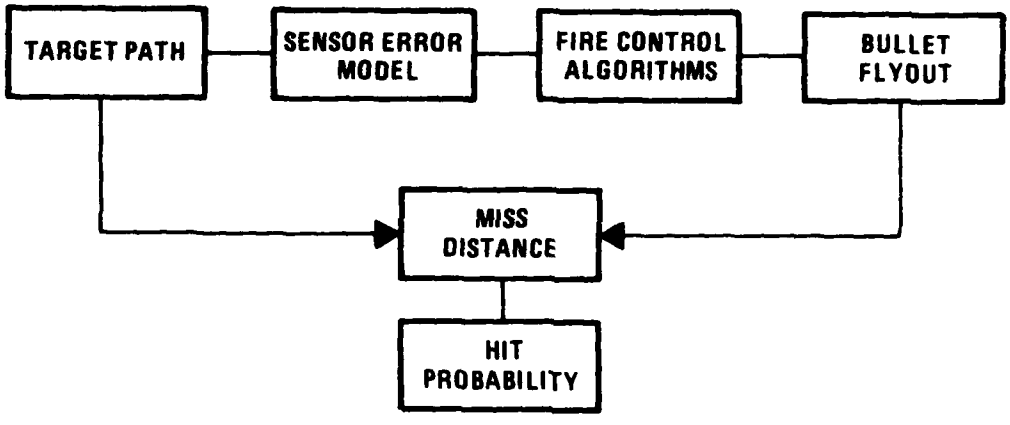
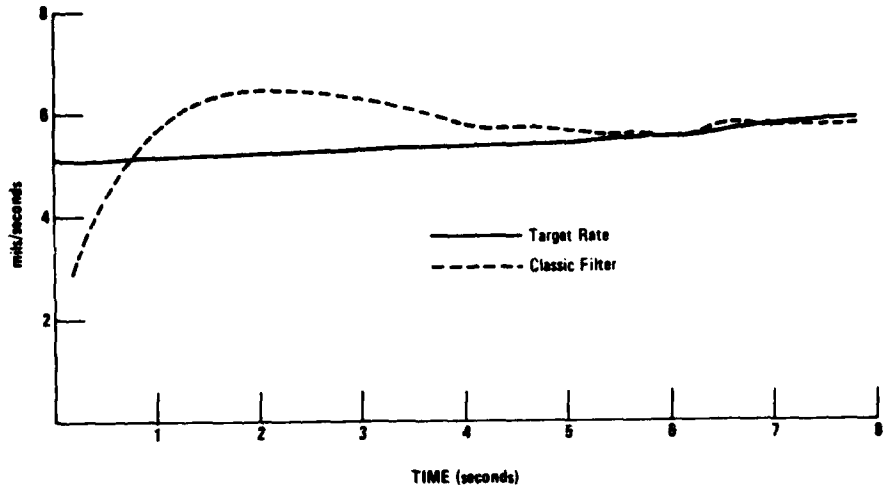


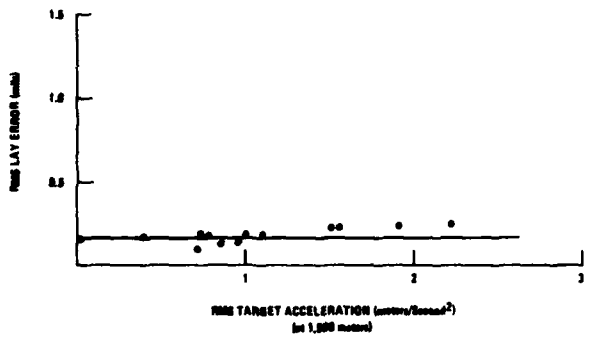
Figure 6. Fire Control Effectiveness Simulation Modes

PERFORMANCE OF CLASSICAL FIRE CONTROL

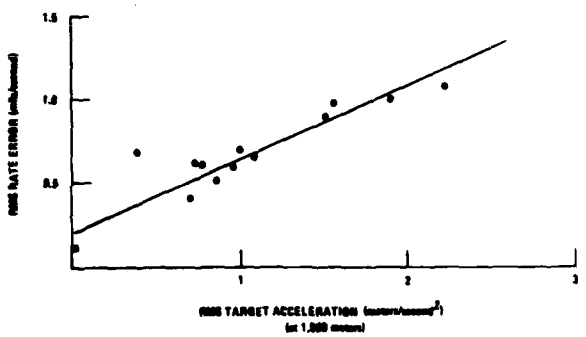
Classical fire control performance was evaluated by examining the HIMAG autotracker fire control settling time, lay error, rate estimation error, and target-induced error. Figure 7a shows that the settling time is between 5 and 6 seconds. It was found not to be highly dependent on target acceleration. Figure 7b shows the autotrack lay error as a function of target acceleration. Note that increasing target acceleration has no appreciable effect on laying accuracy. Rate estimation errors, as affected by level of target maneuver, are shown in Figure 7c. These errors increase with target acceleration.



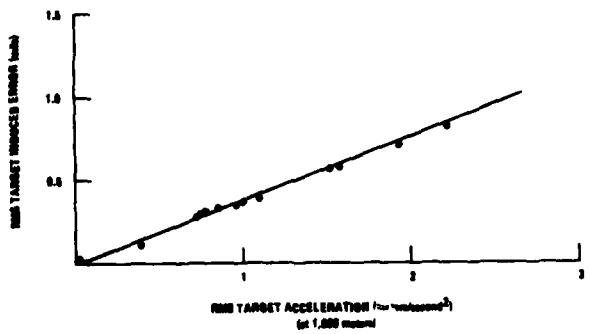
a. Settling Time



b. Laying Accuracy



c. Rate Estimation Accuracy



d. Target-Induced Error

Figure 7. Classical Fire Control Performance

An analysis of target induced error is useful in that it establishes the upper limit of performance for a given round and level of target maneuver. Figure 7d shows target induced error as a function of target acceleration level, assuming the time of flight (t_f) of the 75 mm AP round. The values derived in Figure 7d (0.0 to 0.84 mils)$_2$ were found to be within $\pm$0.03 mils of the theoretical value, $at_f^2/2$.

PERFORMANCE OF MODERN FIRE CONTROL

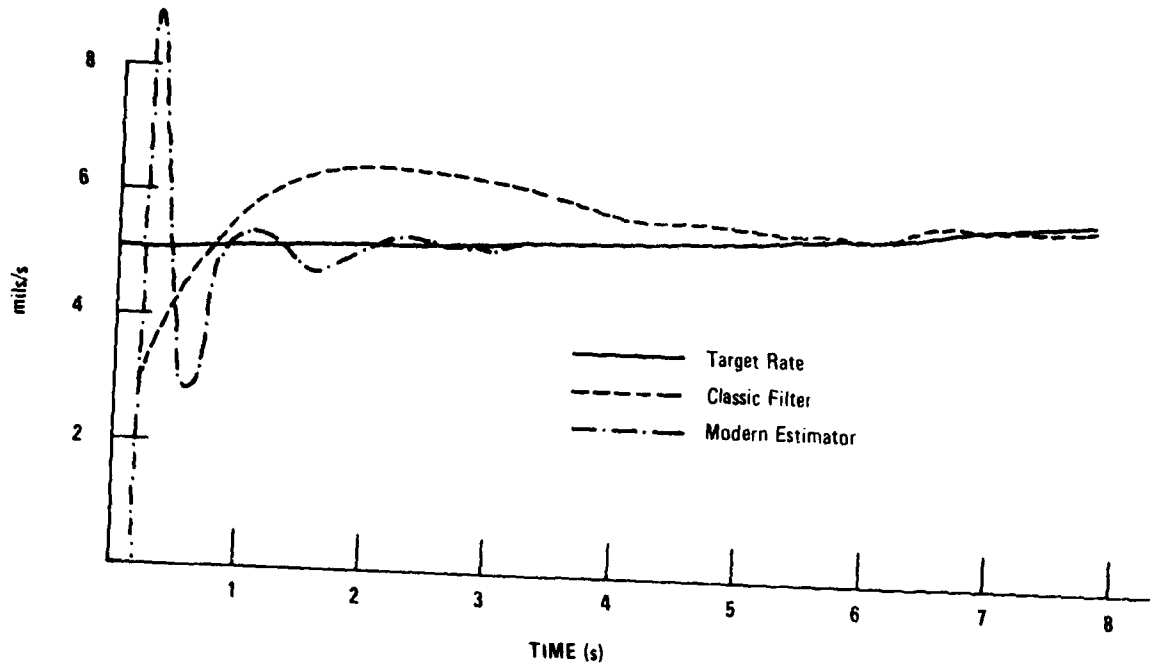
The substantial improvement in settling time achieved by the modern estimator is illustrated in Figure 8a, which shows a change from 5 to 6 seconds for the classical versus 2 seconds for the modern. Similarly, the improvement in rate estimation accuracy is illustrated in Figure 8b. Note the greater than 1 second lay in the classical fire control estimates. Figure 8c translates improved estimator performance into hit probability against the standard NATO 2.3 by 2.3-meter target, 75mm round-to-round dispersion, typical alignment and environmental effects errors, and the HIMAG first order predictor.

Higher order prediction is made feasible by the accurate target acceleration estimates provided by the modern target state estimator. Figure 9 provides a typical example of the reduction in target-induced error achieved with a second order predictor over a first order predictor against a highly evasive target (AMSAA 1500 path). The statistical, one sigma, target-induced errors over the entire path are:

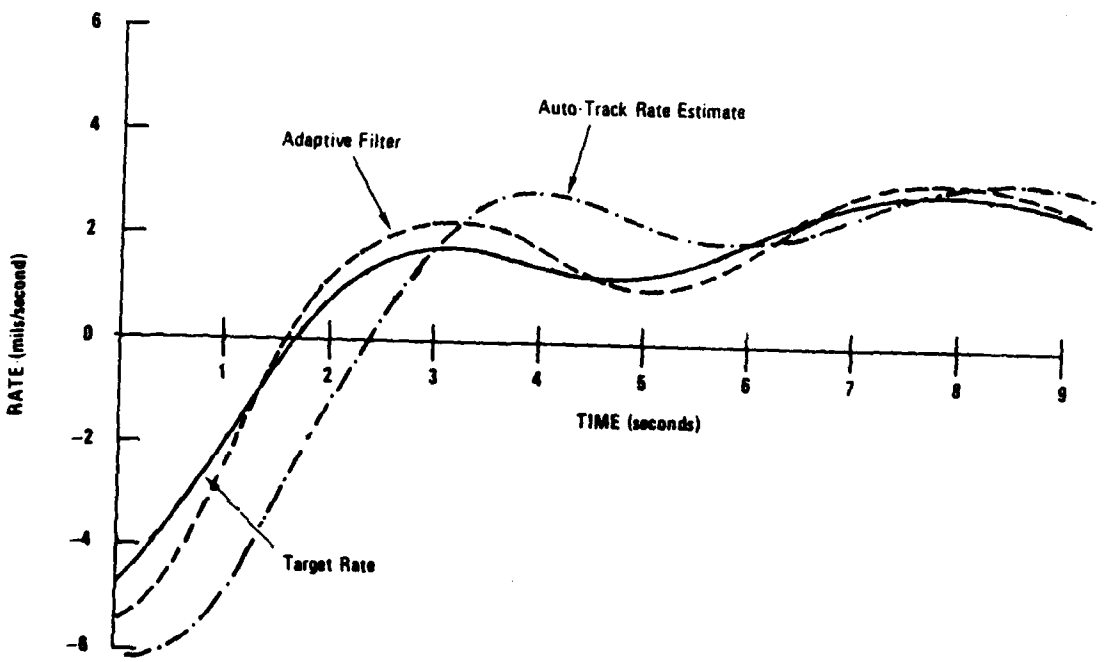
- First Order 0.69 mrad
- Second Order 0.36 mrad.

While the 2 to 1 reduction is impressive, there are other considerations. When combined with the standard quasi-combat error budget, the 100 percent difference in target-induced error results in only a 25 percent difference in hit probability. Even more significant, both predictions offer the same number of opportunities for effective fire. (Note, however, that they are of larger duration for the second order predictor.) Either predictor can result in a target kill if the weapon is fired during a fortunate time window. Hence, the measures of "opportunities for effective fire (cued and uncued)" and "effective fire window size" must be added to the measures of settling time, estimator/predictor accuracy, and hit probability when comparing the military worth of alternative fire control.

Figures 10a and 10b quantify the maximum difference in hit probability among first, second, and third order predictors as a function of target maneuver. For each acceleration level, the target is moving in a coordinated maneuver at the indicated range. While the considerations of the previous paragraph make concrete statements difficult, the figures do suggest that high order predictors have a large potential for improving hit probability against evasive targets.

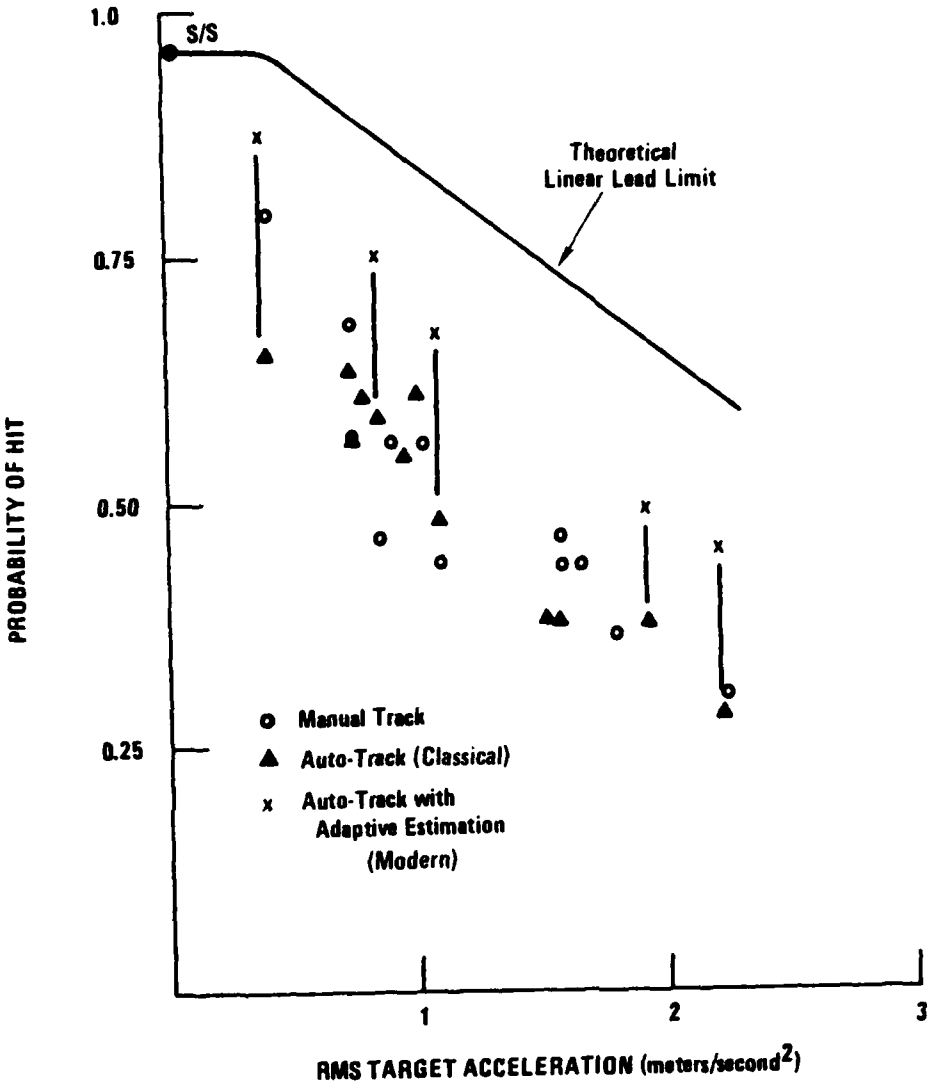


a. Settling Time Comparison



b. Estimator Comparison

Figure 8. Modern Estimator Versus Classical Filter



c. Hit Probability Comparison

Figure 8. Modern Estimator Versus Classical Filter

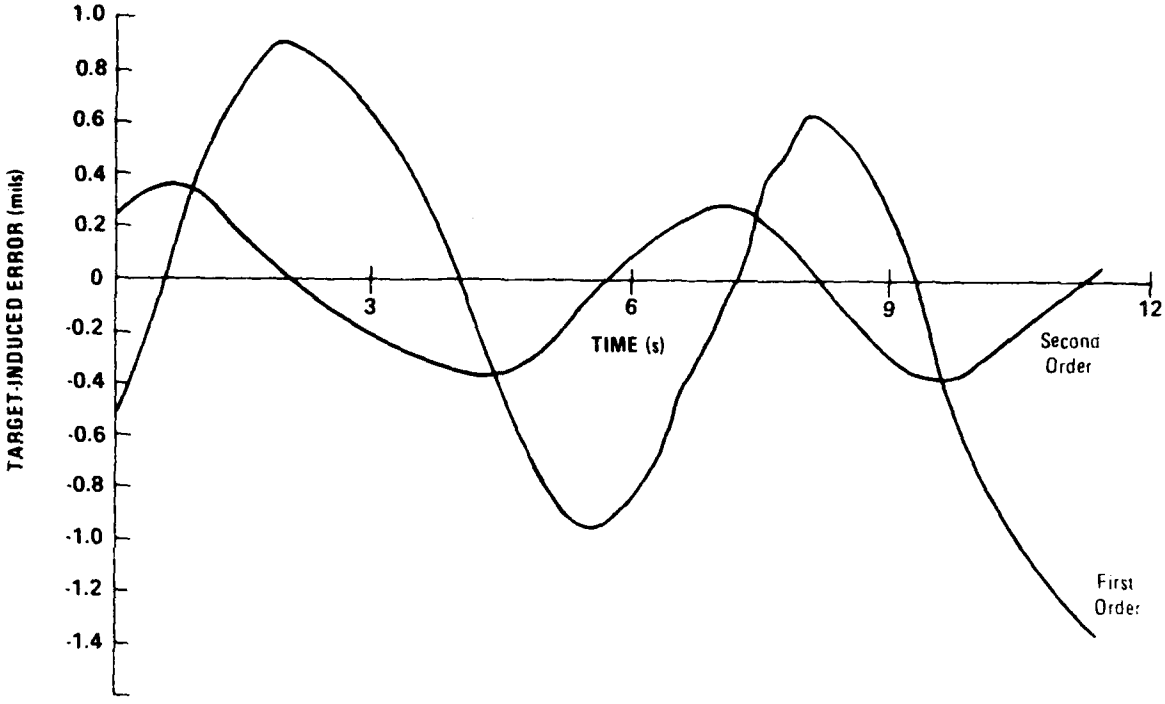


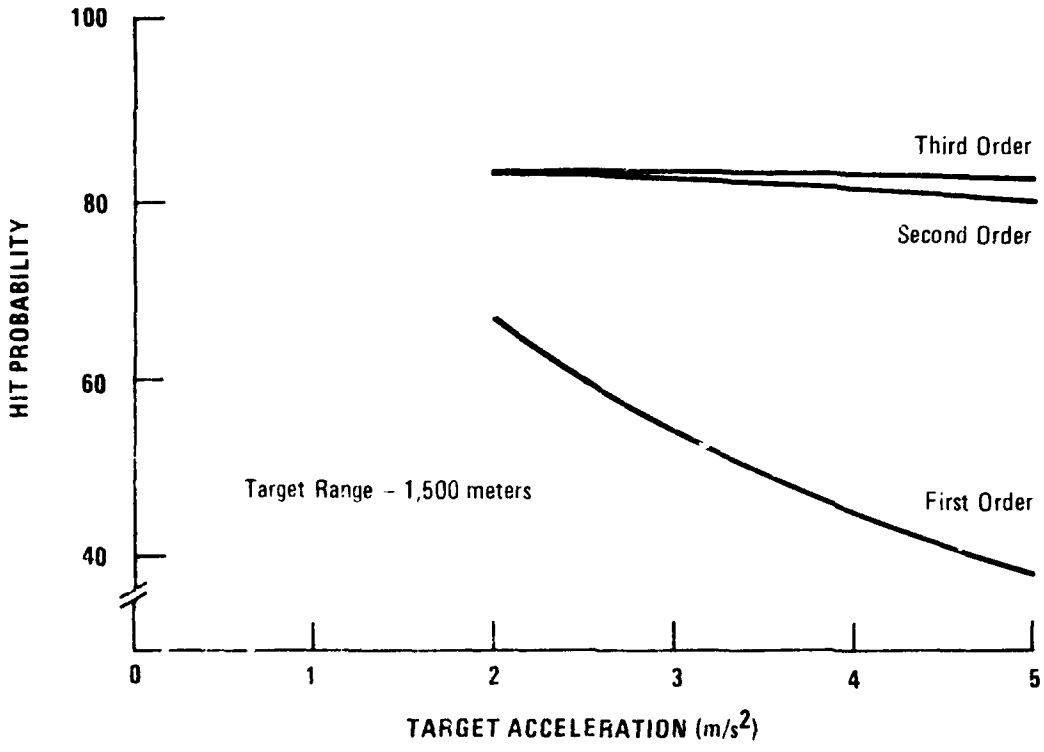
Figure 9. First Order Versus Second Order Prediction

CONCLUSIONS

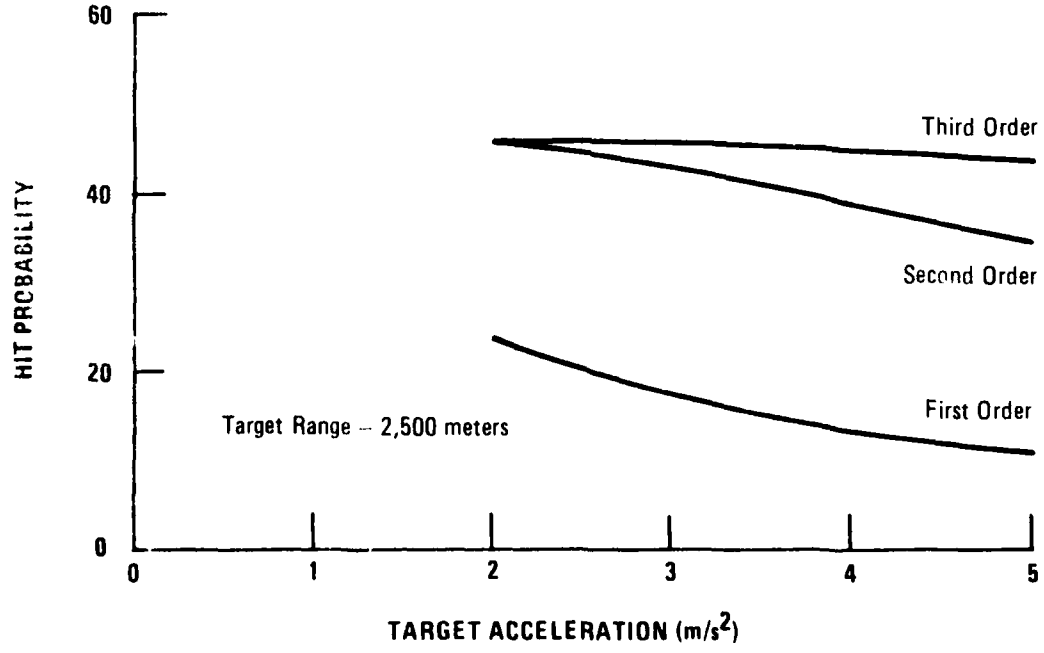
1. Modern fire control outperformed classical fire control against every measure of military worth considered.

2. Classical fire control suffers from long reaction times against all targets and poor hit probability against evasive targets. Modern fire control does not suffer these deficiencies.

3. Fire control measures of military worth should include opportunities to fire (cued and uncued) as well as settling time and hit probability. Lay error is not a good opportunity to fire cue.



a. Target Range 1,500 Meters



b. Target Range 2,500 Meters

Figure 10. Comparison of Target Predictors

AD P001088

MANEUVERING VEHICLE PATH SIMULATOR

T. R. Perkins
H. H. Burke
J. L. Leathrum
Army Materiel Systems Analysis Activity Aberdeen
Proving Ground, Maryland

ABSTRACT

The mobility and agility of land combat vehicles provide countermeasure tactics against gun fire control systems. Improvements in the performance of fire control systems engaging maneuvering vehicles can be realized by upgrading the system's ability to accurately estimate the threat's line-of-sight motion and predict future position. A quantitative description of the maneuvering threat motion is needed to evaluate prediction concepts and system performance. Field test to obtain the data base would be too costly because threat maneuvers constitute a large set of possibilities even when constrained by tactical doctrine and vehicle capabilities.

In lieu of field test, an analytic approach describing maneuvers is presented in this paper to provide the needed data base for evaluating the performance of fire control system engaging maneuvering targets. A two dimensional maneuvering vehicle path simulation capable of generating position, velocity and acceleration is presented. Intentional vehicle operator commands and random disturbances are included in its structure. In addition to the intent to maneuver, a vehicle is required to go from one place to another. The model deals with this goal oriented activity by constraining the maneuvers within angle limits about the instantaneous line from the vehicle to the objective.

INTRODUCTION

The purpose of this paper is to provide an alternative to field test data required for the evaluation of the performance of fire control systems engaging maneuvering targets. Maneuvering vehicle modeling methodology, including background, and model structure are presented. A computer program incorporating features which permit different vehicle mobility and agility characteristics is supplemented with a user's guide.

MANEUVERING VEHICLE MODELING METHODOLOGY

The critical motion parameters of maneuvering vehicle paths that degrade the performance of predictive fire control systems have been identified as small cyclic oscillations

occurring at frequencies that are within the maneuvering capabilities of tactical land vehicles.[1] This type of vehicle maneuver has been incorporated into the M1 Materiel Need Document.[2,3] The XM-1 Materiel Need Document specifies a requirement that the fire control system perform satisfactorily when presented with selected experimentally obtained paths. These same paths are also in use on the C-Field "Hardison" Simulator at Aberdeen Proving Ground. The number of such available paths is limited by the generation and formatting costs. Thus, in the assignment of fire control system performance one is often faced with the availability of only a few selected engagement scenarios.

Improvements in the performance of fire cotrol systems operating against maneuvering targets can be realized by upgrading their ability to estimate the threat's line-of-sight movement and predict its future position. A quantitative description of the maneuvering threat is needed to evaluate the extent of the performance degradation.[4] It is necessary to consider both mobility and agility characteristics of threat vehicle movements. A thorough description of all anticipated maneuvering seems to defy identification because threat maneuvers constitute a large set of possibilities even when constrained by tactical doctrine and vehicle capabilities. An analytic approach describing maneuvers views each maneuver as being composed of elements from an idealized group of movements. An empirical approach views maneuvers as having occurred during limited tests of different types of maneuvering vehicles. Neither of these approaches provide a maneuver description, but a combination of these two approaches offers some advantages and is the rationale adopted. The analytic approach partially overcomes the incompleteness of the empirical data base while the empirical data will offset mathematical idealizations of the analytic methodology.

EMPIRICAL APPROACH

When using empirical data to demonstrate the performance of a gun fire control system, baseline performance can be determined with no concerns arising from idealization of the maneuvers. Since the number of maneuvers usually available will be constrained, they provide insufficient information about both the robustness of a fire control design methodology and the pathology when the fire control system begins to degrade. The procedure for the acquisition of experimental data will often dictate the accuracy and frequency of the data values. Matching these to the data acquisition of the system being evaluated often requires some data editing and even augmentation. Subtle tradeoffs often arise between the maintenance of the parity of the experimental data and the re-synchronization or other massaging of the data to make it resemble field acquired data. Thus, even systems which are evaluated in the context of experimentally obtained data will often be subjected only to preprocessed data. This lack of integrity

of empirical data often leaves the analyst in a dilemma with respect to the appropriate value of test data during the systems design and simulation activities.

ANALYTIC APPROACH

As a supplement to the empirical approach, the analytic approach may be used to investigate sensitivity effects for a larger group of vehicle movements. Simulating new or pathological maneuvers using the analytic approach requires the superposition of maneuvers arising from random disturbances and intentional vehicle driver commands.

Random Disturbances

Random disturbances may be represented in terms of time histories or power spectral densities. The time history approach is based on the development of a mathematical model of vehicle movement influenced by terrain effects and arbitrary driving habits of individual drivers. It is assumed that for no random effects caused by terrain irregularities or driver input, the vehicle would proceed along a straight line-constant speed path. Maneuvers are viewed as perturbations about this straight line-constant speed path. Apparent acceleration a(t), accounts for the vehicle's deviation from a straight line path. Maneuver capability is expressed by three quantities: the variance σ^2 of a(t), the cyclic maneuver frequency ω and the time constant of the maneuver $1/\beta$. The apparent vehicle acceleration is correlated in time. If the target is accelerating at time t, it is likely to be accelerating at $t + \tau$ for sufficiently small τ. A representative model of the auto-correlation function, $\phi(\tau)$, associated with the apparent acceleration is

$$\phi(\tau) = \sigma^2 e^{-\beta|\tau|} \cos(\omega|\tau|)$$

where β = reciprocal of maneuver acceleration time constant.(5) The auto correlation function for a periodic random acceleration is shown in Figure 1.

INTENTIONAL VEHICLE DRIVER COMMANDS

Motion of a specific land vehicle over particular terrain is complicated and is not treated in this report. However, it is recognized that interaction between vehicle horsepower, weight, suspension, and locomotion concepts do combine with terrain over which a vehicle moves, providing different levels of mobility and agility.

Agility is closely related to mobility and yet it is a slightly different description of vehicle motion. Whereas mobility describes the movement of a vehicle from one location

to another location in a given period of time, agility describes the vehicle's ability to alter its mean path during that time period. These two components of vehicle motion are evident when a vehicle travels from A to B in 100 seconds (mobility) while executing several deceleration, acceleration and oscillatory movements (agility).

A major component of the agility of a vehicle arises from the driver's intent to maneuver. This is a product of training and the perception of threat. Any analytical approach to modeling the motion of a maneuvering vehicle will inevitably encounter a requirement to represent this intentional motion. The phenomenon is so important that it deserves independent description and verification.

MANEUVERING VEHICLE MOTION

The path traversed by a maneuvering vehicle proceeding from point A to point B can be thought of as being generated by moving on circular arcs connected by straight line segments as shown in Figure 2. The radii of these circles vary from 10 meters to infinity. The speed of the evasive vehicle is $\leq$15 meters/sec as it moves through the circular arcs. The angle of circular arc traversed, the radius of each arc and the speed variation over the interconnecting straight segments between the circular arcs determines the mobility/agility of the evasive vehicle. Orientation of the engaging gun fire control system will establish a reference frame from which the apparent motion of the evasive vehicle can be observed. Figure 2 describes the relationships that exist for head-on maneuvering of a threat vehicle. The apparent velocities and accelerations for paths of this nature are considerably different than for continuous sinusoidal motion.

As shown in Figure 3, the random and intentional accelerations are summed to obtain resultant forcing functions. The apparent motion of the combined model may be used instead of empirical data to evaluate the performance of fire control systems. Effects of vehicle parameter variations are readily observed without resorting to extensive field testing.

A MODEL FOR MANEUVERING THREAT VEHICLES

Target tracking and fire control system design studies are replete with attempts to compare the motion of a tracking device with the true target behavior. Such comparisons often require analysis of target rate and acceleration profiles in order to ascertain the real differences of movement between the tracking device and the target. When only target position data are available, complete descriptions of target motion must be obtained numerically, thus, performance analysis of the tracking device regresses to a comparison of the device's performance and a numerical differentiation algorithm.

The model for maneuvering targets developed in this report is intended to address these issues. Target behavior is generated in such a way that numerical differentiation is not required. Whether the model represents plausible behavior is debatable, and there will always be latitude for refinement and improvement. Therefore, validation procedures are being developed to authenticate model output.

The model attains its plausibility from the fact that the inputs to the model are physically equivalent to the actions of the driver of a maneuvering vehicle. Limitations on the inputs correspond to vehicle design limitations or human factors related to driver comfort.

STRUCTURE OF THE MODEL

The model for a maneuvering vehicle being developed acknwledges three fundamental features of the motion: (a) Intentional Maneuver, (b) Involuntary Maneuver, and (c) Goal Oriented Motion. The relative importance of these three features is subject to judgment, both by the vehicle driver and to the modeler. The model deals with each of the features separately and superimposes them to obtain the total motion of the vehicle.

The intentional part of the maneuver is designed to represent voluntary or evasive target motion. The driver is expected to select levels of lateral and tangential accelerations and their time durations. The selection is done from a set of possibilities constrained by vehicle capabilities. The choice of acceleration may be determined by a probability model which may or may not be symmetric about zero. A Poisson model for time durations is a reasonable possibility. Observed behavior of maneuvering vehicles suggests accelerations distributed between $\pm$ 1 g and time durations of 3 to 6 seconds are reasonable.

Involuntary maneuvering is included to capture that part of the motion which is not under the driver's direct control. It may arise from terrain roughness, steering drift or looseness, and driver inattention. It is likely to be correlated in time and may be mathematically modeled as the output of a linear dynamical system driven by white noise. The parameters and noise levels may be set to approximate the power spectra of the off-nominal behavior of observed empirical data.

In addition to an intent to maneuver, the driver must also consider goals or objectives which must be achieved at the completion of the motion. This part of the motion is usually stated informally as "go from point A to point B." The model deals with this goal oriented activity by allowing the driver to maneuver within an angular sector. The center line of the angular sector passes through the objective and the vertex angle shrinks as the objective is approached. Including such a feature in the model insures that the goal is reached. When the velocity vector points outside the allowable angular

sector, free selection of accelerations gives way to a proportional steering law for the vehicle.

DISCRETE EQUATIONS OF MOTION

As indicated in the previous section, the maneuvering vehicle will be modeled in several parts. The intentional motion and the involuntary motion come together in a difference equation of the form

$$\underline{X}_{i+1} = \phi_i \underline{X}_i + \underline{B}_i \underline{U}_i$$

with the two types of motion described in U_i, i.e.,

$$U_i = [a_S + a_R]_i$$

where a_S = Selected (intentional) acceleration in vehicle coordinates

a_R = Random (involuntary) acceleration in vehicle coordinates

The state of the vehicle in inertial coordinates is represented by

$$\underline{X}_i = [x \quad y \quad V_x \quad V_y \quad V]_i^T$$

where:

X, Y = Position components
V_x, V_y = Velocity components
V = Vehicle speed

Each of the acceleration terms is represented by a lateral and a tangential component, i.e.,

$$(U_L)_i = [(a_L)_S + (a_L)_R]_i$$
$$(U_T)_i = [(a_T)_S + (a_T)_R]_i$$

The motion between the times corresponding to i and i+1 is approximated by an arc of a circle with a mean radius of curvature, i.e.

$$\bar{R} = \bar{V}/\omega = (V_i + U_T \cdot \Delta t/2) \cdot \frac{\Delta\tau}{\Delta\theta}$$

where

$$\Delta\theta = \frac{U_L}{U_T} \ln \left(\frac{V_i + U_T \Delta t}{V_i}\right)$$

$\bar{V}$ = mean speed

The displacement and velocities in vehicle coordinates (see Figure 4a) can be represented as

$$X_{i+1} = X_i + R \sin \Delta\vartheta$$

$$Y_{i+1} = Y_i + \bar{R} (1-\cos\Delta\vartheta)$$

$$(V_x)_{i+1} = V_{i+1} \cos\Delta\vartheta$$

$$(V_y)_{i+1} = V_{i+1} \sin\Delta\vartheta$$

$$V_{i+1} = V_i + U_T \Delta t$$

$(V_x)_{i+1}$ and $(V_y)_{i+1}$ are in the vehicle coordinate frame. The orientation of this frame to an inertial frame is determined by the components of velocity at time i in the inertial frame of reference as shown in Figure 4b. The transformation from vehicle to inertia coordinates is accomplished by the operator, T

$$T = \begin{bmatrix} \cos\alpha & -\sin\alpha \\ \sin\alpha & \cos\alpha \end{bmatrix}$$

where $\alpha = \tan^{-1} \dfrac{(V_y)_i}{(V_x)_i}$

In inertial coordinates, the same equations appear as

$$\begin{bmatrix} x \\ y \end{bmatrix}_{i+1} = \begin{bmatrix} x \\ y \end{bmatrix}_i + T \begin{bmatrix} \frac{\sin\Delta\vartheta}{\Delta\vartheta} \\ \frac{1-\cos\Delta\vartheta}{\Delta\vartheta} \end{bmatrix} . V_1 \Delta t + T \begin{bmatrix} \frac{\sin\Delta\vartheta}{\Delta\vartheta} \\ \frac{1-\cos\Delta\vartheta}{\Delta\vartheta} \end{bmatrix} . U_T . \frac{\Delta t^2}{2}$$

$$\begin{bmatrix} V_x \\ V_y \end{bmatrix}_{i+1} = T . \begin{bmatrix} \cos\Delta\theta \\ \sin\Delta\theta \end{bmatrix} V_i + T \begin{bmatrix} \cos\Delta\vartheta \\ \sin\Delta\vartheta \end{bmatrix} U_T . \Delta t$$

$$V_{i+1} = V_i + U_T \Delta t$$

The role of the accelerations is now apparent. The lateral accelerations enter in the definition of $\Delta\vartheta$. The tangential accelerations arise both in $\Delta\vartheta$ and as forcing on the equation of motion. A complete separation may be obtained by approximating $\Delta\vartheta$ with

$$\Delta\theta \approx \lim_{U_T \to 0} \left\{ \frac{U_L}{U_T} \ln [(V_i + U_T \Delta t)/V_i] \right\} = \frac{U_L}{V_i} \Delta t$$

The U_L part of U_i is now a time varying parameter in the ϕ_i and B_i matrices. The forcing function is thus collapsed to

$$U_i = (U_T)_i;$$

which is the tangential acceleration.

INVARIANCE OF TOTAL VELOCITY

The form of the model presented in the previous section is, in part, dictated by a requirement that the lateral acceleration must leave the total velocity (speed) invariant. A crude form of the model would represent the velocity in vehicle coordinates as

$$(V_X)_{i+1} = (V_X)_i + U_T \cdot \Delta t$$

$$(V_Y)_{i+1} = (V_Y)_i + U_L \cdot \Delta t$$

In the absence of tangential accleration ($U_T = 0$), the total velocity at i+1 would be

$$V_{i+1} = [(V_X)^2_i + ((V_Y)_i + U_L\Delta t)^2]^{1/2} \neq V_i$$

where

$$V_i = [(V_x)^2_i + (V_y)_i^2]^{1/2}$$

Thus, a long term bias in lateral acceleration would force the total velocity to diverge. This divergence is eliminated from the model if a new state variable, V_i (total speed), is introduced.

$$V_{i+1} = V_i + U_t\Delta t$$

which forces invariance when U_T is zero, i.e.,

$$V_{i+1} = V_i$$

The components of velocity in the vehicle coordinates, are then obtained from geometry

$$(V_x)_{i+1} = V_{i+1} \cdot \cos\Delta\theta$$

$$(V_x)_{i+1} = V_{i+1} \cdot \sin\Delta\theta$$

$$(V_x)_{i+1} = V_{i+1} \cdot \sin\Delta\theta$$

These definitions effectively supplement the cruder form stated above.

This model of circular motion handles straight line motion correctly provided $\bar{R}\sin\Delta\theta$ and $\bar{R}(1-\cos\Delta\theta)$ are computed correctly in the limit as $\Delta\theta \to 0$.

A MODEL FOR INVOLUNTARY ACCELERATION

The discrete equations for the maneuver model left the involuntary acceleration, a_R, unspecified. It was noted in the discussion of the overall structure that it may be convenient to model this part of the motion as a linear dynamical system driven by white noise. If the linear system is of sufficiently high order, the correlation and power spectral properties of the random acceleration can be matched to desired specifications or actual data of vehicles moving over terrain.

A reasonable compromise between order of the model and flexibility in the choice of model parameters to obtain the desired specification may be achieved with a second order model of the form

$$\dot{X}_1 = X_2 + U$$
$$\dot{X}_2 = -\alpha^2 X_1 - 2\beta X_2 + (\alpha - 2\beta)U$$

Where U is a Gaussian white noise sequence with zero mean and variance $2\beta\sigma^2$. Gelb[5] provides a detailed analysis of the spectral properties of x as a function of the parameters, α and β. The auto-correlation function for this model is discussed previously in this paper.

A discrete form of the involuntary motion is most easily integrated with the maneuver model. The conversion to discrete motion is represented by the following definitions.

$$X_{k+1} = \Phi_k X_k + W_k$$

$$\Phi_k \equiv \begin{bmatrix} \cos\omega\Delta t + \frac{\beta}{\omega}\sin\omega\Delta t & \frac{1}{\omega}\sin\omega\Delta t \\ -\frac{\alpha^2}{\omega}\sin\omega\Delta t & \cos\omega\Delta t - \frac{\beta}{\omega}\sin\omega\Delta t \end{bmatrix} e^{-\beta\Delta t}$$

where $\omega^2 = \alpha^2 - \beta^2 \geq 0$

The forcing vector, W_k, is discrete Gaussian noise with mean and variance of

$$E(W_k) = 0$$
$$E(W_k W_k') \tilde{=} 2\beta\sigma^2 BB'\Delta t$$

where $B = \begin{bmatrix} 1 \\ \alpha - 2\beta \end{bmatrix}$

The output of this part of the model is a_R in the overall model

This form of the involuntary motion could be used to create both the lateral and tangential components of a_R perhaps with different α, β and σ^2 parameters.

CONSTRAINING THE DIRECTION OF TRAVEL

As noted earlier, an essential part of this model is the goal directed ability. True free play of intentional motion would be unrealistic because the vehicle can be expected to have a destination. The modeling of this goal directed component of the motion must capture the expectation that, as the objective is approached, the free play is diminished so that the vehicle passes directly over the objective. The relationship between the state of the vehicle and the allowable motion is illustrated in Figure 5. So long as $-\alpha \leq \beta \leq \alpha$, the vehicle is free to use its current intentional accelerations. If the direction of travel exceeds these limits, a new selection of accelerations is required such that the vehicle turns back into the allowable state space.

Such a policy of constraining the motion is easily realized in a model provided it can be specified and provided appropriate action can be taken to restore the direction of motion once it exceeds the limit. The latter problem arises under sudden changes of objective such as when an unusually fast turn is executed to restore allowable free play.

The limits of free play motion are modeled by allowing α to be a function of range. A convenient functionality is achieved by

$$\alpha = SA \cdot [\ln (D + 1)/\ln (300.)]$$

Where D is the distance to the objective and SA is the starting angle which is a function of maneuverability.

When the vehicle is outside of the allowable state space or very close to the objective, the model would allow the driver to select any turning acceleration up to the maximum possible for the vehicle. The acceleration chosen would be proportional to the angular rate with respect to the objective (this policy is commonly called proportional navigation). The desired control acceleration would be

$$a_c = -K_p V \omega$$

where $\omega = V(\sin\beta)/D$

K_p = proportional navigation constant

This acceleration is a lateral acceleration which is applied in the direction necessary to turn the velocity vector toward the line-of-sight.

SELECTING INTENTIONAL MANEUVERS

The proposed model of intentional motion of the vehicle requires specifying a probability model for changes in acceleration and in acceleration levels. The acceleration levels are specified by either a density function of the levels, p(a), or a discrete grid of acceleration levels and probabilities.

Those points in time at which new accelerations are selected are further defined by a Poisson probability model with densities

$$P(t) = \frac{1}{\lambda} e^{-t/\lambda}$$

where λ is the mean duration.

IMPLEMENTATION AND USER PROCEDURES FOR SIMULATION

The mathematical models and concepts, as previously described, are programmed in standard Fortran IV computer code. The resulting computer program (simulation) is capable of generating maneuvering paths which capture the characteristics of actual vehicle motion The program allows considerable flexibility in establishing and controlling the agility and mobility of simulated vehicle motion.

The maneuvering path simulator is designed to be user dependent. User dependent and interaction are emphasized in the effort to maximize the prob ability of generating realistic maneuvering paths. The user must decide on the general layout and characteristics of the intended path. Basic considerations for establishing these general characteristics are:

(a) Total path length

(b) Nominal time to complete path

(c) Number and locations of the objectives

(d) Level of maneuvering (agility) for each leg

(e) Variability of vehicle speed

Execution of the program will produce a maneuvering path which passes through or very close to each specified objective. The amount of maneuvering will depend on the distance between objectives, the nominal speeds, and the values chosen for lateral accelerations for each leg of the path. In the example shown in Figure 6, the basic information for determining the general layout of the path are:

(a) Total path length - approximately 1000 meters

(b) Time to complete path - 2.5 minutes

(c) Number of objectives - 5

(d) Level of agility - $\pm$ 1 m/s^2 and $\pm$ 2 m/s^2

(e) Vehicle speed - varies from one leg to another.

The positions (xy coordinates) of the maneuvering vehicle are generated every 0.1 second (program input parameter, Δt). The maximum speed and lateral accelerations in the xy coordinates frame are indicated on the figure for each leg of the path. The simulated path starts at the initial locations, (0, -2000) meters, and procedes in sequential order to objectives A through E.

CONCLUSIONS

The purpose of this paper has been to describe a methodology and and the computer program that will generate maneuvering threat vehicle movements. The versatility of the approach makes it a feasible tool for tactical planners interested in studying relationships between agility, mobility and fire control system performance. A demonstrated application is the incorporation of a maneuvering vehicle path on the APG C Field Moving Target Simulator.

REFERENCES

1 AMSAA TR-234, Investigation of the Performance of Fire Control Systems Engaging Maneuvering Threats, Aug 1978.

2 US Army Armor Center, Report on The Development of Main Gun Accuracy Requirements for the XM1 Tank Against Maneuvering Targets, Aug 1978.

3 TRADOC Document ACN20337, Revised Materiel Need Document XMI MBT, 1980.

4 Fire Control System Performance Degradation When a Tank Gun Engages a Maneuvering Threat, XVII AORS, November 1978, Ft. Lee, VA.

5 Gelb, A., Applied Optimal Estimation, MIT Press, Boston, MS, 19174.

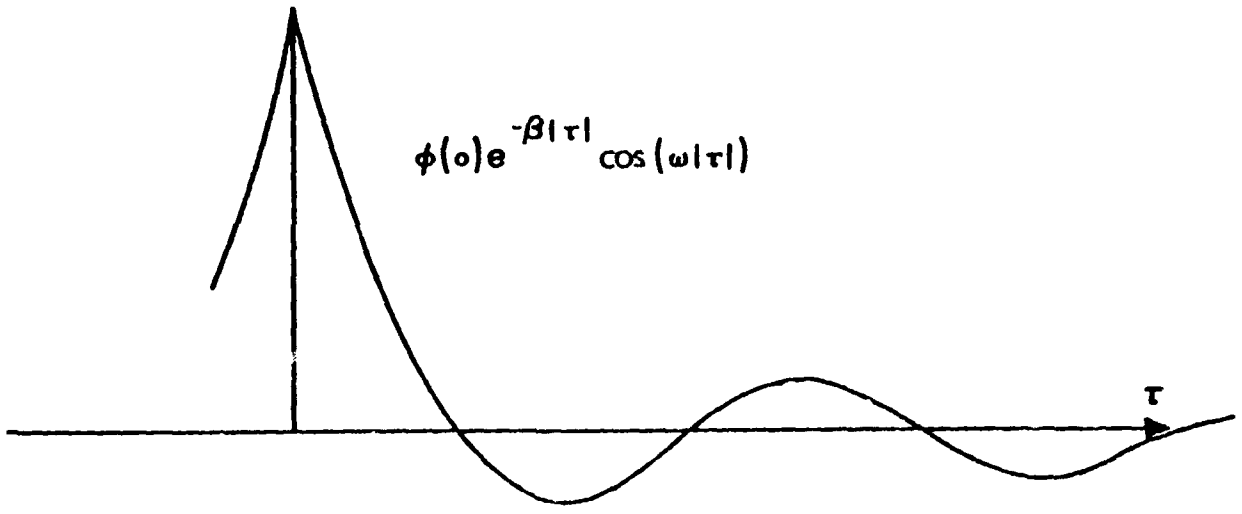


Figure 1. Auto-Correlation Function of Target Random Acceleration.

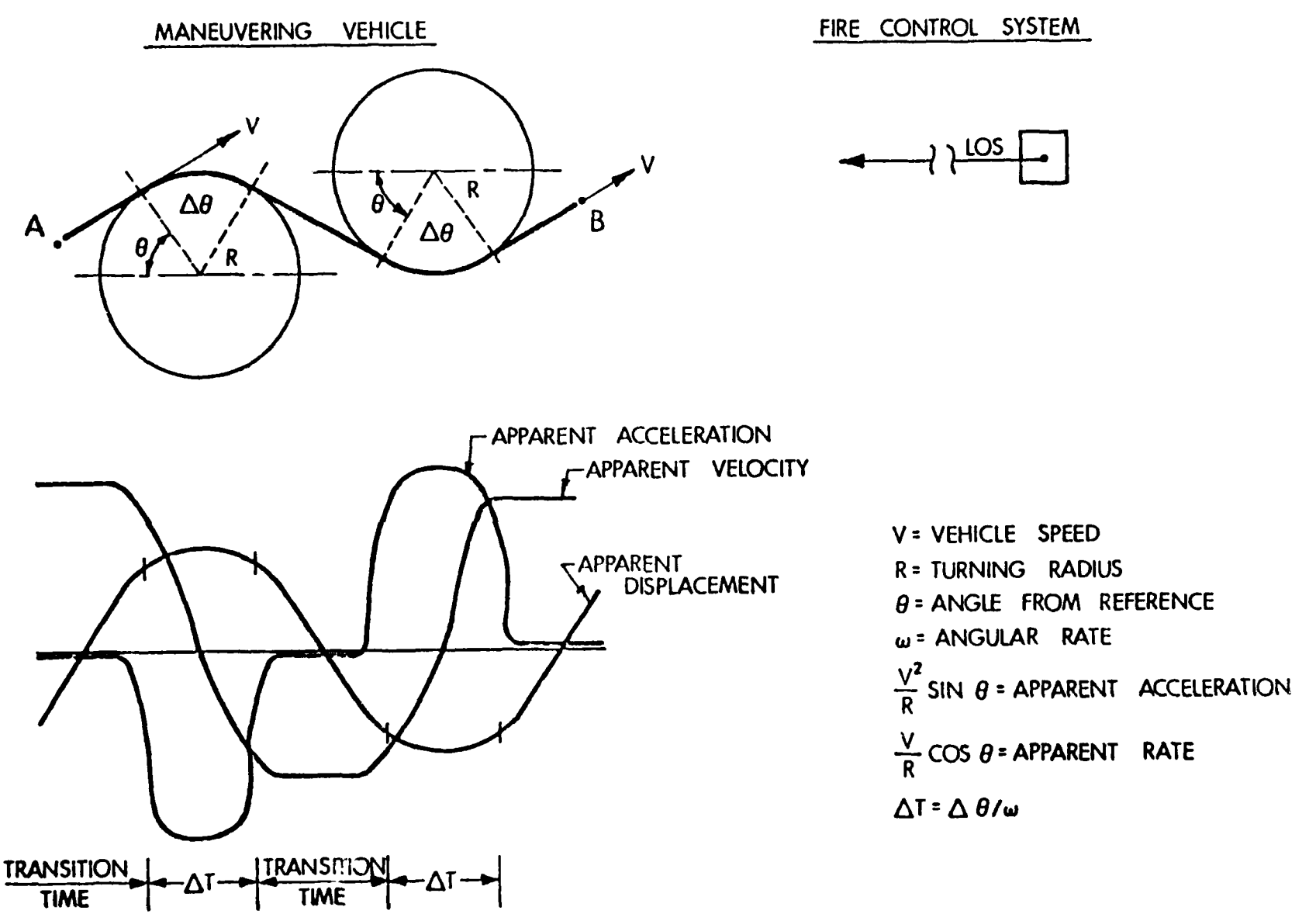


Figure 2. Intentional Maneuvers and Apparent Vehicle Movement.

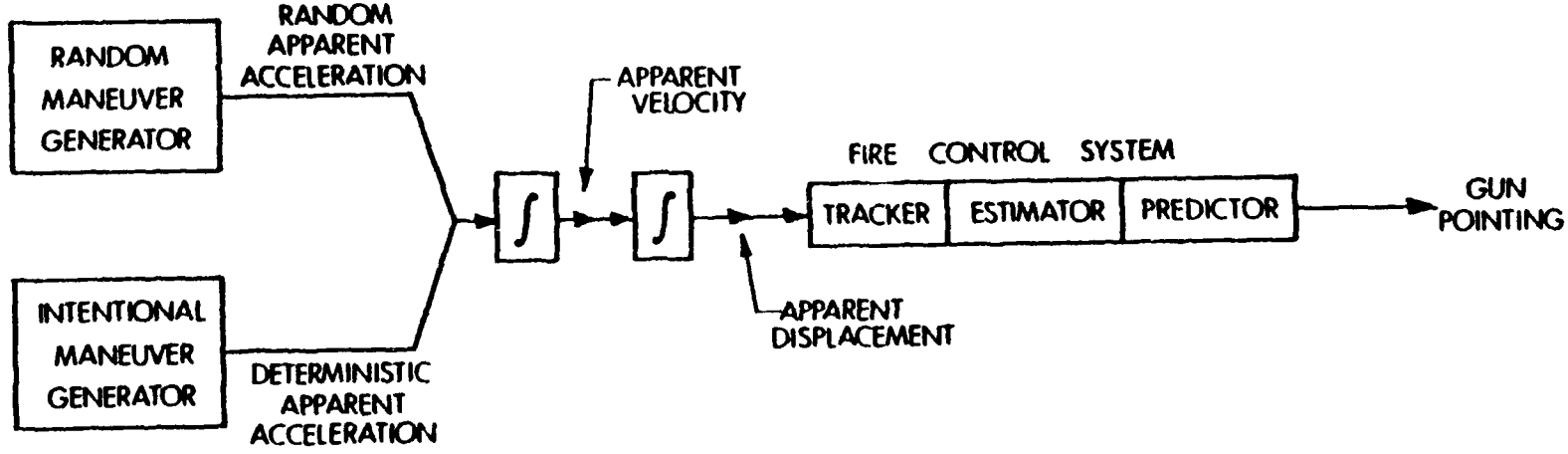


Figure 3. Total Analytic Maneuver.

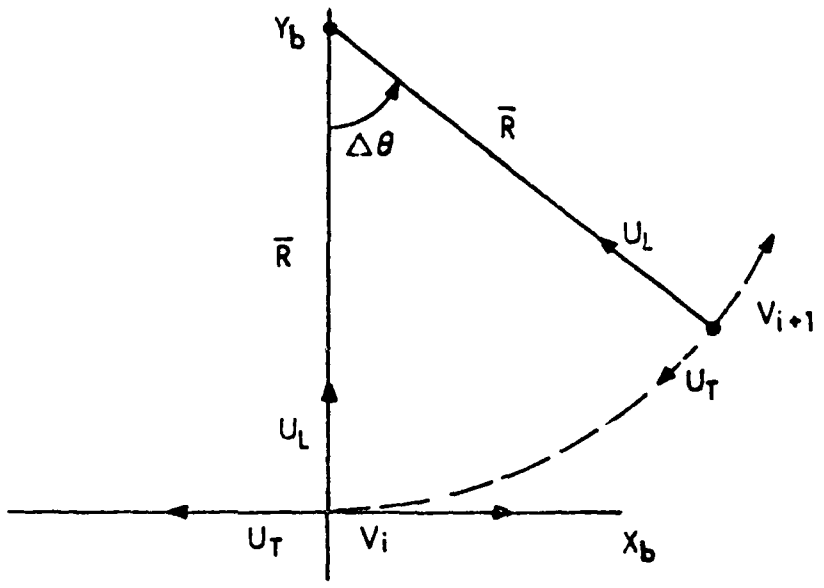


Figure 4a. Representative Vehicle Motion in Vehicle Coordinates.

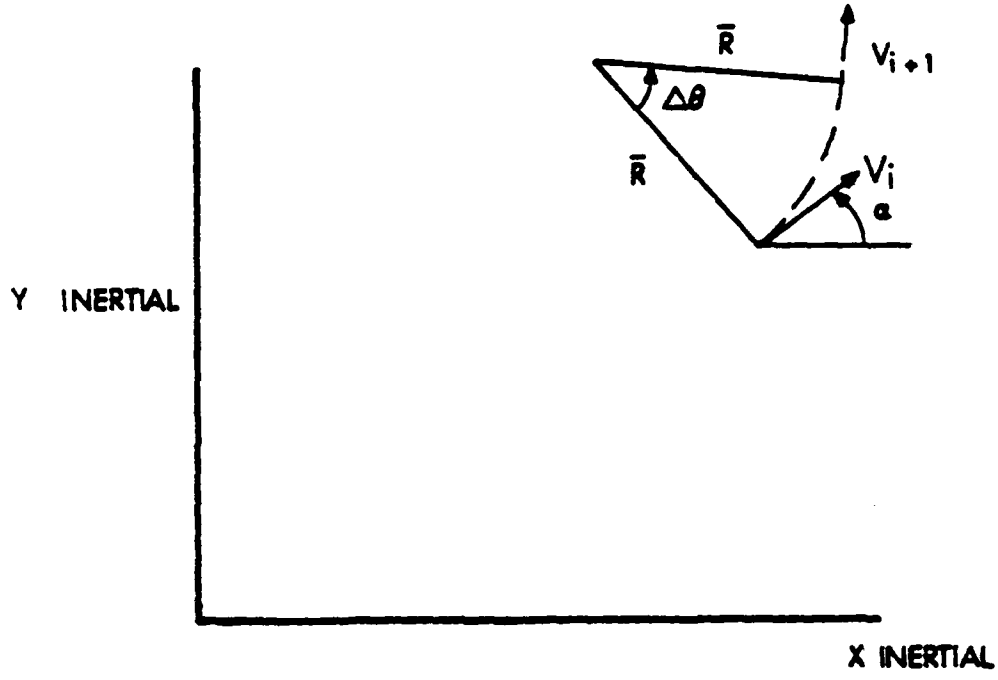


Figure 4b. Orientation of the Vehicle Coordinate System.

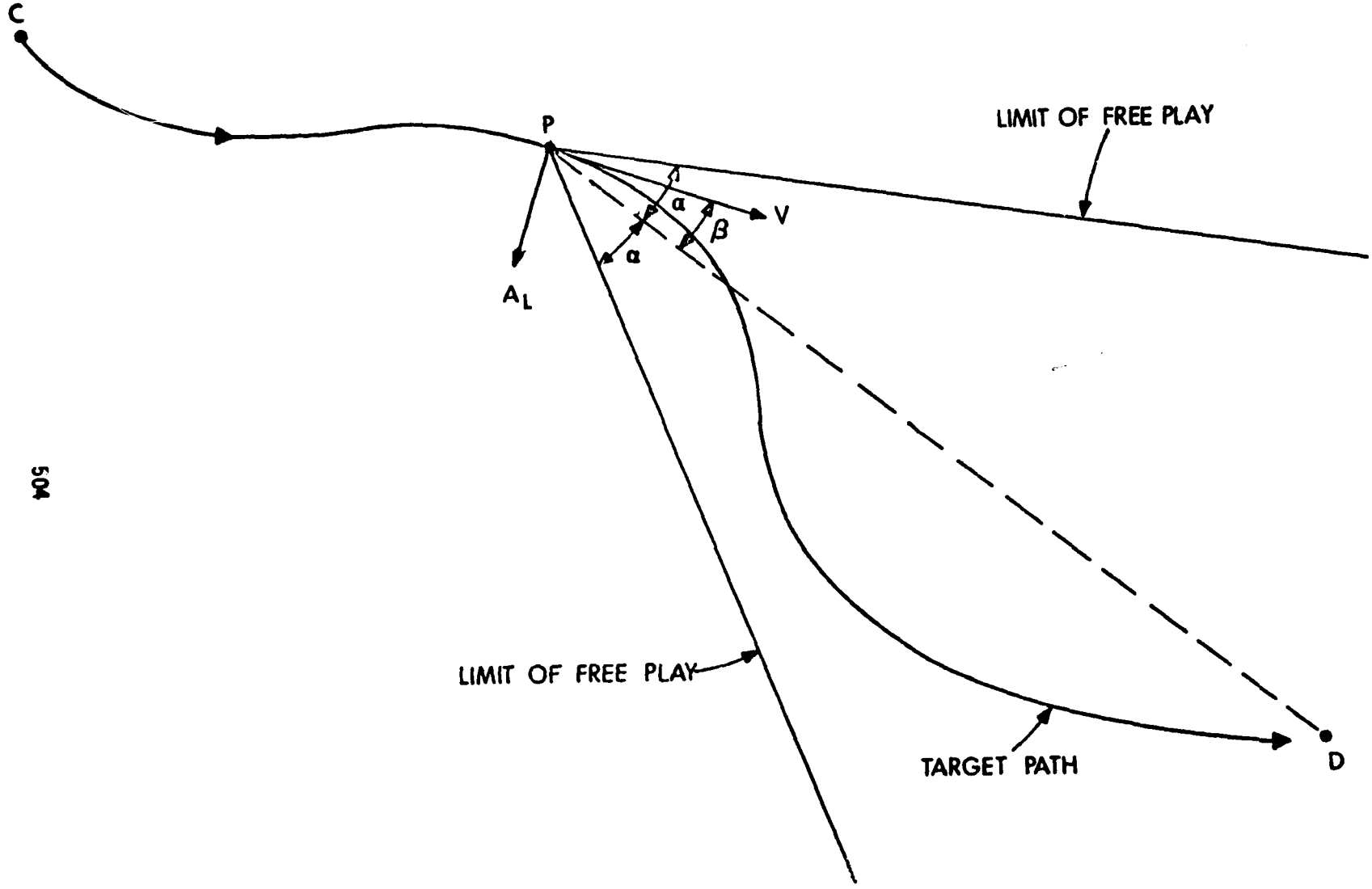


Figure 5. Target Motion Description.

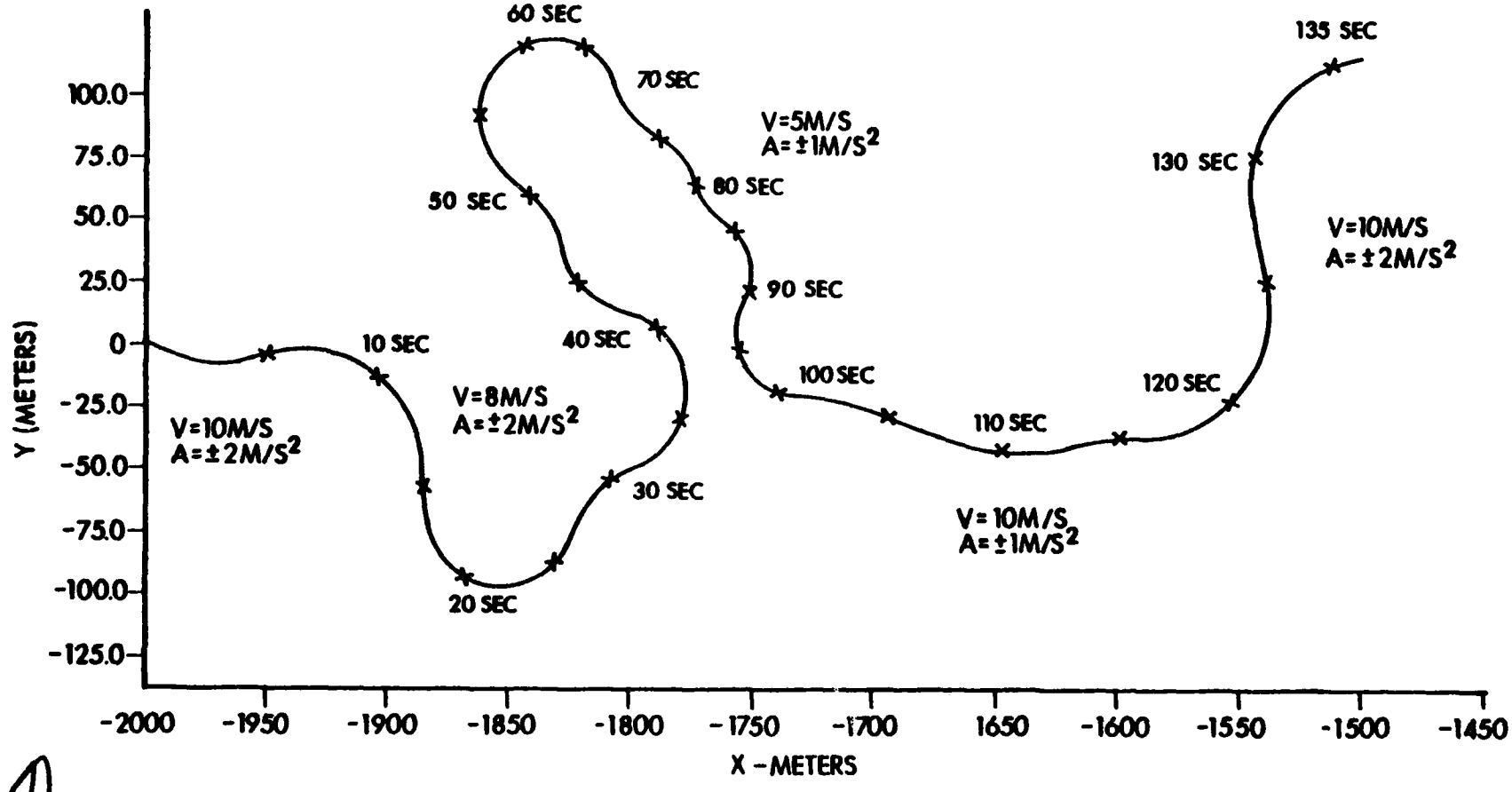


Figure 6. Analytical Maneuvering Vehicle Path.

505

Next page is blank.

AD P001089

IMPROVING AIR-TO-GROUND GUNNERY USING AN ATTACK AUTOPILOT AND A MOVEABLE GUN

Dr. Edward J. Bauman
Department of Electrical Engineering
University of Colorado, Colorado Springs 80907
and
Captain Randall L. Shepard
Department of Astronautics
USAF Academy, Colorado 80840

INTRODUCTION

Recent analysis (Reference 1) indicates that an attack autopilot and moveable gun combination can improve air-to-ground survivability and effectiveness. A pursuit guidance technique is applied to a simplified point mass attacker. The attacker then pursues a psuedo (ficticious) target. The gun is moved in the opposite direction to the attacker motion to keep the rounds on the target. In this way the attacker can continue to accelerate and be less vulnerable to AAA during the attack maneuver. The moveable gun with this technique was also shown to be effective during piloted full scale simulation. For this reason an attack autopilot was designed for a realistic aircraft using modern control theory. The attack autopilot is now being implemented on the full scale simulation.

MANEUVER GENERATION FOR A CONSTANTLY TURNING ATTACK

This section briefly describes the entire engagement scenario, but it concentrates on the attack guidance phase, a constantly turning maneuver.

ENGAGEMENT SCENARIO

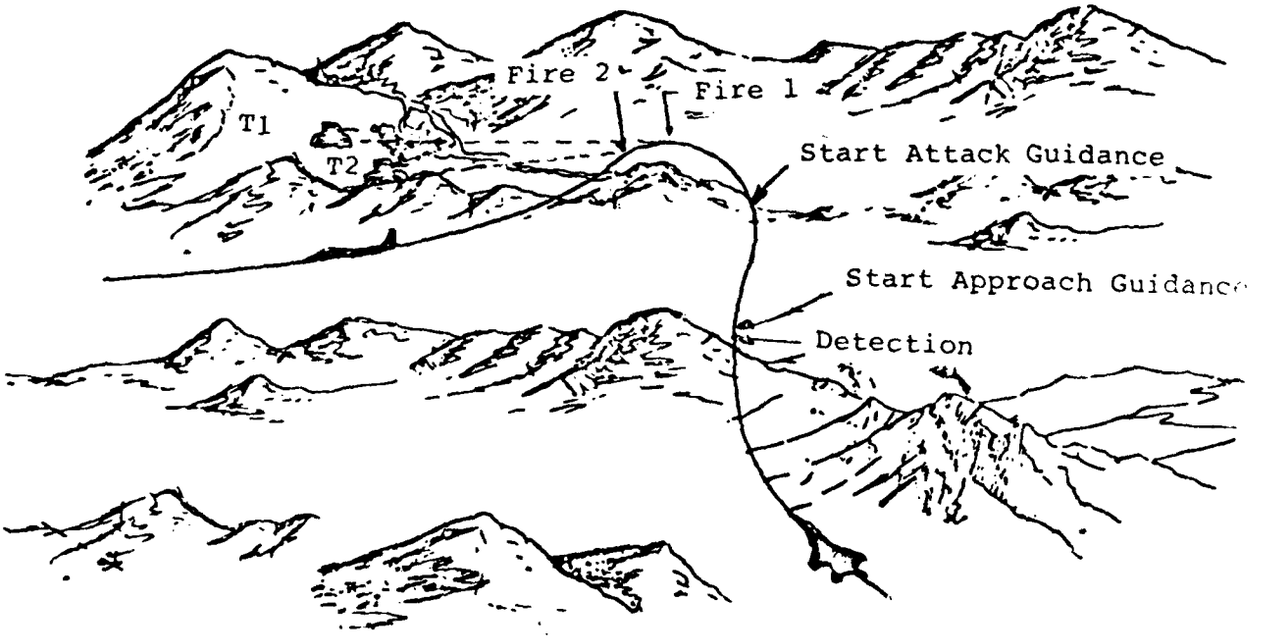
The engagement scenario is shown in Figure 1. The detection and acquisition phase is where the targets are first detected and a sensor is locked onto one or more of them. The inertial position of the targets is also stored in the attacker computer. The approach guidance phase gives the pilot steering cues to bring him to the point of attack. The attack phase generates a constantly turning maneuver which is described in the next section.

Attack Phase

Appendix A shows the derivation of two guidance techniques,

Figure 1

Engagement Scenario



proportional navigation and pursuit guidance. Proportional navigation leads to a non-turning trajectory and, therefore, is not useful for our application. Pursuit guidance leads to an accelerating trajectory against a target moving rapidly at some angle to the attacker. However, ground targets are relatively slow and, therefore, a pursuit course again would also lead to nearly a non-turning trajectory. The key idea to our guidance scheme is:

Provide a rapidly moving pseudo ground target which moves along the line formed by the actual targets.

The pilot tracks this pseudo target using pursuit guidance and thus generates a constantly accelerating path which passes his rounds through the actual targets.

The second key idea of this study is:

As the aircraft moves its aim point across the target, the moveable gun holds the rounds on the target while the aircraft continues to accelerate.

The essence of this system's effectiveness is:

The attacker is always accelerating to minimize vulnerability while the moveable gun takes out this motion to keep the rounds hitting the target.

Figure 2 shows the x-y projection (ground trace) of a typical point mass attacker trajectory using pursuit guidance against the moving pseudo target which passes through the actual targets. This pseudo target initially starts at x=3000 ft. and moves at -300 fps. For this simplified analysis the gun line and rounds are assumed along the attacker velocity vector (i,e, no ballistics). The velocity vector (predicted round impact point) follows the pseudo target as shown in Table 1.

The present pursuit guidance shows an x overshoot and a slight oscillation around the pseudo target after the initial conditions are imposed. However, the y position tracks the pseudo target which means the predicted round impact line exactly follows the line of the actual targets. A gain adjustment on the guidance law would take out the oscillation.

Figure 3 graphically portrays the accelerating maneuver. This is essentially an altitude versus cross-range trjectory (z versus x) of the attacker as seen by the target (or AAA). If the AAA is a linear predictor, it will see a rapidly changing velocity vector as the attacker closes in range. This changing attacker velocity vector will cause the AAA to miss. The attacker firing points are again shown as ●'s on its trajectory plot. The attack is disengaged at the last firing point.

Figure 4 shows the z versus y trajectory projection, essentially

Figure 2

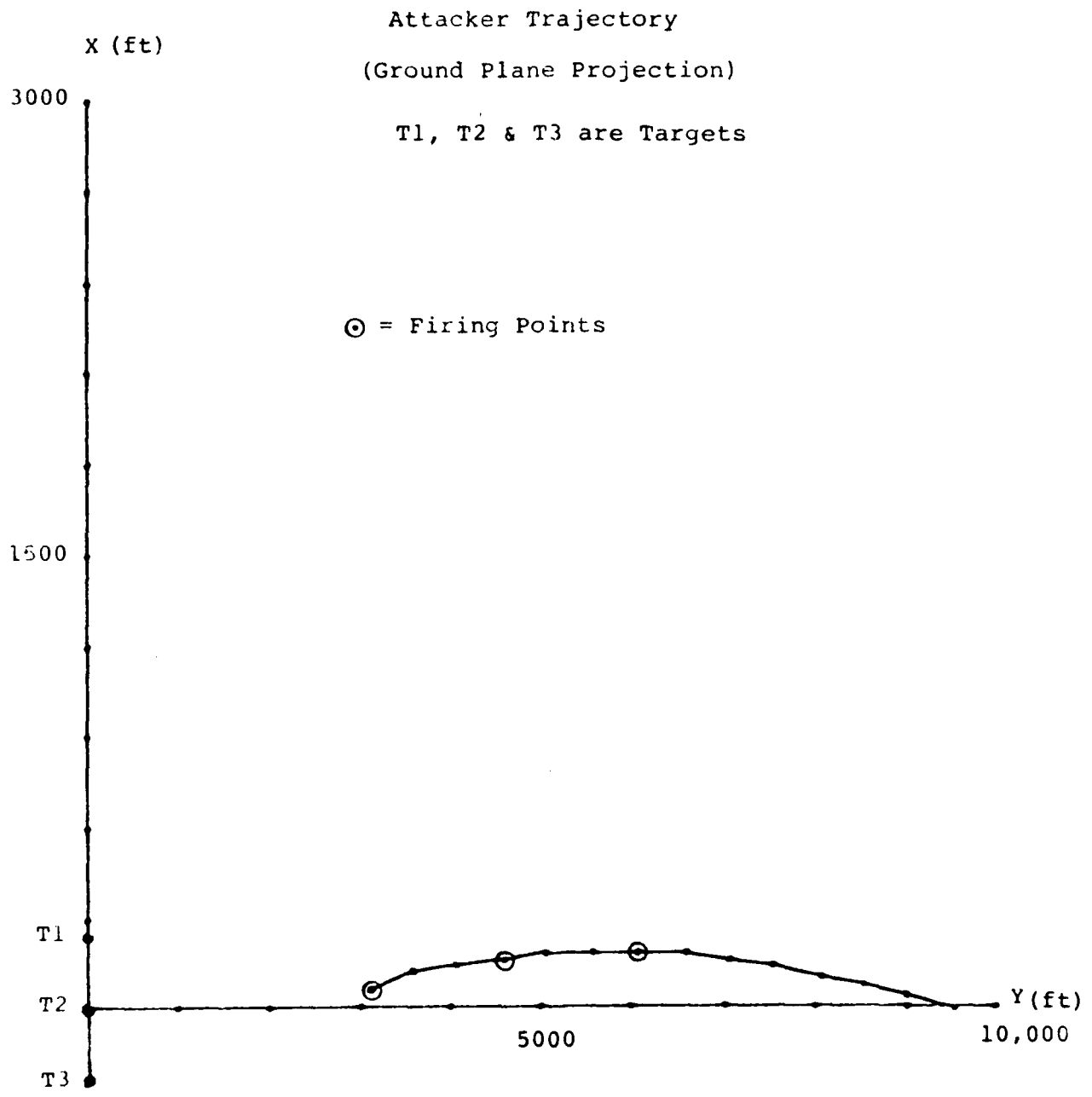

Attacker Trajectory
(Ground Plane Projection)
T1, T2 & T3 are Targets
X (ft)
3000
1500
⊙ = Firing Points
T1
T2
T3
5000
Y (ft)
10,000

Table 1

PSEUDO TARGET POSITION AND PREDICTED ROUND IMPACT POINTS

Time (sec)	Pseudo Target x (Ft.)	Predicted Impact x (Ft.)	Pseudo Target y (Ft.)	Predicted Impact y (Ft.)
0	3000	3000	0	0
1	2700	2607	0	0
2	2400	2350	0	0
3	2100	2073	0	0
4	1800	1786	0	0
5	1500	1494	0	0
6	1200	1191	0	0
7	900	901	0	0
8	600	603	0	0
9	300	303	0	0
10	0	3	0	0
11	-300	-298	0	0
12	-600	-599	0	0
13	-900	-901	0	0

Figure 3

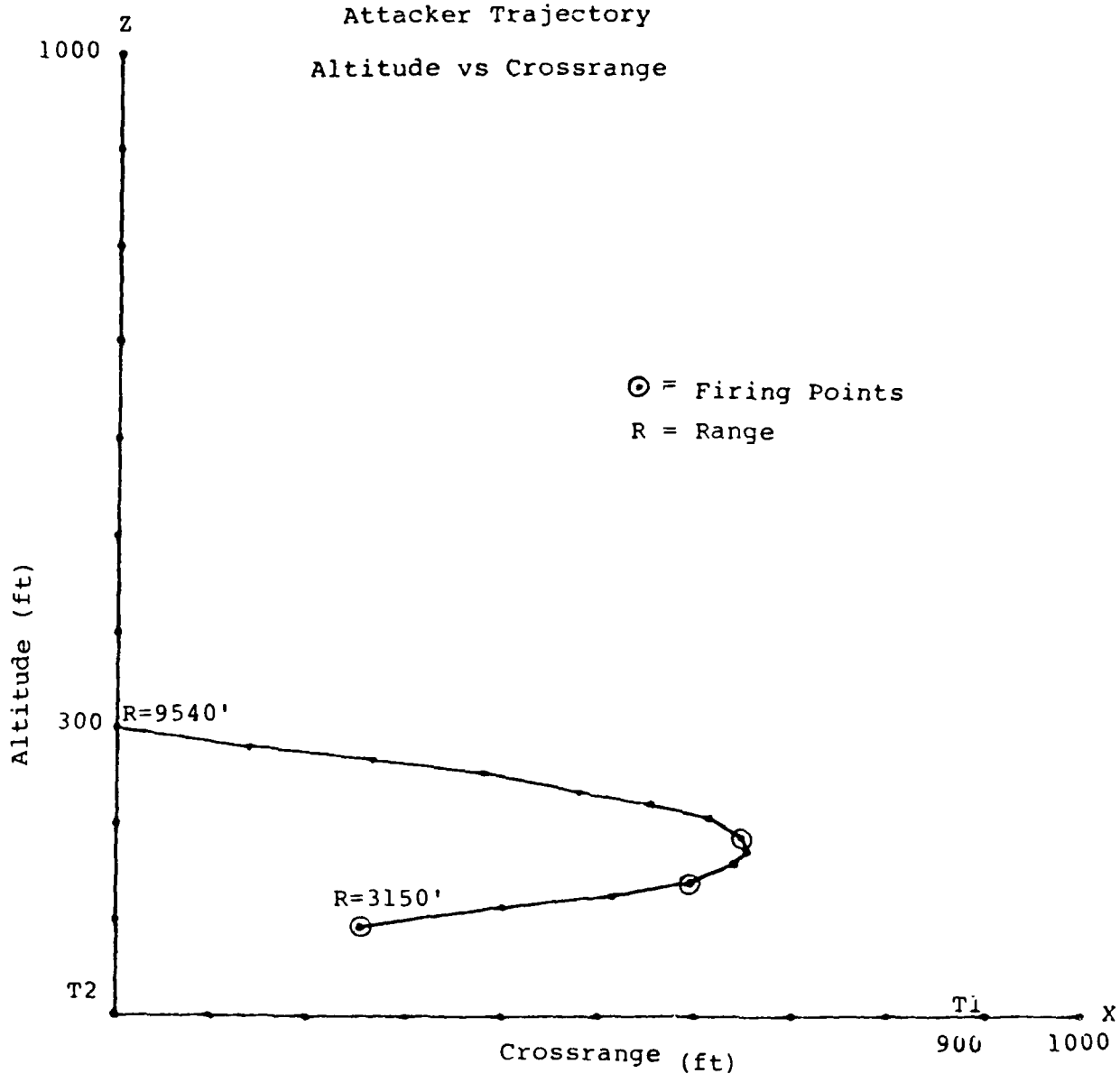
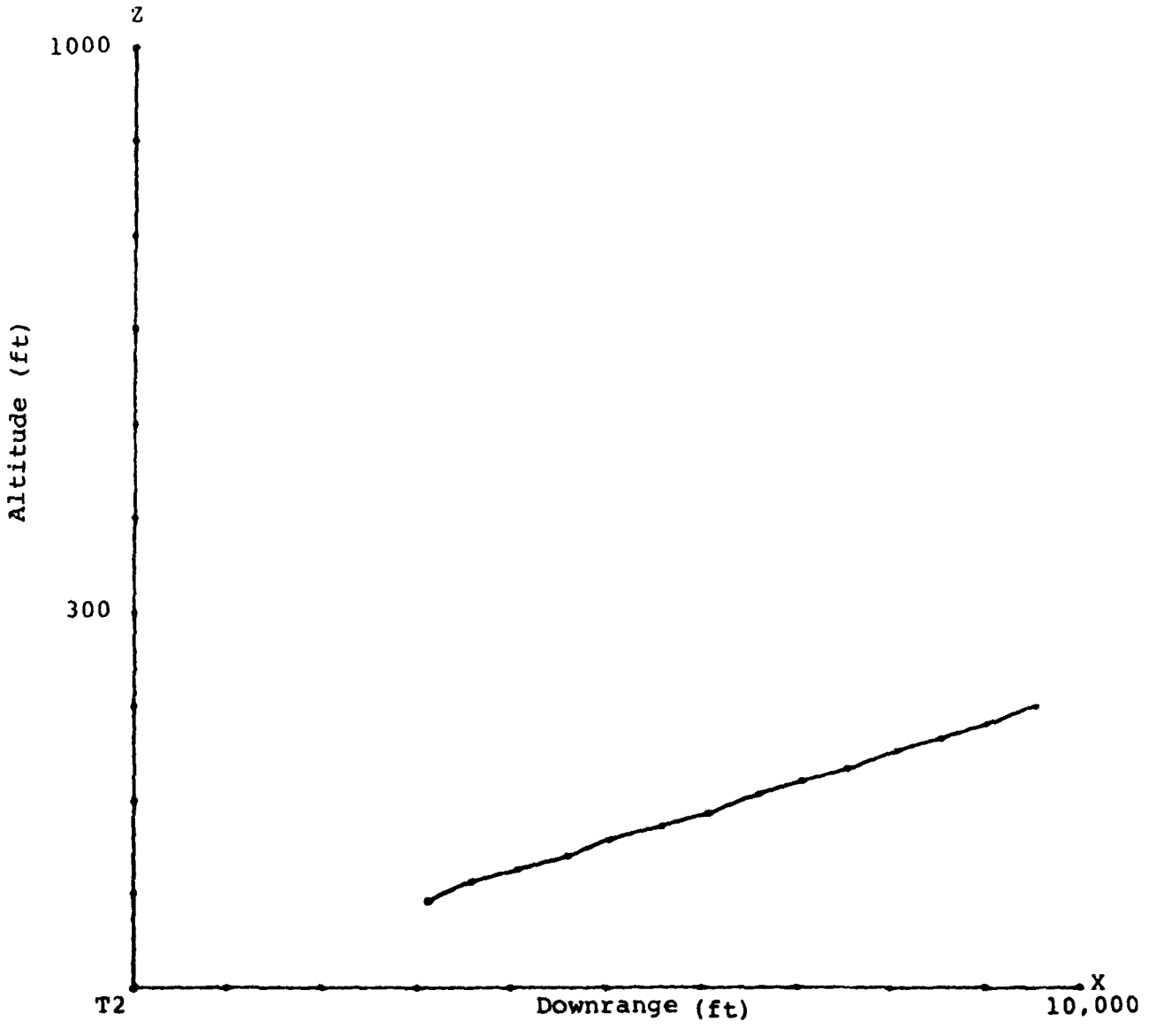

Attacker Trajectory
Altitude vs Crossrange
Z
1000
⊙ = Firing Points
R = Range
Altitude (ft)
300
R=9540'
R=3150'
T2
Ti
X
900
1000
Crossrange (ft)

Figure 4

Attacker Trajectory

Altitude vs Downrange

(Note Axes Scale not the same)



altitude versus down-range. For minimizing vulnerability, some attention needs to be given to changing this trajectory to a curved path. If AAA is situated away from the targets and in position to fire at this aspect it sees nearly a straight line trajectory. However, the attacker is accelerating along the line. Note at the lower portion of attack, the effect of the turn in the y-z plane is to cause the points along the line to decelerate. This effect will cause the AAA to miss.

Figure 5 shows the attacker acceleration versus time. The acceleration is constantly changing and increases as the attacker approaches the target. A desirable feature to minimize vulnerability to AAA.

Finally, Figure 6 shows the angular rate magnitude, $|\underline{\omega}_L|$ of the line adjoining the target (or AAA) and the attacker. This is the angular rate the AAA uses to predict future attacker position. If $\underline{\omega}_L$ is constant, the AAA can well predict the attacker's future position. However, if it changes rapidly, then the AAA will miss the attacker. After seven seconds the $\underline{\omega}_L$ changes very rapidly and at 10 seconds goes through zero. (Since we are plotting the magnitude of $\underline{\omega}_L$, it reverses direction.)

AUTOPILOT ATTACK WITH A MOVEABLE GUN

Reference 2 gives the results of the pursuit autopilot using a moveable gun and a simplified point mass attacker. This reference also gives results for a full scale, simulation using a 6 degree of freedom attacker against a ground target defended by a AAA. In this later case an attack autopilot was not available for the simulation. The results are summarized below.

SIMPLIFIED ATTACKER AUTOPILOT RESULTS

To determine the probability of killing the target for a given gun angle (total gun travel) several trajectories were flown using the simplified simulation. The "baseline," fixed gun trajectory was a 3 g sweep, with a 2 second straight-line firing segment. The firing commenced at a range of 4000 feet and ended at a range of 3000 feet. The simulated trajectory ended when firing ceased. The 3 g approach was chosen because essentially no hits are scored by the AAA prior to the straight-line firing segment. The gun angle is zero and the probability of killing the target (P_K) is about 0.45. During the 2 second straight-line firing segment, the AAA scored 5.6 hits on the attacker. The simulation was run for 1, 2,3, and 4 g's and stopped at the end of firing. In each case, the firing range was centered around 3500 feet. The moveable gun countered the motion of the attacker and kept the rounds on the target. The results show that a 2 g sweep will also get a 0.45 P_K if the gun can move

Figure 5

Attacker Acceleration

vs.

Time

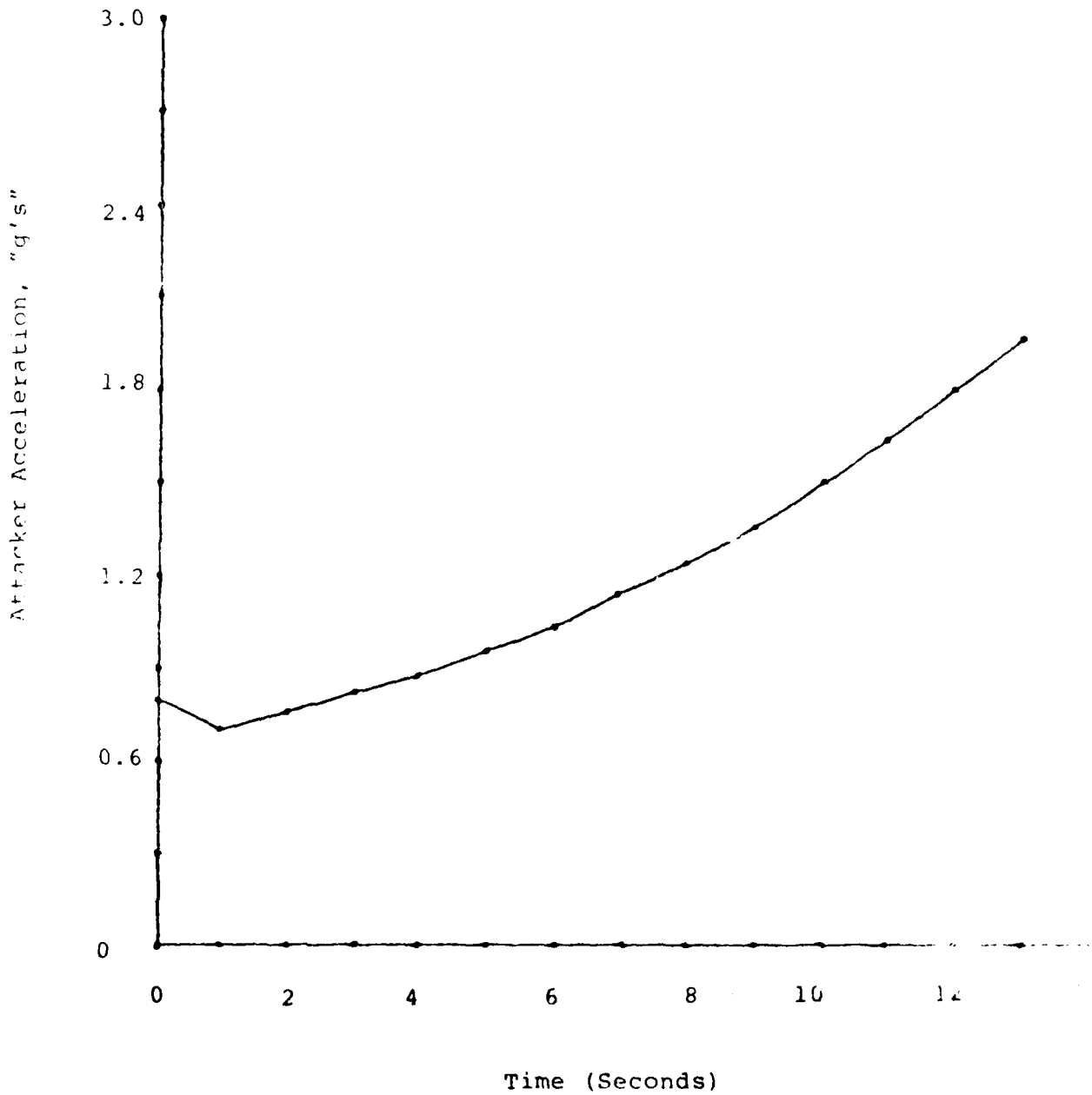


Figure 6

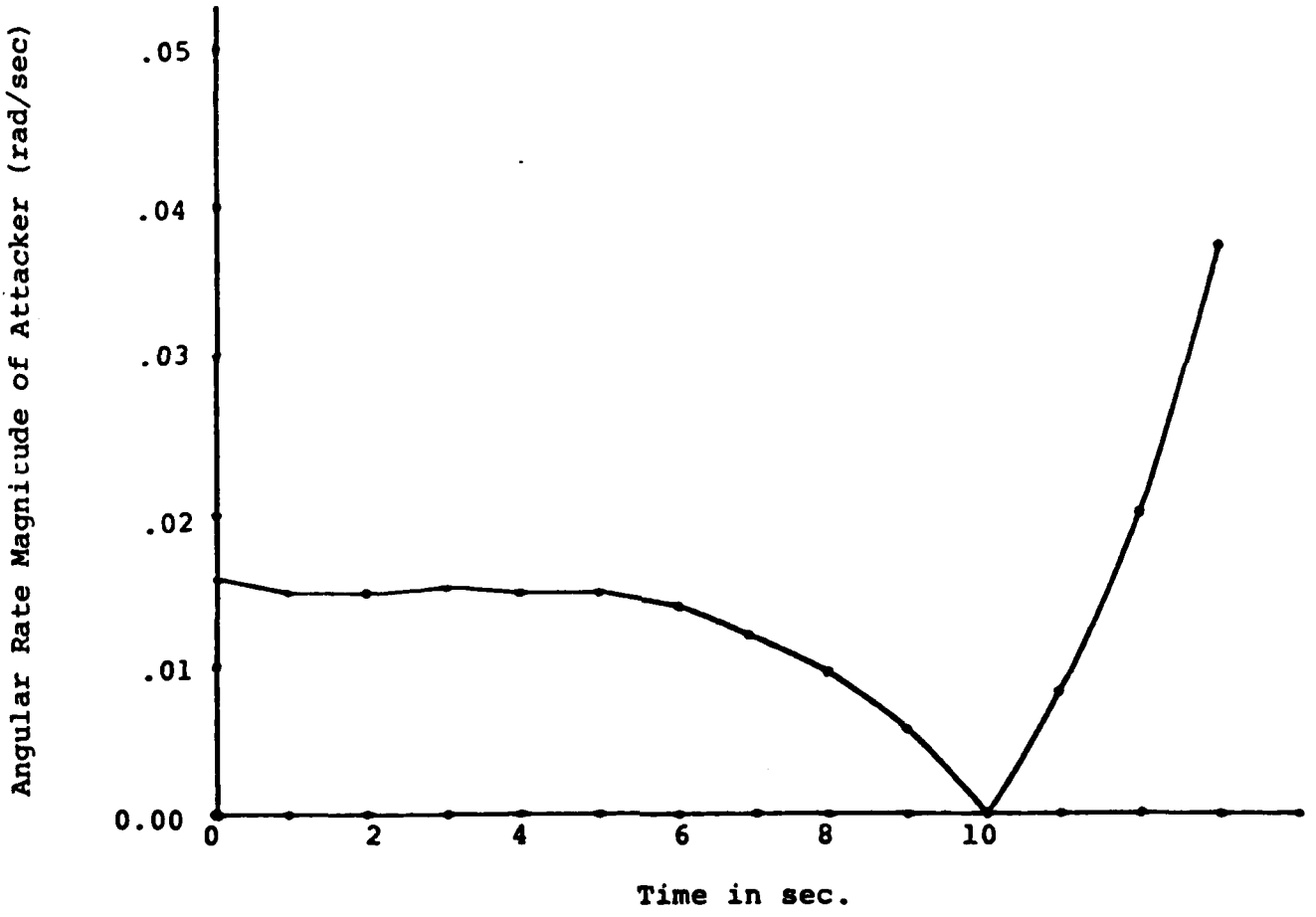
Angular Rate Magnitude of Attacker

vs

Time

As viewed from AAA

(or Target)



approximately 18 degrees (plus or minus 9). The advantage gained by the moveable gun is survivability. The number of hits on the attacker is reduced by a factor of 15 compared to the straight-line firing segment (from 5.6 hits to 0.38 hits)! The helix firing maneuver described in reference 1 gives over a 0.4 P_K. During firing about one hit was scored on the attacker or about 5 times less than the baseline trajectory. For this trajectory the gun was offset 4.8 degrees with a 3 degree travel about that offset.

FULL SCALE PILOTED SIMULATION RESULTS

An accelerating sweep scenario was flown by 2 pilots on the Air Force Academy's flight simulator using A-10 type dynamics. The attacker starts at 300 feet altitude and pulls up slightly turning away from the target. The attacker then begins a gradual dive doing an accelerating sweep to pass his gun sight through the target.

Three different firing techniques are used:

The pilot alters the attacker's trajectory at firing to a straight line to employ the fixed gun.

He continues his sweep through the target and employs a ±11 degree moveable gun which keep the rounds on the target during the sweep.

He changes the sweep to a partial helix around the target during firing and employs a ±3 degree moveable gun.

The simulation pass is stopped during egress when the attacker has turned 90 degrees away from the target, i.e., the target is on the attacker's beam.

Two significant results were evident from the simulation passes:

The moveable gun solution doubled the probability of killing the target while receiving less than one half the number of AAA hits when compared to the fixed gun.

The sweep with a helix type maneuver during firing gave nearly identical results to the pure sweep across the target. The advantage was the helix type fire maneuver reduced the necessary gun travel angle from ±11 degrees to ±3 degrees.

ATTACK AUTOPILOT FOR REALISTIC AIRCRAFT

Because of the promising results with the autopilot for the simplified point mass attacker, an autopilot was designed for a realistic A-10 type air to ground aircraft. The translational and rotational equations of motion are:

$$\begin{bmatrix} F_x \\ F_y \\ F_z \end{bmatrix} = m \begin{bmatrix} \dot{u}+qw-rv \\ \dot{v}-pw+ru \\ \dot{w}+pv-qu \end{bmatrix} = \begin{bmatrix} -QC_D+T \\ QC_y \\ -QC_l \end{bmatrix}$$

where: F_x, F_y and F_z are the forces along the aircraft axes, x, y, z.

m = mass of the aircraft

u, v, w are the inertial velocities along x, y, z

p, q, r are the inertial rotational rates around x, y, z

Q = dynamic pressure

T = thrust

C_D, C_y, C_l are the resultant aerodynamic translational coefficients along the aircraft axes

$$\begin{pmatrix} L \\ M \\ N \end{pmatrix} = \begin{bmatrix} I_x\dot{p}-\dot{r}J_{xz}+qr(I_z-I_y)-pqJ_{xz} \\ I_y\dot{q}+pr(I_x-I_z)+(p^2-r^2)J_{xz} \\ I_z\dot{r}-\dot{p}J_{xz}+pq(I_y-I_x)qrJ_{xz} \end{bmatrix} = \begin{bmatrix} QBC_L \\ QCC_M \\ QBC_N \end{bmatrix}$$

where: L, M, N are the torques about the aircraft axes

I_x, I_y, I_z are the moments of inertial about the aircraft axes

J_{xz} is the cross product of inertia

B = wing span

C = mean chord length

C_L, C_M, C_N are the resultant aerodynamic rotational coefficients around the aircraft axes

These equations are then linearized about a nominal flight condition.

The aerodynamic coefficients contain δ_a, δ_r, δ_e, the control surface deflections.

The linearized state equations are of the form:

$$\delta\dot{\underline{x}} = \left.\frac{\partial \underline{f}}{\partial \underline{x}}\right|_{\substack{\underline{x}_n \\ \underline{u}_n}} \delta\underline{x} + \left.\frac{\partial \underline{f}}{\partial \underline{u}}\right|_{\substack{\underline{x}_n \\ \underline{u}_n}} \delta\underline{u}$$

where: $\underline{x} = \begin{pmatrix} u \\ v \\ w \\ p \\ q \\ r \end{pmatrix}$ and $\underline{u} = \begin{pmatrix} \delta a \\ \delta e \\ \delta r \\ T \end{pmatrix}$

(units are ft, sec, radians, and pounds)

The linearization was done around the condition:

$$\underline{x}_c = \begin{pmatrix} 489 \\ 0 \\ 52 \\ 0 \\ .13 \\ 0 \end{pmatrix} \text{and } \underline{u}_c = \begin{bmatrix} 0 \\ .03 \\ 0 \\ 16500 \end{bmatrix}$$

A pole placement design method (reference 3) was used to place the closed loop poles at -2, -1.5, -1.0, -0.8, -0.6 and -0.5 .

The resulting feedback gain matrix is:

$$K = \begin{bmatrix} 0 & 6.3\text{x}10^{-4} & 0 & -.142 & 0 & .217 \\ 9.6\text{x}10^{-5} & 0 & 1.06\text{x}10^{-3} & 0 & .946 & 0 \\ 0 & 6.4\text{x}10^{-4} & 0 & .0257 & 0 & -.221 \\ 873 & 0 & 88.6 & 0 & 40176 & 0 \end{bmatrix}$$

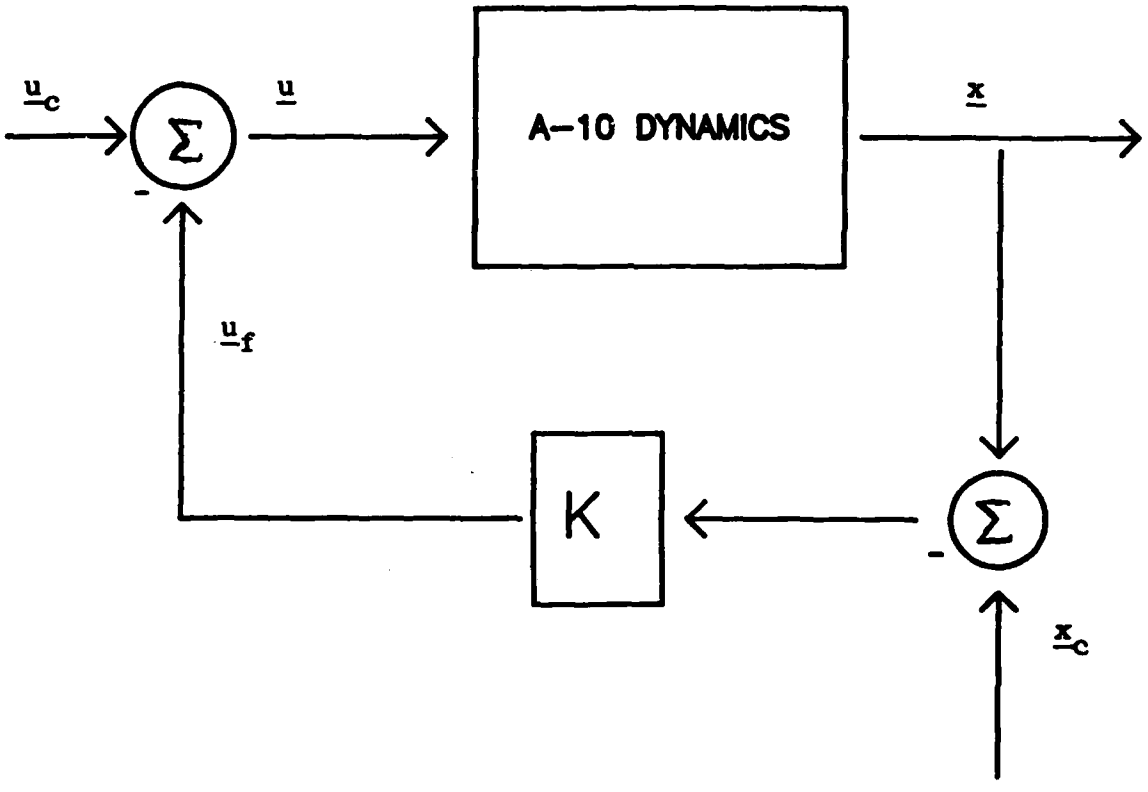
These gains multiply the state deviations from $\underline{x}_c$ and add to the nominal controls, u_c, as shown in Figure 7. The nominal attack conditions approximate a 2 "g" sweep maneuver. To test the control scheme the initial state vector was perturbed to:

$$x = \begin{pmatrix} 500 \\ 20 \\ 0 \\ .1 \\ 0 \\ .1 \end{pmatrix}$$

Figures 8 to 13 show the resulting state responses. The system behaves quite well except it is a little more oscillitory than expected. Presently this attack autopilot is being refined and programmed into the Air Force Academy flight simulator to test the full scale simulation including pursuit guidance against a pseudo target.

Figure 7

State Feedback Autopilot for an A-10 Type Aircraft



$\underline{u}$, the input vector

$\underline{u}_f$, the feedback control vector

$\underline{u}_c$, the nominal control vector

$\underline{K}$, the feedback gain matrix

$\underline{x}$, the state variable

$\underline{x}_c$, the nominal state variable vector

Figure 8

Forward (x) Velocity Versus Time

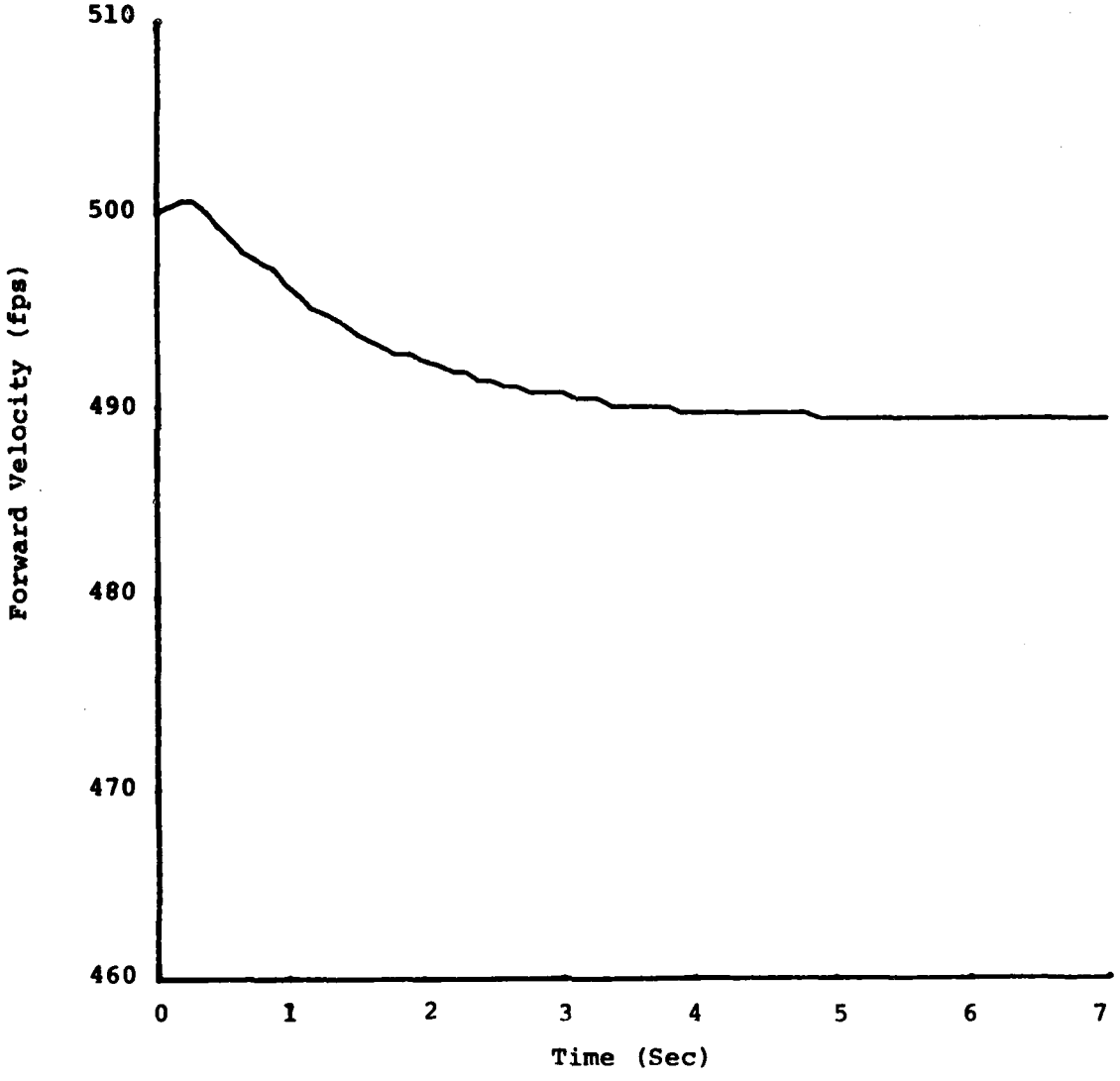


Figure 9

Side (y) Velocity versus Time

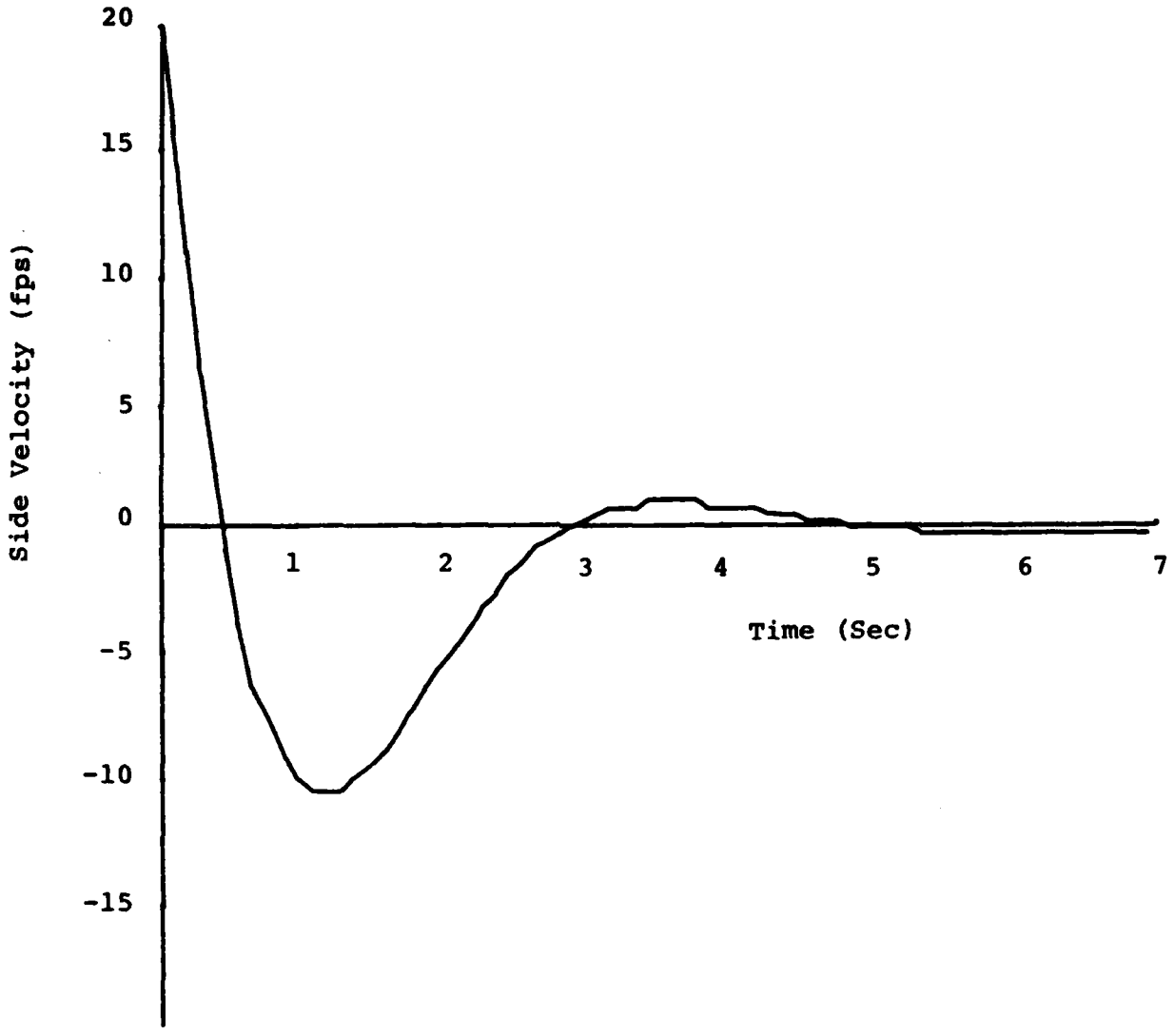


Figure 10

Vertical (z) Velocity Versus Time

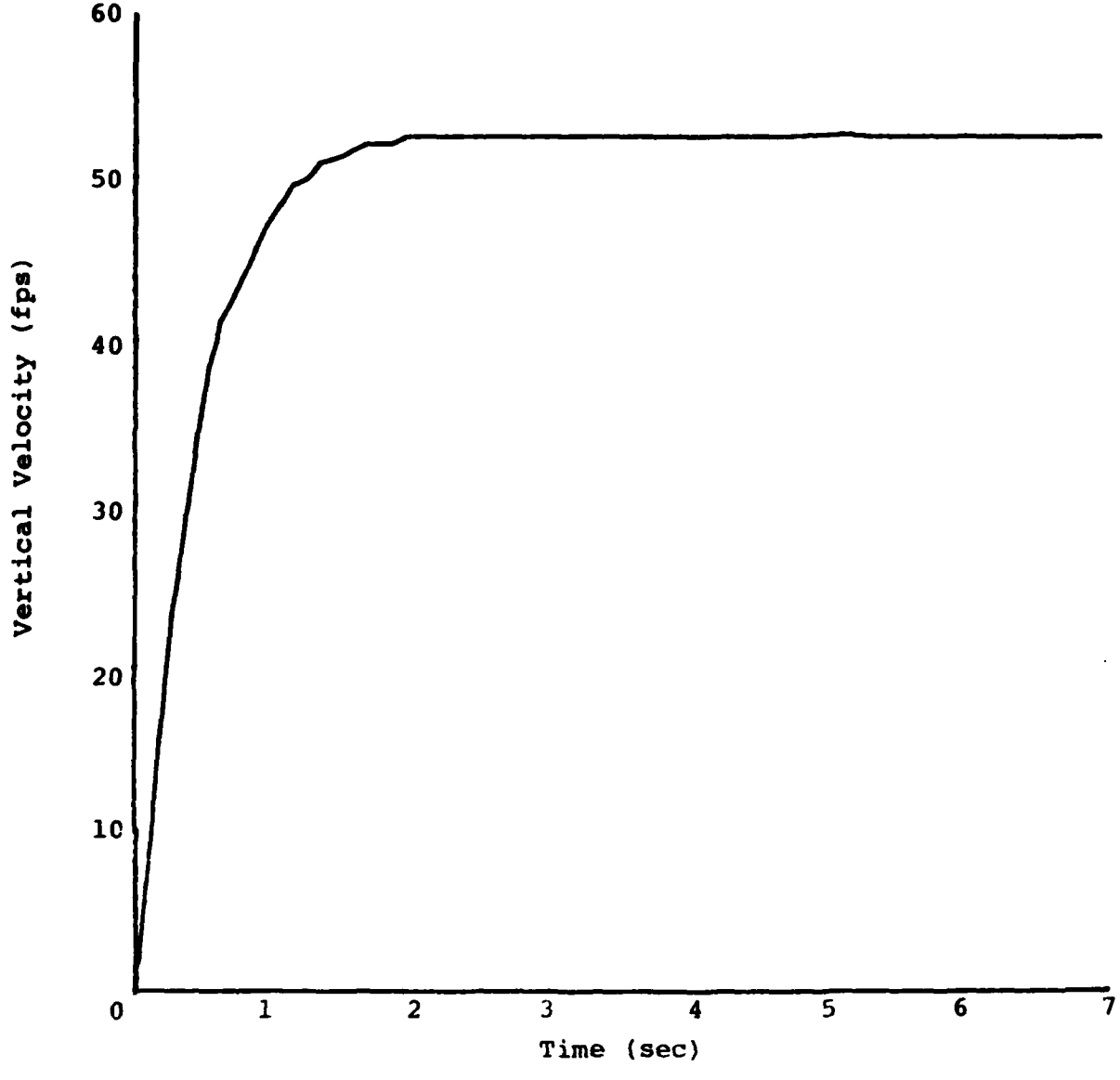


Figure 11

Roll Rate (p) versus Time

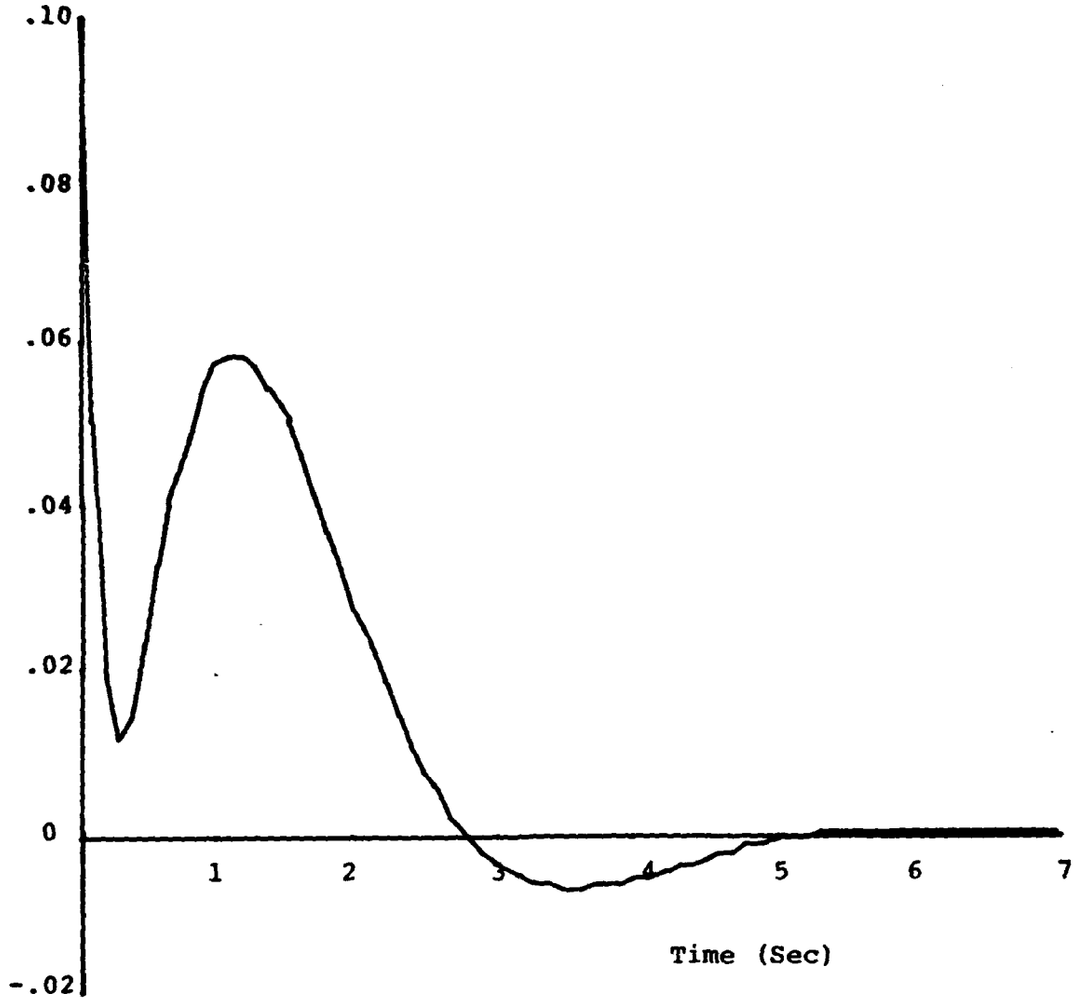


Figure 12

Pitch Rate (q) versus Time

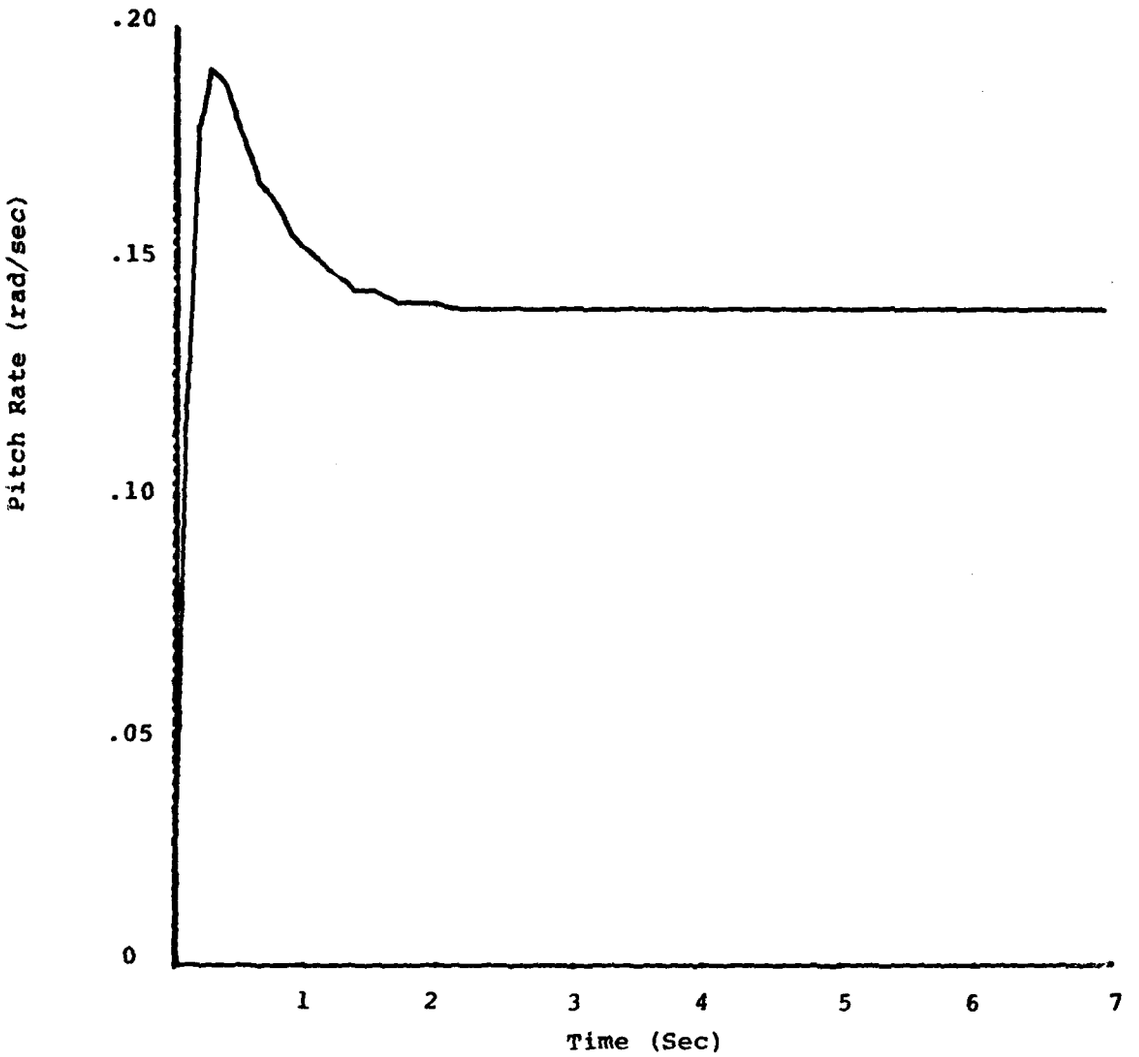
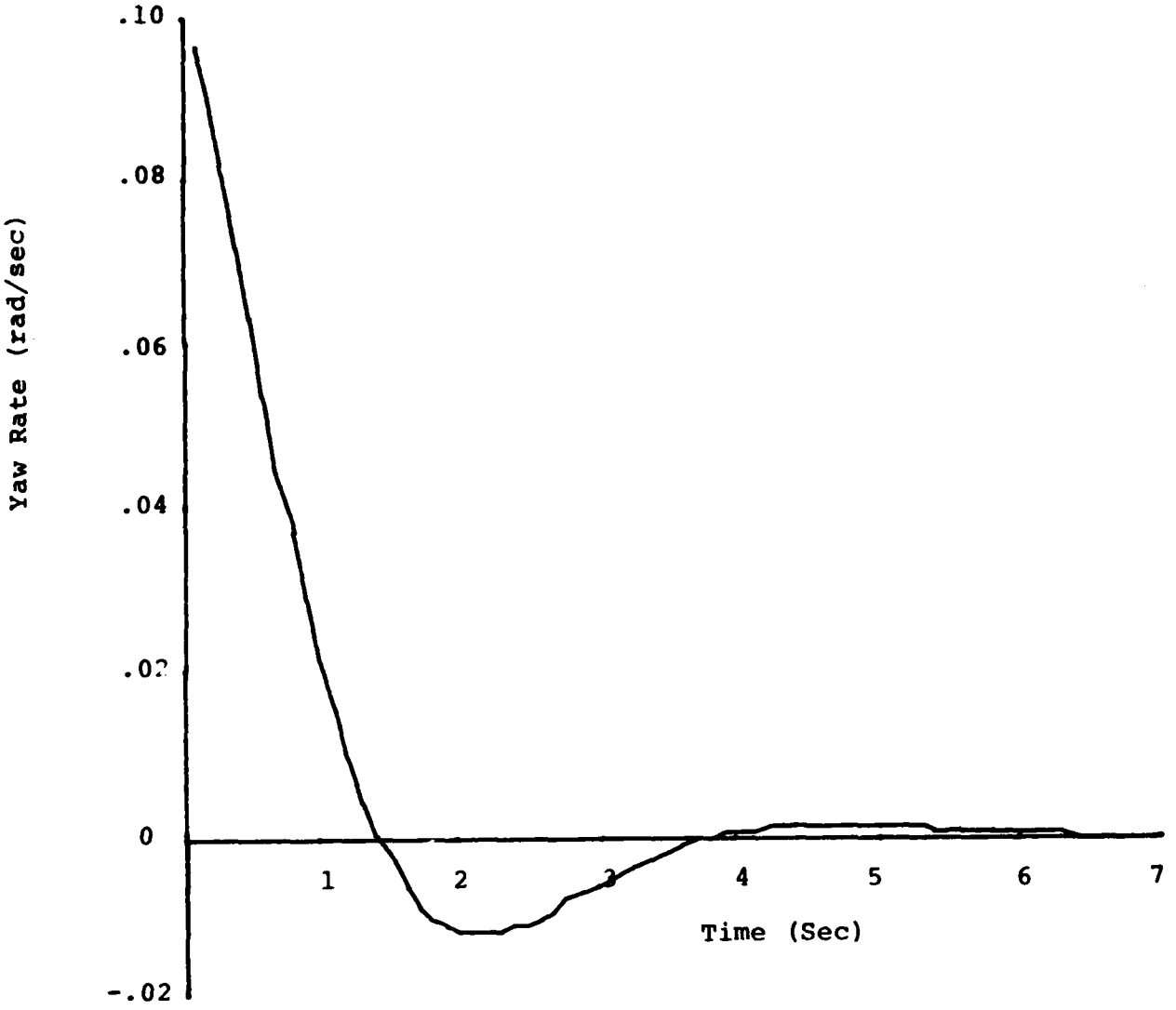


Figure 13

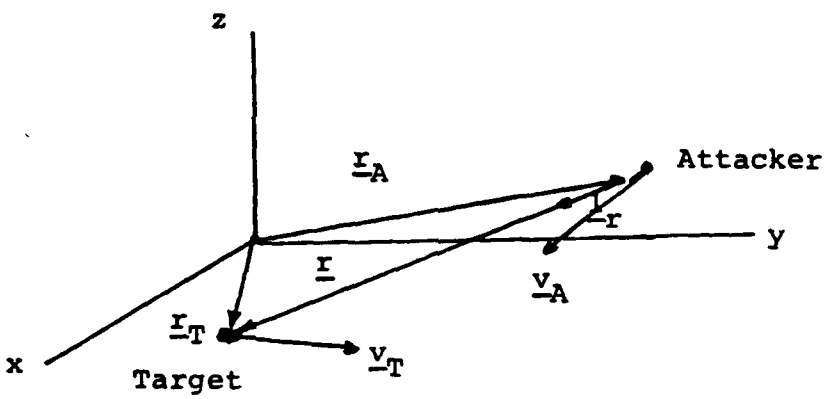
Yaw Rate (r) versus Time



APPENDIX A

Deriviation of Three Dimensional Proportional Navigation and Pursuit Guidance Simulation Equations

Proportional Navigation Derivation



$$\underline{r}_T - \underline{r}_A = \underline{r} = r\underline{1}_r$$

$$\dot{\underline{r}} = \underline{v} = \dot{r}\underline{1}_r + r\dot{\underline{1}}_r = \dot{r}\underline{1}_r + r(\underline{\omega}_L \times \underline{1}_r)$$

$$\therefore \quad \underline{v} - \dot{r}\underline{1}_r = \underline{\omega}_L \times \underline{r} \qquad \text{(A1)}$$

We wish to solve for $\underline{\omega}_L$ (angular rotation rate of the line of sight). However, since angular rotation parallel to $\underline{r}$ (the LOS) will not produce any effect on $\underline{v}_T$ or $\underline{v}_A$, a direct solution of (A1) cannot give a unique solution (e.g., if we rewrite (A1) as:

$$\underline{v} - \dot{r}\underline{1}_r = \begin{bmatrix} o & z & -y \\ -z & o & x \\ y & -x & o \end{bmatrix} \begin{pmatrix} \omega_x \\ \omega_y \\ \omega_z \end{pmatrix} \quad \text{where: } \underline{r} = \begin{pmatrix} x \\ y \\ z \end{pmatrix} \quad \underline{\omega}_L = \begin{pmatrix} \omega_x \\ \omega_y \\ \omega_z \end{pmatrix}$$

$$= B\underline{\omega}_L$$

The matrix, B, is singular, showing the problem encountered. To get around this we assume that

$\underline{\omega}_L$ is orthogonal to $\underline{r}$

(i.e., no rotation parallel to $\underline{r}$)

Now cross $\underline{r}$ with both sides of (A1)

$$\underline{r} \times \underline{v} - \overbrace{\underline{r} \times \dot{r}\underline{1}_r}^{=0} = \underline{r} \times (\underline{\omega}_L \times \underline{r})$$

$$= \overbrace{(\underline{r} \cdot \underline{r})\underline{\omega}_L - (\underline{r} \cdot \underline{\omega}_L)\underline{r}}^{=0} \text{ (by assumption)}$$

$$\therefore \underline{r} \times \underline{v} = r^2 \underline{\omega}_L$$

$$\underline{\omega}_L = \frac{1}{r^2} (\underline{r} \times \underline{v}) \qquad \text{(A2)}$$

Now let us examine the acceleration of the attacker:

$$\underline{v}_A = v_A \underline{1}_A$$

$$\dot{\underline{v}}_A = \underline{a}_A = \dot{v}_A \underline{1}_A + v_A \dot{\underline{1}}_A$$

$$\underline{a}_A = \dot{v}_A \underline{1}_A + (\underline{\omega}_v \times \underline{v}_A) \qquad \text{(A3)}$$

But we desire the rotation rate of the attacker to be a constant times the rotation rate of the LOS:

(Proportional Nav)

$$\underline{\omega}_v = K\underline{\omega}_L \qquad \text{(A4)}$$

Substituting (A4) into (A3)

$$\underline{a}_A = \dot{v}_A \underline{l}_A + K(\underline{\omega}_L \times \underline{v}_A)$$

or

$$\underline{a}_A = \dot{v}_A \underline{l}_A + \frac{K}{r^2} (\underline{r} \times \underline{v}) \times \underline{v}_A \qquad \text{(A5)}$$

Now we examine that portion of $\underline{a}_A$ which is orthogonal to $\underline{l}_A$ (the velocity vector direction); a special case would be if v_A is held constant; i.e., $\dot{v}_A = 0$, then $\underline{a}'_A \triangleq \underline{a}_A$.

$$\underline{a}'_A = \frac{K}{r^2} (\underline{r} \times \underline{v}) \times \underline{v}_A$$

then

$$\underline{a}'_A = \frac{-K}{r^2} (\underline{v}_A \cdot \underline{v}) \underline{r} - (\underline{v}_A \cdot \underline{r}) \underline{v} \qquad \text{(A6)}$$

where

$$\underline{v} = \underline{v}_T - \underline{v}_A$$

$$\underline{r} = \underline{r}_T - \underline{r}_A$$

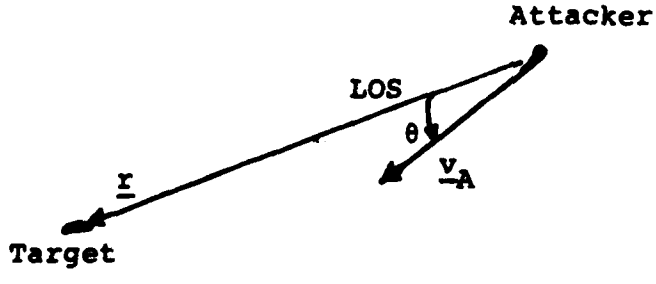
Pursuit Guidance Deviation

For pursuit guidance we want to meet two conditions:

(1) the velocity vector to point at the target

(2) the angular velocity of the attacker to equal the angular velocity of the line of sight (LOS)

Condition 1



We want to drive θ to zero.

$$\underline{\theta} = \sin^{-1}\left|\frac{\underline{r} \times \underline{v}_A}{rv_A}\right|\underline{1}_\theta \qquad \text{(A7)}$$

where $\underline{1}_\theta$ is a unit vector perpendicular to $\underline{r}$ and $\underline{v}_A$, (i.e., $\underline{1}_\theta = \frac{\underline{r} \times \underline{v}_A}{rv_A}$).

The acceleration, $\underline{a}_\theta$, necessary to drive θ to zero must be in a direction perpendicular to $\underline{v}_A$ and $\underline{1}_\theta$. This direction is found by taking a unit vector along the cross product of $\underline{v}_A \times \underline{1}_\theta$.

then

$$\underline{a}_\theta = A\left(\frac{\underline{v}_A \times \underline{1}_\theta}{v_A}\right) = A\left(\frac{\underline{v}_A \times (\underline{r} \times \underline{v}_A)}{rv_A^{\,2}}\right)$$

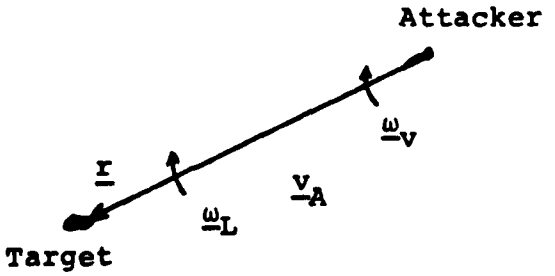
where A is some desired level of acceleration, expanding the triple cross product:

$$\underline{a}_\theta = \frac{A}{rv_A^{\,2}}(\underline{v}_A \cdot \underline{v}_A)\underline{r} - (\underline{v}_A \cdot \underline{r})\underline{v}_A$$

$$\underline{a}_\theta = \frac{A}{rv_A^{\,2}}(v_A^{\,2}\underline{r} - (\underline{v}_A \cdot \underline{r})\underline{v}_A) \qquad \text{(A8)}$$

This acceleration drives our velocity vector to align with the LOS to the target.

Condition 2



We want $\underline{\omega}_L = \underline{\omega}_V$ to keep the velocity vector aligned with the LOS. From our derivation of proportional guidance (A4) we see that K must be unity. Using the special case (A6) we define $\underline{a}_L$:

$$\therefore \underline{a}_L \triangleq -\frac{1}{r^2}\left[(\underline{v}_A \cdot \underline{v})\underline{r} - (\underline{v}_A \cdot \underline{r})\underline{v}\right] \tag{A9}$$

this $\underline{a}_L$ keeps $\underline{\omega}_L = \underline{\omega}_V$.

The total pursuit acceleration is the sum of these two accelerations:

$$\underline{a}_{pur} = \underline{a}_\theta + \underline{a}_L \tag{A10}$$

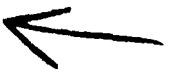
Equation (A10) is used by the attacker in the simulation to follow the pseudo target.

References

1. Definition and Analysis of Sensor Directed Gun System Concepts, Final Report, E. Bauman and C. Fosha, Department of Electrical Engineering and Computer Science, University of Colorado, Colorado Springs, October 1981.

2. "Maximizing Survivability and Effectiveness of Air-to-Ground Gunnery Using a Moveable Gun", E. Bauman and R. Shepard, Proceedings of the IEEE 1982 National Aerospace and Electronics Conference, May, 1982, pp. 908-915.

3. Modern Control Theory, W. Brogan, Quantum Publishers, Inc., 1974, pp. 311-314.



Next page is blank.

SESSION VI: MISSILE STABILIZATION & CONTROL

28 OCT 1982

(MORNING)

ROOM #2

FOURTH MEETING OF THE COORDINATING

GROUP ON MODERN CONTROL THEORY

HOSTED BY: OAKLAND UNIVERSITY
ROCHESTER, MICHIGAN

Next page is blank.

AD P001090

A FIRE COORDINATION CENTER FOR LIGHTWEIGHT AIR DEFENSE WEAPONS

William C. Cleveland
LADS Program Office
Ford Aerospace & Communications Corporation
Newport Beach, California 92660

INTRODUCTION

The objective of an ongoing company sponsored program at Ford Aerospace and Communications Corporation (Aeronutronic Division) is the conduct of conceptual and preliminary design studies on Lightweight Air Defense Systems (LADS). These systems are intended for use in the mid 1980's by Army Light Infantry and Air Mobile Divisions, Marine Corps Infantry Divisions, and other elements of the Rapid Deployment Joint Task Forces. The systems must be lightweight in order to be easily air transportable/air liftable and highly mobile on the ground. They must be self-contained in terms of target sensors, communications and weapons. Operation in a variety of environmemts and theaters is a prime requirement, including deployment in battle areas where attack from enemy air launched anti-radiation missiles is to be expected. The problem addressed in this paper is the configuration of a Fire Coordination Center which can be used at the platoon and/or battery level as an element of a distributed command and control system.

LADS SYSTEM DESCRIPTION

The LADS system, as considered here, is a family of lightweight guns and missiles operating as Division Air Defense Weapons. The primary system requirements and constraints are listed in Figure 1. A weapons control system concept has been developed which is consistent with the listed requirements and constraints.

• Lightweight	- Minimum weight/length for maximum air transportability/ liftability (6,000 and 12,000 pound classes)
• Mobile	- Transported by highly mobile vehicles (HMMWV, LAV)
• Multiple Sensors	- Required for tactical flexibility
• SHORAD C^2 Interface	- To Battalion/Division TOCS
• Short Emplacement/March Order Times	- 2 minutes
• Defend Against Multiple Threats	- Ground Support Fighters/ Helicopters/Ground Vehicles

FIGURE 1. LADS System Requirements and Constraints

FIGURE 1. LADS System Requirements and Constraints (Cont'd)

• Early IOC	- 1985
	- Hardware from current programs/ developments
• P^3I Growth Compatibility	- Sensors
	- Communications

Figure 2 depicts the system concept. An acquisition and tracking radar and several passive sensors are located on a vehicle deployed at the platoon and/or battery level with four to sixteen weapon Fire Units. This Fire Control Center vehicle is connected by two-way data links to the Fire Units. The Fire Control Center also has communication links to other adjacent Fire Control Centers and to Battalion and Division Tactical Operations Centers. The concept is flexible in terms of deployment to accommodate various missions and weapons. The weapons considered in these studies are a mix of lightweight 40mm guns, towed Chaparrals, and Manpads missiles.

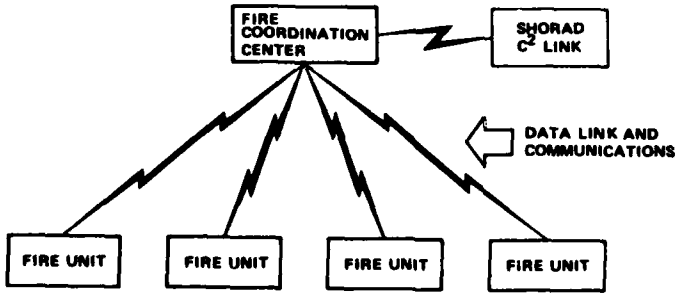


FIGURE 2. LADS System Concept

The principal functions of the Fire Control Center are listed in Figure 3. Target detection is accomplished by the sensor collection which can include radar, FLIR, passive RF and acoustic detectors. The other functions are provided by computers, displays and controls located in the Fire Control Center. The sensors are capable of providing a variety of data with varying degrees of accuracy,

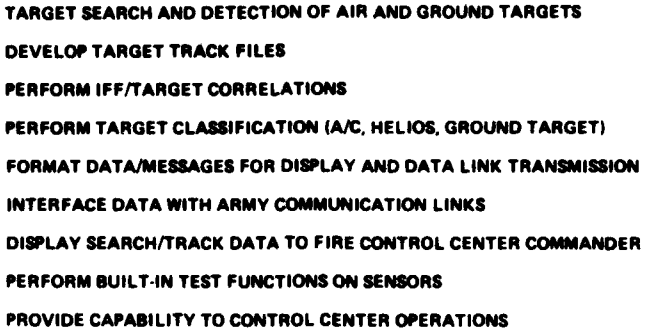


FIGURE 3. Fire Control Center Functions

depending upon the data mode. Figure 4 shows the modes and users of the data organized by target angular data accuracy. Other data such as target range, velocity, type, etc. is also available, depending upon the sensors in use. The radar is utilized to provide data to the Fire Units and weapons during the all weather fire control data modes. The Fire Control Center is manned by a three man crew consisting of Driver, Sensor Operator and Fire Control Commander. Stabilized sensors permit operation while on the move.

To communicate commands and data between the Fire Control Center (FCC) higher level Tactical Operations Centers, other Fire Control Centers and Fire Units, voice communications and data links are required. The general requirements are listed in Figure 5. The FCC design has been developed so that interfaces and data rates are compatible with the present Army VRC-12 family of radios. Provisions are being made for interfacing with new communications equipment such as SINCGARS-V and PACKET radios if they are fielded.

The message content and duration of typical track messages from the FCC to a weapon are shown in Figure 6. The message durations assume a 1200 bit per second data link capability. Fire Units would communicate status to the FCC with short messages (300 bits) every one to ten minutes.

- VOICE/DIGITAL DATA TRANSMISSION

  TO CONTROL CENTERS

  - DIVISION/CORP. TOCS
  - BATTALION CPS

  TO WEAPONS

  - LIGHTWEIGHT GUN/TOWED CHAPARRAL
  - MANPADS MISSILES
- ADAPTIVE UPDATE RATES
- SECURE (ENCRIPTION CAPABILITY)
- JAM RESISTANT
- MULTIPLE DATA FORMAT COMPATIBILITY
- REDUNDANT LINKS THROUGH NETTING
- BUILT-IN TEST AND ERROR DETECTION CAPABILITY

FIGURE 4. Fire Control Center Data Modes

- ALERTING/CUEING (TO FIVE DEGREES)
  - STINGER
  - TOWED CHAPARREL
  - LIGHT WEIGHT GUN
  - PASSIVE RF ANTENNAS
- ACQUISITION/POINTING (1^{o} TO 2^{o})
  - NIGHT CHAPARRAL FLIR
  - LIGHTWEIGHT-GUN SIGHT/FLIR
- FIRE CONTROL (TO SEVERAL MILS)
  - LIGHTWEIGHT GUN
  - CHAPARRAL MISSILE SEEKER
  - LASER RANGE FINDER

FIGURE 5. LADS Communications Requirements

- CONTENT
  - UNIT ADDRESS
  - TARGET IDENTITY/FIRE STATUS
  - TARGET POSITION (ALERTING, CUEING)
  - TARGET VELOCITY
  - TARGET ALTITUDE/ELEVATION
  - TARGET HEADING (ALERTING, CUEING)
  - TARGET DIRECTION COSINES (TRACKING)
  - CONTROL WORD/ENCRYPTION
- MESSAGE DURATION (MSEC)
  - ALERTING 140
  - CUEING 140
  - TRACKING 223
- MESSAGE RATE
  - ALERTING 1/2 SEC/TARGET
  - CUEING 1/2 SEC/TARGET
  - TRACKING 4.5/SEC/CHANNEL/TARGET

FIGURE 6. FCC Message Structure

Figure 7 shows a block diagram of the equipment required in the Fire Control Center to perform the functions listed in Figure 3. The equipment is grouped functionally according to purpose; Sensors, Computation, Communications, or Display.

The characteristics of typical passive sensors are tabulated in Figure 8. The active radar sensor characteristics are classifed.

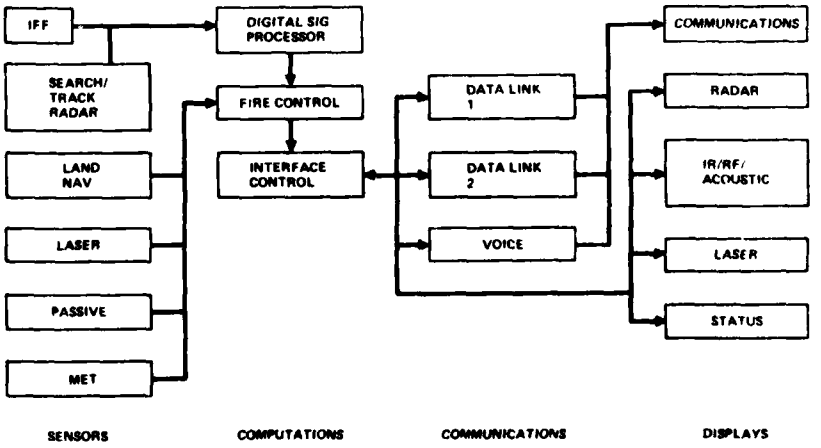


FIGURE 7. FCC Block Diagram

FLIR	
FOV	– 6^{o} X 6^{o} AND 2^{o} X 2^{o}
RESOLUTION	– 0.1 TO 0.33 MRD
SENSITIVITY (NET)	– 0.2°C
DEFECTION RANGE	– <10 km
RF FREQUENCY	– 5-18 GHz
AZIMUTH COVERAGE	– 360°
ELEVATION COVERAGE	– 20°
DF ACCURACY	– < 1° RMS
TRACK RATE	– 20°/SEC
I FIELD OF VIEW	– ≠ 45°
ACOUSTIC	
DETECTION RANGE (HIND-D)	– 10 km
CLASSIFICATION CAPABILITY	– ROTOR BLADES
AZIMUTH ERROR (RMAX)	– < 10° RMS
AZIMUTH ERROR RMAX/5	– 2° RMS

FIGURE 8. Passive Sensor Characteristics

In order to compute and communicate the position of targets in a universal map grid system for transmission to Fire Units, the FCC must have accurate knowledge of its geographical location and attitude. This information is provided by a strapdown three axis inertial sensor system: the requirements and accuracy of typical available lightweight systems are listed in Figure 9. A compilation of system error sources and magnitudes from the active and passive sensors in the FCC is given in Figure 10. These accuracies allow achievement of the target positions as listed in Figure 4.

- REQUIREMENTS
  - PROVIDE ATTITUDE REFERENCE FOR SENSORS AND WEAPONS
  - PROVIDE AXIMUTH/ALTITUDE REFERENCE FOR TARGET POSITION COMPUTATIONS
  - COMPUTE FIRE CONTROL CENTER AND FIRE UNIT POSITIONS
  - MEASURE GUN TUBE AZIMUTH AND ELEVATION NOTES
- ACCURACY (1σ VALUES)

ATTITUDE	1 MIL
AZIMUTH	0.54 MIL INITIAL PLUS 1 MIL/HR DRIFT
POSITION (NORTHING AND EASTING)	< 0.25% DISTANCE (20 km TRAVEL)
ALTITUDE	0.025% DISTANCE (20 km TRAVEL)

- INITIALIZATION METHODS
  - GYROCOMPASSING
  - KNOWN REFERENCE POINT
  - COMMON SIGHTING POINT
  - LINE OF SIGHT

FIGURE 9. Land Navigation Unit Characteristics

FIRE CONTROL CENTER TARGET SENSORS (RMS)		
ACTIVE (SEARCH)		1° AZ/EL
ACTIVE (TRACKING AND CUEING)		1-2 MRD
PASSIVE (CUEING)		
	ACOUSTIC	5°
	RF	1°
	IR	0.1
FIRE CONTROL CENTER/FIRE UNITS POSITION/ ATTITUDE SENSOR (1σ) (10 km TRAVEL)		
ATTITUDE REFERENCE		1 MIL
POSITION REFERENCE		20 METERS
ALTITUDE		2.5 METERS
DIGITAL DATA LINK		NEGLIGIBLE WITH ERROR CORRECTIN CODE
COMPUTATIONS		16 BIT MICROPROCESSOR ERRORS NEGLIGIBLE

FIGURE 10. System Errors

The design concepts described in this paper have been implemented in a partially functional mockup as illustrated in Figure 11. The fiberglass shelter containing the equipments shown was mounted on a prototype High Mobility Multipurpose Wheeled Vehicle furnished by the General Dynamics Land Systems Division. The complete Platoon Coordination Center, as it was named, is pictured in Figure 12. All equipments illustrated were functional except for the radar and land naviation unit. This unit was trucked to the Army Firing Center at Yakima, Washington in April 1982 where it participated in the Ninth Infantry Division's Field Training Exercise "Goldenblade". The Control Center was deployed on a hilltop overlooking the edge of the exercise battlefield. Figure 13 illustrates the inputs from various radar sensors located nearby to the Division Operations Van (OPNS Van) and Air Battle Management Operator's Van (ABMOC). The radar track data was automatically input to the Briefcase Terminals (described in Figure 11) which were located in the two vans and the Platoon Coordination Center (PCC) via the Command Net Data links. The track data was then relayed to the Lightweight Gun, Towed Chaparral and Dual and Dual Purpose Manpads Missile (SABER) over the Fire Unit data net.

The track data was used to cue the mini-FLIR mounted on the roof of the PCC for target acquisition. Operations were conducted by the contractor-trained Army crews during the entire five-day exercise period. All equipment in the Fire Coordination Center (PCC) worked very well.

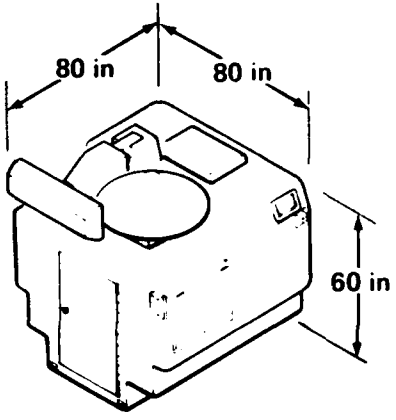
The conclusions drawn from PCC operation during the Yakima Field Exercise were as follows:

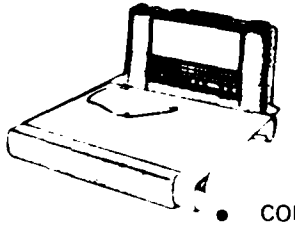
1. The feasibility of the prototype mobile distributed C^2 center was demonstrated. This center has the following advantages:

   - Command and Control capability can be placed in the hands of the Light Division Platoon/Battery Commander.

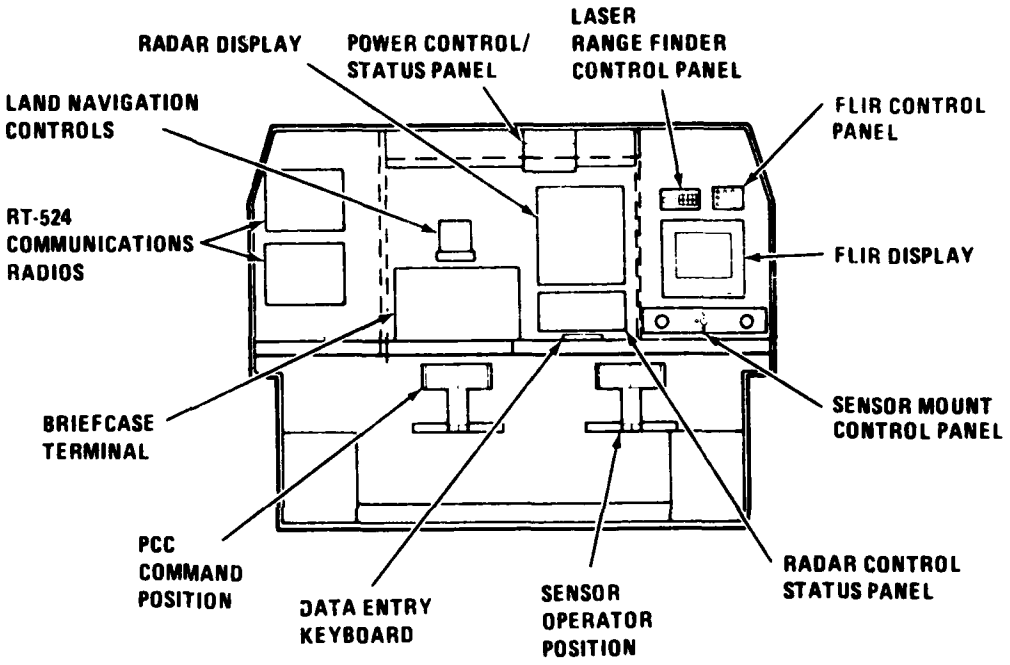
PCC SHELTER

- CONSTRUCTED OF FIBERGLASS ON WELDED ALUMINUM FRAME
- DIMENSIONS





PCC OPERATORS CONSOLE



Briefcase Terminal (BCT) Is Key Interactive Display Device That Provides Digital Data Interface With BCTs At Btry CP, ABMOC, And Other PCCs And With Digital Communications Terminals (DCTs) At Individual Weapons

- COMPACT LIGHTWEIGHT INTELLIGENT TERMINAL
- LED INTERACTIVE DISPLAY
- ONE 16-BIT MICROPROCESSOR (256K BYTES OF RAM)
- FIVE 8-BIT MICROPROCESSORS (32K BYTES OF RAM)
- UP TO 6 PROGRAMMABLE MODEMS
- THREE HIGH SPEED INTERFACES

FIGURE 11. PCC MOCKUP AT YAKIMA REPRESENTS A FIRST-STEP PROTOTYPE OF AN AUTOMATED DIGITAL PLATOON COORDINATION SYSTEM

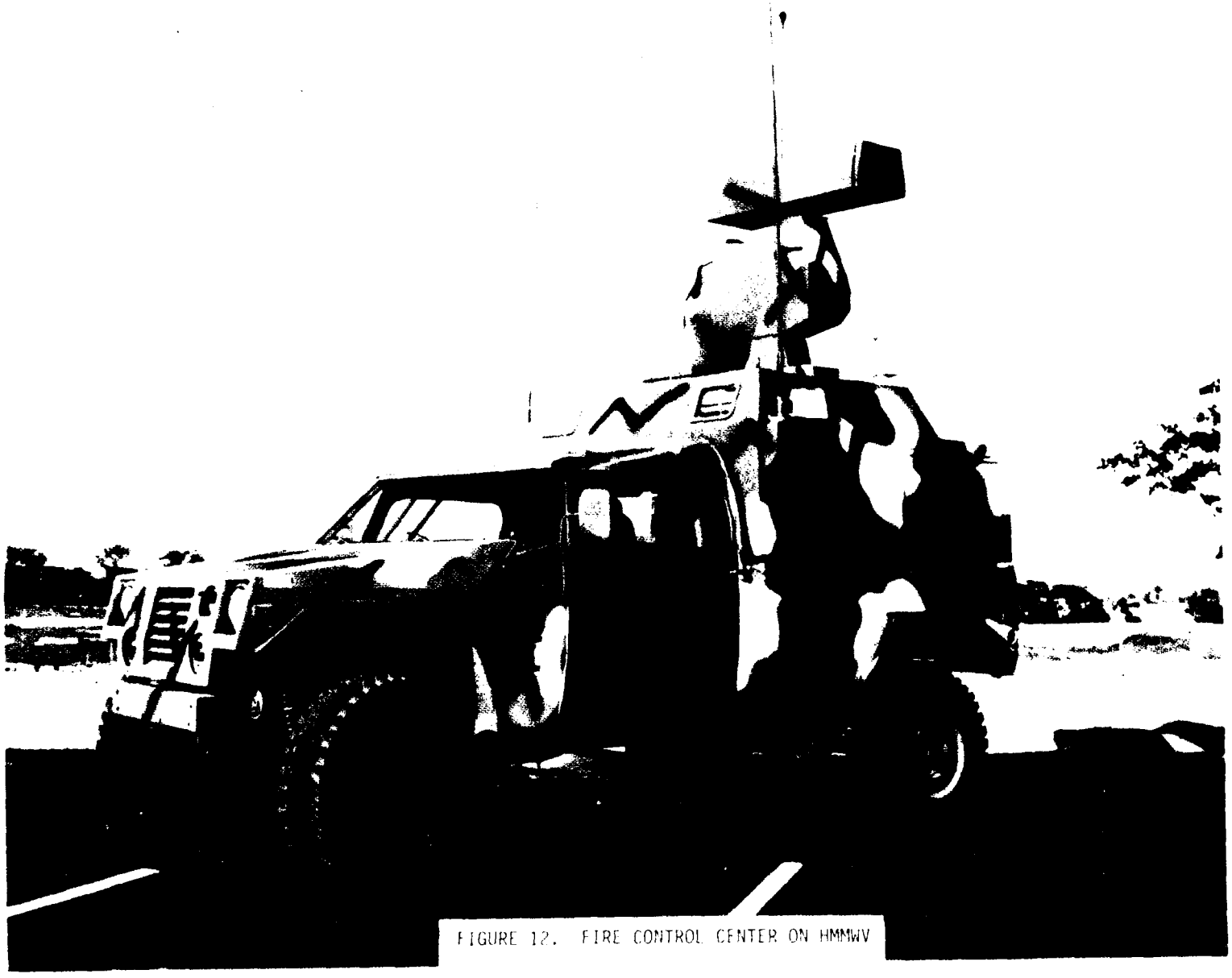


FIGURE 12. FIRE CONTROL CENTER ON HMMWV

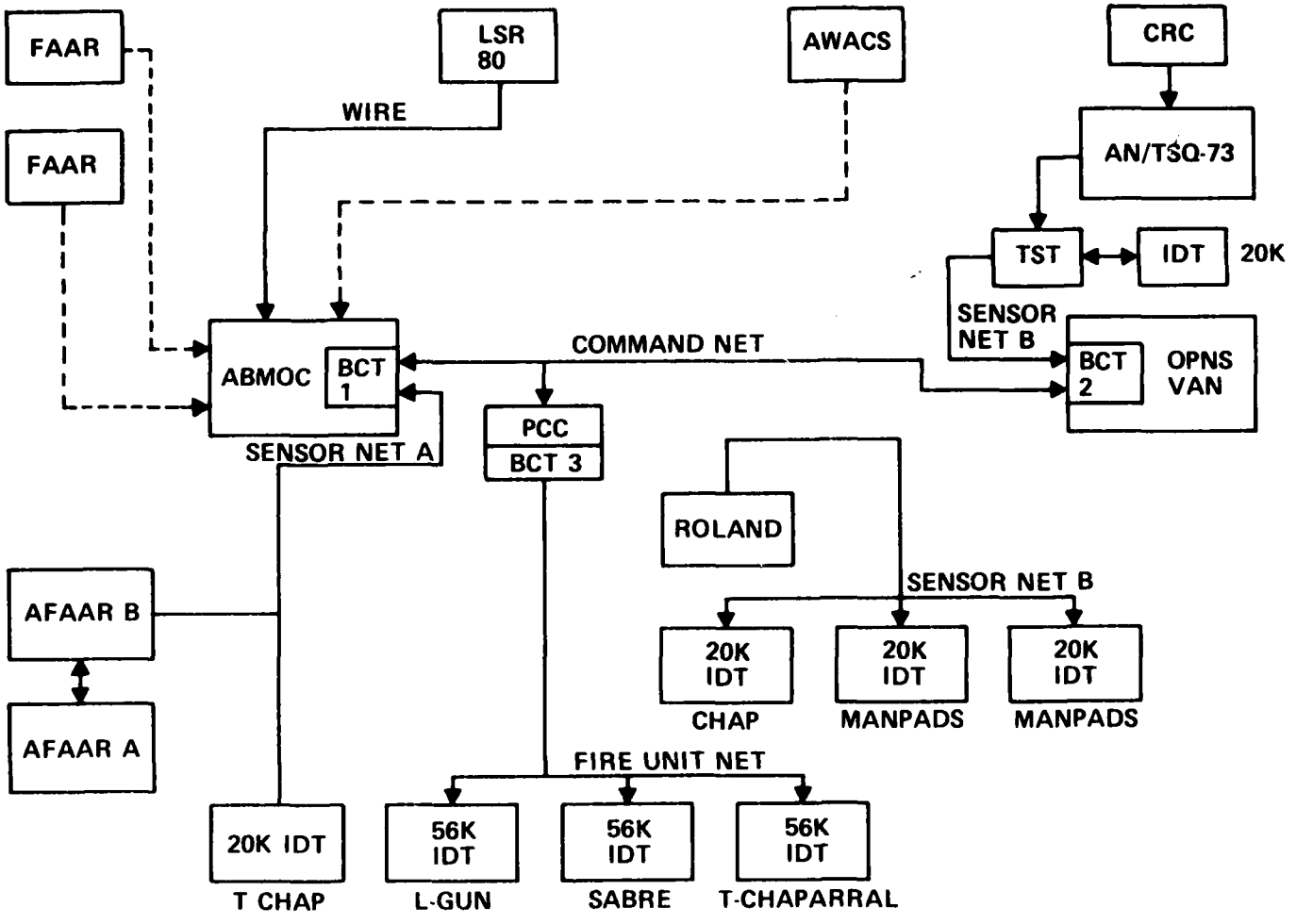
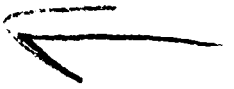


FIGURE 13. YAKIMA MAY DEMONSTRATION

- Flexibility is provided by combining active and passive sensors
- C^2 tie into Battalion and Division TOCs is provided
- Multiple Fire Unit types (guns, Chaparrals, Manpads) can be controlled by the PCC
- Platoon/Battery Coordination Centers can be netted to provide data redundancy and active emitter blinking and shutdown control

2. The PCC mounted on a HMMWV is a highly mobile air liftable center.
   - Limited road testing was performed at Yakima
   - Shelter dematability and UH60B Blackhawk liftability was demonstrated at Ft. Lewis, Washington following the Yakima Field Training Exercise
   - The PCC can keep up with highly mobile ground forces and operate on the move



Next page is blank.

AD P001091

CLOSED-FORM CONTROL ALGORITHM FOR CONTINUOUS-TIME DISTURBANCE-UTILIZING CONTROL INCLUDING AUTOPILOT LAG

Jerry Bosley
Wayne Kendrick
Computer Sciences Corporation

INTRODUCTION

Missile dynamic time lag is a major factor contributing to excessive terminal miss distances resulting from short range intercept trajectories. The objective of this paper is to describe a linear closed loop guidance law which compensates for this lag. Disturbance-Utilizing Control (DUC) theory [1] is applied to the terminal homing missile intercept problem as described in [2] except that the plant model is extended to include the missile dynamics, represented as a single time lag. The final form of the guidance law is identical with the result of Cottrell [3], and extends the results of [5] which discusses the relations between DUC and some well known guidance laws. The results described in this paper are applicable to problems in which the external disturbances have waveform structure (e.g. target maneuvers or wind gusts). Further work is under way to derive controllers which can drive the missile to the target in the face of both waveform and noise-type disturbances.

PLANAR HOMING INTERCEPT

The geometry of the missile-intercept problem to be considered is shown in Figure 1. The missile is assumed to have been placed near a reference line-of-sight (REF LOS) by some satisfactory midcourse guidance scheme. The REF LOS is established prior to terminal guidance initiation at an angle α_h from the horizontal. The control objective is to guide the missile along the REF LOS to the target with as little control effort as possible in the face of a given class of waveform disturbances. Several assumptions are made to simplify the problem. First assume the missile's velocity and position are known throughout the missile's trajectory and the velocity parallel to the REF LOS is known and constant during the terminal phase of the missile's flight. Furthermore assume that both control and disturbance forces are restricted to act perpendicular to the REF LOS. Moreover, assume the control force experiences a first order lag ($1/\tau$) from the commanded acceleration. The dynamics of the problem can now be restricted to the dynamics of the displacements of the missile from the REF LOS.

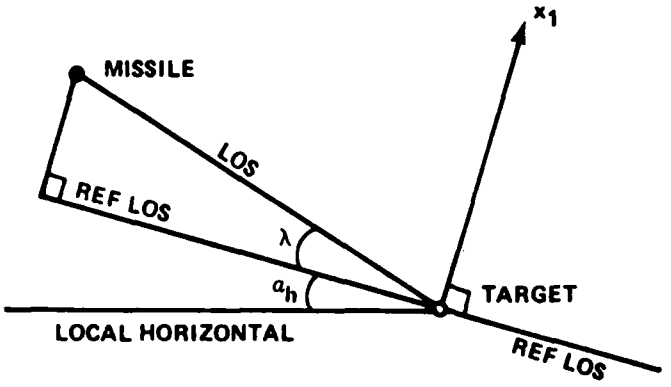


Figure 1. Relative Intercept Geometry.

The dynamics of the missile's displacement from the REF LOS are modeled by

$$\dot{x} = \begin{bmatrix} \dot{x}_1 \\ \dot{x}_2 \\ \dot{x}_3 \end{bmatrix} = \begin{bmatrix} 0 & 1 & 0 \\ 0 & 0 & 1 \\ 0 & 0 & -1/\tau \end{bmatrix} \begin{bmatrix} x_1 \\ x_2 \\ x_3 \end{bmatrix} + \begin{bmatrix} 0 \\ 0 \\ 1/\tau \end{bmatrix} u(t) + \begin{bmatrix} 0 \\ 1 \\ 0 \end{bmatrix} w(t) \qquad (1)$$

where

$x_1(t)$ = missile displacement from RLOS,

$x_2(t)$ = missile velocity normal to RLOS,

$x_3(t)$ = missile acceleration normal to RLOS,

$u(t)$ = missile acceleration command,

$w(t)$ = missile disturbance acceleration,

τ = missile control acceleration time constant.

The disturbance acceleration, w(t), is assumed to be a piecewise continuous sequence of step and ramp functions obeying the dynamical equation

$$\dot{Z} = \begin{bmatrix} \dot{Z}_1 \\ \dot{Z}_2 \end{bmatrix} = \begin{bmatrix} 0 & 1 \\ 0 & 0 \end{bmatrix} \begin{bmatrix} Z_1 \\ Z_2 \end{bmatrix} + \begin{bmatrix} \sigma_1(t) \\ \sigma_2(t) \end{bmatrix} \tag{2}$$

$$w(t) = \begin{bmatrix} 1 & 0 \end{bmatrix} \begin{bmatrix} Z_1 \\ Z_2 \end{bmatrix}$$

where σ_1 and σ_2 are sequences of sparsely spaced impulse functions with random amplitude. According to Johnson [1] the impulse sequences σ_1 and σ_2 can be ignored in order to develop the required control law.

DUC PROBLEM

It is shown in [1] that the zero set-point DUC problem can be formulated as a linear-quadratic regulator problem by using the augmented vector

$$\tilde{x} = \begin{bmatrix} x \\ \hline Z \end{bmatrix}$$

which is a composite of the state vectors of the plant and the disturbance process. The composite system equation may be written as follows:

$$\dot{\tilde{x}} = \tilde{A}\tilde{x} + \tilde{B}u \tag{3}$$

where

$$\tilde{A} = \left[\begin{array}{ccc|cc} 0 & 1 & 0 & 0 & 0 \\ 0 & 0 & 1 & 1 & 0 \\ 0 & 0 & -1/\tau & 0 & 0 \\ \hline 0 & 0 & 0 & 0 & 1 \\ 0 & 0 & 0 & 0 & 0 \end{array}\right] ; \tilde{B} = \left[\begin{array}{c} 0 \\ 0 \\ 1/\tau \\ \hline 0 \\ 0 \end{array}\right]$$

The performance index to be minimized is

$$J = 1/2\ \tilde{x}^T(T)S\tilde{x}(T) + 1/2 \int_{t_o}^{T} \left[\tilde{x}^T(t)Q\tilde{x}(t) + u^T(t)Ru(t)\right] dt \tag{4}$$

where S and Q are known non-negative definite symmetric matrices and T is the terminal time of the missile intercept. T is given by

$$T = t_o + d/v$$

where

t_o = time of terminal phase initiation,

d = displacement of the missile from the target along the REF LOS at time t_o

and v = missile velocity along the REF LOS.

The optimal DUC which minimizes (4) subject to (3) is found using standard linear quadratic methods to be

$$u(t) = -R^{-1}\tilde{B}^T K\tilde{x} \tag{5}$$

where K obeys the matric Ricatti equation

$$\frac{d}{dt} K = -K\tilde{A} - \tilde{A}^T K + K\tilde{B}R^{-1}\tilde{B}^T K - Q, \; K(T) = S \tag{6}$$

Solutions of (6) will be expressed as closed form functions of the time-to-go (tgo) to intercept.

The control objective of the missile-intercept problem is to minimize the final displacement of the missile from the target using a minimum of control force. Selection of S, Q, and R as

$$S = \begin{bmatrix} S & 0 & 0 & 0 & 0 \\ 0 & & & & \\ 0 & & & \underline{0} & \\ 0 & & & & \\ 0 & & & & \end{bmatrix}, \; Q = 0, \; R = 1$$

is consistent with these objectives. The solution for the optimal control law as a function of tgo is to be found where tgo is defined as

$$tgo = T - t$$

The optimal control law is thus

$$u(tgo) = -R^{-1}\tilde{B}^T K(tgo)\, \tilde{x}(tgo) \tag{7}$$

and K obeys the matric Ricatti equation

$$\dot{K} = K\tilde{A} + \tilde{A}^T K - K\tilde{B}R^{-1}\tilde{B}^T K + Q, \; K(0) = S \tag{8}$$

where $\dot{(\;)}$ designates the operator $\frac{d}{d\,tgo}$

DUC PROBLEM SOLUTION

Using (3) and (4) the Hamiltonian is constructed

$$H = 1/2(\tilde{x}^T Q\tilde{x} + u^T Ru) + \lambda^T(\tilde{A}\tilde{x} + \tilde{B}u)$$

Then, the necessary conditions for an optimal trajectory are

$$\lambda = -\frac{\partial H}{\partial \tilde{x}} = -Q\tilde{x} - \tilde{A}^T\lambda \tag{9}$$

with boundary condition

$$\lambda = S\tilde{x}(T)$$

and

$$\frac{\partial H}{\partial u} = 0 = Ru + \tilde{B}^T\lambda \tag{10}$$

Solving (10) explicitly, we get

$$u(t) = -R^{-1}\tilde{B}^T\lambda$$

Now we can rewrite (3) and (9) and combine them in matrix notation

$$\begin{bmatrix} \dot{\tilde{x}} \\ \dot{\lambda} \end{bmatrix} = \left[\begin{array}{c|c} \tilde{A} & -\tilde{B}R^{-1}\tilde{B}^T \\ \hline -Q & -\tilde{A}^T \end{array}\right] \begin{bmatrix} \tilde{x} \\ \lambda \end{bmatrix} \tag{11}$$

Assume a solution for λ of the form

$$\lambda = K\tilde{x} \tag{12}$$

where, at tgo = 0

$$\lambda(0) = S\tilde{x}(0)$$

The general solution to (11) can be written

$$\begin{bmatrix} \tilde{x}(tgo) \\ \lambda(tgo) \end{bmatrix} = \begin{bmatrix} \Phi(tgo) \end{bmatrix} \begin{bmatrix} \tilde{x}(0) \\ \lambda(0) \end{bmatrix} \tag{13}$$

where

$$\Phi(tgo) = \left[\begin{array}{c|c} \Phi_{xx}(tgo) & \Phi_{\lambda x}(tgo) \\ \hline \Phi_{x\lambda}(tgo) & \Phi_{\lambda\lambda}(tgo) \end{array}\right]$$

is the state transition matrix of (11).

CLOSED FORM ALGORITHM FOR GUIDANCE LAW

Substituting the general solutions for x(tgo) and λ(tgo) into (12) we can obtain K(tgo) in the form

$$K = \left[\Phi_{\lambda x} + S \Phi_{\lambda\lambda} \right] \left[\Phi_{xx} + S \Phi_{x\lambda} \right]^{-1} \tag{14}$$

let

$$\bar{A} = \left[\begin{array}{c|c} \tilde{A} & -\tilde{B}R^{-1}\tilde{B}^T \\ \hline -Q & -\tilde{A}^T \end{array}\right] \tag{15}$$

then

$$\Phi(tgo) = e^{\bar{A}t} = I + \bar{A}t + (1/2)\bar{A}^2t^2 + (1/6)\bar{A}^3t^3 + \ldots$$

Solving for $\Phi(tgo)$ we find

$$\Phi_{xx}(tgo) = \begin{bmatrix} 1 & -tgo & \tau^2(e^N-N-1) & tgo/2 & tgo/6 \\ 0 & 1 & \tau(1-e^N) & -tgo & tgo/2 \\ 0 & 0 & e^N & 0 & 0 \\ 0 & 0 & 0 & 1 & -tgo \\ 0 & 0 & 0 & 0 & 1 \end{bmatrix} \tag{16}$$

$$\Phi_{\lambda\lambda}(tgo) = \begin{bmatrix} 1 & 0 & 0 & 0 & 0 \\ tgo & 0 & 0 & 0 & 0 \\ \tau^2(e^{-N}+N-1) & \tau(1-e^{-N}) & e^{-N} & 0 & 0 \\ tgo^2/2 & tgo & 0 & 1 & 0 \\ tgo^3/6 & tgo^2/2 & 0 & tgo & 1 \end{bmatrix} \tag{17}$$

$$\Phi_{\lambda x}(tgo) = 0 \tag{18}$$

$$\Phi_{\lambda x}(tgo) = \begin{bmatrix} \tau^3F_1/2-tgo^3/6-\tau^2tgo & \tau^2F_2/2-tgo^2/2-\tau^2 & \tau F_1/2-tgo & 0 & 0 \\ -\tau^2F_2/6+tgo^2/2+\tau^2 & tgo - \tau F_1/2 & 1-F_2/2 & 0 & 0 \\ \tau F_1/2 - tgo & -1 + F_2/2 & F_1/2\tau & 0 & 0 \\ 0 & 0 & 0 & 0 & 0 \\ 0 & 0 & 0 & 0 & 0 \end{bmatrix} \tag{19}$$

Where $N = tgo/\tau$,

$$F_1 = e^N - e^{-N} \text{ and } F_2 = e^N + e^{-N}$$

Substituting (16), (17), (18) and (19) into (14) we obtain K(tgo) as follows

$$K = \frac{1}{\Delta} \begin{bmatrix} 1 & tgo & F_3 & tgo^2/2 & tgo^3/6 \\ tgo & tgo^2 & tgoF_3 & tgo^3/2 & tgo^4/6 \\ F_3 & tgoF_3 & F_3^2 & tgo^2F_3/2 & tgo^3F_3/6 \\ tgo^2/2 & tgo^3/2 & tgo^2F_3/2 & tgo^4/4 & tgo^5/12 \\ tgo^3/6 & tgo^4/6 & tgo^3F_3/6 & tgo^5/12 & tgo^6/36 \end{bmatrix} \quad (20)$$

Where $F_3 = \tau^2(e^{-N} + N - 1)$

$$\Delta = -tgo^2\tau \left[(1/2N^2)\, e^{-2N} + (2/N)\, e^{-N} - N/3 + 1 - 1/N - 1/2N^2 - 1/S\tau tgo^2 \right]$$

Finally substituting (20) into (5) we obtain the DUC law as

$$u = \frac{-F_3}{\tau R\Delta} \left[x_1 + tgox_2 + F_3x_3 + tgo^2Z_1/2 + tgo^3Z_2/6 \right]$$

or in long form

$$u = \frac{(e^{-N}+N-1) \left[x_1+tgox_2+\tau^2(e^{-N}+N-1)x_3 + tgo^2Z_1/2+tgo^3Z_2/6 \right]}{Rtgo^2 \left[(1/2N^2)\, e^{-2N} + (2/N)\, e^{-N} - N/3 - 1/N - 1/2N^2 - 1/S\tau tgo^2 + 1 \right]} \quad (21)$$

If R is set to 1, S is set to a very large number and the second order disturbance term is dropped we obtain

$$u = \frac{(e^{-N} + N - 1) \left[x_1 + tgox_2 + \tau^2 (e^{-N} + N - 1)\, x_3 + tgo^2Z_1/2 \right]}{tgo^2 \left[(1/2N^2)\, e^{-2N} + (2/N)\, e^{-N} - N/3 + 1 - 1/N - 1/2N^2 \right]} \quad (22)$$

which is the general form of the optimal guidance law given by Cottrell [3] for an accelerating target.

If τ is set to zero in (21) we obtain

$$u = \frac{-tgo\ (x_1 + tgox_2 + tgo^2Z_1/2 + tgo^3Z_2/6)}{(1/S + tgo^2/3)} \quad (23)$$

which is equivalent to the result of Garber [4] for the case when the target acceleration and its time-derivative "jerk" are taken into account.

OTHER WAVEFORMS

While the present paper is concerned with demonstrating the similarity between DUC and other guidance approaches, certain distinguishing characteristics may be noted. The DUC design technique provides a straight forward way to deal with rather complex disturbance waveforms consisting of piecewise combinations of functions such as C_1t^2, C_2e^{-at}, C_3te^{-at} and $C_4\cos at$, where the C_i are not known a priori and may jump in value from time to time.

CONCLUSION

A closed-form guidance algorithm has been derived for the homing missile intercept problem using the Disturbance-Utilizing Control approach. The control gains are given as closed form functions of time-to-go to intercept. Special cases of the guidance algorithm are similar to those obtained by Cottrell [3] and Garber [4] . Other special cases of DUC are related to some well-known guidance laws in [5] . Such identifications are analogous to previous results [1] in which special cases of the disturbance cancellation mode may be identified with classical control forms such as integral control and disturbance feedforward control.

REFERENCES

1. Johnson, C. D., "Theory of Disturbance Accommodating Control", Control and Dynamic Systems Advances in Theory and Application, Vol. 10 Academic Press, New York, 1976.

2. Kelly, W. C., "Theory of Disturbance - Utilizing Control With Application to Missile Intercept Problems", U.S. Army Missile Command Report RG-80-11, 12 Dec 1979.

3. Cottrell, R. G., "Optimal Intercept Guidance for Short-Range Tactical Missiles," AIAA Journal, Vol. 9, No. 7, July 1971, pp. 1414, 1415.

4. Garber, V., "Optimal Intercept Laws for Accelerating Targets," AIAA Journal, Vol. 6, No. 11, Nov 1968, pp. 2196-2198.

5. Kelly, W. C., "Relations Between Disturbance-Utilizing Control and Certain Well Known Homing Missile Guidance Laws", Proceedings of Southeastcon 82, Destin, Florida, April 1982.

AD P010092

CONTROL OF A SPINNING PROJECTILE

N.A. Lehtomaki
J. E. Wall
Honeywell Systems and Research Center
2600 Ridgway Parkway
Minneapolis, Minnesota 55413

ABSTRACT

Powerful multivariable robust control synthesis techniques which have recently been devised [1] are applied to a tracking problem for a spinning projectile. A linearized lateral axis model of the projectile is used to design a reduced order LQG compensator to command angle of attack and sideslip using only fixed plane pitch rate and yaw rate measurements. Singular values of various transfer function matrices are used to explain the design procedure to obtain robust compensation that recovers the full state feedback guaranteed gain and phase margins.

INTRODUCTION

In this paper the design of a robust tracking feedback system for a spinning projectile is presented. A spinning projectile undergoing external forces behaves like a top in that it has two characteristic types of motion, namely, precession and a higher frequency epicyclic deviation about the precessional motion .termed nutation. Either of these motions may be unstable under certain conditions or at least underdamped. Therefore, without modifying the projectile geometry or weight, an active control system is necessary to steer the projectile and damp out the precession and nutation.

The precessional and nutational and other characteristics of the projectile along with control system objectives are discussed in the first section. The following section describes the design methodology which utilizes singular values of various transfer matrices and LQG loopshaping techniques.

Finally, the design for the projectile is described and illustrated with a number of frequency and time domain plots. The performance and stability robustness of the design to trim variations in sideslip angle and modelling uncertainty is discussed and multiloop stability margins are computed.

PROJECTILE CHARACTERISTICS AND CONTROL OBJECTIVES

The projectile under consideration weighs about 100. lbs and is spun at a rate of 70 to 180 rad/sec. It has thrusters located behind the center of gravity directed perpendicular to the spin axis which are capable of delivering about 100 lbs. of thrust. To manuever the projectile, the thrusters are fired to produce attack and sideslip angles (defined in aeroballistic non-spinning axes) allowing aerodynamic forces to be used in conjunction with the translational forces produced by the thrusters to steer the projectile. This requires a less powerful thruster than if the thrusters were located at the cg and did not pitch and yaw the projectile. With this arrangement, 50 lbs. of thrust yields about 5^{o} attack angle and 100 lbs. about 10^{o} (at the flight condition of interest). It is desired to be able to manuever the projectile to about $\pm$ 15^{o} in attack or sideslip angles to meet the guidance objectives. However, in some cases as the attack or sideslip angles approach 10^{o} the projectile becomes unstable in either precessional or nutational motion. Figure 1 depicts a typical transient response to a step in vertical thrust. The precession is indicated by the spiral motion and the nutation by the epicyclic deviation from the spiral motion at high frequency.

The basic control objective is to design a tracking system in which attack and sideslip angles may be commanded independently. The control system must sufficiently damp the precessional and nutational modes to provide well damped step responses with rise times of approximately 1/2 second. This performance must be maintained over the entire manuevering envelope. The most significant variation in this envelope occurs with sideslip angle. For sufficiently positive sideslip angles the nutational motion is unstable while for sufficiently negative sideslip angles the precessional motion is unstab... Thus for right and left turns the characteristic response is very different. The tracking system must handle these variations as well as unknown modelling errors that grow with increasing frequency. It will be assumed that these modelling errors will be small for frequencies less than 200 rad/sec (twice the nutational frequency). At 300 rad/sec the control

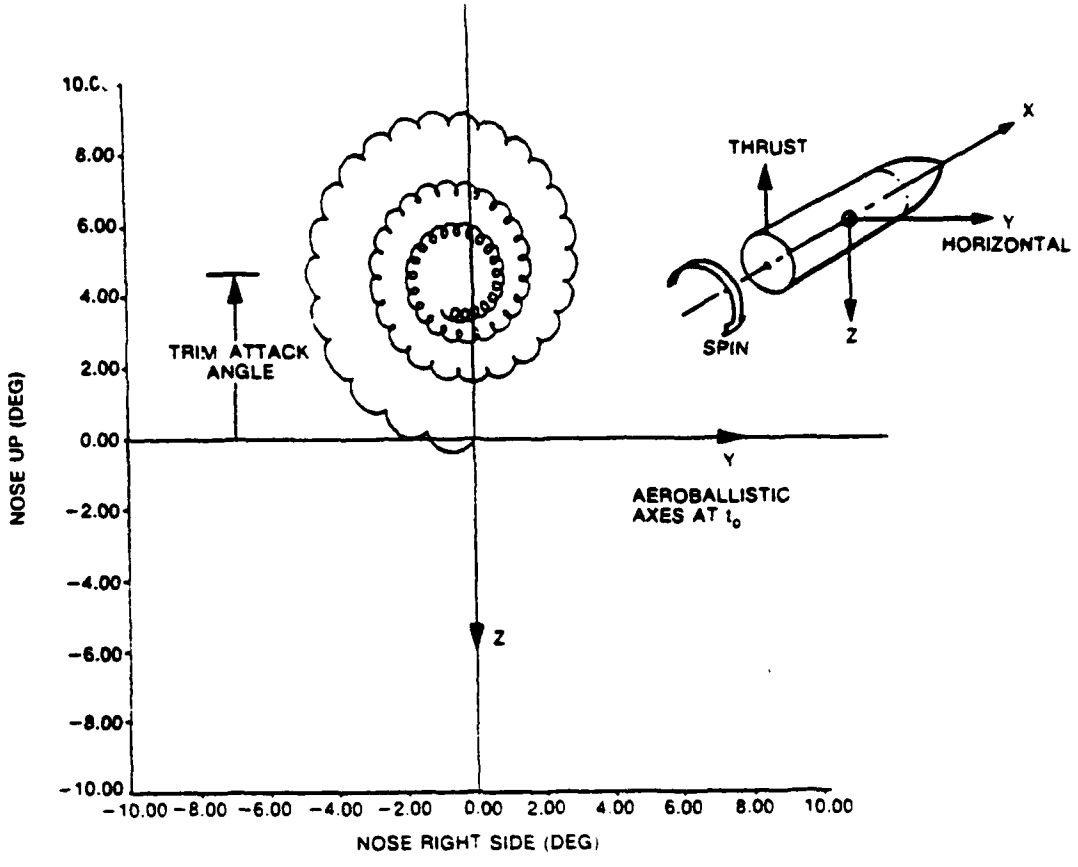


Figure 1: Typical Transient Response to Step in Vertical Thrust

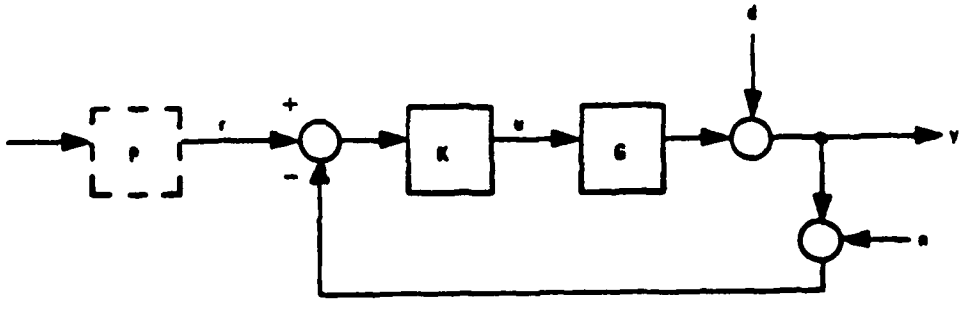


Figure 2: Standard Feedback Configuration

system loops should well rolled off. Below 200 rad/sec it will be assumed that the standard linear quadratic state feedback guaranteed gain and phase multiloop margins [7]-[10] (-6dB to $+\infty$ and $\pm$ 60° respectively) are adequate.

DESIGN METHODOLOGY

SINGULAR VALUE EXTENSIONS OF CLASSICAL CONTROL

Our objective will be to design a dynamic compensator for the generic feedback loop shown in Figure 2. We have a plant (G) with input vector (u), output vector (y), disturbance vector (d) as seen at the output, and measurement noise vector (n). Our compensator is designated as K. For convenience, K is shown in the generic forward path location from command vector (r), i.e., unity feedback. More general situations with K in the return path from y or with K split between the forward and return paths are equivalent to the forward-path location if appropriate pre-fliters (P) are used to shape the commands. Since P does not affect feedback properties, however, we will not deal with its design issues here.

The plant G is a real physical system. Hence, its detailed behavior must be expected to be quite complicated--nonlinear, infinite dimensional, time-varying, etc. Nevertheless, we will assume that G can be approximated by a finite dimensional, linear, time invariant (FDLTI) model with transfer function, G(s). The inevitable errors which this model makes will be represented by unstructured multiplicative perturbations of the form [2]

$$G'(s) = [I + L(s)]G(s). \qquad (1)$$

Here G'(s) is a possible "true" system, and L(s) is a FDLTI system with known bounded maximum gain, $\ell_m(s)$. Any L(s) which does not exceed this maximum gain generates another potential "true" system. Hence, equation (1) actually describes an entire family* of plants for which our compensator must be designed.

---

*For deep technical reasons discussed in [3], the number of unstable poles of G'(s) must be known for all members of this family. We will assume that this number is constant and equal to the numbers of unstable poles of G(s).

The design problem will be to provide good command-following (i.e., small errors, e=y-r, in response to commands), good disturbance rejection (i.e., small errors in response to disturbance excitation), and small responses to sensor noise, all subject to the constraints imposed by modelling errors in (1). Doyle [2] has shown that these various design objectives can be interpreted as conditions on the loop transfer function matrices GK(s), evaluated at real frequencies $s=j\omega$. We need large loop transfer matrices in the frequency range where commands and/or disturbances are large, small loop transfer matrices in the frequency range where modelling errors are large, and well-behaved crossover regions in between. "Well-behaved" crossovers are those which achieve nominal stability and maintain reasonably large return difference matrices, $I+GK(j\omega)$, and inverse return difference matrices, $I+[GK(j\omega)]^{-1}$. These frequency domain requirements of multivariable feedback design are summarized in Figure 3 [1].

Classical feedback designers will recognize that the frequency domain interpretations above are completely analogous to the classical single-input single-output design methodology [References 4, and 5 for example]. The only distinction, in fact, is that different measures are used to judge when transfer functions are "large" or "small." For scalar transfer functions, the absolute value serves as a single measure of size. The scalar gk is large if $|gk| << 1$, and it is small if $|gk| >> 1$. For multivariable systems, on the other hand, two singular values serve as measures of size. The matrix, GK, is large if its smallest singular value (smallest gain) is large, i.e., if $\underline{\sigma}[GK] >> 1$. It is small if its largest singular value (largest gain) is small, i.e., $\bar{\sigma}[GK] << 1$. More discussion of singular values and their interpretations are given in [1, 2, 6, 14]. The key point to note here is that singular values reduce the multivariable feedback design problem, in concept, to the familiar frequency domain loop-shaping problem of classical control.

The discussion to this point has focused, for convenience, on breaking the loop at the ouput y assuming it was the tracking variable of interest. This need not be the case. One could design the system to track prefiltered commands r that enter additively at the output of the compensator and the input to the plant. This simply requires the corresponding constraints involving GK become constraints involving KG. In fact, in the rest of this paper this latter approach is taken since the commanded variables are not the measured variables and the designer has the option to choose whether to design GK or KG and then use an appropriate prefilter to shape the commands that enter the feedback loop.

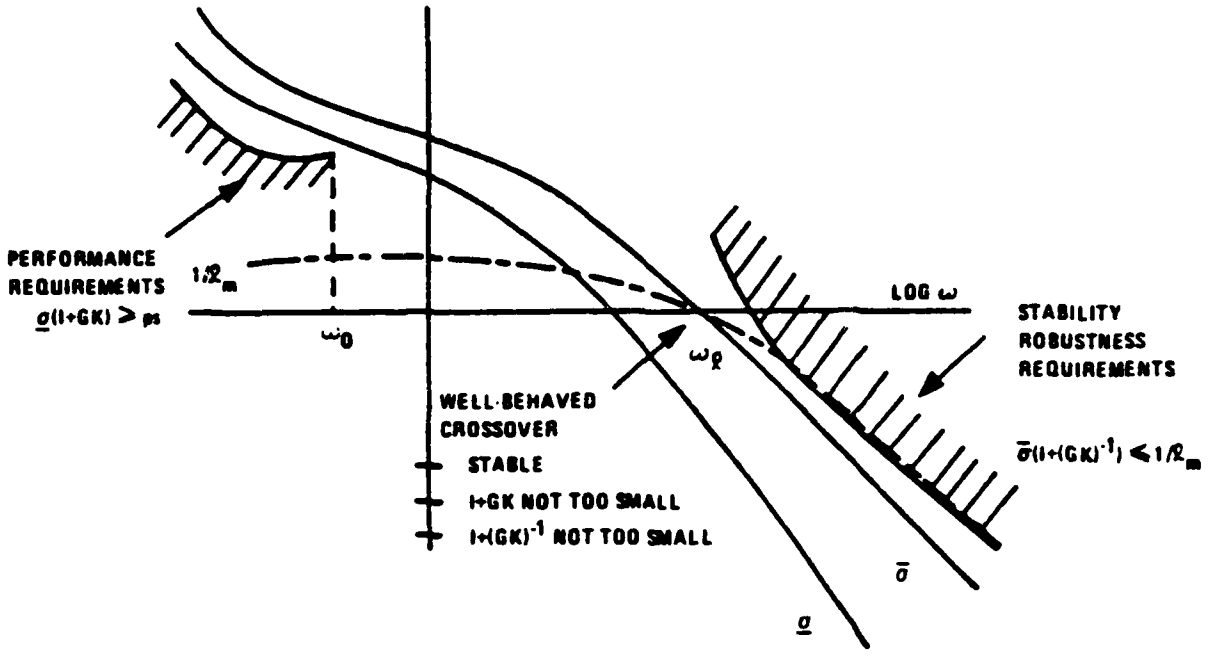


Figure 3: Frequency Domain Requirements
for Multivariable Feedback Systems

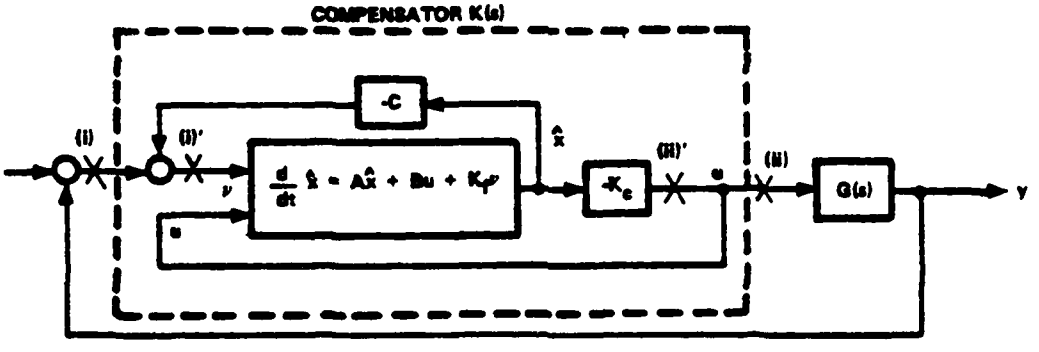


Figure 4: The LQG Feedback Loop

LQG LOOP-SHAPING

The LQG design methodology can be a remarkably effective tool for achieving the loop-shaping demanded by Figure 3. A detailed description of the manner in which LQG can be used to solve multivariable control problems is given by Doyle and Stein [1]. The properties of LQG loops which make effective for multivariable control design are briefly summarized below.

We will deal with the standard LQG controller configuration shown in Figure 4. This has the same structure as the generic control system introduced earlier in Figure 2. In this figure, the controller is treated as an ordinary finite dimensional linear compensator with a special internal structure consisting of a Kalman-Bucy Filter (KBF) cascaded with a linear-quadratic state feedback regulator (LQR). Standard symbols will be used to represent these elements; i.e., the state space realiziation of G(s) is composed of the matrix triple A,B,C, the control gains are denoted by matrix K_c, the filter gains by K_f, and the weighting and noise intensity matrices by Q, R, and Ξ, θ, respectively.

The loop transfer properties of interest are those corresponding to loop-breaking points (i) and (ii) of the figure. Two other loop-breaking points, (i)' and (ii)' also are shown in the figure. These are internal to the compensator and therefore have little direct significance. However. They have desirable loop transfer properties which can be related to the properties of points (i) and (ii). We will concentrate on points (ii) and (ii)' and present the theory for these points. We will return to points (i) and (i)' at the end of this section.

FACT 1. The loop transfer function obtained by breaking the LQG loop at point (ii)' is the LQR loop transfer function $K_c(sI-A)^{-1}B$.

FACT 2. The loop transfer function obtained by breaking the LQG loop at point (ii) is KG. It can be made to approach the LQR loop transfer function $K_c(sI-A)^{-1}B$ arbitrarily closely by designing the KBF according to a full-state loop transfer recovery procedure.*

---

* This requires the assumptions that G(s) is minimum phase and has at least as many outputs as inputs.

The significance of these two facts is that we can design LQG transfer functions on a full-state feedback basis and then approximate them adequately with a recovery procedure.

Full-State Loop Transfer Design

The intermediate full-state design step is worthwhile because LQR loops have good classical properties [7]-[10]. The basic result is that LQR loop transfer matrices satisfy the following return difference identity [8] for all frequencies ω:

$$T(s) = K_C(sI-A)^{-1}B \tag{2}$$

$$[I+T(j\omega)]^* R[I+T(j\omega)] = R + [H(j\omega I-A)^{-1}B]^* [H(j\omega I-A)^{-1}B] \tag{3}$$

where $H^TH=Q\geq 0$ is the state weighting matrix. When the control weighting matrix is a scalar times the identify, $R = \rho I$, the singular values of the transfer function T satisfy*

$$\sigma_i[T(j\omega)] \approx \sigma_i[H(sI-A)^{-1}B]/\sqrt{\rho} \tag{4}$$

whenever the right-hand-side is much greater than unity. This means we can choose ρ and H explicitly to satisfy the low frequency performance conditions shown in Figure 3**

The return difference identify (3) also guarantees that the LQR return difference always exceeds 1, i.e.,

$$\underline{\sigma}[I+T(j\omega)] \geq 1 \tag{5}$$

for all frequencies. This is a multivariable generalization of avoiding the -1 critical point on the Nyquist Diagram for

---

*Non-identity R matrices can be subsumed in B by letting $B' = BR^{1/2}$.

**It also may be necessary to append additional dynamics. For example, to achieve zero steady-state errors may require additional integrators in the plant. This is equivalent to "frequency-dependent" weighting.

scalar systems. It implies that LQR loops provide reasonable transition or "crossover" between the low and high frequency regions shown in Figure 3.

Finally, we note that at high frequencies the LQR loop approaches

$$\bar{\sigma}[T(j\omega)] \approx \frac{\bar{\sigma}[HB]}{\rho\omega} \qquad (6)$$

This shows how the high frequency roll-off characteristics are related to and H. This is a relatively slow attenuation rate and is the price the regulator pays for its excellent return difference properties. We recognize that no physical system can maintain indefinitely a $1/\omega$ characteristic. This is not a concern since T(s) is only a design function and will be approximated by the full-state loop transfer recovery procedure.

Full-State Loop Transfer Recovery

As mentioned earlier, the full-state loop transfer function designed above for point (ii)' can be recovered at point (ii) by a modified KBF design procedure.* Special noise statistics are used for the KBF design. The driving noise intensity matrix is modified as $\Xi = qBB^T$ where Ξ is the nominal noise intensity matrix and q is a scalar parameter. Then as q becomes large, we know that the filter gain K_f behaves in such a way to yield loop transfer recovery for point (ii). Mathematically [11],

$$K(s)G(s) \rightarrow K_c(sI-A)^{-1}B \text{ as } q \rightarrow \infty \qquad (7)$$

Based on the above summary of properties of LQG controllers, the following simple loop-shaping procedure suggests itself.

---

*The required theoretical assumptions are that the plant have at least as many outputs as inputs and be minimum phase. In practice, the recovery procedure is effective as long as G(s) has no right-half-plane zeros below the crossover frequency. The limitations on the achievable performance of feedback systems because of non-minimum zeros is discussed in Reference [12].

Step 1. Design a LQR with a ρ and H selected such that the loop transfer function T(s) meets performance and stability robustness requirements (Figure 3).

Step 2. Design a sequence of KBF's with modified driving noise intensity matrix and the parameter q allowed to take on consecutively larger values.

Step 3. Select an element of the resulting sequence of transfer fucntions.

$$K(s)G(s) \rightarrow T(s), \quad q \rightarrow \infty$$

which adequately approximates the desired function over the frequency range of interest.

All design objectives including nominal stability are then assured. Our conclusion is that LQG represents a powerful, general tool for obtaining multivariable control designs.

We have just discussed designing a full-state regulator and then recovering the full-state properties with a Kalman-Bucy Filter. We followed this approach because this is the usual sequence one considers for LQG design. We note that the procedure also applies to loop-breaking point (i) in Figure 4. For this point, however, the role of the filter and the controller are reversed. We begin by designing a KBF whose loop transfer function $C(sI-A)^{-1}K_f$ (at point (i)') has good loop properties. Then we design a sequence of LQR's which serve to recover this function at point (i) [1]. The equations for this alternate procedure are mathematical "duals" of the ones given above. The subtle differences between the two procedures are discussed in Reference [12].

PROJECTILE CONTROL SYSTEM DESIGN

LINEARIZED MODELS

A four state linearized design model of lateral axis of the projectile was calculated at the equilibrium condition for zero total angle of attack, .97 mach, 60° descent angle and a spin rate of 166 rad/sec. For evaluation purposes two other linearized models were computed at the same equilibrium condition except that the equilibrium value of the sideslip

angle, β_e, was changed from zero to $\pm$ 15°. For these two models, however, the aerodynamics were linearized about zero total angle of attack.

All of the models are of the form

$$\dot{x} = Ax + Bu \tag{8}$$
$$y = Cx \tag{9}$$
$$z = Hx \tag{10}$$

where

$$x^T = [\alpha, \beta, q, r] = \text{states} \tag{11}$$

$$u^T = [F_{yc}, F_{zc}] = \text{controls} \tag{12}$$

$$y^T = [q, r] = \text{measurements} \tag{13}$$

$$z^T = [\alpha, \beta] = \text{controlled variables} \tag{14}$$

with the x, u, y, z variables representing deviations from their equilibrium values. Here α and β are the angles of attack and sideslip (in radians), q and r are pitch rate and yaw rate (in rad/sec) and F_{yc} and F_{zc} are the y and z axis control forces (in lbs.). It is assumed that α and β are not measured but that q and r are the only measurements available. The matrices B, C and H do not change with the value of β_e with C and H defined by (13) and (14) and B given by

$$B = \begin{bmatrix} 0 & 3.921E\text{-}4 \\ 3.921E\text{-}4 & 0 \\ 0 & .0897 \\ -.8097 & 0 \end{bmatrix} \tag{15}$$

The value of the design A matrix for $\beta_e = 0$ is given by

$$A = \begin{bmatrix} -.2160 & 0 & 1.0 & 0 \\ 0 & -.2160 & 0 & -1.0 \\ 797.0 & -19.19 & -.2850 & -112.4 \\ -19.19 & -797.0 & 112.4 & -.2850 \end{bmatrix} \tag{16}$$

For $\beta_e = 15^o$ A is as in (16) except that $a_{12}=a_{21}= .1322$, $a_{34} = a_{43}= -112.7$ and $a_{14}=-.2197$. For $\beta_e=-15^o$ A is as in (16) except that $a_{12}=a_{21}=-.1322$, $a_{34}=a_{43}= -112.1$ and $a_{14}=.2197$. The open loop eigenvalues for $\beta_e=0$, -15^o and $+15^o$are given respectively by $\{-.0135 \pm j\ 7.605, -.4879 \pm j\ 104.8\}$, $\{.8917 \pm j\ 7.545, -1.393 \pm j\ 104.5\}$ and $\{-.9106 \pm j\ 7.551, .4096 \pm j\ 105.1\}$. The precessional mode corresponds to the eigenvalue with the smaller imaginary part and the nutational mode to the other. In all cases the models are minimum phase. Notice that the design model is stable but the other two evaluation models are unstable.

FEEDBACK DESIGN

This design will proceed in two steps. First a state feedback tracking system is designed with a high loop gain at low frequency. Next, since only pitch and yaw rates (q and r) are assumed to be measurable quantities, a Kalman filter must be used to construct a state estimate to be fed back. However, inserting the Kalman filter in the feedback loop can destroy the stability margins and tracking performance (that the state feedback design possessed) by changing the loop transfer shape. Therefore, the Kalman filter design is not designed to provide "optimal" estimates of the states but to recover the original loop transfer shape of the state feed-back design that in turn provides enhanced stability and good tracking performance.

As a first step in the state feedback design the precessional and nutational modes are further damped. This provides insensitivity to the variation of the model with β_e. The first part state feedback design is accomplished with linear quadratic regulator using a method proposed by O. Solheim [13]. This method allows one to move poles independently to semicircles in the left half plane of any desired radius larger than the radius of the semicircle passing through their initial location. Without this prestabilization step the designed feedback system becomes unstable when β_e varies between $\pm 15^o$.

The next step is to use linear quadratic proportional plus integral feedback around the prestablized system. This amounts to simply adding the state feedback gains of the two LQ designs to obtain the overall state feedback gain. The necessity of integral control is obvious from Figure 5.

Figure 5 shows the open loop transfer matrix singular values where the outputs are q and r. Obviously, the gain at low frequency must be significantly raised by the compensation for good tracking in the face of model variations. To do this, integrators are appended to the states α and β and their outputs used for feedback. This is a well known procedure to provide infinite loop gain at $\omega=0$ for zero steady state tracking error.

To achieve the desired speed of response (0.5 sec rise time) the desired crossover frequency is approximately 10 rad/sec. Figure 6 shows the resulting loop transfer singular values from a regulator design that weights the integrals of α and β. The recovery of this loop transfer is shown in Figure 7, 8 and 9 where a sixth order Kalman filter has been inserted in the feedback loop to estimate the state that now includes the integrals of α and β. The process noise intensity matrix Ξ is chosen as qBB^T and successively larger values of q are used until with $q = 10^6$ (Figure 9), the recovery of the state feedback loop transfer is almost perfect. In the filter design the integrators are stabilized slightly to ensure the detectability condition required for solution of the filter Riccati equation.

The cascade of the state feedback gain and the Kalman filter gives a sixth order compensator with inputs q, r, α_c and β_c where α_c and β_c are the commanded values of α and β. The singular values of the compensator are shown in Figure 10. This sixth order compensator can be reduced to fourth order by modal residualization. The resulting compensator singular values are shown in Figure 11. Modal residualization simply replaces the fast system modes by their steady state contribution and retains the slow system modes.

Loop transfer singular values using the reduced order compensator are shown in Figure 12 which when compared to the state feedback case are almost identical. Figures 13 and 14 give the singular values of the return differences and closed loop transfers at the input to the projectile. These plots indicate that the feedback system has at least -13 dB to + ∞ gain margin and $\pm$ 60 degree phase margin simulatneously in both loops at the F_{yc} and F_{zc} inputs of the projectile. Recall, however, that the bandwidth limitation limits the realistic upward gain margin.

The reduced order LQG controller has the form

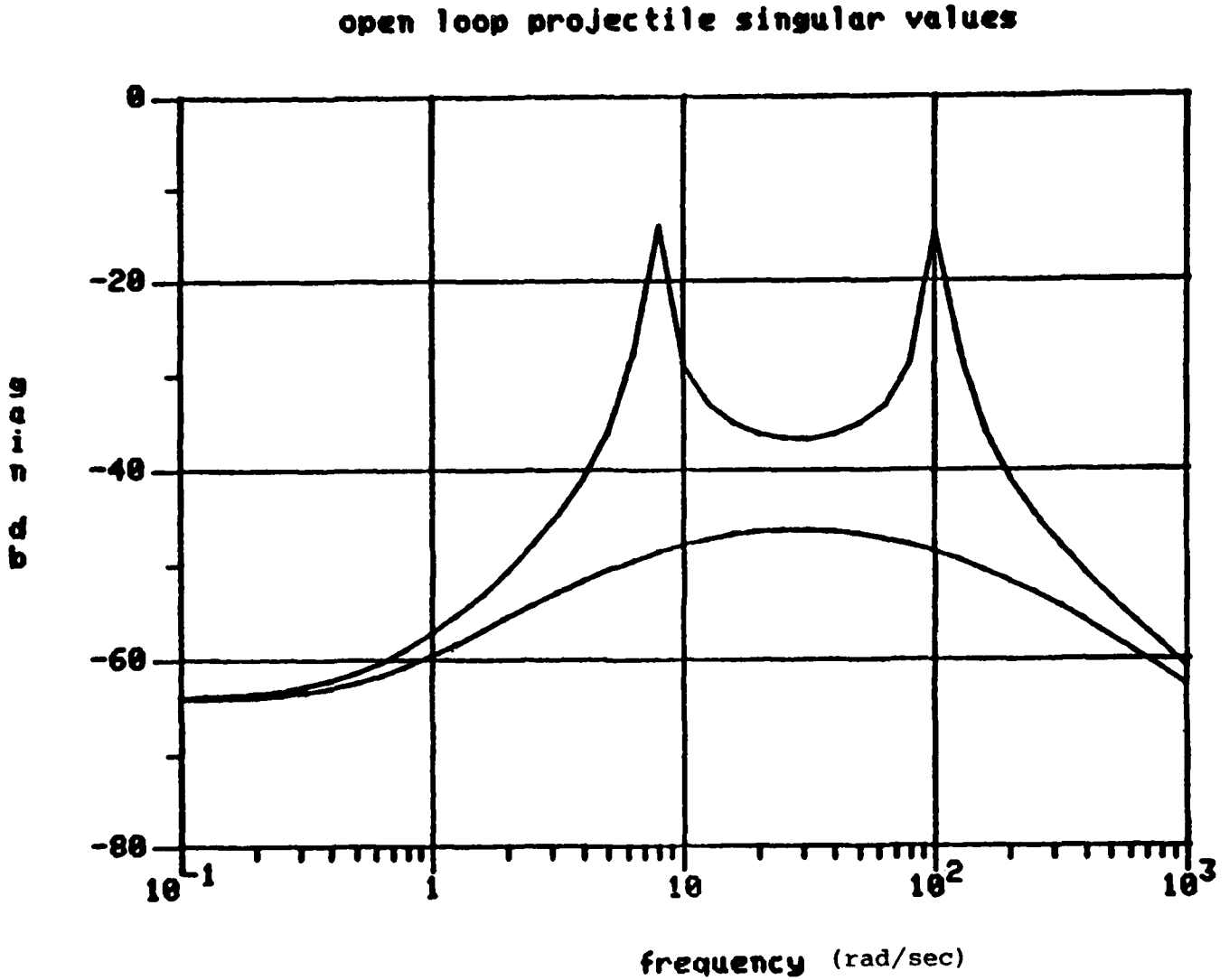


Figure 5: Singular Values of $C(Is-A)^{-1}B$

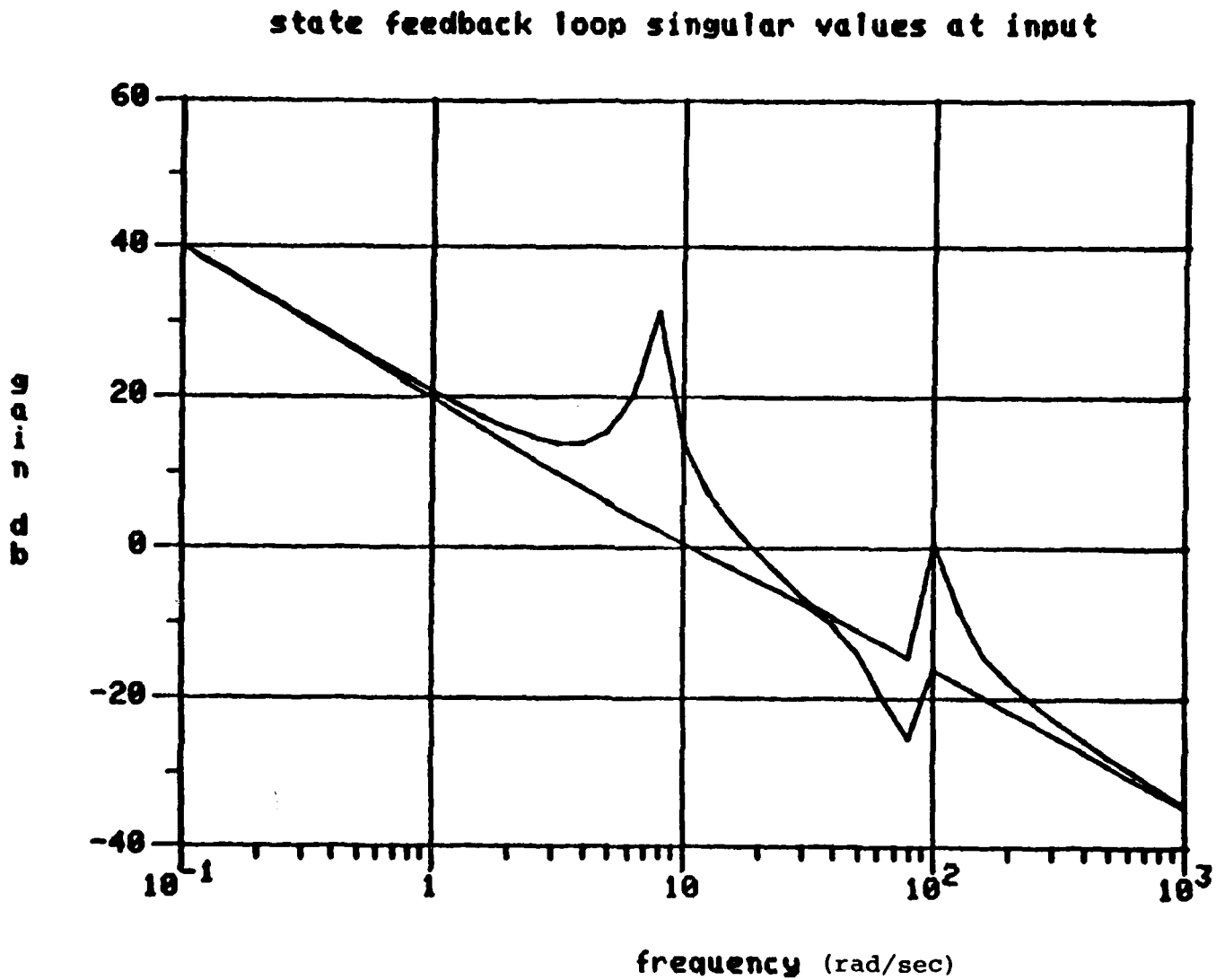


Figure 6: Singular Values of $K_c(Is-A)^{-1}B$

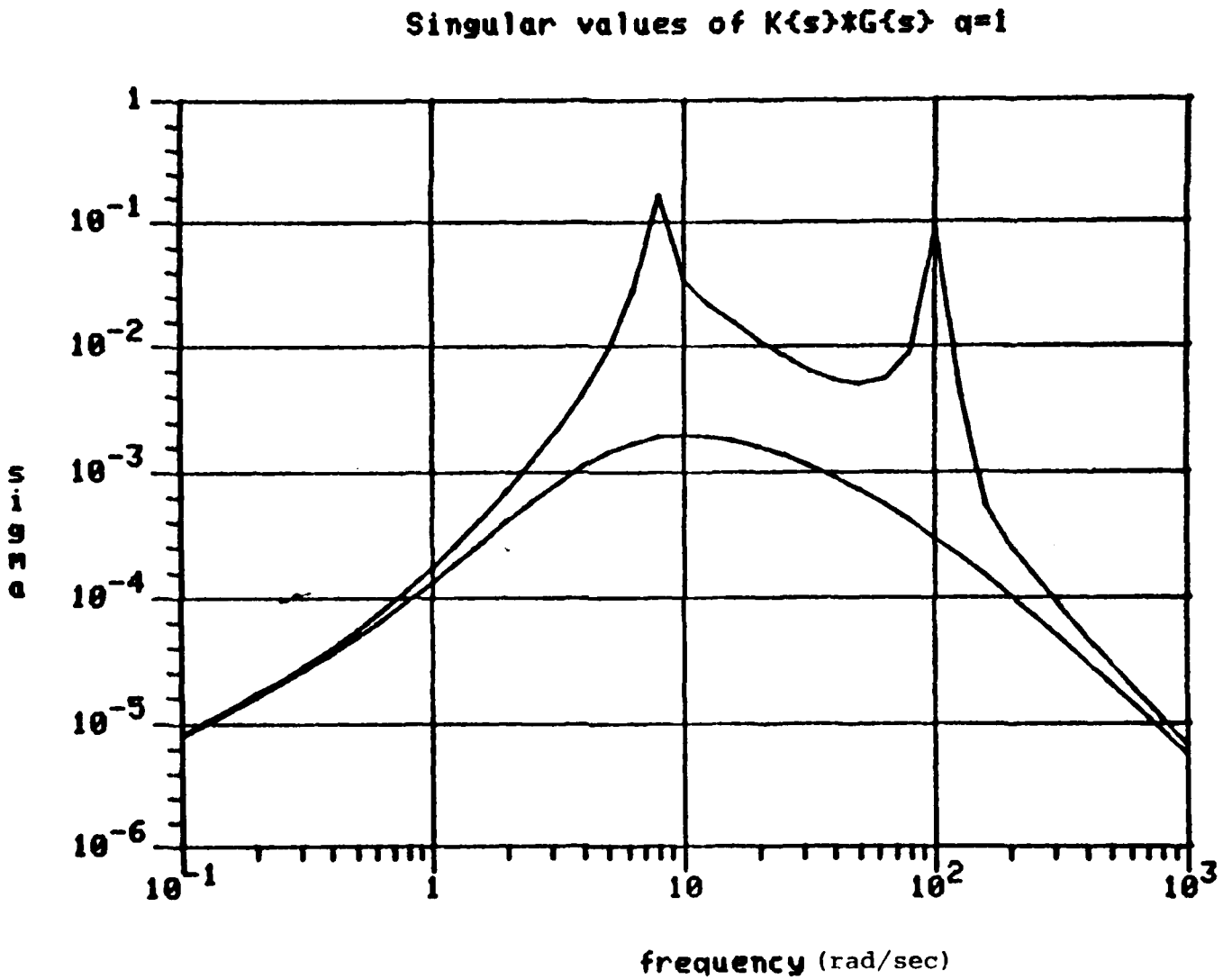


Figure 7: Singular Values of Loop Transfer

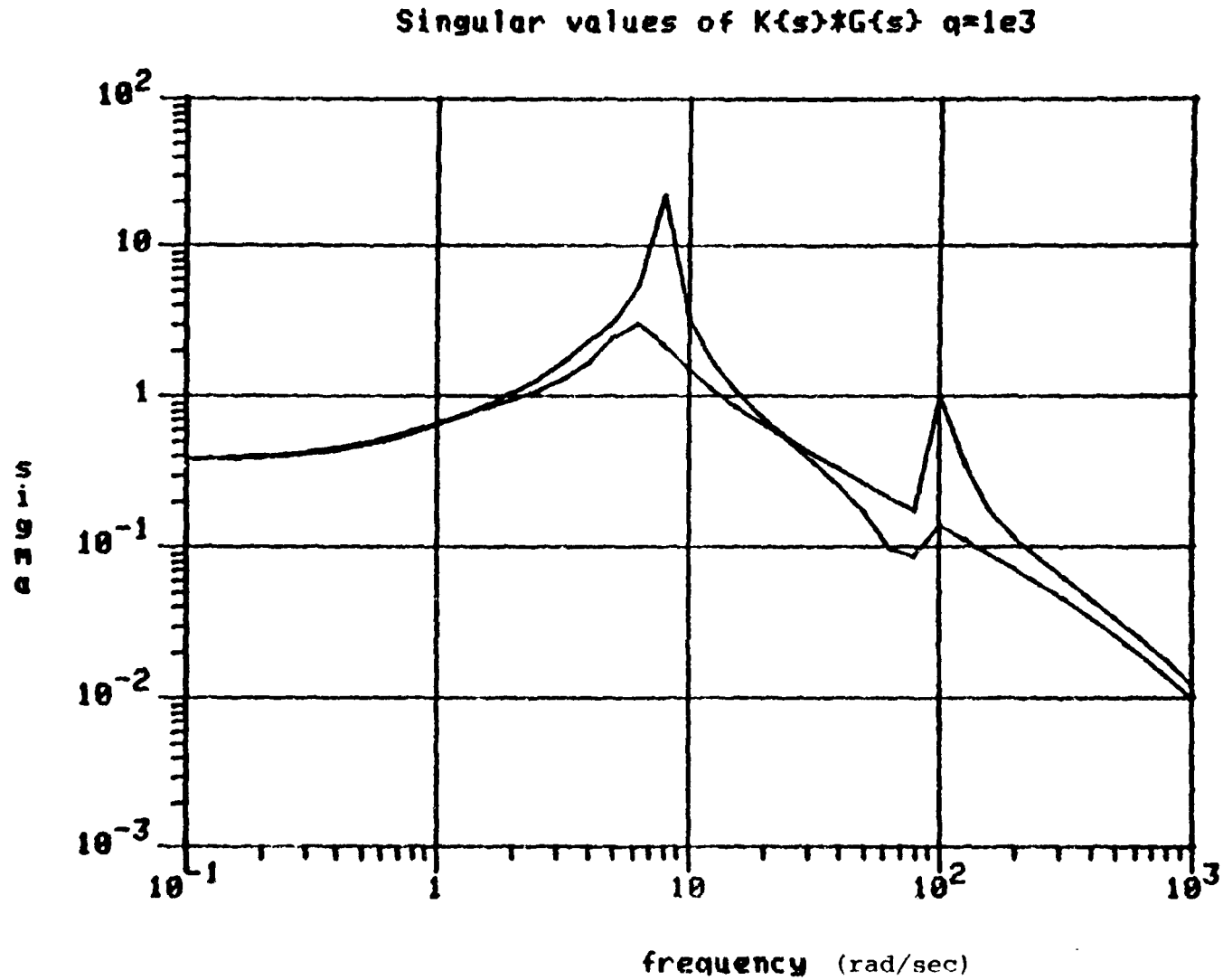


Figure 8: Singular Values of Loop Transfer

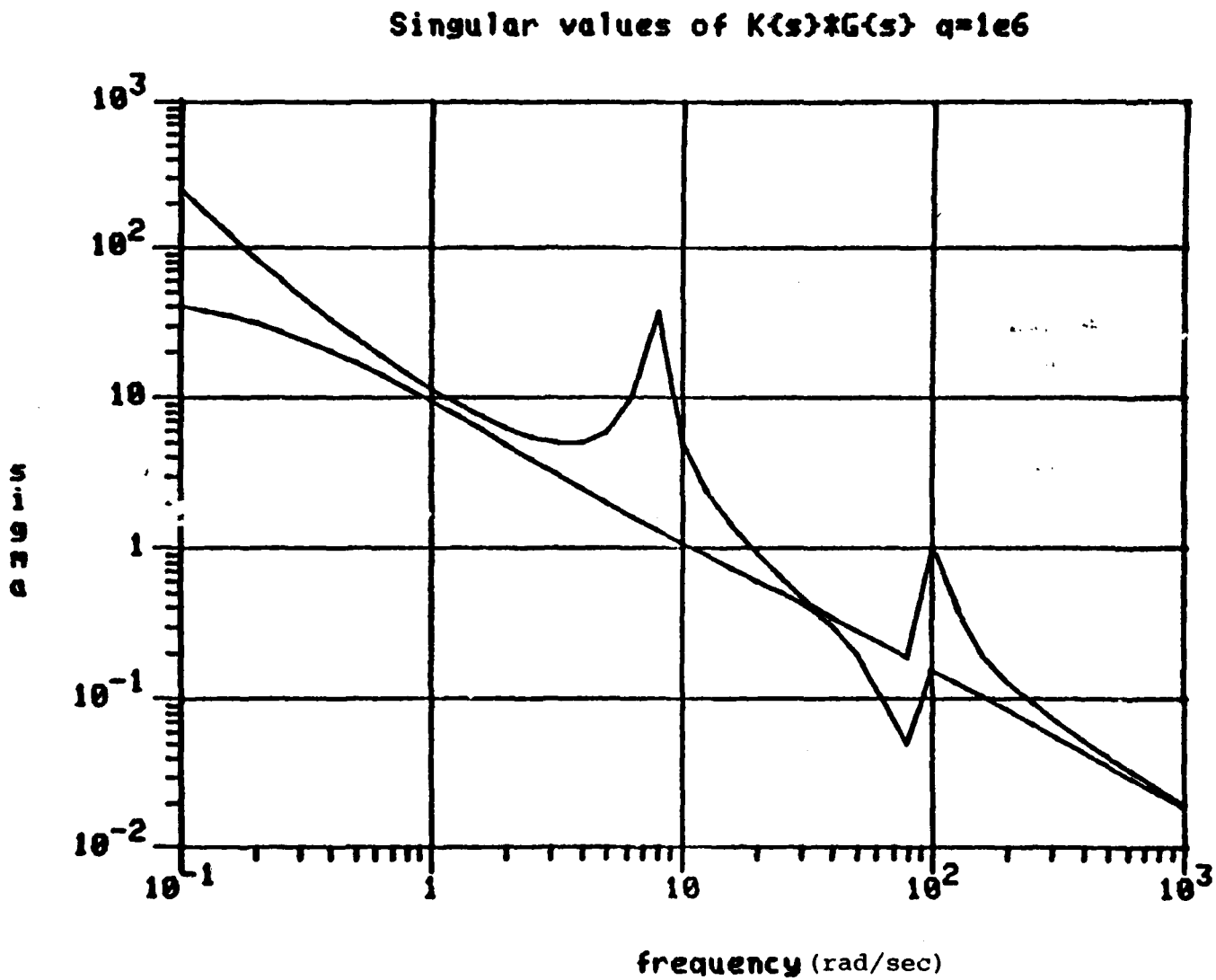


Figure 9: Singular Values of Loop Transfer

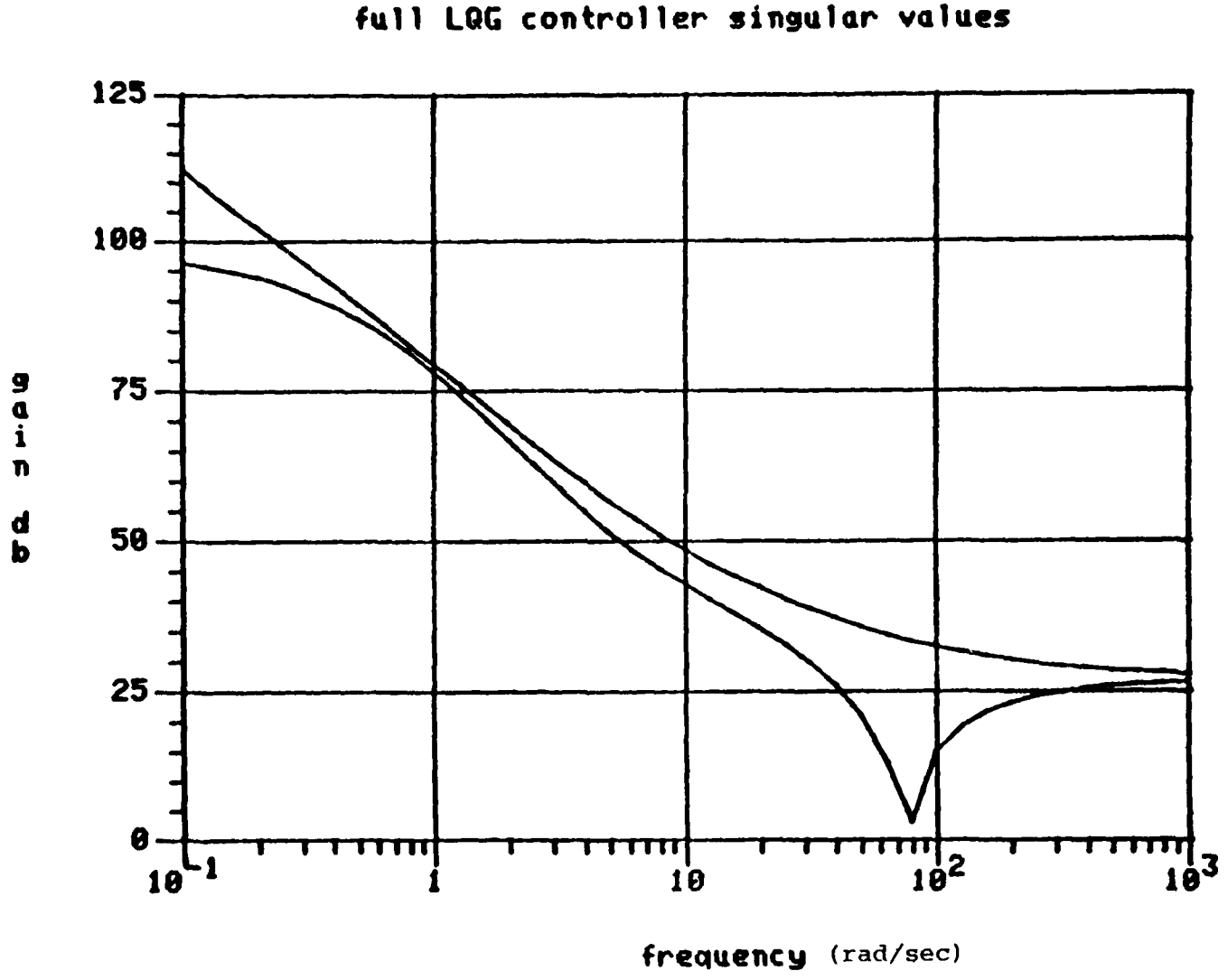


Figure 10: Singular Values of $K_c(Is-A+BK_c+K_fC)^{-1}K_f$

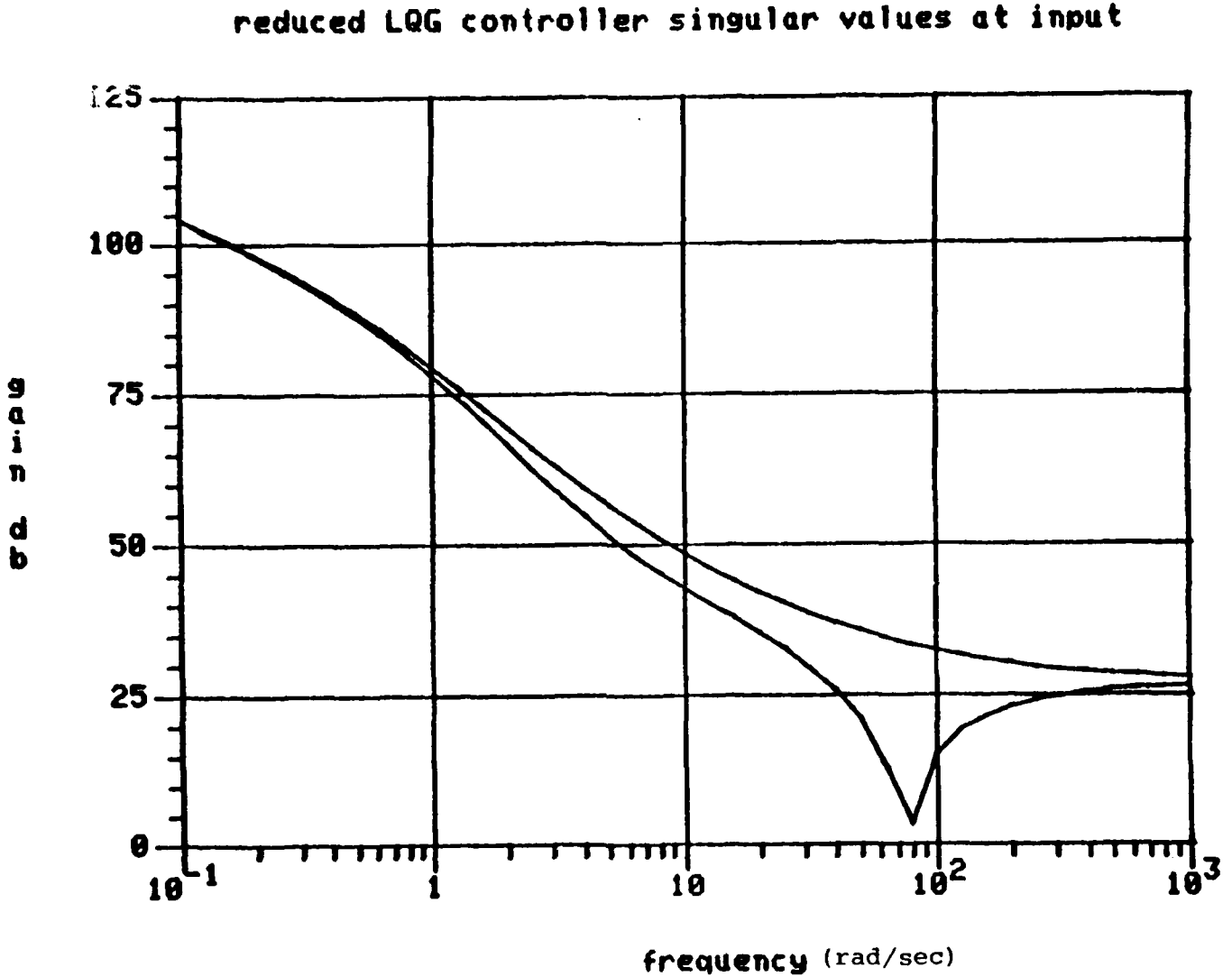


Figure 11: Singular Values of Reduced Order Controller

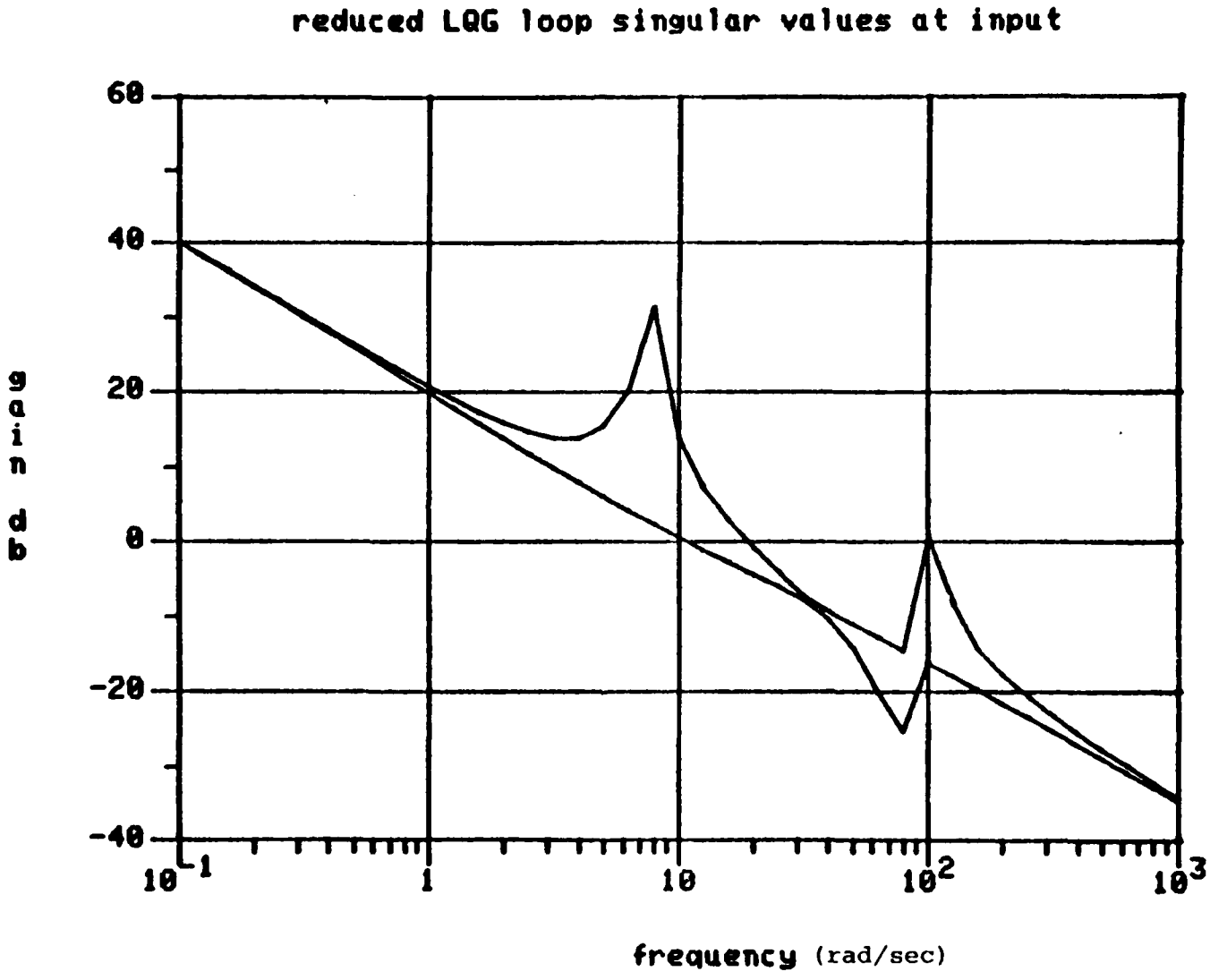


Figure 12: Singular Values of Loop Transfer with Reduced Order Controller

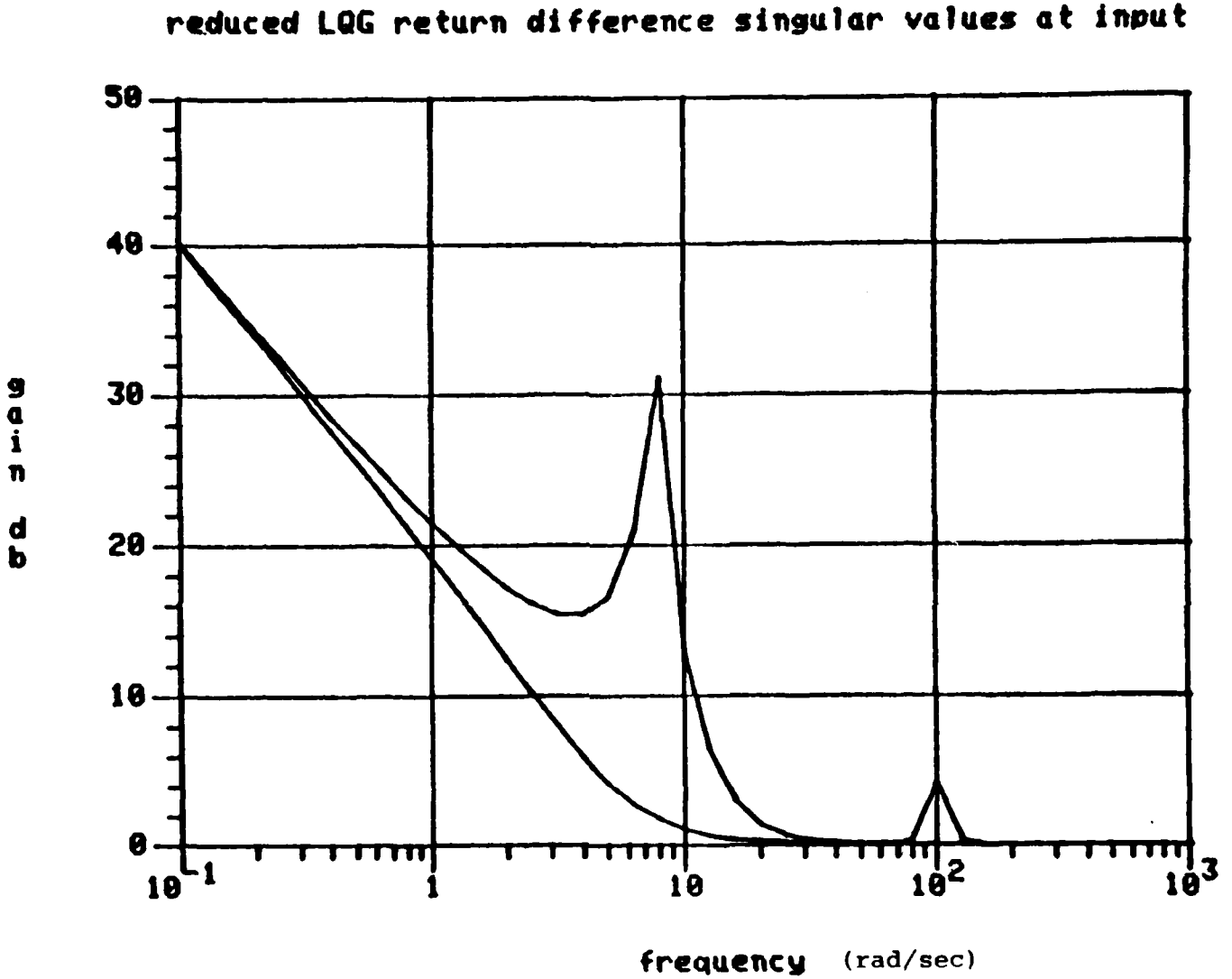


Figure 13: Singular Values of (I+KG)
KG = Loop Transfer

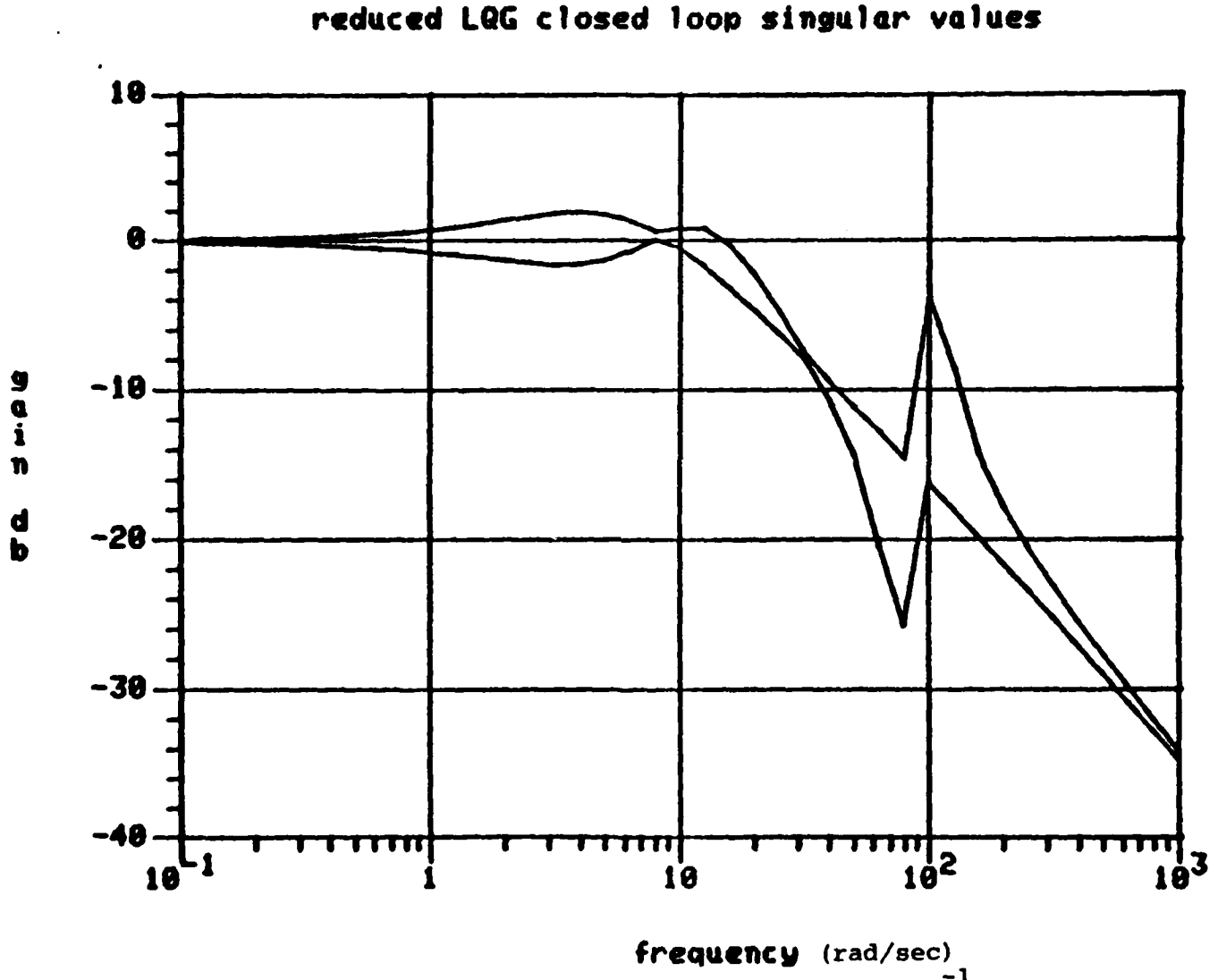


Figure 14: Singular Values of $KG(I+KG)^{-1}$
KG = Loop Transfer

$$\dot{x}_l = A_l x_l + B_l \begin{bmatrix} y \\ z_c \end{bmatrix} \tag{17}$$

$$-u = C_l x_l + D_l \begin{bmatrix} y \\ z_c \end{bmatrix} \tag{18}$$

where $z_c^T = [\alpha_c, \beta_c]$, the commanded value of z. The matrices A_l, B_l, C_l and D_l are given by

Number of rows = 4
Number of columns = 4

$$A_l = \begin{bmatrix} -1.0011E-02 & 2.4916E-05 & -5.8538E-08 & 8.7288E-09 \\ -2.4850E-05 & -1.0011E-02 & -7.1433E-09 & 1.0219E-10 \\ 4.0193E-09 & 2.6958E-08 & -6.0194E-01 & 9.3037E-03 \\ 1.0712E-08 & 7.1853E-08 & -9.3038E-03 & -6.0194E-01 \end{bmatrix} \tag{19}$$

Number of rows = 4
Number of columns = 4

$$B_l = \begin{bmatrix} 2.3581E+00 & 4.0751E-01 & -1.4020E+00 & 1.8685E-01 \\ -4.0708E-01 & 2.3577E+00 & 1.8660E-01 & 1.4018E+00 \\ 5.1940E-01 & 2.7309E+00 & -3.7349E-05 & 9.4636E-06 \\ 2.7309E+00 & -5.1941E-01 & -9.4322E-06 & -3.7336E-05 \end{bmatrix} \tag{20}$$

Number of rows = 2
Number of columns = 4

$$C_l = \begin{bmatrix} 6.8899E+03 & 1.5886E+03 & -3.3038E+03 & -4.4206E+03 \\ -1.5894E+03 & 6.8904E+03 & -4.4206E+03 & 3.3038E+03 \end{bmatrix} \tag{21}$$

Number of rows = 2
Number of columns = 4

$$D_l = \begin{bmatrix} -3.3271E-07 & -2.3376E-01 & -2.7031E-07 & 1.0138E-07 \\ 2.3376E-01 & -3.3271E-07 & 1.0138E-07 & 2.7031E-07 \end{bmatrix} \tag{22}$$

DESIGN EVALUATION

In order to evaluate the control system performance transient responses to step commands in α and β, bode plots of the transfer functions from z_c to z and closed loop eigenvalues were calculated for the design model and the two evaluation models corresponding to $\beta_e = \pm 15^o$. Only some of the representative plots are given here.

The closed loop feedback system was stable with all three models. With the design model the closed-loop precessional eigenvalues are $-7.81 \pm j10.2$ and the closed-loop nutational eigenvalues are $-6.18 \pm j105$. With the other two models the real parts of the precession or nutation closed-loop eigenvalues is less than -5 with the imaginary parts (frequency) changing only slightly.

The transient responses given here are for the open loop and closed-loop systems using the design model with $\beta_e = 0$ (time is in seconds). A .1 rad step command in α is given to both systems. Figures 15 to 18 show the α, β, q, and r underdamped responses respectively of the open loop system which must eventually reach $\alpha = .1$ and $\beta = 0$. The required control forces to maintain this equilibrium are $F_{yc} = 5.97$ lbs. and $F_{zc} = -98.1$ lbs. Figures 19 to 24 give the α, β, q, r, F_{yc} and F_{zc} responses respectively of the closed loop system to a .1 rad α command. Figure 19 shows a 1/2 second rise time step response in α and Figure 20 shows that β is bounded by approximately .01 rad. Figures 21 and 22 show that the q and r responses are much better damped than in Figures 17 and 18 of the open loop responses. Figures 23 and 24 show smooth fairly low bandwith control actuation thruster commands of less than 100 lbs. A .1 rad = 5.7^o step command thus generates a 100 lbs. of control thrust which is much higher than predicted by the nonlinear analysis due to linearizing the aerodynamics at $\alpha_e = \beta_e = 0$. Transient plots with β commands yeild similar results.

Transient plots with $\beta_e = \pm 15^o$ models give similar step responses in the .1 rad α command but the cross coupling between α and β is a little more pronounced but in all cases $|\beta| < .011$ rad. The situation for .1 rad step commands in β is somewhat worse when $\beta_e = \pm 15^o$ where β has about a 5% overshoot and $|\alpha|$ is much larger and the control forces are somewhat larger.

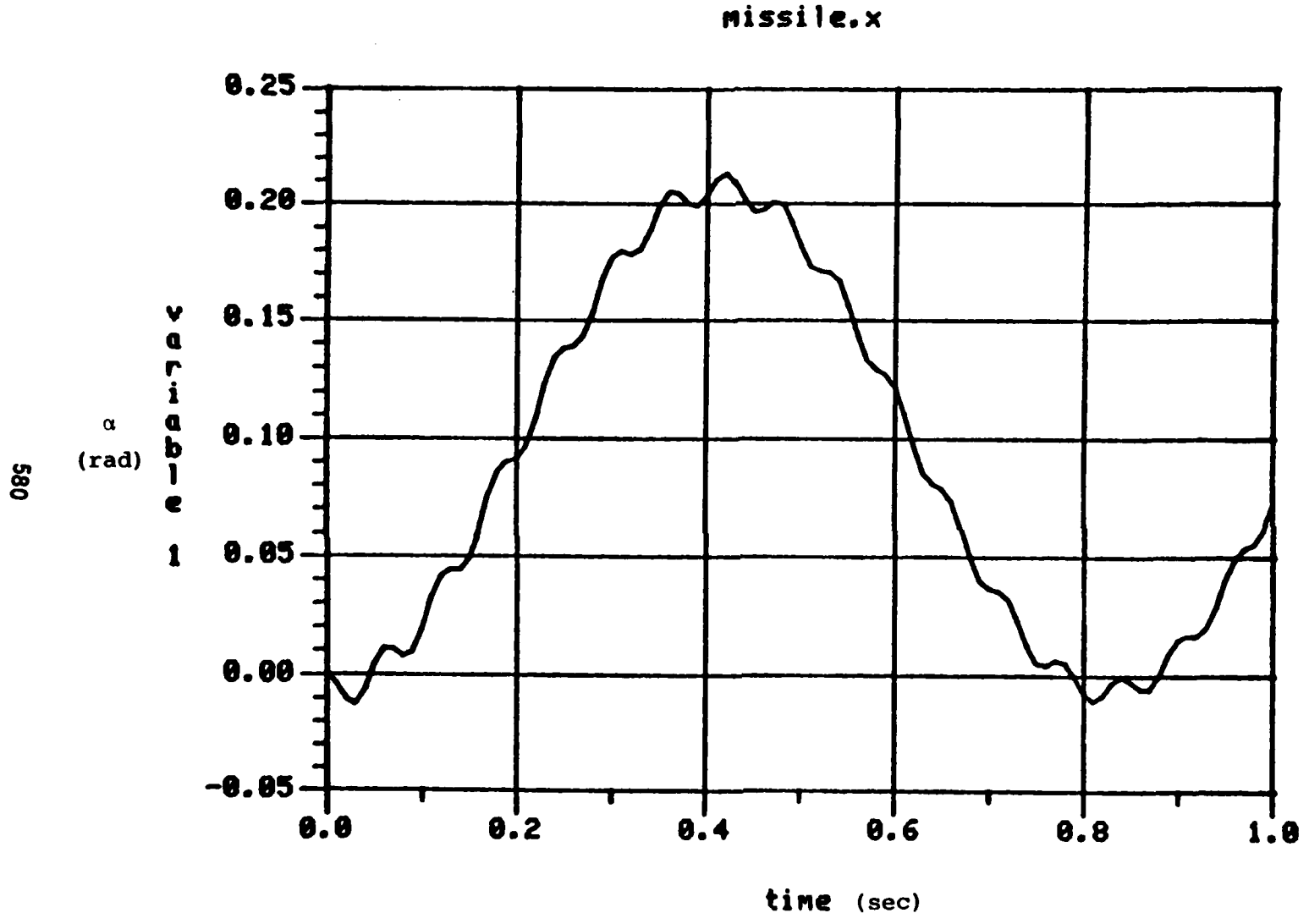


Figure 15: Open Loop Response to α_c = .1 step

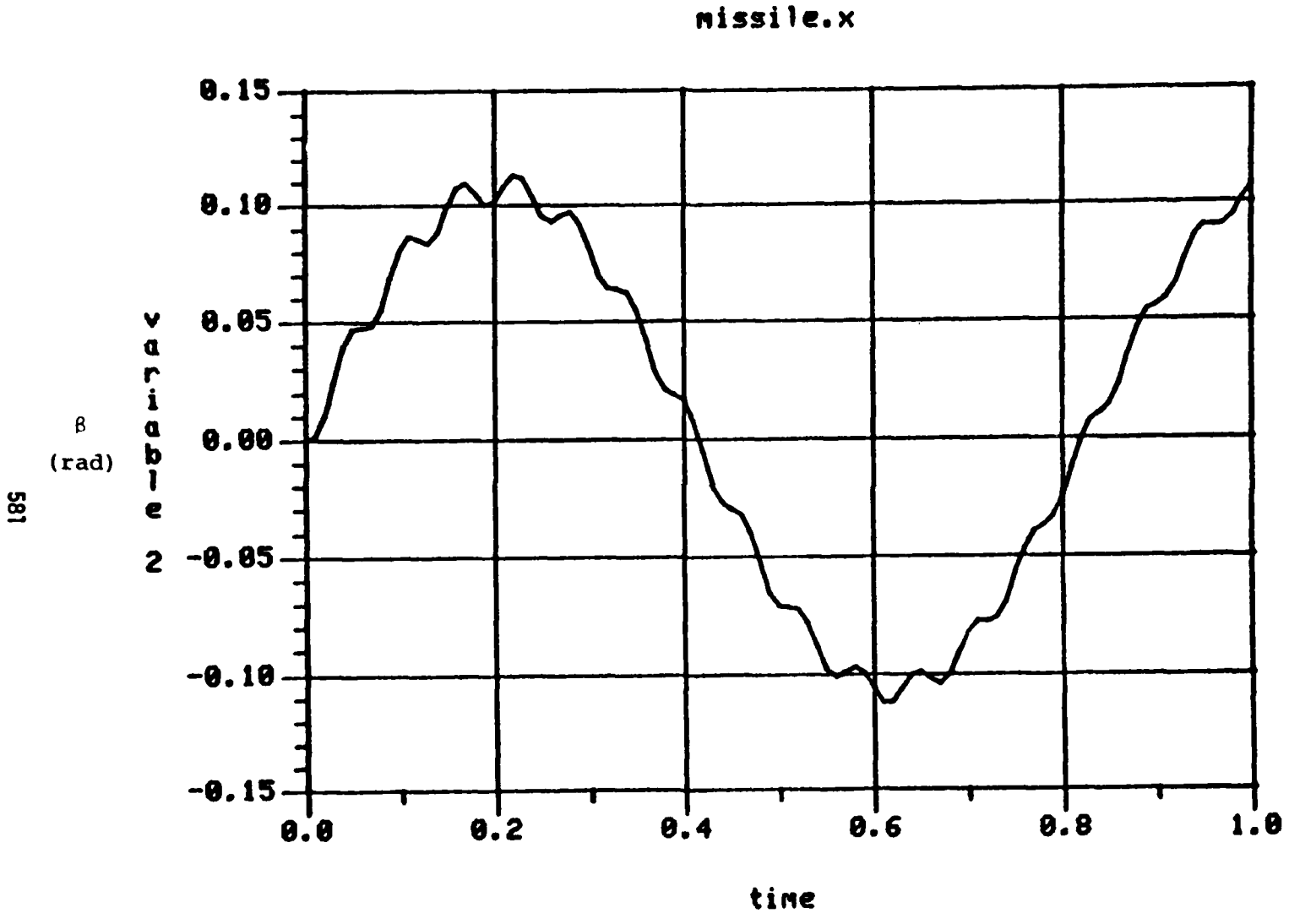


Figure 16: Open Loop Response to α_c = .1 step

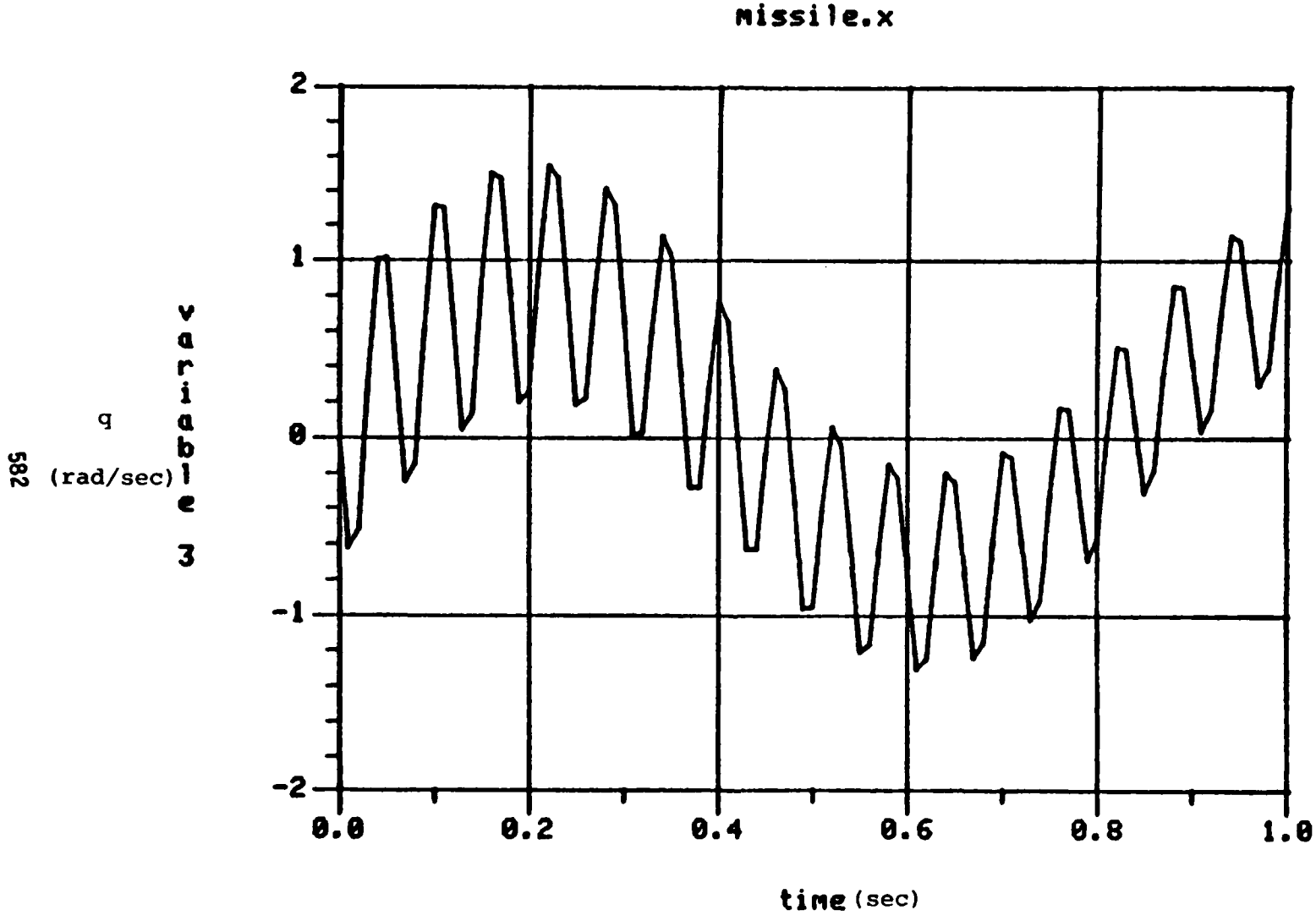


Figure 17: Open Loop Response to α_c = .1 step

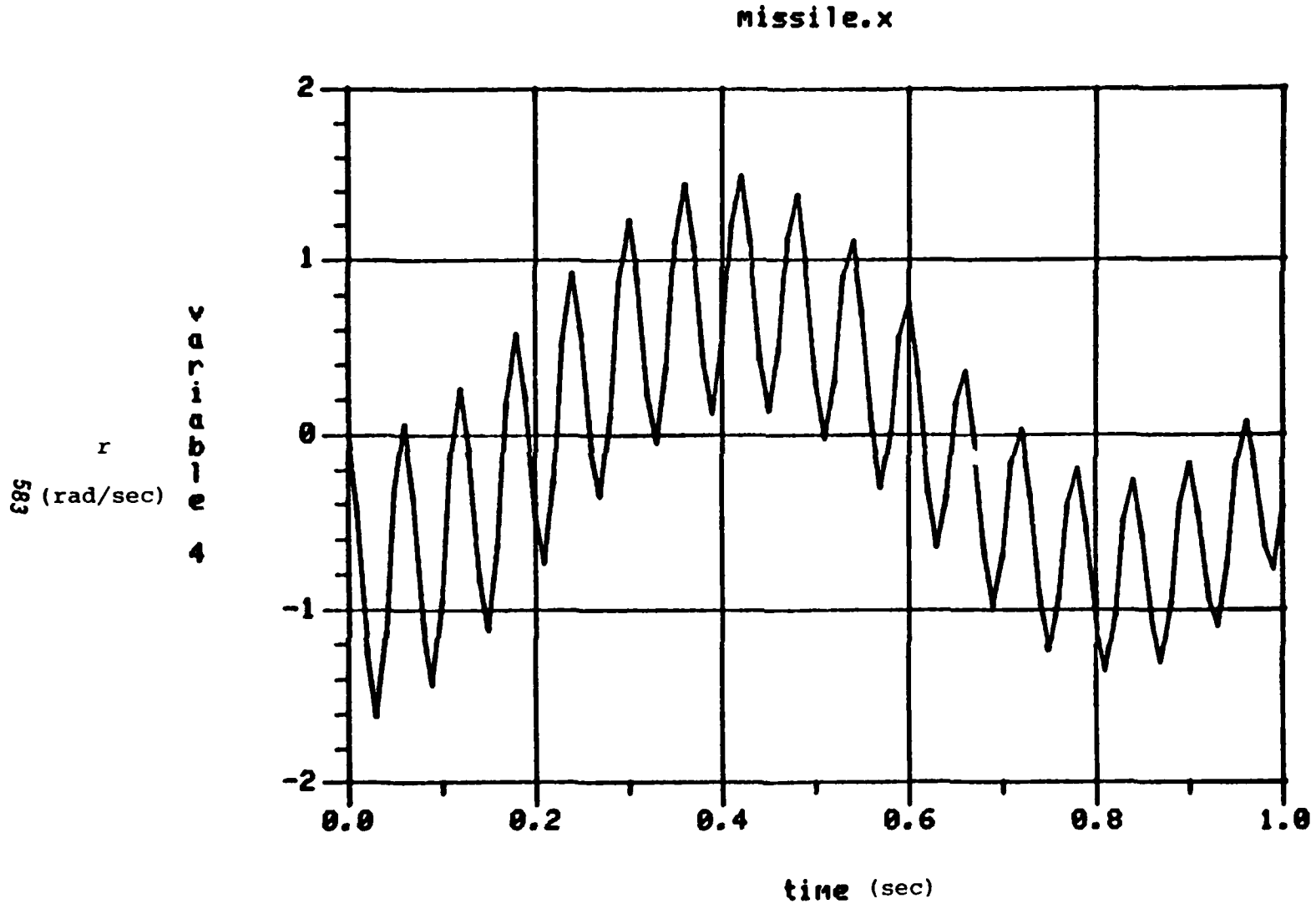


Figure 18: Open Loop Response to α_c = .1 step

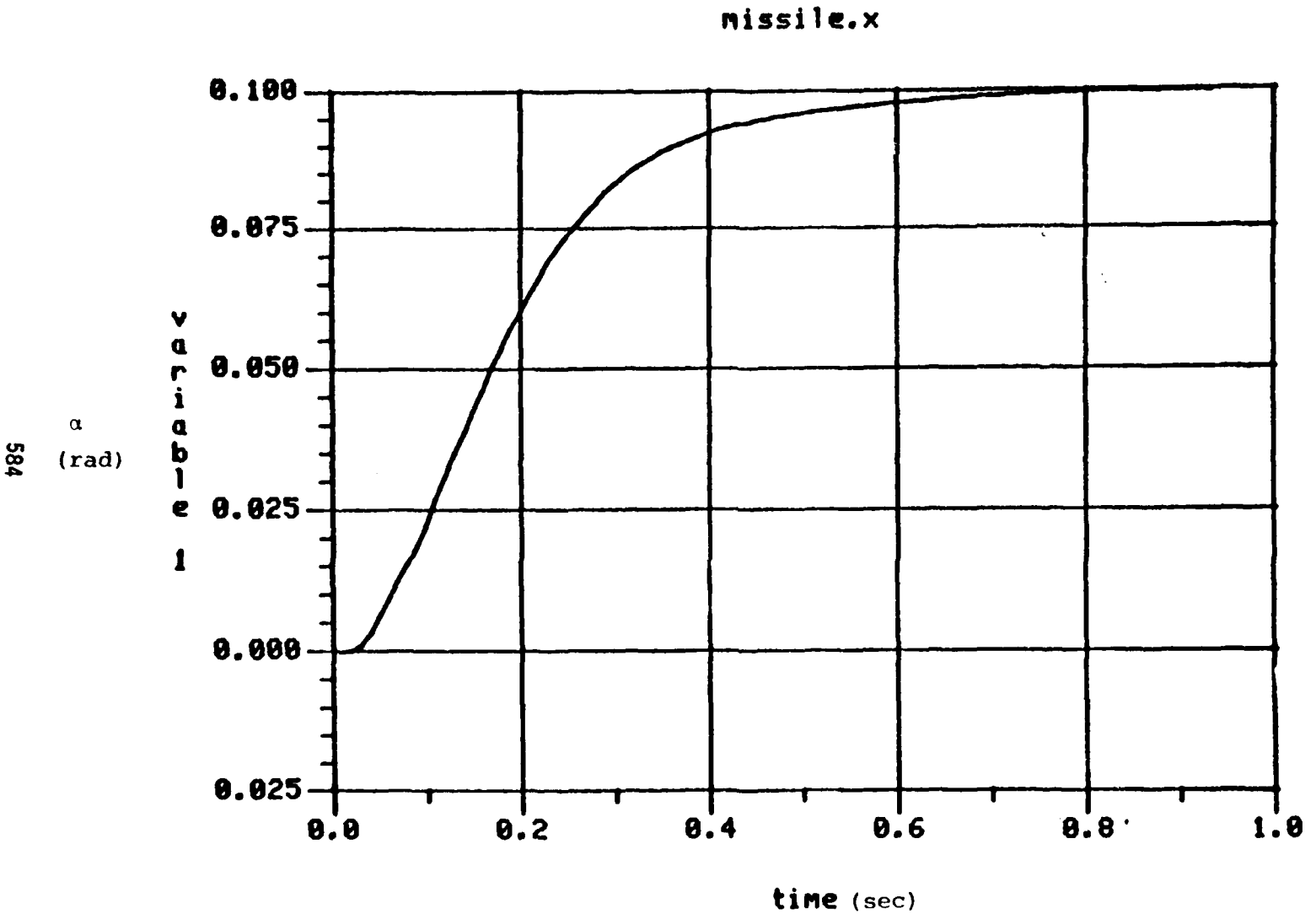


Figure 19: Closed Loop Response to α_c = .1 step

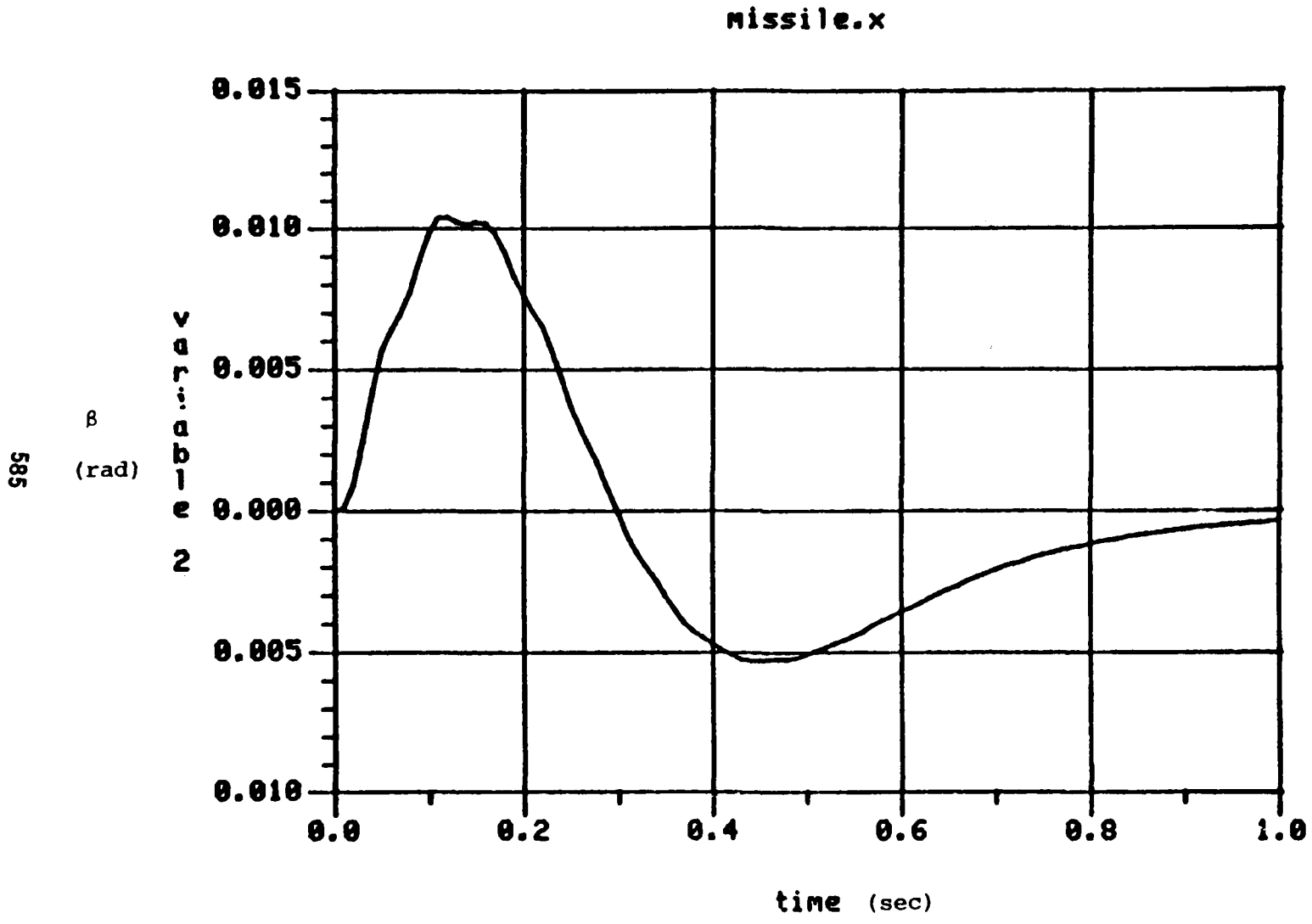


Figure 20: Closed Loop Response to α_c = .1 step

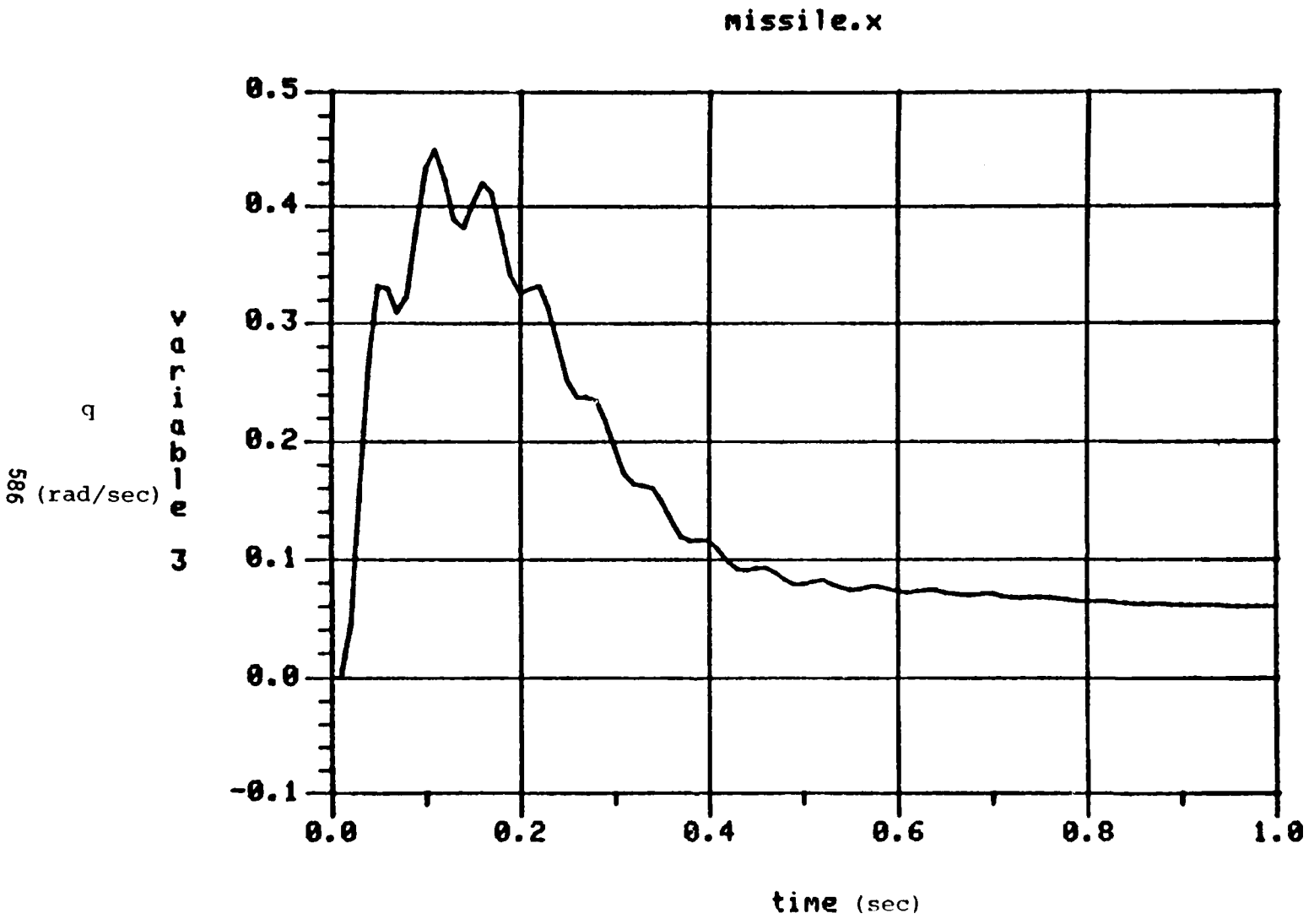


Figure 21: Closed Loop Response to α_c = .1 step

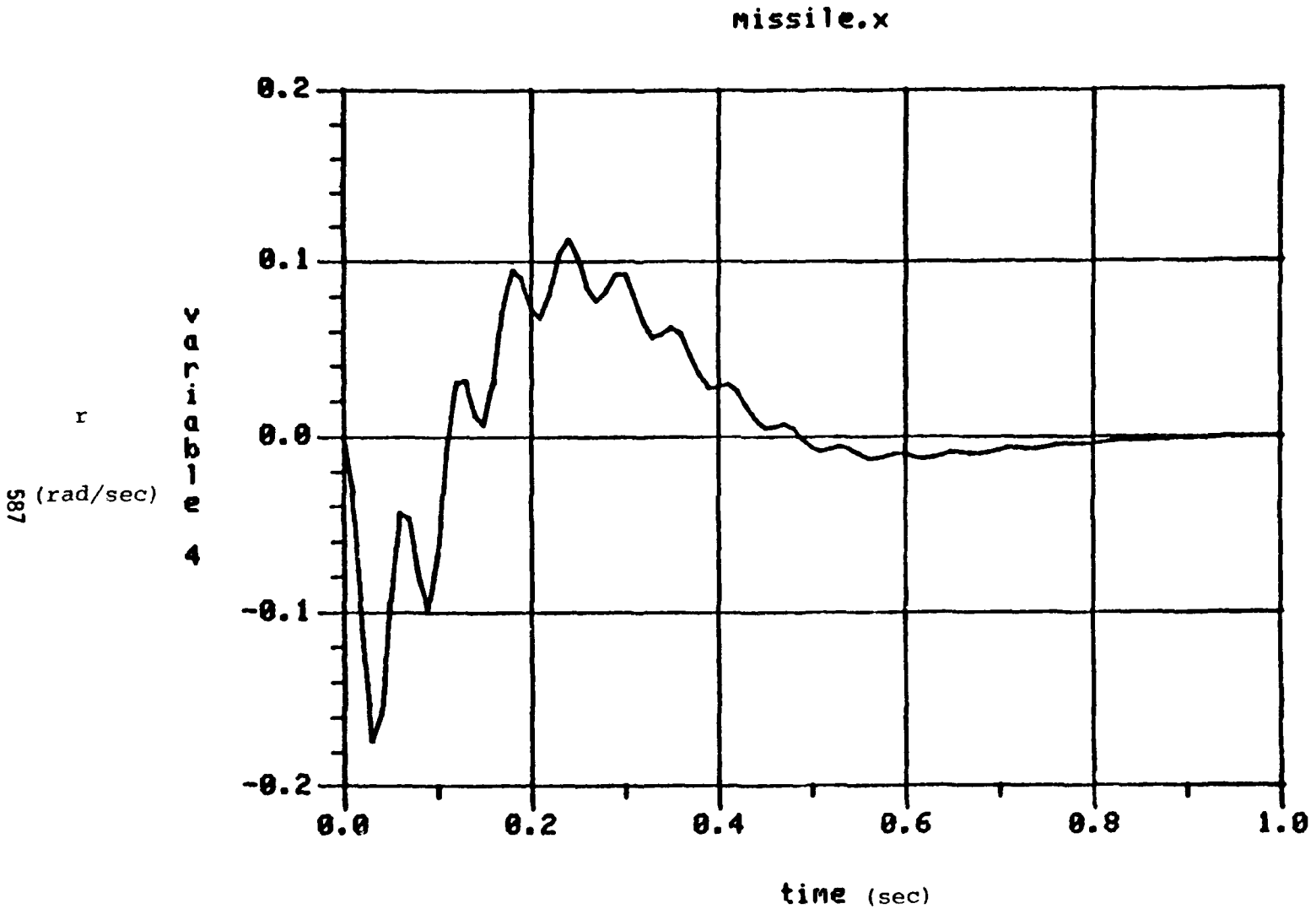


Figure 22: Closed Loop Response to α_c = .1 step

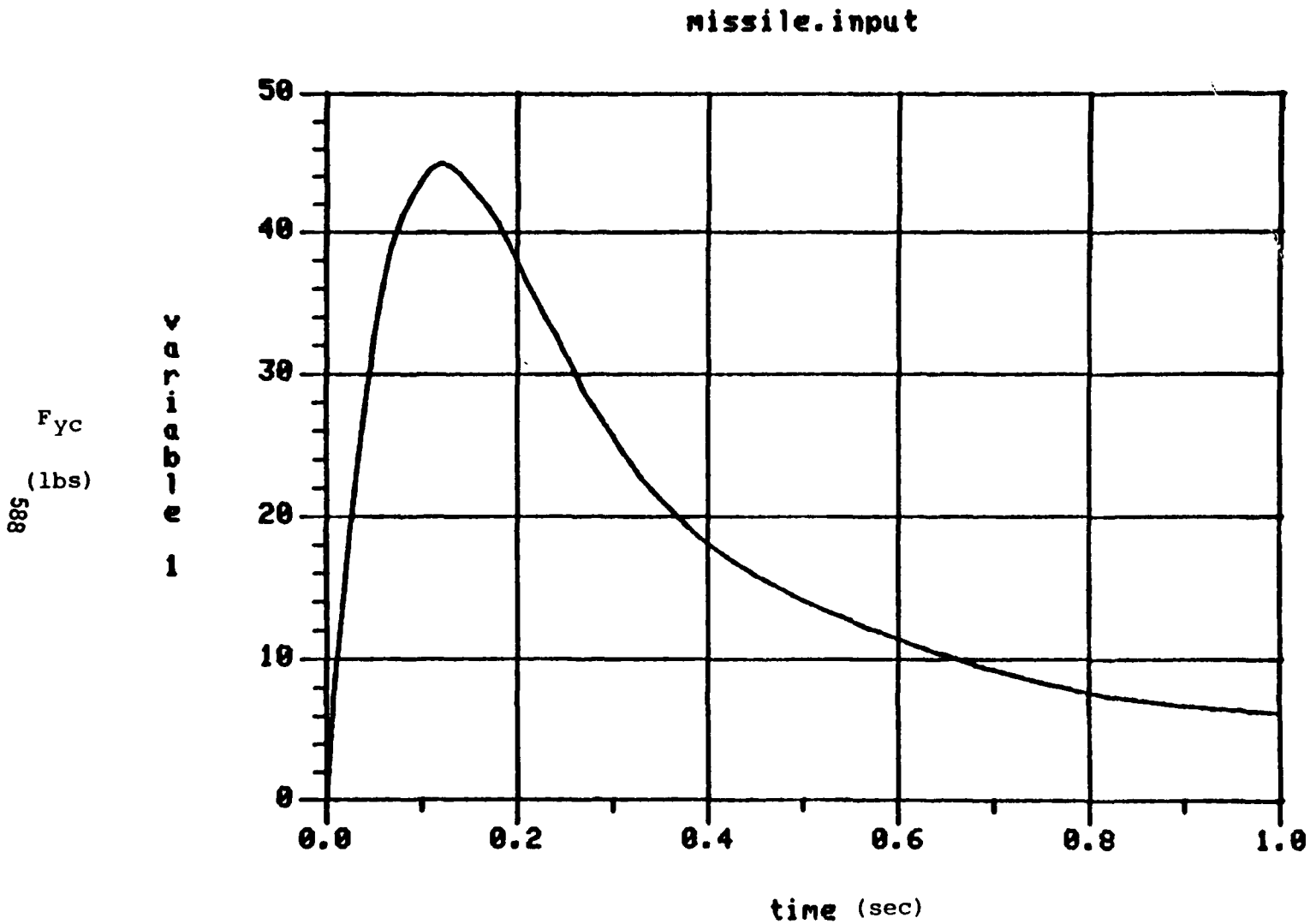


Figure 23: Closed Loop Response to α_c = .1 step

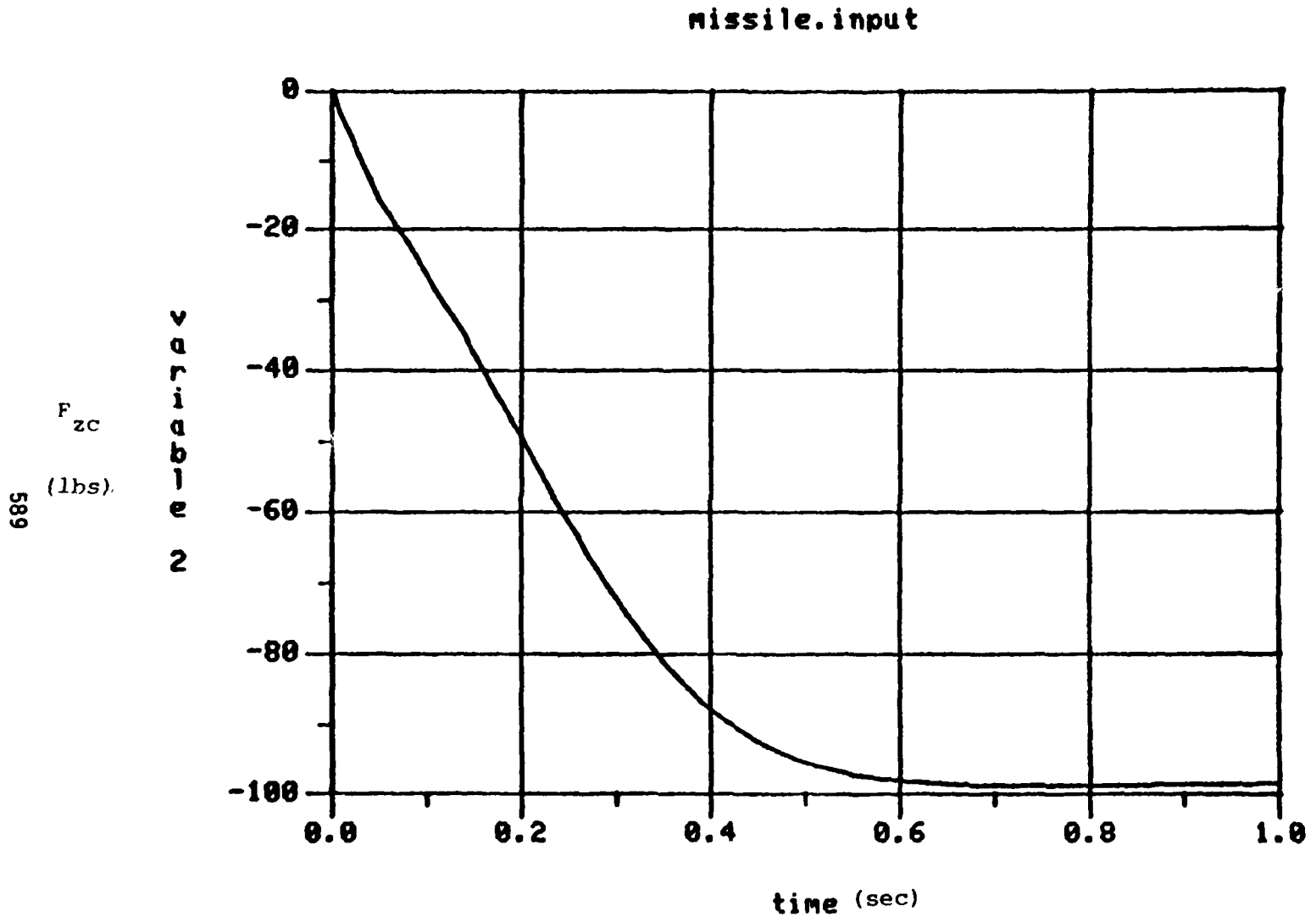


Figure 24: Closed Loop Response to α_c = .1 step

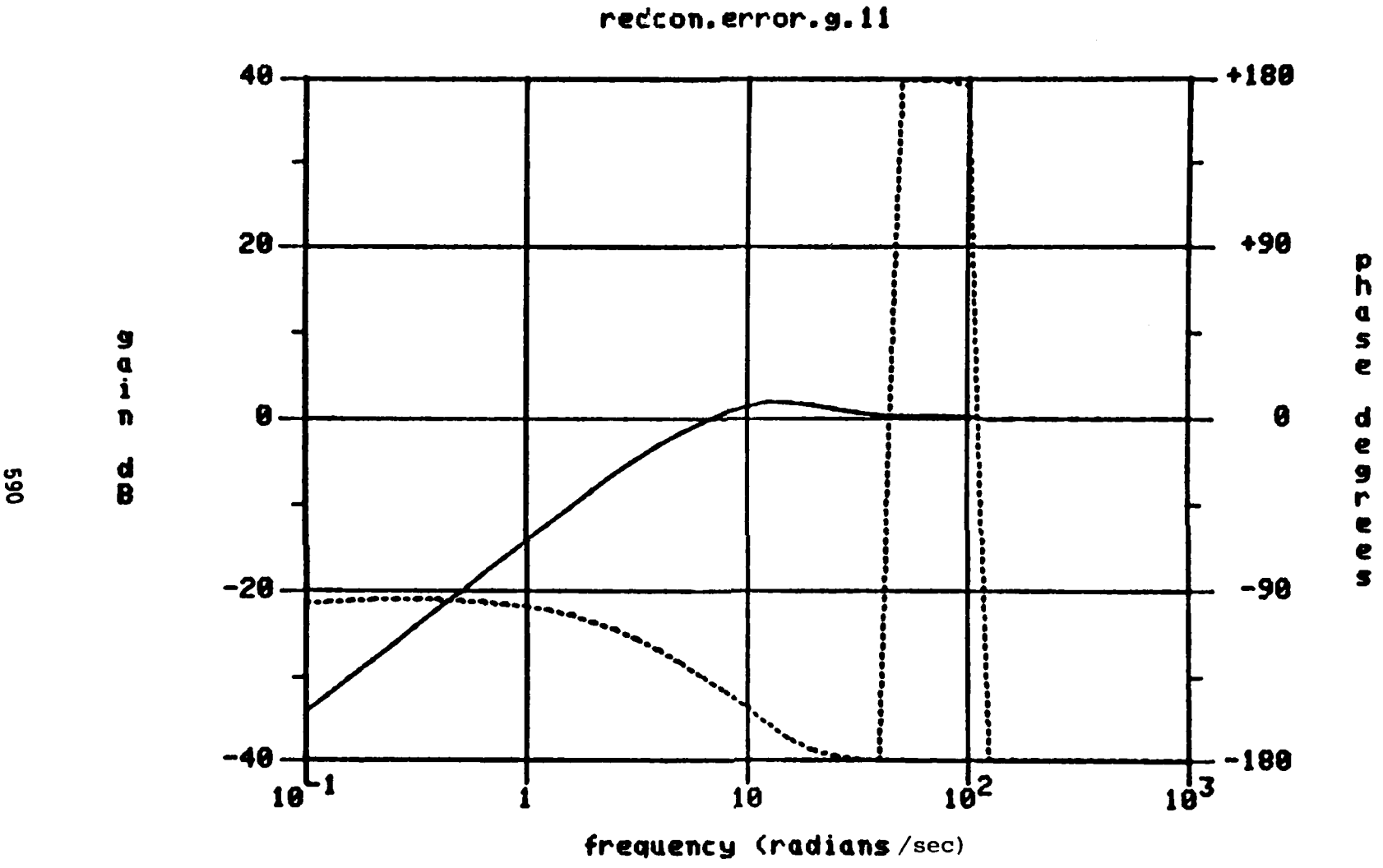


Figure 25: Transfer Function $(\alpha-\alpha_c)/\alpha_c$, $\beta_e = 0$

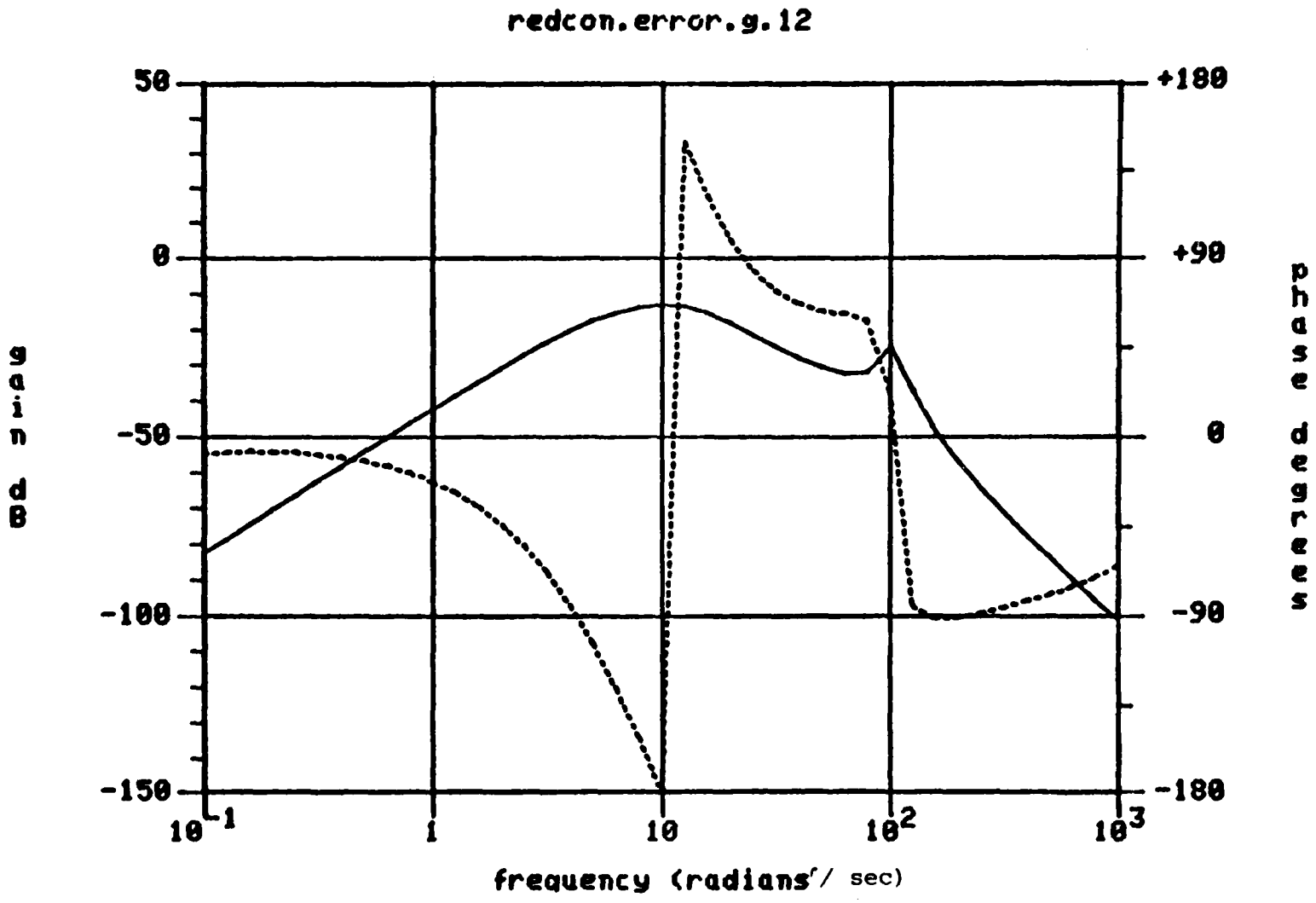


Figure 26: Transfer Function $(\alpha - \alpha_c)/\beta_c$, $\beta_e = 0$

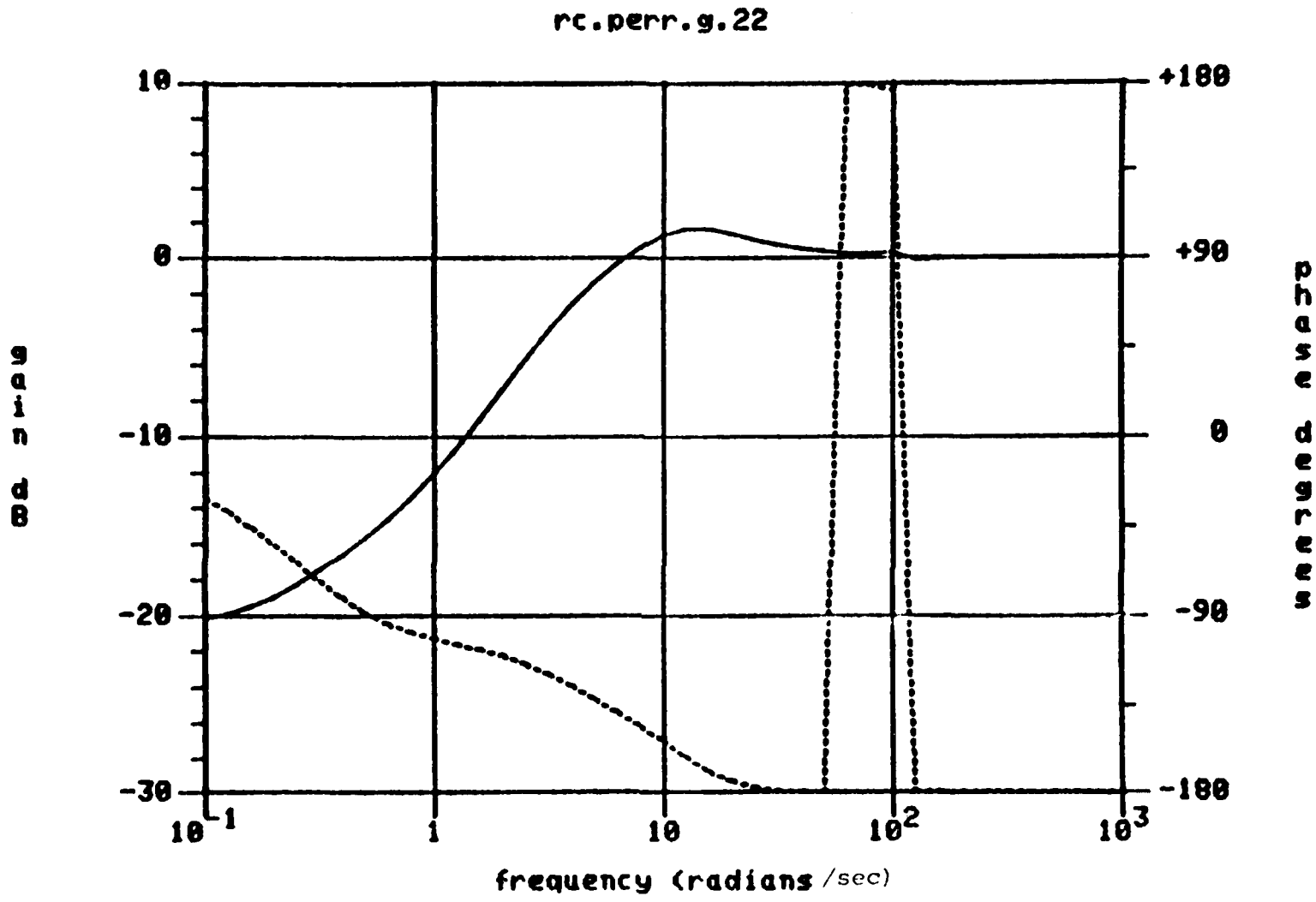


Figure 27: Transfer Function $(\beta - \beta_c)/\beta_c$, $\beta_e = 15^o$

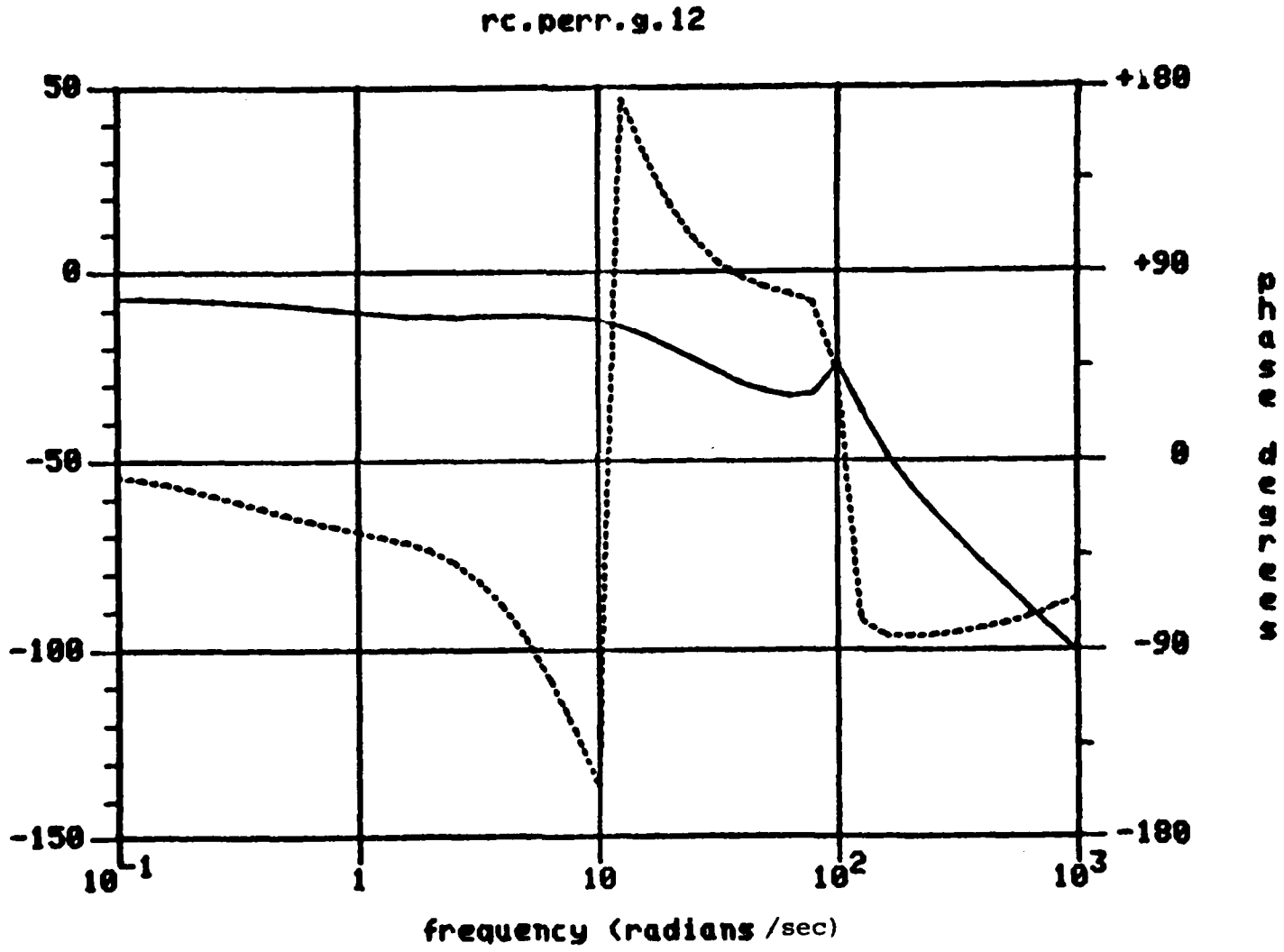


Figure 28: Transfer Function $(\alpha-\alpha_c)/\beta_c$, $\beta_e = 15^o$

An alternative way to evaluate the performance of the controller for various values of β_e is to plot the transfer functions of the command error transfer matrix T(s) where $(z-z_c) = T(s)\ z_c$. For good tracking performance T(s) should be small over the frequency range of interest. Figures 25 and 26 show the transfer functions $(\alpha-\alpha_c)/\alpha_c$ and $(\alpha-\alpha_c)/\beta_c$ respectively for $\beta_e = 0$. Due to symmetry $(\beta-\beta_c)/\beta_c = (\alpha-\alpha_c)/\alpha_c$ and $(\beta-\beta_c)/\alpha_c = (\alpha-\alpha_c)/\beta_c$. Figures 27 and 28 show the transfer functions $(\beta-\beta_c)/\beta_c$ and $(\alpha-\alpha_c)/\beta_c$ for $\beta_e = 15^o$. The remaining cases are very similar. As is evident the cross coupling in commands to outputs is probably unacceptable and points to a need for scheduling the controller on β_e, even though the modes remain well damped throughout the manuevering envelope.

CONCLUSIONS

In this paper we have demonstrated the design of a robust tracking system for the lateral axis of a spinning projectile which may be open-loop unstable in certain manuevering envelopes. The angles of attack and sideslip can be commanded independently with the available measurements being only pitch rate and yaw rate. Essential features of the design are the use of LQ pole prestabilization and LQG loopshaping procedures. The multiloop guaranteed stability margins are -13dB to $+\infty$ in gain and $\pm\ 60^o$ in phase determined from various singular value plots.

ACKNOWLEDGEMENT

The authors would like to thank Don Stilley of Honeywell Defense Systems Division for providing linearized projectile models and nonlinear simulation results.

REFERENCES

[1] Doyle, J.C. and Stein, G., "Multivariable Feedback Design: Concepts for a Classical/Modern Synthesis," IEEE Trans. Auto Control, AC-26, pp. 4-16, Feb. 1981.

[2] Doyle, J.C., "Multivariable Design Techniques Based on Singular Value Generalization of Classical Control," AGARD Lecture Series No. 117, Multivariable Analysis and Design Techniques.

[3] Zames, G. And A. El-Sakkary, "Unstable Systems and Feedback," Proceedings of the 18th Allerton Conference, October 1980.

[4] Bode, H. W., Network Analysis and Feedback Amplifier Design, D. Van Nostrand, Princeton, 1945.

[5] Horowitz, I.M., Synthesis of Feedback Systems, Academic Press, New York, 1963.

[6] Stewart, G.W., Introduction to Matrix Computations, Academic Press, New York, 1973.

[7] N.A. Lehtomaki, N.R. Sandell, Jr., and M. Athans, "Robustness Results in LQG Based Multivariable Control Designs," IEEE Trans. on Automatic Control, Vol. AC-26, No. 1, February 1981.

[8] Kalman, R.E., "When is a Linear System Optimal?," Trans. ASME Ser. D.J. Basic Eng., Vol. 86, pp. 51-60, 1964.

[9] Anderson, B.D.O. and Moore, J.B., Linear Optimal Control, Prentice-Hall, 1971.

[10] Safonov, M.G. and Athans, M., "Gain and Phase Margin of Multiloop LQG Regulators," IEEE Trans. Auto. Control, April 1977.

[11] Doyle, J.C., and Stein, G., "Robustness with Observers," IEEE Trans. on Automatic Control, August 1979.

[12] Wall, J.E., Harvey, C.A., and Doyle, J.C., "Tradeoffs in the Design of Multivariable Feedback Systems," Eighteenth Allerton Conference, 10/8-10/80.

[13] O.A. Solheim, "Design of Optimal Control Systems with Prescribed Eigenvalues," Int. Journal Control, Vol. 15, No.1, 143-160, 1972.

[14] N.A. Lehtomaki, "Practical Robustness Measures in Multivariable Control System Analysis," PhD Dissertation, Massachusetts Institute of Technology, May 1981.

Next page is blank

AD P001093

INFORMATION ENHANCEMENT AND HOMING MISSILE GUIDANCE

Jason L. Speyer and David G. Hull
Department of Aerospace Engineering and Engineering Mechanics
University of Texas
Austin, Texas 78712

Guidance laws currently in use in today's tactical missiles may be inadequate for the envisioned battlefield environment. The major sources of system deterioration are high-acceleration targets which stress the guidance laws and/or the autopilot and electronic countermeasures which degrade sensor accuracy. Although the ultimate goal for the missile guidance system is to produce minimum terminal miss, enhancement of information or system observability in a highly-stressed environment is critical to this goal. Observability is enhanced by the fundamental structure of the filter, the on-line determination of the required statistics necessary for the filter calculations, and the modulation of the guidance trajectory. Since the modulation of the guidance trajectory enhances the observability necessary for minimal terminal miss, this complex interaction between the guidance law and filter performance must be included in guidance law development. These issues are addressed, and the present status of development is given.

INTRODUCTION

All homing missile guidance is based upon the simple but effective control law called proportional navigation. The basic notion is that, if the line-of-sight rate is nulled, the missile (for non-maneuvering, constant-velocity targets) is on a collision course. If the target is considered to have acceleration capability perpendicular to the line-of-sight, then variations on the basic theme of proportional navigation as increased navigation ratio and biasing give improved performance. These improvements ensured that significant nonlinearities do not occur. However, with new high-performance targets, drastic maneuvers can result, forcing nonlinearities which degrade significantly system performance. This stress along with electronic countermeasures which degrade sensor accuracy, motivate the need for more sophisticated guidance laws and estimation techniques which can be realized by current microprocessor technology.

In its most general formulation, the homing missile problem can be represented as a stochastic control problem which can be solved by dynamic programming formalism. However, this approach is not computationally feasible. The task of decomposing this problem into tractable problems giving suboptimal performance may take the form of a nonlinear filter followed by a deterministic guidance law. This notion has some theoretical base in that the guidance law is a function of the conditional probability density of the state given the measurement history. This

means that the present estimation process is not influenced by the guidance process but that the guidance process is influenced by the estimation process. Based upon this observation, our research efforts have focused upon developing filter structures tailored to the homing missile engagement and performance criteria which will reflect relative filter observability and also be compatible with current homing guidance law development.

The present status of our work is described in this paper after presenting the system model in the second section, on which much of the work is based. First, a filter structure is described which seems to combine the best of the extended Kalman filte (EKF) and the pseudo-measurement observer (PMO). This filter, called the modified gain extended Kalman filter (MGEKF), retains the global convergence properties of the PMO with the seemingly unbiased estimation of the EKF. Initial results given in the third section indicate remarkable performance.

An assumption made in producing the numerical results for the MGEKF is that the measurement noise and process noise variances are known a priori. Since this is not the case, on-line estimation of the unknown variances is required. A sliding-window average scheme is described, and the results of numerical tests of the algorithm on a six-degree-of-freedom simulation are presented in the fourth section. Miss performance with the adaptive EKF shows remarkable improvement over that of the uncompensated EKF.

The above emphasizes our development of a filter structure and an adaptive noise variance algorithm to improve the estimation process. In the fifth section, trajectory modulation is proposed as a means of improving observability and, therefore, enhancing the estimation process. An observability measure is proposed, and the resulting deterministic trajectory which maximizes this measure is determined. The improvement in filter performance is demonstrated by operating the EKF along the maximum observability path and along a path generated by proportional navigation guidance. Again, significant improvements occur in reducing estimation errors when the modulated path is followed. This improvement occurs because the proportional navigation guidance procedure attempts to null the line-of-sight angle rate which causes some of the dynamic states not to be observable. The information performance criterion developed here is significantly simple so as to form the basis for guidance law development without the usual separation assumption.

Finally, in the sixth section, conclusions are presented, and the perceived direction of future work is given.

SYSTEM MODEL FOR FILTER/GUIDANCE LAW DERIVATIONS

The system dynamics and measurement process used to derive the EKF filter and guidance law are simplified by the assumption that the missile acceleration is measured very accurately by accelerometers and that the autopilot dynamics are negligible. The equations of relative inertial motion between the missile and target are given by the linear kinematic equations (the engagement geometry is shown in Figure 1).

$$\dot{S}_r = V_r \ , \quad \dot{V}_r = A_T - A_M \tag{1}$$

In these equations, S_r is the relative position vector, V_r is the relative velocity vector, A_T is the target acceleration vector, and A_M is the missile acceleration vector, all in three-dimensional inertial coordinates. The target acceleration is modeled as the first-order Gauss-Markov process

$$\dot{A}_T = -\lambda_T A_T + w_T \tag{2}$$

where λ_T is the target maneuver time constant and w_T is the maneuver uncertainty (Gaussian white noise with a zero mean and a power spectral density q_T). The parameters λ_T, q_T are chosen so that the autocorrelation function for a Poisson process for some given average switch time λ_T and maximum acceleration is the same as the autocorrelation function for this Gauss-Markov process.

In rectangular coordinates relative to an inertial reference frame, the scalar components of the above quantities are given by (see Figure 1)

$$S_r^T = [x_r \quad y_r \quad z_r] \qquad V_r^T = [\dot{x}_r \quad \dot{y}_r \quad \dot{z}_r]$$

$$A_T^T = [a_{T_x} \quad a_{T_y} \quad a_{T_z}] \qquad A_M^T = [a_{M_x} \quad a_{M_y} \quad a_{M_z}] \tag{3}$$

$$w_T^T = [w_{T_x} \quad w_{T_y} \quad w_{T_z}]$$

In terms of the nine-component state vector

$$x^T = [x_r \quad y_r \quad z_r \quad \dot{x}_r \quad \dot{y}_r \quad \dot{z}_r \quad a_{T_x} \quad a_{T_y} \quad a_{T_z}] \ , \tag{4}$$

the dynamics of the system are defined by the linear equation

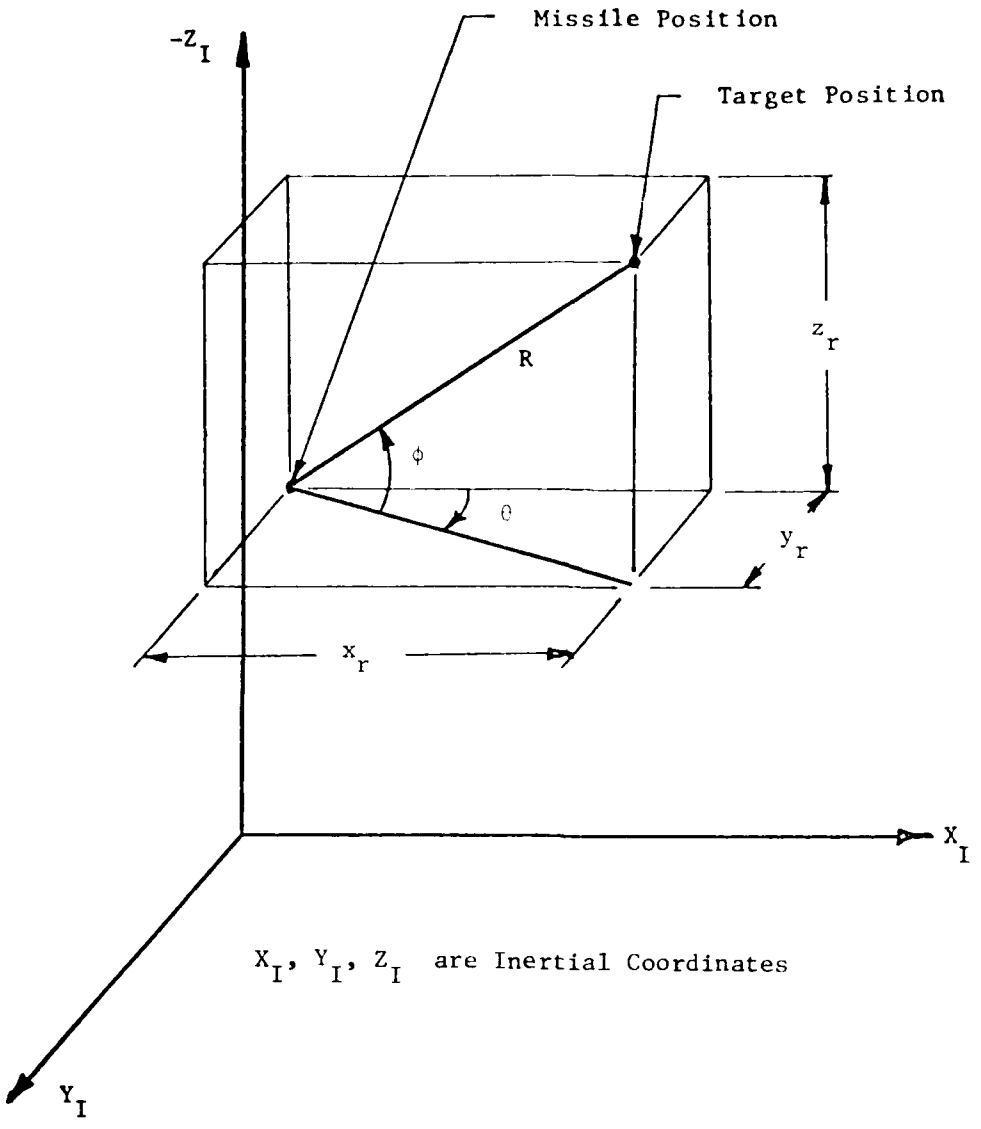


Figure 1. Intercept Geometry and Measurement Angles.

$$\dot{x} = Fx + GA_M + w \tag{5}$$

where, if I_3 is the 3×3 identity matrix,

$$F = \begin{bmatrix} 0 & I_3 & 0 \\ 0 & 0 & I_3 \\ 0 & 0 & -\lambda_T I_3 \end{bmatrix}, \quad \begin{aligned} G^T &= [0 \quad -I_3 \quad 0] \\ w^T &= [0 \quad 0 \quad w_T^T] \end{aligned} \tag{6}$$

For angle-only measurements, the nonlinear measurement-state relations are given by

$$z_\theta = \theta + v_\theta \quad , \quad z_\phi = \phi + v_\phi \tag{7}$$

where

$$\theta = h_\theta(x) \triangleq \tan^{-1}(y_r/x_r) \tag{8a}$$

$$\phi = h_\phi(x) \triangleq -\tan^{-1}[z_r/(x_r^2 + y_r^2)^{1/2}] \tag{8b}$$

The random sequences v_θ and v_ϕ represent independent noise sources with zero means and the following variances:

$$V_{\theta\theta} = q_\theta/\Delta t \quad , \quad V_{\phi\phi} = q_\phi/\Delta t \quad . \tag{9}$$

where Δt is the sample period. The power spectral densities q_θ and q_ϕ are modeled as

$$\begin{aligned} q_\theta &= q_{-1,0}/R^2 + q_{0,\theta} \\ q_\phi &= q_{-1,0}/R^2 + q_{0,\phi} \end{aligned} \tag{10}$$

where R is the range and the remaining parameters have been assumed known. The adaptive feature, to be described in the fourth section, estimates $V_{\theta\theta}$ and $V_{\phi\phi}$ on line.

In general terms, the measurement vector at time t_i is $z_i \triangleq [z_\theta(t_i), z_\phi(t_i)]^T$, the measurement vector function is $h(x_i) \triangleq [h_\theta(x_i), h_\phi(x_i)]^T$ where $x_i \triangleq x(t_i)$, and the measurement noise vector is $v_i \triangleq [v_\theta(t_i), v_\phi(t_i)]^T$. Therefore, (7) is rewritten as

$$z_i = h(x_i) + v_i \tag{11}$$

where the zero-mean, independent noise sequence v_i has variance $V(t_i)$ with only the diagonal elements given by (9) being nonzero.

The EKF is formulated in discrete time. Therefore, the discrete form of (5) is required. Since F and G in (6) are sufficiently elementary, the required transition matrix Φ and convolution integral B are obtained in closed form as

$$\Phi = \begin{bmatrix} I_3 & (\Delta t) I_3 & \frac{1}{\alpha^2}(e^{-\alpha \Delta t} + \alpha \Delta t - 1) I_3 \\ 0 & I_3 & (\frac{1}{\alpha} - \frac{1}{\alpha} e^{-\alpha \Delta t}) I_3 \\ 0 & 0 & e^{-\alpha \Delta t} I_3 \end{bmatrix} \tag{12}$$

$$B = [[-(\Delta t)^2/2] I_3 \quad (\Delta t) I_3 \quad 0]^T$$

where Φ and B are dependent upon the sample interval Δt but not on the sample time t_i, i.e., $\Phi = \Phi(\Delta t) = \Phi(t_{i+1} - t_i)$. The discrete form of the equations of motion is

$$x_{i+1} = \Phi x_i + B A_{xi} + w_{di} \tag{13}$$

where the w_{di} is the discrete form of the process noise having zero mean and variance

$$E[w_{di} w_{dj}] = 0 \quad , \quad i \neq j$$

$$= W = \int_{t_i}^{t_{i+1}} \Phi(t_{i+1} - \tau) G Q G^T \Phi^T(t_{i+1} - \tau) d\tau \quad , \quad i = j \tag{14}$$

where Q_c is the power spectral density of w_c in (6) where only the last three elements along the diagonal are nonzero and equal to q_c.

A NEW FILTER STRUCTURE FOR THE HOMING ENGAGEMENT

For the bearing-only estimation problem formulated in rectangular coordinates (second section), it has been recognized [1,2,3] that the nonlinear form of the angle measurements (8) can be manipulated into a linear function of the rectangular states where the coefficient matrix is a nonlinear function of the observations. For example, if $v_{\beta} = 0$ in (7), then (8a) can be manipulated into the form

$$v_1 = \sin z_\alpha \, x_r - \cos z_\alpha \, y_r \tag{15}$$

where v_1, called the pseudomeasurement, is identically zero. By using this form, observability requirements are established rigorously [3]. If the original measurements are corrupted by additive white

noise, the estimates resulting from linear filter structures are biased [2]. In [4] the performance of the EKF is improved for bearing-only measurements by modifying the gains of the EKF on the basis of a comparison of the structure of the EKF with a linear filter based upon the pseudomeasurements (PMO). In [4] the measurements have been assumed noiseless so that the comparison has been made by considering these filters as observers. The nonlinear structure of the EKF for the bearing-only problem can be manipulated into the linear structure of the PMO. The difference between these two observers is seen to be in the algorithm for updating the gains. By updating the gains in a manner suggested by the PMO, the gains of the EKF are modified although the gains of these two observers are still not the same. The difference seems to be quite important. In the PMO, the gains are a function of the present measurement while in the modified gain EKF (MGEKF) the gains are an explicit function of only past measurements. This seems to have a significant effect on the performance of the estimators when noise measurements are used where the error response of the PMO is quite biased from its noiseless error response and the MGEKF is not.

The results shown in [4] are for a two-dimensional problem. In the results to be shown here, the three-dimensional formulation is used, requiring both noisy elevation and azimuth angle measurements. The gain modifications for the two cases are slightly different because an additional assumption is made in the three-dimensional case.

The results presented are preliminary but hopefully indicate the performance improvements that can be achieved with a more sophisticated simulation. The simulation here had imposed an environment which was identical to that assumed in the filter. Furthermore, in order to compare performance of the various filters, the paths were generated using a linear-quadratic-Gaussian (LQG) guidance rule operating on the simulation states rather than the estimates.

The launch scenario is given by

$$x_r = 3000 \text{ ft} \quad , \quad y_r = 1000 \text{ ft} \quad , \quad z_r = 500 \text{ ft}$$

$$\dot{x}_r = -900 \text{ ft/sec} \quad , \quad \dot{y}_r = -50 \text{ ft/sec} \quad , \quad \dot{z}_r = -20 \text{ ft/sec}$$

$$a_{T_x} = 10 \text{ ft/sec}^2 \quad , \quad a_{T_y} = 10 \text{ ft/sec}^2 \quad , \quad a_{T_z} = 10 \text{ ft/sec}^2,$$

and the initial estimates (where $\hat{x}$ denotes the estimate of x) are assumed to be

---

*The analysis and simulation results were obtained by Tack L. Song.

$$\hat{x}_r = 2500 \text{ ft} \quad , \quad \hat{y}_r = 850 \text{ ft} \quad , \quad \hat{z}_r = 600 \text{ ft}$$
$$\dot{\hat{x}}_r = -800 \text{ ft/sec} \quad , \quad \dot{\hat{y}}_r = -100 \text{ ft} \quad , \quad \dot{\hat{z}}_r = -100 \text{ ft}$$
$$\hat{a}_{T_x} = 0 \text{ ft/sec}^2 \quad , \quad \hat{a}_{T_y} = 0 \text{ ft/sec}^2 \quad , \quad \hat{a}_{T_z} = 0 \text{ ft/sec}^2$$

The filter is initialized with a diagonal error covariance matrix with 10,000 ft^2 for each of the position elements, 10,000 ft^2/sec^2 for each of the velocity elements, and 100 ft^2/sec^4 for each of the acceleration elements. The value in (10) of $q_{0,\theta}$ and $q_{0,\phi}$ is zero, and the value of $q_{-1,\theta}$ and $q_{-1,\phi}$ is .1 . The values of the elements of the matrix W in (14) are all zero although $\lambda_T = 1$ in (2). The performance of the filter is measured here in terms of the range tracking error

$$\text{Range Error} \triangleq [(x_r - \hat{x}_r)^2 + (y_r - \hat{y}_r)^2 + (z_r - \hat{z}_r)^2]^{1/2} \qquad (16)$$

The preliminary results of simulating the PMO, MGEKF, and EKF are shown in Figures 2 and 3. In Figure 2 the behavior of all three filters is shown where the measurements are noiseless. The response of the PMO and the MGEKF are quite similar where the PMO performs a bit slower than the MGEKF. If the initial errors were reversed in sign, then the PMO performs a bit faster than the MGEKF. Clearly, the EKF performs poorly for these large initial-condition errors. Figure 3 shows a realization of the range error for each filter when the measurements are noisy. The range error of the PMO is biased away from the deterministic range error profile as shown in Figure 2. This is the case for all the realizations that have been made. The range error realization of the MGEKF, although a bit raggedy, as expected, essentially follows the deterministic range error profile. The range error realization of the EKF remains poor. Similar results occur for the velocity error, while the effect on acceleration is not as pronounced. For a number of cases performed, the behavior shown here persists. For the case where the initial state errors are small, all three filters perform equally for noiseless measurements. However, for noisy measurements, the PMO shows a divergence, whereas both the MGEKF and EKF perform similarly although the EKF seems slightly better.

The essential conclusion is that the MGEKF has the global filter characteristics of the PMO for noiseless measurements as well as the unbiased behavior of the EKF for noisy measurements. A possible explanation for the seemingly robust performance of the MGEKF is that the gain structure is based upon the algorithm used for the PMO, thereby producing global behavior. However, the current gains are not an explicit function of the current noisy measurement as in the EKF, thereby avoiding the biased performance of the PMO.

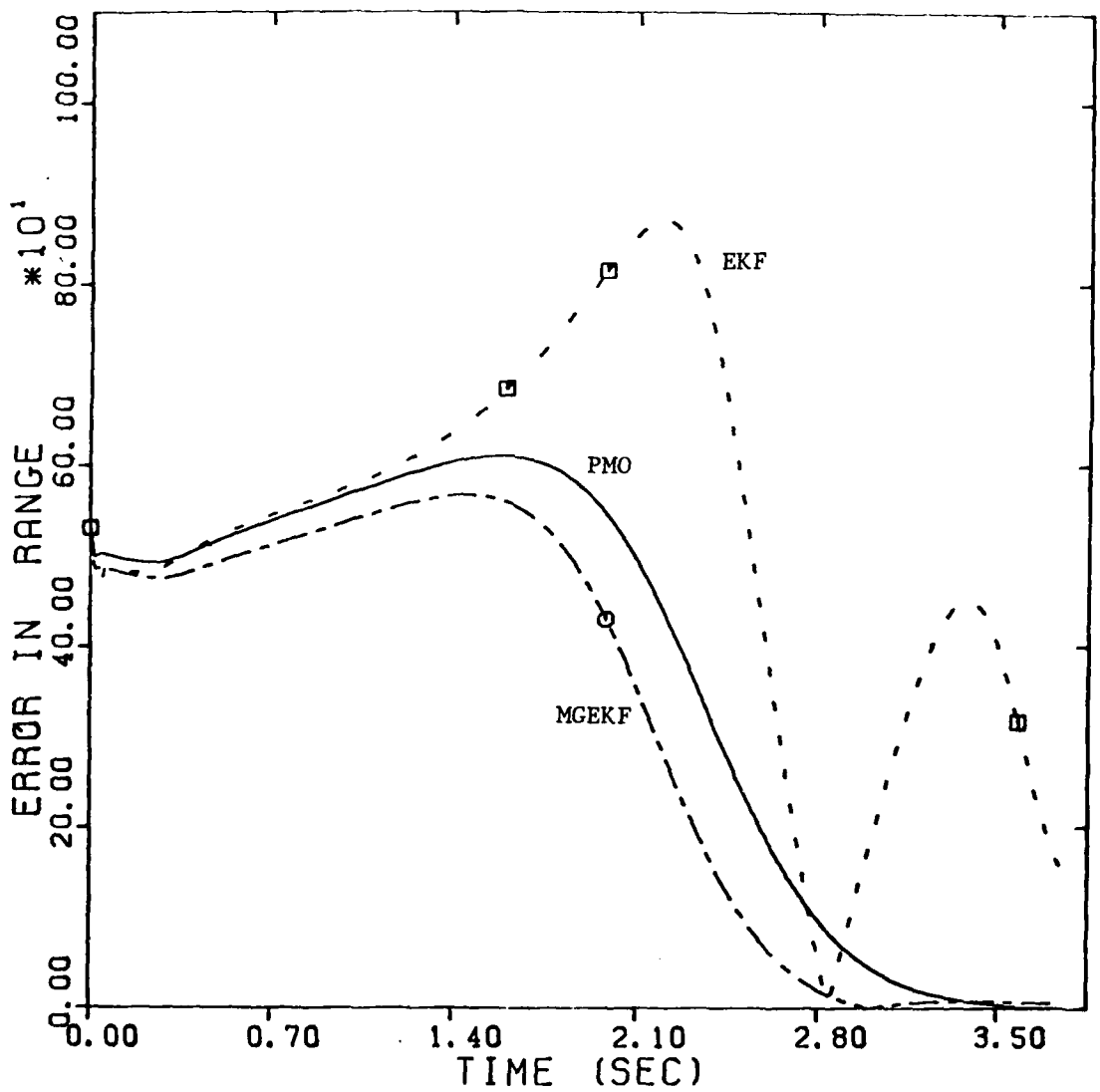


Figure 2. Response of the PMO, MGEKF, and EKF for Noiseless Measurements.

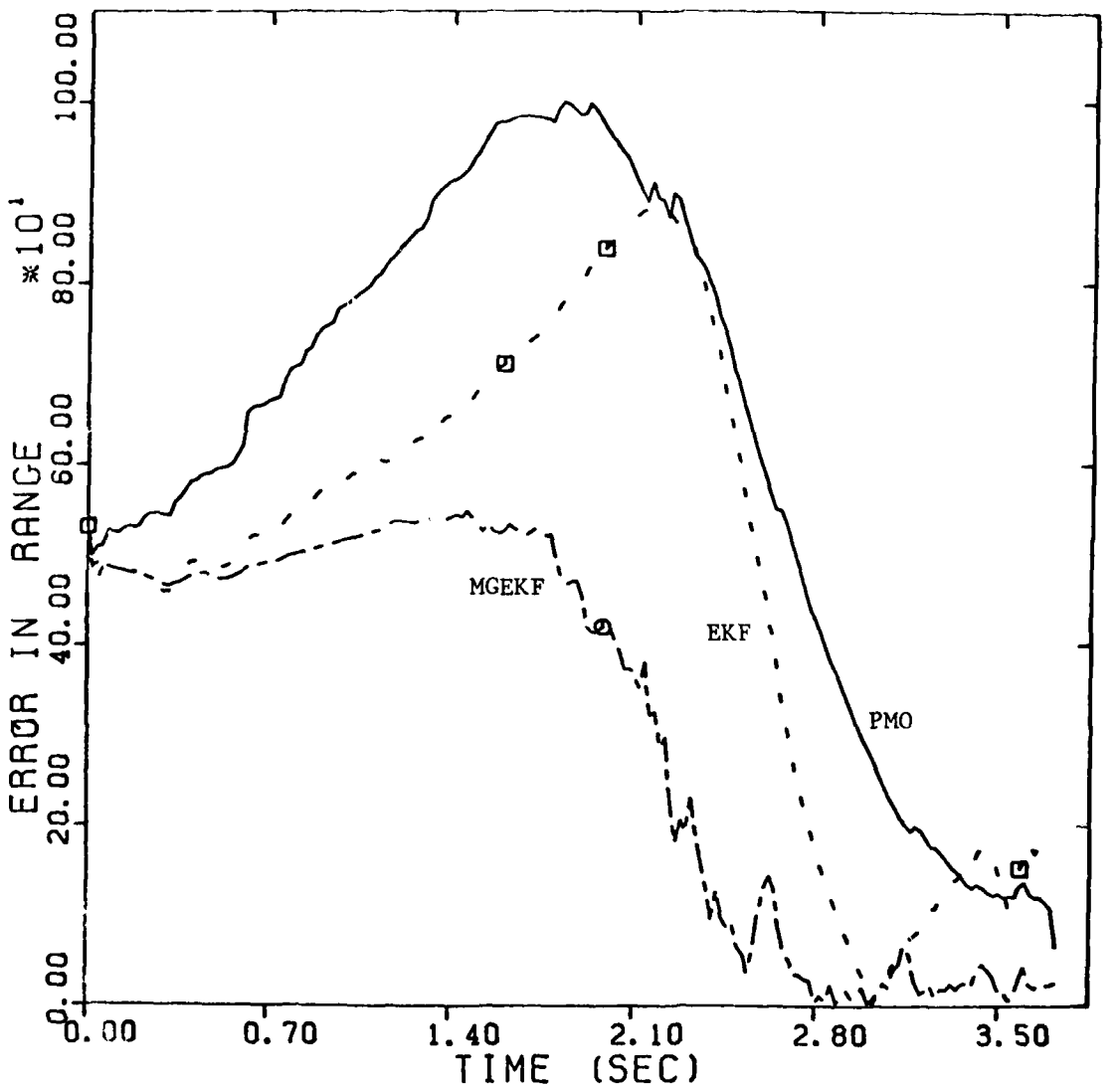


Figure 3. Response of the PMO, MGEKF, and EKF for Noisy Measurements.

ADAPTIVE NOISE VARIANCE ESTIMATION

As the basis for the development of adaptive techniques for noise variance estimation, a missile guidance system composed of the EKF followed in cascade with a guidance law formed using LQG theory [5,6] is used. The following results show that the miss distance produced by this guidance system is very sensitive to the values of the measurement noise variance. A scheme for estimating the measurement noise variance from the residuals of the EKF is given in [7] and used in [8] to improve miss distance performance. The results of [8] are partially reproduced here.

The measurement noise variance estimator developed for the homing engagement is a limited-memory scheme utilizing a sliding window to incorporate the most recent noise sample and to discard the oldest. The number of samples in the average, N, is chosen empirically. The on-line mean and covariance of the measurement noise are determined using statistical sampling theory, assuming stationarity and independence of the EKF measurement residuals over the sample window. The EKF gains are adjusted to the on-line estimate of the measurement variance, and the estimation equation includes the on-line estimate of the measurement bias.

Prior to the buildup of the sliding window, the adaptive filter behaves as the unmodified EKF using the assumed a priori values of the measurement noise variance. At the sample time immediately following the initial adaptive estimate, the filter begins using the recursion relations for the estimate of the measurement noise mean and variance.

COMPUTER SIMULATION

A six-degree-of-freedom missile simulation [9] has been used to test the adaptive noise estimator. This simulation contains the interception of a maneuvering target by a short-range, air-to-air missile. The airframe aerodynamics and the autopilot of a bank-to-turn missile are included in the simulation as well as the digital filter and the guidance system. Each is a separate component capable of being modified without changing the rest of the program. The adaptive filter can be added to the extended Kalman filter in a straightforward manner.

An engagement begins with the firing of the missile from a launch aircraft which provides the true state vector. The target is assumed to be a constant-speed point mass which can change direction instantaneously. Initially, the target flies straight and level at the launch altitude. When the missile reaches a range of 6000 ft, the target commences a 9g maneuver 45 deg up and to the right relative to its original heading. When the estimated time-to-go reaches 1 sec, the target executes a second 9g maneuver straight down. The missile itself is capable of 100g's normal acceleration. An engagement ends when the closing velocity becomes negative or when a preset time limit is exceeded.

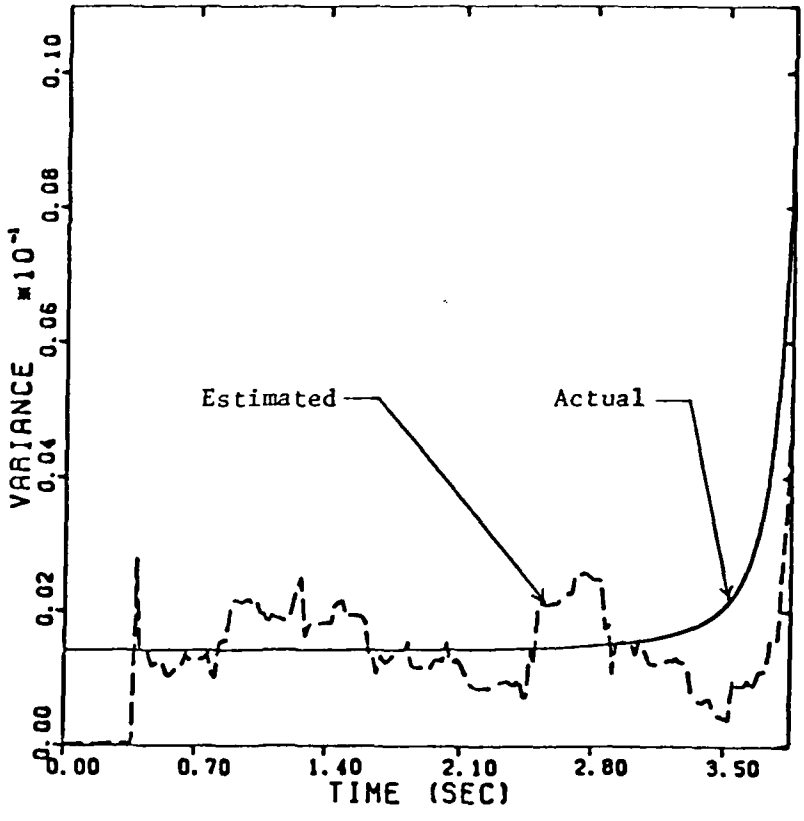


Figure 4. Azimuth Measurement Variance Estimate for $\sigma = 50$ and $N = 20$.

The actual measurement variance is obtained by multiplying $V_{\theta\theta}$ and $V_{\phi\phi}$ given in (9) by a parameter σ which is called the mismatch parameter allowing the true variance to be of a different order of magnitude than the value assumed in the filter. The value used in (10) for $q_{-1,\theta} = q_{-1,\phi}$ is .25 $rad^2 ft^2 sec$, and the value for $q_{0,\theta} = q_{0,\phi}$ is 56.25×10^{-8} $rad^2 sec$.

The launch conditions are the same for all simulations performed in this study and are given by the following:

Missile and Target Mach	.9
Altitude	10,000 ft
Range	7,000 ft
Off-Boresight Angle	0 deg
Aspect Angle	60 deg

The filter inputs which remain unchanged are the a priori error covariance matrix, M_o , and the process noise spectral density matrix, Q . The filter is always initialized with the true state vector; however, uncertainty is introduced by assigning values to the diagonal elements of M_o and Q . The nonzero values are the following:

Parameter	Value
$M_o(1,1), M_o(2,2), M_o(3,3)$	10 ft^2
$M_o(4,4), M_o(5,5), M_o(6,6)$	10 ft^2/sec^2
$M_o(7,7), M_o(8,8), M_o(9,9)$	25,000 ft^2/sec^4
$Q(7,7), Q(8,8), Q(9,9)$	50,000 ft^2/sec^5

ADAPTIVE FILTER TESTING

The limited-memory filter (LMF) is compared with the uncompensated extended Kalman filter (EKF) for nine different cases representing three values of the noise mismatch (σ = 1.,50.,.02) and three values of the sample window size (N = 15,20,25). A Monte Carlo simulation containing ten realizations of the measurement noise process is performed for each case. The performance of the filters is evaluated based on the mean and standard deviation of the miss distance distribution.

The effect of the adaptive noise estimation can be seen in the tracking histories of the estimated variance for azimuth and elevation versus the actual variance. Figure 4 shows the typical behavior of the estimated measurement variance for σ = 50 and N = 20 . The elevation profile is quite similar. Figure 5 shows the typical behavior of the estimated measurement variance for σ = .02 and N = 20 .

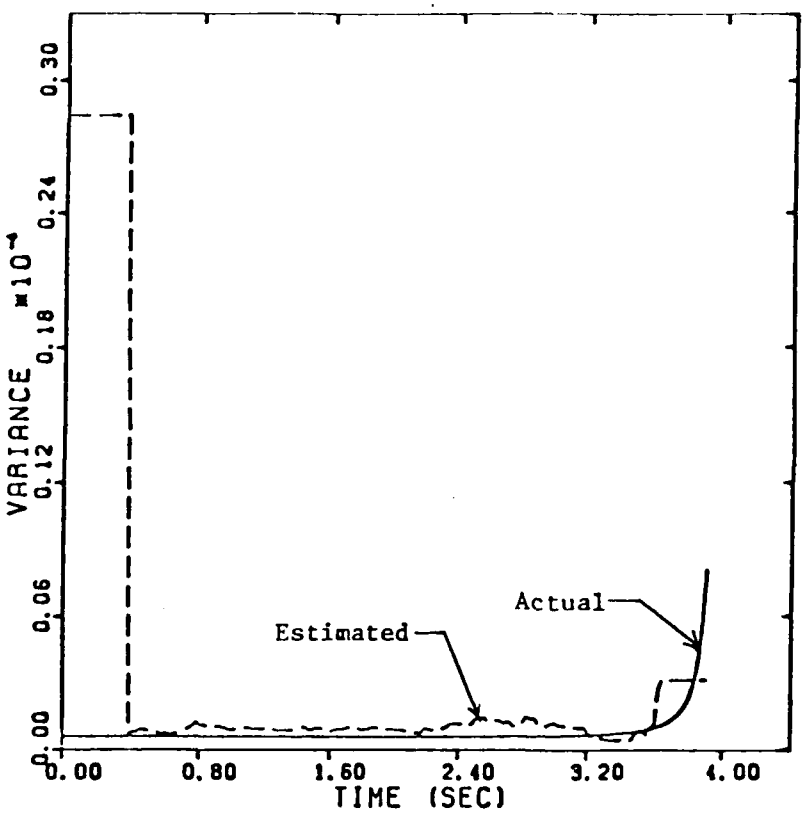


Figure 5. Elevation Measurement Variance Estimate for $\sigma = .02$ and $N = 20$.

The azimuth profile is quite similar. In Figures 4 and 5 it can be seen how the estimated variance remains at the a priori value until the sample size of 20 is reached. Then, at .4 sec, the filter begins using the value computed by the adaptive noise estimator. The estimates are then on the same order of magnitude as the actual variance. Near termination the actual variance begins to rise sharply, and the estimates tend to lag behind. For $\sigma = .02$ this effect is more evident, and in fact, the estimates level off and become constant as seen in Figure 4. These constant values are caused by logic in the program which chooses the last value of the estimate if the present measurement noise covariance matrix is found to be nonpositive definite.

The means and standard deviations of the miss distance distributions are shown in Table 1. The adaptive filter is clearly performing better than the EKF when the noise mismatch is different from one. When $\sigma = 1$ the difference is not as great because the adaptive filters are estimating the same level of noise that the EKF is assuming. It is interesting to note that when $\sigma = 1$ and when $\sigma = 50$, the statistics of the adaptive filter degrade when N changes from 15 to 20 and then improve again when $N = 25$. The trend is different when $\sigma = .02$. In these cases the statistics for the LMF degrade for increasing sample size. The more desirable miss distance statistics displayed by the adaptive filter when $\sigma = .02$ are due to the lower value of the actual measurement noise.

TABLE 1. MEANS AND STANDARD DEVIATIONS OF MISS DISTANCE DISTRIBUTIONS*

$\sigma = 1.$						
	MEAN	STANDARD DEVIATION				
EKF	9.35	9.32				
	N = 15		N = 20		N = 25	
LMF	12.13	6.64	20.21	35.66	19.33	37.26
$\sigma = 50.$						
	MEAN	STANDARD DEVIATION				
EKF	117.37	33.71				
	N = 15		N = 20		N = 25	
LMF	51.17	31.49	64.23	30.46	61.98	29.62
$\sigma = .02$						
	MEAN	STANDARD DEVIATION				
EKF	31.93	31.54				
	N = 15		N = 20		N = 25	
LMF	4.00	2.85	7.16	10.57	11.29	22.22

*All distances are in feet.

ESTIMATION ENHANCEMENT BY TRAJECTORY MODULATION

In the past two sections, improved estimation has been obtained by either the development of new filter structures or by the addition of adaptive features. For bearing-only measurements, the observability of the states depends upon the changing geometry of the engagement. This aspect of the homing engagement can be investigated by transforming the original measurements into pseudomeasurements where linear observability theory holds. Those geometries producing poor observability can be avoided by trajectory shaping using the control variables. If this type of scheme were to be implemented, the guidance scheme would have the dual role of driving the terminal miss to small values while enhancing the observability needed for estimation.

The objective here is to present a performance measure of observability which has a particularly simple form due to the properties of the homing problem. This performance index is maximized subject to the nonlinear equations of motion of a point mass model of a bank-to-turn missile. The additional constraints are zero terminal miss, a limit on the off-boresight angle, and a limit on angle-of-attack. The results of this section are a summary of [10].

INFORMATION PERFORMANCE CRITERION

A commonly used measure of accuracy in determining unknown parameters from a sequence of measurements is the Fisher information matrix [11]. The Fisher information matrix can be related to the missile intercept problem through the local observability Gramian when no process noise is considered and the additive measurement noise is white and Gaussian. For this case the inverse of the error covariance of the linearized filter about a given nominal is the local observability Gramian. The local observability Gramian for the missile problem is a 9×9 symmetric matrix convolution integral involving the transition matrix defined in (12) where Δt is replaced with $\tau - t_f$ (τ is the dummy variable and t_f is the terminal time), the partial derivative of the measurement function $h(x)$ (given in the second section) with respect to the state, and the power spectral densities q_θ and q_ϕ also given in the second section. The local observability Gramian is reduced by first multiplying it by a weighting matrix L which is a function of the terminal time so that certain state terms will not dominate others. Finally, the trace operation is used to reduce the Gramian to a scalar. Furthermore, the trace being a linear operation commutes with the integral of the observability Gramian so that the standard Bolza form for the cost functional is produced for the optimization problem. After a good deal of simplification the following simplified and elegant form of the information performance criterion is obtained:

$$J = \int_{t_o}^{t_f} [(q_{-1,\theta} + q_{0,\theta} R_{az}^2)^{-1} + (q_{-1,\phi} + q_{0,\phi} R_{el}^2)^{-1}]$$
$$\cdot [L_{11}\, \Phi_{11}^2(\tau - t_f) + L_{44}\, \Phi_{14}^2(\tau - t_f) + L_{77}\, \Phi_{17}^2(\tau - t_f)]d\tau \qquad (17)$$

where Φ_{ij} represents the ij element of Φ defined in (12). The azimuth range R_{az} is $(x_r^2 + y_r^2)^{1/2}$ and the elevation range R_{el} is $(x_r^2 + y_r^2 + z_r^2)^{1/2}$. This performance index is to be maximized subject to the dynamics of the missile-target engagement and other constraints.

PHYSICAL MODEL USED FOR OPTIMIZATION

To complete the formulation of the optimization problem, it is necessary to discuss the modeling of the missile and the target, the boundary conditions, and the inequality constraints.

The bank-to-turn missile is modeled as a point mass, and hence, its motion is governed by a set of nonlinear differential equations. These equations are the three kinematic equations giving the inertial position of the missile center of gravity and the three dynamic equations giving the magnitude and direction of the missile velocity vector. The earth is assumed to be flat with a constant acceleration of gravity and a standard atmosphere. The thrust has a constant magnitude for 2.6 seconds, and the mass flow rate is assumed constant so that the mass is a known function of time. The aerodynamics are typical of a theoretical bank-to-turn missile and are presented in tabular form as functions of Mach number and angle of attack. These tables are read by linear interpolation. Finally, the control variables are chosen to be the yaw and pitch angles of the body centerline.

The target is assumed to have zero acceleration. Hence, it is traveling in a straight line at constant speed.

The initial conditions are those for a co-altitude, co-speed launch with a given range to the target. Also, the target off-boresight is assumed to be zero and the aspect angle has been taken to be 30 degrees. The prescribed final conditions are that the final relative positions be zero (zero terminal miss).

Several inequality constraints exist for this model. First, the angle of attack and the normal acceleration are limited. Second, in an attempt to model the seeker, the boresight angle (the angle between the line of sight to the target and the missile centerline) is limited to 60 degrees.

THE OPTIMIZATION PROBLEM

In general, the optimization problem is to maximize the information performance index subject to a set of differential constraints (equations of motion) with known initial conditions, a set of prescribed final conditions (zero terminal miss), and some control variable inequality constraints (angle of attack, normal acceleration, and boresight angle). To simplify the problem, each inequality constraint is converted into a penalty-type constraint, which, in turn, can be reduced to a differential constraint and an equality final condition.

At this point, the optimal control problem is reformulated as a nonlinear programming problem. This is accomplished in two steps. First, the time is normalized with respect to the final time, making t_f a parameter. Second, each control history is replaced by a set of nodal points and some form of interpolation. In this study, interpolation has been performed with cubic splines, and since the initial and final slopes are unknown, they are included as unknown parameters. In summary, the unknown p parameters are the final time, the nodal points of each control history, and the initial and final slopes of each control history. Once a set of these parameters is given, the differential equations can be integrated to obtain the final state as a function of the parameters. This means that the performance index and the final conditions can be considered as functions of the unknown parameters.

In view of the above discussion, the form of the nonlinear programming problem considered here is the following: Find the p-vector y of parameters which minimizes the performance index $J = F(y)$ subject to the m-vector of equality constraints $C(y) = 0$. A maximization problem is converted into a minimization problem by multiplying the performance index by a minus sign.

MAXIMUM-INFORMATION TRAJECTORY

The particular method which has been chosen to solve the optimization problem is known as the augmented-Lagrangian method [12]. It is a penalty function method which allows convergence to be achieved without having to drive the weights to infinity. The particular code used has been obtained from the Atomic Energy Research Establishment in Harwell, England. Derivatives needed to perform the optimization are computed numerically by central differences.

The co-altitude, co-speed launch occurs at 10,000 feet and 0.9 Mach while the range is 3000 feet. As stated previously, the off-boresight angle is 0 degrees, and the aspect angle is 30 degrees. Each control history has been represented by five parameters: three nodes and two slopes. The results are summarized in Table 2. Also presented in Table 2 for comparison are the characteristics of the trajectory using proportional navigation guidance [6] which is essentially a minimum-time path.

TABLE 2. INTERCEPT RESULTS

Trajectory	Flight Time t_f(sec)	Performance Index	Miss Distance (ft) x_R	y_R	z_R
Maximum Information	5.84	16.2	0.011	0.039	0.002
Proportional Navigation	2.66	4.94	0.026	-0.171	-0.218

The geometry of the maximum-information trajectory is shown in Figures 6 and 7. It is seen that this trajectory tries to vary the azimuth and the elevation simultaneously. Furthermore, the initial part of the trajectory is a transient maneuver which puts the missile on the desired intercept path. The value of the performance index is shown in Table 2 along with that calculated along the pro-nav trajectory. It is interesting to note that the maximum information path requires almost twice as much flight time as the proportional navigation path. Obviously, the extra time is being used to modulate the trajectory to improve its information content.

Of all the inequality constraints, only the boresight angle constraint is ever in effect. Also of concern but not included as a constraint is the boresight angle rate. Fortunately, the maximum boresight angle rate encountered along the maximum information path is around 54 deg/sec. This value can be achieved with current seekers.

FILTER PERFORMANCE

In this section, the performance of the extended Kalman filter along the maximum information (max-info) path is compared with that along the proportional-navigation (pro-nav) path. The intent is to show that, for filter problems with nonlinear dynamics and/or measurements, the performance of the filter should be a major consideration in the design of guidance laws.

For a given trajectory, measurements are created at every 0.02 seconds, which is the filter sample time. This is done by adding to the true azimuth and elevation (see (7)) zero-mean white noise with noise variance given by (9) and (10) where R is the true range. By using a prescribed trajectory to form the noisy measurements, the performance of the filter is studied independently of the guidance law.

The physical model on which the filter is based has been presented in the second section. It is assumed that the measurements of missile acceleration are perfect. However, accelerometers can only measure aerodynamic accelerations (due to drag, lift and thrust) so that the missile acceleration components in (1) are given by

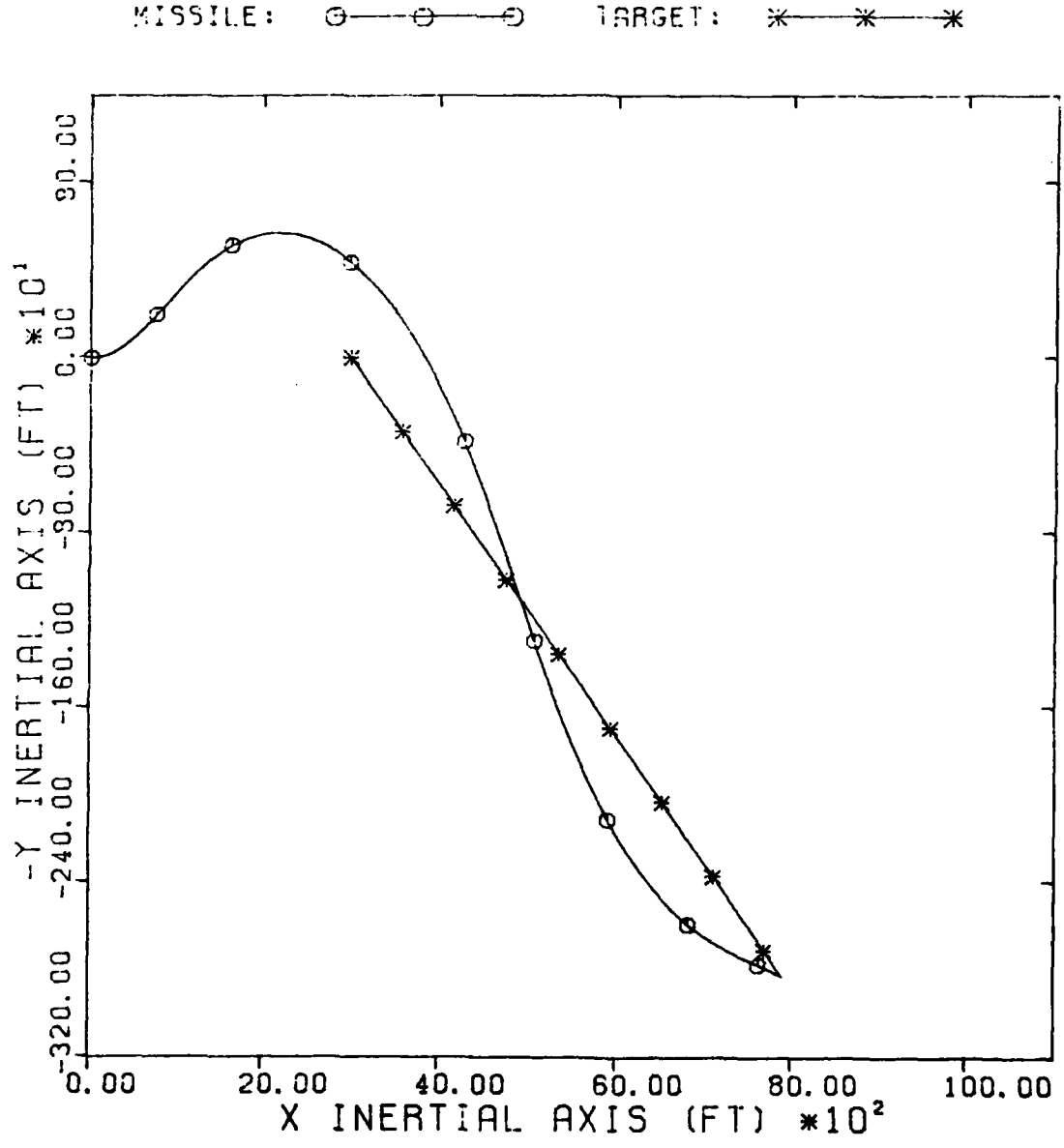


Figure 6. Maximum Information Trajectory, Horizontal Projection.

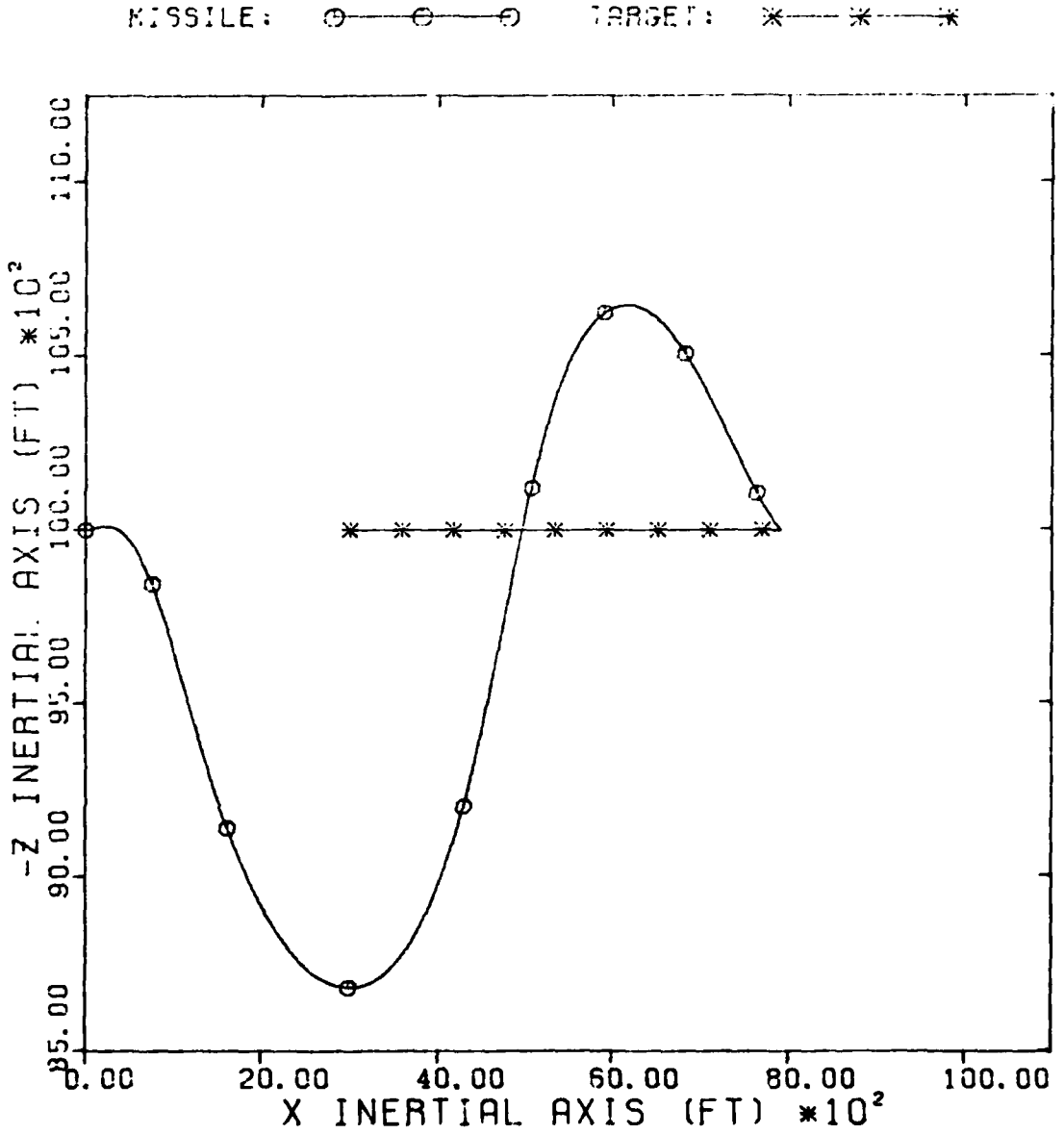


Figure 7. Maximum Information Trajectory, Vertical Projection.

$$A_{M_X} = \bar{A}_{M_X} \quad , \quad A_{M_Y} = \bar{A}_{M_Y} \quad , \quad A_{M_Z} = \bar{A}_{M_Z} + g \qquad (18)$$

where the bar denotes "aerodynamic" and $g = 32.2$ ft/sec^2 . The target maneuver time constant is chosen to be $\lambda_T = 1$. For this study, the process noise associated with the target model is assumed to be zero because the maximum information performance criterion is based on zero process noise. Finally, the measurement noise variance is calculated where $R \triangleq \hat{R} = [\hat{x}_R^2 + \hat{y}_R^2 + \hat{z}_R^2]^{1/2}$.

The range tracking errors (16) are plotted versus a normalized time, t/t_f , where t_f is the final time. All of the results presented here are the averages of 10 Monte Carlo runs. The runs are made, and the results of each sample time are averaged. To have a scale small enough to see the results, it has been necessary to eliminate the last three points from each curve. These points are not important because they are within times-to-go which are much smaller than the time constant of a typical autopilot and, therefore, would not have any effect on guidance accuracy.

For the first set of filter runs, the initial filter statistics are those presented in the previous section on Computer Simulation. The variances for the relative position and relative velocity are representative of measurements made with a good radar. The variances for the target acceleration components are based on a standard deviation of 5g. In Figure 8 the range tracking errors for the max-info path and the pro-nav path are presented. It is seen that range error for the max-info path increases during the first one-third of the trajectory and then steadily goes to zero over the last two-thirds of the path. For the pro-nav trajectory, the range error increases with time, and shows no sign of converging. Initially, the pro-nav path seems to lead to a smaller tracking error than the max-info path. However, if the errors are plotted versus time rather than normalized time, the initial error histories would be similar. In conclusion, the max-info path enables the filter to track the target, whereas the same is not true for the pro-nav path.

Figure 9 shows the effect of a +500-foot error in the relative position component $\hat{x}_R$. The filter uses an initial range of 3500 feet instead of 3000 feet. The conclusions reached are the same as those when there is no initial error. The max-info path enables the filter to converge to the true results, whereas the pro-nav path causes the filter to diverge on range and range-rate and converge to the wrong result in target acceleration. The results are the same when there are initial biases in velocity or acceleration.

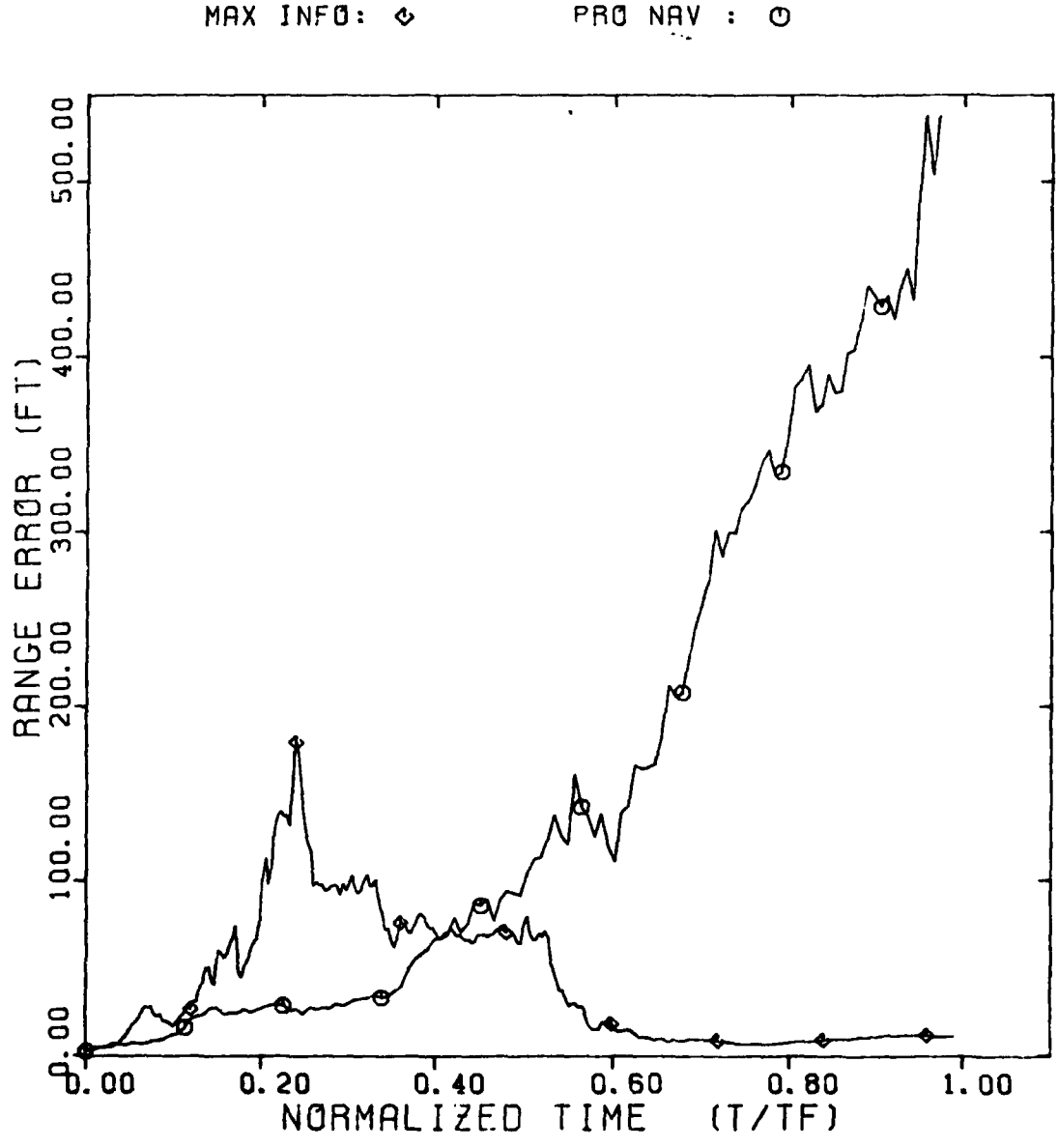


Figure 8. Range-Error History.

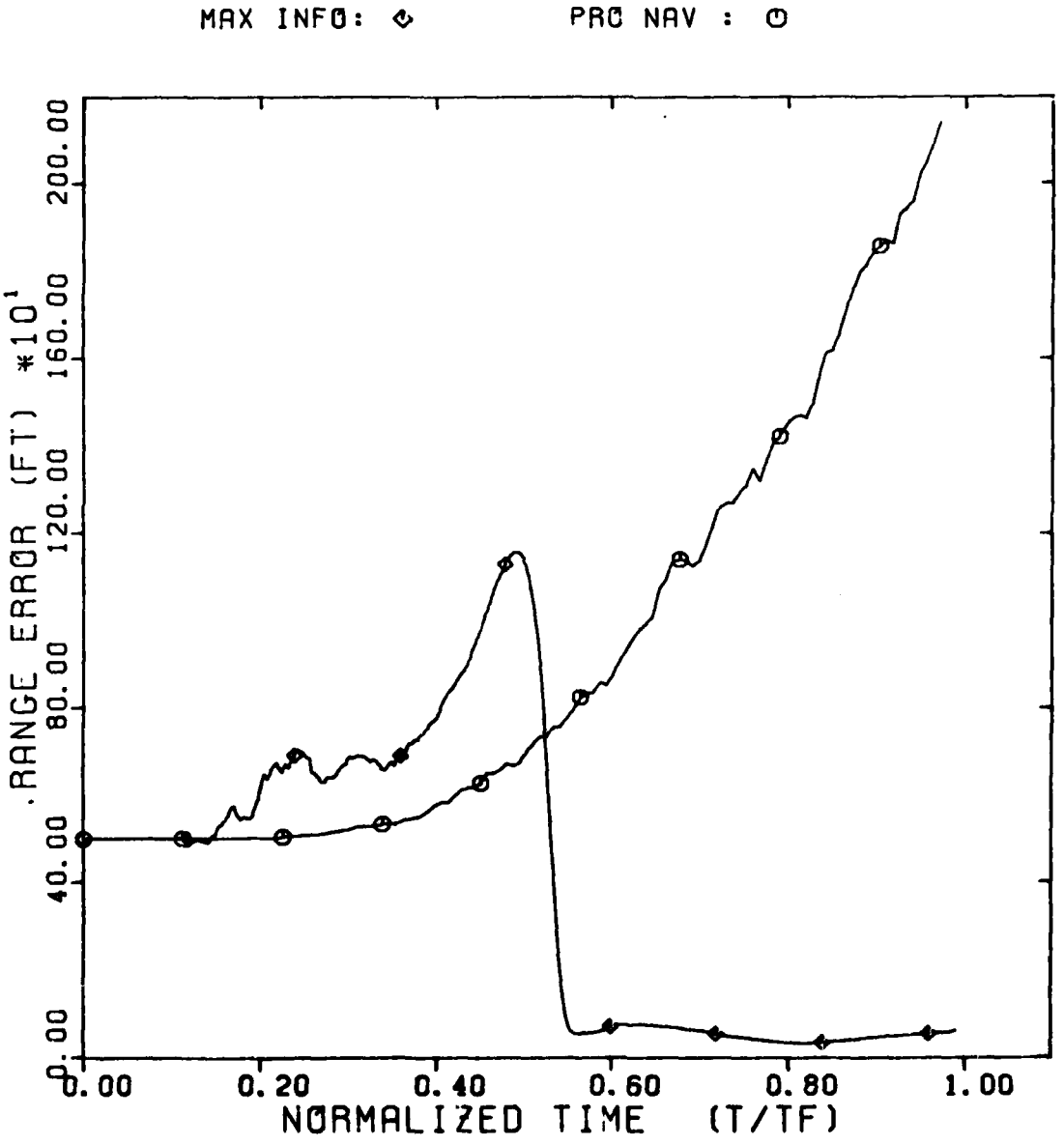


Figure 9. Range Error History, Initial Range Error = +500 ft.

DISCUSSION AND CONCLUSIONS

Three different directions are presented to improve the estimation of the homing engagement state space. First, a new filter structure is suggested which has global estimation capability, and in the presence of noise seems unbiased. Additional investigations are being performed to fully understand the properties of this new filter which is tailored to the homing engagement. Next, the remarkable improvement in terminal miss for a modern homing missile guidance rule, using an adaptive estimator to determine the measurement mean and variance on line, is discussed. Attempts to estimate the process noise variance associated with the target model on-line failed. This is partly due to the mismatch in models between the Gauss-Markov model assumed in the filter and the acceleration switching algorithm assumed in the simulation. Furthermore, the estimation of target acceleration still remains a problem. Possibly a combination of the use of the MGEKF, the inclusion of higher fidelity target models into the filter, and trajectory modulation may help elevate this difficulty. Possibly some type of event detection used in failure detection might also have some impact. Finally, trajectory modulation is shown to enhance the performance of the EKF. This aspect is extremely appealing in that the results of the section on Filter Structure showed that even for the noiseless case the EKF could not converge along the proportional navigation path when the initial errors are large. By increasing the observability, as done in the section on Estimation Enhancement, the region of convergence for the EKF enlarges. If trajectory modulation enhances the EKF, then it should also improve the MGEKF performance.

Our goals are to first establish the MGEKF as the standard filter for the homing engagement. Then, adaptive noise estimation will be used with the MGEKF to enhance its performance. Finally, the information performance index which is tailored for the EKF used in the homing engagement will be modified for the MGEKF where the observability Gramian is not local in the sense that the measurement function is linearized, although the observability Gramian is path dependent.

To realize the potential improvement in estimation by modulating the flight path, the guidance system has to be designed with this feature included. The information performance criterion developed here, although reasonably simple, does not lend itself to the development of easily implementable guidance laws. Furthermore, the property of enhanced estimation reduces the energy advantage between the missile and the target. Therefore, trajectory modulation should only be used when sufficient sensor degradation is perceived (which would be detected on-line). Furthermore, additional constraints must be imposed, such as terminal energy constraints, to ensure good terminal miss performance. Nevertheless, this type of information measure should be used to form the basis for guidance law development without the usual separation assumption.

REFERENCES

1. Aidala, V. J., "Behavior of the Kalman Filter Applied to Bearings-Only Target Motion Analysis," Advances in Positive Tracking, Vol. 1, NPS-62TS 77001, Naval Postgraduate School, May, 1977.

2. Lindgren, G. and Gong, F., "Position and Velocity Estimation Via Bearing Observations," IEEE Trans. on Aerospace and Electronic Systems, Vol. AES-14, No. 4, July 1978.

3. Nardone, S. C. and Aidala, V. J., "Observability Criteria for Bearing-Only Target Motion Analysis," IEEE Trans. on Aerospace and Electronic Systems, Vol. AES-17, No. 2, March 1981.

4. Speyer, J. L. and Song, T. L., "A Comparison Between the Pseudomeasurement and Extended Kalman Observers," Proceedings of the 20th IEEE Conference on Decision and Control.

5. Bryson, A. E. and Ho, Y.-C., Applied Optimal Control, Waltham, Massachusetts, Blaisdell, 1969.

6. Speyer, J. L. and Hull, D. G., "Comparison of Several Extended Kalman Filter Formulations for Homing Missile Guidance," Proceedings of the AIAA Guidance and Control Conference, August 11-13, 1980.

7. Myers, K. A., Filtering Theory Methods and Applications to the Orbit Determination Problem for Near-Earth Satellites, AMRL 1058, Applied Mechanics Research Laboratory, The University of Texas at Austin, 1973.

8. Speyer, J. L., Greenwell, W. M., and Hull, D. G., "Adaptive Noise Estimation and Guidance for Homing Missiles," Proceedings of the AIAA Guidance and Control Conference, August 1982.

9. Smith, R. C., "A Six-Degree-of-Freedom Computer Simulation of an Air-to-Air Missile Intercept," M.S. Thesis, The University of Texas at Austin, May 1979.

10. Speyer, J. L. and Hull, D. G., "Estimation Enhancement by Trajectory Modulation for Homing Missiles," Proceedings of the 1982 American Control Conference, Arlington, Virginia, June 1982.

11. Mehra, R. K., "Optimal Input Signals for Parameter Estimation in Dynamic Systems--Survey and New Results," IEEE Trans. on Automatic Control, Vol. AC-19, No. 6, pp. 753-768, 1974.

12. Fletcher, R., "An Ideal Penalty for Constrained Optimization," J. Inst. Maths. Applics., Vol. 15, pp. 319-342, 1975.

AD P001094

ROBUSTIFYING THE KALMAN FILTER VIA PSEUDO-MEASUREMENTS

DR. G. A. HEWER
and
ROBERT J. SACKS
RF Anti-Air Branch
Weapons Synthesis Division
Naval Weapons Center
China Lake, California 93555

ABSTRACT

This is a preliminary report on the current research on the applicability of robust Kalman filtering in monopulse radar tracking systems. (An estimation procedure is robust if small perturbations in the noise model from the assumed (Gaussian) noise model result in only small changes in the mean-squared-error of estimate.)

INTRODUCTION

In Hewer [1] a rationale for robust Kalman filtering in a monopulse radar tracking system was outlined. The primary purpose of this paper is to outline some subsequent research that complements the previous study.

The paper begins with a discussion of a basic pointing error control system. The purpose of the discussion is to outline the role of Kalman filter and to define pseudo-measurements. Next, within the context of pseudo-measurements, the robust statistical estimates of location and scale are outlined. For a Gaussian distribution location is equivalent to the mean and scale the equivalent to the standard deviation. Subsequently, some steady state Kalman filter analysis is introduced to indicate how the Kalman gain can be influenced by pseudo-measurements. Next, an executive summary of a planar simulation is highlighted. Finally, some plots of Kalman performance using robust and non robust pseudo-measurements are included.

BACKGROUND

Optimal guidance laws for accelerating targets depend on adequate estimates of key states such as line-of-sight rate and target normal accelerations. When optimum state estimates of these parameters are available, superior missile performance can be demonstrated. These estimates are usually provided by some Kalman filter algorithm. In the classical Kalman filter, noise sources are characterized by uncorrelated Gaussian statistics. Unfortunately, as the research of Masreliez and Martin [2] demonstrates, the behavior of Kalman filter algorithms can be severely degraded when

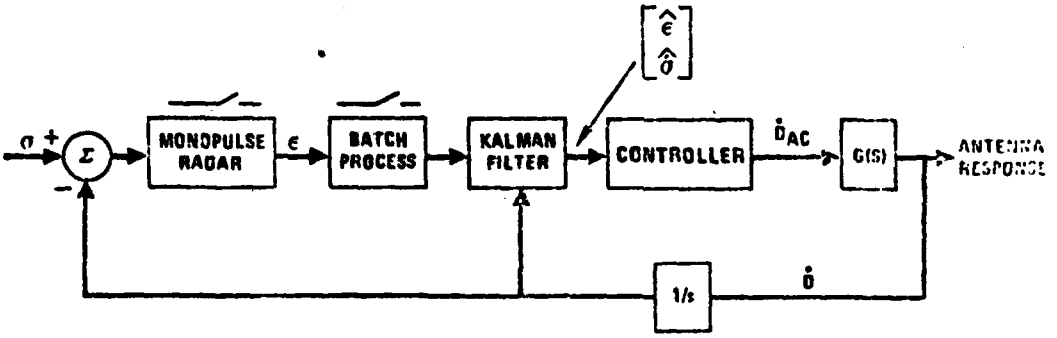
the actual noise disturbances are non-Gaussian, particularly when the non-Gaussian behavior is heavy tailed. The latter behavior is characterized by outliers. In monopulse radars this heavy tailed non-Gaussian behavior is present in the angle tracking signals because of target glint. A monopulse tracker will turn until the central axis of the receiver antenna is aligned with the normal of the incoming (scattered) wavefront. For a point target the scattered wavefront is spherical, and thus the gradient is always along a radial vector directed from the receiver aerial to the target. A complex target is composed of a number of spatially separated scatterers and thus the spherical wavelets from the individual "point" scatterers will interfere. As a result of this interference, the phase of the received signal will not, in general, be independent of the target aspect. The component of the phase gradient vector orthogonal to the radial direction is directly related to tracking error. It is this type of error that constitutes glint. Since the phase of a complex target varies as a function of target aspect and motion, the statistics for the Kalman filter are non-stationary. Thus, the Kalman filter must adapt to the non-stationary glint statistics.

The basic angle tracking loop is defined in Figure 1 which is based on the discussion by Pearson and Stear [3]. In their paper they did not explicitly include any discussion of the batch processing block. In fact, the batch processing block is purely optional in a tracking loop unless the pulse repetition rate of the radar is much higher than the requisite tracking rate and the block is included to facilitate digital processing requirements. For whatever reason, whenever the input to the Kalman filter is a set of statistics derived from a sample of the radar measurements, these measurement statistics will be called pseudo-measurements. This is to distinguish the altered measurements from the basic measurements that are available directly from the radar.

The angles in Figure 1 are defined in Figure 2. These angles are defined, respectively, as the angle pointing (boresight) error epsilon, the line of sight to the target sigma and the dish (antenna) angle D. In Figure 1 a pseudo-measurement of epsilon is the single input to the Kalman filter, while the output is an estimate of epsilon and a reconstructed estimate of the line of sight rate sigma. This is combined in a linear fashion as outlined by Pearson and Stear [3] and is a command input to the antenna. The loop is then closed as indicated in Figure 1 and discussed in Hewer [1]. Mehra [4] has addressed the problem of identifying the measurement noise for an autonomous multi-variable discrete linear Kalman filter.

ROBUSTIFYING THE KALMAN FILTER

A statistical procedure is resistant if the value of estimate is insensitive to a small change in all of the data values or to large changes in a few of the data values. According to Huber [5] this is a working definition that can be used to define robustness.



ϵ – ANGLE POINTING ERROR

σ – LOS RATE

$\dot{D}$ – ANTENNA RATE

$\dot{D}_{AC}$ – COMMANDED ANTENNA RATE

FIGURE 1. Pointing Error Control System.

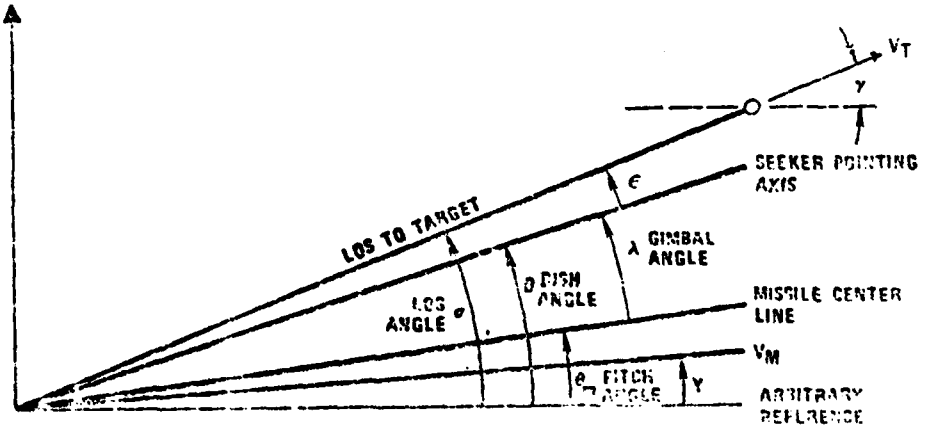


FIGURE 2. Two Dimensional Geometry.

In Hewer [1] a plot of linear glint is presented which clearly exhibits the presence of outliers (glint spikes) that are intrinsic in the glint signature. The glint was generated for a complex target using a radar target model developed by Mumford [6]. Mumford's model computes the backscatter from a complex target by decomposing the complex target into simple component shapes for which scattering solutions have been derived. This modeling technique is known informally as "N-shape" modeling. Angular glint is defined as the linear displacement of the center of radar reflection from the defined physical center of the target measured along a line in the plane passing through the target center, at right angles to the sightline, to the physical center. Its magnitude is equal to the tangent of the angle between the true and apparent directions of the target times the range. Linear glint is simply range independent angular glint. Thus, the strategy of robustifying the Kalman filter is based on making it resistant to glint spikes. There are at least two ways to implement this strategy. The first way is to preprocess the monopulse radar pulses in a robust manner using summary statistics as inputs to the pointing error control system flowcharted in Figure 1. This is a natural approach in tracking radars, since the radar pulse rate is much higher than the requisite tracking rate. The second way is based on the robustified Kalman filter developed by Masreliez and Martin [2] and refined by Martin [7]. Both of these techniques rely on influence functions that are outlined in this section.

Generally, for a complex target, the resulting glint signature is a non-stationary time series. Thus, both robust techniques rely on adaptive noise estimates of the input noise statistics. For the moment we ignore the interaction of target maneuver and the glint signature. The two pseudo-measurements of the input noise that are required are an estimate of location and scale. For a symmetric distribution estimate of location is the center of the distribution, while an estimate of scale is the spread of the distribution. For a Gaussian distribution the maximum likelihood estimate of location is the mean, and scale is the standard deviation. For the moment in this discussion, the correlation structure in the glint signature is also ignored. As amply demonstrated by Tukey [8] for non-Gaussian heavy tailed symmetric distributions, these classical estimates are unsafe.

Following Martin [9], the following definitions are introduced for completeness. Let $x_1, \ldots, x_n$ denote a univariant data sample. A statistic is simply a function of the data $T(X) = T(x_1, \ldots, x_n)$. An estimator is a statistic whose value is supposed to provide an indication of a parameter in a parametric model for the data. A real scalar-valued estimate is translation invariant if, for any real number C and the constant n-dimensional unit vector 1

$$T(X + C1) = T(X);$$

translation equivariant if

$$T(X + C1) = T(X) + C;$$

scale invariant if for any real constant $C > 0$

$$T(CX) = T(X);$$

and scale equivariant if

$$T(CX) = CT(X).$$

The sample mean

$$T(X) = \frac{1}{N} \sum_{i=1}^{N} X_i$$

is translation and scale equivariant. The sample standard deviation

$$S(Y) = \frac{1}{N-1} \sum_{i=1}^{N} (X_i - T(Y))^2$$

is translation invariant and scale equivariant. The robust estimate of scale CMADM = Median Absolute Deviation from the Median = median $|X_i$ - median $(Y)|/.6745$ is translation invariant and scale equivariant. The divisor .6745 makes CMADM a consistent estimate of the standard deviation if the sample is drawn from a normal population. This is an appealing feature of CMADM since an operating principle of this robust filter study is that the robust estimates should protect against glint spikes and yet provide a good sampling efficiency on Gaussian noise. Recall that at long ranges, thermal noise will be predominate while at close range glint noise will be dominant [10]. Thus, estimators that are effective over a class of distributions are required. A definition of relative efficiency and the effect of distribution shape on the relative efficiency of an estimator is discussed in Mosteller and Tukey [11, p. 17]. Other guidelines of efficiency for different estimators are found in the studies by Andrews et al [12], Gross [13], Martin and Goodfellow [14] and Lax [15]. For exploratory data analysis an operational definition of relative efficiency is the ratio of the minimum estimator to other compatible estimators. This ratio can be established by Monte Carlo studies or for some estimators by direct analysis. As an example, the median provides a more robust estimate of location than the mean on non-Gaussian heavy tailed distributions, and yet both estimators converge in probability to the mean on Gaussian distributions. For large samples from a Gaussian distribution, the sample mean has a variance of about σ^2/N, and the median has a variance of about $\pi\sigma^2/2N$. Thus, the relative efficiency of the median is about $2/\pi \approx .64$, which means that the median requires a sample of 100 to give the same level of precision as mean with a sample of 64.

Relative efficiency is gauge of the number of samples required for a class of estimators to do the same job. Fortunately, other estimators of location and scale exist that show better relative efficiency than the median and CMADM over a given set of distributions.

Before introducing these estimators, the concept of an influence function is introduced. In this discussion only some heuristic aspects of an influence function will be noted. A more complete discussion of influence functions is found in Huber [5] and Hampel [16]. In exploratory data analysis the influence function displays the general shape of the effect of one value of x on each estimator. Some plots of common influence functions are found in Figures 3 and 4 in Mostellar and Tukey [11]. Consider the sample mean which can be written in the simple form

$$\frac{1}{N}\sum_{i=1}^{N} X_i = \frac{1}{N}\left(\sum_{i=1}^{N-1} X_i + X_N\right)$$

for a fixed sample size N. Clearly, the variation in the value of the sample mean varies linearly without bound as one value of the sample is changed. Suppose the expectation of the sample is zero and consider the variance of the sample

$$\frac{1}{N}\sum_{i=1}^{N} X_i^2 = \frac{1}{N}\left(\sum_{i=1}^{N} X_i^2 + X_N^2\right).$$

For a fixed sample size, as the absolute value of one sample goes to infinity, eventually the variance becomes unbounded at a quadratic rate. Some influence functions are graphed in Figure 3. The linear influence curve in Figure 3(i) is the influence curve for the sample mean, and shows that the sample mean is directly affected by a change in one data point. The influence curve labeled (Figure 3(ii)) is Huber's monotone function and the influence curve (Figure 3(iii)) is Hampel's two-part redescending function. The role of these influence functions in robust statistics is discussed in Huber [5]. Both of the latter influence functions ignore changes in measurement outside of a band and respond within the band; thus, outliers outside the acceptance band are rejected. The influence curve (Figure 3(ii)) is a light limiter, which could correspond to a common robustifying policy of setting outliers beyond a certain value, say 3 sigma, to a constant. Another influence function is a "hard rejection" which is defined by

$$\psi(t) = \begin{cases} t & |t| \leq C \\ 0 & |t| > C \end{cases}.$$

The parameter C is called the cutoff parameter. It governs the role that an influence function will have in weighting or rejecting data values.

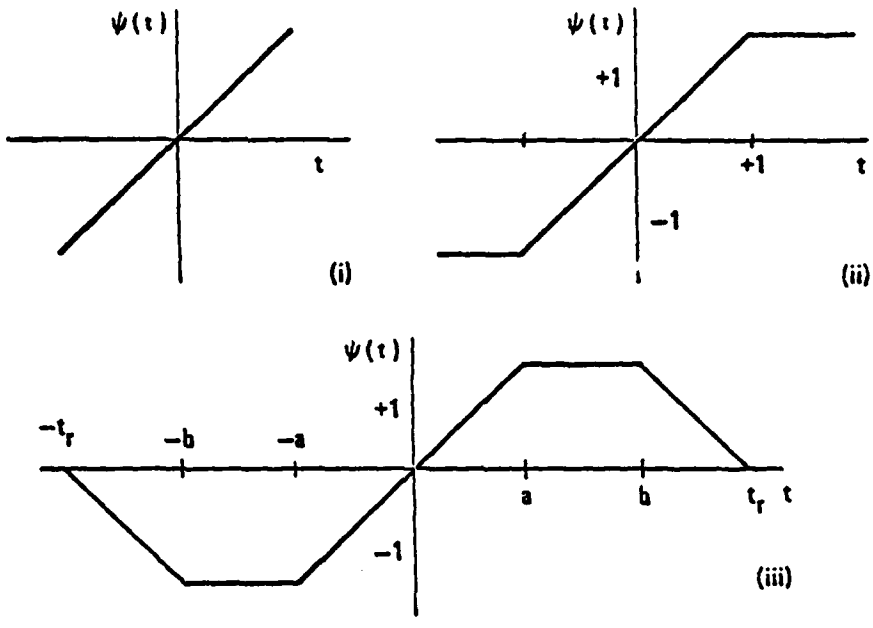


FIGURE 3. Influence Functions.

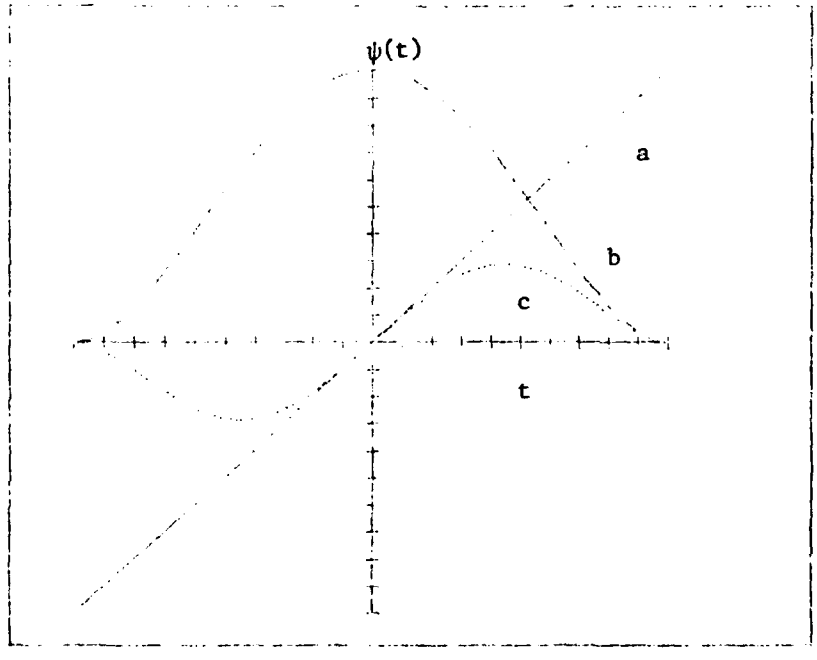


FIGURE 4. Influence Functions.

Two other important influence functions are Tukey's "bisquare"

$$\psi(t) = \begin{cases} t(1 - (t/C)^2)^2, & |t| \leq C \\ 0 & |t| > C \end{cases}$$

and "biweight"

$$\psi(t) = \begin{cases} (1 - t^2)^2, & |t| < 1 \\ 0 & \text{elsewhere} \end{cases}$$

Curves labeled a, b and c in Figure 4 represent, respectively, the linear, biweight and bisquare influence functions.

An M estimate is defined by Huber to be a solution of the equation

$$\sum_{i=1}^{N} \psi(X_i - T(X)/CS) = 0$$

where C is a scale parameter, S is a translation invariant and scale equivariant estimate of scale and $\psi(\cdot)$ is an influence function. Clearly, the influence functions included in the preceding paragraph are not always continuous or monotone. Their properties as real variables will govern the existence and characteristics of an M estimate. However, for completeness, we note that Hampel [16] proposed that a robust estimate should have an influence curve which is bounded, continuous and have compact support (i.e., the function is identically zero outside a finite region). Boundedness prevents a single observation from having a large (literal) influence on the estimate. Note that the influence curves of the mean and variance are not bounded. A continuous influence function insures that rounding and grouping produce only small changes in the estimate. Compact support ensues that ridiculously large observations have no effect on the estimate. Other rigorous matters about M estimates are discussed in Huber [5].

The biweight estimate, which is an abbreviation for bisquare weight, is the most promising pseudo-measurement for location.

The biweight estimate is an M estimate that uses a bisquare influence function. The estimates T and S are taken as simultaneous solutions of

$$\sum_{i=1}^{N} \psi((X_i - T)/CS) = 0$$

and

$$S = \text{median}|X_i - T|.$$

The asymptotically correct Tukey [11, p. 208] variance for the biweight estimate T of location is

$$V = \frac{(CS_0)^2 \sum_{i=1}^{N} \psi^2(U_i)}{\left(\sum_{i=1}^{N} \psi'(U_i)\right)\left(-1 + \sum_{i=1}^{N} \psi'(U_i)\right)}$$

where $U_i = (X_i - T)/CS_0$ with S_0 taken as an estimate of the scale of the sample and C a positive cutoff parameter. Note that the derivative is

$$\psi'(t) = \begin{cases} (1 - t^2)(1 - 5t^2), & |t| < 1 \\ 0 & \text{elsewhere} \end{cases}.$$

If the data is "clustered" near the estimate of location T as determined by the scale S_0 and cutoff C, so that U_i^2 becomes negligible over all the samples, then V becomes approximately equal to

$$\frac{1}{N(N-1)} \sum_{i=1}^{N} (X_i - T)^2,$$

which is a reasonable formula for the variance of T. Note that if $\psi(U) = u$, then V reduces to the variance of the mean. These estimates are also discussed in Gross [13] and Lax [15]. When pseudo-measurements are used to adaptively adjust the Kalman gain, then the location estimate of boresight error and estimated variance V of T are the input statistics to the Kalman filter. When the noise is Gaussian, then these estimates are the sample mean and the standard error $S(X)/\sqrt{N}$. When the data is non-Gaussian, then the meaning of the standard error is dependent on how much information resides in the tails. For this reason, biweight variance formula is appealing because it reduces to known quantities. On the other hand, CMADM asymptotically is an estimate of the standard error for Gaussian distributions. However, CMADM is ancillary estimate of scale when used with biweight and not a direct measure of its variability.

Thus, a Kalman filter can be robustified in at least two ways. The first is to imbed an influence function within the Kalman derivation or to use influence functions to obtain the pseudo-measurements. The latter approach is taken in this paper; while the approach is conceptually simple, a rigorous framework for this methodology is apparently incomplete. The former approach is developed in Masreliez and Martin [2] and will be investigated elsewhere.

SIMULATION DESCRIPTION

This section provides an executive summary of the planar simulation with specific details to appear elsewhere. Figure 5 depicts a flow chart of the simulation components. The target is modeled as a point mass and is coplanar with the interceptor. The target kinematics block specifies target motion with respect to an inertial reference frame. This information is combined with the missile velocity in the kinematics block to provide range, closing velocity and line of sight to target (LOS). The dish angle D is subtracted from the LOS angle to provide pure boresight error ε. As in Hewer [1] ten percent contaminated normal noise is added to the boresight error signal. The contaminated model was generated as the mixture of two normal distributions, each with zero mean and one with variance equal to observation variance and one with ten times the first variance. Let us denote these distributions as N(0,R) and N(0, 10R), respectively, The mixture of the two distributions defined as

$$F(x) = pN(0,R) + (1 - p)N(0, 10R) \quad 0 < p < 1$$

generates the contaminated normal distribution. The random variable X with this distribution can be generated by first taking a uniform deviate U; if U < p, X is generated by independent samples from N(0, R) and otherwise choose N(0, 10R).

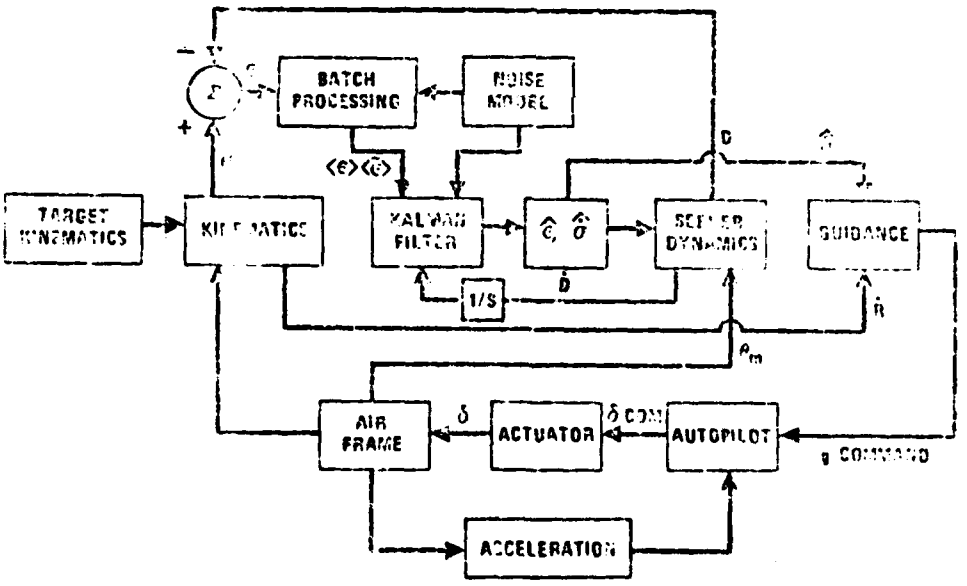


FIGURE 5. Simulation Flow Chart.

The guidance law used is proportional navigation, wherein commanded gees is proportional to the product of the closing velocity and the estimated LOS rate. A commanded wing deflection angle is provided by the autopilot block. The commanded deflection rate is

modeled as a linear combination of the error signal between commanded gees and actual gees and the missile body angular rate. The specific gains are functions of missile altitude. The commanded rate is then integrated and limited to provide the deflection angle command.

The actuator model computes the slew rate $\dot{\delta}$ from the net torque on the control surface. The total torque is given as the difference between the applied torque, which is modelled as a limited term proportional to the difference between commanded and actual deflection angle, and the sum of the aerodynamic hinge torque and a damping torque proportional to $\dot{\delta}$. The total torque is divided by the wing and actuator inertia, integrated, limited, and integrated again to obtain the deflection angle δ.

The airframe block computes the aerodynamic lift and drag forces and torques, gravitational forces and thrust forces acting on the missile body. The lift and drag forces are composed of two components. One component represents the force exerted by the discrepancy between the airflow direction and the missile body orientation. The second component represents the control force exerted by the angular difference of the airflow direction and the wing orientation. Specific models for the aerodynamic forces and torques are given elsewhere. The sum of the lift force and the components of gravity and thrust perpendicular to the missile velocity vector is computed to provide the normal acceleration which turns the missile (actual gees). The aerodynamic pitching moment is computed, divided by the missile inertia and integrated to obtain body angular rate used by the seeker control loop. The missile velocity used in the kinematics block is obtained from the velocity components in inertial space. The velocity components are obtained from the inertial components of the total force acting on the missile.

DISCUSSION OF THE ANGLE-TRACKING FILTER MODEL

The dynamics of the angle track filter used in the 3 DOF simulation is a discretization of Equation 1 given by

$$\dot{x} = Fx + Ga \tag{1}$$

with

$$x = \begin{pmatrix} \varepsilon \\ \dot{\sigma} \end{pmatrix}, \quad F = \begin{bmatrix} 0 & 1 \\ 0 & 0 \end{bmatrix}, \quad G = \begin{bmatrix} 0 \\ 1 \end{bmatrix}$$

and a(t) is a white noise process with variance q. The above "random walk velocity" model is discussed by Fitzgerald [16] as a limiting case of the exponentially correlated velocity model as the correlation time parameter approaches infinity.

The associated measurement model is given by

$$Z = Hx + v$$

with $H = [\ 0 \quad 1\ ]$ and $v(t)$ is a white noise process with variance r. The associated state covariance matrix P solves the continuous Riccati equation

$$\dot{P} = FP + PF^T - PH^T R^{-1} HP + Q$$

with $R = r$ and $Q = \begin{bmatrix} 0 & 0 \\ 0 & q \end{bmatrix}$. The Kalman filter gain vector

$K = \begin{bmatrix} K_1 \\ K_2 \end{bmatrix}$ is then given by

$$K = PH^T R^{-1}.$$

The steady state gains are computed by setting $\dot{P}=0$, solving for P and then computing k. The steady state gains are found by Fitzgerald [17] to be given by

$$K_1 = \sqrt{2}\ (q/r)^{1/4}$$

$$K_2 = (q/r)^{1/2}.$$

These equations show that the steady state gains are a function of the process noise variance and the measurement noise variance solely through their ratio. This is a desirable property as the size of the gains determine the degree to which the state predictions are adjusted by the discrepancy between prediction and measurement. They exhibit that the adjustments are determined by the relative credibility of the state model and the measurement model.

The sampled data version of Equation 1 is found by discretizing the continuous state solution given by

$$x(t) = e^{Ft}x(0) + \int_0^t e^{F(t-w)}Ga(w)dw$$

so that

$$x(K) = \Phi(K-1,K)x(K-1) + u(K)$$

with sampling interval Δt, when

$$\Phi(K-1,K) = e^{\Phi \Delta t}$$

$$u(K) = \int_{(K-1)\Delta t}^{K\Delta t} e^{F(K\Delta t - w)}Ga(w)dw.$$

The state transition matrix is $\Phi(t) = \begin{bmatrix} 1, & t \\ 0, & 1 \end{bmatrix}$.

The process noise covariance matrix Q(K) is obtained as

$$Q(K) = E[u(K)u^T(K)]$$

$$= \int_{(K-1)\Delta t}^{K\Delta t} \int_{(K-1)\Delta t}^{K\Delta t} \begin{bmatrix} K\Delta t-w \\ 1 \end{bmatrix} [K\Delta t-v \quad 1] E(a(w)a(v))dwdv$$

$$= q \int_{(K-1)\Delta t}^{K\Delta t} \begin{bmatrix} (K\Delta t-w)^2 & K\Delta t-w \\ K\Delta t-w & 1 \end{bmatrix} dw$$

as

$$E(a(w)a(v)) = \begin{cases} 0 & \text{if } w \neq v \\ q & \text{if } w=v. \end{cases}$$

Upon integrating,

$$Q(K) = \begin{bmatrix} 4/3\ q(\Delta t)^3 & 1/2q(\Delta t) \\ 1/2\ q(\Delta t)^2 & q(\Delta t) \end{bmatrix}.$$

The dependence of the steady-state Kalman gain values on the noise variance ratio is preserved in the sampled model. This is proven below for a more general model. Let the discrete steady-state covariance and gain propagation equations be given by

$$P = \Phi P \Phi^T + Q \tag{2}$$

$$K = PH^T[HPH^T + R]^{-1} \tag{3}$$

$$P = [I-KH][\Phi P \Phi^T + Q] \tag{4}$$

Theorem I:

If P and K are solutions for the discrete Kalman filtering problem with the dimension of H 1 x N, process covariance matrix Q and noise variance r=1, then r'P and K are solutions with process covariance matrix r'Q and noise variance r'.

Proof:

Multiplying Equation 4 by r' shows that r'P and K satisfy Equation 4 if P and K are steady-state solutions with Q replaced by r'Q. Assuming that r'P and K are steady-state solutions to a Kalman filtering problem, then substitution of these quantities into Equation 2 implies that the resulting steady-state prediction covariance matrix is r'P where P is the corresponding matrix for the pair

(P,K). The pair (r'P,K) satisifies Equation (3) since

$$r'PH^T[Hr'PH^T + r']^{-1} = PH^T[HPH^T + 1]^{-1} = K.$$

Thus (r'P,K) is a steady-state solution to the Kalman filtering problem with process covariance matrix r'Q and noise variance r'.

The above result implies that for a discrete Kalman filter, keeping the elements of the process noise covariance matrix Q in fixed ratio to the measurement noise variance leads to the same value for the Kalman gain vector.

Figures 6 and 7 exhibit the dependence of K_1 and K_2 on the quantity L = log (q/r) for a specific sampling time. Steady state values were achieved by running through several iterations of the Bierman UD Kalman filter algorithm. This algorithm is not bothered by numerical stability and is guaranteed to give the correct steady state solution.

RATIONALE FOR USE OF ROBUST STATISTICS IN THE KALMAN TRACKING FILTER

It is well known that the sample mean and sample variance are optimal estimators of location and scale for Gaussian samples. Here optimality refers to the property of possessing, minimum variance among the class of unbiased estimators. These estimators are not minimum variance when the samples are symmetric heavy-tailed non-Gaussian.

The effect of glint spikes on the batched processed sample mean and standard deviation is discussed in Hewer[1]. Therein the N shape scatterer models of Mumford [6] are used to represent models of non-Gaussian boresight error data contaminated by glint. When large glint spikes occur, the batch averaged boresight error can be pulled off, and the standard deviation can be inflated by as much as an order of magnitude. The effect on the Kalman filter is twofold: (1) a misleading filter innovation will arise in the correction equation due to the glint spikes, and (2) the inflated estimate of the boresight error variance r will reduce the value of the Kalman gains perhaps to the point where the filter can no longer track a maneuver. This simple example illustrates that non robust pseudo-measurements can adversely effect the Kalman gains.

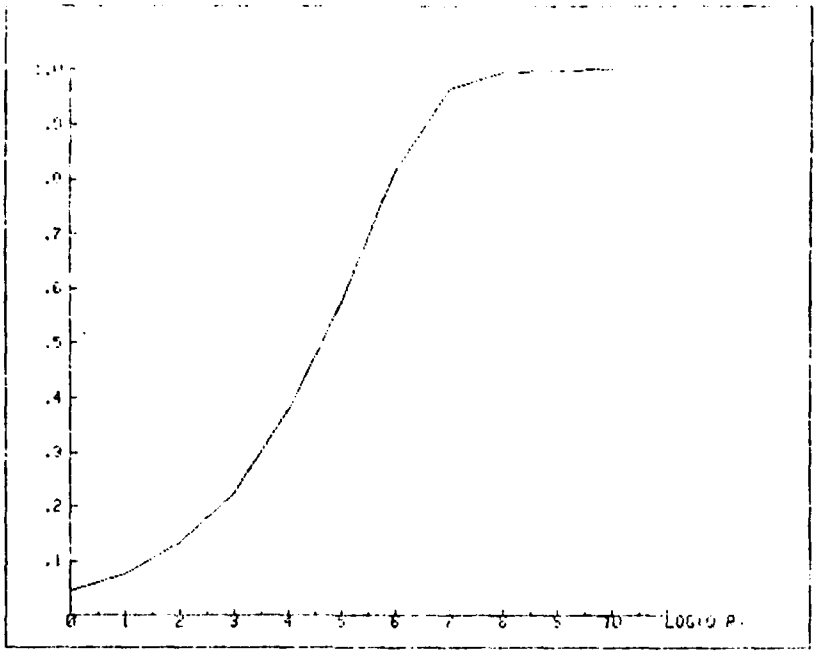


FIGURE 6. K_1 Vs Log Q/R.

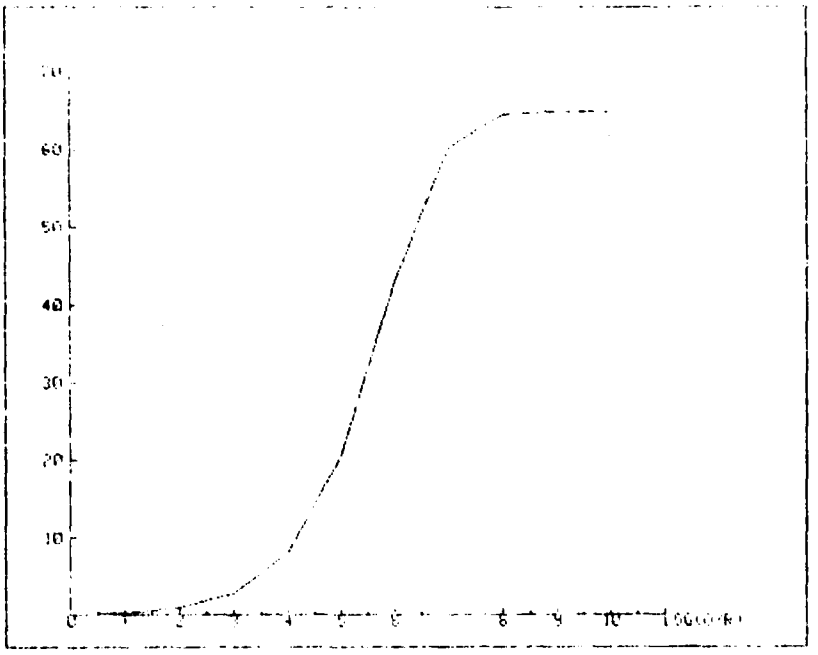


FIGURE 7. K_2 Vs Log Q/R.

SIMULATION RESULTS

In this section, some tentative but suggestive simulation results are presented. These results are not intended to be statistically significant. They do, however, suggest that results in Hewer [1] and this paper are indicative of the difference between robust and non robust pseudo-measurements in a given system. For this study a sample size of twenty was selected for the batch processor, primarily because it corresponds to the sample size of Gross [13], Lax [15] and Martin [14] in their small sample Monte Carlo studies. In addition, a typical segment of this result is presented simply to indicate the Kalman filter behavior.

Figures 8 and 9 are plots of the pseudo-measurements of location, while Figures 10 and 11 are pseudo-measurements of its associated scale. Since these are self scaling plots the range of the estimators properly reflected by the plots. The first consistent pattern that had been predicted by Hewer [1] is that robust estimator of scale CMADM is resistent to the outliers generated by the contaminated normal noise model. In fact, by colocating the outliers from the scale plots, corresponding location values can be compared. These plots also indicate that biweight is generally more resistent to outliers. This conclusion is consistent with the plots in Hewer [1] using the Mumford [6] N-shape target model glint signatures. Since the location and scale pseudo-measurements determine the corresponding filter gains, they exhibit a similar behavior, namely, the robust gains are generally larger and are not severely reduced by outliers.

CONCLUSION

Based on this very preliminary sample, the robust pseudo-measurements perform in a planar simulation as predicted. A more definitive conclusion will be based on more typical target signatures and maneuvers. In addition, future simulations will incorporate the asymptotically consistent biweight estimator of scale, instead of ancillary estimate of scale CMADM.

ACKNOWLEDGMENT

The author would like to acknowledge Dr. E. B. Royce, Head, Research Department (Code 38), Naval Weapons Center, China Lake, California and Dr. Gerhard Heiche, Naval Air Systems Command (NAVAIR-03C), Washington, D. C. for their financial support of this research.

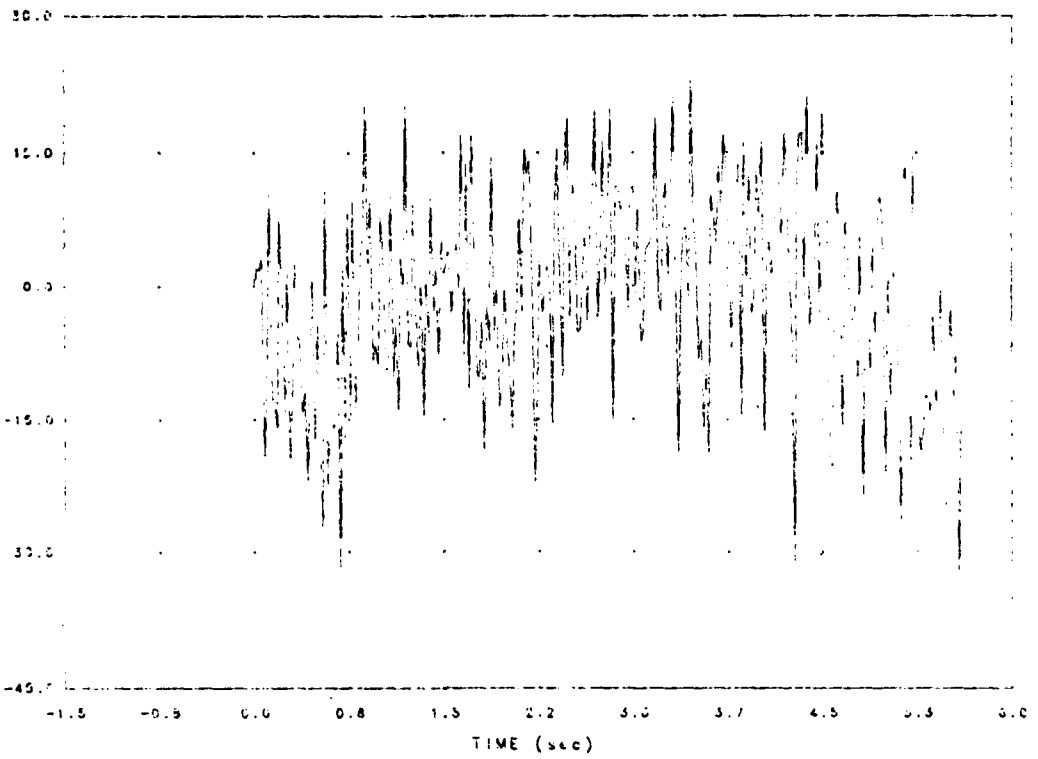


FIGURE 8. Boresight Error (Mean).

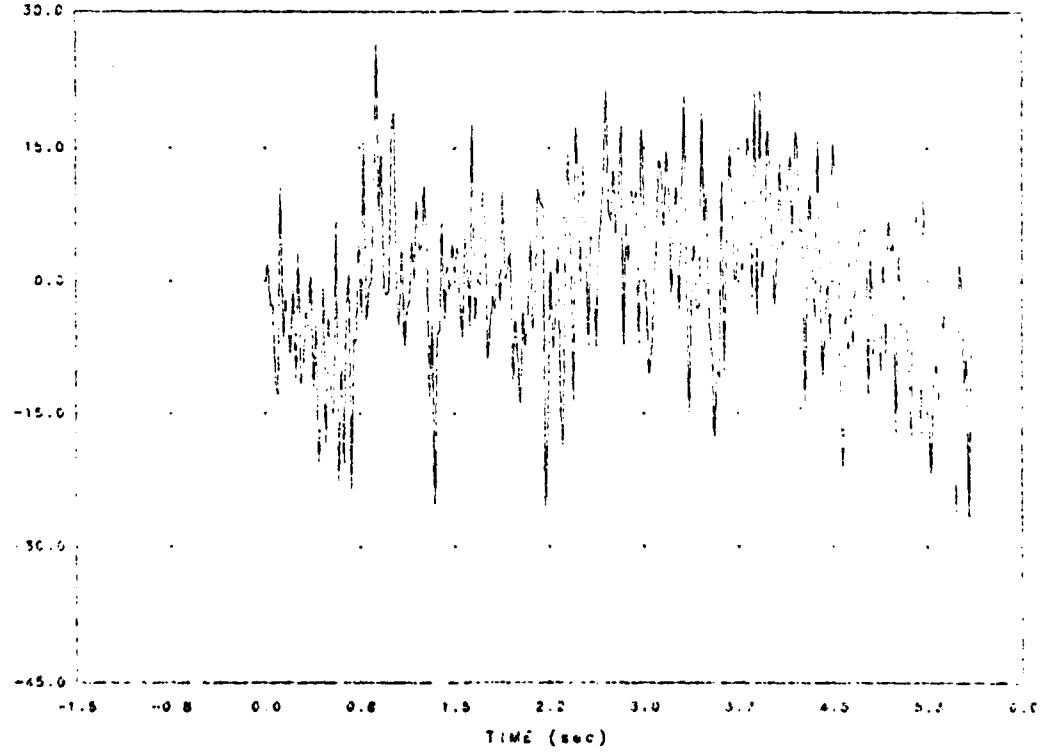


FIGURE 9. Boresight Error (Biweight).

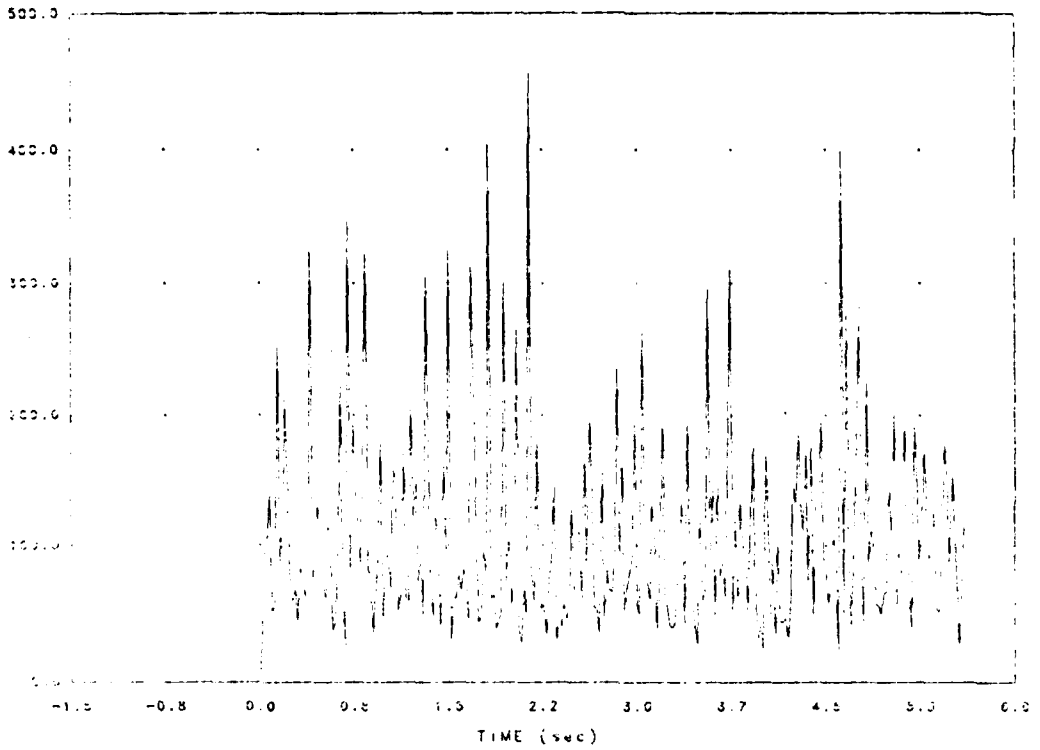


FIGURE 10. Scale Estimate (Variance).

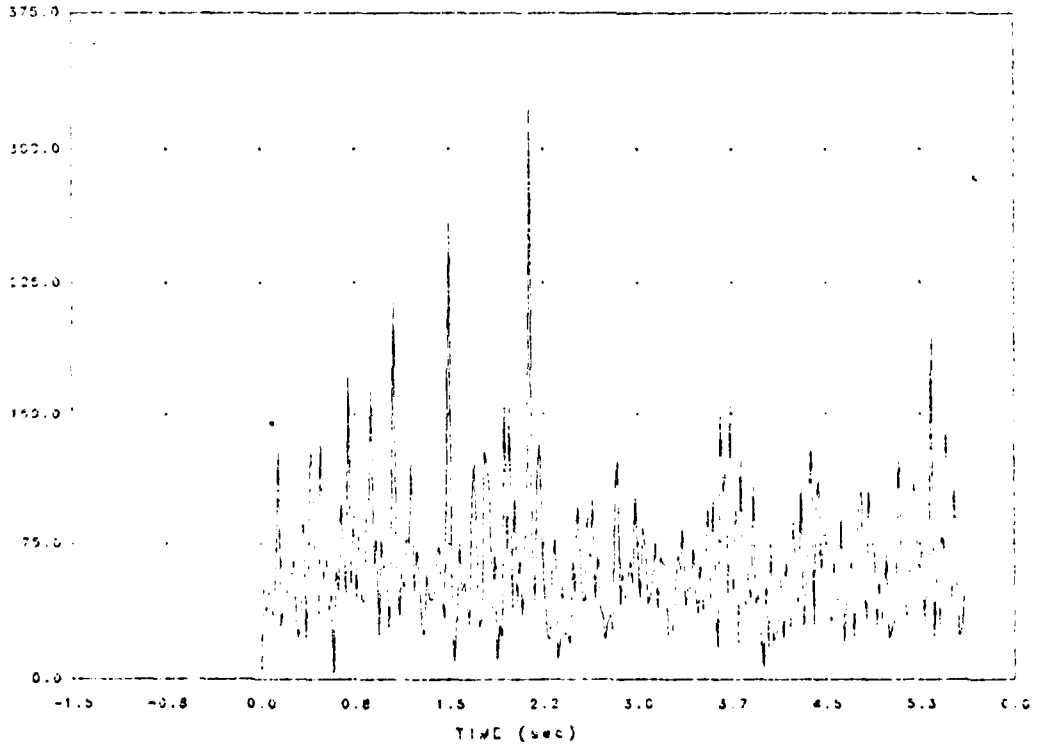


FIGURE 11. Scale Estimate (CMADM).

REFERENCES

1. Hewer, G. A. "Robust Kalman Filtering," Proceeding of the Third Meeting of the Coordinating Group on Modern Control Theory, AD A109134, Oct. 1981.

2. Masreliez, C. J. and R. D. Martin. "Robust Bayesian Estimation for the Linear Model and Robustifying the Kalman Filter," IEEE Trans. on Auto. Control, AC-22, pp. 361-371.

3. Pearson, J. B. and E. B. Stear. "Kalman Filter Applications in Airborne Radar Tracking," IEEE Trans. on Aero and Elec. Systems, AES-10, 1972, pp. 319-329.

4. Mehra, R. K. "On the Identification of Variances and Adaptive Kalman Filtering," IEEE Trans. Auto. Control, AC-15, April 1970, pp. 175-184.

5. Huber, P. I. "Robust Statistics," John Wiley, New York, 1981.

6. Mumford, M. L. "Reflections Upon Target Modeling," Naval Weapons Center, Technical Memorandum 4124, Naval Weapons Center, China Lake, CA, 1980.

7. Martin, R. D. "Approximate Conditional Mean Type Smoothers and Interpolators," Heidelberg Workshop on Smoothing Techniques for Curve Estimation, Heidelberg, Germany, 1979.

8. Tukey, J. W. "A Survey of Sampling from Contaminated Distributions," Contributions to Probability and Statistics, Ed. Olkin, Ingram and others, Stanford University Press, Stanford, CA, 1960.

9. Martin, R. D. Unpublished Lecture Notes, Dept. of Statistics, University of Washington, Seattle, Washington, 1980.

10. Barton, D. K. "Radar System Analysis," Artech House, 1979.

11. Mosteller, F. and J. W. Tukey. Data Analysis and Regression, Addison-Wesley, London, 1977.

12. Andrews, D. F., et al. "Robust Estimators of Location: Survey and Advances," Princeton Univ. Press, Princeton, NJ, 1972.

13. Gross, A. M. "Confidence Interval Robustness with Long-Tailed Sysmetric Distributions," Jour. of Amer. Stat. Assoc., Vol. 71, 1976, pp. 409-416.

14. Martin, R. D. and D. M. Goodfellow. "Small Sample Behavior of Robust Stochastic Approximation and Iterated Weighted Least Squares Estimates for Location," Private Communications, 1981.

15. Lax, D. A. "Robust Estimators of Scale: Finite-Sample Performance in Long-Tailed Symmetric Distributions," Private Manuscript, 1982.

16. Hampel, F. "The Influence Curve and Its Role in Robust Estimation," Jour. of Amer. Stat. Assoc., Vol. 69, pp. 383-393.

17. Fitzgerald, R. J. "Dimensionless Design Data for Three-State Tracking Filters," Proc. J. Auto. Cont. Conf., 1971.